Biophysical investigation of the membrane and nucleic acids interactions of the transfection peptide LAH4-L1 : molecular mechanisms of complex formation and cellular entry

Nataliia Voievoda

UNIVERSITÉ DE STRASBOURG

UNIVERSITÉ DE STRASBOURG

EDSC

BIOZENTRUM
Universität Basel
The Center for
Molecular Life Sciences

ÉCOLE DOCTORALE SCIENCES CHIMIQUES

Institut de Chimie de Strasbourg

Institut de Chimie de Strasbourg UMR 7177

EN CO-TUTELLE AVEC

UNIVERSITÉ DE BALE

BIOZENTRUM

THÈSE présentée par :

Nataliia VOIEVODA

soutenue le : **25 juin 2014**

pour obtenir le grade de : **Docteur de l'Université de Strasbourg**

Discipline/ Spécialité : CHIMIE

BIOPHYSICAL INVESTIGATION OF THE MEMBRANE AND NUCLEIC ACIDS INTERACTIONS OF THE TRANSFECTION PEPTIDE LAH4-L1.

Molecular mechanisms of complex formation and cellular entry

THÈSE dirigée par :

M. BECHINGER Burkhard	Professeur, Université de Strasbourg
M. SEELIG Joachim	Professeur, Université de Bâle

RAPPORTEURS :

M. KELLER Sandro	Professeur , Université de Kaiserslautern
Mme SIZUN Christina	HDR, Université Paris-Sud 11

AUTRES MEMBRES DU JURY :

M. HILLER Sebastian	Professeur, Université de Bâle
Mme LEIZE-WAGNER Emmanuelle	HDR, Université de Strasbourg

ABSTRACT

Gene and RNA-based therapies have a great promise as the methods for the treatment of a great variety of genetic disorders and viral infections, but also it is a versatile tool for the investigation of the genetic and epigenetic mechanisms underlying the proper functioning or dysfunctioning of the cells and complex organisms. However, intracellular delivery of nucleic acids remains a major hurdle for the implementation of these therapies. In spite of the recent progress in the field, there is limited number of the non-viral transfection agents that passed to the clinical phase of the drug development.

An efficient transfection agent forms a complex (usually non-covalent) with nucleic acids, which is stable in the extracellular environment, in particular in the blood plasma. Furthermore, it should promote the cellular delivery by interacting with the plasma membrane or negatively charged glycosaminoglycans and inducing the endocytic uptake of the transfection complex. Finally transfection agent should enhance the endosomal escape and unpacking of the nucleic acids from the complex.

Cationic amphipathic cell-penetrating peptide comprise all above-named features as they associate electrostatically with the nucleic acids, they bind efficiently and translocate plasma membrane promoting the cargo uptake. LAH4-L1 is the lysine and histidine-rich designed peptide from LAH4 family, possessing a promising DNA and siRNA transfection activity, which was shown in biological experiments on the cell culture. LAH4-L1 peptide displays different modes of interaction with the membranes at neutral and acidic pH, which is one of the most important features that assure an efficient nucleic acid release to the cytoplasm.

This works is dedicated to the investigation of structural and thermodynamic characteristics of the pH-dependent LAH4-L1 association with model membranes and nucleic acids, such as generic DNA and siRNA. The variety of the biophysical techniques, as nuclear magnetic resonance, circular dichroism, isothermal titration calorimetry, dynamic light scattering and calcein efflux assay, were used to unravel the mechanism of efficient cellular transfection by LAH4-L1 peptide.

The orientation of the LAH4-L1 peptide in the POPC/POPS and POPC lipid bilayers is studied by ^{15}N static oriented solid state NMR. ^{2}H static NMR helps us to understand the mechanism of the peptide penetration into membranes and its association with negatively charged lipids.
Circular dichroism spectroscopy allows estimation of the peptide secondary structure changes upon the association with lipid bilayers, which, in turn, enables the construction of binding curves and calculation of the association constants.
Isothermal titration calorimetry is used for study of the energetics of the macromolecular interactions. Thus determination of the thermodynamic parameters of LAH4-L1 association with membranes and nucleic acids would allow comparison of the strength of such interactions. However, complex character of the calorimetric isotherms, which characterise peptide - membrane interactions, did not allow the calculation of the thermodynamic parameters. Yet the calorimetric isotherms were

used for characterisation of the process occurring upon peptide association with model membranes and nucleic acids.

Heteronuclear recoupling methods, in particular REDOR MAS solid-state NMR technique, allow calculation the distances between the pairs of heteroatoms, such as ^{31}P and ^{13}C, or ^{31}P and ^{15}N. The technique was used to estimate the proximity of the LAH4 peptide residues to the DNA phosphates. It was determined previously that only lysine residues are in a direct contact with DNA phosphates. In the present work lysine - phosphate proximity was investigated by REDOR in the LAH4 - DNA complexes, prepared at pH 5.5 and pH 7.4. The method of REDOR multispin simulation was developed and applied to the experimental results.

L’ABSTRAIT

Les thérapies basées sur les gènes et les ARN sont très prometteuses en tant que méthodes de traitement d'une grande variété de troubles génétiques et d'infections virales, mais aussi un outil polyvalent pour l'étude des mécanismes génétiques et épigénétiques qui sous-tendent le bon fonctionnement ou le dysfonctionnement de Les cellules et les organismes complexes. Cependant, l'administration intracellulaire d'acides nucléiques reste un obstacle majeur pour la mise en œuvre de ces thérapies. En dépit des progrès récents sur le terrain, il y a un nombre limité d'agents de transfection non virale qui sont passés à la phase clinique du développement de médicaments.

Un agent de transfection efficace forme un complexe (habituellement non covalent) avec des acides nucléiques, qui est stable dans l'environnement extracellulaire, en particulier dans le plasma sanguin. En outre, il devrait favoriser la distribution cellulaire en interagissant avec la membrane plasmique ou les glycosaminoglycanes à charge négative et en induisant l'absorption endocytique du complexe de transfection. Enfin, l'agent de transfection devrait améliorer l'échappement endosomal et le déballage des acides nucléiques du complexe.

Le peptide de pénétration de cellules amphipathiques cationiques comprend toutes les caractéristiques mentionnées ci-dessus car elles associent électrostatiquement avec les acides nucléiques, elles se lient efficacement et transposent la membrane plasmatique favorisant l'absorption de la cargaison. LAH4-L1 est le peptide conçu par la lysine et le complexe histidine de la famille LAH4, possédant une activité de transfection des ADN et des ARN prometteuse, qui a été démontrée dans des expériences biologiques sur la culture cellulaire. Le peptide LAH4-L1 présente différents modes d'interaction avec les membranes au pH neutre et acide, qui est l'une des caractéristiques les plus importantes qui assurent une libération efficace d'acide nucléique dans le cytoplasme.

Ce travail est consacré à l'étude des caractéristiques structurelles et thermodynamiques de l'association LAH4-L1 dépendante du pH avec des membranes modèles et des acides nucléiques, tels que l'ADN générique et les siARN. La variété des techniques biophysiques, comme la résonance magnétique nucléaire, le dichroïsme circulaire, la calorimétrie de titrage isotherme, la diffusion dynamique de la lumière et l'essai d'efflux de calcéine, ont été utilisés pour démêler le mécanisme de transfection cellulaire efficace par le peptide LAH4-L1.

L'orientation du peptide LAH4-L1 dans les bicouches lipidiques POPC/POPS et POPC est étudiée par RMN statique orientée ^{15}N. ^{2}H RMN statique nous aide à comprendre le mécanisme de la pénétration du peptide dans les membranes et son association avec des lipides chargés négativement.

La spectroscopie de dichroïsme circulaire permet d'estimer la structure secondaire du peptide en association avec des bicouches lipidiques, ce qui permet à la fois la construction de courbes de liaison et le calcul des constantes d'association.

La calorimétrie de titrage isotherme est utilisée pour étudier l'énergie des interactions macromoléculaires. Ainsi, la détermination des paramètres thermodynamiques de l'association LAH4-L1 avec les membranes et les acides nucléiques permettrait de comparer la force de ces interactions. Cependant, le caractère complexe des isothermes calorimétriques, qui caractérisent les interactions peptide-membrane, n'a pas permis de

calculer les paramètres thermodynamiques. Pourtant, les isothermes calorimétriques ont été utilisées pour la caractérisation du processus survenant lors de l'association peptidique avec des membranes modèles et des acides nucléiques.

Les méthodes de recouplage hétérogéné, en particulier, la technique RMN à l'état solide (REDOR MAS), permettent de calculer les distances entre les paires d'hétéroatomes, telles que ^{31}P et ^{13}C, ou ^{31}P et ^{15}N. La technique a été utilisée pour estimer la proximité des résidus peptidiques LAH4 avec les phosphates d'ADN. On a déterminé précédemment que seuls les résidus de lysine sont en contact direct avec des phosphates d'ADN. Dans le présent travail, la proximité de la lysine - phosphate a été étudiée par REDOR dans les complexes LAH4 - ADN, préparés à pH 5,5 et pH 7,4. La méthode de la simulation multispine de REDOR a été développée et appliquée aux résultats expérimentaux.

“Education is the most powerful weapon which you can use to change the world”

……

Nelson Mandela

To one of the world’s bravest men, who knew that the way to freedom is a long way, but this path lies only through the peace, dignity and forgiveness.

I dedicate this work to all Ukrainian people, who want to live a decent life they deserved, and were brave enough to stand up for their rights.

ACKNOWLEDGMENTS

First and foremost I would like to express my gratitude to Prof. Burkhard Bechinger for giving me a chance to pursue my doctoral studies in one of the best European Universities, to work on the extremely interesting and actual topic and for creating the conditions for learning a variety of biophysical methods, especially solid-state NMR. Frankly, it was a risky deal to take for the project a student with degree in organic synthesis and only a little notion of the biophysical investigations, so thank you very much for that. Thank you also for the thoughtful review of this thesis manuscript, including the correction of all of my english grammar mistakes.

I'm truly thankful to Prof. Joachim Seelig for the possibility to work in the Biozentrum of Basel and to learn the calorimetry techniques, for the fruitful and interesting discussions, and for providing highly valuable comments and corrections on the manuscript.

I also would like to acknowledge the people without whom this work literally would not be realised. Thanks a lot, Christopher, for being always beside when I needed a help whether it was setting up an experiment and discussing the results, or managing the laboratory hardware.

Elise, without you our lab would fall apart! Thank you very much in the first place for organising our laboratory lives, but also for your help with the biological experiments, which I had difficulties to accomplish, for all of the discussions and for nice time spent together.

Thank you, Philippe, for enrolling and supervising me at such interesting REDOR project and for your appreciable teaching method. Only because you believed I'm able to set up the experiment by myself, I did it and I learn it.

Well, the learning process was not possible without small accidents, as damage of an expensive NMR probe. So, thank you very much, Jesus, first of all for your patience, for the great sense of humour, the valuable advices, and for introducing me to the solid-state NMR hardware.

Thank to Arnaud for the help with mastering DLS, CD and for the assistance with setting up the contacts. Thanks to Evgeniy for the help with NMR experiments.

I would like to acknowledge all other people who assured the proper performance of my experiments, in particular to Dr. Therese Schulthess for her assistance with the ITC experiments, and Dr. Martine Heinrich for the help with CD and the fluorescence measurements. Thank you, Delphine, for the peptide synthesis and purification and for all other work about laboratory organisation.

I would love to thank Anna for her support, she is still helping me with the advices even being far away. Thank you, Barbara, for the fun days at work and outside the work, and for constantly producing a fresh ideas how to spend a great time.

A separate thank to my other PhD days comrades, Omar, Patricia and Hiba for sharing our time and experience. Thanks to Matthias for the help and assistance with variety of the experiments at my really first attempts to do science.

Thank you, Louic, for interesting discussions and your advices. I regret we did not spend more time working together.

A special thank to Caroline, Nadia for saving me a huge amount of time by always helping to solve any kinds of organising issues, and to other chemistry department administrative assistants for creating a comfortable conditions for work.

My special acknowledgments to Collège doctoral européen, who accepted me as a student and hosted in their superb residence. Also I would like to thank CDE for the financial support, which allowed me to finish all the necessary experiments.

Accomplishment of this PhD thesis was made possible with the financial support from the Alsace region, to which I'm grateful for the 3-year full-time funded PhD contract. My full gratefulness to the Institut de Science et d'Ingénierie Supramoléculaires for hosting our laboratory and for providing an excellent working environment during two years of my PhD studies.

I'm indeed grateful to the Career development centre of the University of Strasbourg ('Espace Avenir') for the great programs and events they organise to guide the PhD students in their search for the professional avenir.

Many many thanks to all Addal members for all the events and lovely activities that they organised and we organised together. I'm really happy and proud for being part of this organisation. The improvement of my French speaking skills I owe primarily to the participation in the Addal activity.

I also would like to thank the University sport centre, who were responsible for my good physical shape and for the nice time after-work.

My warm-hearted gratitude to my family for their love, patience and ever-present support. They always encouraged me in all of my initiatives. I'm really-really appreciate that they let me leave home at 13-years old in order I could pursue my lyceum studies in the far-away Kiev. I'm more than sure that this determine largely who I am today, so I owe this degree to my family.

Tons of thanks to my dear friends, especially to my ukrainian friends in Strasbourg, with whom we приємно згаяли lots of time, and hopefully will do much more! Thank you, guys, for your help and for that you are as you are!

Table of Contents

INTRODUCTION AND MOTIVATIONS

In the following chapters the rational design of the peptidic transfection vectors LAH4-L1 will be discussed. It will be shown how particular structural features, such as position of the positively charged amino acids and hydrophobic angle, determine the peptide performance in the transfection experiments on the cellular culture. The overview of the biophysical investigations of the LAH4-L1 (LAH4) peptide complexes with DNA, done previously, will be provided.

Afterwards the introduction to the biophysical techniques will be provided, in particular to solid state NMR and isothermal titration calorimetry methods for the study of peptide - membrane interaction. The calorimetric signatures of the membrane association for various peptide classes will be discussed in greater detail.

The value of isothermal titration calorimetry for the investigation of cationic polymers complexes with nucleic acids will be show as well.

We will discuss which structural features in proteins determine the specific or non-specific association with nucleic acids, and the NMR methods that allow investigation of the protein - DNA/RNA complexes. In particular, it will be shown how dipolar decoupling solid-state NMR methods are used for the intermolecular distance measurements.

Finally, the structure and composition of the natural and model membranes will be reviewed briefly.

I. LAH4 AND LAH4-L1, THE PEPTIDES WITH A POTENT TRANSFECTION ACTIVITY.

LAH4 and LAH4-L1 physicochemical properties.

LAH4 is a cationic amphipathic histidine-rich peptide of 26 amino acids long (KKALL ALALH HLAHL ALHLA LALKKA), which was first designed to evaluate the structural characteristics of peptides with antimicrobial activity and to better understand the energetic contributions that determine their membrane topology (Bechinger, 1996). The LAH4 peptide hydrophobic core consists of leucine and alanine residues, interrupted by four histidines. Four lysines on the termini ensure good solubility in aqueous environments. The helical wheel analysis (Schiffer and Edmundson, 1967) represents schematically the amino acids distribution when the peptide is in an alpha-helical conformation (***Figure I-1***) where the distribution of amino acid side chains determines the polar angle and the angle subtended by the cationic residues, which for an ideal alpha-helix equals 100° for LAH4. The pKa of the histidine imidazole ring is about 6.0. The precise pK values of LAH4 histidines were determined in the presence of dodecylphosphocholine micelles using solution NMR spectroscopy by following the ^{1}H chemical shift of the imidazole protons (pK values found are 5.4, 5.8, 5.9, and 6.0). The secondary structure of LAH4 peptide in DPC micelles was determined by ^{1}H homonuclear multi-dimensional correlation NMR spectroscopy in solution (Georgescu et al., 2010). It was found that LAH4 forms an α-helix spanning residues 9–24 at pH 4.1 with the N- and C-terminal residues remaining largely disordered. At pH 6.1 the peptide undergoes conformational transitions and adopts a helix-loop-helix structure, where two helical domains are formed encompassing residues 3–9 and 14–24. At pH 7.8 LAH4 reverts to a long α-helix including residues 4–21. It was suggested that such helix transition from C-terminus to N-terminus *via* loop formation might facilitate the in-planar-to-transmembrane re-orientation of the peptide. The corresponding structures could be found in Protein Data Bank under the items 2KJN (pH 4.1) and 2KJO (pH 6.1).

LAH4-L1 (KKALL AHALH LLALL ALHLA HALKKA) is a related peptide from same family designed to improve the transfection capacity (Mason et al., 2006a). The rationale for peptide design will be discussed below. LAH4-L1 possesses a reduced polar angle when compared to LAH4 (80°, ***Figure I-1***). Both LAH4-L1 and LAH4 peptide change nominal charge from 9 at acidic pH to 5 at pH around 7 similarly to LAH4, as illustrated in a ***Figure I-1.***

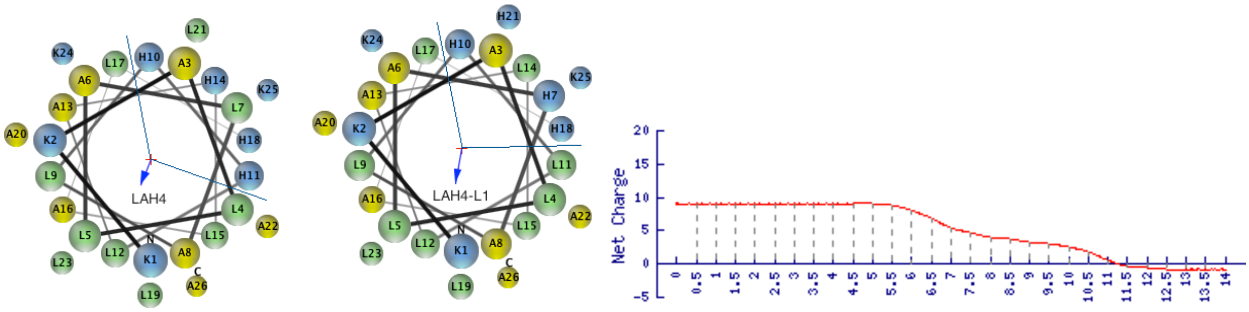

Figure I-1. Helical wheel representation of LAH4 and LAH4-L1 peptides, created with Membrane Protein Explorer (MPEx) tool (Stephen White, Craig Snider, Sajith Jayasinghe, & Kalina Hristova, UC Irvine), which could be found at http://blanco.biomol.uci.edu/mpex/; LAH4-L1nominal charge, calculated with the on-line tool developed by GenScript USA Inc. (USA), available at https://www.genscript.com/ssl-bin/site2/peptide_calculation.cgi.

This pH-controlled protonation of histidines has been used previously to modulate the membrane insertion of the model peptide LAH4, since its orientation in the target membrane depends on the charge

distribution in the peptide (Vogt and Bechinger, 1999). At acidic pH, when the histidines are protonated, the LAH4-helix adopts an in-plane orientation along the membrane surface, when at neutral pH the uncharged histidine residues render a more hydrophobic helix such that the peptide adopts a transmembrane orientation with the lysine residues acting as anchors at the membrane surfaces. LAH4 membrane alignment was found to influence its antimicrobial activity. Thus at low pH (≈5) LAH4 exhibits 2 orders of magnitude higher antibiotic activity than at neutral pH. Moreover, membrane-disruption activity is five time more pronounced at pH 5, which was shown by calcein release assay on POPC and mixed POPC/POPG model membranes (Vogt and Bechinger, 1999). Therefore, LAH4 antimicrobial activity was associated to its membrane *in-planar* alignment via a 'detergent-like' mechanism of action.

Further in this chapter I provide the overview of development the efficient nucleic acid delivery agent on the base of LAH4 peptide. The motivation for biophysical characterisation of LAH4-L1 peptide interaction with model membranes and nucleic acids will be revealed. The emphasis is made on the rationale of transfection peptide design, because those investigations uncover many important details about the mechanism of LAH peptides interaction with lipid bilayers.

Rational design of gene delivery peptides.

Short anionic lysine-rich peptides such as KALA (Wyman et al., 1997) and ppTG20 (Rittner et al., 2002), and C-terminal domain of HIV type 1 Viral protein R ($Vpr_{52–96}$) (Kichler et al., 2000) exhibit high potential as gene delivery agents. They have capacity to bind DNA and destabilize membranes at the same time, the properties that are indispensable for efficient gene transfer *in dividing cells*. These transfecting peptides adopt an α-helical conformation under interaction with membranes with positively charged lysines or arginines positioned on one face of the helix. The LAH4 peptide possesses similar structural characteristics when inserted in lipid bilayers. The angle subtended by the histidine residues in the LAH4 α-helical conformation equals to 100°.

Poly-L-lysine was the first synthetic reagent possessing transfection capacity (Wu and Wu, 1987). For an overview over the chemical vectors for gene delivery please see the dedicated publication (Midoux et al., 2009). Plasmid DNA – polylysine complexes increase the uptake of DNA by mammalian cells, but plasmid molecules are then often trapped inside endosomal vesicles where they cannot escape to reach the nuclear machinery. Substitution of about 35% of ε-amino groups by histidine residues allowed the increase the polymer transfection capacity. The drastic inhibition of transfection activity in the presence of bafilomycin A1 indicates that the protonation of the imidazole groups in the endosome lumen favour the delivery of pDNA into the cytosol (Midoux and Monsigny, 1999).

LAH4 peptide possesses the structural and physicochemical properties that allow it to be considered as the promising transfection agent. First of all the peptide is rather well soluble in the water and in buffers of varied salt concentration. It associates with zwitterionic POPC membranes (Vogt and Bechinger, 1999). It possessed different charge at pH 5 and pH 7.4, and different membrane topology. It was assumed that the lysines in the LAH4 peptide sequence might serve then for DNA condensation and the histidine residues might favour endosomal escape of the DNA.

Cell transfection assays.

The series of transfection experiments *in vitro* was performed, in which *luciferase* reporter gene activity was used to quantify the delivery efficiency. The structural characteristics of the efficient transfection peptide were determined. It was shown that the sole presence of histidine and lysine residues is not sufficient to obtain an efficient transfection agent. The number of histidine residues, their position

in the sequence, and the pH at which the peptides change from an in-planar to a transmembrane alignment are all crucial parameters that determine the transfection capacity (Kichler et al., 2003a).

In a first step of evaluation several members of LAH peptides family with varied number of histidine residues were chosen for transfection activity test. All these peptides consist of four terminal lysines, a hydrophobic core represented by leucines and alanines, and certain number of histidines in the middle of the peptide sequence (***Table I-1***). The peptides that contain 1 to 3 histidine residues (LAH1–LAH3) were found to be at least 10 times less efficient in plasmid DNA delivery than LAH4 or LAH5.

Table I-1. LAH peptide family members used for transfection capacity evaluation (Kichler et al., 2003b).

LAH1	KKLALALALAL**H**ALALALALKKA	23*aa*
LAH2	KKLA**H**LALALALGLALA**H**LAKKA	23*aa*
LAH3	KKALALGL**H**LA**H**LAL**H**LALALKKA	24*aa*
LAH4	KKALLALAL**HH**LA**H**LAL**H**LALALKKA	26*aa*
LAH5	KKALLALAL**HH**LA**H**LA**HH**LALALKKA	26*aa*

In the next evaluation step LAH4 derivatives and salivary antimicrobial peptide histatin-5 were used to show how different structural properties of peptides influence their transfection capacity.

The summary of transfection and gel retardation assay test results are provided in a ***Table I-2*** and the helical wheel representation of peptide's sequences is given in a ***Figure I-2***. In gel retardation assay the plasmid DNA and peptide were mixed at certain molar ratio and deposited on the agarose gel. Then a minimum amount of peptide capable to completely retard the DNA migration was determined and provided in the table.

Table I-2. Amino acid sequence and transfection efficiency of LAH4 peptides. Adapted from (Kichler et al., 2003a)

Peptide	Sequence	Retardation assay, μg of peptide*	Transfection efficiency**	Optimal ratio, μg of peptide / μg of DNA***
LAH4	*KKALLALAL**HH**LA**H**LAL**H**LALALKKA*	*2.5*	*1 000*	*6*
LAK4	KKLAKALAKALAKALKLALALAKK	2.5	≤1	2.5
Histatin-5	DS**H**AKR**HH**GYKRKFHEK**HH**S**H**RGY	>50	<1	7.5
LAH4-L3	KKALLALAL**HH**LALLA**HH**LALALKKA-NH2	<2.5	1 150	6
LAH4-L4	KKALLALAL**HH**LALLA**H**LLAL**H**LKKA-NH2	1	510	4
LAH4-A6	KKKKALA**H**L**H**ALAA**H**L**H**ALAAAALKKK	2.5	140	15
LAH4-L6	KKKKALL**H**L**H**LLAL**H**L**H**LLALLALKKK	2.5	10	12
LAH4-G6	KKKKALG**H**L**H**GLAG**H**L**H**GLAGGALKK	>50	≤1	7.5
H4-LAK4	**HH**ALLALALKKLAKLALKLALAL**HH**A	1	20	5

*The indicated amount of peptide is the minimal amount required to completely retard 1 μg of plasmid DNA.
**The value 1,000 was given to the luciferase activity obtained with LAH4. Transfection experiments were performed on HepG2 cells.
***Amount of peptide per μg of DNA that gives the highest reporter gene expression.

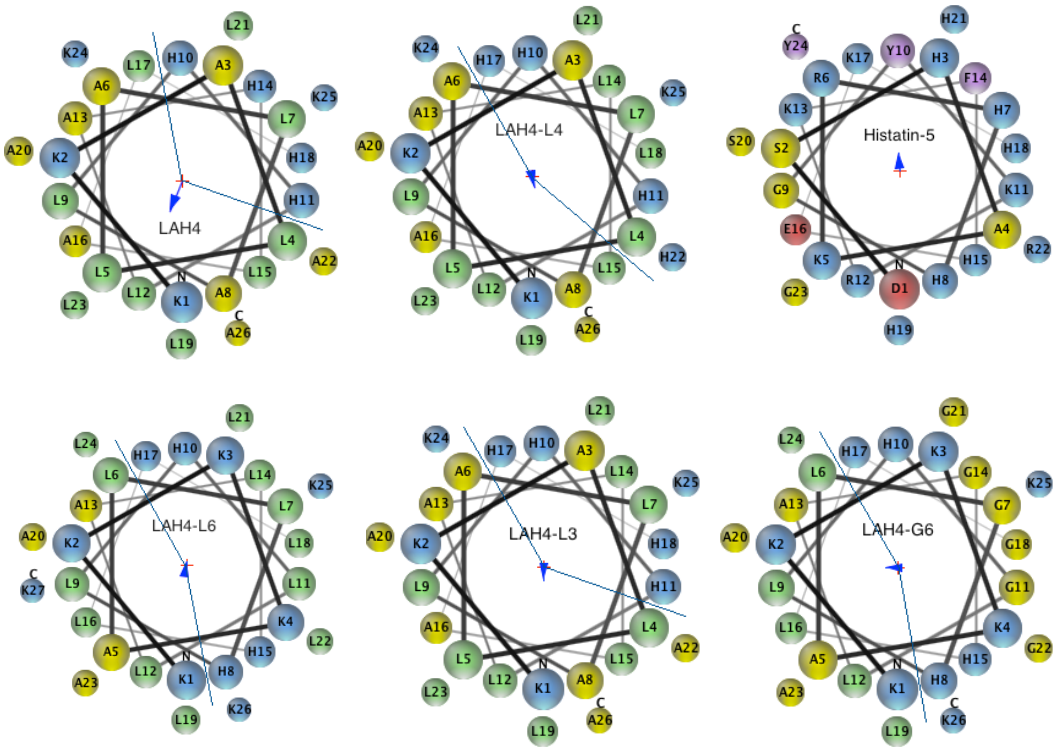

Figure I-2. Helical wheel representation of some LAH4 peptides used in the test and histatin-5.

The transfection and gel retardation assays on the LAH4 peptide and its derivatives allowed discerning the principal structural elements that assure high transfection activity of peptides. Those structural characteristics can be summarized as follows:

- *histidine presence is essential*. LAK4 showed very poor transfection activity;
- *presence of a well defined hydrophobic face*. Histatin-5, which has equal distribution of hydrophilic residues along the surface, shows poor transfection activity and low DNA retardation capacity. The ability of the peptides to complex DNA is then not only linked to the global charge of the peptide, but requires specific structural motifs.
- *the position of the four histidine residues in the hydrophilic face*. LAH4-L4 shows slightly lower luciferase activity level than LAH4 and LAH4-L3, suggesting that optimal transfection efficiency requires four histidines to be placed within defined angle, which is formed when peptide adopts α-helical structure. LAH4-L3, LAH4-L4, and LAH4 peptides with the angles of 120°, 160° and 100° respectively, all show pronounced transfection efficiencies, indicating that the position of the histidine residues within the polar face is important, though minor modifications can be tolerated. However when this angle was reduced to 60°, rather big loss of activity was observed (LAH4-L0, Mason et al., 2006)
- *in-plane to transmembrane reorientation of peptide with increasing pH*. For LAH4 the midpoint of the IP to TM transition was determined at $pH_{50} = 6.1$ in POPC membranes (Bechinger, 1996)> Three other mutants with different transition points were tested: LAH4-L6 with $pH_{50} = 4.8$, LAH4-A6 with $pH_{50} = 6$, and LAH4-G6 with $pH_{50} > 8.5$. Table II.2 shows that LAH4-L6 and -A6 were able to complex DNA efficiently and to retard its electrophoretic migration, when LAH4-G6, which is considerably more hydrophilic, was unable to fully retard the migration of DNA. In transfection experiments the three mutants are significantly less efficient than LAH4, but LAH4-

A6, the peptide having the closest transition midpoint to LAH4, was also the most efficient when compared with LAH4-L6 or -G6.

- *the histidine residues have to be positioned in the core of the peptide*. H4-LAK4 with inverted positions of lysines and histidines was significantly less active in gene transfer than LAH4 (Kichler et al., 2003a).
- *number of positively charged residues.* LAH4 analogue with two extra lysines on each terminus K2-LAH4-K2 (KKKKALLALAL**HH**LA**H**LAL**H**LALALKKKK) was synthetized to evaluate the influence of increased charge on transfection activity. Two parameters were measured and compared with those of LAH4. First the DNA uptake by the cell was quantified. It was found that K2-LAH4-K2 delivers about three fourths of the DNA amount found with LAH4. But the transfection capacity observed by reporter gene expression, was about 24 600 times smaller for K2-LAH4-K2 (Kichler et al., 2007). The difference was explained by elevated lytic activity of K2-LAH4-K2 even at neutral pH. The increased destabilization of membranes affects only little the uptake process, but the peptide is then much more cytotoxic for the cells. Also, too tight association with DNA therefore lack of membrane lysis upon pH decrease.
- *ability to adopt α-helical structure.* LAH4 peptide mutant with the proline incorporated into the middle of sequence (P15) was synthetized and tested as well. It is known that proline lacks the ability to form an α-helical conformation. Therefore when placed right in the middle of the sequence it modifies the secondary structure of peptide. LAH4-P15 was found to be 1500 times less active in transfection experiments. Also LAH4-P15 peptide was able to deliver 25 times less genetic material than LAH4. It is not more toxic to the cells than LAH4, as was shown by cell viability test. It means that the ability of peptide to form α-helix is one of the key factors to successful delivery (Kichler et al., 2007).
- *peptide length.* Increase of the peptide length to 30aa by adding more hydrophobic residues, as leucines or alanines, cause the slight decrease of activity, even though it helps to reduce the peptide/DNA complex size (Mason et al., 2007a). But depletion of hydrophobic amino acids either on C-terminus, or on N-terminus leads to the activity reduction by about 20 times (Kichler et al., 2007).

To summarize this investigation, the two peptides with quite close structural characteristics – LAH4 and LAH4-L3 – proved to be the most promising transfection agents among all the peptides tested.

In a final step LAH4 transfection efficiency was compared to that of commercial reagents pLys180 and 25-kDa PEI. LAH4 was found to be significantly more efficient than polylysine with four various cell lines and was about as active as PEI (Kichler et al., 2003a).

In another experiment LAH4 gene delivery capacity was compared with activity of some cell-penetration peptides, such as KALA (WEAKLAKALAKALAKHLAKALAKALKA), TAT47-57 (YGRKKRRQRRR), ppTG20 (GLFRALLRLLRSLWRLLLRA) and Vpr55-91 (TGVEALIRILQQLLFIHFRIGCRHSRIGIIQQRRTRN) and the commercial agent DOTAP (Prongidi-Fix et al., 2007). The result of transfection test shows clear precedence for LAH4 peptide over the rest of tested compounds.

Effect of the outer membrane composition. Hereinafter in a transfection experiment on transformed cells LAH4 showed about 2 orders of magnitude higher activity on human hepatocarcinoma (HepG2) and transformed HEK 293 cells as compared with other eukaryotic tissues (mouse fibroblasts NIH 3T3 and rabbit aorta smooth muscle cells Rb1). The outer membrane of transformed cell possess elevated fraction

of negatively charged POPS lipid, with suggest the preferable association of LAH4 – pDNA transfection complex with anionic membrane surfaces (Kichler et al., 2003a).

Agarose gel retardation assay. pH effect. Agarose gel electrophoresis allows to monitor that plasmid DNA (SMD2-LucΔITR, 7.6 kbp) retardation occurs at a LAH4/DNA *w/w* ratio of 1.75 at acidic pH (5.2), whereas a ratio of approximately 2.5 is required to inhibit the migration of plasmid DNA at neutral pH (Kichler et al., 2007).

Suggested mechanism of transfection complex uptake and endosomal escape induced by LAH4.

At the first step of endocytic uptake peptide would be either inserted into endosomal membrane in its transmembrane orientation or/and associated with the DNA complex. As soon as uptake of DNA-LAH4 complex occurs from the outer membrane, it stays in contact with outer membrane, which has low fraction of anionic lipids. I would like to draw your attention to the fact that LAH4/plasmid DNA ratio, which promotes the highest reporter gene expression, is 6/1*w/w* (Kichler et al., 2003a). But the peptide/pDNA ratio of only 2.5/1*w/w* is required to inhibit the migration of plasmid DNA at neutral pH (Kichler et al., 2007). It means that in transfection complex there will be quite large amount of peptide available to interact with membranes.

Inside early endosomes the pH is about 6.2 – 6, but it drops to about 5.5 – 5 when the endosome matures (Huotari and Helenius, 2011). The histidine imidazole groups become protonated at these conditions, and less peptide associates with the DNA complex. Therefore the peptide is available to insert into the membrane where it adopts in-planar orientation, in which its membrane disruption activity is more pronounced. It was suggested that at this step LAH4 causes flip-flop of anionic lipids from the cytoplasmic facing monolayer of endosomal membranes (Mason et al., 2006a). Anionic lipids will then attract the LAH4 peptide from transfection complexes, and together with enhanced membrane destabilization, it will provoke the release of oligonucleotide into the cytoplasm(Mason et al., 2006a).

Correlation between transfection capacity and membrane destabilization activity.

At the following stage the investigations were supplemented with ^{2}H solid-state NMR measurements (Mason et al., 2006a). Four LAH4–derived peptides of similar amino acid sequence, but with varied angles subtended by the histidine side chains, were designed for this experiment. Peptide sequences are given in a ***Table I-3***.

Table I-3. LAH4–derived peptides with varied angles subtended by the histidine side chains.

LAH4	KKALLALAL**HH**LA**H**LAL**H**LALALKKA	100°
LAH4-L0	KKALLA**H**ALA**H**LALLAL**H**LAL**H**LKKA	60°
LAH4-L1	KKALLA**H**AL**H**LLALLAL**H**LA**H**ALKKA	80°
LAH4-L2	KKALLALAL**HH**LALLAL**H**LA**H**ALKKA	100°
LAH4-AL6	KKALL**H**LALALLAL**H**A**H**ALAL**H**LKKA	180°

As it was show previously that the presence of anionic lipids plays the important role in mediation of transfection complex uptake and DNA release into cytoplasm, the series of biophysical experiment was performed to show how peptide associates with mixed anionic peptides. Wide line ^{2}H NMR on chain deuterated analogues of POPS or POPC has provided a more detailed view of how LAH4 disrupts mixed POPC/POPS/cholesterol lipid bilayers at pH 5 and has shown that the PS chain order parameter profiles are more readily disordered by LAH4 than those of PC. Among the LAH4 derivatives with varied angles subtended by the histidine side chains, their effect on POPS order perturbation was rather segment-

specific. Such all four LAH4 isomers perturbed the lipid chains to a similar extend in the region toward the lipid head group (between chain position 2 and 10). However, the lower part of the chain, in the hydrophobic core, was much more selectively affected by LAH4 isomers. LAH4-L2 and -L1 have a similar effect on chain order and both disrupt the lower part of the chains more effectively than LAH4-L0, while LAH4-AL6 had comparably weak effect. The results suggested that the depth of bilayer penetration of the LAH4 peptides is modulated by the distribution of hydrophobic residues in the helix.

Also clear relationship was observed between the POPS chain-order disruption activity and the transfection efficiency of those peptides, with LAH4-L2 and -L1 being the most active in transfection experiments.

Further the transfection activity of the most promising delivery peptides LAH4 and LAH4-L1 was investigated in the presence of foetal calf serum (Mason et al., 2007a). Again a series of LAH4 and LAH4-L1 derivatives with various properties was prepared for test. Their structures and brief characteristics are provided in a ***Table I-4***. Various structural characteristics were incorporated by design. For example the number of histidines in LAH4-L1 was increased to 6, yielding a peptide with decreased hydrophobic surface LAH6-L1. Other peptide conserves the angles of LAH4-L1, but has 6 histidines and increased length (LAH6-L1-80). LAH4-L1-30 conserves the number of histidines and angle, subtended by histidine residues, but has increased length. The peptides, in which amino acids were partially or completely substituted by D-analogues were also tested.

Table I-4. The structures and properties of LAH4 and LAH4-L1 derivatives. Adapted from (Mason et al., 2007a)

Peptide	Sequence	Peptide length	DNA retardation	Angle
LAH4	KKALLALAL**HH**LA**H**LAL**H**LALALKKA	26	2.5	100
LAH4-L1	KKALLA**H**AL**H**LLALLAL**H**LA**H**ALKKA	26	2.5	80
LAH6-L1	KKALLA**H**AL**HH**LALLA**HH**LA**H**ALKKA	26	2.5	120
LAH6-L1-80	KK**H**LLA**H**AL**H**LLALLAL**H**LA**H**ALA**H**LKKA	29	2.5	80
LAH4-D	*KK*ALLALAL**HH**LA**H**LAL**H**LALAL*KK*A	26	2.5	100
LAH4-L1-30	KKALLAA**H**AL**H**LLAALLA**H**LL**H**ALLALKKA	30	5	80
LAH4-L1-30-D	*KK*ALLAA**H**AL**H**LLAALLA**H**LL**H**ALLAL*KK*A	30	2.5	80
D-LAH4	*KKALLALAL**HH**LA**H**LAL**H**LALALKKA*	26	1.75	100

[a]*Amount of peptide (μg) needed for complete retardation of 1 μg of plasmid DNA.*

Results of the transfection in the serum-free medium. The lead peptide LAH4-L1 was shown again to be the most effective vector for each of the tested cell lines. LAH6-L1-80, where the charged residue angle at acidic pH is maintained, was also effective transfection agent with expression levels close to LAH4-L1. LAH6- L1 had reduced efficiency, and the longer versions of LAH4-L1 or peptides with incorporated D-amino acids had shown quite low transfection efficiency across all cell lines.

Transfection in the presence of serum. The presence of 20–25% serum in the transfection medium reduces the transfection efficiency of all peptide vectors. However the effects varied considerably according to the structural properties of peptides. LAH4-L1 and LAH6-L1-80 were affected the least by the presence of serum. The transfection capacity of LAH6-L1 peptide was almost completely suppressed by the presence of serum. The transfection efficiency, mediated by peptides containing terminal D-amino acids, was noticeably reduced too in serum media, such incorporation of D-amino acids at the peptide

termini does not protect against the serum degradation effect. Transfection capacity of D-LAH4 was also weak (Mason et al., 2007a).

Therefore **efficient peptidic vector** has following structural characteristics:

- it adopts α-helical structure under the interaction with membranes.
- it possesses histidine residues that becomes protonated when pH drops from 7.4 to 5,
- it possesses optimal number of positively charged (at neutral pH) residues, such has a capacity to condense DNA. However, by increasing the number of positively charged amino acids it was not possible to improve peptide's transfection capacity, because it increases its toxicity.
- it has well defined angle, subtended by positively charged amino acid residues, because the latter determines the peptide's membrane destabilization properties at acidic pH. Such the peptides which are characterized by rather small angle of 100° (LAH4, LAH4-L2, LAH4-L3) or 80° (LAH4-L1, LAH4-L1-30, LAH6-L1-80) were the most promising transfection agent, with LAH4-L1 being the leader compound.
- augmentation of the number of histidines does not affect the transfection ability, as soon as the angle, subtended by histidines, is conserved.
- the peptide should have optimal length (26-29aa) and hydrophobic-to-hydrophilic residues ratio.

Biophysical characterization of transfection complexes.

Isothermal titration calorimetry. The energetics of LAH4 association with low molecular weight salmon sperm DNA (around 300 base pairs) was studied by ITC (Prongidi-Fix et al., 2007). The measurements were performed in phosphate-saline buffer (10mM phosphate, 137mM NaCl) at various temperatures (288, 298, 308K). The thermodynamic parameters as free energy of binding (ΔG), association constant (Ka), entropy change (ΔS) and the stoichiometry (N), were calculated from the calorimetric isotherms, assuming 'single set of binding sites' model. DNA-peptide association reaction was exothermic at pH 7.5 and endothermic at pH 5.5, such at pH 5.5 the process was more entropy-driven. The stoichiometry of association was determined to be 148±39 LAH4 per DNA (300bp) at pH 7.5 and 98±10 at pH 5.5 (Prongidi-Fix et al., 2007). The results indicate that a very high molar ratio of LAH4 is required to saturate the binding sites of DNA, therefore there cannot be specific interaction with LAH4 peptide. It was suggested that the lysine residues of the peptide are associated electrostatically with neighbouring DNA strands, which promotes DNA condensation and formation of big globular aggregates.

Structural investigations by solid-state NMR. LAH4 samples labelled

with ^{15}N and/or ^{13}C selectively and/or uniformly were prepared in order to test by REDOR solid-state NMR technique which of the peptide side chains exhibit close proximities (<8Å) to the ^{31}P nuclei of the DNA inside the transfection complex (Bechinger et al., 2011; Vidovic, 2011). The transfection complexes were prepared at pH 5.5, and the optimal peptide/salmon sperm DNA ratio was chosen on the basis of previous investigations – agarose gel electrophoresis, ITC, centrifugation assay (Prongidi-Fix et al., 2007). The first REDOR test on the peptide with a specific ^{13}C label at the β-positions of Ala-6 and Ala-13 indicated that these residues do not reside in the proximity of the DNA phosphates. Then the REDOR effect was measured using $^{13}C/^{15}N$ uniformly labelled peptides, the close distances were found between the ^{15}N and ^{13}C nuclei of the lysine side chains and the ^{31}P nuclei of DNA phosphate groups, but not for any of the other side chains. The distances in the range of 5Å were detected between terminal amino group nitrogens and phosphate groups. Furthermore, the REDOR measurements were performed on the LAH4/DNA complexes, where one of the lysines was uniformly labelled with ^{15}N, thus the distances to DNA phosphate groups were resolved for each lysine side chain. The closest proximity to

DNA phosphates (4Å) was detected for terminal amino group nitrogens of 2nd and 24th lysines. Therefore, the model where DNA – LAH4 association is governed by electrostatic attraction, and exclusively lysine side chains are interacting with DNA was confirmed by NMR structural measurements.

ITC and gel shift assay have shown different stoichiometry of DNA – LAH4 complex at various pH (5.5 and 7.5). We were interested if the structure of transfection complex would be also different at pH 7.5, therefore REDOR NMR investigation were carried on in present work (Chapter XI).

Macroscopic parameters. The size and charge of transfection complexes, formed by various peptides, were assessed by DLS and ζ-potential measurements (***Table I-5***). All of the transfection complexes carry positive charged at peptide/DNA ratio that exhibits the highest transfection levels. The size of complexes is considerably increased in the buffers with high (150mM) ionic strength. In the presence of 25% serum there was no consistently observable increase or reduction in complex size as was expected taking into account the effect of serum on complex size for histidylated polylysine, where the size of complexes were reduced approximately 10-fold in the presence of more than 5% serum, which were only around 100 nm in diameter (Bello Roufaï and Midoux, 2001).

Table I-5. Size and zeta-potential of the peptide/DNA complexes. Adapted from (Mason et al., 2007a).

Peptide	Peptide/DNA (w/w ratio)	+/- ratio	Zeta-potential (mV)	Size in water (nm)	Size in 150mM NaCl (nm)	Size in 150mM NaCl +25% FCS (nm)
LAH4	6/1	3.6	26	229	994	1488
D-LAH4	3.75/1	2.25	24	257	1470	1853
LAH4-D	10/1	6	27	ND	2904	2330
LAH4-L1	6/1	3.6	33	87	1502	1395
LAH4-L1-30	7.5/1	3.9	37	121	246	351
LAH4-L1-30-D	7.5/1	3.9	40	120	207	249
LAH6-L1-80	9/1	4.7	35	103	1422	2553
LAH6-L1	5/1	2.9	22	140	1533	1788

[a]The peptide/DNA that were used to perform the size and zeta-potential measurements correspond to the ratios that gave the highest expression on HepG2 cells. [b]As all the peptides are C-terminally amidated, the LAH4 lysines and the N-terminus are the only positively charged amino acids, conferring a nominal charge of +5 to the peptides at pH 7.5.

Membrane order perturbation and antimicrobial properties of LAH4 family peptides.

It was shown that LAH4 peptide inhibits the *E. coli* grows more efficiently at pH 5.5 than at neutral pH (7.2) (Vogt and Bechinger, 1999). Mason and co-workers have expanded the investigation of antibacterial properties on other LAH family peptides, including LAH4-L1 (Mason et al., 2006b). The activities of LAH peptides were compared with the activity of antibacterial peptide magainin 2. In particular, LAH6-L1 peptide (KKALL A**H**AL**H** **H**LALL A**HH**LA **H**ALKKA, 120°), which possesses two extra histidines, was found to be the most efficient agent against wide range of Gram-positive and Gram-negative bacteria, and its efficiency was almost as pronounced at pH 7.2 as it was at pH 5.5. LAH4-L1 (KKALL A**H**AL**H** LLALL AL**H**LA **H**ALKKA, 80°), similarly to LAH4 peptide, has shown more promising activity at pH5.5 than at neutral pH, with ten times bigger efficiency at pH 5.5. In contrast, the addition of phenylalanine residues to the sequence (LAH4-L1-F4, KKALL A**H**FF**H** LLALL

AL**H**FF **H**ALKKA, 80°) reduced drastically the antibiotic efficiency of the peptide, especially at pH 7.2. The peptide's activity reaches the level observed for magainin 2, which is also enriched in phenylalanine residues (GIGKFL**H**SAKKFGKAFVGEIMNS).

The order perturbation of deuterated acyl chains of POPE and POPG lipids in mixed POPE/POPG=75:25 membranes by LAH peptides was investigated by ^{2}H static solid-state NMR spectroscopy (Mason et al., 2006b). Thus LAH6-L1 has shown great disruption effect on PE as well as PG acyl chains at acidic pH, but caused very weak order perturbation effect at pH 7.5. LAH4-L1 induced a slight reduction of POPE and POPG acyl chain

order at pH 7.5, yet it was smaller compared with the effect at pH 5.5. Similarly order perturbation induced by LAH4-L1 peptide was more pronounced for POPG than POPE acyl chains. Finally, the behavior of LAH4-L1-F4 was really close to that of LAH4-L1 peptide.

Future development of LAH4-L1 as transfection agent.

siRNA transfection capacities of LAH4-derived peptides were investigated on six peptide sequences, all 26*aa* long, possessing the charge +5 at pH 7.5 with varied degree of hydrophobicity (Langlet-Bertin et al., 2010):

LAH4 KKALLALAL**HH**LA**H**LAL**H**LALALKKA,
LAH4-Leu KKALLAL*L*L**HH**L*L***H**ALL**H**L*L*LALKKA,
LAH4-L1 KKALLA**H**AL**H**LLALLAL**H**LA**H**ALKKA,
LAH4-L1-R RRALLA**H**AL**H**LLALLAL**H**LA**H**ALRRA,
LAH4-L1-Leu KKALLA**H***L*L**H**LLLAL*L*L**H**L*L***H**ALKKA,
LAH4-L1-F **FF**KKLA**H**AL**H**LLALLAL**H**LA**H**ALKKA.

All six peptides were active in siRNA and plasmid DNA transfection, however some differences were observed. LAH4, LAH4-L1 and LAH4-Leu possess were highly active in DNA transfection, while LAH4-L1-F has shown moderate activity. On the contrary, LAH4-L1-F was the most active siRNA transfection agent comparing with other peptides and commercially available compound (DOTAP, Lipofectamine and B-PEI). It was suggested that pDNA delivery requires an interaction with the transfection agent sufficiently strong to ensure the safe transport across the cytoplasm and delivery into the nucleus. In contrast, siRNA need to be released from endosomes and from transfection complex sufficiently early as it is acting in the cytoplasm. From the other hand, LAH4-L1 and LAH4-Leu peptides were shown to be the most tolerant to the cells, and promoted the higher cell viability rates than other peptides and commercial agents.

It was also found that about 3.2 times more peptide is required to complex the siRNAs when compared with plasmid DNA. The explanation was proposed that, in contrast to DNA, siRNA cannot be condensed, and the peptide-siRNA complex formation lacks cooperativity (Langlet-Bertin et al., 2010).

The subsequent investigation of mechanism of siRNA delivery by LAH4-L1 peptide and derivatives is pursued by Dr. James Mason and the colleagues. In particular, the histidines residues of LAH4-L1 and analogues were substituted by 2,3-diaminopropionic acid in order to better tune the peptides functional pH response (Abbate et al., 2013; Lan et al., 2010).The conformational changes of LAH4 and LAH6 derivatives were studied by circular dichroism upon the binding to nucleic acids, and also at in the solutions at varied pH (Iacobucci et al., 2012). The mechanism of cellular entry by LAH4-L1 complexes with nucleic acid was investigated using confocal live cell imaging. Thus it was shown that both siRNA and pDNA – peptide complexes are internalised via endocytosis, but the difference was that siRNA particles entered via a cholesterol dependent mechanism, in contrast to DNA transfer which was associated with clathrin dependent endocytosis (Lam et al., 2012). In another work an efficient method

based on western blotting technique was developed for evaluation the efficiency of siRNA delivery mediated by LAH4-L1 peptide (Liang et al., 2013).

In the present work we will concentrate exclusively on the biophysical characterisation of LAH4-L1 (and partially LAH4) peptide interactions with model membranes and nucleic acids.

Conclusions.

LAH4 peptides combine the antimicrobial and cell transfection properties, which make them very interesting candidates for development of the drugs for genetic disorders treatment (Kichler et al., 2003a).

The peptides property to alter their net charge under pH change and therefore mode of interaction with model membranes and nucleic acids, was shown to have great advantage in realising the transfection complex uptake by the cell and its subsequent endosomal escape. LAH peptide-mediated nucleic acid

delivery involves condensation of the nucleic acid by peptide at neutral pH, adhesion to the cell membrane and stimulation of cellular uptake via endocytosis pathways. During endocytosis, the acidification of the endosomal lumen promotes the increase of the pH responsive peptides charge, which causes the substantial amount of peptide to be released from the peptide–nucleic acid complex (Iacobucci et al., 2012; Prongidi-Fix et al., 2007). Peptides released from the complex are able to access the surface of the endosomal membrane and disrupt the membrane, facilitating release of the endosomal contents into the cytosol.

LAH4-L1 has shown the highest DNA transfections capacity among other LAH peptides, along with its relatively low toxicity. This peptide was chosen as the model sequence for subsequent gene delivery development (by Mason and colleagues), and also for further biophysical investigations with the goal to understand how the particular structural characteristics determine the mechanism of peptide interaction with membranes and nucleic acids and its cellular entry (Mason, Bechinger and co-workers).

I. LAH4 et LAH4-L1, les peptides avec l'activité de transfection.

Les propriétés physico-chimiques de LAH4 et LAH4-L1.

LAH4 est un peptide riche en histidine amphipathique cationique de 26 acides aminés (KKALL ALALH HLAHL ALHLA LALKKA), qui a d'abord été conçu pour évaluer les caractéristiques structurelles des peptides avec activité antimicrobienne et pour mieux comprendre les contributions énergétiques qui déterminent leur topologie membranaire (Bechinger, 1996). Le noyau hydrophobe peptide LAH4 consiste en résidus de leucine et d'alanine, interrompus par quatre histidines. Quatre lysines sur les extrémités assurent une bonne solubilité dans des environnements aqueux. L'analyse de la roue hélicoïdale (Schiffer et Edmundson, 1967) représente schématiquement la distribution des acides aminés lorsque le peptide est dans une conformation alpha-hélicoïdale (Figure I-1) où la distribution des chaînes latérales d'acides aminés détermine l'angle polaire et l'angle sous-tendu par Les résidus cationiques, qui pour une alpha-hélice idéale est égal à 100 ° pour LAH4. Le pKa de l'anneau histidine imidazole est d'environ 6,0. Les valeurs précises de pK des histidines LAH4 ont été déterminées en présence de micelles de dodécylphosphocholine en utilisant la spectroscopie RMN en solution en suivant le changement chimique 1H des protons d'imidazole (les valeurs de pK trouvées sont de 5,4, 5,8, 5,9 et 6,0). La structure secondaire du peptide LAH4 dans les micelles DPC a été déterminée par une spectroscopie RMN de corrélation multidimensionnelle 1H homonucléaire en solution (Georgescu et al., 2010). On a constaté que LAH4 forme une hélice α dans les résidus 9-24 à pH 4.1 avec les résidus N- et C-terminaux restant largement désordonnés. À pH 6.1, le peptide subit des transitions conformationnelles et adopte une structure hélice-boucle-hélice, où deux domaines hélicoïdaux sont formés englobant les résidus 3-9 et 14-24. À pH 7.8, LAH4 revient à une longue hélice α, y compris les résidus 4-21. Il a été suggéré qu'une telle transition hélice de la terminaison C à la terminaison N par la formation d'une boucle pourrait faciliter la réorientation d'in-planar à transmembranée du peptide. Les structures correspondantes ont été trouvées dans Protein Data Bank sous les éléments 2KJN (pH 4.1) et 2KJO (pH 6.1).

LAH4-L1 (KKALL AHALH LLALL ALHLA HALKKA) est un peptide apparenté de la même famille conçu pour améliorer la capacité de transfection (Mason et al., 2006a). La raison d'être de la conception des peptides sera discutée ci-dessous. LAH4-L1 possède un angle polaire réduit par rapport à LAH4 (80 °). Le peptide LAH4-L1 et LAH4 modifient la charge nominale de 9 à pH acide à 5 à pH autour de 7, de manière similaire à LAH4.

Cette protonation contrôlée par le pH des histidines a été utilisée précédemment pour moduler l'insertion membranaire du peptide modèle LAH4, car son orientation dans la membrane cible dépend de la distribution de charge dans le peptide (Vogt et Bechinger, 1999). Au pH acide, lorsque les histidines sont protonées, l'hélice LAH4 adopte une orientation dans le plan le long de la surface de la membrane, lorsque, à pH neutre, les résidus d'histidine non chargés rendent une hélice plus hydrophobe telle que le peptide adopte une orientation transmembranaire avec les résidus de lysine Agissant comme ancre sur les surfaces de la membrane. L'alignement de la membrane LAH4 a influé sur son activité antimicrobienne. Ainsi, à faible pH (≈5) LAH4 présente 2 ordres de grandeur une activité antibiotique plus élevée qu'à pH neutre. En outre, l'activité de perturbation de la membrane est cinq fois plus prononcée au pH 5, ce qui a été démontré par l'essai de libération de la calcéine sur les membranes modèles POPC et POPC / POPG (Vogt et Bechinger, 1999). Par conséquent, l'activité antimicrobienne de LAH4 a été associée à son alignement planaire membranaire via un mécanisme d'action "détergent".

En plus, dans ce chapitre, je présente l'aperçu du développement de l'agent efficace d'administration d'acide nucléique sur la base du peptide LAH4. La motivation pour la caractérisation biophysique de

l'interaction du peptide LAH4-L1 avec les membranes modèles et les acides nucléiques sera révélée. L'accent est mis sur la raison d'être de la conception des peptides de transfection, car ces recherches révèlent de nombreux détails importants sur le mécanisme de l'interaction des peptides LAH4 avec les bicouches lipidiques.

Conception rationnelle des peptides d'administration de gènes.

Des peptides riches en lysine anionique courtes tels que KALA (Wyman et al., 1997) et ppTG20 (Rittner et al., 2002) et le domaine C-terminal de la protéine virale de type 1 du virus HIV (Vpr52-96) (Kichler et al. , 2000) présentent un potentiel élevé en tant qu'agents de délivrance de gènes. Ils ont la capacité de lier l'ADN et de déstabiliser les membranes en même temps, les propriétés indispensables pour un transfert efficace des gènes dans la division des cellules. Ces peptides transfectants adoptent une conformation α-hélicoïdale sous interaction avec des membranes avec des lysines chargées positivement ou des arginines positionnées sur une face de l'hélice. Le peptide LAH4 possède des caractéristiques structurelles similaires lorsqu'il est inséré dans des bicouches lipidiques. L'angle sous-tendu par les résidus d'histidine dans la conformation α-hélicoïdale LAH4 est égal à 100 °.

La poly-L-lysine a été le premier réactif synthétique possédant une capacité de transfection (Wu et Wu, 1987). Pour un aperçu des vecteurs chimiques pour l'administration des gènes, veuillez consulter la publication dédiée (Midoux et al., 2009). Les complexes ADN-polylysine du plasmide augmentent l'absorption de l'ADN par des cellules de mammifères, mais les molécules de plasmide sont alors souvent piégées dans les vésicules endosomales où elles ne peuvent échapper pour atteindre les machines nucléaires. La substitution d'environ 35% des groupes ε-amino par des résidus d'histidine a permis d'augmenter la capacité de transfection du polymère. L'inhibition drastique de l'activité de transfection en présence de bafilomycine A1 indique que la protonation des groupes imidazole dans la lumière de l'endosome favorise l'administration d'un ADNp dans le cytosol (Midoux et Monsigny, 1999).

Le peptide LAH4 possède les propriétés structurelles et physico-chimiques qui lui permettent d'être considéré comme l'agent de transfection prometteur. Tout d'abord, le peptide est plutôt soluble dans l'eau et dans des tampons de concentration de sel variée. Il s'associe aux membranes POPC zwitterioniques (Vogt et Bechinger, 1999). Il possédait une charge différente à pH 5 et pH 7,4, et une topologie de membrane différente. On a supposé que les lysines dans la séquence peptidique de LAH4 pourraient servir alors à la condensation d'ADN et que les résidus d'histidine pourraient favoriser l'échappement endosomique de l'ADN.

Dosages de transfection cellulaire.

La série d'expériences de transfection in vitro a été effectuée, dans laquelle l'activité du gène rapporteur de la luciférase a été utilisée pour quantifier l'efficacité de la livraison. Les caractéristiques structurelles du peptide de transfection efficace ont été déterminées. Il a été démontré que la seule présence de résidus d'histidine et de lysine n'est pas suffisante pour obtenir un agent de transfection efficace. Le nombre de résidus d'histidine, leur position dans la séquence et le pH auquel les peptides passent d'un alignement planaire à un alignement transmembranaire sont tous des paramètres cruciaux qui déterminent la capacité de transfection (Kichler et al., 2003a).

Dans une première étape d'évaluation, plusieurs membres de la famille de peptides LAH avec un nombre varié de résidus d'histidine ont été choisis pour le test d'activité de transfection. Tous ces peptides se composent de quatre lysines terminales, un noyau hydrophobe représenté par les leucines et les alanines et un certain nombre d'histidines au milieu de la séquence peptidique (Tableau I-1). On a trouvé que les peptides

qui contiennent 1 à 3 résidus d'histidine (LAH1-LAH3) étaient au moins 10 fois moins efficaces dans l'administration d'ADN plasmidique que LAH4 ou LAH5.

In Dans la prochaine étape d'évaluation, les dérivés de LAH4 et le peptide antimicrobien salivaire histatine-5 ont été utilisés pour montrer comment différentes propriétés structurales des peptides influencent leur capacité de transfection.

Le résumé des résultats du test de dosage de la transfection et du retard de gel est fourni dans un Tableau I-2 et la représentation de la roue hélicoïdale des séquences du peptide est donnée dans une Figure I-2. Dans un essai de retard de gel, l'ADN plasmidique et le peptide ont été mélangés au rapport molaire et déposés sur le gel d'agarose. Ensuite, une quantité minimale de peptide capable de retarder complètement la migration de l'ADN a été déterminée et fournie dans le tableau.

Les analyses de transfection et de retard de gel sur le peptide LAH4 et ses dérivés ont permis de discerner les principaux éléments structurels qui assurent une haute activité de transfection des peptides. Ces caractéristiques structurelles peuvent être résumées de la manière suivante:

- *La présence d'histidine est essentielle.* LAK4 a montré une activité de transfection très faible;
- *Présence de la surface hydrophobe bien défini.* L'histatine-5, qui a une répartition égale des résidus hydrophiles le long de la surface, présente une faible activité de transfection et une faible capacité de retard d'ADN. La capacité des peptides à complexe l'ADN n'est pas seulement liée à la charge globale du peptide, mais nécessite des motifs structurels spécifiques.
- *La position des quatre résidus d'histidine dans la face hydrophile.* LAH4-L4 montre un niveau d'activité de luciférase légèrement inférieur à celui de LAH4 et LAH4-L3, ce qui suggère que l'efficacité de transfection optimale requiert que quatre histidines soient placées dans un angle défini, ce qui se forme lorsque le peptide adopte une structure a-hélicoïdale. Les peptides LAH4-L3, LAH4-L4 et LAH4 avec les angles de 120 °, 160 ° et 100 ° respectivement, montrent tous des gains d'efficacité de transfection prononcés, ce qui indique que la position des résidus d'histidine dans la face polaire est importante, bien que des modifications mineures puissent Être toléré. Cependant, lorsque cet angle a été réduit à 60 °, une perte d'activité assez importante a été observée (LAH4-L0, Mason et al., 2006).
- *Réorientation du peptide d'in-plane à transmembranaire avec un pH croissant.* Pour LAH4, le point médian de la transition IP à TM a été déterminé à pH_{50} = 6,1 dans les membranes POPC (Bechinger, 1996). Trois autres mutants ayant différents points de transition ont été testés: LAH4-L6 avec pH_{50} = 4,8, LAH4-A6 avec pH_{50} = 6 , et LAH4-G6 avec pH_{50}> 8.5. Le tableau II.2 montre que LAH4-L6 et -A6 ont réussi à complexer l'ADN efficacement et à retarder sa migration électrophorétique, lorsque LAH4-G6, qui est considérablement plus hydrophile, n'a pas été capable de retarder complètement la migration de l'ADN. Dans les expériences de transfection, les trois mutants sont significativement moins efficaces que LAH4. Néanmoins, LAH4-A6, le peptide ayant le point médian de transition le plus proche de LAH4, était également le plus efficace par rapport à LAH4-L6 ou -G6.
- *Les résidus d'histidine doivent être positionnés dans le noyau du peptide.* H4-LAK4 avec des positions inversées de lysines et d'histidines était significativement moins actif dans le transfert de gènes que LAH4 (Kichler et al., 2003a).
- *Nombre de résidus chargés positivement.* L'analogue LAH4 avec deux lysines supplémentaires sur chaque extrémité K2-LAH4-K2 (KKKKALLALALHHLAHLALHLALALKKKK) a été synthétisé pour évaluer l'influence d'une charge accrue sur l'activité de transfection. Deux paramètres ont été

mesurés et comparés à ceux de LAH4. D'abord, l'absorption de l'ADN par la cellule a été quantifiée. On a constaté que K2-LAH4-K2 délivre environ les trois quarts de la quantité d'ADN trouvée avec LAH4. Mais la capacité de transfection observée par l'expression du gène rapporteur était environ 24 600 fois plus petite pour K2-LAH4-K2 (Kichler et al., 2007). La différence a été expliquée par une activité lytique élevée de K2-LAH4-K2 même à pH neutre. La déstabilisation accrue des membranes affecte peu le processus d'absorption, mais le peptide est alors beaucoup plus cytotoxique pour les cellules. En outre, une association trop étroite avec l'ADN ne nécessite donc pas de lyse de la membrane lors de la diminution du pH.

- *Capacité d'adopter une structure α-hélicoïdale.* Le mutant peptidique LAH4 avec la proline incorporée au milieu de la séquence (P15) a été synthétisé et testé également. On sait que la proline n'a pas la capacité de former une conformation α-hélicoïdale. Par conséquent, lorsqu'il est placé juste au milieu de la séquence, il modifie la structure secondaire du peptide. LAH4-P15 a été jugé 1500 fois moins actif dans les expériences de transfection. Aussi le peptide LAH4-P15 a été capable de délivrer 25 fois moins de matériel génétique que LAH4. Il n'est plus toxique pour les cellules que LAH4, comme l'a montré le test de viabilité cellulaire. Cela signifie que la capacité du peptide à former α-hélice est l'un des facteurs clés de la réussite de la délivrance cellulaire (Kichler et al., 2007).
- *Longueur du peptide.* L'augmentation de la longueur du peptide à 30aa en ajoutant plus de résidus hydrophobes, en tant que leucines ou alanines, entraîne une légère diminution de l'activité, bien qu'elle contribue à réduire la taille du complexe peptide / ADN (Mason et al., 2007a). L'épuisement des acides aminés hydrophobes soit sur l'extrémité C-terminale, soit sur l'extrémité N-terminale conduit à la réduction de l'activité d'environ 20 fois (Kichler et al., 2007).

Pour résumer cette enquête, les deux peptides présentant des caractéristiques structurelles assez proches - LAH4 et LAH4-L3 - se sont révélés être les agents de transfection les plus prometteurs parmi tous les peptides testés.

Dans une étape finale, l'efficacité de transfection LAH4 a été comparée à celle des réactifs commerciaux pLys180 et 25-kDa polyéthylènimine (PEI). LAH4 a été jugé significativement plus efficace que la polylysine avec quatre lignées cellulaires différentes et était à peu près aussi actif que le PEI (Kichler et al., 2003a).

Dans une autre cas, la capacité de délivrance du gène LAH4 a été comparée à l'activité de certains peptides de pénétration cellulaire, tels que KALA (WEAKLAKALAKALAKHLAKALAKALKA), TAT47-57 (YGRKKRRQRRR), ppTG20 (GLFRALLRLLRSLWRLLLRA) et Vpr55-91 (TGVEALIRILQQLLFIHFRIGCRHSRIGIIQQRRTRN) et l'agent commercial DOTAP (Prongidi-Fix et al., 2007). Le résultat du test de transfection montre une nette préséance pour le peptide LAH4 sur le reste des composés testés.

Effet de la composition de la membrane extérieure. Ci-après, dans une expérience de transfection sur des cellules transformées LAH4 a montré environ 2 ordres de grandeur d'activité supérieure sur l'hépatocarcinome humain (HepG2) et des cellules HEK 293 transformées par rapport à d'autres tissus eucaryotes (fibroblastes de souris NIH 3T3 et cellules de muscle lisse de l'aorte de lapin Rb1). La membrane externe de la cellule transformée possède une fraction élevée de lipides POPS chargés négativement, suggérant l'association préférable du complexe de transfection LAH4-pDNA avec des surfaces membranaires anioniques (Kichler et al., 2003a).

Test de retardement du gel d'agarose. Effet du pH. L'électrophorèse sur gel d'agarose permet de surveiller le retard de l'ADN plasmidique (SMD2-LucΔITR, 7,6 kbp) à un rapport LAH4 / DNA m/m de 1,75 à pH

acide (5,2), alors qu'un rapport d'environ 2,5 est requis pour inhiber la migration de ADN plasmidique au pH neutre (Kichler et al., 2007).

Le mécanisme suggéré d'absorption de complexe de transfection et d'échappement endosomal induit par LAH4.

Lors de la première étape du peptide d'absorption endocytaire, il serait soit inséré dans la membrane endosomale dans son orientation transmembranaire, soit associé au complexe d'ADN. Dès que l'absorption du complexe ADN-LAH4 se produit à partir de la membrane externe, elle reste en contact avec la membrane externe, qui a une faible fraction de lipides anioniques. J'aimerais attirer votre attention sur le fait que le rapport d'ADN de LAH4 / plasmide, qui favorise l'expression du gène rapporteur le plus élevé, est de 6/1 m/m (Kichler et al., 2003a). Mais le rapport peptide / pDNA de seulement 2,5/1 m/m est nécessaire pour inhiber la migration de l'ADN plasmidique au pH neutre (Kichler et al., 2007). Cela signifie que dans le complexe de transfection, il y aura une quantité assez grande de peptide disponible pour interagir avec les membranes.

À l'intérieur des endosomes précoces, le pH est d'environ 6,2 à 6, mais il descend à environ 5,5 à 5 lorsque l'endosome mûrit (Huotari et Helenius, 2011). Les groupes histidine imidazole se protonnent à ces conditions, et moins de peptide associe au complexe d'ADN. Par conséquent, le peptide est disponible pour insérer dans la membrane où il adopte une orientation plane, dans laquelle son activité de rupture de la membrane est plus prononcée. Il a été suggéré que, à cette étape, LAH4 provoque une flip-flop de lipides anioniques à partir de la monocouche de membrane cytoplasmique des membranes endosomales (Mason et al., 2006a). Les lipides anioniques vont alors attirer le peptide LAH4 à partir de complexes de transfection, et avec une déstabilisation améliorée de la membrane, cela provoquera la libération d'oligonucléotide dans le cytoplasme (Mason et al., 2006a).

Corrélation entre la capacité de transfection et l'activité de déstabilisation de la membrane.

À l'étape suivante, les enquêtes ont été complétées par des mesures de RMN de 2H à semi-conducteurs (Mason et al., 2006a). Quatre peptides dérivés de LAH4 d'une séquence d'acides aminés similaire, mais avec des angles variés sous-tendus par les chaînes latérales d'histidine, ont été conçus pour cette expérience. Les séquences peptidiques sont données dans un Tableau I-3.

Comme il a été démontré précédemment que la présence de lipides anioniques joue un rôle important dans la médiation de l'absorption du complexe de transfection et la libération d'ADN dans le cytoplasme, la série d'expériences biophysiques a été réalisée pour montrer comment le peptide associe aux peptides anioniques mixtes. La largeur de la ligne ^{2}H RMN sur les analogues deutérone de chaîne de POPS ou POPC a fourni une vue plus détaillée de la façon dont LAH4 perturbe les bicouches lipidiques POPC / POPS / cholestérol mixtes au pH 5 et a montré que les profils des paramètres de l'ordre de la chaîne PS sont plus facilement désordonnés par LAH4 que Ceux de PC. Parmi les dérivés de LAH4 avec des angles variés submergés par les chaînes latérales de l'histidine, leur effet sur la perturbation de l'ordre des POPS était plutôt spécifique au segment. Tous ces quatre isomères LAH4 ont perturbé les chaînes lipidiques à une extension similaire dans la région vers le groupe de tête lipidique (entre la position de chaîne 2 et 10). Cependant, la partie inférieure de la chaîne, dans le noyau hydrophobe, a été beaucoup plus sélectivement affectée par les isomères LAH4. LAH4-L2 et -L1 ont un effet similaire sur l'ordre de la chaîne et tous deux perturbent la partie inférieure des chaînes plus efficacement que LAH4-L0, tandis que LAH4-AL6 a eu un effet comparativement faible. Les résultats ont suggéré que la profondeur de la pénétration bicouche des peptides LAH4 est modulée par la distribution de résidus hydrophobes dans l'hélice.

On a également observé une relation claire entre l'activité de rupture de l'ordre de la chaîne POPS et l'efficacité de transfection de ces peptides, avec LAH4-L2 et -L1 étant les plus actives dans les expériences de transfection.

De plus, l'activité de transfection des peptides d'administration les plus prometteurs LAH4 et LAH4-L1 a été étudiée en présence de sérum de veau foetal (Mason et al., 2007a). De nouveau, une série de dérivés LAH4 et LAH4-L1 avec diverses propriétés a été préparée pour le test. Leur structure et leurs caractéristiques brèves sont fournies dans un tableau I-4. Diverses caractéristiques structurelles ont été incorporées par la conception. Par exemple, le nombre d'histidines dans LAH4-L1 a été augmenté à 6, ce qui a donné un peptide avec une surface hydrophobe diminuée LAH6-L1. L'autre peptide conserve les angles de LAH4-L1, mais possède 6 histidines et une longueur accrue (LAH6-L1-80). LAH4-L1-30 conserve le nombre d'histidines et d'angle, submergé par les résidus d'histidine, mais a augmenté la longueur. Les peptides, dans lesquels les acides aminés ont été partiellement ou complètement substitués par des D-analogues ont également été testés.

Résultats de la transfection dans le milieu sans sérum. Le peptide principal LAH4-L1 a de nouveau été le vecteur le plus efficace pour chacune des lignées cellulaires testées. LAH6-L1-80, où l'angle de résidu chargé à pH acide est maintenu, était également un agent de transfection efficace avec des niveaux d'expression proches de LAH4-L1. LAH6- L1 avait une efficacité réduite et les versions plus longues de LAH4-L1 ou des peptides avec des D-aminoacides incorporés avaient une efficacité de transfection relativement faible dans toutes les lignées cellulaires.

Transfection en présence de sérum. La présence de 20 à 25% de sérum dans le milieu de transfection réduit l'efficacité de transfection de tous les vecteurs peptidiques. Cependant, les effets variaient considérablement en fonction des propriétés structurales des peptides. LAH4-L1 et LAH6-L1-80 ont été les moins affectés par la présence de sérum. La capacité de transfection du peptide LAH6-L1 a été presque complètement supprimée par la présence de sérum. L'efficacité de transfection, médiée par des peptides contenant des acides aminés D terminaux, a également été sensiblement réduite aussi dans les milieux sériques, cette incorporation d'acides aminés D au niveau des peptides ne protège pas contre l'effet de dégradation du sérum. La capacité de transfection de D-LAH4 était également faible (Mason et al., 2007a).

Par conséquent, le **vecteur peptidique efficace** présente les caractéristiques structurelles suivantes:

- il adopte une structure α-hélicoïdale sous l'interaction avec les membranes.
- il possède des résidus d'histidine qui se protonent lorsque le pH passe de 7,4 à 5,
- il possède le nombre optimal de résidus chargés positivement (à pH neutre), tels qu'ils ont une capacité à condenser l'ADN. Cependant, en augmentant le nombre d'acides aminés chargés positivement, il n'était pas possible d'améliorer la capacité de transfection du peptide car cela augmente sa toxicité.
- il a un angle bien défini, submergé par des résidus d'acides aminés chargés positivement, car ce dernier détermine les propriétés de déstabilisation de la membrane du peptide au pH acide. De tels peptides qui sont caractérisés par un angle de 100 ° (LAH4, LAH4-L2, LAH4-L3) ou 80 ° (LAH4-L1, LAH4-L1-30, LAH6-L1-80) étaient l'agent de transfection le plus prometteur, Avec LAH4-L1 étant le composé principal.
- l'augmentation du nombre d'histidines n'affecte pas la capacité de transfection, dès que l'angle, submergé par les histidines, est conservé.

- le peptide doit avoir une longueur optimale (26-29aa) et un rapport hydrophobe-hydrophile.

Caractérisation biophysique des complexes de transfection.

Calorimétrie de titrage isotérmique. L'efficacité de l'association LAH4 avec l'ADN du sperme de saumon de bas poids moléculaire (environ 300 paires de bases) a été étudiée par ITC (Prongidi-Fix et al., 2007). Les mesures ont été effectuées dans du tampon phosphate-sérum physiologique (10 mM de phosphate, 137 mM de NaCl) à différentes températures (288, 298, 308K). Les paramètres thermodynamiques comme énergie libre de liaison (ΔG), constante d'association (Ka), changement d'entropie (ΔS) et stoechiométrie (N), ont été calculés à partir des isothermes calorimétriques, en supposant un modèle unique de sites de liaison. La réaction d'association ADN-peptide était exothermique à pH 7,5 et endothermique à pH 5,5, de sorte à pH 5,5, le processus était plus entraîné par l'entropie. On a déterminé que la stoechiométrie d'association était de 148 ± 39 LAH4 par ADN (300 pb) à pH 7,5 et 98 ± 10 à pH 5,5 (Prongidi-Fix et al., 2007). Les résultats indiquent qu'un rapport molaire très élevé de LAH4 est nécessaire pour saturer les sites de liaison de l'ADN, il ne peut donc pas y avoir d'interaction spécifique avec le peptide LAH4. Il a été suggéré que les résidus de lysine du peptide sont associés électortiquement avec des brins d'ADN voisins, ce qui favorise la condensation de l'ADN et la formation de grands agrégats globulaires.

Enquêtes structurelles par RMN à l'état solide. Des échantillons de LAH4 marqués avec ^{15}N et / ou ^{13}C sélectivement et / ou uniformément ont été préparés afin de tester par une technique RMN à l'état solide REDOR quelles chaînes latérales peptidiques présentent des proximités proches (<8 Å) aux noyaux ^{31}P de l'ADN à l'intérieur de la coxplexe de transfection (Bechinger et al., 2011; Vidovic, 2011). Les complexes de transfection ont été préparés à pH 5,5, et le rapport optimum peptide / ADN de sperme de saumon a été choisi sur la base d'études précédentes - électrophorèse sur gel d'agarose, ITC, dosage de centrifugation (Prongidi-Fix et al., 2007). Le premier test REDOR sur le peptide avec un marqueur ^{13}C spécifique aux positions β de Ala-6 et Ala-13 indique que ces résidus ne résident pas à proximité des phosphates d'ADN. Ensuite, l'effet REDOR a été mesuré à l'aide de peptides uniformément marqués $^{13}C/^{15}N$, les distances proches ont été trouvées entre les noyaux ^{15}N et ^{13}C des chaînes latérales de lysine et les noyaux ^{31}P des groupes phosphate d'ADN, mais pas pour aucune des autres chaînes latérales. Les distances dans la plage de 5Å ont été détectées entre les groupes nitrogènes du groupe amino terminal et les groupes phosphate. En outre, les mesures REDOR ont été effectuées sur les complexes LAH4/ADN, où une des lysines était uniformément marquée avec ^{15}N, de sorte que les distances avec les groupes phosphate d'ADN étaient résolues pour chaque chaîne latérale de lysine. La proximité la plus proche des phosphates d'ADN (4 Å) a été détectée pour les nitrogènes terminaux du groupe amino des 2èmes et 24èmes lysines. Par conséquent, le modèle où l'association ADN-LAH4 est régie par une attraction électrostatique, et exclusivement les chaînes latérales de lysine interagissent avec l'ADN, a été confirmée par des mesures structurelles RMN.

L'ITC et le dosage par changement de gel ont montré une stéchiométrie différente du complexe ADN/LAH4 à différents pH (5,5 et 7,5). Nous étions intéressés si la structure du complexe de transfection serait également différente à pH 7,5, par conséquent, l'étude de REDOR RMN a été menée dans le présent travail.

Paramètres macroscopiques. La taille et la charge des complexes de transfection, formés par divers peptides, ont été évaluées par des mesures de potentiel de DLS et ζ (Tableau I-5). Tous les complexes de transfection semblent être chargés positivement au rapport peptide/ADN qui présente les niveaux de transfection les plus élevés. La taille des complexes est considérablement augmentée dans les tampons à haute résistance ionique (150mM). En présence de 25% de sérum, il n'y avait pas d'augmentation ou de réduction systématiquement observable de la taille complexe comme prévu en tenant compte de l'effet du

sérum sur la taille complexe pour la polylysine histidylée, où la taille des complexes a été réduite d'environ 10 fois en présence de plus de 5% de sérum, qui ne disposait que d'environ 100 nm de diamètre (Bello Roufaï and Midoux, 2001).

Perturbation de l'ordre des membranes et propriétés antimicrobiennes des peptides de la famille LAH4.

Il a été démontré que le peptide LAH4 inhibe le *E. coli* plus efficacement à pH 5,5 qu'à pH neutre (7.2) (Vogt and Bechinger, 1999). Mason et ses collègues ont élargi l'étude des propriétés antibactériennes sur d'autres peptides de la famille LAH, y compris LAH4-L1 (Mason et al., 2006b). Les activités des peptides de LAH ont été comparées à l'activité du peptide antibactérien *magainin 2*. En particulier, le peptide LAH6-L1 (KKALL A**H**AL**H** **H**LALL A**HH**LA **H**ALKKA, 120°), qui possède deux histidines supplémentaires, s'est avéré être l'agent le plus efficace contre le large Gamme de bactéries Gram-positives et Gram-négatives, et son efficacité était presque aussi prononcée à pH 7,2 qu'à pH 5,5. LAH4-L1 (KKALL A**H**AL**H** LLALL AL**H**LA **H**ALKKA, 80°), de manière similaire au peptide LAH4, a montré une activité plus prometteuse à pH 5,5 qu'à un pH neutre, avec une efficacité dix fois plus grande à pH 5,5. En revanche, l'addition de résidus de phénylalanine à la séquence (LAH4-L1-F4, KKALL A**H**FF**H** LLALL AL**H**FF **H**ALKKA, 80°) a réduit considérablement l'efficacité antibiotique du peptide, en particulier à pH 7,2. L'activité du peptide atteint le niveau observé pour la magainine 2, qui est également enrichie en résidus de phénylalanine (GIGKFL**H**SAKKFGKAFVGEIMNS).

La perturbation de l'ordre des chaînes d'acyle deutériées des lipides POPE et POPG dans les membranes mixtes (POPE / POPG = 75: 25) par des peptides LAH a été étudiée par spectroscopie RMN statique statique ^{2}H (Mason et al., 2006b). Ainsi, LAH6-L1 a montré un excellent effet de perturbation sur le PE ainsi que les chaînes d'acyle PG au pH acide, mais a provoqué un effet de perturbation de l'ordre très faible à pH 7,5. LAH4-L1 a induit une légère réduction de l'ordre de la chaîne acyle POPE et POPG à pH 7,5, mais elle était plus petite par rapport à l'effet à pH 5,5. De même, la perturbation de l'ordre induite par le peptide LAH4-L1 était plus prononcée pour le POPG que les chaînes acyle du POPE. Enfin, le comportement de LAH4-L1-F4 était très proche de celui du peptide LAH4-L1.

Développement futur de LAH4-L1 en tant qu'agent de transfection.

Les capacités de transfection de siRNA des peptides dérivés de LAH4 ont été étudiées sur six séquences peptidiques, toutes les 26 aa de longueur, possédant la charge +5 à pH 7,5 avec un degré varié d'hydrophobicité (Langlet-Bertin et al., 2010):

LAH4 KKALLALAL**HH**LA**H**LAL**H**LALALKKA,
LAH4-Leu KKALLAL*L*L**HH**L*L***H**ALL**H**L*L*LALKKA,
LAH4-L1 KKALLA**H**AL**H**LLALLAL**H**LA**H**ALKKA,
LAH4-L1-R RRALLA**H**AL**H**LLALLAL**H**LA**H**ALRRA,
LAH4-L1-Leu KKALLA**H***L*L**H**LLLAL*L*L**H**L*L***H**ALKKA,
LAH4-L1-F **FF**KKLA**H**AL**H**LLALLAL**H**LA**H**ALKKA.

Tous les six peptides étaient actifs dans la transfection d'ARNsi et d'ADN plasmidique, mais certaines différences ont été observées. LAH4, LAH4-L1 et LAH4-Leu ont été très actifs dans la transfection de l'ADN, tandis que LAH4-L1-F a montré une activité modérée. Au contraire, LAH4-L1-F était l'agent de transfection de siRNA le plus actif comparé à d'autres peptides et au composé commercialement disponible (DOTAP, Lipofectamine et B-PEI). Il a été suggéré que la délivrance d'ADNp nécessite une interaction avec l'agent de transfection suffisamment solide pour assurer un transport sûr à travers le cytoplasme et l'administration dans le noyau. En revanche, le siRNA doit être libéré des endosomes et du complexe de transfection assez tôt car il agit dans le cytoplasme. D'autre part, les peptides LAH4-L1 et LAH4-Leu se sont

révélés être les plus tolérants aux cellules et ont favorisé les taux de viabilité cellulaire supérieurs à ceux des autres peptides et agents commerciaux.

On a également constaté qu'environ 3,2 fois plus de peptide est nécessaire pour complexer les ARNsi par rapport à l'ADN plasmidique. L'explication a été proposée que, contrairement à l'ADN, l'ARNsi ne peut pas être condensé, et la formation du complexe peptide-ARNi-Si manque de coopération (Langlet-Bertin et al., 2010).

L'étude ultérieure du mécanisme de délivrance de siRNA par le peptide LAH4-L1 et ses dérivés est poursuivie par le Dr James Mason et ses collègues. En particulier, les résidus d'histidines de LAH4-L1 et les analogues ont été substitués par de l'acide 2,3-diaminopropionique afin de mieux adapter la réponse au pH fonctionnel des peptides (Abbate et al., 2013; Lan et al., 2010). Les changements conformationnels Des dérivés LAH4 et LAH6 ont été étudiés par dichroïsme circulaire lors de la liaison aux acides nucléiques, et également dans les solutions à pH varié (Iacobucci et al., 2012). Le mécanisme d'entrée cellulaire par les complexes LAH4-L1 avec l'acide nucléique a été étudié en utilisant l'imagerie cellulaire confocale. Ainsi, il a été démontré que les complexes de siRNA et de pDNA-peptide sont internalisés par endocytose, mais la différence était que les particules de siRNA sont entrées par un mécanisme dépendant du cholestérol, contrairement au transfert d'ADN qui était associé à une endocytose dépendante de la clathrine (Lam et al., 2012). Dans un autre travail, une méthode efficace basée sur une technique Western Blot a été développée pour évaluer l'efficacité de l'administration d'ARNs médiée par le peptide LAH4-L1 (Liang et al., 2013).

Dans le présent travail, nous nous concentrerons exclusivement sur la caractérisation biophysique des interactions peptidiques LAH4-L1 (et partiellement LAH4) avec des membranes modèles et des acides nucléiques.

Conclusions.

Les peptides LAH4 combinent les propriétés de transfection antimicrobienne et cellulaire, ce qui les rend très intéressants pour le développement des médicaments pour le traitement des troubles génétiques (Kichler et al., 2003a).

La propriété des peptides pour modifier leur charge nette sous changement de pH et donc le mode d'interaction avec les membranes modèles et les acides nucléiques a montré un grand avantage à réaliser l'absorption du complexe de transfection par la cellule et son échappement endosomal subséquent. La délivrance d'acide nucléique médiée par un peptide LAH implique la condensation de l'acide nucléique par peptide au pH neutre, l'adhésion à la membrane cellulaire et la stimulation de l'absorption cellulaire par voie endocytose. Au cours de l'endocytose, l'acidification de la lumière endosomale favorise l'augmentation de la charge de peptides sensible au pH, ce qui provoque la libération de la quantité substantielle de peptide du complexe peptide-acide nucléique (Iacobucci et al., 2012; Prongidi-Fix et al. , 2007). Les peptides sortis du complexe peuvent accéder à la surface de la membrane endosomale et perturber la membrane, ce qui facilite la libération des contenus endosomaux dans le cytosol.

LAH4-L1 a montré la plus grande capacité de transfections d'ADN parmi d'autres peptides de LAH, ainsi que sa toxicité relativement faible. Ce peptide a été choisi comme séquence modèle pour le développement ultérieur de l'administration de gènes (par Mason et ses collègues), ainsi que pour d'autres recherches biophysiques dans le but de comprendre comment les caractéristiques structurelles particulières déterminent le mécanisme de l'interaction peptidique avec les membranes et les acides nucléiques et son cellulaire Entrée (Mason, Bechinger et collègues).

II. METHODS

In this chapter the insight into biophysical methods used in the present work will be discussed. Isothermal titration calorimetry technique and its application for investigation of peptide – lipid and peptide – nucleic acid interaction will be reviewed in more details. The reason for that is the complex character of the data we obtain by ITC. Despite of the recent advancement in application of ITC to the complex biological systems, there is still no general method or reference database set for analysis of ITC data for the peptide – membrane and peptide – nucleic acid systems, which makes the analysis to be more complicated and unambiguous. The other methods that will be discussed are circular dichroism of polypeptides and solid-state nuclear magnetic resonance. Solid-state NMR has found its broad application for the investigation of biological, as well as inorganic materials. Therefore the large number of methods and associated techniques were developed so far. In this chapter however I will focus exclusively on the description of methods, which were employed in present work.

1. Thermodynamics of membrane – peptide interactions by isothermal titration calorimetry.

In the present section of manuscript the theory and application of isothermal titration calorimetry will be discussed with the emphasis on its application for the investigation of peptide – membrane interaction. A short introduction to the ITC experimental design will be provided as well. First the general approach to the analysis of calorimetric isotherms is described. Afterwards, several examples from the literature are given to illustrate the application of the method. Also the examples of the complex ITC isotherms will be discussed with respect to the information about mechanism of peptide – lipid interactions, which was possible to obtain by analyzing those isotherms.

Theoretical background of microcalorimetry.

Isothermal titration calorimetry is employing power compensation principle to measure the energy that is absorbed or emitted by the system, during chemical reactions such as association (dissociation) of molecules. The most common ITC application nowadays is the measurement of the enthalpy of *non-covalent binding* reactions that takes place between the macromolecule possessing defined binding site, such as protein, and the ligand, which can occupy this site. But of course, ITC technique has a much broader range of applications. Recently it became to be more widely used for measurements of non-specific interaction taking place between the polyelectrolytes, protein with surfaces, during the self assembly of amphiphiles, or solvation of biological molecules, *etc.* (reviewed in Ball and Maechling, 2009). And it is certainly a valuable technique when investigating the interactions with lipid membranes (Heerklotz, 2004; Seelig, 2004).

The equilibrium of the intermolecular interaction between the species, like ligand and macromolecule, is characterized by dissociation constant $K_D = [L][M]/[LM]$, which is related to the free energy of binding ΔG *via* the equation $\Delta G = RT\ln K_D$, where R is the universal gas constant (1.98 cal mol^{-1} K^{-1}) and T is the temperature in Kelvin.

When discussing the thermodynamics of macromolecular interactions very often the association constant is provided instead to characterize the binding $K_A = 1/K_D$ ($\Delta G = -RT\ln K_A$). The association constant is expressed in M^{-1}.

Free energy consist of enthalpy and entropy term: $\Delta G = \Delta H - T\Delta S$, where $\Delta G \leq 0$ for a spontaneous reaction to occur.

The more negative the free energy is, the higher is affinity between the species. ΔH, the enthalpy change, is the parameter directly measured in the ITC experiment. The enthalpy change of association between the molecules usually results from the multiple processes, such as solvation (usually hydration), proton exchange, hydrogen bonds formation or breaking, conformational changes, *etc*. Even though the enthalpy contributions from these processes are not resolved in single ITC experiments, various methods were developed in order to discern the contributions, which enable the determination of the energetics that drive the particular interaction (Baker and Murphy, 1996; Ren et al., 2000). The thermodynamic parameters associated with a protonation/deprotonation processes during the formation of a biomolecular complex could be determined by performing titrations over a range of pH, while the understanding of the electrostatic contribution can be obtained by performing the ITC experiment over a range of salt concentrations. The uptake or release of

ions can be deduced from the relation of the K_A with the concentration of salt (Bergqvist et al., 2004; Ladbury, 2004). Hydrogen bond formation and proton exchange are usually major contributors to the

enthalpy, when hydrophobic interactions and the conformational changes are entropy-driven processes (Ball and Maechling, 2009).

The observed enthalpy change is dependent on the temperature at which the measurement was performed. Therefore, performing the experiments at several temperatures allows the calculation of the heat capacity of binding: $\Delta C_p = \delta(\Delta H)/\delta T$, and this value is usually negative. C_p measurement is useful for understanding the nature and extent of binding interfaces especially during protein complex formation where water displacement from the protein surface is significant (Falconer and Collins, 2010).

Experimental design.

There are several steps to running the ITC experiment, such as planning the experiment (simulations), preparing the ligand and macromolecule solutions, collecting the raw ITC data, collecting the blank (ligand solution dilution), correcting the raw ITC data, nonlinear regression of the corrected titration data to provide estimates of the thermodynamic parameter values, and interpretation of the model data (Freyer and Lewis, 2008).

The usual mode of ITC operation is titration. The system works by comparing the thermocoupled sample and reference cells. The typical ITC instrument (***Figure II-1***) consists of the measurement cell, which is maintained at a constant temperature (isothermal), the syringe, from which the binding partner is supplied, and the temperature control unit. Any interactions between molecules that take place in the calorimetric cell generate (or absorb) heat, which is sensed by control unit. Subsequently the power applied to the control heater will be reduced (or increased). The raw ITC signal is the power (µcal/sec or µJ/sec) applied to the control heater that is required to keep the calorimeter cell from changing temperature as a function of time. The enthalpy is then calculated by integrating the heater power over the time (sec), the time required for the control heater power to return to a baseline value. Modern ITC instruments make it possible to measure heat as small as 0.1 µcal (0.42 µJ), allowing the determination of binding constants as large as 10^8–$10^9 M^{-1}$.

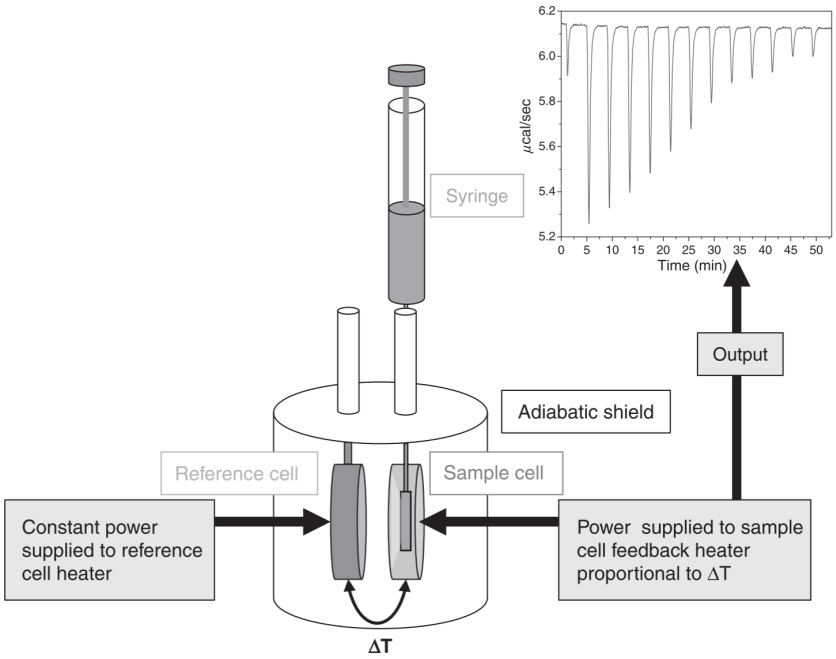

Figure II-1. The scheme of typical ITC instrument. The diagram shows a simplification of how the power applied by the instrument to maintain constant temperature between the reference and sample cells is measured. The resulting ITC signal, measured in µcal/sec over the time, is shown on the graph. Adapted with permission from the ref. (Freyer and Lewis, 2008).

The measured signal is then integrated and plotted against the ligand/macromolecule molar ratio as shown in a ***Figure II-2***. The binding enthalpy ΔH, entropy ΔS, stoichiometry *n*, and association constant can be the determined from ITC isotherm when appropriate fitting model is applied.

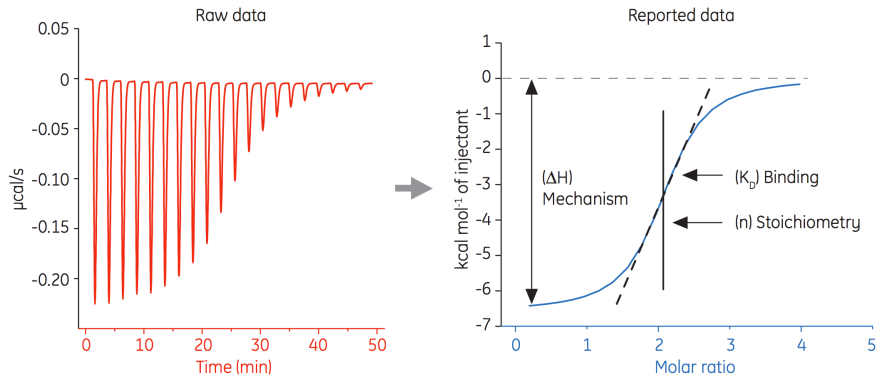

Figure II-2. The results of the ITC signal collecting and processing by MicroCal Origin® software. The sample graphs are adapted from GE Lifesciences application note 28-9782-62 AD (2011).

To be more specific, the association reaction that takes place after each injection of the binding partner, promotes the release or absorption of a certain amount of heat (Δh_i) proportional to the amount of ligand that binds to the protein in a particular injection

($V_0 \times \Delta l_i$) and the characteristic binding enthalpy (ΔH) for the reaction: $\Delta h_i = V_0 \times \Delta l_i \times \Delta H$, where V_0 is the volume of the reaction cell and Δl_i represents the difference between the concentration of bound ligand between the ith and (i–1)th injections. Because the amount of unbound macromolecules progressively decreases after each successive injection, the magnitude of the peaks becomes smaller until complete saturation is achieved (***Figure II-2***). When the saturation is reached, subsequent injections produce similar peaks corresponding to dilution or mechanical effects that need to be subtracted from all the injection peaks before analysis.

The amount of bound ligand in each injection depends on the mode of interaction between species. The successful extraction of thermodynamic parameters relies on the use of nonlinear least squares curve fitting while employing an appropriate model. In the case when monovalent ligand binds to the macromolecule with single binding site, Δl_i could be represented as follows:

$$\Delta l_i = [M] \times \left(\frac{K_A[L]_i}{1 + K_A[L]_i} - \frac{K_A[L]_{i-1}}{1 + K_A[L]_{i-1}} \right)$$

where K_A is the association constant and [L] is the concentration of free ligand (Leavitt and Freire, 2001). The solutions to this equation as well as to other more complicated binding models in terms of the total ligand concentration has been published (Freire et al., 1990; Wiseman et al., 1989) and are integrated in the modern MicroCal software. Also the corrections for volume displacement and titrate dilution are integrated in the Origin® program, and are therefore taken into account automatically in the construction of the binding isotherm. The mathematical background for these corrections can be found in the Microcal iTC200 user manual http://www.gelifesciences.com/webapp/wcs/stores/servlet/productById/en/GELifeSciences/28428955, and in dedicated publications (Brown, 2009).

It is possible to obtain all three parameters (K_A, n, ΔH) only if calorimetric titration is performed under the optimal conditions. Those conditions are sufficient heat response, which anticipates high enough concentrations of reagents, the optimal ratio between titrant and titrate in order to obtain complete calorimetric isotherm, and the slope of titration curve, which depend on the concentration of titrate and

association constant. In 1989, Wiseman and co-workers (Wiseman et al., 1989) have shown that the product of the total protein concentration in the calorimeter cell, [P], and the

association constant, K_A, a parameter known as $c = K_A \times [P]$, must be lower than 1000 in order to measure directly by ITC the binding of the ligand. This restriction sets an upper limit of 10^8–10^9 M^{-1} for the association constant.

Figure II-3 illustrates how the *c* value modulates the shape of titration curve. *c* values between 5 and 500 are generally considered to be good (Peters et al., 2009). When the *c* value is too high, ΔH and the stoichiometry can be determined accurately but not K_D. Wen it is too low, the stoichiometry cannot be determined accurately (***Figure II-4***). However, these considerations are valid for simple cases, when the macromolecule possesses one binding site, or a the set of non-interacting binding sites ($c = nK_A[M]$). When cooperative, or even more complex molecular association takes place, this mathematical form of the *c* parameter wouldn't make sense (MicroCal iTC200 user manual).

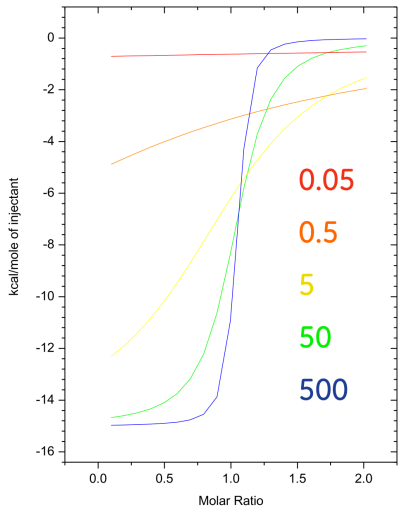

Figure II-3. Calorimetric isotherms with various *c* values. Adopted with permission from 'Isothermal titration calorimetry: Principles and experimental design', GE Healthcare tutorial (Stoyan Milev, Ph.D, 2013).

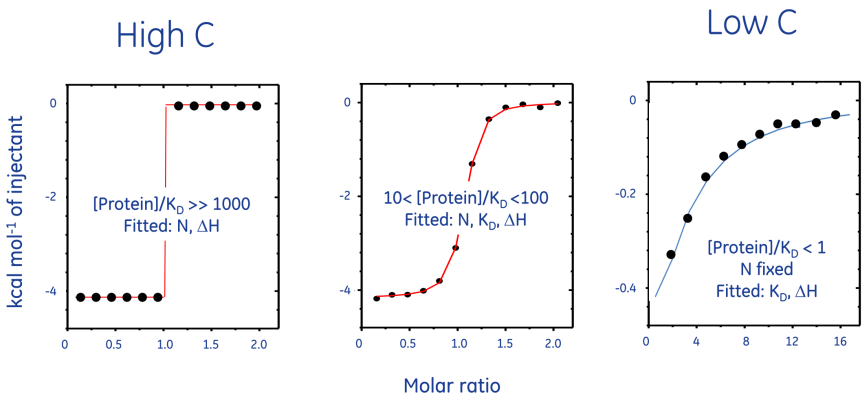

Figure II-4. Relation between c value and the accuracy of thermodynamic parameters determination. Adapted with permission from 'Isothermal titration calorimetry: Principles and experimental design', GE Healthcare tutorial (Stoyan Milev, Ph.D, 2013).

ITC practical considerations.

As it was already mentioned above, proton exchange makes a substantial contribution to the binding enthalpy. Such processes could accompany the calorimetric titrations, but they are not necessarily related

to the binding itself. Therefore, buffers with low ionization enthalpies are preferred for ITC experiment (phosphate, acetate, formate, citrate, sulfate), whereas quaternary amines have high ΔH_{ion} (e.g. HEPES ΔH_{ion} = 4.97 kcal mol^{-1}, Tris ΔH_{ion} = 11.4 kcal mol^{-1}). Also one should consider the dialysis of material as a way to equilibrate the buffer composition and to avoid the pH mismatches between the solution in the calorimetric cell and the syringe. The control experiment that accounts for the injectant and/or buffer dilution enthalpy is performed by titrating syringe content into the corresponding buffer. The signal needs to be subtracted from the calorimetric isotherm.

Even if above-mentioned buffer requirement are fulfilled, it is critical to understand that heat of protonation still contributes to the ΔH_{obs}, as the protons can be released or taken up during the binding event (Falconer and Collins, 2010). For an accurate estimate of the intrinsic enthalpy $\Delta H°$ and entropy $\Delta S°$ it is important to correct for the contribution of proton transfer. This can be done by measuring ITC signal in the buffers of different ionization enthalpies. Plotting ΔH_{obs} versus ΔH_{ion} should give a straight line according to $\Delta H_{obs} = \Delta H° + [nH^+ \times \Delta H_{ion}]$, where nH^+ is the number of protons transferred during the interaction. The intrinsic enthalpy can be estimated

by extrapolating to $\Delta H_{ion} = 0$, and the slope of the line determines the number of protons either released or taken up during association.

The time spacing between injections should be sufficiently long to allow the power to return to its baseline level. And finally the injection volume should be chosen to obtain the detailed enough binding isotherm, but in the same time to keep good signal-to-noise ratio.

Microcalorimetry of peptide – membrane interactions. Introduction.

The application of ITC for investigation of membrane association of membrane-active peptides was pioneered by Prof. Joachim Seelig and co-workers in the early 90's (Beschiaschvili and Seelig, 1992; Georgi Beschiaschvili, 1990; Seelig et al., 1993; Terzi et al., 1995).

The set of thermodynamic parameters (ΔH, ΔS, K_A) can be also determined from calorimetric titrations. However in case of membrane – peptide association the unspecific interactions between the peptide molecules and lipid surface occurs, that's why we are talking rather about adsorption or partitioning, than binding (Seelig, 1997, 2004). Peptide interaction with lipid bilayers can be divided in several consributions. In the first step electrostatic attraction takes place between charged species such as cationic peptides and anionic membranes, which creates an elevated peptide concentration near the bilayer surface. Electrostatic attraction is not a prerequisite

for binding, as there are also uncharged membrane-active peptides that interact with pure zwitterionic membranes. The peptide may remain electrostatically attracted the to membrane surface, but in the second step most amphipathic peptides tend to penetrate deeper into the hydrophobic core of the lipid bilayer. Finally the third contribution to association is related to conformational changes. Most of the membrane-active peptides adopt α-helix or β-sheet structures in lipid bilayer environment. It was shown in the experiments with several antimicrobial peptides and their D-analogues that α-helix formation is an exothermic process (reviewed in Seelig, 2004). It is possible that peptide association with the membrane and helix formation have the opposite sign for the enthalpy value. In this case at a certain temperatures we may observe only a very small calorimetric response from peptide – membrane association, as ΔH (adsorbtion) ≈ ΔH (helix formation).

There are two strategies of performing such ITC measurements (Seelig, 1997). In the first approach the peptide is titrated into a vesicles suspension. The lipids are in large excess, so one would anticipate the complete binding of the peptide. The binding enthalpy ΔH can be determined directly from the titrations. In the second step the vesicles are loaded in the syringe and titrated into the peptide solution.

When the concentrations of reagents in the cell and the syringe are carefully selected, the binding isotherm can be constructed such that peptide association is complete at the end of the titration. The binding enthalpy could also be determined from this type of titration using:

$$\Delta H = \sum_{1}^{n} \Delta h_i \, / n_P$$

where n_P is the molar amount of peptide in the calorimeter cell after n injections. This value should be identical to the obtained by the first method, but additionally we can evaluate the binding constant from the second type of titration isotherm.

After *i* injections, the fraction of bound peptide can be expressed as follows:

$$X_i(P) = \frac{n_i(P)}{n(P)} = \sum_{1}^{i} \Delta h_i \, / \sum_{1}^{n} \Delta h_i$$

where $n_i(P) = X_i(P) \times n(P)$ is the molar amount of bound peptide after

i injections and n(P) is the total amount of

peptide in the calorimeter cell after *n* injections. Intuitively we consider n(P) to be equal to $n_0(P) = c_0 \times V_0$, initial molar amount of peptide in the calorimetric cell. But one should take into account the volume displacement effect, as the heat is sensed from the reactions that occur in the well-defined volume (V_o). Thus the molar amount of peptide after *n* titrations will be slightly smaller. This concentration recalculation is integrated in MicroCal Origin® algorithm.

The free peptide concentration in the calorimeter cell, $c_i(P_f)$ at each point of the titration can

f

be calculated according to $c_i(P_f) = c_o(P) \times (1 - X_i(P))$, where $c_o(P)$ refers to the initial peptide concentration in the calorimetric cell.

The molar amount of lipid after *i* injections equals to $n_i(L) = i \times V_{inj.} \times c_o(L)$, where $c_o(L)$ is the concentration of vesicles suspension in the syringe, $V_{inj.}$ – injection volume.

Thus the fraction of bound peptide at *i*th titration step can be derived: $X_i(P_b) = n_i(P) / (n_i(P) \times \gamma)$, γ is introduced to correct on the exclusive binding to the outer membrane. $X(P_b)$ is hence a function of the free peptide concentration $c(P_f)$. The exact form of the function will depend on the nature of peptide – lipid interactions (Seelig, 1997).

In case of interaction of uncharged peptide with lipid membrane the simple partitioning of the peptide into the bilayer is considered. The fraction of bound peptide, $X(P_b)$, is related linearly to the concentration of free peptide, $c(P_f)$, via the association constant: $X(P_b) = K_A \times c(P_f)$.

When the peptide is charged, the electrostatic interactions modulate the peptide – membrane association, even in the case when the membrane consists only of zwitterionic lipids. The association constant K_A depends then on the concentration of charged peptide, and is called apparent binding constant K_{app}. The binding constant can be corrected on the electrostatic attraction using Gouy-Chapman theory. This approach was elaborated by Seelig and co-workers and explained in details in the corresponding publications (Seelig, 1997, 2004; Seelig et al., 1993; Wieprecht et al., 1999a). The general principle is that the concentration of peptide near the membrane surface is elevated due to the electrostatic attraction, therefore the fraction of bound peptide is in the equilibrium with the peptide near the membranes surface rather than bulk peptide. But the electrostatic attraction of cationic peptide to negatively charged membrane will diminish progressively when more peptide is getting bound. The relation between the fraction of bound peptide and the concentration of peptide near the membrane surface then take a linear form (***Figure II-5***).

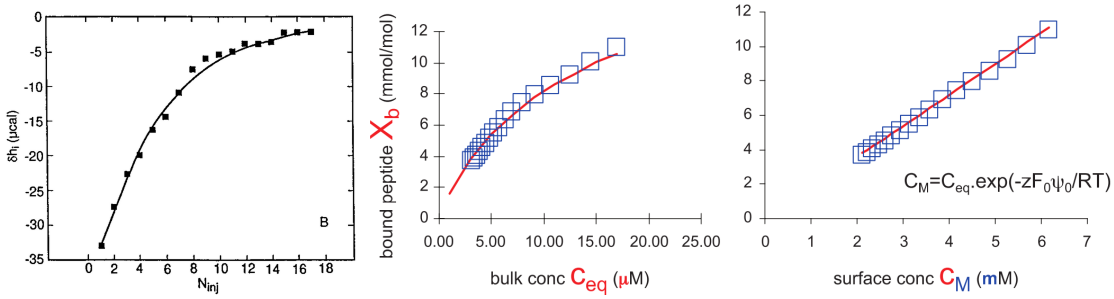

Figure II-5. *Left*) ITC curve of nisin Z peptide association with POPC/POPG=3:1 vesicles; *Middle*) Binding isotherms obtained by plotting the fraction of bound peptide against peptide bulk concentration; *Right*) Binding isotherm corrected on electrostatic attraction. The thermodynamic parameters for the experiment shown are K_0=1.8 M^{-1} and $\Delta H° = -8.5$ kcal/mol (at 28°C). Adapted with permission from the references (Breukink et al., 2000; Seelig, 2004).

The surface concentration is related to the bulk concentration *via* the membrane surface potential ψ_0: $c(P_M) = c(P_f) \times \exp(-z_P F_0 \psi_0 / RT)$, where z_P is the peptide net charge, F_0 – Faraday constant, RT – thermal energy. The membrane potential ψ_0 cannot be measured directly, but it is connected with the membrane surface charge density, σ, which is linearly related to the extent of binding X_b. The surface charge density σ is given by the sum of contributions of anionic lipid, bound cationic peptide, and all other bound cations such as Na^+ (Seelig et al., 1993). This approach allows calculating of the intrinsic binding constant K_0, which is not dependent on the electrostatic attractions.

Very often the regular sigmoidal shape of ITC isotherm is not obtained when performing the experiment on peptide – lipid system, which indicates that peptide association with membrane is accompanied by various processes which have opposite enthalpy sign and/or occur at different lipid-to-peptide ratio. The irregular calorimetric signal hampers the subsequent isotherm analysis and often the calculation of thermodynamic parameters become impossible. From the other hand, that particular calorimetric trace can provide the additional information about the mechanism of peptide – membrane interaction, especially when compared to the available structural data. In the following sections such interactions viewed by ITC will be illustrated. In the view of their complex character the original ITC traces adapted from the corresponding publications will be provided in order to facilitate the discussion. In this manuscript section the author aims to give an overview of the processes that accompany peptide insertion into membrane and their appearance on the ITC isotherm.

Peptide aggregation on lipid membranes – pore formation.

The approach to ITC curve analysis that has been described above can be applied when peptide association with membranes occurs via partitioning or electrostatic attraction-modulated partitioning. However, the calorimetric response from other processes that occur upon peptide – membrane association are also observed. The example of such processes is peptide aggregation in the lipid bilayer environment with subsequent pore formation. Wenk and Seelig observed that along with an exothermic process which characterizes magainin 2 peptide association with mixed POPC/POPG=75:25 *mol/mol* membranes, some endothermic process occurs. The magnitude of this endothermic process depends strongly on the peptide concentration and was subsequently referred to peptide aggregation on the membrane surface (Wenk and Seelig, 1998). This process is reversible, and the heat that was absorbed at the initial titration steps (at low L/P ratios) is returned as an exothermic process of peptide disaggregation at higher L/P ratio. The similar calorimetric traces were obtained when melittin (Klocek et al., 2009) and mastoparan X (Henriksen and Andresen, 2011) peptides were titrated with mixed anionic vesicles. Those ITC results and the relation to

structural characteristics of peptide – membrane association will be reviewed in General discussion (p. 146) with respect to ITC traces obtained with LAH4-L1.

Membrane association of arginine-rich cell-penetrating peptides.

The **pAntp** peptide (or penetratin RQIKIWFQNRRMKWKK) was the first

member of a rapidly expanding family of peptide-based cellular transporters. It is able to spontaneously cross the cell membrane in a receptor-independent manner and with high efficiency and low lytic activity although it is water-soluble. Penetratin does not belong to the family of amphipathic helical peptide, which are able to translocate membranes by pore formation. It was shown experimentally and by molecular modeling that penetratin is not sufficiently hydrophobic to insert deeply into the phospholipid model membranes, but remains at the interface between the phospholipid bilayer and the aqueous environment instead (Drin et al., 2001). Most of the studies show that penetratin peptides cross the cell membrane and deliver the cargo *via* an endocytic pathway (Madani et al., 2011). ITC technique was applied to characterize factors that affect pAntp peptide internalization into mixed anionic lipid vesicles (Binder and Lindblom, 2003). Penetratin possesses a small hydrophobic moment, and the intrinsic constant for penetratin binding to DOPC/DOPG membranes (K_b) of $80M^{-1}$ is typical for weakly hydrophobic peptides (Persson et al., 2001).

The electrostatic nature of penetratin interaction with lipid membranes was shown by performing the experiments with the DOPC/DOPG small unilamelar vesicles with varied DOPG content and at various salt concentrations. The interaction of penetratin with DOPC membranes produces only a small exothermic signal, but this signal grows when the DOPG content is increasing (***Figure II-6***, left columns). Peptide is completely bound to the vesicles with elevated DOPG content at the smaller lipid-to-peptide ratio (about 20 for PC/PG-75%). The increased ionic strength also suppresses largely the peptide association to the vesicles (***Figure II-6***, right columns). In the reverse series of titrations (***Figure II-7***) the endothermic signals of peptide were also produced upon peptide – membrane association, however the calorimetric trace revealed a rather complex character of interaction with highly charged vesicles. It was assumed that the membrane permeabilization of such weakly hydrophobic peptide requires high surface negative charge density, and also some critical P/L ratio, at which translocation takes place. In a ***Figure II-7***, which is adapted from the original publication, the zones of permeability determined by calorimetric peptide-to-lipid titrations are shown. The mechanism was named ‘‘electroporation-like’’ internalization (Binder and Lindblom, 2003).

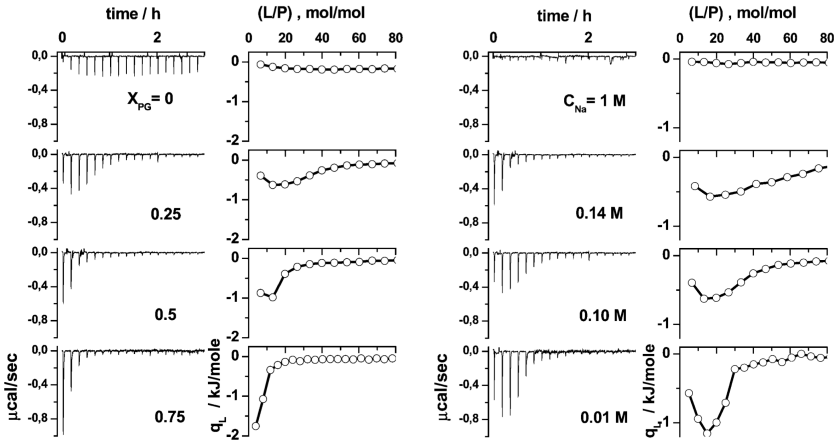

Figure II-6. Calorimetric titrations of 15mM DOPC/DOPG SUV of varied PG content into 12.5µM pAntp peptide solution, Tris – 100mM NaCl (left); calorimetric titrations of 15mM DOPC/DOPG-25% SUV into 12.5µM pAntp peptide solution in Tris buffer with varied salt concentration. Adapted with permission from (Binder and Lindblom, 2003).

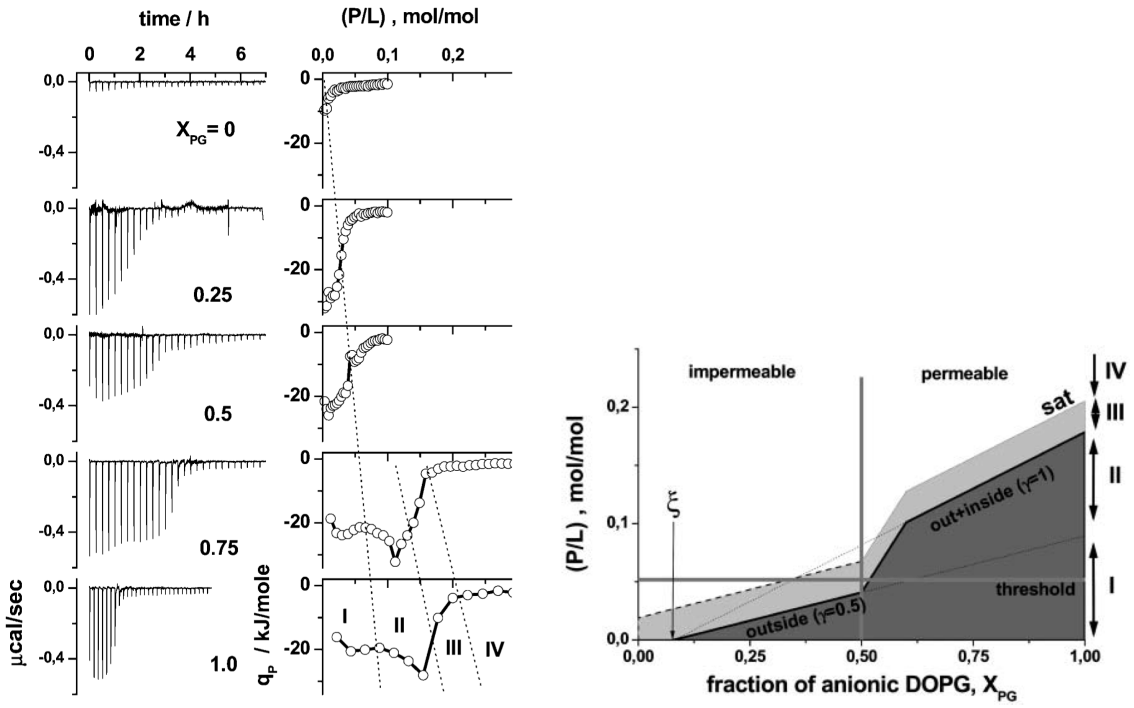

Figure II-7. *Left)* Calorimetric titration of 0.2-0.4mM penetratin solution into 0.2-0.4mM DOPC/DOPG SUV with varied PG content. *Right)* Penetratin permeabilization through the DOPC/DOPG membranes. The horizontal and vertical lines define the internalization threshold, (P/L) threshold and X_{PG} threshold, respectively. The dark gray region refers to the strong binding regime where virtually all peptide binds to the negatively charged surface of the vesicles. Adapted with permission from (Binder and Lindblom, 2003). For definition of the parameters and the ITC analysis please see original reference.

Membrane association of the **HIV-1 TAT** protein transduction domain (YGRKKRRQRRR) was investigated by ITC and other biophysical methods (Ziegler et al., 2003). Rather regular shape of calorimetric isotherm was obtained upon the titrations of POPC/POPG small unilamelar vesicles with varied PG content into the peptide solution at neutral pH. TAT peptide association with membranes was accompanied by the negative enthalpy signal. The apparent association constant K_{app} was determined from the binding isotherm, and after the correction on electrostatic attraction using Gouy-Chapman theory the intrinsic binding constant K_A was derived. Electrostatic interactions account for about 77% of the free energy of TAT-PTD peptide association to POPC/POPG-25% SUV ($\Delta G° = -5.2$ kcal/mol include $\Delta G_{el} = -4.0$ kcal/mol and $\Delta G_h = -1.2$ kcal/mol). TAT-PTD peptide does not undergo the conformational changes upon membrane association (Mitchell et al., 2000; Ziegler et al., 2003), and therefore its membrane association is not driven by α-helix formation, as it is for majority of cationic amphipathic peptides. Also TAT-PTD does not perturb the lipid acyl chain order upon the association, as shown by ^2H NMR spectroscopy, however it binds preferentially to POPG head groups. In contrast to previous investigation with penetratin, any membrane translocation by TAT peptide was registered neither by ITC, nor by the dye leakage assay. Also TAT peptide does not induce the lipid domain separation. It was concluded that the cell membrane translocation by TAT-PTD occurs via glycosaminoglycans binding rather than by the direct association with plasma membrane lipids.

Special cases.

1) The interaction of high molecular weight polylysines with negatively charged large unilamelar vesicles was assessed by ITC (Reuter et al., 2009). Polylysine (PLL402, Sigma) solution was titrated into DPPG and DPPG/DPPC=1:1 vesicles suspension. The titrations were performed at two

temperature conditions – below and above the gel to liquid-crystalline phase transition. Polylysines form large aggregates with lipid vesicles. The authors concluded that at lower temperatures (membrane in gel phase) primarily the electrostatic association takes place, but at 60°C also the translocation through the membrane (in its fluid phase), which is confirmed but different calorimetric responses.

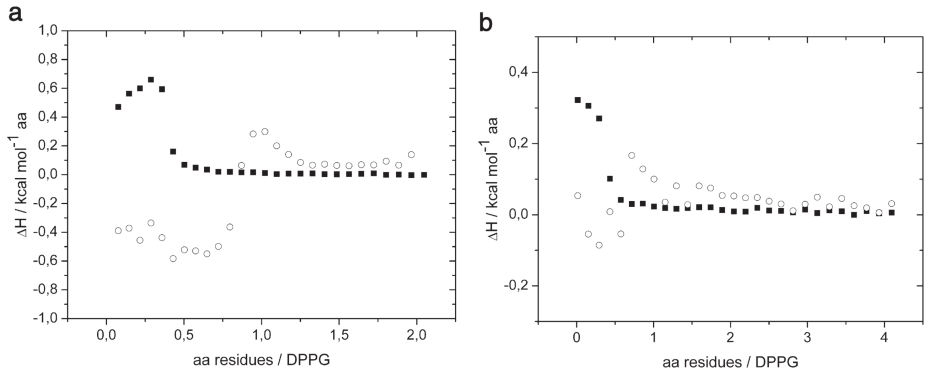

Figure II8. ITC binding curves for PLL 402 to PG membranes. a) Reaction heats for the titration of 20mM PLL402 into a *a*) 2mM DPPG suspension and *b*) a 2mM DPPG/DPPC (1/1mol/mol) suspension at 20°C (■) and 60°C (○). Adapted with permission from (Reuter et al., 2009).

2) ITC was used to determine the degree of interaction of highly charged cationic peptides and lipopeptides with negatively charged constituents of bacterial cell walls, which regulate peptides' access to the membrane of Gram-negative and Gram-positive bacteria (Epand et al., 2010).

Peptide Name	**Sequence**	**Net charge at neutral pH**
Magainin 2	GIGKFLHSAKKFGKAFVGEIMNS	+3.5
MSI-78 (Pexiganan)	GIGKFLKKAKKFGKAFVKILKK-NH2	+10
MSI-103	KIAGKIAKIAGKIAKIAGKIA-NH2	+7
MSI-469	Octyl-KIAGKIAKIAGKIAKIAGKIA-NH2	+6
MSI-843	Octyl-OOLLOOLOOL-NH2	+6
MSI-1254	Octyl-XXLLXXLXXL-NH2	+6

O=Ornithine; X=2,4 diaminobutyric acid (Dab)

In the series of ITC experiments the peptide solutions was titrated in suspension of lipopolysaccharides (LPS) from E. coli O111:B4, either into lipoteichoic acid (LTA) from Staphylococcus aureus (Epand et al., 2010). The calorimetric traces are shown below (***Figure II-9***). The enthalpy observed by ITC was reported to arise from the following processes: the exothermic processes of peptide helix-formation, membrane insertion, intermolecular salt-bridge formation and peptide aggregation, also the endothermic contributions from disaggregation of the macromolecule, the break up of hydrogen bonds, and in LPS displacement of Mg2+ ions or removal of water from phosphate groups in Lipid A. The interactions of cationic peptides and lipopeptides with those negatively charged macromolecules produce the calorimetric traces of rather complex character. It was shown that two of the peptides (MSI-78 and MSI-1254) aggregate strongly with lipopolysaccharides at some critical concentration, producing large exothermic signal (***Figure II-9***, left). Their binding to LTA was much weaker, producing the exothermic signal at low peptide-to-lipid ratio, even though both are negatively charged species with high sugar content. The thermodynamic parameters were not derived due to the complexity of titrations curves

(Epand et al., 2010).

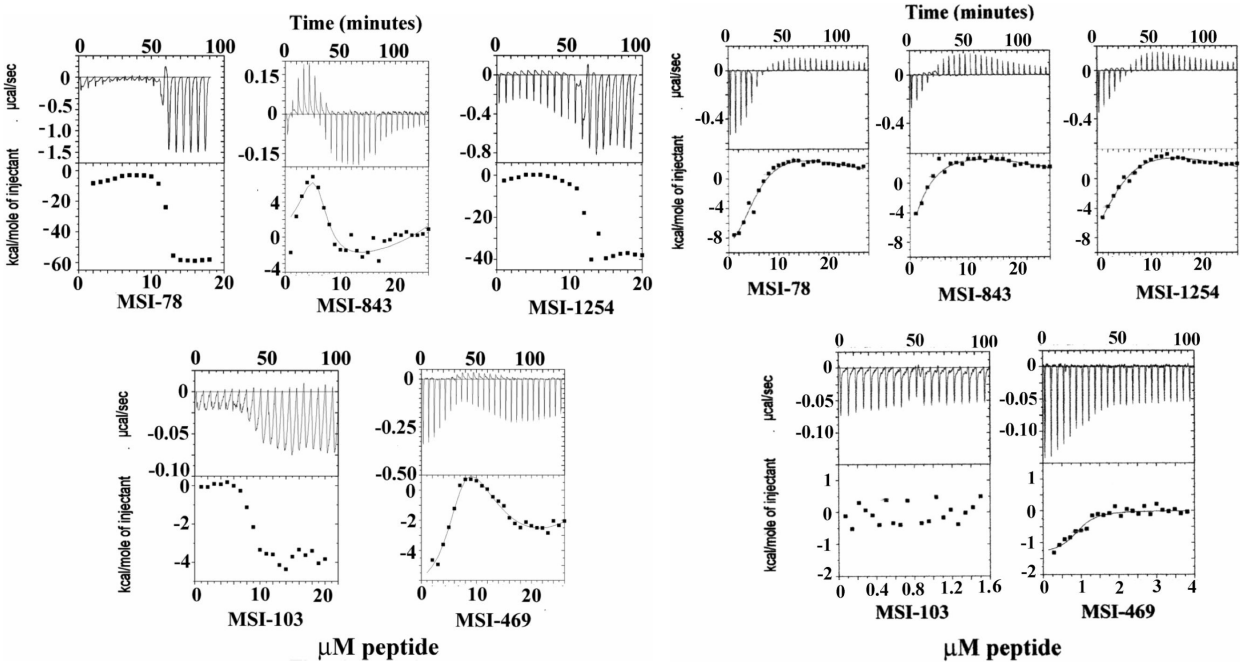

Figure II-9. *Left*) ITC of 125 µg/mL LPS with 10 µL injections of a solution of 200 µM peptide in the syringe, 10 mM HEPES, 0.14 M NaCl, pH 7.4, at 30°C; *Right)* LTA in calorimetric cell, same conditions. Adapted with permission from (Epand et al., 2010).

3) An interesting approach was used by Reshetnyak and co-workers (Reshetnyak et al., 2008) to investigate pH-dependent peptide insertion into lipid bilayer. pHLIP peptide (AEQNPIYWARYADWLFTTPLLLLDLALLVDADEGT) is negatively charged protein domain and potent tumour targeting agent, which is water-soluble at physiological pH, but inserts transmembrane adopting α-helical structure at low pH. The stages of peptide insertion into POPC lipid bilayers were investigated by ITC and other biophysical techniques, and displayed in a ***Figure II-10***. The authors have shown that peptide inserts superficially into POPC bilayer with considerable negative enthalpy at near physiological pH. In the second step the vesicles preloaded with peptide at pH 8 were titrated with acid till pH 4. Thus peptide transmembrane insertion, followed by α-helix formation was found to be an exothermic process. For the analysis of ITC isotherms binding equilibrium model was preferred rather than a partition model, as the authors felt it was more appropriate to consider lipids as individual molecules rather than as a phase. The detailed mathematical description of the model can be found in the original publication (Reshetnyak et al., 2008). By using this model for treatment of ITC and tryptophan fluorescence data it was possible also to determine the number of lipids that were affected by the peptide insertion.

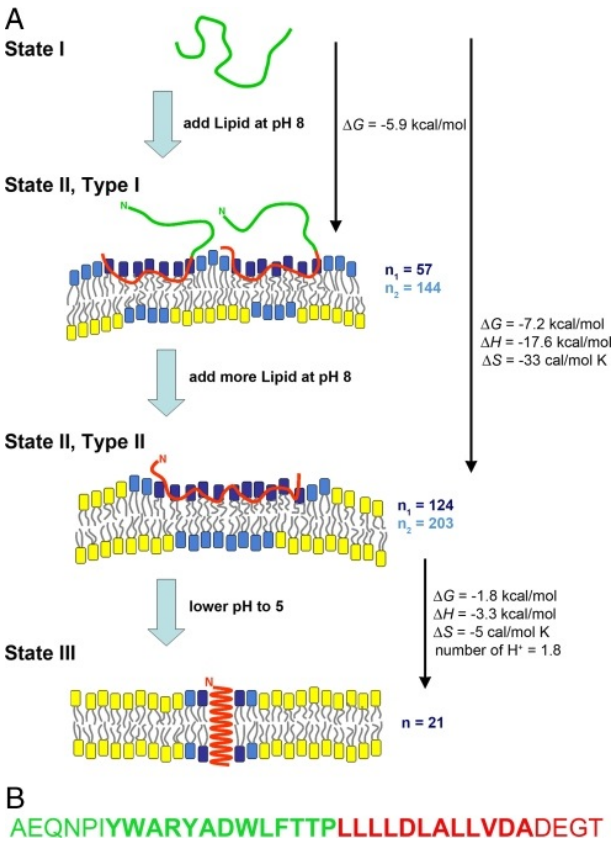

Figure II-10. A schematic representation of pHLIP interaction with a lipid bilayer is shown. (A) In state I, the peptide is in solution at neutral and basic pHs. By addition of vesicles, the unstructured peptide is adsorbed on the membrane surface. State II, type I interactions occur at a low lipid/peptide ratio, when the total accessible membrane surface is not enough to accommodate the full length of peptide on it. The hydrophobic motif near the C terminus is adsorbed first (red sequence in B). By addition of more vesicles, the transition to the type II (state II) interaction is seen, at a high lipid/peptide ratio when there is enough accessible space on a membrane for peptides to freely occupy lipid surface area without competing with each other. In state III, a drop of pH leads to the protonation of Asp residues, increasing peptide hydrophobicity, and resulting in the insertion and formation of a transmembrane α-helix. Adopted with permission from the reference (Reshetnyak et al., 2008).

2. Structural characterisation of membrane-active peptides.

In this section the biophysical methods applied to the peptide – membrane interaction will be discussed, in particular circular dichroism and solid-state nuclear magnetic resonance. The general overview of each method, as well as the examples of its application will be illustrated, however without detailing as it was done for Isothermal titration calorimetry section. The description of theoretical background of the circular dichroism and nuclear magnetic resonance methods will not be provided in this manuscript section, yet can be found in the appropriate literature (for example B.A. Wallace and R.W. Janes "Modern Techniques for Circular Dichroism and Synchrotron Radiation Circular Dichroism Spectroscopy", 2009 and Malcolm H. Levitt "Spin Dynamics: Basics of Nuclear Magnetic Resonance, 2nd Edition", 2008).

Circular dichroism spectroscopy of proteins.

Circular dichroism spectroscopy is widely used to assess secondary structure and folding properties of proteins. The advantage of technique is that measurements can be made on multiple samples in short time and it requires rather small quantity of material. However it does not provide residue-specific structural information. Briefly, circular dichroism is defined as the difference in absorption of left-handed and right-handed circularly polarized light. It occurs when a molecule contains one or more asymmetric light-absorbing groups. The absence of regular structure results in zero CD intensity, but an ordered molecular structure usually results in spectra, which contain both positive and negative signals. Circular dichroism on biological macromolecules is measured over a range of wavelengths in the UV region, typically 260-185nm. Different structural elements of polypeptides have their characteristic CD spectra. For proteins the spectra are decomposed into contributions from α-helix, β-sheet, β-turn and random coil (detailed in Greenfield, 2007). Since CD spectroscopy was well developed as method for the structural investigations of proteins, the substantial collection of data was gathered. The CD spectra of proteins with confirmed secondary structure (usually by X-ray, or NMR) were regrouped into databases, for example SP175 is CD data collection for soluble proteins recorded up to 175 nm, or MP180 that was created recently to regroup the data on membrane proteins (Abdul-Gader et al., 2011). Those database sets are stored in the Protein Circular Dichroism Data Bank (PCDDB) http://pcddb.cryst.bbk.ac.uk/home.php. It is a public repository that archives and freely distributes circular dichroism (CD) and synchrotron radiation CD (SRCD) spectral data and their associated experimental metadata (Whitmore et al., 2011). There are a number of methods which allow the estimate of protein secondary structure from experimental CD data. All this methods assume that the spectrum of a protein can be represented by a linear combination of the spectra of its secondary structural elements, including a noise term, which includes the contribution of aromatic chromophores (detailed in Greenfield, 2007). The characteristic CD traces of protein structural elements are taken from the appropriate reference database set. The web-based tools for protein secondary structure estimate (as Dichroweb http://dichroweb.cryst.bbk.ac.uk/html/home.shtml Whitmore and Wallace, 2004) or CD programs (as CDPro http://lamar.colostate.edu/~sreeram/CDPro/ Sreerama and Woody, 2000) have integrated both the analysis algorithms and the reference database sets.

Most of the antimicrobial and cell-penetrating peptides have rather short sequences of 14 – 30 amino acids. As soon as they usually consist of the same building blocks as proteins, their secondary structure can also be characterized by common structural elements, as α-helix, β-sheet, β-turn and random coil. But many algorithms that are applied for secondary structure assessment of proteins cannot be directly applied to peptide secondary structure determination. But the structure of peptides lacks many of the elements –

such as long-range interactions, extensive and twisted β-sheet segments, and multiple packed, short, and tilted helices – seen in the large globular proteins used in this algorithms (Poschner et al., 2007).

Usually folding of small peptides is associated with their interaction with membranes, DNA, proteins or between peptide molecules. Due to the short sequence peptides are typically found in two co-existing conformations. Depending on the applied external stimuli, we are talking about random coil – α-helix, random coil – β-sheet, or α-helix - β-sheet transitions. A majority of antimicrobial and cell-penetrating peptides adopt α-helical conformation when interacting with lipid bilayers (Galdiero et al., 2013). Linear α-helical peptides represent one of the most important subgroups of the Antimicrobial Peptide Database (almost 317 out of 740 items with known secondary structure; http://aps.unmc.edu/AP/main.php). Typical CD spectra of peptide taken in the presence of membranes consist then of two components – one resulting from random coil conformation and another – from α-helical conformations. A helix content of the peptide secondary structure can then be estimated by deconvolution of the CD spectra. Such deconvolution are often made by applying least-square fitting method using an appropriate spectral reference set (Poschner et al., 2007; Reed and Reed, 1997). The example of procedure will be provided in the Experimental part.

The peptide – lipid interaction are usually investigated on liposomes. Small unilamellar vesicles (≈30nm) are used as membrane model more often than large unilamellar vesicles (100nm) because of the reduced light scattering. However, even at this condition the CD spectrum of peptide could not be recorded in the far UV range (195-170nm), while most of the empirical secondary structure determination algorithms, used for proteins, require the spectra to be taken in the 250 – 180mn range of wavelength. Once more, the adopted method of secondary structure determination has to be used in analysis of the peptides CD spectra.

In an alternative method the fractional helical content (f_α) of membrane-bound peptide can be estimated from the mole residue ellipticity [θ] at 222nm as was first described by Scholtz et al. (Myers et al., 1997). The method is based on the conversion of the measured CD signal at 222nm into a free energy scale using Lifson-Roig helix-coil theory (Lifson S. & Roig A., 1961).

$$f_\alpha = \frac{[\theta]_{222} - [\theta]_{coil}}{[\theta]_{helix} - [\theta]_{coil}}$$

where $[\theta]_{helix}$ and $[\theta]_{coil}$ represent the mole residue ellipticity of a complete helix and coil respectively.

The values for $[\theta]_{helix}$ and $[\theta]_{coil}$ were corrected by Luo and Baldwin (Luo and Baldwin, 1997) and are equal to: $[\theta]_{helix}$ = (-42 500*(1-3/n) + 100t), where n is the number of amino acid residues, and t is the temperature in °C, and $[\theta]_{coil}$ = 640 -45t = -485.

CD spectroscopy of peptide is used not only for structural characterisation of their membrane-bound state, but it can be employed to construct the peptide-to-lipid binding isotherms and calculate the partitioning constant. The fraction of peptide bound is determined in titration experiment using CD measurements, as described in detail by White and co-workers (White, 1998):

$$\Theta_{\text{norm}} = 1 + (\Theta_{\text{m}} - 1)\frac{K_{\text{X}}[L]}{[W] + K_{\text{X}}[L]},$$

where Θ_{norm} is the normalized molar ellipticity of the peptide and Θ_{m} is the increase in the normalized molar ellipticity of the peptide upon binding to the membrane. The equation can be fitted using least-square method in order to obtain peptide – membrane association constant. This method was applied to characterize the membrane association of several antimicrobial peptides (Fernández-Vidal et al., 2011; Wieprecht et al., 1999b, 2000a, 2000b).

Solid-state nuclear magnetic resonance of membranes and membrane peptides (selected methods).

Nuclear magnetic resonance is the spectroscopic method that measures the interactions between the atomic nuclei, however not between any nuclei, only ones that have particular quantum mechanical properties. From one hand the most abundant nucleus found in living world, hydrogen ^{1}H, is NMR active and that is why it is used directly or intermediately in the most of NMR methods. However other abundant nuclei are silent in NMR (^{12}C, ^{14}N, ^{16}O) and the labelling is required. From the other hand sparsed labeling allows to distinguish only the interactions we are interested in.

Solid-state NMR technique has found a wide range of application in the investigation of membrane proteins and membrane-active peptides (Bechinger and Salnikov, 2012; Gehman and Separovic, 2008; Hong and Su, 2011; Judge and Watts, 2011; Murray et al., 2013; Zhao, 2012). The advantage of solid-state NMR is that the biological molecules can be investigated in an anisotropic environment, and a large number of ssNMR methods are based on the asymmetry of the nuclear interactions. By using the specific labelling scheme one can elucidate the structure of large membrane assemblies (Weingarth and Baldus, 2013), the orientation of peptide and proteins in lipid bilayers (Fu and Cross, 1999), and dynamics of membrane proteins (Hong et al., 2012; McDermott, 2009). There are two principal approaches to acquisition of NMR signal from the matherial in solid state. The magic angle spinning technique is used to average the anisotropic interactions between the dipoles, and to obtain narrow signals. From the other hand *chemical shift anisotropy* provides an additional information about the macromolecule structure and orientation, thus static mode is very often used in membrane investigations.

Solid-state NMR is widely employed in membrane-active peptides study because it allows to assess both peptide structure and orientation (Aisenbrey and Bechinger, 2004; Aisenbrey et al., 2010; Bechinger et al., 2004; Drechsler and Separovic, 2003; Su et al., 2013), and membrane structure and dynamics upon peptide association (Bechinger, 2005; Seelig, 1977). Because of a really large variety of methods and applications of solid-state NMR in membrane and membrane polypeptide study in this section only the selected methods will be described, based on the static solid-state NMR technique, while the *magic angle spinning* methods will be discussed in the next section.

a) The alignments of peptides in the oriented lipid bilayers assessed by ^{15}N solid-state NMR.

When peptide adopts a α-helical structure, the hydrogen bonds are formed and the N-H dipole occurs aligned almost parallel to the long axis of the helix (***Figure II-11***).

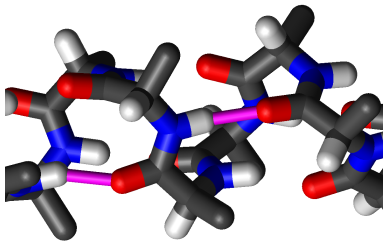

Figure II-11. Schematic representation of α-helix. Nitrogens are in blue, protons – in light grey, oxigens – red, and hydrogen bonds are depicted by magenta line.

This property can be used to determine the peptide helix alignment in uniaxially oriented lipid bilayers (Bechinger and Sizun, 2003; Bechinger et al., 1993; Opella, 1994). For this single or multiple ^{15}N labels are incorporated in the peptide backbone, specifically in the peptide region, which adopts α-helical structure. The peptide is then reconstituted into mechanically uniaxially oriented lipid bilayers, which are inserted between the thin glass plates. For ^{15}N static solid-state experiment the sample is placed into flat

coil such that the bilayer plane is oriented perpendicularly to the magnetic field (B_o). Detailed procedure for sample preparation and the spectra acquisition can be found in the dedicated publication (Aisenbrey et al., 2010).

In order to understand how we can correlate the ^{15}N NMR spectroscopic data with structure and alignment of peptides in lipid bilayers, the theoretical considerations shall be introduced.

Chemical shift tensor. Depending on the local symmetry of electric field around the NMR active nucleus, the magnitude of the chemical shift varies as a function of the molecule orientation with respect to the external magnetic field B_o. This orientation dependence of the chemical shift is called the chemical shift anisotropy (CSA), which is described mathematically using tensor. In the principal axis system (PAS), the chemical shift tensor is described by the three diagonal elements - the principal components σ_{zz}, $\sigma_{yy,}$ σ_{xx}[1] - and the three eigenvectors or Euler angles, which determine the orientation of the principal axes with respect to a laboratory frame (***Figure II-12***). More detailed mathematical description of CSA tensor can be found in the dedicated literature (Bechinger and Sizun, 2003; Saitô et al., 2010).

In addition, various combinations of the principal components (and their orientations) are used to describe the chemical shift tensor. Those terms are organised in the convention systems. The most common CSA systems are Haeberlen[2] and Mehring[3] (adapted by IUPAC) conventions (***Figure II-13***) .

The IUPAC convention describes the chemical shift anisotropy by three values, called principle components of the CSA tensor, which follow the high frequency-positive order: $\sigma_{11} \geq \sigma_{22} \geq \sigma_{33}$. The average value or these is then the isotropic chemical shift $\sigma_{iso} = (\sigma_{11} + \sigma_{22} + \sigma_{33})/3$.

The principle components according to the Haeberlen convention are $|\sigma_{zz} - \sigma_{iso}| \geq |\sigma_{zz} - \sigma_{iso}| \geq |\sigma_{zz} - \sigma_{iso}|$, where $\sigma_{iso} = (\sigma_{11} + \sigma_{22} + \sigma_{33})/3$ is the isotropic chemical shift.

Other terms are defined as reduced anisotropy $\delta = \sigma_{zz} - \sigma_{iso}$,

anisotropy $\Delta = (\sigma_{zz} - (\sigma_{yy} + \sigma_{xx}))/2 = 3\delta/2$,

asymmetry $\eta = (\sigma_{yy} - \sigma_{xx})/\delta$, where $0 \leq \eta \leq 1$.

The chemical shift anisotropy (CSA) is usually obtained from NMR experiments on a solid or a liquid crystalline sample, where the chemical shift tensor component σ_{zz} as is related to components σ_{11}, σ_{22} and σ_{33} in the molecular principal axis system (PAS) frame by $\sigma_{zz} = \sigma_{11}\sin^2\theta\cos^2\varphi + \sigma_{22}\sin^2\theta\sin^2\varphi + \sigma_{33}\cos^2\theta$ (Saitô et al., 2010).

The solid sample contains orientations sampling all directions in three dimensions. When the sample is placed into spectrometer, each magnetic moment of this system can be related for its PAS to the Z axis (B_o) by an angle, θ, and its position in the x y plane given by angle φ. Then the magnetization experienced by the nucleus is the function of Euler angles $B_o^{PSA} = (\sin\theta\cos\varphi, \sin\theta\sin\varphi, \cos\theta)$.

The observed spectral frequency is related to CSA tensor components and can be represented in the Haeberlen convention system:

$\nu_{CS} = -\nu_o\sigma_{iso} - \frac{1}{2}\nu_o\Delta*[3\cos^2\theta - 1 + \eta\sin^2\theta\cos^2\varphi]$, where $-\nu_o\sigma_{iso}$ is the isotropic frequency.

The examples of the spectral line shapes obtained from the powder samples, containing NMR active nuclei with particular CSA Haeberlen parameters are provided in a ***Figure II-14***. In average ^{31}P nuclei in

---

[1] In this chapter symbol σ is used to define chemical shift, while other publications σ is used for the magnetic field shielding constant designation. When σ is defined as shielding constant, then $\sigma_{33} \geq \sigma_{22} \geq \sigma_{11}$ (Saitô et al., 2010).

[2] U. Haeberlen, High Resolution NMR in Solids, Selective Averaging, Academic Press, 1976

[3] M. Mehring, High Resolution NMR in Solids, Springer, 1983

lipids are characterized by asymmetry $\eta = 0$. For ^{15}N in the polypeptides this value is closer to 0.25 (Loth et al., 2005), but of course this value can vary significantly depending on the structure.

CSA is an important source of spin–lattice (T_1) and spin–spin (T_2) relaxation. The contribution of the CSA to T_2, and the width of the resonance increases with magnetic field strength leading to broad, unresolved lines (Saitô et al., 2010).

In the polypeptides the principal values of the ^{15}N chemical shift tensor of the amide bond have equal about 61, 75 and 223 ppm (σ_{11}, σ_{22}, σ_{33}). In α-helical conformation the σ_{11} and σ_{33} components are oriented within the plane of the peptide bond. The N-H dipole vector and the σ_{33} vector form an angle of about 18° (Bechinger and Sizun, 2003), and both vectors are oriented within a few degrees relative to the helix long axis. When reconstituted into membrane, the peptide adopts ideally well-defined alignment. Therefore the chemical shift from ^{15}N-labeled peptide backbone will indicate the orientation of the peptide relative to the magnetic field (B_o). As soon as the lipids in the sample are oriented parallel to magnetic field, the observed chemical shift will indicate the peptide alignment in the lipid bilayer (***Figure II-15***). When the peptide is inserted transmembrane, the ^{15}N chemical shift will be observed around 200ppm, when it is aligned parallel to membrane surface, the CS is < 100ppm (Bechinger and Sizun, 2003).

The alignment of the peptide helix in the oriented lipid bilayer is described by the set of additional parameters, named tilt (δ) and rotational pitch (γ) angles (Aisenbrey and Bechinger, 2004). A given ^{15}N chemical shift may correspond to multiple alignments, described by the set of tilt and pitch angles, but obtained ^{15}N chemical shift restricts the possible tilt angles. Thus in uniaxially oriented samples the transmembrane α-helical peptides with a tilt angle ≤20° show ^{15}N signal >180 ppm (Bechinger et al., 2004).

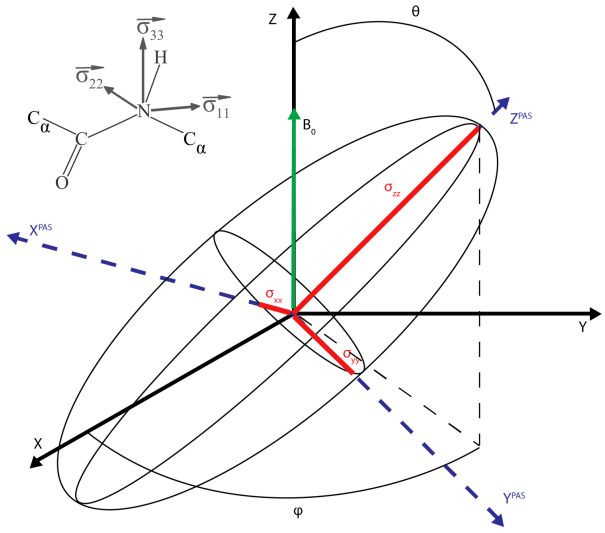

Figure II-12. Graphical representation of the relation of the Principle Axis System (dotted blue lines) to the laboratory frame (black solid lines). The projection of the PAS onto the laboratory frame is indicated by the black dotted line. The principle components of the chemical shift tensor are illustrated using the red lines, which the black ellipses represent the electron field surrounding the nucleus (adapted from http://chemwiki.ucdavis.edu/Physical_Chemistry/Spectroscopy/Magnetic_Resonance_Spectroscopies/Nuclear_Magnetic_Resonance/). The smaller picture in the left upper corner represents the principal parameters of chemical shift tensor for ^{15}N nucleus in the context of the polypeptide backbone.

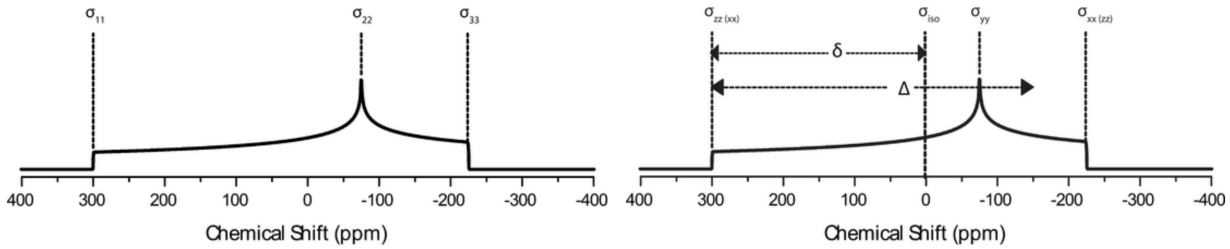

Figure II-13. Convention systems used to represent chemical shift tensor: *left*) Mehring (IUPAC), right) Haeberlen. Adapter from http://chemwiki.ucdavis.edu/Physical_Chemistry/Spectroscopy/Magnetic_Resonance_Spectroscopies/Nuclear_Magnetic_Resonance/).

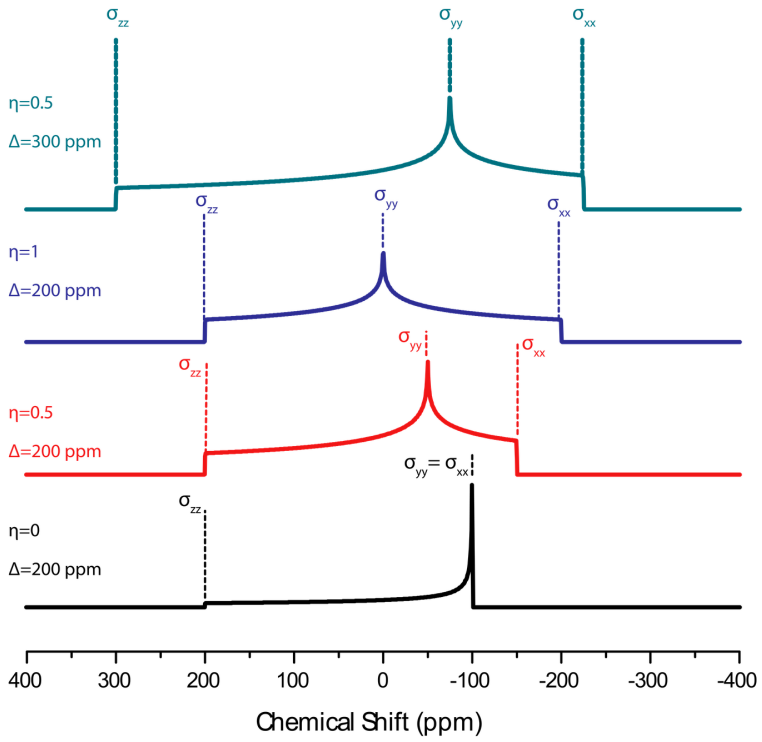

Figure II-14. Comparison of the static NMR signal with changing anisotropy Δ and asymmetry η parameters. The dashed lines are used to show how the principle components the chemical shielding tensor relate the line shape. Adapter from http://chemwiki.ucdavis.edu/Physical_Chemistry/Spectroscopy/Magnetic_Resonance_Spectroscopies/Nuclear_Magnetic_Resonance/).

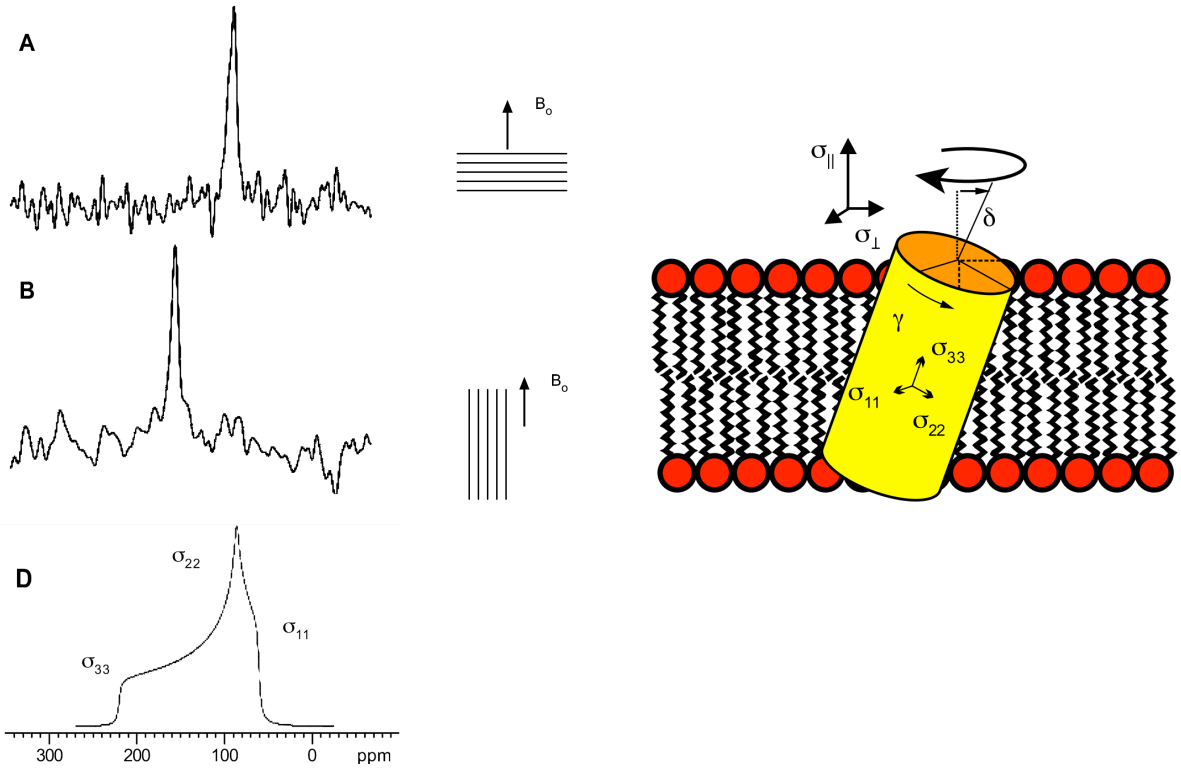

Figure II-15. *left*) Proton-decoupled ^{15}N solid-state NMR spectra of the *in-plane* oriented model peptide LK15 in C20-PC with alignments of the membrane normal parallel (A) and perpendicular (B) to the magnetic field direction. (D) Static simulated powder spectrum. *right*) Transmembrane-inserted helical peptide is represented as a cylinder and the tilt and rotational pitch angles, γ and δ, are indicated. The approximate alignment of the static tensor elements is shown within the helix. Adapted with permission from the reference (Bechinger et al., 2004).

b) Membrane properties investigation by static solid-state NMR.

^{31}P static NMR.

Solid-state NMR spectroscopy proposes the variety of valuable methods to assess the membrane morphology upon peptide association, the depth of peptide insertion, the electrostatic interactions between lipids head groups and cationic compounds. Dr. Mason and co-workers (Mason et al., 2007c) have summarized the number of these methods (Table II-1). The chemical shift of the naturally abundant ^{31}P nuclei provide us several kind of information depending on the method we use. For instance, the measurement of the ^{31}P chemical shifts anisotropy is a sensitive method for assessing the degree of alignment of the phospholipids in mechanically oriented bilayers, and the effect of peptide insertion on the lipids orientation (Aisenbrey et al., 2010).

Table II-1. A comparison of NMR active nuclei commonly present in lipid membranes and the information that is tractable by solid-state NMR methods. Adapted with permission from (Mason et al., 2007c).

Nucleus	Labelling	Interaction	Technique/Information (Time Domain)
^{1}H	Natural abundance	Nuclear Overhauser Effect	MAS/NOESY gives direct measurement of peptide lipids contacts
^{2}H	Headgroup	Quadrupolar coupling (10-100 kHz)	Molecular voltmeter
	Acyl chain		Order parameter profile (μs)
		Relaxation (T_1, T_2)	Acyl chain dynamics (T_1: ns→μs; T_2: ms)
^{13}C	Natural abundance	^{1}H-^{13}C dipolar coupling (2-20 kHz)	Order parameter profile (μs)
^{14}N	Natural abundance	Quadrupolar coupling	Molecular voltmeter
^{31}P	Natural abundance	Chemical shift anisotropy (5-50 ppm)	Membrane morphology (ms→μs)
		Isotropic chemical shift	Molecular voltmeter
		Relaxation (T_1, T_2)	Headgroup dynamics (T_1: ns→μs; T_2: ms)

^{31}P chemical shift tensor.

^{31}P CSA tensor is also defined with three principal elements σ_{11}, σ_{22}, σ_{33}.

The observed ^{31}P chemical shift consists of the isotropic and anisotropic component.

Isotropic component is defined as $\sigma_{iso} = (\sigma_{11} + \sigma_{22} + \sigma_{33})/3$ (in a figure it is marked as ω_{iso} – carrying isotropic frequency).

In order to define the anisotropic component of ^{31}P chemical shift of lipid head groups several assumption have been made. In a liquid crystalline phase lipids undergo rapid diffusional motions about the normal to the membrane surface. These motions generate a tensor of chemical shift with resulting axial symmetry. Lipid bilayers oriented with their normal parallel to the field resonate at $\sigma\|$,whereas bilayers orient with their normal perpendicular to the magnetic field resonate at $\sigma\perp$. By conventions $\sigma\| = \sigma_{11}$, and $\sigma\perp = (\sigma_{22} + \sigma_{33})/2$. The difference $\sigma\| - \sigma\perp$, called anisotropy of chemical shift, is typically 45 ± 5 ppm for fluid lipid bilayers, and depends on the type of lipid (Soubias and Gawrisch, 2007). ^{31}P spectrum of the membrane consists of the signals from individual lipid molecules, the chemical shift of which depends on the lipid orientation relative to the magnetic field B_o. The anisotropic component then takes a view:

$$\Delta\omega_{CSA} = \tfrac{2}{3}(\sigma\| - \sigma\perp)\times(3\cos^2\theta - 1)/2,$$

where θ is the angle between the bilayer normal and the magnetic field B_o.

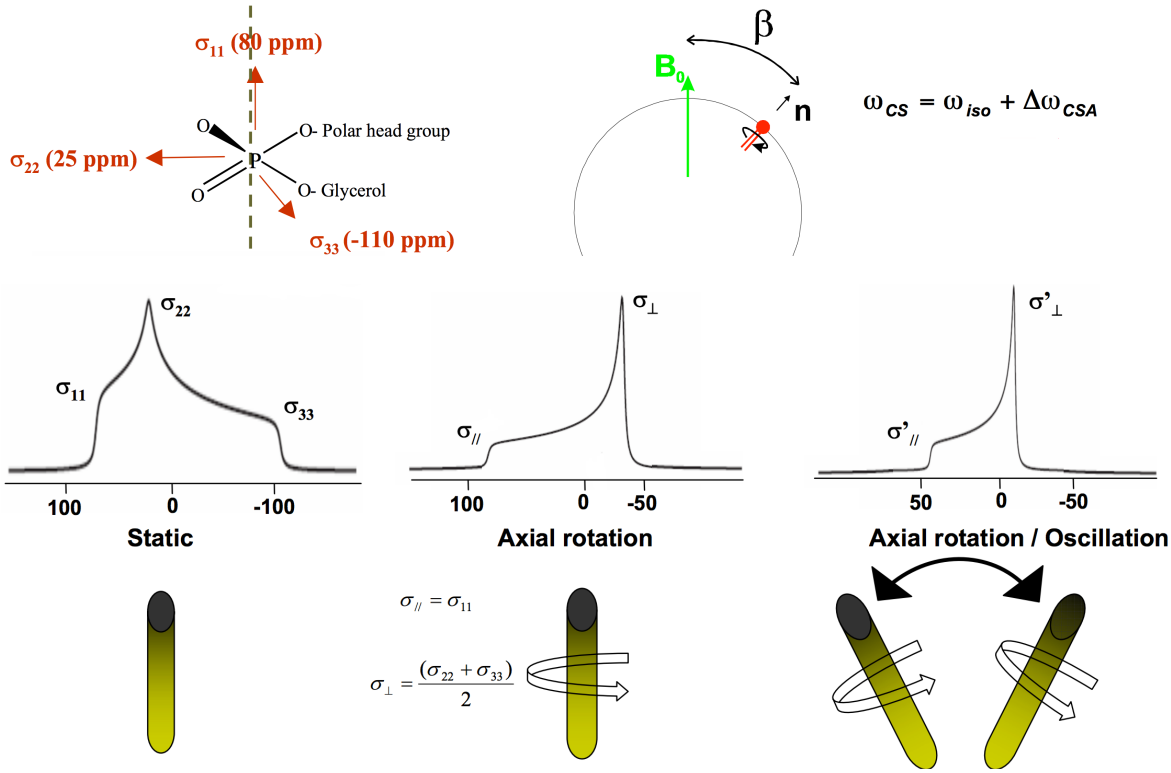

Figure II-16. The *upper left* figure illustrates the principal elements of the chemical shift anisotropy tensor of the phosphorus nucleus that belongs to the lipid headgroup. The *upper right* figure shows the orientational dependence and the elements of the ^{31}P chemical shift. And the picture on the *bottom* shows the effect of axial symmetry and motional averaging on the phosphorus chemical shift anisotropy. Adapted with permission from the tutorial lectures by Michele Auger (http://web.mit.edu/fbml/winterschool2008/talks/Tue4%20-%20Auger_NMR_of_lipids_and_membranes.pdf) and Ludovic Berthelot (http://www.ibpc.fr/UMR7099/Publis/pdf/LudoAlpine99.pdf).

The isotropic chemical shifts of all phospholipids are within a few parts per million of the resonance of 85% phosphoric acid (usually set as the reference at 0ppm). Most lipid bilayers oriented with their normal parallel to the magnetic field (θ= 0) yield narrow signal in ^{31}P ssNMR spectra, resonating at about 30ppm. The intensity at about -15ppm arises results non-oriented lipids. Even in the well-oriented membranes the orientation of certain lipid fraction may deviate from the mean orientation, the phenomenon is called mosaic spread, which introduce the broadening of the NMR signal and may cause a line asymmetry. Mosaic spread of bilayer orientations is measured by comparing the ^{31}P linewidth obtained for the same sample oriented with its bilayer normal parallel to the magnetic field (θ= 0) and oriented at an angle of 45° (Soubias and Gawrisch, 2007).

Therefore ^{31}P NMR spectroscopy is used to determine the lipids phase properties. For instance the gel membrane phase will result in broader spectrum than the liquid phase, because in the liquid phase the lipid molecules possess bigger degree of freedom, as schematically show in a ***Figure II-16***.

Static phosphorus spectra of common lipid structures are shown in a ***Figure II-17.*** For example the pictures B and C show the phosphorus spectra of the perfectly oriented lipid bilayer with the membrane normal parallel to the magnetic field director, and the spectra of lipid bilayer that contain the fraction (50% of integral intensity) of non-oriented lipids.

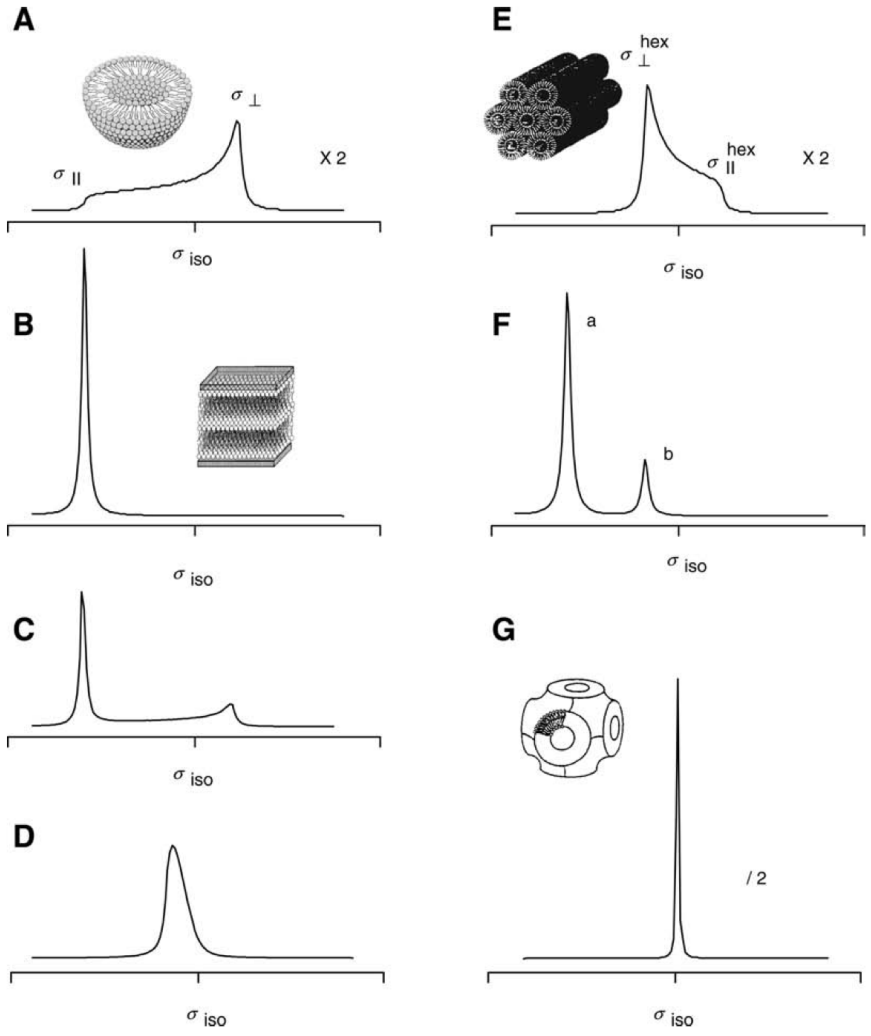

Figure II-17. (**A**) ^{31}P NMR powder pattern for a spherical distribution of bilayer orientations as observed for nonoriented multilamellar liposomes. (**B**) Perfectly oriented sample with the bilayer normal parallel to the magnetic field: the linewidth is determined entirely by spin–spin relaxation, T2 (line broadening = 0.7 ppm). (**C**) Same as in (B) but with a superimposed signal from randomly oriented bilayers. The integral intensity (amount of lipid) in oriented and nonoriented bilayers is equal. The weak resonance at high field is a good indicator for the presence of nonoriented material. (**D**) Resonance signal of a sample oriented with the bilayer normal at 45° to the magnetic field. The sample orientation has a mosaic spread described by a Gaussian distribution with a width of σ= 2.5°. (**E**) ^{31}P NMR powder pattern representative of lipids in an inverse-hexagonal H_{II} phase. (**F**) Same as in (B) with 80% of lipids in a lamellar phase (signal a) and 20% in a H_{II} phase (signal b). (**G**) ^{31}P NMR spectrum of lipids in a cubic phase. In this phase, the anisotropy of chemical shift is completely averaged out, resulting in a single resonance peak at σ_{iso} (simulated with a width at half height of 0.33 ppm).
The spectra were simulated with identical integral intensity. The y-axis of spectra A, E, and G is scaled as indicated.
Adapted with permission from the reference (Soubias and Gawrisch, 2007).

Membrane lipid order determined by ^{2}H static wide-line ssNMR spectroscopy.

The quadrupolar splittings observed in the wide-line static solid-state NMR spectra of the deuterated phospholipids are very sensitive measures of the motional freedom of the corresponding ^{2}H–C bonds belonging to the lipids acyl chains (Seelig, 1977). The method is widely used to probe the peptide – membrane interactions, in particular it allows to probe the formation of torroidal pore structures, the membrane thinning upon the peptide association, the membrane packing in a segment-specific manner, and also it is used along with the ^{31}P NMR spectroscopy to establish lipid phase diagrams in complex mixtures (reviewed in Bechinger and Salnikov, 2012).

The ^{2}H isotope has a spin-quantum number 1, and therefore possesses an electrical quadrupolar moment. The ^{2}H NMR resonance consists of a doublet whose splitting depends on the strength of the interactions between the electric quadrupole moment of the ^{2}H-nucleus and the internal magnetic field gradients in ^{2}H–C bonds. Therefore deuterium quadrupolar splittings of lipid acyl chains are also dependent on the alignment of bilayer normal to the magnetic field. Non-oriented liposomes, which are often used in these types of the experiments, yield powder spectra. The two maxima in the powder pattern result from the lipid bilayer segments that are oriented with their normal perpendicular to the magnetic field (***Figure II-18***).

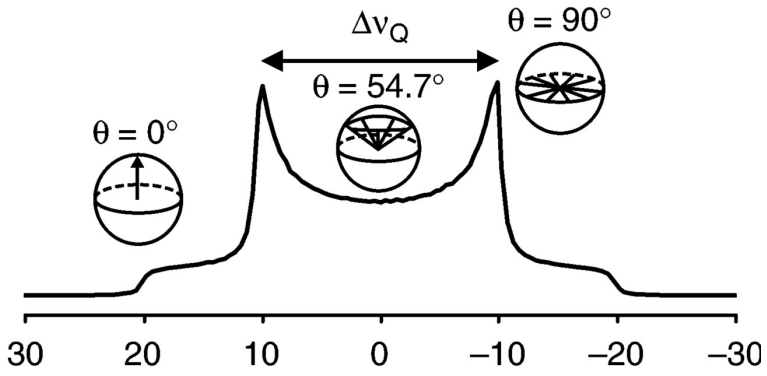

Figure II-18. ^{2}H NMR spectrum of a single labeled –CD_2 group in the lipid bilayers oriented at random to the magnetic field. The distance in kilohertz between two maximum is the quadrupolar splitting ($\Delta\nu_Q$) of this deuteron in the membranes that are oriented with their normal perpendicular to the magnetic field. Adapted with permission from (Soubias and Gawrisch, 2007).

Quadrupolar splitting of the deuterium nucleus.

The observed quadrupolar splitting ($\Delta\nu_Q$) in ^{2}H solid-state NMR spectra results from the interaction between the quadrupolar moment (eQ) and the electric field gradient at the center of the deuterium nucleus (eq). The quadrupolar splitting has an orientational dependence[4]:

$$\Delta\nu_Q = \frac{3}{2}\frac{e^2qQ}{h}\frac{1}{2}\left((3cos^2\theta - 1) + \eta\sin^2\theta cos2\phi\right)$$

$$\eta = \frac{V_{xx} - V_{yy}}{V_{zz}}$$

where V_{zz}, V_{yy} and V_{xx} are the principal components of electric field gradient tensor, by convention $|V_{zz}| \geq |V_{yy}| \geq |V_{xx}|$;

[4] The picture and theoretical introduction are adopted from the tutorial by Michele Auger http://web.mit.edu/fbml/winterschool2008/talks/Tue4 - Auger_NMR_of_lipids_and_membranes.pdf

ϕ and θ are the angles that characterize the principal V_{zz} vector orientation relative to the laboratory frame coordinates;

η – axial asymmetry parameter, which determines the shape of ^2H spectra, as illustrated below (picture is adapted from the tutorial by Michele Auger http://web.mit.edu/fbml/winterschool2008/talks/Tue4 - Auger_NMR_of_lipids_and_membranes.pdf) :

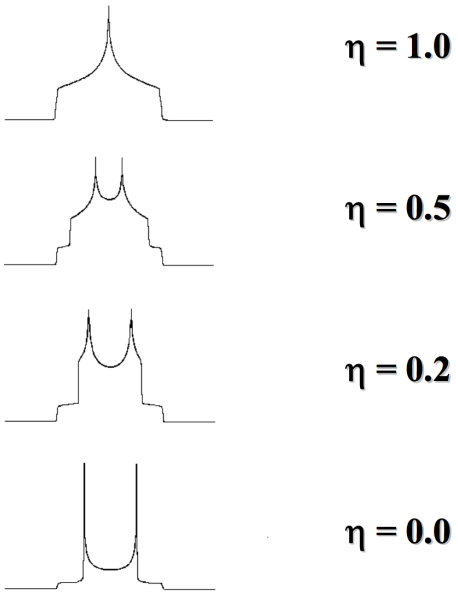

The aliphatic C-D bond possesses the electric field gradient tensor which is axially symmetrical η=0. Aromatic deuterons have quadrupolar coupling tensors that deviate slightly from perfect axial symmetry about the C-D bonds, but the asymmetry parameter is never more than 0.1 (Wann and Harbison, 1994).

$C_Q = e^2qQ/h$ – quadrupolar coupling constant, which equals to about 167 kHz for $–CD_2$ groups that belong to the saturated acyl chains, and about 175 kHz for C–D bond has a neighboring double bond (Seelig, 1977).

When the tensor is uniaxially symmetrical $V_{yy} = V_{xx}$, then

$$\Delta\nu_Q = \frac{3}{2}\frac{e^2qQ}{h}\frac{1}{2}(3cos^2\theta - 1)$$

The maximum splitting is observed, when θ=0° and $(3\cos^2\theta - 1)/2 = 1$. The maximum splitting for paraffinic CD_2 deuterons would be 250 kHz. Then in powder spectra the quadrupolar splitting between the two maximum peaks are 125 kHz, which corresponds to θ=90°.

Deuterium quadrupolar splitting in the context of membranes.

On the practice we don't observe such large quadrupolar splittings as 125 kHz when measuring ^2H NMR on the membrane at room temperatures. Usual quadrupolar splitting for deuterated lipids are within 40 kHz. The observed quadrupolar splitting is related to this theoretical quadrupolar splitting value via the parameter, called order parameter (S) (Seelig, 1977):

$$\Delta\nu_Q = \frac{3}{2}\frac{e^2qQ}{h}S$$

Lipid order parameter S is a measure for the orientational mobility of the C–D bond:

$$S = \langle\frac{3cos^2\Theta - 1}{2}\rangle$$

where Θ is the time dependent angle between the C–D bond vector and a reference axis (for instance

bilayer normal). The angular brackets denote a time and ensemble average. Therefore S depends simultaneously on the lipids disordering in bilayers and on the membrane orientation relative to magnetic field (Seelig, 1977; Vermeer et al., 2007). Lipids disordering includes all the possible effects on quadrupolar splitting averaging resulting from the lipids rotational and wobbling movements. Thus rotations around the bilayer normal causes a reduction of the quadrupolar splitting of the fatty acyl chain C–^{2}H by −1/2, and free rotation of a methyl group reduced its quadrupolar splitting by S = −1/3 by taking into account a tetrahedral angle of 109.4° (Bechinger and Salnikov, 2012).

If the movements in lipid bilayer are independent of each other, the order parameter S can be represented as the product of the quadrupolar splitting averaging effects that come from various sources (Vermeer et al., 2007): $S = S_{CD}S_{bilayer}$, where $S_{bilayer}$ describes the orientation of the bilayer normal with respect to the magnetic field and S_{CD} represents the motional averaging.

S_{CD} also consists of the several contributions with individual angular dependences:

$S_{CD} = S_{coll}\, S_{mol}\, S_{intra}$, where S_{coll} is the fluctuations of the bilayer normal, S_{mol} – reorientations of the molecular director with respect to the bilayer normal, S_{intra} - reorientations of the C–D vector with respect to the molecular director (Vermeer et al., 2007).

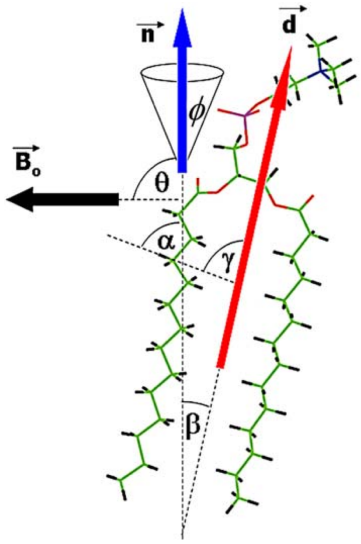

Figure II-19. Visual representation of different contributions to the observed order parameter S. Fast rotations of lipids about the vector normal to the bilayer permit to separate the contribution to the order parameter due to this movement from the contribution due to the overall positioning of the oriented bilayer with respect to the external magnetic field ($S = S_{CD}S_{bilayer}$). The bilayer normal, symbolized by the vector **n**, is oriented at an angle θ to the external magnetic field B_o. The observed CD vector is tilted at an angle α with respect to the bilayer normal. The bilayer normal is subject to fluctuations, shown here as wobbling of the vector **n** within a cone, characterized by an angle ϕ. The molecular director **d** is at an angle β to the bilayer normal. The observed CD vector is at an angle γ with respect to the molecular director. Adapted with permission from the reference (Vermeer et al., 2007).

The angular dependence of each contributor to S can be represented as following:

$$S_{bilayer} = \langle\frac{3cos^2\theta - 1}{2}\rangle, S_{CD} = \langle\frac{3cos^2\alpha - 1}{2}\rangle,$$

$$S_{coll} = \langle\frac{3cos^2\phi - 1}{2}\rangle, S_{mol} = \langle\frac{3cos^2\beta - 1}{2}\rangle, S_{intra} = \langle\frac{3cos^2\gamma - 1}{2}\rangle$$

Usually in a wide-line ^2H NMR spectrum we measure the quadrupolar splitting between the two maxima, which corresponds to the 90° orientation of membrane normal. Hence in the calculation we can neglect $S_{bilayer}$ contribution and calculate only S_{CD}.

When the lipid acyl chain is uniformly deuterated the order parameters S_{CD} are calculated for each segment of the lipid fatty residue. The procedure of ^2H NMR spectra processing will be shown in Material and Methods part of the Chapter IV. This segment specific determination of lipid dynamics allows estimation of the depth and the mode of the peptide insertion (Seelig and Seelig, 1980). The peptide helix intercalates into the water – bilayer interface and increases the space available in the hydrophobic interior of the membrane. The fatty acyl chains fill this space and subsequently increase their freedom by adopting a higher ratio of gauche conformations. The observed changes in order parameter can be translated into a membrane thinning effect according to $\Delta d = 2.5Å \times \Sigma(\Delta S_{CD})$ (Bechinger and Salnikov, 2012).

Large variety of antimicrobial peptides interacting with model membranes was studied using ^2H static NMR spectroscopy (reviewed in Bechinger and Salnikov, 2012). One of the interesting applications of deuterium spectroscopy is that it allows monitoring of lipids domain separation in mixed lipid bilayers induced by membrane-active peptides. In particular LAH4 peptide was shown to interact preferentially with POPS lipids in mixed POPC/POPS/cholesterol membranes (Mason et al., 2006a). The lipid domains separation was even suggested as novel mechanism of action of the arginine-rich antimicrobial peptides (Arouri et al., 2009; Epand and Epand, 2009; Jean-François et al., 2008) and even as the mechanism of cell internalisation of cationic cell-penetrating peptides (Kwon et al., 2013).

NUCLEIC ACID INTERACTION WITH PEPTIDES, PROTEINS AND CATIONIC POLYMERS. SELECTED METHODS.

1. Biophysical investifation of unspecific peptide and polymers – nucleic acid complexes.

Development of the chemical vectors for gene delivery.

Today there exists a large number of the non-viral vector designed to enhance the nucleic acid delivery into the cell. The overview of the various classes of such compounds can be found in dedicated literature (Guo and Huang, 2012). Initially several classes of cationic polymers were developed to efficiently bind and condense the nucleic acid (usually plasmid DNA) and to form compact particles that could be easily taken up by cells via endocytosis. Those compounds include the first commercial transfection agents, as polyethyleneimine (Ogris et al., 2001) and poly(L)lysines (Zauner et al., 1998).

Subsequently it was found that efficient transfection is not possible without effective endosomal escape. Thereby the considerable attention was drawn to the transfection agents that are capable of enhancing the endosomal escape and improving the nucleic acids release. The first compounds in this group were hystidilated polylysines (Bello Roufaï and Midoux, 2001; Chen, 2002; Midoux and Monsigny, 1999). The lysine polymers, which contain about 35-50% of histidine residues, were 3 − 4.5 orders of magnitude more efficient than polylysines alone (Midoux and Monsigny, 1999). The efficiency was related to the ability of HpK polymers to act as a proton sponge when the histidines become protonated at pH < 6 in endosome lumen, but also was considered to have better membrane destabilisation properties.

In this connection the histidine-rich cationic peptides emerged as the class of potent transfection agents (reviewed in Midoux et al., 2009). The peptides have better defined than polymers structures, and most of the amphipathic cationic peptides are membrane active. The first examples of such compounds were peptides that combine anti-tumorous and transfection capacities, for example cRGD-hk peptide (cRGD-$[(H)KKKK]_6$), which comprises lysine and histidine-rich DNA-binding motif with tumor-homing cyclic peptide (Aoki et al., 2001).

The HIV transduction domain arginine-rich Tat peptide (RKKRRQRRRR) is a well-known cell-penetrating peptide, which promotes the cellular uptake of a large variety of molecules including nucleic acids (Brooks et al., 2005). But the complexes of Tat with DNA were found to be unstable, especially in cell culture media that limited their usage as transfection vehicles. Hence the C terminus of Tat has been modified by addition of ten histidine residues (Tat-10H) and as high as 7000-fold improvement in transfection efficiency was obtained (Lo and Wang, 2008). Subsequently similar peptide was designed with five histidines and one cysteine at each terminus of Tat peptide, which in addition to endosome destabilization properties showed the enhanced DNA complex stability in the presence of serum (Lo and Wang, 2008).

An interesting approach towards transfection vehicles design was proposed by Hatefi and co-workers, where the recombinant technique was employed to biosynthesize the protein with the fused HK units (Hatefi et al., 2006). This rather sophisticated carrier contained lysine and histidine residues for stable DNA complexes formation and for assuring the endosomal escape, and fibroblast growth factor (FGF2) to specifically target the cells over-expressing corresponding receptor.

LAH4 and LAH4-L1 peptides also belongs to the class of cationic histidine-rich peptides, which efficiently complex DNA and associate with zwitterionic and negatively charged membranes, but in the same time have low cytotoxicity (Kichler et al., 2003a; Mason et al., 2007c). The rational design of LAH4 and LAH4-L1 vectors has been discussed in a detail in the Chapter I.

Those are only few examples of peptide-like delivery vectors. Of course, many more transfection vehicles were developed by date based on membrane-active peptides, including various classes of Arg-rich cell-penetrating and cationic amphipathic antimicrobial peptides (Copolovici et al., 2014; Hoyer and Neundorf, 2012; Mann et al., 2008).

The most common techniques used for biophysical characterization of transfection complexes are dynamic light scattering for particles size characterization (Goparaju et al., 2009; Prevette et al., 2007; Québatte et al., 2013; Ziegler and Seelig, 2007), gel retardation assay (Kichler et al., 2003a; Langlet-Bertin et al., 2010; Prongidi-Fix et al., 2007) and Western blotting (Liang et al., 2013) for evaluation of the nucleic acid binding by delivery vectors, confocal microscopy imaging for localization of transfection complexes cell internalization (van Asbeck et al., 2013), and, of course, ITC technique that have been used for thermodynamic characterization of the nucleic acids interaction with cationic polymers and peptides. The examples of ITC utilization for transfection complexes characterization will be discussed subsequently in more detail.

NMR technique has also been employed for investigation of unspecific nucleic acid complexes, however it is not a widely used techniques for transfection performance characterization. In particular, $^{1}H-^{15}N$ heteronuclear single quantum coherence (HSQC) NMR was used to investigate the protonation state of selectively ^{15}N-labeled histidines of branched His-Lys polymers in solution and within the complex with siRNA (Chou et al., 2014). ^{13}C solid-state NMR magic angle spinning technique allowed characterization of the LAH4 peptide binding with DNA (Prongidi-Fix et al., 2007), and REDOR ssNMR technique enables the detailed complex structure characterization on an atomic level (Bechinger et al., 2011; Vidovic, 2011). The letter techniques will be discussed in more detail later in the introductory, as well as in the experimental part of this work.

Thermodynamics of nucleic acid interaction with cationic peptides and polymers.

Isothermal titration calorimetry as a method for investigation of unspecific interactions between nucleic acids and the counterparts (such as cationic polymers, peptides and some proteins) has emerged relatively recently as evidenced by the growing number of publications on this topic in the past ten years (D Wettig, 2012; Ghai et al., 2012; Okhrimenko and Jelesarov, 2008). Due to these investigations we have much better insight to the processes that occur upon nucleic acid association with cationic polymers or polypeptides, and how this processes could be revealed by ITC. These processes include electrostatic attraction at first place, as nucleic acid strands possess multiple negatively charged phosphate residues. However in some studies it was found that Coulombic attraction is purely entropic component of the free energy of binding (Privalov et al., 2011). Still it is believed that the electrostatic attraction is a major driving force for the interactions in such systems, as nucleic acids – cationic polymers complexes (Kaur et al., 2011). However the enthalpy that we measure by ITC may result from the successive to the electrostatic attraction processes, such as proton exchange or in general ions displacement, either conformational changes. Despite the considerable advancement in understanding of the calorimetric signature of those processes, there is still no general methodology for the analysis of binding isotherms. Some researchers treat the DNA (RNA) as the macromolecule that possesses the finite number of binding sites and cationic polymer, or peptide, as a ligand. This approach enables the use of the available binding models (as single set of identical binding sites and two sets of binding sites), or their combination by applying the appropriate corrections (Kim et al., 2006). Another approach includes the methods where the nucleic acid is regarded as one-dimensional lattice-like macromolecule to which the ligands are bound in the cooperative, anti-cooperative or independent manner (Ma et al., 2009; Matulis et al., 2000; Velázquez-Campoy, 2006).

Several examples of ITC isotherms will be illustrated below. The original calorimetric traces are provided to display the complex character of the interactions, which possess however rather similar elements when comparing different examples. The range of compounds, which complexation with DNA was investigated by ITC, varies from small polycations to the cell-penetrating peptides.

Characterisation of cationic polymer – DNA transfection complexes by ITC.

a) The first to my knowledge publication that discusses the isothermal calorimetry of cations binding to the DNA refer to the study by Bloomfield and co-workers (Matulis et al., 2000). The authors have shown that the binding of small polyvalent cations as cobalt (III) hexamine and spermidine to the nucleic acid is accomplished in two stages. First the cations complex with extended DNA strand, replaces the smaller monovalent counter-ions (Na^+), and secondly the DNA condensation takes place when positive-to-negative charge ratio reaches some critical value. The two processes were endothermic and rather well resolved on ITC curve. The mathematical solution of the calorimetric isotherm was proposed by Bloomfield and colleagues, which is based on the electrostatic theory (Matulis et al., 2000).

b) The cationic linear and branched polymers, as polyethyleneimines (PEI) and mixed polyethyleneimines – polyethyleglycoles (PEI-PEG), poly-L-lysines (PLL), have been widely investigated as potent DNA transfection systems (Midoux et al., 2009). They have been found to condense efficiently long DNA strands, and facilitate its intracellular delivery. The paper of Kim and co-workers (Kim et al., 2010) reviews the possible mechanisms of cationic polymers – DNA interaction and its thermodynamic signature. These mechanisms include a fluctuation of condensed counterions, a charge-ordered structure, a release of structured water or of low molar mass counterions, or/and a delocalization of condensed counterions, which can be classified into two groups. In the first group, electrostatic interaction plays the predominant role in DNA condensation, while in the other group the increase in entropy is the dominant factor. The authors argue that when DNA condensation is induced by electrostatic interaction, the exothermic heat would be observed by ITC, whereas the increase in entropy is accompanied by endothermic heat.

In their work (Kim et al., 2010) the authors have investigated the influence of the salt concentration and polymers length on the energetics of PEG-PLL binding to plasmid DNA. The ITC curves (***Figure II-20***) show two distinctive endothermic binding processes: the first was referred to PEG-PLL binding to the elongated pDNA, and the second – to the binding that accompanied by the conformational transition of pDNA. After the fitting of calorimetric isotherms it was found that the binding of PEG-PLL to pDNA was accompanied by a small increase in enthalpy, a large increase in entropy, and a large decrease in free energy.

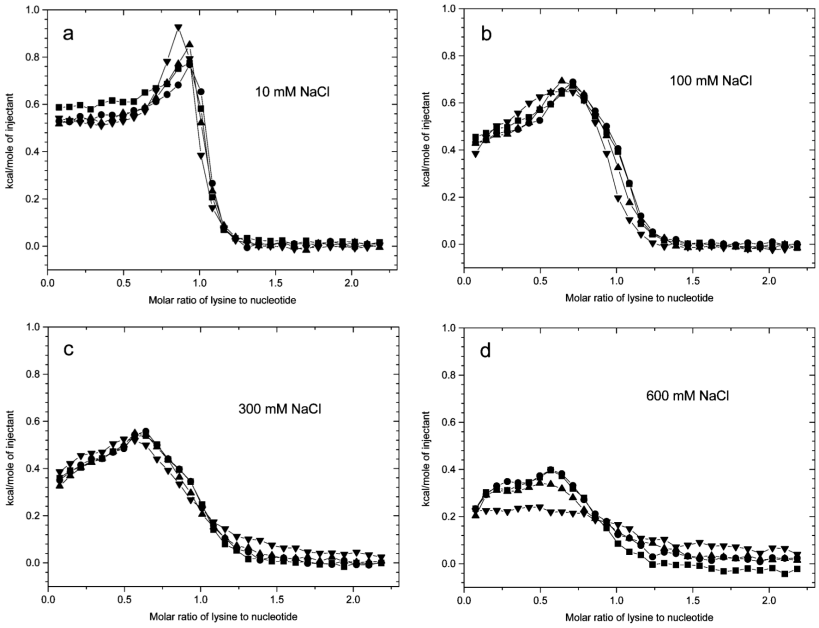

Figure II-20. Dependence of integrated ITC curves of PEG-PLL binding to pGL3 DNA on degree of polimerization of PLL in various NaCl concentrations: (a) 10 mM, (b) 100 mM, (c) 300 mM, and (d) 600 mM; PEG-PLL (12-109), PEG-PLL (12-73), PEG-PLL (12-47), PEG-PLL (12-20). Adapted with permission from (Kim et al., 2010).

Of special interest is the author's approach to the ITC curves fitting for such complex system, that was elaborated initially for modeling the small cations interaction with DNA (Kim et al., 2006). The approach is based on the single set of identical binding sites (SSIS) model published earlier (Freire et al., 1990) and now integrated into MicroCal Origin® ITC analysis software. SSIS implies that a general ITC isotherm should be produced as a decreased sigmoidal curve depending on the three parameters, the ratio of the occupied binding sites to the total binding sites (stoichiometry) N, the molar heat of ligand binding ΔH and the association constant K. The ITC curves by DNA titration with monomeric cations and polycations were fitted by the sum of two functions corresponding to the initial and second binding stages. When the function for the initial binding stage was defined by the set of three parameters, N1, K1, and ΔH1, the function for the second binding stage is defined by the set of six parameters, N1, K1, ΔH1, N2, K2, and ΔH2. The parameters were defined in this way because during the transition region from elongated to collapsed DNA, the increase in the population of collapsed DNA leads to the decrease in the fraction of ligands bound to the elongated DNA and the residual ligands not involved in the initial binding stage would contribute to the second binding stage. All nine parameters were simultaneously fitted using non-linear fitting tool, integrated in Origin® software. The approach allows taking into account the effect of pDNA conformational change on ligand binding. This fitting method, unlike the conventional ones such as the "two sets of independent sites" (TSIS) model, is not restricted to the condition that the binding constant for the first binding process (K1) is greater than that for the second (K2) and, therefore, has greater applicability. The same method was employed by other investigator for the fitting of calorimetric isotherms of other cationic polymers interaction with DNA (Alatorre-Meda et al., 2010; Utsuno and Uludağ, 2010).

c) In the earlier study the thermodynamic parameters of calf thymus DNA interaction with cationic polymer poly(bis-acryloylpiperazine-2-methyl-piperazine), p(BAP-2MP), were determined by ITC (Ehtezazi et al., 2003). This example is particularly interesting because the simple sigmoidal calorimetric isotherm was obtained and the association process between macromolecules was

essentially exothermic, in contrast to all other examples of ITC isotherms provided in this overview. The negative enthalpy of binding and rather small negative value of entropy (calculated when appropriate model was applied) were taken as the indicators of hydrogen bond formation between polycations and DNA. Despite of the apparent simpler character of the binding isotherm, the author treated the ITC data considering the same two-stage binding process. However, the mathematical model, that they used to derive thermodynamic parameters, was different from those described above. The nonspecific site size exclusion model, developed earlier by McGlee and von Hippel (McGhee and von Hippel, 1974), was applied assuming that the complex formation stage of p(BAP-2MP) interaction with DNA is a noncooperative process, but the model admit the cooperative behavior of ligands in the subsequent condensation step (Ehtezazi et al., 2003).

d) In another recent publication the authors has shown that the calorimetric response from the DNA – cationic polymer association can vary from purely exothermic to purely endothermic, depending on the nature of the polymer molecule (Samsonova et al., 2013). The polymeric cations, such as commercial transfection agent polyethylenimine (PEI) and designed copolymers of the poly(2-dimethylaminoethyl methacrylate) (PDMAEMA) and poly(2-hydroxyethyl methacrylate) (pHEMA), were titrated into solution of herring testes DNA at pH 7. The calorimetric traces are shown in a ***Figure II-21***. On the contrast to the previous hypothesis, which explains biphasic appearance of the calorimetric trace by cations binding followed by the DNA condensation, the authors proposed an alternative explanation. They argued that observed heat change results from the electrostatic attraction plus polymer conformational changes upon its association with DNA. The initial conformation of each polymer was assessed by molecular dynamic simulations. Thus branched polyethylenimine is a less flexible polymer, and the spatial accessibility of its cationic amino groups to DNA does not change over the titration process. The pDMAEMA115, in contrast, starts from an energetically unfavorable arrangement and thus maintains the binding process by spending energy for the unfolding process from the very beginning, as the molecules were more densely folded in water prior to interaction with DNA. For the two other co-polymers the initial exothermic phase of the ITC profile was suggested to represent the interaction of DNA with the polymer in its ‘solution’ state. Afterwards the binding of additional polymer molecule was not possible without inducing polymer conformational changes due to reduced access to DNA. The unfolding, that is induced by electrostatic attractions to make the nitrogen atoms more available to DNA, was an endothermic process. This enthalpically unfavorable step was compensated by an increase in entropy (Samsonova et al., 2013). None fitting model was applied for the analysis of calorimetric isotherms, thus ITC curves were presented in descriptive view.

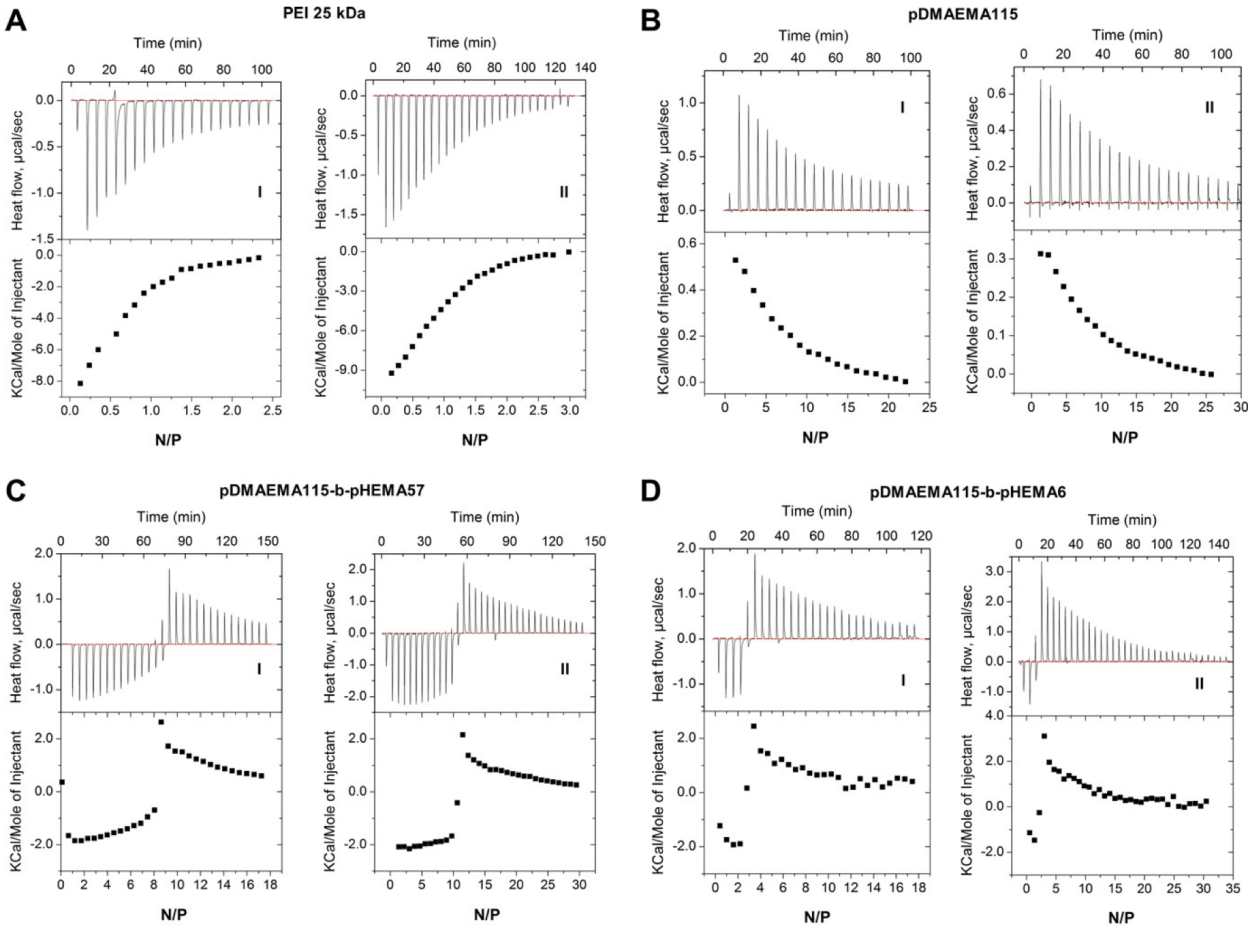

Figure II-21. Isothermal titration calorimetry profiles presented in duplicates (I + II) of 0.03mM DNA titrated with polymers: 0.55mM PEI 25 kDa (A I, II); 5.5mM pDMAEMA115 (B I and II); 2.75mM (C I) and 5.5mM pDMAEMA115-b-pHEMA57 (C II); 4mM (D I) and 5.5mM pDMAEMA115-b-pHEMA6 (D II). Adapted with permission from the reference (Samsonova et al., 2013).

e) Similar investigation was performed with poly-ε-lysines and the analogues possessing incorporated amino acids of varied hydrophobicity (Arg, Leu, Tyr) (Korolev et al., 2009). It has to be emphasized that even if those macromolecules have the chemical compositions close to polypeptides, they lack the ability to adopt secondary structures, as α-helix, and therefore behave rather like polymers than peptides. The ITC traces of polylysines titration into pDNA solution were quite similar to those obtained with other polycations, showing two (or even three) binding stages (***Figure II-22***). The processes are also characterized by positive enthalpy. The ITC curves have rather complex character, but, surprisingly, the authors used simple one-site binding model to derive the thermodynamic parameters of association. On the contrary, they have developed a sophisticated model to correlate the degree of polymerization of DNA binding partner and salt concentration with the DNA condensation rate (for the details please see the original reference Korolev et al., 2009).

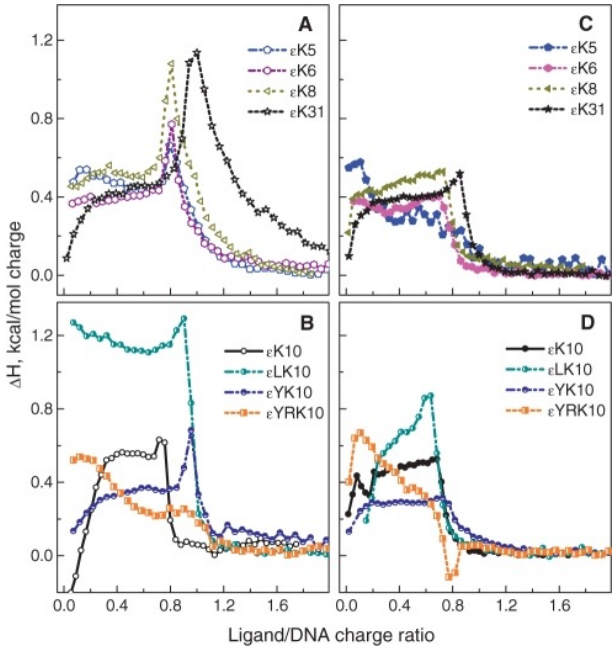

Figure II-22. Results of ITC showing enthalpy at 298K plotted versus ratio of added ligand charge to charge of the DNA. Panels (A) and (B) show the results obtained in 10mM KCl; panels (C) and (D) present similar data determined in 100mM KCl; DNA concentration 400mM in all measurements. (A) and (C). Influence of degree of polymerization of ε-oligolysines on enthalpy of ligand–DNA interaction. (B) and (D) The influence of side chain of the εK10 derivatives on enthalpy of ligand–DNA interaction. Adapted with permission from (Korolev et al., 2009).

f) In another study the polyplex formation between cationic polyamidoamine dendrimers (PAMAM 7, about 420 positive charges/per molecule) and siRNA was examined by ITC (Jensen et al., 2010). Similar as in the above-described examples, a biphasic titration curve was observed, where association reaction was exothermic at low dendrimer/siRNA ratio, but changes to endothermic when the concentration of dendrimer increases. It was shown by dynamic light scattering that the aggregation of polyplexes occurs at high dendrimer/siRNA ratio, thus the change from exothermic to endothermic ITC signal was explained by aggregation. The enthalpy of binding was assessed from the ITC signal at the first titration steps, where as it was suggested the binding is not yet perturbed by polyplexes aggregation. However no model was applied to fit the data and the set of thermodynamic parameters as ΔS, ΔG, K_A was not calculated.

Cationic peptides – nucleic acid transfection complexes studied by ITC.

a) Mixon and co-workers investigated the role of hydrogen bonding on the stability and performance of siRNA polyplexes (Chou et al., 2014). The authors have shown that ITC can be used to elucidate the types of interaction that govern the polyplex formation (hydrogen bonding *vs.* electrostatic). In the series of ITC experiments the branched polylysines, and branched mixed lysine – histidine (KH) and lysine – asparagine (KN) polymers were titrated into siRNA solution. For histidine and asparagine containing polymers ITC traces consisted of an exothermic component, which was observed at low polymer/siRNA total ratio, and a smaller endothermic component at higher KH polymer concentration. But for the polymer that consist of lysines only the endothermic component of ITC isotherm was observed. Also the magnitude of endothermic, as well as exothermic process was smaller for asparagine containing polymer than for two other transfection polymers. The authors suggested that the endothermic signal results from the hydrogen bonds formation between histidine and asparagine residues and the hydrogen-accepting groups of siRNA, such as –OH, P-O^-

of phosphate, or tertiary nitrogen. The authors reasoned also that the observed exothermic heat is smaller for KN polymer, because the capability of asparagine amide for the hydrogen bonding is smaller than that for histidines' imidazole group. The appearance of endothermic component at higher polymer/siRNA ratio they explained by the formation of bigger polyplex aggregates, during which some conformational changes can occur.

As far as the branched amino acid polymers can be more prone to hydrogen bond formation because of bigger accessibility of hydrogen donating groups to siRNA, the authors carried out similar experiment with linear KH peptide to check if they perform as well as branched ones. It was shown that the linear KH polymers produce the same ITC profile upon binding to siRNA as branched ones, and the magnitude of the exothermic process is related to the number of histidines. When in the linear polymer all the histidines were replaced with alanines, only endothermic signal was observed by ITC. Therefore the authors concluded that the endothermic ITC signal is observed when lysines are interacting with phosphate groups of siRNA, and ionic bonds are forming by replacing smaller counterions and disrupting the hydration layer. This process is enthalpically unfavorable, and therefore is entropy-driven. The hydrogen bond formation is on the contrary enthalpy-driven, and histidines were shown to govern and stabilize the interactions between polymer and siRNA via hydrogen bonding. Additionally the hydrogen bonds formation was shown by ^{1}H two-dimensional NMR spectroscopy with labeled histidines (Chou et al., 2014).

The dependence of polyplex formation by lysine-histidine branched polymers on pH of solution and subsequently on degree of histidines protonation was investigated as well (Chou et al., 2014). It was shown that histidine protonation promotes even more active hydrogen bond formation, as indicated by increase of the exothermic signal (**Figure II-23**). Also there was much more polymer needed to completely bind siRNA.

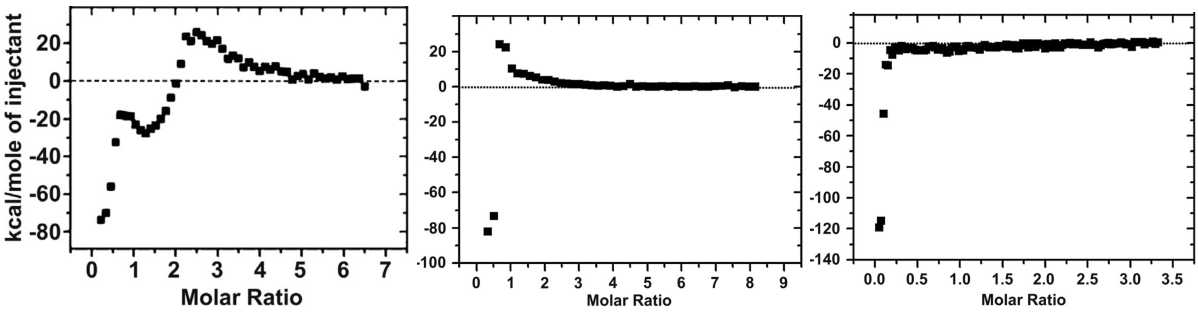

Figure II-23. pH dependence of measured enthalpy of branched lysine-histidine polymer H3K(ϸH)4b binding to siRNA. Representative ITC data for H3K(ϸH)4b addition to siRNA in 10 mM MES buffer at pH 7.0 (*left*), pH 6.0 (*middle*) and 5.0 (*right*).

b) The complex formation between cationic cell-penetration peptide, HIV 1 TAT protein transduction domain YGRKKRRQRRR, and salmon sperm DNA was assessed by ITC among other biophysical methods (Ziegler and Seelig, 2007). As a result of the peptide titration into DNA solution in 30mM phosphate-saline buffer, the exothermic sigmoidal curve was obtained. The plateau region, characterized the same intensity of ITC signal, was observed till the DNAbp/peptide ratio equal three, that indicates complete binding of DNA, such the enthalpy of binding ΔH was determined directly. After DNAbp/peptide = 3 the ITC signal steeply decreased. The complete set of thermodynamic parameters was calculated by applying multiple sites binding model. The stoichiometry of reaction is about four DNA base pairs per TAT peptide molecule assuming complete binding. Interestingly that TAT peptide – DNA complexes were also prone to aggregation, as shown

by static light scattering method. SLS experiment was also performed by titrating DNA into the peptide solution. Thus the optical perturbation of the solution increased with increasing of DNA concentration, indicating the complex formation. The intensity of scattered light went to the plateau when DNAbp/peptide ratio reached 4, which was in excellent agreement with stoichiometry of the reaction determined by ITC. It was assumed also that most of the reaction enthalpy originates from the release of hydration water and counter-ions during the DNA complexation. The ITC measurements were performed at several temperatures. The temperature dependence of $\Delta H°_{CPP}$ was characterized by a negative molar heat capacity of ΔC_P. The authors reasoned that a negative heat capacity indicates the binding, which is dominated by changes in solvent-accessible surface area (dehydration), in contrast to a positive heat capacity observed when the reaction is driven by an electrostatic interaction (Ziegler and Seelig, 2007).

c) The complexation of DNA by riDOM (retro-inverso dioleoylmelittin) was investigated by ITC (Québatte et al., 2013). riDOM is the hybrid compound consisting of antimicrobial peptide mellitin, which is bound covalently to dioleoylphosphatidylethanolamine-N-[3-(2- pyridyldithio)propionate moiety. It is potential transfection agent with low toxicity. In solution it forms stable nanoparticles of about 13nm, but upon DNA addition it complex and condense DNA strands. The titration of salmon testes DNA (≈2000bp) into riDOM solution results in the endothermic heat of reaction, which consist of two components (***Figure II-24***). The authors discern the different processing by fitting the ITC curve corresponding to the association with multisite binding model (red). Thus the endothermic reaction was referred to the association between riDOM molecules and DNA (green), and the exothermic – to DNA condensation (blue). When the thermodynamics of melittin (GIGAVLKVLTTGLPALISWIKRKRQQ) binding to DNA was measured by ITC, the similar profile was observed. The authors concluded that binding of melittin and its more hydrophobic analogue to DNA is thus entropy-driven process, and indicated the possible sources of entropy gain, as release of the counter-ions from DNA (Na^+), as well as form peptide surface (Cl^-); the shrinking of hydration surface due to the tight binding between molecules with subsequent water release; conformational changes as DNA condensation, for which the negative enthalpy was observed, but determination of the precise entropy change value was not possible; also the aggregation between transfection particles leaded to the release of hydration water from their surfaces (Québatte et al., 2013).

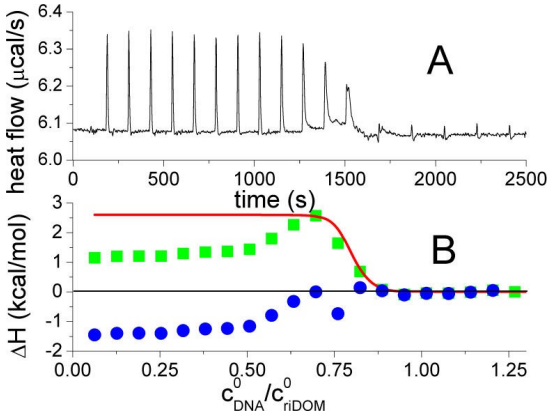

Figure II-24. Isothermal tiration calorimetry of riDOM nanoparticles with DNA. The calorimeter cell contained riDOM (107 µM). A DNA solution (0.765 mM) was injected in 1.8 µL aliquots. (A) Heat flow. (B) Heats of injection. The solid line corresponds to the multisite binding model. The corresponding parameters are ΔH (riDOM) = 2.0 kcal/mol, K =6 × 107 M−1, and n = DNA(bp)/riDOM = 0.77. Temperature 30 °C. (■) Experimental heats of injection, hi, obtained by integration of heat flow shown in (A). (●)Difference between experimental h_i and theoretical prediction. Adapted with permission from (Québatte et al., 2013).

Conclusions. All the described above examples indicate that it is possible to use isothermal titration calorimetry to elucidate the thermodynamics of nucleic acid interaction with cationic counterparts, as polymers, peptides and lipopeptides. Remarkably, most of those interactions result in the biphasic titration curve, however the explanation of the origin of the calorimetric signal differs when reviewing various puclications. The most common hypothesis is that DNA condensation together with polymer association creates the appearance of biphasic titration isotherm. Other authors argue that it is polymer conformational change that is the major component to observed enthalpy. Interestingly, in the experiment with siRNA the biphasic character of ITC diagram also was observed. Thus, negative component of observed enthalpy was referred to hydrogen bond formation, and positive – to the polyplexes aggregation. It is believed that the enthalpy of association reaction results from multiple processes occurring on the interfaces between the interacting macromolecules, as hydrogen bond or/and ionic pairs formation, release of hydrating water, release of counterions, conformational changes. Each of those processes has its enthalpic and entropic component. But unfortunately it still does not exist any reference system for ITC results analysis that would allow the researcher to refer this or another calorimetric signature to particular type on interaction between macromolecules, such as nucleic acids and cationic polymers / peptides.

2. Investigation of the nucleic acid – polypeptides interactions. NMR methods.

DNA-binding proteins. An overview.

In this manuscript section a short overview of the structural features of DNA-binding motifs will be given with an accent on the cationic protein domains.

Usually the proteins that are capable of the specific DNA binding possess particular structural motifs. The most common types of those domains are helix-turn-helix motif, that characterize lambda repressor-operator complex (1LMB), zinc finger proteins with the common binding motif X_3-Cys-X_{2-4}-Cys-X_{12}-His-X_{3-4}-His-X_4 (1TF6), leucine zippers (1YSA), and other non-classified motifs (Luscombe et al., 2000).

Two main factors contribute to the specific recognition of DNA by proteins: the formation of hydrogen bonds to specific nucleotide donors and acceptors in the major groove, and the sequence-dependent deformations of the DNA helix to altered shapes with increased affinity of protein ligands (educational resource).

Nucleotide sequence-specific interactions involve the formation of hydrogen bonds between amino acid side chains and hydrogen bond donors and acceptors of individual base pairs. Nearly two-thirds of the direct read-out of DNA sequences involves complex networks of hydrogen bonds, which enhance specificity (Luscombe et al., 2001). It has been shown that every base pair has its unique hydrogen bonding signature in the major groove but the same assumption was not valid for the minor groove (Rohs et al., 2009; Seeman et al., 1976).

Luscombe and co-workers have examined the hydrogen bond formation within 129 protein-DNA complexes. The authors have found that the formation of the hydrogen bonds with the DNA backbone (*i.e.* with phosphate groups and sugars) typically is not implicated in specificity. Nevertheless, the two-thirds contribution found in these dataset highlights importance of such hydrogen bonding in stabilizing protein–DNA complexes (Luscombe et al., 2001). Those interactions are independent of the DNA sequence, which emphasize their non-specific nature. Of note, 97% of these interactions are with phosphate group, while only 3% with sugars.

One third of the hydrogen bonds dataset account for the interaction with the DNA bases (Luscombe et al., 2001). Guanine was found to have the biggest propensity to the hydrogen bonding (180, *cf.* original reference for the meaning of this value), much bigger than the other nucleic bases (adenine – 66, cytosine – 56, and thymine – 53).

On the protein side, the polar and charged amino acids are more prone to hydrogen bond formation (Luscombe et al., 2001). Thus arginine (375), lysine (165), serine (113) and threonine (92) accounts for the 70% of the contacts, with asparagine (88) and glutamine (70) that follows, but histidine has rather low capacity to hydrogen bond formation (40). The asparagine and glutamine hydrogen bonds formation is hampered by the unfavorable electrostatic effects. Of the non-polar amino acids, only glycine (41) shows a significant number of interactions (Luscombe et al., 2001). Certain amino acids show clear preference for hydrogen bonding with particular functional groups. Thus >80% of serine and threonine hydrogrn bonds are with DNA backbone, it is much above the average when comparing with 67% displayed by other amino acids. The short side chains have limited access to bases and therefore contribute to stability rather than specificity (Luscombe et al., 2001).

Specific deformations of DNA helix may be promoted by the proteins from one hand, like the integration host factor (Rice Phoebe, 1996, 1IHF); or by the presence in the DNA sequence the specific motifs, such as TATA box (Kim et al., 1993) or A-tract (Stefl et al., 2004). The characteristic of the A-tract motifs is the ability to adapt the twisting conformations that cause inter-base-pair hydrogen bonding in

the major grooves, resulting in the narrowing of minor grooves. This property is assured by the high contents of AT base pairs that are concentrated in narrow minor grooves (width <5.0Å compared to 5.8Å in an ideal B-DNA), while CG base pairs are mostly found in the wide minor grooves (Stefl et al., 2004). Narrowing of the DNA minor grooves enhance the negative electrostatic potential of the DNA in those specific domains and makes it more recognizable by the proteins (Rohs et al., 2009). For example the arginine-rich domains of T3c Transposase proteins (1U78, 1TC3) are accommodated specifically in these narrowed minor grooves (van Pouderoyen et al., 1997; Watkins et al., 2004). Generally, the arginines account for 28% of all amino acid residues that contact the minor groove, of which 60% of the amino acid residues found in narrow minor grooves of specific protein-DNA complexes were arginines, while 22% in minor grooves that are defined as not narrow (Rohs et al., 2009). Arginine sequences are preferred over the lysines since the effective radius of the charge in arginine is greater than of the charge carrier by lysine (Honig and Nicholls, 1995). It was shown by the free energy calculations of desolvation using DelPhi program that the arginines have decreased desolvation energy compared to lysine residues, which enhances their binding to the narrowed major groove (Rohs et al., 2009). This type of the DNA recognition based on shape is used by a number of DNA-binding proteins.

Therefore, the distribution of the surface electrostatic potential plays a great role in the DNA recognition by the proteins. In a ***Figure II-25*** there is illustrated the electrostatic potential distribution of three DNA forms (A, B and Z). By the way he great majority of protein-DNA complex structures contain DNA that is essentially B-form, with some degree of bending and deformation (Garvie and Wolberger, 2001). It was also shown that non-specific electrostatic interactions are often the major constituent of the binding free energy of DNA-protein complexes (Privalov et al., 2011). However, the statistical analysis of the structures of non-homologous protein-DNA complexes revealed that actually ionic pairs formed between charged protein side chains and DNA account only for 8% of all contacts (Lejeune et al., 2005).

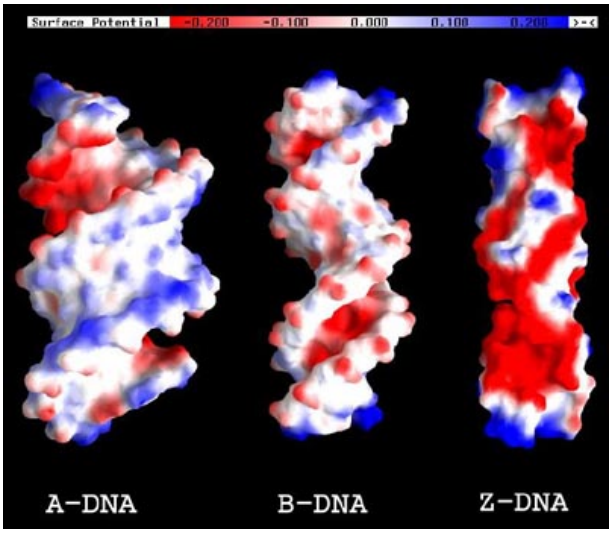

Figure II-25. The electrostatic potential map of the solvent-induced polarization response density (the difference between the DNA electron density that is polarized by solvent and the unpolarized density of an isolated DNA molecule) of A, B and Z-form DNA. Adapted from http://www.chem.umn.edu/netstep/2001/january/10york.html

The extensive statistical analysis was performed on the two datasets of the high-resolution structures of DNA- (139 structures) and RNA (49) complexes with proteins (Lejeune et al., 2005). All the detected intermolecular contacts were classified into four categories: electrostatic interactions between atoms with opposite charges, H-bonds (classic XH-Y H-bonds, where both X and Y are electronegative atoms, but

also CH-O H-bonds), and van der Waals interactions, among which a fourth category was classified, namely hydrophobic interactions involving atom pairs with low electronegativity difference. The friquences of the interactions are shown in a Table II-2. The distributions for DNA and RNA are quite similar with the clear preference for hydrogen bonding. Also the participation of the amino acids and nucleic bases was classified and shown in a ***Figure II-26***. The interactions with phosphate are twice less frequent in RNA complexes (22%) as in DNA complexes (47%). Of the 47% DNA phosphate interactions, only 16% are salt bridges, while of the 22% RNA phosphate interactions salt bridges comprise 31% of interactions. Thus the difference results in a similar occurrence of salt bridges in both kinds of complexes (Lejeune et al., 2005).

In DNA complexes, 62% of the H-bonds involve nucleic phosphate atoms, while in the RNA complexes hydrogen bonds with phosphates are only 27% of all H-bonds. The results show that hydrogen bonds, not salt bridges, are responsible for the twice more frequent contacts of proteins with DNA than with RNA phosphates.

Hydrophobic interactions are the main type of contacts of sugar. Approximately 63% of the DNA-deoxyribose and 42% of RNA-ribose interactions are hydrophobic contacts. This type of interaction could have a stabilizing role in the protein–nucleic acid complexes. 22% of protein–DNA interactions, and 27% of protein–RNA interactions belong to other types of van der Waals interactions (Table II-2). On the nucleotide side, these van der Waals interactions mainly involve the sugar–phosphate backbone of nucleic acids (62% in protein–DNA and 60% in protein–RNA interactions). The presence of an additional hydroxyl group on the ribose cycle of RNA explains the higher incidence of this type of interactions in protein–RNA complexes (Lejeune et al., 2005). On the amino acid side the involvement of the protein backbone atoms into van der Waals bonding makes 43% of the protein–DNA interactions and only 27% in the protein–RNA complexes.

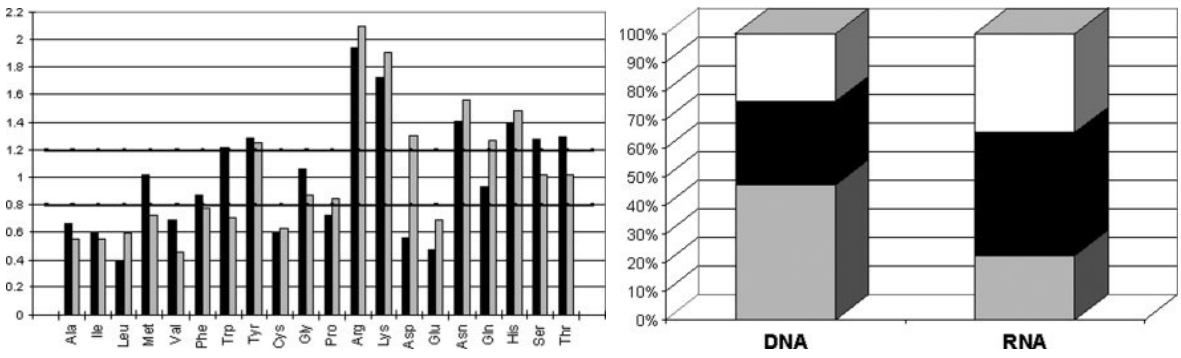

Figure II-26. *left*) Amino acid propensities to interact with nucleotides. The propensity values correspond to the frequency of an amino acid in the interaction sites divided by the frequency of the same amino acid in the whole database. Values for DNA are represented with black bars and values for RNA with gray bars. Propensity values higher than 1.2 correspond to favored amino acids, while disfavored amino acids have values lower than 0.8.
right) Frequency distribution of interactions with different nucleic acid parts. Atom types are colored as follows: white, base edge; black, sugar; and gray, phosphate atoms.
Adapted from (Lejeune et al., 2005).

Table II-2. Distributions of interaction types in the interaction sites of protein-DNA and protein-RNA complexes. Adapted from (Lejeune et al., 2005).

Interaction type	% (number)	
	DNA	RNA
H-bonds	51 (3912)	47 (1582)
Electrostatic interactions	8 (614)	7 (236)
Hydrophobic interactions	19 (1457)	19 (640)
Other van der Waals	22 (1688)	27 (909)

The most favored residue pairs were determined by statistical analysis. Those pairs were ordered by the frequency of appearance in protein – nucleic acid complexes. For DNA the sequence is following Arg-G >> Arg-C > Lys-G > Lys-T >> Arg-T >> Lys-A >> His-G > Trp-C > Asn-C > Tyr-G > Asn-T > Arg-A > Ser-T > Thr-T > Thr-C > Lys-C > His-T > Thr-G > Tyr-T > Asn-G > Ser-G, and for RNA Arg-C > Arg-G >> Lys-C > Asp-G >> Arg-U > Tyr-U > Asn-U > Lys-G > Gly-G > His-G > Lys-A > His-U > Arg-A (Lejeune et al., 2005). Regarding the interactions involved into formation of most populated residue pairs, the amine group of arginines are involved in 80% of all Arg-G interactions, of which the electrostatic interactions make up about 20% and hydrogen bonding about 55%.

All those statistical analysis results suggest that cationic amino acids play a significant role in binding to DNA and RNA. Some classes of proteins contain so-called nuclear localization signal (NLS) motifs, which are characterized by a cluster of basic residues. Not all proteins that contain such domains are DNA-binding proteins, but analysis shows that about quarter of the proteins have DNA-binding and NLS overlapped, in particular PDB entries 1a02, 1an2, 1an4, 1akh, 1au7, 1b8i, 1cdw, 1fos, 1hlo, 1hry, 1hwt, 1lat, 2lef, 1mdy, 1nk2, 1nk3, 1oct, 1pdn, 1pue, 1tgh; 1ftz, 1ign (Cokol et al., 2000). Here we explore in more detail few examples of the available crystal structures of such domains, in order to show how cationic amino acid residues are accommodated by the DNA strands.

Figure II-27 displays the DNA-binding motif of the NFAT – AP-1 – DNA quaternary complex (Chen et al., 1998). Fos-Jun protein, which is the part of the complex and belongs to the type zipper of DNA-binding proteins, possesses a motif that consists primarily of the positively charged amino acids – arginines and lysines. This binding motif is inserted into major groove of DNA. Distance measurements, performed in PyMol program (http://www.pymol.org/), reveal the tight contacts between the DNA backbone phosphate groups and positively charged residues of the protein. The distances between nitrogen atoms of guanidinium and amine groups and phosphorus atoms of DNA are in the range of 3.7 to 5.1Å.

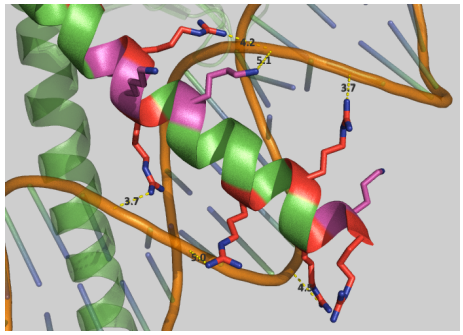

Figure II-27. DNA-binding motif (RKRMRNRIAASKSRKRK) from the quaternary complex, constructed by the nuclear factor of activated T cells (NFAT) and the AP-1 heterodimer, Fos–Jun. Jun helix is highlighted on the picture. The figure was created using PyMol software (http://www.pymol.org/) and the PDB item 1A02. The distances between the guanidinium residue of arginines / amine residue of lysines and phosphorus atom of DNA backbone were measured using the same program.

Next example is the structure of the bipartite DNA-binding domain of Tc3 transposase bound to transposon DNA (Watkins et al., 2004). Its arginine/lysine-rich motif is shown in a ***Figure II-28***. Two arginine residues are buried into the DNA narrowed minor groove, and the rest of the cationic amino acids side chains are exposed to the solvent. The distance between the lysines and phosphate groups of DNA backbone is more than 6Å, however it is possible that those cationic residues stabilize the binding by forming solvent mediated hydrogen bonds (Reddy et al., 2001). Unlike the previous structure, the specific DNA recognition in this complex is assured, among other things, by the hydrogen bonding between the arginines and nucleic bases. As it was mentioned previously, the arginine residues are often preferred over the lysines when the peptide domain interacts with DNA minor grooves (Rohs et al., 2009).

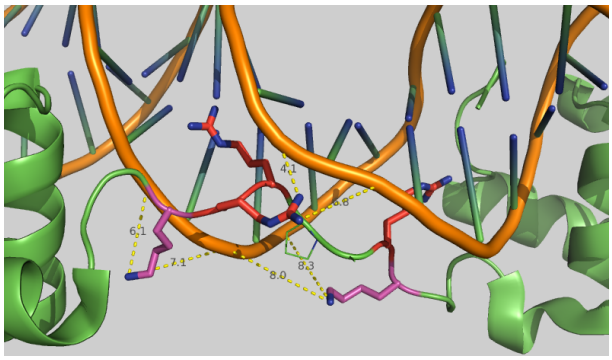

Figure II-28. The structure of the bipartite DNA-binding domain of Tc3 transposase bound to transposon DNA. KRAPRRKA motif, which is tightly incorporated into DNA major groove, is highlighted on the picture. The figure was created using PyMol software (http://www.pymol.org/) and the PDB item 1U78. The distances between the guanidinium residue of arginines / amine residue of lysines and phosphorus atom of DNA backbone were measured using the same program.

There are examples where the specific interaction between DNA and protein is assured by simultaneous binding to major and to minor grooves, as it is realized in the VND/NK-2 homeodomain/ DNA complex (Gruschus et al., 1997). The cationic KRKRR (lysines-arginines) motif is inserted into the narrowed minor groove, where one lysine and one arginine are bound to the nucleic bases, and other cationic amino acids are exposed to the solvent. The binding to the major groove is provided by QN--YK motif (glutamine-asparagin--tyrosine-lysine). Possibly the association with major groove of DNA is also

realized by the hydrogen bonding to nucleic bases, including water-mediated hydrogen bonds, which often characterize glutamine and asparagine interactions with nucleic bases (Reddy et al., 2001).

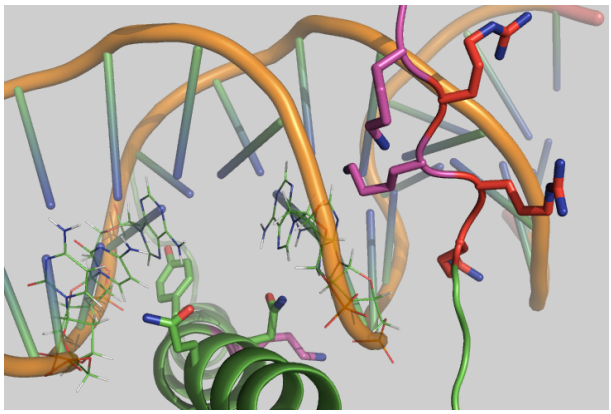

Figure II-29. Structure of DNA binding motif in VND/NK-2 homeodomain/DNA complex. KRKRR motif is inserted in the minor groove and QNHRYK in the major groove of DNA. The figure was created using PyMol software (http://www.pymol.org/) and the PDB item 1NK2.

Much fewer examples of the naturally occurring DNA-binding peptides can be found in the literature. Usually the investigations are performed on the specific DNA-binding protein domains (Aravind, 1998), or on the unspecific peptide-DNA complexes for transfection application (Keller et al., 2002; Prongidi-Fix et al., 2007; Ziegler and Seelig, 2007). Few examples of natural DNA-binding peptides include antimicrobial peptides, for which DNA association was shown as one of the mechanism of action, for example indolicidine with the tryptophane-proline reach sequence ILPWKWPWWPWRR (Fojan et al., 2011; Hsu et al., 2005). Also there are DNA-binding antimicrobial peptides that represent certain protein domains, such as cationic NK-18 peptide (KILRGVCKKIMRTFLRRI) (Yan et al., 2013).

NMR methods for investigation of protein – nucleic acids interactions.

There is a vast number of liquid and solid-state NMR methods for the investigation of specific protein – nucleic acid complexes developed by date (Campagne et al., 2011; Jamin and Toma, 2001; Kaptein, 2013). Two kinds of information can usually be obtained, ambiguous restraints generally derived from interaction surface mapping; and unambiguous restraints provided by intermolecular nuclear Overhauser effects (NOEs), residual dipolar couplings and paramagnetic relaxation enhancement (PRE) experiments. In the majority of methods the NMR signals from protein are detected, however nowadays there exist the versatile methods for production of labeled nucleic acids as well (Campagne et al., 2011). The methods shortly summarized below are mostly performed in a liquid state.

The mapping of protein-binding interfaces is realized for instance by recording ^{15}N HSQC spectra of the free and the bound ^{15}N-labelled protein, with subsequent calculations of normalized chemical shift perturbations (CSPs). Usually the proximity of DNA phosphates or the ring currents induced by aromatic bases are responsible for important CSPs (Campagne et al., 2011; Yamasaki et al., 2004). In addition the development of TROSY method (transverse relaxation-optimized spectroscopy) allowed the acquisition of NMR spectra for large complexes with high spectral resolution (Pervushin et al., 1997).

Another methods of DNA-protein contacts mapping, called cross-saturation, is based on selective saturation of protons from one molecule partner that promotes transfer of the saturation to the other partner, which subsequently leads to decrease of the signal intensity from the biding partner (Campagne et al., 2010).

Nuclear Overhauser effect (NOE) is widely employed for calculation of short-range intermolecular distances restrains. Spatial proximity of certain residues to the protein–DNA interface promotes intermolecular dipole–dipole interactions which are sufficiently large for creating measurable NOEs (Campagne et al., 2010). The resonances of both binding partners are assigned prior to identification of the intermolecular NOEs. Proton frequencies of the protein, which is usually $^{15}N/^{13}C$ uniformly labeled, are generally assigned using a combination of classical triple-resonance experiments (HNCA, HNCACB) and TOCSY and nuclear Overhauser spectroscopy (NOESY) experiments (three-dimensional ^{15}N HSQC-NOESY, three-dimensional ^{15}N HSQC-TOCSY, three-dimensional HCCH-TOCSY, three-dimensional ^{13}C HSQC-NOESY).

Structural determination of DNA using the NOE method is hampered by low proton density, which together with the elongated shape of the DNA molecule leads to a small number of long-range NOE restraints (Campagne et al., 2011). In order to improve the reliability of determination of long-range intermolecular distance restraints, the measurements of residual dipolar couplings are realized by restricting the complex movements to a preferred direction relative to the magnetic field (Murphy et al., 2001).

Another method to detect the long-range contacts between atoms in protein-DNA complexes is paramagnetic relaxation enhancement (Campagne et al., 2011). PRE effect can be observed at distances up to 35Å, while NOE is limited to 5Å, however in the former case the paramagnetic spin label has to be conjugated to one of the macromolecules (usually DNA) (Cai et al., 2007).

NMR relaxation studies are largely implied to study the dynamics inside DNA – protein complexes (Jamin and Toma, 2001), but the description of these methods will be skipped in this introduction.

Instead the introduction to the long-range distance measurements in biological solids, including nucleic acid complexes, will be presented in the following part of this manuscript chapter.

Distance measurements in biological solids. REDOR NMR.

Rotational echo double resonance (REDOR) is a solid-state NMR technique that provides a direct measure of short and long-range heteronuclear dipolar couplings. The technique was introduced by Terry Gullion and Jacob Schaefer in 1989 (Gullion and Schaefer, 1989).

Below the physical background of REDOR experiment will be shortly introduced.

The strength of the dipole–dipole couplings between the magnetic moments of neighbouring spins can be described as:

$$d_{kl} = \frac{\mu_0}{4\pi}\frac{\gamma_I\gamma_S\hbar}{r_{kl}^3}\left(\frac{3cos^2\theta_{kl}-1}{2}\right)$$

The orientation independent term, called dipolar constant, is:

$$D_{kl} = \frac{\mu_0}{4\pi}\frac{\gamma_I\gamma_S\hbar}{2\pi r_{kl}^3}$$

where μ_0 – is vacuum magnetic permeability, γ_I and γ_S – are the gyromagnetic ratios of the spins; *k* and *l* – the labels for the spins of type I and S, respectively, where S is being by convention more abundant nucleus; θ_{kl} – angle between *kl* dipole and the magnetic field.

The internuclear distance can be deduced directly from the coupling strength, and the latter can be measured through the evolution of the spin system caused by the underlying dipolar coupling Hamiltonian H_{IS} (Webb et al., 2006). The dipolar coupling Hamiltonian H_{IS} in the high-temperature approximation is represented as:

$$H_{IS} = -\sum_{k<l} 2\pi d_{kl} 2I_{z,k} S_{z,l}$$

where I and S are the spin operators of the coupling spins.

It is difficult to read directly the coupling strength, because in solid-state a number of interactions, as chemical shift anisotropy and homonuclear dipolar couplings cause substantial line broadening. Magic angle spinning technique facilitates the acquisition of high-resolution solid-state nuclear magnetic spectra by effectively averaging the anisotropic parts of nuclear spin interactions: chemical shifts and through-space dipole–dipole couplings for spin-1/2 systems, and heteronuclear recoupling techniques were designed to selectively reintroduce the dipolar couplings between the nuclei of interest (Jaroniec, 2009).

The basic idea behind recoupling techniques is that the averaging of spatial-dependent parameter such as dipolar couplings under MAS can be removed if radiofrequency pulses are applied in rotor-synchronized mode (REDOR).

The physical basis of REDOR experiment can described as following (Webb et al., 2006).

(*MAS effect*) The orientation-dependent factors of NMR interactions, such as the dipolar coupling strength d_{kl}, become time-dependent under sample spinning:

$$d_{kl}(t) = D_{kl}\frac{1}{2}\left[sin^2\beta_{kl}cos2\left(\alpha_{kl} + \frac{2\pi t}{T_R}\right) - \sqrt{2}sin^2\beta_{kl}cos\left(\alpha_{kl} + \frac{2\pi t}{T_R}\right)\right]$$

where β and α are two of the Euler angles describing the rotation of the dipolar principal axis frame of the current molecular orientation into a rotor-fixed frame, and T_R – is the rotor period (Melinda J. Duer, 2002). Time integral of $d_{kl}(t)$, vanishes over each rotor period, therefore the dipolar coupling is not affecting the NMR signal.

(*RF effect*) Besides averaging by sample spinning, radiofrequency (RF) pulses provide another means to influence the contributions to the NMR signal. The RF pulses are applied to the spin-part of the dipolar Hamiltonian (I_zS_z) whereas MAS only influences the spatial part ($3\cos2\theta - 1$).

For instance, π-pulse irradiated at either the I- or S-spin resonance frequency will invert the I or S spins, respectively, and can hence be used to manipulate the evolution of the spin system. Inverting either I or S spin is equivalent to an evolution under a Hamiltonian H_{IS}, but with inverted sign ($I > -I$ or $S > -S$) (Webb et al., 2006). Such the average over each rotor period will differ from zero:

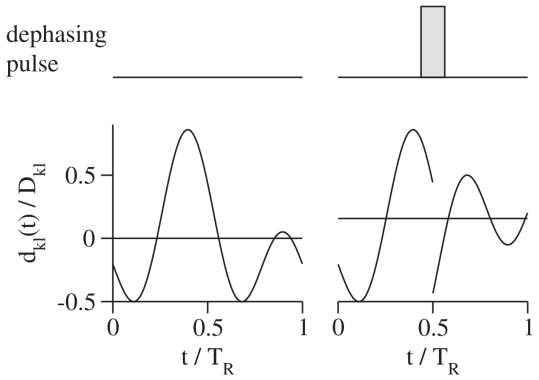

Figure II-30. (*left*) magic-angle sample spinning renders the dipolar coupling time-dependent. Averaged over a full rotor cycle the dipolar interaction vanishes (=0, average denoted with a straight line). (*right*) with the aid of radiofrequency (RF) pulses effecting one of the two coupled spins, the sign of the dipolar interaction is inverted. MAS is no longer averaging the dipolar coupling to zero, but a finite average (denoted by a straight line) remains. Adapted from the reference (Webb et al., 2006).

The REDOR experiment represents a series of π-pulses, spaced every half rotor cycle of a dephasing time, to recouple the heteronuclear dipolar interaction. The signal which is dephased by the heteronuclear couplings is then measured after this period. To separate the influence of the dipolar coupling from the influence of relaxation on the NMR signal, two experiments are performed. In the main experiment the dephasing pulses are switched on, and a reduced signal S is obtained. In the control experiment those π-pulses are switched off and the full signal S_0 is measured. As the relaxation is contributing to both signals equally, the relaxation does not affect the ratio $(S_0 - S)/S_0$.

Therefore, a series of dephasing-on / dephasing-off experiments are performed where the NMR signal from observed nuclei is measured after certain number of rotor pulses. REDOR-curve $(S0(nT_R) - S(nT_R))/S0(nT_R)$ is obtained as a function of dephasing time nT_R. The corresponding internuclear distances are then evaluated by fitting with theoretical curves (Webb et al., 2006). The REDOR-curve depends on the product of dephasing time and the orientation-independent part of the dipolar coupling $D_{kl}nT_R$. Other parameters, such as the pulse sequence or couplings in a spin network also influence the dephasing behaviour.

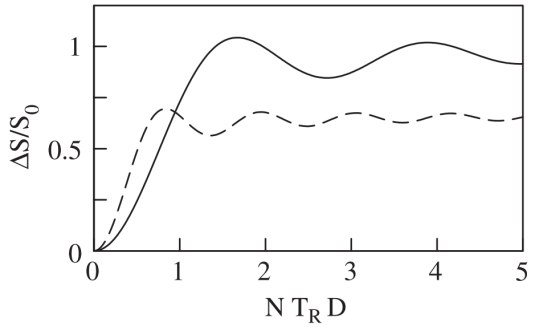

Figure II-31. The dephased signal follows a universal function of the product of the time nT_R, during which RF pulses are applied, and the dipolar coupling constant D. The REDOR curve depends on the spin of the dephasing nucleus. The dephased signal (S0-S)/S0 approaches 1 for long dephasing times if the observed spin is coupled to a spin-1/2 nucleus (solid line). The dephasing by a spin-1 nucleus is twice as fast and (S0-S)/S0 reaches only 2/3 (dashed line), as only 2/3 of the spins contribute to dephasing. Adapted from (Webb et al., 2006).

Distance measurement limitations. The first limitation, which is common for all NMR experiments, is the sensitivity of the participating nuclei. For this reason ^{19}F and ^{31}P are often used in REDOR experiments. Another advantage of ^{31}P isotopes is its 100% natural adundance. The problem with low sensitivity of commonly used isotopes as ^{15}N and ^{13}C is solved by cross polarization as is shown below.

Second limitation is the relaxation rate. As soon as spin-spin relaxation times (T_2) are much shorter in solids than spin-lattice relaxation times (T_1), it is transverse relaxation (T_2) that determines the limit of the REDOR measurement. Slow relaxation allows the acquisition of NMR signal at longer evolution times, which in turn allows building more complete REDOR curves and more accurate long distances determination, as can be seen from the simulations (***Figure II-32***). Relaxation depends on the molecular architecture of the matter under the study, and dynamic properties of the system.

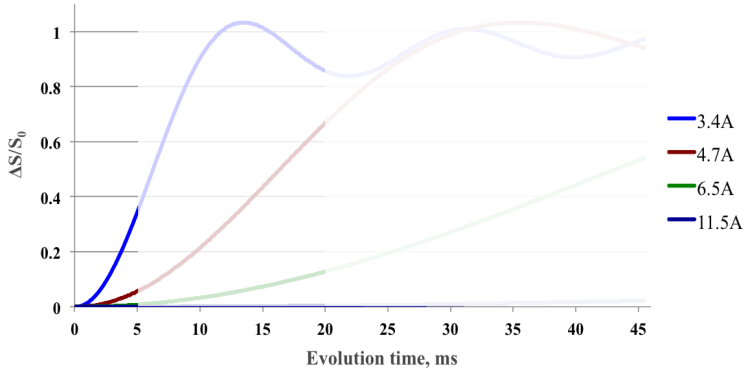

Figure II-32. The simulations of REDOR curves for the isolated pair of interacting ^{31}P – ^{15}N nuclei. The curves were created using SIMPSON program http://nmr.au.dk/software/simpson/. Semi-transparent areas show the effect of REDOR curve cut-off due to the short relaxation times.

As soon as dipolar constant D depends on the properties of the interacting nuclei, there will be different distance measurement limits for each separate nuclei pair, as shown in a ***Figure II-33***.

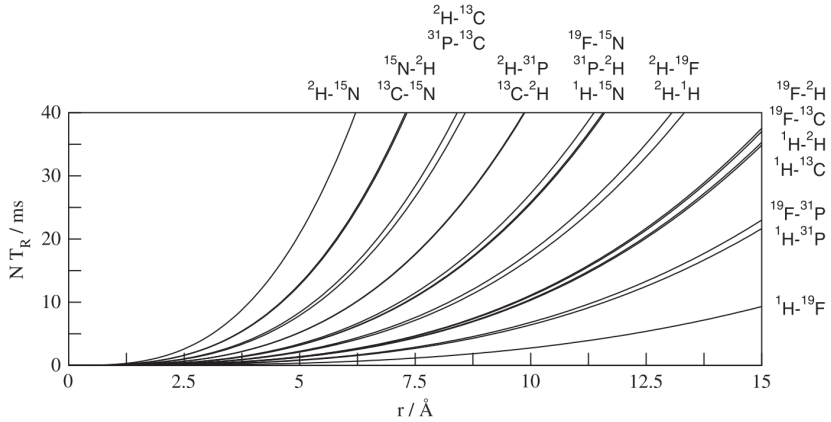

Figure II-33. The distance range accessible in a REDOR experiment for various nuclei types. The dephasing time needed to achieve a dephasing (S0-S)/S0 of 10% is plotted as a function of the internuclear distance for spin-pairs typically used in biological applications. For the quadrupolar nuclei (^2H) the difference in limitation arise depending whether it is used as observed, or dephasing nucleus. Adapted from (Webb et al., 2006).

REDOR pulse sequence as it was introduced by Terry Gullion and Jacob Schaefer begins with a cross polarization from proton spins to the *observed* spins, or with a π/2–pulse at the resonance frequency of the spins to be observed (I spins). A sequence of π-pulses at the resonance frequency of the non-observed nuclei (S spins) are placed after every half-rotor period, which 'dephase' the observed signal if there is I–S dipolar interaction. The dephasing pulse in the centre is omitted and replaced by a refocusing π-pulse on the I-spin channel. The additional pulse on the observe channel assures that the isotropic chemical shift is refocused at the end of the dephasing period. This one of the ways for REDOR pulse sequence implementation, but depending on the properties of interacting nuclei, or NMR hardware requirements the REDOR pulse may be realized in other ways (***Figure II-34***).

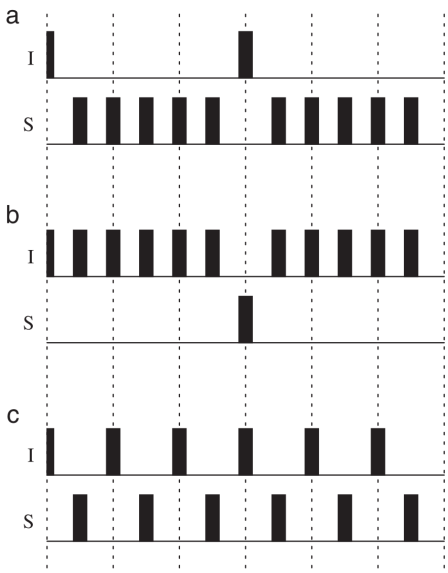

Figure II-34. The REDOR pulse sequence implementation. The RF pulses can be distributed mainly on the dephasing channel (a), on the observed channel (b), or in an alternating fashion (c). Adapted from (Webb et al., 2006).

In parallel to the pulses on the I and S channel, ^{1}H-decoupling is applied during the dephasing and acquisition time of most biological REDOR experiments to reduce linewidth and enhance signal/noise (Webb et al., 2006). From the practical point of view it means that triple resonance NMR probe is required to perform REDOR experiment with proton channel to be obligatory present. In a typical experiment (***Figure II-33***) first the cross polarization technique is applied to transfer the magnetization from the most abundant ^{1}H nuclei to the observed nuclei (^{13}C) by using a long low power pulse on both channels (labelled mix, ***Figure II-35***). In the exemplary pulse sequence (***Figure II-35***) cross polarization is then followed by the series of rotor-synchronized π-pulses on both observed and non-observed nuclei under proton decoupling conditions. The signal acquisition is made also ^{1}H decoupling.

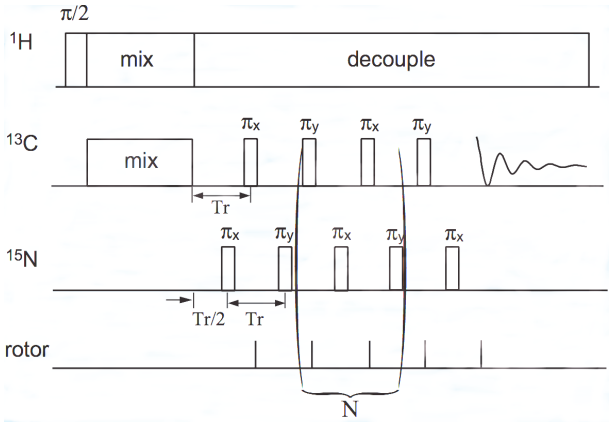

Figure II-35. ^{13}C−{^{15}N} REDOR pulse sequence. Adapted from http://www.tecmag.com/pdf/REDOR.pdf

Multiple spin labels. In some cases the selective labelling of material can not be achived. For instance in DNA molucules ^{31}P is present in its 100% abundance, and the distances between phosphorus nuclei in B-DNA are 5.8-6Å. It means that the interacting nuclei that appears between two phosphate groups in of DNA molecule will be coupled equally to both ^{31}P nuclei, or even to the whole group of all neighboring spins. Also, when protein is obtained by the recombinant expression, it is usually ^{15}N/^{13}C uniformly labelled (depending on the goal of the experiment). In such cases, the homonuclear couplings within the

spin can obscure the results of the REDOR experiment. On the other hand, using a coupling network can be beneficial in elucidating molecular structures. Isolated, equally distant spin pairs lead to the ideal REDOR dephasing curve, such as shown in a ***Figure II-32***. Very often we deal with the spins network rather than with isolated spins, where various interaction schemes could be realized (***Figure II-36***).

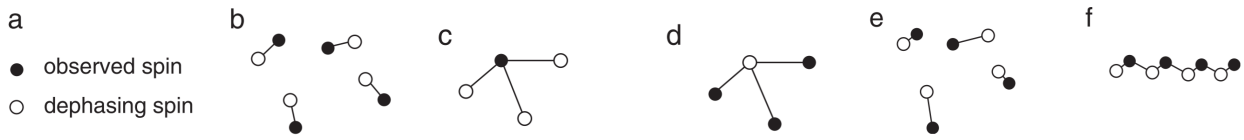

Figure II-36. The coupling network of observed and dephasing spins, such as isolated, identical spin (b); observed spin is dephased by several spins (c) or a single spin dephases several sites (d). With isolated spin pairs, structural heterogeneity of macromolecule can lead to a distribution of distances (e). In molecules, which are built of repetitive units, the couplings of within each unit might be influenced by couplings between neighbouring units (f). Adapted from (Webb et al., 2006).

If several spins are responsible for the dephasing of the signal, the resulting REDOR curve is not necessarily a mere sum of the individual dephasing contributions. Homonuclear couplings as well as scalar couplings among the observed spins can embarrass a quantitative analysis or cause additional signal decay in multiple spin systems. Homonuclear couplings are averaged to zero by MAS if the spinning speed is fast enough. However, the coupling of directly bonded ^{13}C nuclei of about 2 kHz, and scalar couplings which can be of the order of 100Hz for directly bonded ^{13}C are nearly not affected by MAS. Also, homonuclear couplings could be partially reintroduced if the chemical shift separation is close to the spinning frequency (Webb et al., 2006).

Various pulse sequence schemes were developed in order to suppress unwanted homonuclear couplings for the cases when magic angle spinning averaging does not work. For instance, Schaefer and co-workers have introduced MREV pulse scheme on the observed ^{13}C channel (Schaefer, 1999), which allows the decoupling of homonuclear couplings during the dephasing time in the ^{13}C spin clusters.

In case when weak inter-molecular couplings have to be measured, but they are damped by strong intra-molecular couplings, a DSQ–REDOR experiment has been introduced in which ‘double single-quantum’ coherences between strongly coupled intra-residue ^{13}C–^{15}N pairs are created and subjected to dephasing by a REDOR pulse sequence. In such way only the weak ^{13}C–^{15}N inter-residue couplings of interest evolved (Chan et al., 2005; Webb et al., 2006).

Background signal in REDOR. The natural abundance of one of the most useful isotope in structural biology ^{13}C is 1.1%. But considering that it is second most populated nucleus in biological material, the use of ^{13}C is often restricted due to a natural abundance background. Various techniques have been developed to select specifically the signal of interest from the background signal (Webb et al., 2006).

One approach is based on the change of the environment of the observed nuclei by chemical modifications. The use of selectively thiolated phosphate derivatives in the synthesis of a DNA quadruplex allowed the distinction of the phosphothioate ^{31}P signal from the phosphate ^{31}P signal in ^{31}P-observed REDOR experiments on the basis of their different chemical shifts (Webb et al., 2006).

In some cases the distinguishing of the signal due to different chemical environment is not possible. The example of sophisticated REDOR scheme was introduced for calculation of the torsion angles restrictions in peptides (Neeraj Sinha, 2003). ^{13}C-detected N–H REDOR and ^{15}N- or ^{13}C-detected C–H REDOR methods were designed, in which the proton of interest is selected via its directly bonded heteronuclear spin Y, which differs from the X-spin in the REDOR spin pair. Thus REDOR signal was

read out via the third nucleus. Technically it was achieved by applying TEDOR (Transferred-Echo Double Resonance (Jaroniec, 2009) transfer step following the REDOR pulse sequence.

Another approach uses the REDOR experiment itself to select the signal of a particular label of interest. Thus the REDOR experiment applied for the actual distance measurement is combined with a second REDOR experiment, in which the observed nucleus is dephased by a spin only adjacent to the observed nucleus of interest (Webb et al., 2006). This scheme of selecting a particular site has been used for the observation of ^{13}C in the peptide or protein backbone, where the neighbouring amide nitrogen is ^{15}N labelled (Beusen et al., 1995).

REDOR techniques has indeed a broad range of applications in solid-state NMR on biological material. More detailed overview of modern REDOR methodologies can be found in dedicated publications (Kovacs et al., 2007; Toke and Cegelski, 2011; Vega, 2005; Webb et al., 2006).

In particular, ^{31}P resonances are frequently employed to investigate the DNA and RNA conformational changes, or the localization and binding of ^{19}F-labelled small drug molecules (Olsen, 2003; Olsen et al., 2005).

One of the examples of REDOR application to DNA conformation determination is the characterization of DNA packaging in Bacteriophage T4 by Schaefer and co-workers. By analyzing ^{15}N-$\{^{31}P\}$ and ^{31}P-$\{^{15}N\}$ REDOR curves of uniform ^{15}N-labeled T4, specific [ε-^{15}N]lysine-labeled T4, and $^{15}NH4$+-exchanged unlabeled phage T4, the authors were able to show that packaged T4 DNA has a B-form conformation and that the DNA phosphate negative charges are partially balanced by lysyl amines (3.2%), polyamines (5.8%), and monovalent cations (40%) (Yu and Schaefer, 2008). The N–P distance between nitrogen atoms of the lysine side chains and the nearest-neighbor DNA phosphates were determined to be 3.5 Å, consistent with N–H…O–P hydrogen bonding. The dephasing maximum occuring at 16 ms of dipolar evolution is 11%, meaning that 11% of all lysyl amines are hydrogen-bonded to phage T4 DNA phosphates. The REDOR curve of uniformly labeled bacteriophage reveals that there is second more distant population of lysyl residues, which were classified by authors as secondary charge-balance contributors. In contract no contact was observed between histidine and arginine side chains and DNA phosphates, which is clear indicator that those amino acid moieties do not participate in the DNA packaging (Yu and Schaefer, 2008).

NATURAL AND MODEL LIPID MEMBRANES.

The membranes of living cells are highly dynamic structure, composed mostly of the proteins and lipids undergoing continuous reorganization. Lipid composition of membranes affects the proteins structure, and vice versa the proteins modulate membrane properties, such as curvature, permeability, fluidity. Lipids and proteins undergo free lateral movement within the membrane, and this property enables most of the membrane functions.

Structure and composition of eukaryotic plasma membrane.

The plasma membrane is a thin (approximately 40Å) hydrophobic layer, which assures the internal structural support for the cell, the exchange between intracellular and extracellular environment, communication between cells and with external stimuli, and cell identification.

The phospholipids accounts for about 75% of the lipids, cholesterol is usually about 20 - 30%, and the glycolipids – about 5% by weight. The plasma membranes of animal cells contain four major phospholipids (phosphatidylcholine, phosphatidylethanolamine, phosphatidylserine, and sphingomyelin), which together account for more than half of the lipid in most membranes. These phospholipids are asymmetrically distributed between the leaflets of the membrane bilayer. The outer layer consists predominantly of phosphatidylcholine (about 25%), sphingomyelin (about 20%), phosphatidylethanolamine (≈5-6%) and glycolipids. The inner leaflet contains phosphatidylethanolamine (about 20%), phosphatidylcholine (about 15%), sphingomyelin (≈3%), negatively charged phosphatidylserine (12-13%) and less abundant phosphatidylinositol (Op den Kamp, 1979; Vance, 2008). The glycolipids are found exclusively in the outer leaflet of the plasma membrane. Cholesterol is distributed equally between the layers.

The bilayers of naturally occurring phospholipids are viscous fluids. The fatty acids of most natural phospholipids possess one or more double bonds, which introduce conformational ‘kinks’ into the hydrocarbon chains. The hydrocarbon chains of the fatty acids then move freely giving the flexibility to the membrane. Membrane lipids occur in various phases depending on their structure and environment. These phases have specific properties, which determine the mobility of membrane lipids and proteins, and therefore affect membrane functionality. There is no unique macroscopic phase of plasma membrane. Instead, the lipids of biological membranes exist in multiple possible lamellar phase states. The adopted phase depends on lipid structure. When saturated hydrocarbon chains of sphingomyelin (SM) promote the formation of solid-like phases, the glycerophospholipids with unsaturated hydrocarbon chains that are often found in liquid phases (liquid-crystalline L_α and liquid-disordered L_d). Sterols do not form bilayer phases alone, but together with a bilayer-forming lipid they adopt liquid-ordered phase L_o. Phosphatidylcholine (PC) with cholesterol can adopt two coexisting fluid phases: liquid-ordered (L_o) and liquid-disordered (L_d) (Recktenwald and McConnell, 1981). α-helical segments of membrane-anchored proteins often prefer the liquid phase over the solid phase (van Meer et al., 2008).

More information could about membrane structure and properties can be found in dedicated reviews (van Meer et al., 2008; 2000).

The role of phosphatidylserine in cellular membranes.

Phosphatidylserine (PS) is the most abundant negatively charged phospholipid in eukaryotic membranes. In spite of its relatively low abundance among other lipids, phosphatidylserine plays important physiological roles. Phosphatidylserine is known to have an important role in the regulation of apoptosis (programmed cell death) in response to particular calcium-dependent stimuli. The presence of appreciable amounts of phosphatidylserine on the cytosolic leaflet of endosomes and lysosomes enables

these compartments to dock with proteins with specific phosphatidylserine-binding domains, including several important signalling and fusogenic effectors (http://lipidlibrary.aocs.org/Lipids/ps/index.htm).

The chemical structure of naturally occurring 1-palmitoyl-2-oleoyl-sn-glycero-3-phospho-L-serine can be found in a ***Figure II-38***. PS lipids consist of *L*-serine, which is linked to negatively charged phosphate group, and the phosphatidyl moiety is attached to glycerol ester at the position *sn*-3. PS provides membranes with a negative electrostatic potential that concentrates soluble cations in the electrical double layer in proportion to their charge. It makes PS enriched surfaces the preferred target of proteins with specialized motifs and domains. Some of those proteins are not selective and interact with anionic phospholipids in general. Another group of selective towards PS proteins bear specific C2 domains (for review see (Leventis and Grinstein, 2010). The examples of proteins that bind PS-enriched domains are human coagulation factor V discoidin-like domain (RCSB entries 1CZT, 1CZS) and Bovine Lactadherin C2 Domain (2PQS), which exhibits l-serine stereospecific Ca2+-independent binding mechanism. Those proteins possess substantial number of positively charged lysines and arginines exposed to the protein surface. However high affinity of the lactadherin C2 domain for phosphatidylserine is assured by the proline/threonine-enriched domain (Shao et al., 2008).

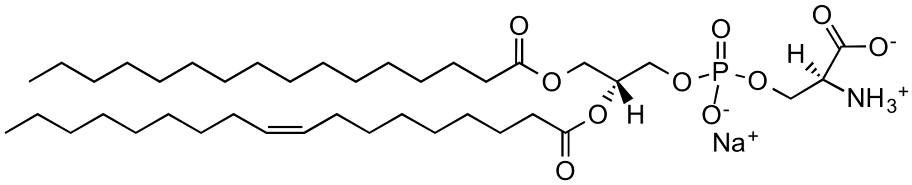

Figure II-38. Chemical structure of 1-palmitoyl-2-oleoyl-sn-glycero-3-phospho-L-serine.

Among the organelles, the plasma membrane is most enriched in PS, followed by early endosomes. As it was mentioned before phosphatidylserine is found preferentially in the inner leaflet of the plasma membrane. But most studies of PS function are related to the extracellular exposure of phosphatidylcholine. Thus the appearance of PS on the surface of apoptotic cells and its role in signalling phagocytosis has been studied extensively (Williamson and Schlegel, 2002; Wu et al., 2006; Zwaal et al., 2005). Phosphatidylserine membrane asymmetry promotes membrane tubulation and regulates endocytic sorting and recycling (Chen et al., 2010). The distinct role of phosphatidylserine in phagosome maturation was shown recently (Yeung et al., 2009). By bringing onto the phagosomal surface a considerable negative charge, PS will contribute to the recruitment of cationic proteins like proto-oncogene tyrosine-protein kinase *c-Src*. This unique property of the cells to expose PS under specific conditions enables the development of large variety of biomarkers (Schutters and Reutelingsperger, 2010).

The regulation mechanisms described above concern healthy cells. In the pathological cell the regulation of PS distribution between inner and outer leaflet of plasma membrane is disturbed. It was shown that PS expression in the outer leaflet of the tumorigenic cell lines was 3-7-fold higher than the expression of PS exposed on the outer membrane leaflet of the Primary Normal Human Epidermal Keratinocytes (NHEK) (Utsugi et al., 1991). On this basis the number of PS-targeting anti-cancer agents were developed recently, as amphipathic peptoids (Huang et al., 2014), phosphatidylserine-targeting antibodies (Beck et al., 2006; Huang et al., 2013) and PS-recognizing synthetic peptides (Jin et al., 2013; Thapa et al.).

Therefore, phosphatidylserine containing model membranes are suitable system to study binding not only specific proteins, but also the agents with potential anti-tumorous activity.

Model membrane systems for investigation of membrane-active peptides.

The most common model membrane systems that are used in the study of antimicrobial and cell-penetrating peptide properties, are liposomes (multilamellar vesicles MLV, small unilamellar vesicles SUV, large unilamellar vesicle LUV), bicelles, micelles and supported lipid bilayers (Eeman and Deleu, 2010).

Lipid composition can determine the membrane's shape and mechanoelastic properties. For instance cholesterol addition increases 1-palmitoyl-2-oleoyl-*sn*-glycero-3-phosphocholine (POPC) lipid order. Such lipid bilayer is mimicking outer plasma membrane properties and is often used to modulate lipid rafts formation (de Almeida et al., 2003). The addition of negatively charged POPS to POPC/cholesterol mixture can be a convenient model to investigate the processes occurring on the membrane of pathological cells (Lin and London, 2014) or to study mechanism of membrane translocation by cell-penetrating peptides (Gupta et al., 2013; Yandek et al., 2007, 2009).

Outer bacterial membranes contain more negatively charged lipids than the eukaryotic outer plasma membrane. Most of antimicrobial peptides bear positive charge. That's why the mixtures of zwitterionic and anionic lipids, such as dimyristoylglycerophosphocholine and dimyristoylglycerophosphoglycerol (DMPC/DMPG), dimyristoylglycerophosphoethanol and dimyristoylglycerophosphoglycerol (DMPE/DMPG), as well as palmitoyloleoylglycerophosphoethanol and palmitoyloleoylglycerophosphoglycerol (POPE/POPG=7:3 according to lipid composition of E. coli inner membrane) are often used to investigate the properties of antimicrobial peptides (Cheng et al., 2009; Dathe et al., 2002; Hall et al., 2011) and are the most commonly used bacterial membrane models. Gram-negative bacteria have different from gram-positive bacteria outer membrane composition. Dipalmitoylphosphatidylcholine (DPPC) and lipopolysaccharides (LPS) mixture is used to mimic the outer membrane of gram-negative bacteria (Clifton et al., 2013).

Therefore model membranes often represent simple two or three component system with defined characteristics as charge, bilayer thickness and fluidity. Model membrane composition influences the behaviour of membrane-active peptide, and has to be chosen accordingly. For instance, the relation between peptide helix size and membrane thickness determines if the peptide could span the lipid bilayer or not (Bobone et al., 2013; Cheng et al., 2009). For comparison, the hydrophobic thicknesses for the most common model membranes DMPC and POPC, as determined by neutron scattering and related methods, equals ~26.2 Å (Kucerka et al., 2004; Nagle and Tristram-Nagle, 2000) and ~27.7 Å (Gawrisch et al., 2007) in the liquid crystalline phase, respectively.

Structural parameters of the series of model membranes, consisting of PC or PE lipids with various hydrocarbon chains, were reviewed in corresponding publication (Nagle and Tristram-Nagle, 2000). The extract concerning the hydrophobic thickness is given in a Table II-3.

Table II-3. Hydrocarbon thickness of various single-component membranes in their fully hydrated state.

Lipid	DPPC	DPPC	DMPC	DOPC	EPC	DLPE	DLPE
Temperature	20°C	50°C	30°C	30°C	30°C	20°C	35°C
Hydrophobic thickness, Å	34.4	28.5	26.2	27.1	27.1	30	25.8

Molecular dynamic simulations provide also some quantitative characteristics of model membranes. MD-derived parameters of some single-component membranes are provided in a ***Table II-4***. In the contrast to the previous table, the membrane thickness in provided here as the distance between the phosphorus atoms. Polyansky and co-workers have shown by MD simulations that the DOPC membrane head group

region is more prone to water penetration than the DOPS membrane and, as a consequence, the DOPC membrane is characterized by smaller packing density of lipids, also smaller thickness and ordering of acyl chains (Polyansky and Efremov, 2005).

Table II-4. The characteristics of single-component model membranes provided by molecular dynamics simulations. Table is adapted with the author's permission from http://model.nmr.ru/index.phtml?page=work.projects.md-puremembr

Table 1. Structural parameters of model bilayers and micelles.

Bilayer	**T, °C***	**A_L, Å²****	**D_{p-p}, Å**	**S_{cd}**
Dimyristoylphosphatidylserine (DMPS)[128]	42 (36)	47.1	41.2	0.326
Dimyristoylphosphatidylcholine (DMPC)[128]	52 (24)	59.7	35.2	0.184
Dipalmitoylphosphatidylcholine (DPPC)[128]	52 (41.5)	59.0	39.0	0.187
Palmitoyloleoylphosphatidylglycerol (POPG)[288]	42 (−4)	56.5	39.4	0.185 / 0.176[#]
Palmitoyloleoylphosphatidylethanolamine (POPE)[128]	42 (26)	57.0	39.9	0.197 / 0.185
Palmitoyloleoylphosphatidylcholine (POPC)[128]	27 (−3)	63.7	37.3	0.183 / 0.149
Palmitoyloleoylphosphatidylserine (POPS)[128]	27 (14)	57.2	41.0	0.185 / 0.178
Dioleoylphosphatidylcholine (DOPC)[128]	27 (−22)	70.5	35.8	0.104
Dioleoylphosphatidylserine (DOPS)[128]	27 (−11)	63.6	39.0	0.138

Micelle	**T, °C**	**A^L, Å²**	**R^s, Å**	**S^{cd}**
Dodecylphosphocholine (DPC)[60]	27	91.5	20.9	0.064
Sodium dodecylsulfate (SDS)[60]	50	77.2	19.2	0.091
Lysomyristoylphosphatidylglycerol (LMPG)[72]	42	100.6	24.0	0.101
Lysopalmitoylphosphatidylglycerol (LPPG)[72]	42	105.3	24.6	0.070
Lysopalmitoylphosphatidylglycerol (LPPG)[125]	42	86.7	29.4	0.086

Superscript indexes indicate the number of lipid molecules in the bilayer or micelle.
* — Temperature of MD simulations, temperature of gel–liquid crystal phase transition is given in brackets.
** — Description of parameters: A_L — average area per lipid molecule; D_{p-p} — average bilayer thickness (distance between peaks of electron density for phosphorus atoms); S_{cd} — average value of order parameter for acyl chains. R_s – radius of micelle;
# — Values of S_{cd} are given separately for saturated and unsaturated acyl chains, respectively.

BIOPHYSICAL CHARACTERISATION OF LAH4-L1 INTERACTION WITH MODEL MEMBRANES.

As it was discussed in the introductory part of the manuscript, LAH4 and LAH4-L1 peptides bear considerable promise as transfection agents. The efficiency of peptides to deliver nucleic acids into the cells relies on the peptide's membrane pH-dependent activity and on the strength of peptide – nucleic acids interactions. LAH4 and LAH4-L1 appeared to be most efficient (Kichler et al., 2003a; Mason et al., 2006a, 2007c) delivery vehicles from whole LAH family (family of lysine – histidine rich amphipathic peptides) due to their particular structural characteristics, such as placement of four positively charged lysines at the peptide termini and four histidines in the core. Histidines change their protonation state at pH about 6, therefore rendering more hydrophobic peptide surface at neutral pH, and producing the helix with well-defined positively charged surface at pH 5 (the angle subtended by histidines is 80-100°).

It will be shown in the following chapters by solid-state NMR that LAH4-L1 peptide, similarly as LAH4, adopts preferably transmembrane alignments in the lipid bilayer at neutral pH, but in-planar orientation at acidic pH. Also, it will be shown that LAH4-L1 peptide disturbs the order of mixed anionic membranes more efficiently at pH 5 than at pH 7.4. Those investigations confirm previously suggested mechanism of transfection complex uptake and endosomal escape (Mason et al., 2006a) that in the endosomal compartments where pH is about 5.5, peptide become protonated and therefore it disturbs more the membrane of the endosome, causing the vesicle swelling and the release of DNA cargo. At pH 7.4 (serum medium) the histidines are deprotonated, and peptide inserts transmembrane in the outer membrane assuring uptake, but not being too toxic for the cells (Mason et al., 2007a).

In order to assess the thermodynamic characteristics of this pH-dependent association of LAH4-L1 peptide with zwitterionic and negatively charged membranes, the series of isothermal titration calorimetry measurements was performed. ITC experiment together with deuterium solid-state measurements reveal the preferable association of LAH4-L1 peptide with anionic lipids in mixed POPC/POPS membranes. The preliminary peptide – membrane association constants were assessed by circular dichroism titrations, where binding curve was built on the basis of peptide secondary structure changes.

And finally dynamic light scattering techniques was used to monitor the POPC/ POPS vesicles aggregation upon peptide association.

III. LAH4-L1 ALIGNMENTS IN MODEL MEMBRANES.

Oriented solid-state NMR spectroscopy can be used to follow the alignment of helical peptides in membranes. The ^{15}N chemical shift is a sensitive indicator of helical tilt angles when α-helices are incorporated in oriented phospholipid bilayers oriented with the normal parallel to the magnetic field direction. The measurement of chemical shifts <100 ppm is indicative of helix orientations parallel to the membrane surface, whereas resonances >180 ppm agree with transmembrane helix alignments. Previously the pH-dependent alignment of the LAH4 peptide in mechanically oriented zwitterionic POPC membranes has been studied in the pH range from 3 to 8 (Bechinger, 1996) and pH6 (Salnikov et al., 2010). The LAH4 orientation in mixed POPC/POPG, DMPC and DMPC/DMPG lipid membranes was also investigated at pH 5 and pH7 at various peptide-to-lipid ratios (*Barbara Perrone, PhD thesis 2011*).

In this work the alignment of LAH4-L1 in *oriented* mixed lipid bilayers was tested at pH 5 and pH 7.4. POPC lipid bilayers with various fraction of negatively charged POPS (0%, 10%, 14% and 25%) were used in the study as membrane model system in order to test the effect of charge and POPS content in particular on the LAH4-L1 membrane topology. To this end 1D proton-decoupled ^{15}N spectra were recorded, and the measured ^{15}N chemical shift was analysed.

MATERIALS AND METHODS

Peptide synthesis and chemicals

The LAH4-L1 peptide (KKALLAHALHLLA^{15N}LLALHLAHALKKA-CONH2) was prepared by solid-phase synthesis using standard Fmoc chemistry on a Millipore 9050 automated peptide synthesizer. A single ^{15}N-labelled leucine was incorporated at position 14 (in the middle of sequence). The purity and identity of the products was controlled by MALDI-TOF mass spectrometry (MW=2780Da) and HPLC. After the purification by reverse phase liquid chromatography (C18; Gilson inc., Middleton), the trifluoroacetate counterions were exchanged on acetate counterions as follows. The peptide powders were placed into 4% acetic acid, the solutions were frozen with liquid nitrogen and subjected to lyophilization at high vacuum overnight.

The lipids (POPC *1-palmitoyl-2-oleoyl-sn-glycero-3-phosphocholine*, POPS *1-palmitoyl-2-oleoyl-sn-glycero-3-phospho-L-serine (sodium salt)*, POPG 1-*palmitoyl-2-oleoyl-sn-glycero-3-phospho-(1'-rac-glycerol) (sodium salt)*) were from Avanti Polar Lipids Inc. (Alabaster, AL, USA) and used without further purification. Chloroform, methanol and trifluoroethanol (TFE) were from Sigma Aldrich (Lyon, France).

Sample preparation for solid-state NMR spectroscopy

The samples were prepared following previously described protocols (Bechinger et al., 2008). The lipids were mixed in the ratio POPC/POPS=3:1 (25*mol* % POPS), POPC/POPS=6:1 (14*mol* % POPS), POPC/POPS=9:1 (10*mol* % POPS). The corresponding amount of peptide was dissolved in 300-500uL TFE, and added to the lipid mixtures in chloroform-methanol=4:1*v/v*. The pH was adjusted by the addition of microliter amounts of 100mM NaOH – 1mM EDTA. The pH was controlled with indicator strips by drying some amount of lipid-peptide mixture on the stripe, and hydrating it with water. Then solvent was partially evaporated and the mixture was dried onto 20-25 glass plates, first for 10min on air, then at least for 3h under high vacuum to remove any traces of organic solvent. The glass plates were placed in a hydration chamber at 93% relative humidity at ambient temperature for at least 10h. The pH value of the lipid/peptide samples was again tested from a small part of the sample that was mixed with 100µl of deionized water. After equilibration, the glass plates were stacked on top of each other, wrapped with Teflon tape and sealed in polymer barrier film *Escal*^{TM} (Mitsubishi gas chemical company, Inc.,

Japan). The proper sealing of the sample is essential for a successful experiment, because good isolation material prevents the membrane sample from dehydration.

The total amount of lipids that were used for sample preparation in each individual experiments varied between 45 and 80mg depending to the size of the glass plates (8mm*21mm or 6mm*11mm). The size and number of glass plates were chosen to fit into the NMR coil.

Solid-state NMR experiments.

The solid-state NMR experiments were performed on Bruker Avance 500 and Bruker Avance 400 spectrometers, equipped with static solid-state NMR probes with a flattened coil for mechanically oriented samples. Proton-decoupled ^{15}N spectra were acquired with cross polarization using a contact time of 800 µs. Nitrogen and proton fields were swept trough the Hartmann-Hahn condition using a standard CP sequence (Waugh, 1976). The B1 fields were in the range 35-43 kHz, the recycle delay 2sec, the spectral width 32000Hz, and the pre-acquisition delay 20usec. Before Fourier transformation, an exponential apodization function corresponding to a line broadening of 200 Hz was applied.

The pulse program schematic view is given below:

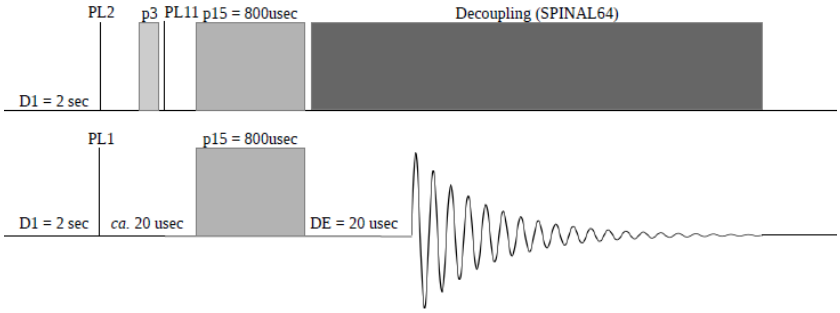

PL1 (X contact power level), PL2 (proton p90 power level) and PL11 (proton contact power level) were in the range of 5-6dB; p3 – proton 90 degree pulse.

The acquisition parameters were optimised before each experimental session using a powder of $^{15}NH4Cl$ sample, and the chemical shift of this reference sample was set to 41.5ppm.

The lipid bilayer orientation was assessed by recording a solid-state NMR ^{31}P spectrum prior to each ^{15}N static NMR measurement. ^{31}P-NMR spectra were acquired using a phase-cycled Hahn-echo pulse sequence with gated broadband proton decoupling (Rance and Byrd, 1983). The ^{31}P 90° pulses were 4 µsec, the echo delay 40 µsec, and the recycle delay 2 sec. During processing the first 4 points were removed in order to start Fourier transformation at the top of the echo. Phosphorous chemical shifts were referenced relative to external 85% H_3PO_4 (0 ppm).

RESULTS.

Static oriented ^{15}N solid-state NMR spectra on the LAH4-L1 peptide embedded in mixed POPC/POPS or zwitterionic POPC membranes at pH 7.4 are shown in a ***Figure III-1*** (left column), as well as the corresponding ^{31}P solid-state NMR spectra (right column), which are used to control the lipid orientation. The ^{31}P NMR signal at around 30ppm indicates that most of the POPC lipids are oriented with their long axes parallel to the magnetic field. For mixed POPC/POPS membranes we usually see another component at around 35ppm, which corresponds to the POPS lipids at the parallel orientation. In contrast, the signal in the range of -15…-17ppm are indicative for lipids in a perpendicular orientation as they occur predominantly in the powder pattern NMR spectra of e.g. spherical liposomes. For some membrane compositions, such as POPC/POPS-25%, for unknown reason, it was more complicated to prepare well-

oriented lipid bilayer, and the POPS component of the ^{31}P signal is hidden under POPC peak (***Figure III-1***, B and ***Figure III-2***, B).

The ^{15}N spectra of 2*mole%* LAH4-L1 embedded into POPC/POPS-25% or POPC/POPS-14% membranes at *pH 7.4* show at least two components (***Figure III-1***, A and B, *left*). Whereas the resonance around 190-210ppm corresponds to the *transmembrane* (TM) orientation of a peptide helix, the component in the range 80-100ppm may belong to a fraction of peptide that adopts multiple alignments around an *in*-planar (IP) orientation. Alternatively, the second peak could represent a powder spectra component of misaligned sample. Generally, ^{15}N powder spectra component appears when the lipid bilayer is oriented in a random fashion relative to the magnetic field direction. As shown on ^{31}P spectra of corresponding POPC/POPS-25% and POPC/POPS-14% membranes (***Figure III-1***, A and B, *right*) there is indeed a considerable fraction also of non-oriented lipids.

Although the phosphorus spectra depicted in a ***Figure III-1***, C and D indicate that most of the lipid is well oriented with the long axes parallel to the membrane normal, the corresponding ^{15}N spectra (Figure III-1, C and D, *left*) are dominated by a spectral component of a transmembrane helical alignment which are quite broad (line width at half-height is 1590Hz for *C*, and 2390Hz for *D*). The Lorentzian broadening of 200Hz, which was applied during ^{15}N spectra processing, cannot account for this line shape (width at half-height is 420Hz for most sharp ^{15}N signals from whole experimental series). Therefore, the main source of the peak broadening is the peptide *mosaic spread*. Even if peptide adopts predominantly transmembrane alignment, some uncertainty in helix alignment is present. Considering sufficient sample hydration, the presence of multiple LAH4-L1orientations in oriented membrane could be referred rather to the behaviour of peptide upon its binding to the membrane than to poor quality of sample preparation.

When the peptide is reconstituted into mixed negatively charged (***Figure III-2*** A, B, C) and zwitterionic (D) membranes at *pH 5* at the same 2 mole% concentration LAH4-L1 resonances around 80ppm are observed and indicative for in-planar alignments (***Figure III-2***). For POPC/POPS-10% the ^{15}N and ^{31}P signals are especially sharp (line width at half-height was 620Hz for ^{15}N signal and 350Hz for ^{31}P peak at 30ppm, ***Figure III-2,*** *C*), indicating that the peptide adopts a well-defined in-planar orientation in the membrane with little disturbance of the membrane order.

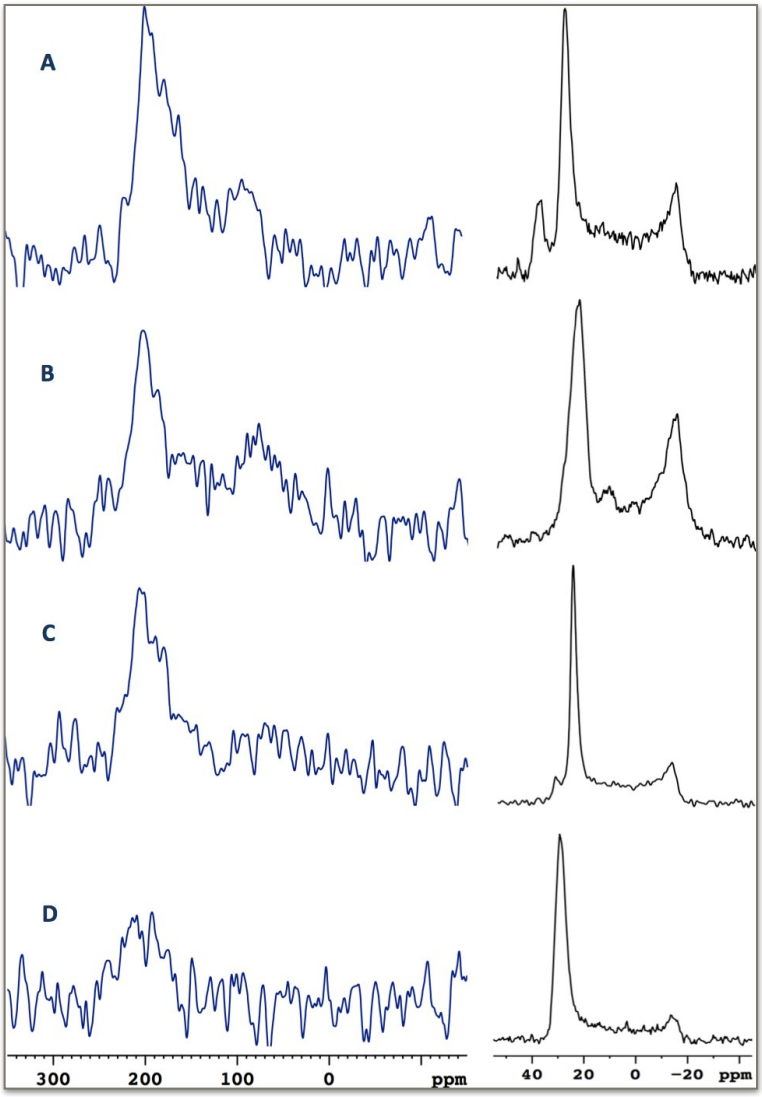

Figure III-1. Solid-state NMR spectra of 2mole% [^{15}NLeu14]-LAH4-L1 reconstituted into bilayers oriented with the membrane normal parallel to the magnetic field direction, pH 7.4
A - POPC/POPS-25%, B - POPC/POPS-14%, C - POPC/POPS-10%, D – POPC (1% LAH4-L1).
Proton decoupled ^{15}N solid-state NMR spectra on the left and the corresponding ^{31}P solid-state NMR spectra to the right.

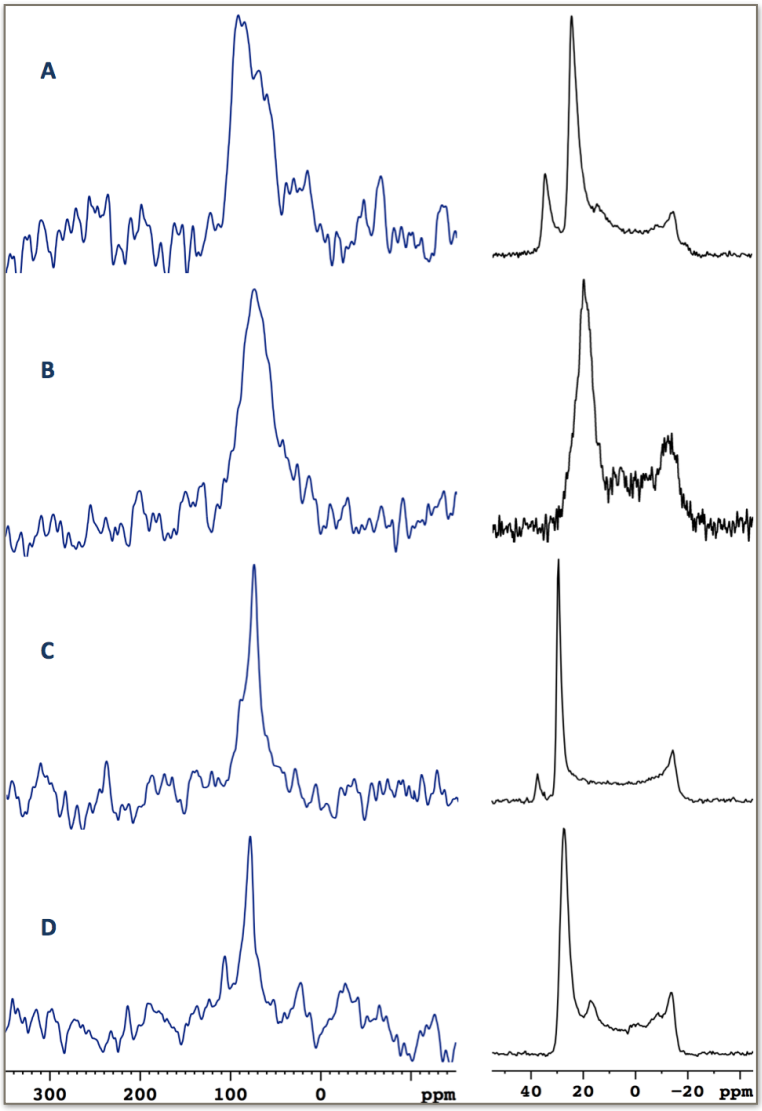

Figure III-2. Solid-state NMR spectra of 2mole% [^{15}NLeu14]-LAH4-L1 reconstituted into bilayers oriented with the membrane normal parallel to the magnetic field direction, pH 5
A - POPC/POPS-25%, B - POPC/POPS-14%, C - POPC/POPS-10%, D – POPC (1% LAH4-L1).
Proton decoupled 15N solid-state NMR spectra on the left and 31P spectra on the right.

In order to test the dependence of peptide alignment on the peptide-to-lipid ratio samples were prepared with 4*mole*% LAH4-L1 in POPC/POPS-25% or POPC oriented lipid bilayers. Doubling the peptide concentration in POPS/POPC-25% lipid bilayers at pH 7.4 *does not* augment the powder pattern contribution of the peptide, as one might expect (***Figure III-3****, B*). On the contrary the preparation of rather well oriented bilayer succeeded indicated by small ^{31}P peak at -15ppm. The peak corresponding to transmembrane alignment is around 200ppm.

Even more surprising is the behaviour of LAH4-L1 at pH 5, when the molar ratio of peptide associated with POPC/POPS-25% lipid bilayers is increased (***Figure III-4****, B*). The enlargement of the ^{31}P signal at -15ppm clearly indicates that in the presence of 4*mole*% LAH4-L1 the lipid bilayer is considerably disturbed when at the same time the ^{15}N solid-state NMR resonance at around 85ppm indicates that the peptide adopts a more homogenous in-planar alignment. There can be well present some fraction of non-oriented peptide, but the powder spectrum is hidden under the noise.

Under the particular conditions (decrease of pH/increase of peptide concentration) the LAH4-L1 peptide considerably disturbs the POPC/POPS lipid bilayer packing, when at the same time this is not

reflected in the ^{15}N solid-state NMR spectrum. Therefore, the ^{31}P spectra alone cannot serve as an absolute reference to the quality of sample preparation. To assure good sample quality it is important to reach sufficient lipid bilayer hydration and to avoid the water loss during the NMR measurement that usually lasts 1-2 days. It will be shown later in deuterium solid state NMR experiment on deuterated lipids (Chapter IV) that indeed the peptide disturbs the lipid order more at pH 5 than at pH 7.4.

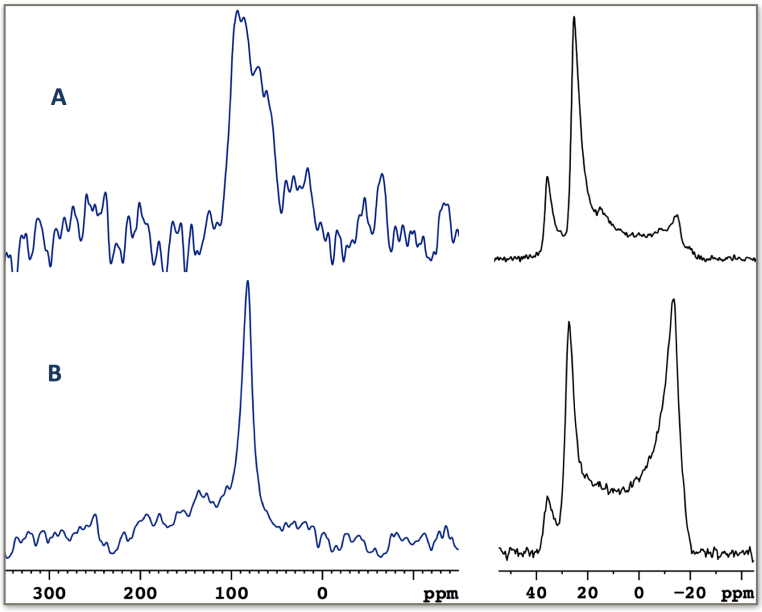

Figure III-3. Solid-state NMR spectra of [^{15}NLeu14]-LAH4-L1 reconstituted in POPC/POPS-25% bilayers oriented with the membrane normal parallel to the magnetic field direction, **pH 7.5**
A – 2mole% LAH4-L1, B – 4mole% LAH4-L1
Proton decoupled 15N solid-state NMR spectra on the left and 31P spectra on the right.

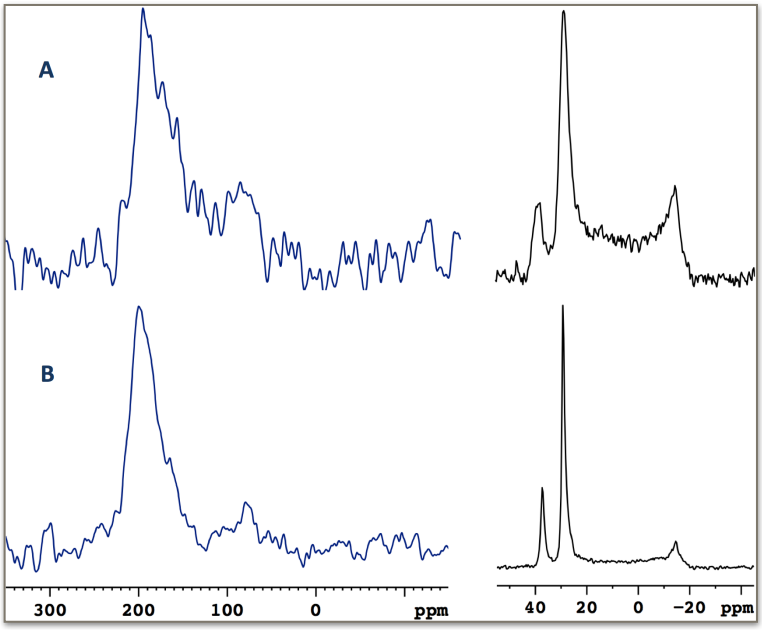

Figure III-4. Solid-state NMR spectra of [^{15}NLeu14]-LAH4-L1 reconstituted in POPC/POPS-25% bilayers oriented with the membrane normal parallel to the magnetic field direction, **pH 5**
A – 2mole% LAH4-L1, B – 4mole% LAH4-L1
Proton decoupled 15N solid-state NMR spectra on the left and 31P spectra on the right.

Solid-state NMR spectra of LAH4-L1 reconstituted into POPC lipid bilayers are displayed in the ***Figure III-5*** (pH 7.4) and ***Figure III-6*** (pH 5). When compared to the POPC/POPS-25% membranes the concentration of LAH4-L1 in the POPC samples are lower, 1% and 3% against 2% and 4%, because the association of peptide with zwitterionic membranes is weaker, as will be shown by other methods.

Increasing of peptide molar ratio at pH 7.4 promotes a larger distribution of alignments (***Figure III-5***, B). LAH4-L1 along with its transmembrane fraction (^{15}N signal around 185pppm) presumably adopts multiple alignments, confirmed by appearance of large powder spectrum component with its maximum around 90ppm. When the ^{31}P solid-state NMR spectrum of the same sample is analysed the phosphorus signal at -13ppm slightly augments, indicating the increase of non-oriented lipids fraction, but this augmentation is not drastic. Taking into account the fraction of membrane lipids, which are not oriented parallel to the membrane normal from the ^{31}P solid-state NMR spectrum, one would expect to obtain a much smaller powder pattern component in the ^{15}N spectrum.

At pH 5 an increase in the molar concentration of peptide does not promote the augmentation of non-oriented lipids fraction, as viewed by ^{31}P signal at -13ppm (***Figure III-6***, B, right column). However, upon increase in the peptide-to-lipid molar ratio the peptide adopts both transmembrane as well as in-planar alignments with a 1:1 ratio (***Figure III-6***, B). Even if, because of the spread of the signal over a much broader frequency range, the signal-to-noise ratio is reduced two separate signal intensities centred at around 190-192ppm (TM) and 82ppm (IP) can be distinguished.

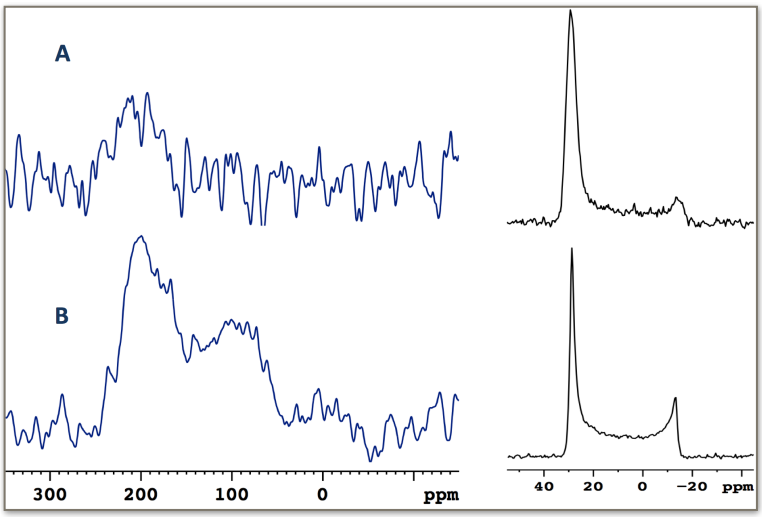

Figure III-5. Solid-state NMR spectra of [^{15}NLeu14]-LAH4-L1 reconstituted in zwitterionic POPC bilayers oriented with the membrane normal parallel to the magnetic field direction, **pH 7.4**
A – 1mole% LAH4-L1, B – 3mole% LAH4-L1
Proton decoupled 15N solid-state NMR spectra on the left and 31P spectra on the right.

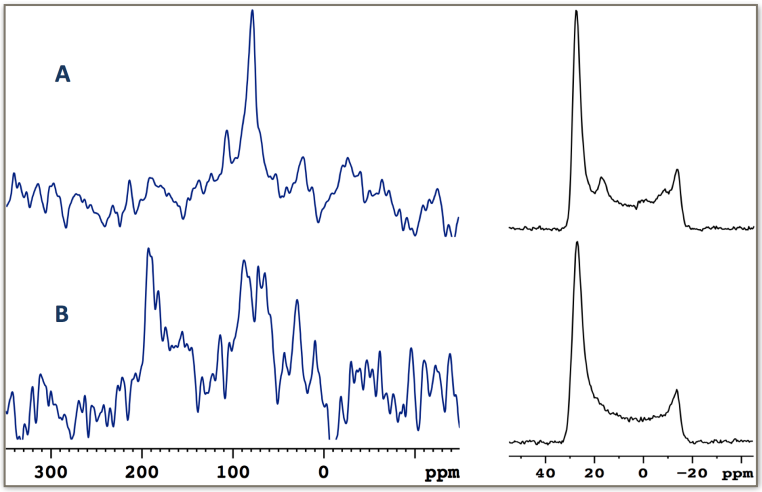

Figure III-6. Solid-state NMR spectra of [^{15}NLeu14]-LAH4-L1 reconstituted in zwitterionic POPC bilayers oriented with the membrane normal parallel to the magnetic field direction, **pH 5**
A – 1% molar LAH4-L1, B – 3% molar LAH4-L1
Proton decoupled 15N solid-state NMR spectra on the left and 31P spectra on the right.

Finally, the behaviour of the LAH4-L1 peptide in two types of negatively charged mixed membranes POPC/POP**S**-25% and POPC/POP**G**-25% (***Figure III-7***) was compared. When reconstituted into these mixed membranes the ^{15}N solid-state NMR spectra of LAH4-L1 exhibits broad resonances with maximum at about 200ppm indicating predominantly transmembrane alignments with some powder pattern component.

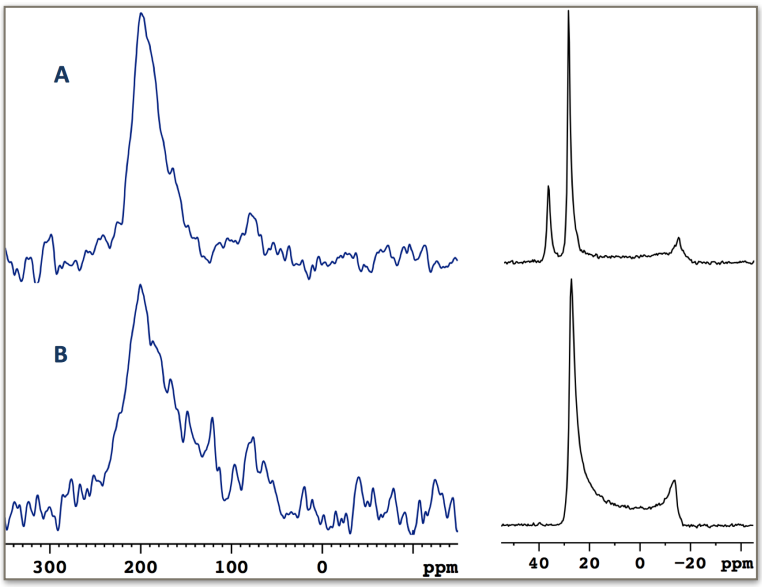

Figure III-7. Solid-state NMR spectra of 4mole% [^{15}NLeu14]-LAH4-L1 reconstituted in negatively charged bilayers oriented with the membrane normal parallel to the magnetic field direction, **pH 7.4**.
A –POPC/POPS-25% (TM – 200÷2ppm), POPC/POPG-25% (TM – 196±2ppm)
Proton decoupled 15N solid-state NMR spectra on the left and 31P spectra on the right.

Table III-1 brief summarizes the conclusions drawn from the oriented ^{15}N solid-state NMR spectra presented in this chapter including the spectral characteristics such as peak position in *ppm* and peak half width in *Hz* (HW). Furthermore the signal to noise ratios (s/n) in relation to the number of scans (ns) are given in order to assess and to compare the spectral quality. Signal to noise ratio in each given case depends on amount of labelled peptide in the sample, number of scans and acquisition parameters' setup.

Table III-1. Proton decoupled ^{15}N solid-state NMR spectra description summary.

	POPC	POPC/POPS-25%	POPC/POPS-14%	POPC/POPS-10%
pH 7.4	*1mole% LAH4-L1*	*2mole% LAH4-L1*	*2mole% LAH4-L1*	*2mole% LAH4-L1*
		Around 75% TM and 25% of IP (powder)	Around 65% TM and 35% of IP (powder)	
	TM=204±8ppm HW=2390Hz s/n=1.88 ns=36462	TM=196±3ppm IP (or powder) = 90±2ppm HW(TM)=1980Hz s/n=11.7 ns=20514	TM=201±3ppm HW(TM)=1560Hz IP (or powder) = 76±4 ppm s/n=4.5 ns=16038	TM=203±2ppm HW=1590Hz s/n=5 ns=55661
	3mole% LAH4-L1	*4mole% LAH4-L1*		
	Around 55-60% TM and 45-40% of IP (powder)	Around 85% TM and 15% of IP (or powder)		
	TM=184±10ppm IP (powder) = 90-100ppm s/n=5.87 ns=32768	TM=200±2ppm HW(TM)=1250Hz IP (or powder)=79±2 s/n=1.88 ns=36462		
pH 5	*1mole% LAH4-L1*	*2mole% LAH4-L1*	*2mole% LAH4-L1*	*2mole% LAH4-L1*
	IP=80±1ppm HW=420Hz s/n=9 ns=29533	IP=85±3ppm HW=1800Hz s/n=12 ns=23651	IP=75±2ppm HW=1350Hz s/n=12 ns=90643	IP=77±2ppm HW=620Hz s/n=11.6 ns=15083
	3mole% LAH4-L1	*4mole% LAH4-L1*		
	Around 50% TM / 50% IP	Probably there is some fraction of non-oriented peptide (hidden)		
	TM=192±5 ppm IP=82±5 ppm s/n=5.37 ns=23408	IP=83±1ppm HW=490Hz s/n=25.7 ns=5930		

Simulation of the ^{15}N solid-state NMR spectra.

For some of the spectra, notably those where LAH4-L1 adopts more than one well defined alignment, the spectra were deconvoluted by spectral simulations using the TopSpin Solid line shape analysis module provided with the instrumental software of the NMR spectrometer. Whereas one component was assumed to arise from a powder pattern contribution, a second NMR resonance from transmembrane peptides was included in the simulation protocol. Lorentzian and Gaussian broadening was included as variable parameters. Please note that for spectra processing the Lorentzian broadening was applied and equal to 200Hz, and that the magnitudes of line broadening parameters are bigger for the simulated spectra. Taking into account that ^{1}H decoupling was applied thereby abolishing broadening effects from heteronuclear dipolar couplings the major factors that remain to cause line broadening are mosaic spread and T_2 relaxation.

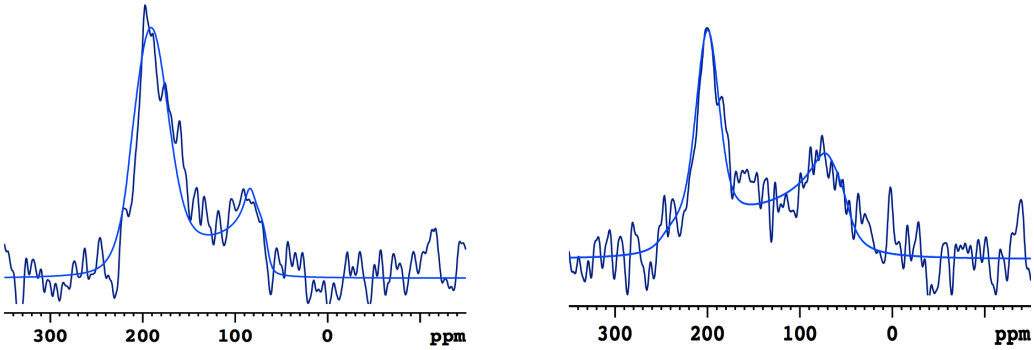

Figure III-8. Experimentally obtained and simulated 15N spectra of 2mole% [^{15}N-Leu14]-LAH4-L1 embedded into POPC/POPS-25%lipid bilayer at pH7 (left figure) and into POPC/POPS-14% lipid bilayer at pH7 (right figure).

The corresponding simulation parameters are given in the table III-2.

Table III-2. The simulations of the ^{15}N chemical shift tensor for 2% [^{15N}Leu14]-LAH4-L1 reconstituted in POPC/POPS-25% lipid bilayers (left) and POPC/POPS-14% lipid bilayer (right).

NUCLEUS	1 (powder)	2 (TM)
Iy	7014524*	20514070*
δ(iso)	125.7*	194
δ(CSA)	92.7*	
η(CSA)	0.2	
δ(11)	218.5	
δ(22)	88.7	
δ(33)	70.1	
LB	178*	508*
GB	255*	1523*

NUCLEUS	1 (powder)	2 (TM)
Iy	7106558*	12822740*
δ(iso)	123*	200
δ(CSA)	125.6*	
η(CSA)	0.2	
δ(11)	248.6	
δ(22)	72.8	
δ(33)	47.7	
LB	1179*	507*
GB	0*	1210*

Nucleus 1 – powder pattern component
Nucleus 2 – transmembrane component
Iy – integral under corresponding simulated peak
** simulation variables*

Chemical shift anisotropy parameters are determined as following (Saitô et al., 2010):

$\delta_{iso} = 1/3(\sigma_{11} + \sigma_{22} + \sigma_{33})$, isotropic shielding

$\delta_{aniso}(CSA) = \sigma_{33} - \delta_{iso}$, anisotropic shielding

$\eta(CSA) = (\sigma_{22} - \sigma_{11})/\delta_{aniso}$, asymmetric parameter

The signal intensity, Lorentz and Gaussian broadening were determined as variable parameters, also isotropic and anisotropic shielding parameters were left free to simulate averaged powder pattern line shapes.

The deconvolution of the spectra can help us to estimate the fraction of non-oriented peptide, and gives a better idea about the chemical shifts. However the second component of the ^{15}N ssNMR signal which was for the simulations assumed to arise from a powder pattern contribution could also arise from other orientational distributions with predominantly in-planar alignments. Accordingly to the simulation there is 75% of transmembrane component and 25% of powder spectra component for LAH4-L1 embedded in POPC/POPS-25%. For LAH4-L1 embedded in POPC/POPS-14% the ratios are 65% and 35% correspondingly.

IV. INTERACTION OF LAH4-L1 WITH MEMBRANES VIEWED BY ^{2}H-NMR

In order to monitor changes in the lipid packing induced by peptide insertion, the quadrupolar solid-state NMR spectra are measured from phospholipids possessing deuterated fatty acyl chains. The quadrupolar splitting is a measure of the

average alignment of the C–^{2}H vector and in the case of the fatty acyl chains predominantly reflect the position-dependent dynamic averaging. Such ^{2}H static NMR spectroscopy enables the lipid acyl segment-by-segment analysis of the peptide penetration depth. Mason and co-workers have investigated in details the effect of LAH4 peptide on the lipid order in POPC/POPS/cholesterol=70:15:15 vesicles at pH 5 and pH 7.5 (Mason et al., 2006a). It was found that LAH4 peptide disturbs preferentially the order of POPS lipids, and the disordering effect was much bigger at pH 5. This finding prompts us to conduct the similar study on LAH4-L1 peptide at two pH conditions. In addition the effect of anionic lipid content (POPS) on the mode of LAH4-L1 interaction with mixed membranes was investigated.

Thus POPC and POPS lipid order perturbation by LAH4-L1 peptide embedded into deuterated mixed anionic (and zwitterionic) vesicles was assessed in parallel experiments by ^{2}H solid-state NMR spectroscopy.

MATERIALS AND METHODS

Sample preparation for solid-state NMR spectroscopy

LAH4-L1 peptide (KKALLAHALHLLALLALHLAHALKKA-CONH2) was prepared by automated solid-phase synthesis as described in the Chapter III, with the difference that unlabelled leucine was incorporated in 14th position. The lipids (POPC *1-palmitoyl-2-oleoyl-sn-glycero-3-phosphocholine*, POPS *1-palmitoyl-2-oleoyl-sn-glycero-3-phospho-L-serine (sodium salt)*, POPG 1-*palmitoyl-2-oleoyl-sn-glycero-3-phospho-(1'-rac-glycerol) (sodium salt)*) and their deuterated (-*palmitoyl-d31*-) analogous were bought from Avanti Polar Lipids Inc. (Alabaster, AL, USA) and used without further purification.

For ^{2}H solid-state NMR experiments on the *deuterated* lipids with peptide reconstituted into the large unilamellar vesicles (LUV), the samples were prepared as follows. Unlabelled POPC (POPS) and deuterated lipids POPS-d31 (POPC-d31) were mixed at the ratios given in a ***Table IV-1***.

A total of 8-10 mg of lipids per sample were dissolved and mixed in chloroform:methanol = 3:1v/v. A stock solution of LAH4-L1 was prepared in TFE, and a corresponding aliquot was added to each sample to obtain molar ratios of 0.5%, 1%, 1.5% or 2.5%.

The organic solvents were evaporated using a gentle stream of nitrogen before the lipid films were exposed to high vacuum overnight to remove all organic solvents. The films were then rehydrated with 120-125 µL of corresponding buffer, such as 50mM acetate - 0.5mM EDTA to maintain pH=4.95-5, 20mM HEPES - 0.5mM EDTA (pH=7.3-7.4), both are prepared from deuterium-depleted water (Eurisotop, France). The range of final concentrations was around 0.8 – 2mM for peptide and 80-100mM for LUVs.

The samples were briefly sonicated in a bath sonicator to improve exposure of all lipids to the peptide. Samples were subjected to five freeze (-20^{0}C) - thaw (37^{0}C) cycles for further sample homogenization. For NMR measurements the samples were placed in small 700uL plastic centrifugation tubes (Eppendorf, Hamburg, DE). For NMR measurements the tubes were placed into the solenoid coil of static solid-state NMR probe.

Table IV-1. The lipid composition of membrane models used in study and experimental conditions.

POPC/POPS *mole/mole*	POPC/**POPS-d31**	Total lipids, mg	% [2]	T	pH
9/1	9mg/1mg	10	10	25 / 37	7.4 / 5
6/1	8.3mg/1.4mg	9.7	14	25 / 37	7.4 / 5
3/1	6mg/2mg	8	25	25 / 37	7.4 / 5

POPC/POPS *mole/mole*	**POPC-d31**/POPC/	Total lipids, mg	%	T	pH
9/1	2mg/7mg/1mg	10	20	25 / 37	7.4
6/1	2mg/6.3mg/1.4mg	9.7	21	25 / 37	7.4
3/1	2mg/4mg/2mg	8	25	25 / 37	7.4
POPC only	2mg/6mg/0mg	8	25	25 / 37	7.4 / 5

Solid-state NMR. Experimental setup and spectra analysis.

^{2}H quadrupolar echo experiments for samples containing POPS-d31 or POPC-d31 were performed at 46.10MHz on a Bruker Avance 300MHz spectrometer using a static probe. Deuterium NMR experiments were performed using the quadrupolar echo pulse sequence 90°x-τ-90°y-τ-acq (Davis et al., 1976). Typical acquisition parameters for ^{2}H-NMR experiments were as follows: spectral width of 500 kHz, recycle delay of 0.5s, echo delay of 100μs, acquisition time 33ms, and π/2 pulse width of 4.2μs. Deuterated water was used to set up the reference frequency. The temperature was maintained stable at 298K or/and 310K to keep the bilayers in their liquid-crystalline phase. As this ^{2}H NMR experiment is essentially the measurement of the acyl chain dynamics, the temperature was kept stable during whole experiment (298K/310K). During processing the first 32 points were removed in order to start Fourier transformation at the top of the echo. Spectra were zero-filled to 8192 points, and 200Hz exponential line broadening was applied before Fourier transformation. The quadrupolar splitting was measured between the corresponding well-defined peaks.

For deuterated POPS the lipid structure is shown in a ***Figure IV-1***. ^{2}H-solid-state NMR powder pattern spectra of phospholipids uniformly deuterated at the palmitoyl acyl chain in the liquid-crystalline phase (L_α) reveal a distribution of the splittings, for which the largest values correspond to the segment closest to the lipid polar head group with a progressive decrease along the lipid acyl chain (Seelig and Seelig, 1974). The movement of -CH_2- group is sterically hindered near lipid head group, so the larger quadrupolar splitting is observed. Usually upon the insertion into lipid bilayer the peptide disturbs the lateral chain packing of *neighbouring* lipids, such the freedom of -CH_2- groups movement increases. This results in decreasing of quadrupolar splitting (the exemplary spectra are depicted in a ***Figure IV-2***).

From the measured ^{2}H quadrupolar splittings (Δν) the order parameters S_{CD} for each -CD_2- group have been therefore calculated according to equation:

The order parameters for each -CD_2- group were calculated accordingly to equation:

$S_{CD} = \Delta\nu / (3/4)(e^2qQ/h)$,

where e^2qQ/h is defined as a -CD_2- static quadrupolar coupling constant that found to be equal 167kHz for paraffin chains (Burnett, 1971; Seelig, 1977),

Δν – observed quadrupolar splitting.

Such quadrupolar splitting for each type of deuterium nuclei was divided by (3/4)*(e^2qQ/h) (=125125Hz) and plotted against its position on the lipid acyl chain for each LAH4-L1 concentration series in order to obtain order parameter profiles.

By plotting the resulting deuterium order parameter against its position on the lipid acyl chain and as a function of LAH4-L1 concentration we obtain lipids order profiles. Those deuterium atoms that belong to

carbon atoms 2-6/7-8 give the quadrupolar splittings that could not be resolved separately. Therefore the same quadrupolar splittings were assigned to several -CD2- groups (example in a ***Figure IV-3***).

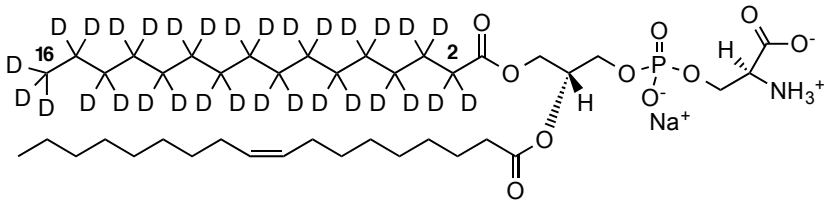

Figure IV-1. Deuterium-labelled 1-palmitoyl-2-oleoyl-*sn*-glycero-3-phospho-L-serine. Numbers 2 and 16 shows the –CD_2- residue numeration.

RESULTS.

Table IV-1 brief summarizes the sample composition and the conditions for all experimental series measured. The order perturbation of mixed POPC/POPS and of zwitterionic POPC membranes by LAH4-L1 peptide was tested at two different temperatures and two pH conditions. Thereby the effect of the negatively charged lipid POPS on the membrane order perturbation by LAH4-L1 was investigated. Also, the effect of peptide-to-lipid ratio, pH and temperature were investigated.

Spectral analysis and presentation of the results.

Below there are examples of deuterium solid-state NMR spectra of deuterated palmitoyl chain in POPC model membranes with varied LAH4-L1 peptide concentration (***Figure IV-2***). There are nine well-resolved peaks in deuterium spectrum of POPC/POPC-d31 membranes without peptide. Six peaks in the middle were attributed to the -CD_2- groups that belong to 11…16th acyl residues on POPC palmitoyl chain. The rest of peaks were splitted into three groups, and attributed to 9-10th, 7-8th and 2nd-6th positions on the palmitoyl chain, as it has been done previously (Salnikov et al., 2009). The splittings between well resolved peaks were measured and the order parameter profiles (***Figure IV-3***) for this measurement series were constructed following the procedure described in Materials and Methods part.

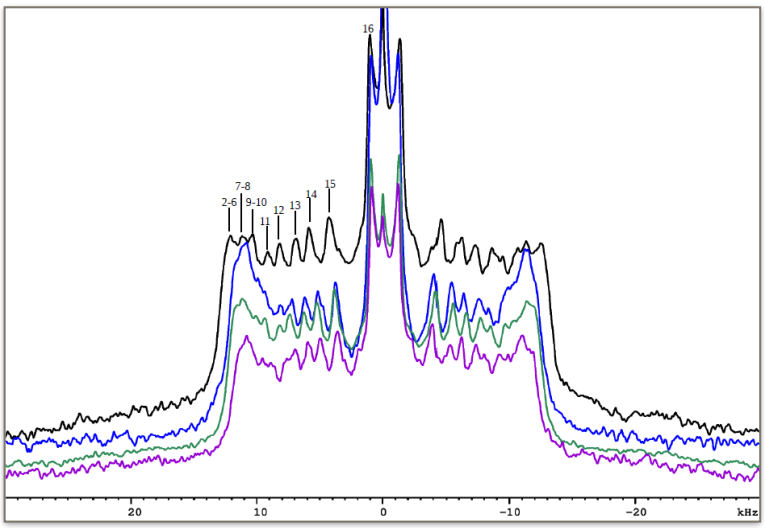

Figure IV-2. Wide line ^{2}H-NMR spectra of perdeuterated palmitoyl chain in POPC/POPC-d31 (6mg/2mg) large unilamellar vesicles as a function of LAH4-L1 peptide-to-lipid ratio, pH 5, 298K
black line – 0% peptide, blue line – 1%, green line – 1.5%, magenta line – 2.5%.

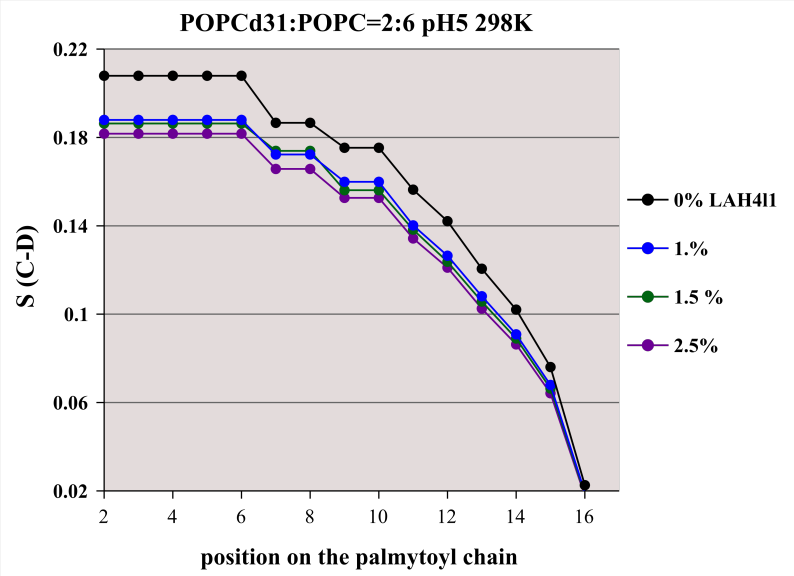

Figure IV3. Order parameters profile of POPC/POPC-d31 (6mg:2mg) mixed large unilamellar vesicles under the interaction with LAH4-L1 peptide (0%, 1%, 1.5%, 2.5mole%) at pH 5 and 298K.

The quadrupolar splitting profiles (***Figure IV-3***) indicate that peptide indeed disturbs the POPS lipid order under its binding with the membrane, as the quadrupolar coupling constants ($S_{C\text{-}D}$) are getting smaller upon addition of peptide. Such disruptions of the lateral chain packing of neighbouring lipids and the corresponding increase in motions of the -CH2- groups has been observed previously upon insertion of amphipathic peptides into the lipid bilayer interface (Kwon et al., 2013; Mason et al., 2006a, 2006b, 2007b; Salnikov et al., 2009).

In order to analyse the data quantitatively one needs to take into account that the physicochemical characteristics of the membrane such as fluidity, temperature of phase transition, and subsequently the acyl chain dynamics, will change with temperature, pH and also the addition of the negatively charged POPS lipid. Therefore, to better compare the results between different measurement series, the changes in quadrupolar splitting are displayed as *relative order parameter* S_{CD} (x% LAH4-L1) / S_{CD} (0% LAH4-L1) as illustrated in a ***Figure IV-4***. In this representation the effect of peptide binding on the dynamics of each segment of palmitoyl chain, the quadrupolar splitting of which is well resolved, can be assessed in a direct manner. If the relative quadrupolar splitting is around 1 the insertion of the peptide does not affect the order of the lipid segment. In case of LAH4-L1 insertion into POPC membrane at pH 5 (***Figure IV-4***), the first addition of peptide (1 mole%) causes relatively big distortion in lipid order (0.90-0.92), whereas the addition of more peptide does not decrease the bilayer order in the same manner (0.86-0.88 in the presence of 2.5% LAH4-L1).

In the following I skip the displaying of original ^{2}H solid-state NMR spectra, so the membrane order perturbation by peptide will be illustrated by *relative order parameter* profiles exclusively.

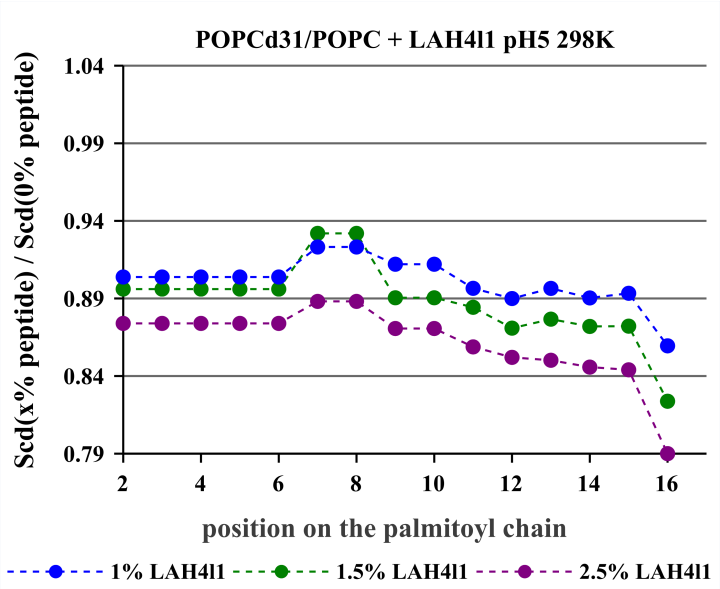

Figure IV-4. *Relative* order parameters profile of POPC/POPC-d31 (6mg:2mg) mixed large unilamellar vesicles under the interaction with LAH4-L1 peptide (1%, 1.5%, 2.5mole%), pH 5, 298K.

Temperature and pH effect on the membrane lipids order.

Before starting the series of experiment where few parameters, as lipid composition, temperature, pH or peptide concentration, will be varied simultaneously, the series of measurements were carried out where the effect of pH and temperature on lipids order was assessed. In order to illustrate how much POPC membrane order is affected by temperature increase for POPC lipid bilayer, the order parameter profiles for POPC-d31/POPC membranes at two temperature and pH regimes were constructed (***Figure IV-5***). The graphs above are actual order parameter profiles and the graphs below show the relative changes of membrane order when temperature increases from 298K to 310K, obtained by dividing order parameter of corresponding -CH_2- residue at 310K on that obtained at 298K. The effect of temperature on the POPC-d31 lipid order could such be compared for various pH, which is slightly bigger at neutral pH (relative order parameters are obtained in the range of 0.93 – 0.97) than at acid pH (0.96 – 0.98). Usually the calculated order parameters for 16th and for 2nd…6th acyl groups carry quite substantial mistake, the former because of small quadrupolar splitting value, and the latter because of the difficulty to determine the precise peak position. That is why the values of -CD_2- group order parameters from the middle of acyl chain are more reliable and suitable for the analysis.

In another experiment the effect of temperature and pH was tested on the mixed POPC/POPS large unilamellar vesicles with varied POPS content. The order parameters were constructed as previously, but the results are displayed in little different manner (***Figure IV-6***). On the same graph POPS-d31 lipid order parameters are displayer for the membrane with various POPS content. The effect of temperature increase can be assessed by comparison of the left and the right graph, and pH change effect may be compared on the corresponding upper and lower graphs. Order parameters scale ($S_{C\text{-}D}$, Y axes) was zoomed in order to better distinguish between various quadrupolar splittings. At pH 7.4 and 298K (25°C) the POPS-d31 quadrupolar splittings are practically not resolved for various lipid compositions (***Figure IV-6***, A), but at increased temperature (37°C) the POPS lipid ordering depends strongly on POPS content (***Figure IV-6***, B). Such temperature rise has virtually no effect on the POPC/POPS-10% membranes (on its deuterated POPS lipid component, to be more precise), but in the same time relative order parameter decrease is about 0.91 for POPC/POPS-d31-25% membrane. Of course, this effect can result from the fact that bigger

concentration of reporter lipid was used in the latter case. As indicated in a ***Table IV-1***, the deuterated POPS lipid content varies for various membrane compositions from 10% of total lipid to 25%. But this dependence was not subsequently confirmed by analogous experiment at pH 5 (***Figure IV-6***, C and D), where there was no correlation with POPS content observed, and effect of temperature was rather small. It probably means that the lipid organization is also affected by pH, which should be taken into account when analysing the peptide order perturbation effect at various pH and temperatures.

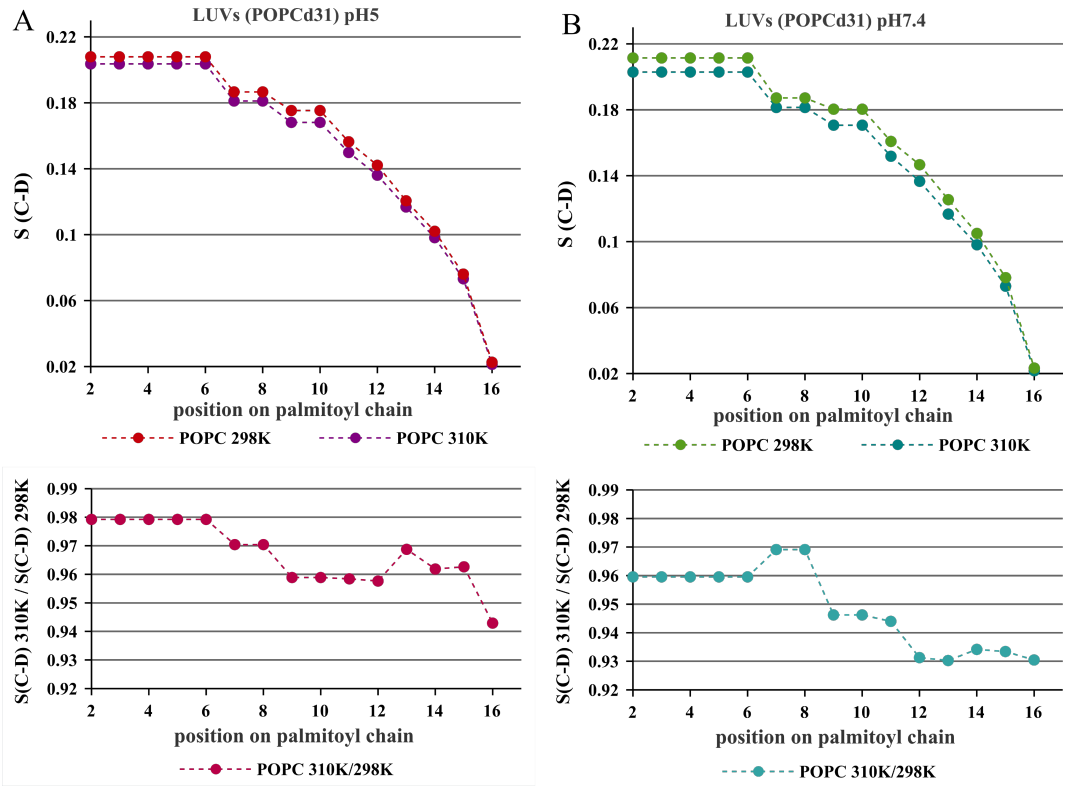

Figure IV-5. The effect of the temperature on the POPC membrane order.
A – pH 7.4, B – pH 5,
The figures below show the relative changes of membrane order when temperature increases from 298K to 310K.

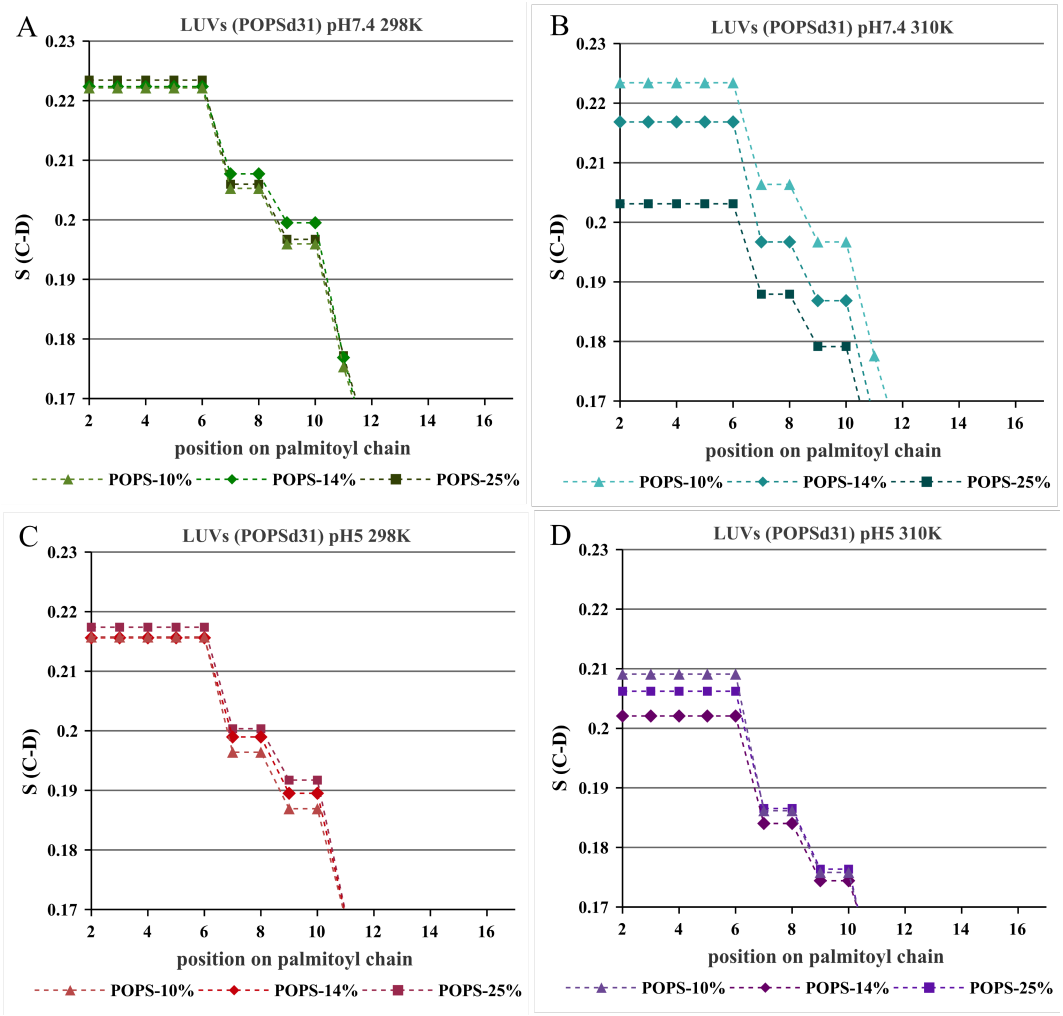

Figure IV-6. The effect of the varied temperature and pH on POPS lipid order in POPC/POPS mixed membranes.
A – pH 7.4 298K,
B – pH 7.4 310K
C – pH 5 298K,
D – pH 5 310K.

POPC-d31 lipid order perturbation by LAH4-L1 in zwitterionic membranes at various temperature and pH conditions.

The series of deuterium static solid-state NMR experiments on POPC-d31/POPC lipid bilayers was recorded at various peptide concentrations, buffers (pH 7.4/5), temperature conditions (T=25°C/37°C) and the effect of temperature and pH change on the relative order perturbation between different concentration series compared to each other.

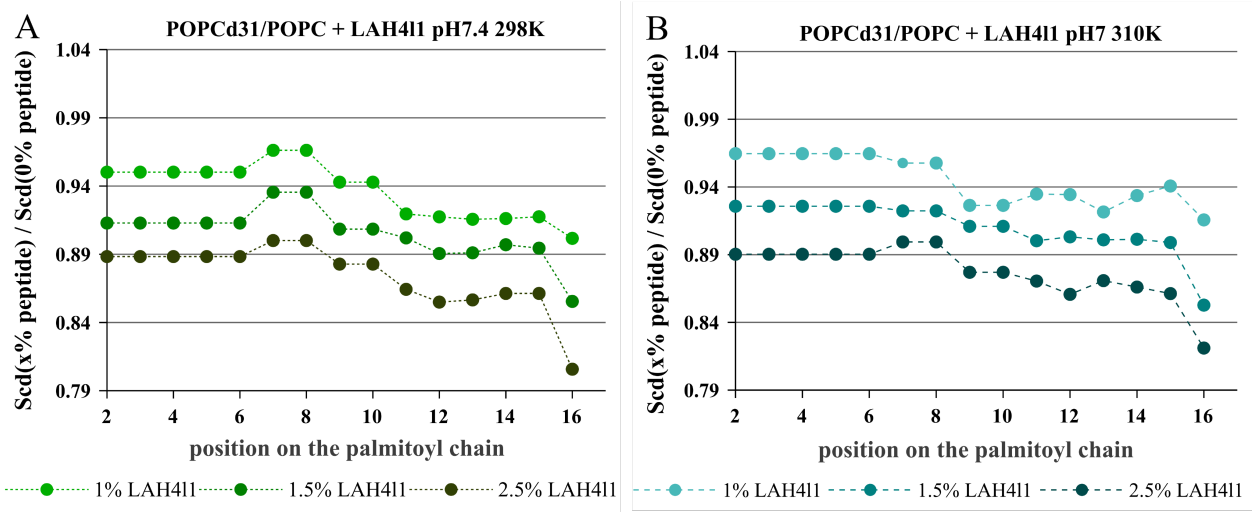

Figure IV-7. The effect of temperature change on the POPC-d31 relative order perturbation. A – 298K, B – 310K

In a ***Figure IV-7*** the POPC-d31 order parameter profiles are displayed for POPC-d31/POPC membrane with 1%, 1.5% and 2.5% *molar* LAH4-L1 peptide embedded at 298K and 310K. The whole order parameters profile is provided thus it can be assessed which segment of the palmitoyl chain is most affected by the presence of peptide. The confidence interval of *relative order parameters* determination is about 0.01-0.02.

Figure IV-7 shows that the temperature increase has quite small effect on the POPC-d31 relative quadrupolar splitting for different LAH4-L1 concentration series. It should be precised that generally the rise of temperature causes the membrane to be more fluid (***Figure IV-5***). By displaying the *relative order parameters* S_{CD} (x% LAH4-L1) / S_{CD} (0% LAH4-L1) the effect from changing membrane fluidity with temperature is already accounted for. Such the effect of temperature on the mechanism of peptide interaction with lipid bilayer was compared, rather than the effect of temperature on the membrane properties. *The preliminary conclusion can be done that the increase of the temperature from 298K to 310K does not influence the mode of peptide interaction with POPC membrane.*

Next the effect of pH change from acidic to neutral on the POPC-d31 relative order perturbation in POPC lipid bilayer was tested as well (***Figure IV-8***). The changes in POPC lipid order perturbation by LAH4-L1 between pH 5 and pH 7.4 are rather small, however there is one noticeable difference. At pH 5 upon adding the first portion of peptide (1 mole%) order parameter drops to around 0.9, but does not change much when incorporating additional portion (1.5 mole%). At pH 7.4 the effect of peptide concentration on the lipid perturbation is more linear (***Figure IV-8***, B).

Those results are consistent with ^{15}N static NMR investigation on peptide inserted in mechanically oriented POPC bilayer. We were able to show that at elevated peptide concentration (3 mole%) at pH 5 LAH4-L1 adopts transmembrane and in-planar alignments simultaneously, but at 1 mole% peptide at pH 5 it adopts only in-planar orientations (***Figure III-6***). At pH 7.4 and in the presence of 1 *mole*% LAH4-L1

the peptide adopts mostly transmembrane alignments (***Figure III-5***), but about 40% of peptides are forced to adopt other orientations (in-planar, mosaic spread) when the concentration of peptide is increased to 3*mol*%. This could explain why the POPC order perturbation by LAH4-L1 at pH 5 and at pH 7.4 differs quite significantly upon addition of small amounts of peptide (***Figure IV-8***) and increases less when the peptide-to-lipid ratio further increases. However it is necessary to mention one important difference in sample preparation for ^{15}N NMR experiment in oriented lipid bilayer and ^{2}H NMR experiment on vesicles. For ^{15}N NMR measurement the peptide is reconstituted into mechanically supported lipid bilayers with only a thin water layer present, thus the peptide is forced to be closely associated with the membrane. In contrast, for ^{2}H experiment concentration of POPC (in form of vesicles) is around 100mM. The suspension is crowded with vesicles, yet the peptide partitioning equilibrium between hydrophilic and hydrophobic phase could be reached. In the case of mixed POPC/POPS vesicles the peptide is attracted to the surface of membrane by additional electrostatic forces.

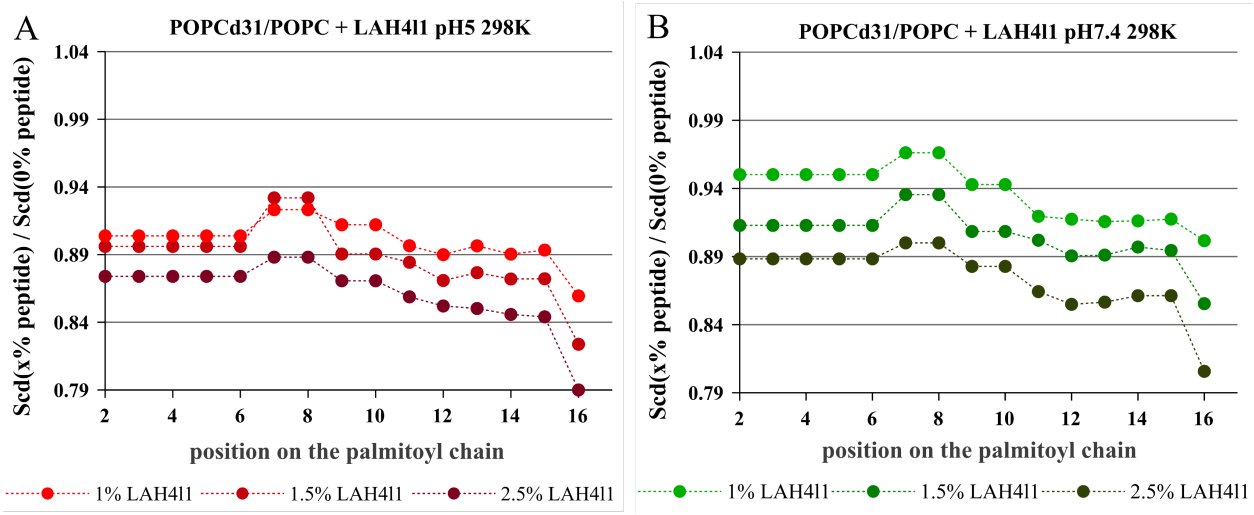

Figure IV-8. The effect of pH change on the POPC-d31 relative order perturbation in POPC lipid bilayer. A – pH 5, B – pH 7.4

POPS-d31 lipid order perturbation by LAH4-L1peptide in mixed POPC/POPS vesicles at various temperature and pH conditions.

In a next step the POPS lipid order perturbation by LAH4-L1 was tested in the series of measurements, when the POPC/POPS lipids molar ratio was varied (10, 14, 25 mole% of POPS). The effect of pH and temperature was investigated as well.

In a ***Figure IV-9*** the POPSd31 order parameter profiles are displayed for POPC/POPS mixed membranes with 0.5 mole% and 1 mole% LAH4-L1 embedded at pH 7.4 and pH 5. On each individual graph the magnitude of the order perturbation by LAH4-L1 was compared for mixed POPC/POPS model membranes with varied POPS fraction.

At pH 5 and a 0.5 mole% peptide concentration the POPS-d31 relative order perturbation is larger for the membranes with smaller POPS fraction (***Figure IV-9***, B). But with 1 mole% of peptide embedded the dependence is inverted (***Figure IV-9***, D). The origin of such behaviour cannot be explained clearly with solely the ^{2}H NMR data available. Please note that the sample of POPC/POPS-25% membranes was prepared with1.5 mole% instead of 1 mole% of LAH4-L1 (***Figure IV-8***, D). It explains much bigger POPS-d31 order perturbation for mixed POPC/POPS-25% membrane.

At pH 7.4 and 298K the relative order parameters don't differ much for various lipid compositions (±0.03) (***Figure IV-9***, A). The magnitude of order perturbation is smaller at pH 7.4 than at pH 5 (***Figure IV-9***, A and

B). Moreover the increase of peptide concentration from 0.5 to 1mole% does not have any noticeable effect on the POPS order perturbation at pH 7.4 (***Figure IV-9***, C), but causes quite significant changes at pH 5. When taking a closer look on the changes in order parameters of each POPS palmitoyl chain segment, one notices that the peptide affects the order especially of the middle and terminal segments at pH 5 when compared to pH 7.4. All those observations taken together reflect the difference in peptide mode of interaction with POPC/POPS mixed membrane at pH 5 and pH 7.4.

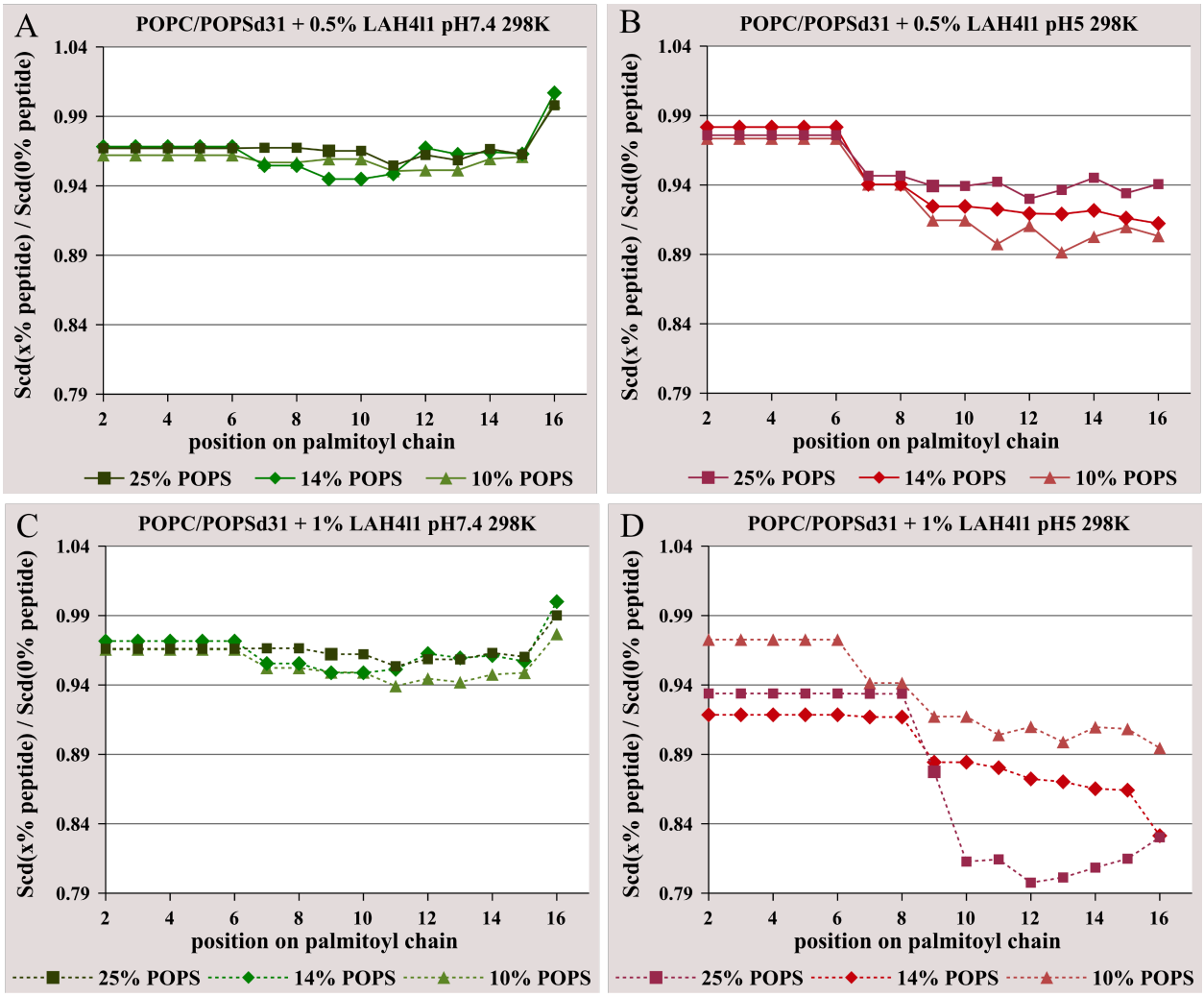

Figure IV-9. Effect of the lipid composition on membrane perturbation by LAH4-L1, and its correlation with pH and the peptide concentration (POPS-d31 quadrupolar splitting was monitored)
A – 0.5% LAH4-L1, pH 7.4
B – 0.5% LAH4-L1, pH 5
C – 1% LAH4-L1, pH 7.4
D - 1% LAH4-L1, pH 5 (1.5% of peptide embedded into POPC/POPS-25% membrane).

Further the effect of temperature increase on the POPS perturbation within the same concentration series was also tested.

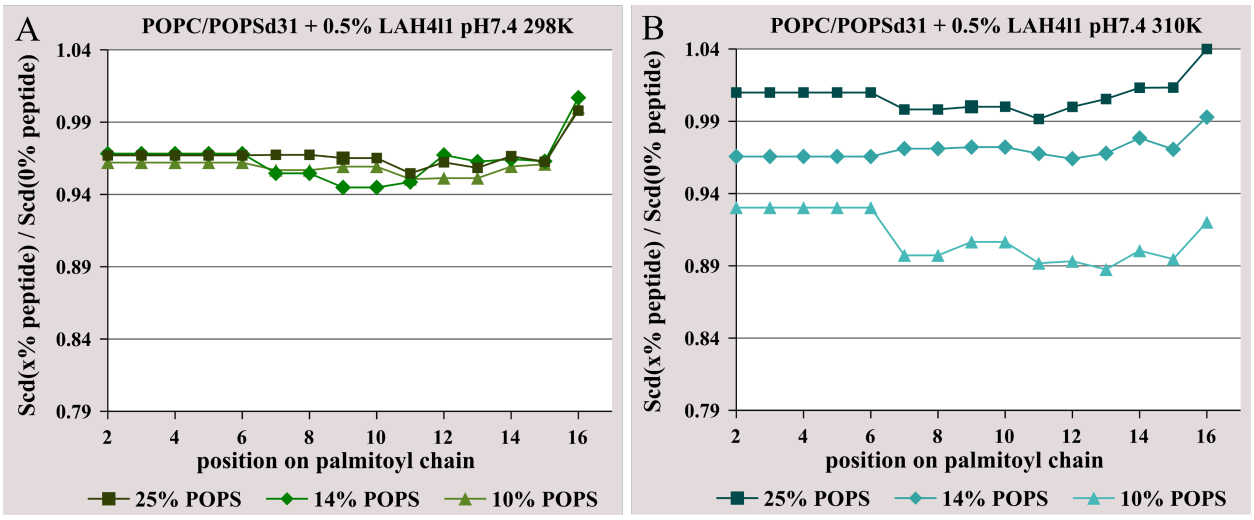

Figure IV-10. Effect of the lipid composition on membrane perturbation of POPSd31 in POPC/POPS membranes by 0.5 mole% LAH4-L1 at pH7.4, as a function of temperature and lipid composition (POPSd31 quadrupolar splitting).
A – 298K, B – 310K.

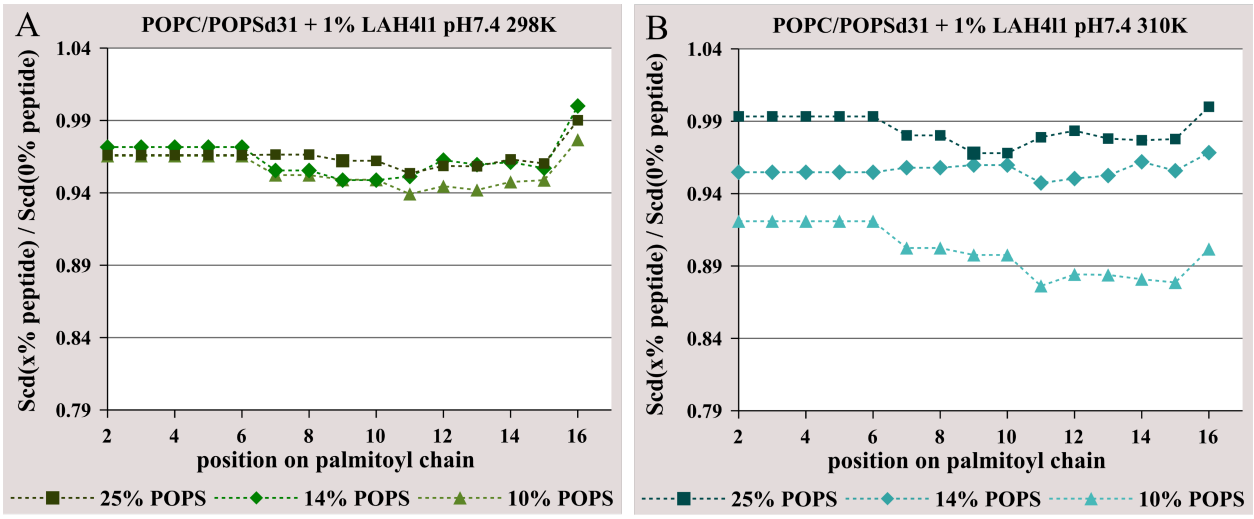

Figure IV-11. Effect of the lipid composition on membrane perturbation of POPSd31 in POPC/POPS membranes by 1 mole% LAH4-L1 at pH 7.4, as a function of temperature and membrane lipid composition (POPSd31 quadrupolar splitting).
A – 298K, B – 310K

The relative order perturbation, caused by LAH4-L1 insertion, differs largely between the membranes with various POPS fraction at 310K and pH 7.4. This difference in relative order perturbation for various membranes is in the range of 0.11-0.12 (***Figure IV-10***, B and ***Figure IV-11***, B). Whereas the order of the POPC/POPSd31-14% membrane changes very little upon temperature increase, the relative order perturbation of POPS-d31 in POPC/POPS-25% *increases* with the temperature (0.99 – 1.02 ***Figure IV-10***, B and 0.98 – 1.01 ***Figure IV-11***, B). In contrast the value of POPS-d31 relative order perturbation *decreases* with the temperature (0.89 – 0.93 ***Figure IV-10***, B; 0.88 – 0.92 ***Figure IV-11***, B). I would like to remind that in previous section it was shown that the temperature increase has literally no effect on POPS order parameters in peptide-free POPC/POPS membranes, but it affects POPC/POPSd31-25%

membranes such order parameters decrease by about 0.91 (***Figure IV-6***). The effect of temperature on membrane order is already accounted in the expression of *relative order perturbation* (S_{C-D} with peptide / S_{C-D} lipids only). Therefore temperature affects the membrane with embedded peptide differently than the membrane alone.

Such at 310K the influence of POPS content on the POPS-d31 *relative* order perturbation by peptide become to be better seen. The smaller is POPS content, the larger is its order perturbation by peptide at same LAH4-L1 molar concentration (***Figure IV-10***, B and ***Figure IV-11***, B). The same dependence was observed at pH 5 and small peptide concentration (0.5mole%, ***Figure IV-9***, B), but at higher peptide concentrations the correlation is inverted (1mole%, ***Figure IV-9***, D).

It will be shown later in this chapter that the peptide associates preferably with POPS lipid, so it seems convenient to recalculate the peptide molar concentration with respect to the POPS lipid. For instance in the sample containing POPC/POPSd31-25% membranes and 0.5mole% LAH4-L1, there will be present one peptide molecule per 200 lipid molecules, but one peptide molecule per 50 POPS lipids (2mole%). Such *re*-calculations for all samples are summarized in the ***Table IV-2***.

Table IV-2. LAH4-L1 concentration series used in ^{2}H NMR experiment.

composition	mole% (per total lipid)	mole% (per POPS)	Total negative/positive charge ratio	
			pH 5	pH 7
POPC/POPS-25%	0.5	2	5.55	10
	1	4		5
	1.5	6	1.85	
POPC/POPS-14%	0.5	3.5	3.17	5.71
	1	7	1.59	2.86
POPC/POPS-10%	0.5	5	2.22	4
	1	10	1.11	2

In the scope of this calculation it does not seem strange that LAH4-L1 perturbs most efficiently POPS lipids order when the fraction of POPS is the smallest (10%), because actual peptide/POPS ratio is bigger in this membrane. But at pH 5 (1mole% peptide) the situation seems to be inverted. It is difficult to give the comprehensive explanation why this relation is different. But there is one thing that should be highlighted. For POPC/POPS membrane samples with 1mole% (1.5mole%) of embedded peptide at pH 5, the negative-to-positive total charge ratios are the smallest among all other preparations, equal 2/1 to 1/1, thereby reducing the electrostatic forces that are responsible for the phase separation into domains enriched by peptide and POPS. As a result under these conditions the peptide may distribute more evenly between POPC and POPS thereby resulting in a local peptide concentration around POPS intermediate between the two values tabulated in ***IV-2***.

Also I would like to remind that in the previous chapter it was shown in ^{15}N ssNMR experiment that LAH4-L1 adopts preferably transmembrane alignment at pH 7.4 and aligns parallel to the bilayer plane at pH 5. This was valid for all membrane compositions tested. Deuterium static NMR experiments confirmed that the effect of POPS order perturbation by LAH4-L1 is bigger at pH 5. So we can conclude that the *in-planar* alignment of peptide is related to the greater membrane order distortion by LAH4-L1. On the contrary the peptide in its transmembrane alignment has a smaller effect on the lipid order.

In a ***Figure IV-12*** one can find the graphical summary of the experimental results presented and discussed so far. The data are re-combined in order to make the presentation clearer. The concentration and pH series are displayed in the same graphs, and the membrane perturbation by LAH4-L1 at two various pH conditions could be assessed through various membrane compositions (POPS content id

decreasing from A to D). For POPS containing membrane the POPS-d31 lipid order profiles were measured, when for POPC membrane order parameters of POPC-d31 were taken.

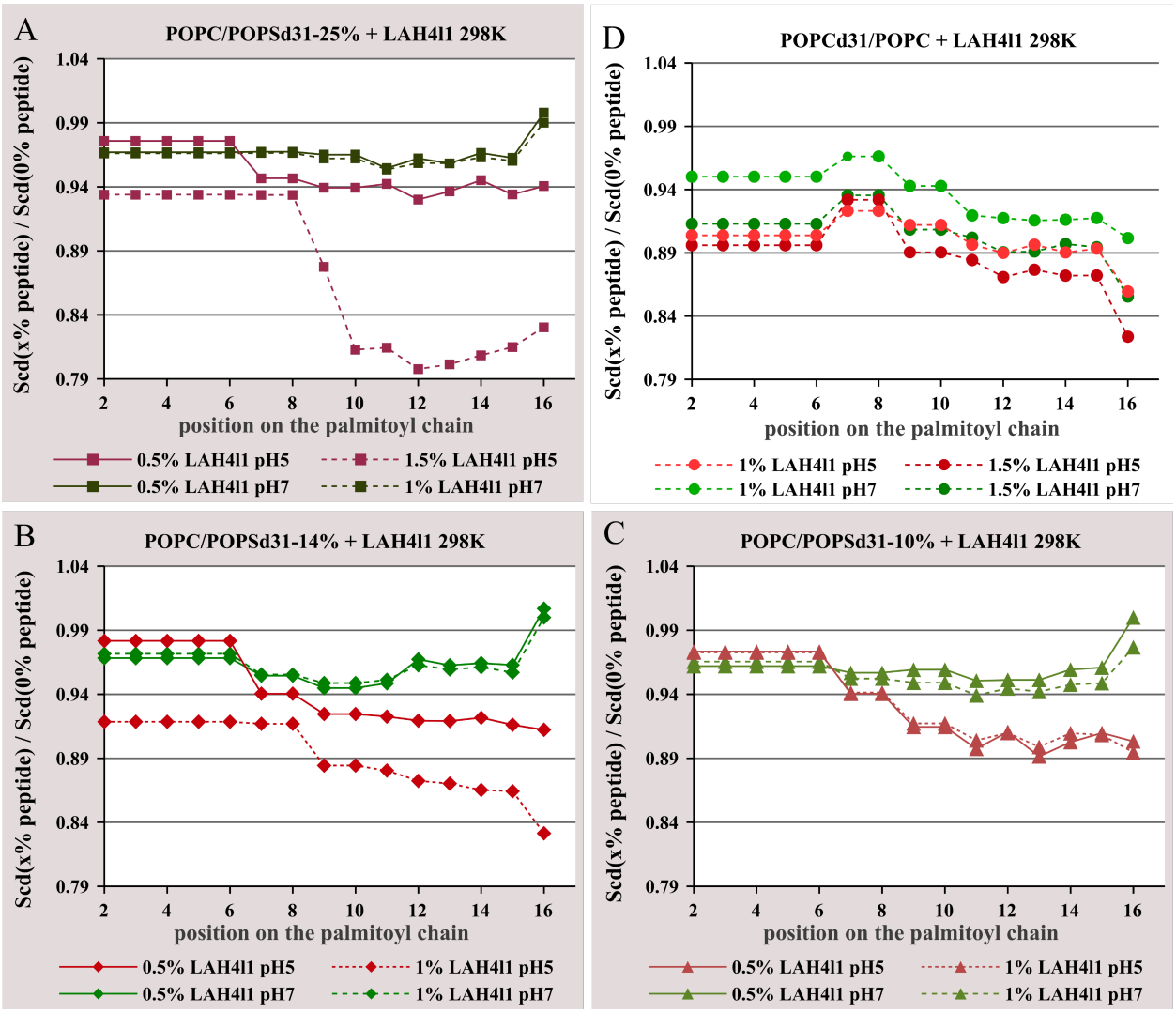

Figure IV12. Effect of pH and LAH4-L1 peptide molar concentration on POPC/POPS-d31 and POPC/POPC-d31 order parameters.
A – POPC/POPS-25%, pH 7.4/pH 5
B – POPC/POPS-14%, pH 7.4/pH 5
C – POPC/POPS-10%, pH 7.4/pH 5
D – POPC, pH 7.4/pH 5

The most important conclusions that could be drawn from this investigation are next. The membrane perturbation by LAH4-L1 peptide is bigger at pH 5 than at pH 7.4, and this observation is valid for all membrane compositions tested. Of note is that the middle and terminal segments of POPS acyl chain are more affected at pH 5 than at pH 7.4 (***Figure IV-12***, A-C), but the same relation cannot be expanded on the acyl segment near lipid head group.

For POPC/POPS mixed membranes at pH 7.4 and 298K the incorporation of additional portion of peptide (from 0.5% molar to 1% molar) practically does not increase the order perturbation (***Figure IV-12***, A-C). While for POPC zwitterionic membranes at pH 7.4 the increase of order perturbation by additional portion of peptide, as well as the values of *relative order perturbation,* are more noticeable (***Figure IV-12***, D). At pH 5 the incorporation of additional amount of lipid cause quite important POPS-d31 relative order parameters decrease for POPC/POPS-25% and POPC/POPS-14% (***Figure IV-12***, A and B), however

1.5mole% of peptide was added to POPC/POPS-25% LUV at pH 5, while only 1mole% to POPC/POPS-14% and POPC/POPS-10% LUV.

POPC-d31 lipid order perturbation by LAH4-L1 into mixed POPC/POPS LUV at pH7.4

So far only POPS-d31 lipids order parameters in the POPC/POPS mixed membranes were analysed, as well as POPC-d31 order parameters in POPC lipid bilayers. In order to complete the picture, the series of samples where POPC palmitoyl chain in POPC/POPS mixed membranes was labelled with ^{2}H (***Table IV-1***). The results were combined with those obtained for POPS-d31 order perturbation in POPC/POPS membranes and POPC-d31 orders in POPC membranes.

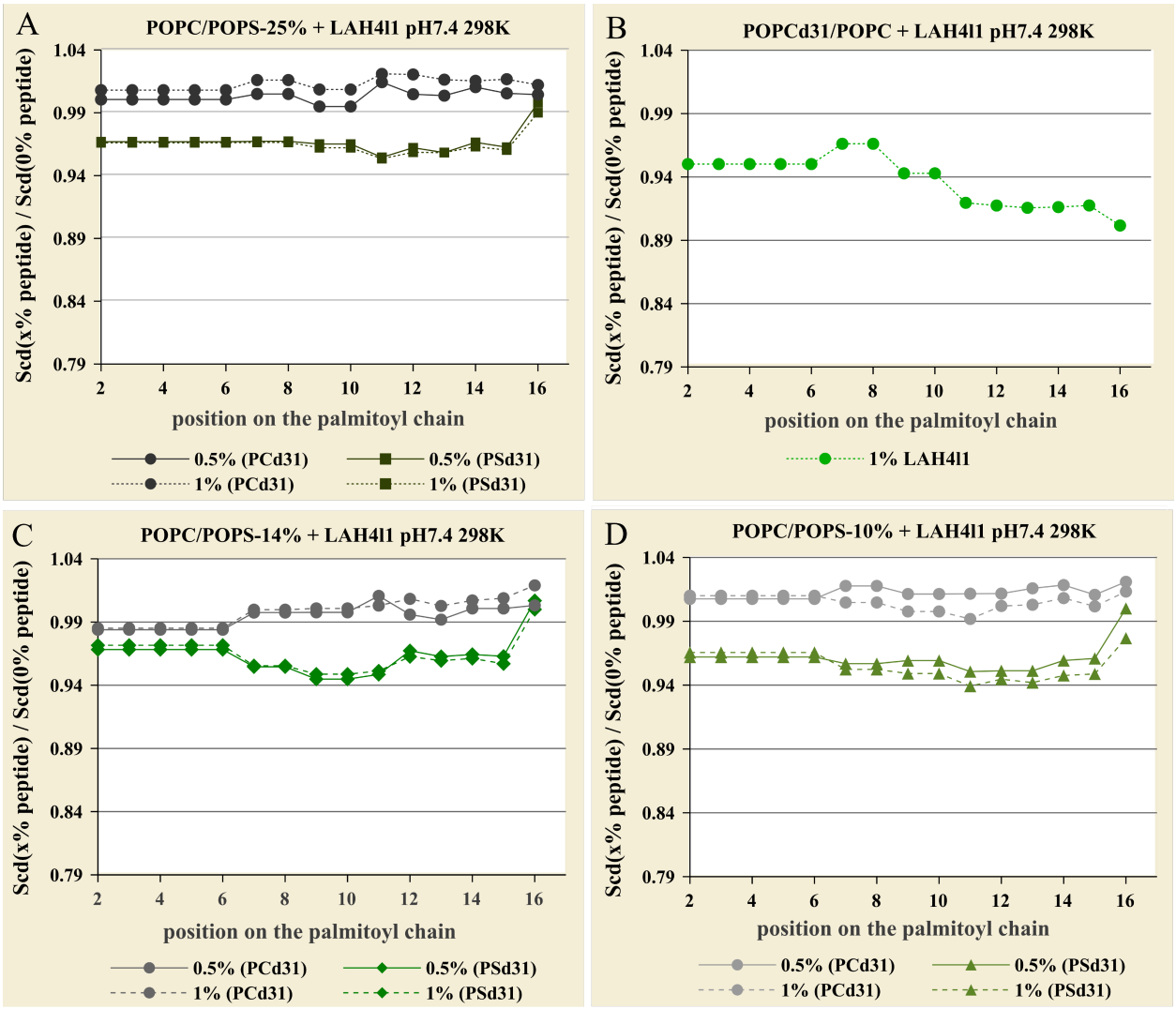

Figure IV-13. Effect f the lipid composition on membrane perturbation by LAH4-L1 at varied peptide concentrations (POPS-d31 and POPC-d31 lipid monitoring), pH 7.4, 298K.
A – POPC/POPS-25% membrane
B – POPC
C – POPC/POPS-14%
D – POPC/POPS-10%

The results (***Figure IV-13***) clearly show that LAH4-L1 peptide interacts preferably with POPS lipid molecules. POPC-d31 relative order parameters are above 1 for almost entire acyl chain in POPC-d31/POPS mixed membranes. It means that when interacting preferably with POPS lipid molecules LAH4-L1 peptide increase the dynamics of POPS -CH2- residues, but restricts the movement of POPC lipid tails.

Though this 'ordering effect' may be within error bar for this type of experiment, and it has to be double-checked.

DISCUSSION (structural characteristics of LAH4-L1 – membrane interaction).

The alignment of LAH4-L1 in uniaxially *oriented* mixed lipid bilayers was tested at pH 5 and pH 7.4 by ^{15}N and ^{31}P solid-state NMR spectroscopy. POPC lipid bilayers with various fractions of negatively charged POPS (0%, 10%, 14% and 25%) were used in the study as membrane model system in order to test the effect of charge, and POPS content in particular, on LAH4-L1 membrane alignment at pH 5 and pH 7.4.

It was shown previously that the parent peptide LAH4 adopts predominantly transmembrane alignment at pH around 7 in POPC oriented lipid membranes, and at pH 5 the helices are oriented parallel to the membrane surface (Bechinger, 1996; Bechinger et al., 1999). The tendency to adopt in planar to membrane helix orientation was confirmed for LAH4 reconstituted into mixed anionic POPC/POP**G**-25% membranes at various peptide concentrations (1mole%, 2mole% and 4mole%). Remarkably, that in oriented lipid bilayers consisting of 100% anionic lipid POPG LAH4 does not switch to transmembrane orientation when pH rises to 7.5 (*Barbara Perrone, PhD thesis 2011*). In present investigation the anionic component is presented by POPS lipid, and maximum anionic lipid content of 25%.

The results of proton decoupled ^{15}N solid-state NMR measurements with LAH4-L1 peptide confirm general tendency of LAH4 peptides to switch the membrane alignment from transmembrane to in planar when the pH decreases from 7 to 5. At pH 7.4 the major fraction of peptide is oriented transmembrane in all four types of lipid bilayers tested, but there is another component of solid-state ^{15}N proton decoupled spectra, which may be referred to LAH4-L1 mosaic spread around all possible orientations.

Quite interesting behaviour of LAH4-L1 was observed when increasing peptide molar concentration. In mixed POPC/POPS-25% lipid bilayer at pH 7.4 peptide does not cause bigger membrane order perturbation when additional portion of peptide was incorporated (from 2 to 4mole% LAH4-L1, observed by ^{31}P NMR). On the contrary, it seems that this promotes the refinement of peptide transmembrane alignment. At pH 5 increase of peptide-to-lipid ratio (up to 4mole%) causes a huge membrane disordering at the level of the phospholipid head group when at the same time LAH4-L1 remains oriented predominantly parallel to the bilayer surface. The behaviour of LAH4-L1 peptide in mixed POPC/POP**G**-25% membranes at pH 7.4 is rather similar to that in POPC/POPS mixed membrane (Figure III.7), which suggests that rather surface charge is important, than any specific interaction with lipids.

The behaviour of the peptide under the condition of high peptide surface concentration is quite different in zwitterionic POPC membranes. By increasing the molar concentration of LAH4-L1 from 1mole% to 3mole% the peptide is forced to partially switch its orientation toward in planar at pH 7.4, and to augment its transmembrane component at pH 5 (***Figures III-5, III-6***). Surprisingly, none of this peptide orientation shifts does not cause big membrane order destabilization, as shown by ^{31}P NMR spectra. Those results suggest that the mechanisms of peptide permeation into neutral POPC and mixed negatively charged POPC/POPS membranes are different. It has been shown previously by tryptophan fluorescence and linear dichroism spectroscopy that addition of anionic lipid POPG to POPC vesicles stabilizes melittin peptide in-planar alignment, whereas in pure POPC membranes melittin goes transmembrane at high peptide surface concentration (more than 3mole%) (Svensson et al., 2011). Therefore the presence of negatively charged lipids stabilizes the cationic peptides in-planar orientation.

The ^{15}N peak that corresponds to peptide transmembrane alignment appears in the range of 190 – 205ppm, and the peak corresponding to in-planar alignment – in the of 75 – 90ppm (Table III.1). The tensor parameters σ_{11}, σ_{22}, and σ_{33} were measured previously for [^{15}N-Leu16]LAH4 static powder

(*Barbara Perrone, PhD thesis 2011*). They equals to 219±3, 86±3, and 66±3. The smaller chemical shift that we observed for transmembrane orientation of LAH4-L1 and bigger CS for in-planar alignment indicates that peptide helix does not orient perfectly parallel or perpendicular to lipid bilayer axes (and B_0 correspondingly), but is slightly tilted. The conclusions were drawn assuming that the tensor parameters of [^{15}N-Leu14]LAH4-L1 are close to those measured with its homologue LAH4. In order to calculate the tilt angle more parameters are required and it was out of the scope of present work.

The relation between the membrane disordering capabilities of LAH4 pH-responsive peptides at acidic pH and their gene delivery activity have previously been shown (Mason et al., 2006a). In the present work the ^{2}H wide-line NMR spectroscopy on deuterated POPC and POPC/POPS vesicles was employed to obtain the detailed characteristics of LAH4-L1 insertion into lipid bilayer at pH 5 and pH 7.4, at varied peptide concentration and negatively charged lipid content (% POPS = 0, 10, 14, 25).

Our ^{2}H solid-state NMR data suggest that the order of POPS lipids is distorted more than POPC lipid acyl chains order when LAH4-L1 is inserted into mixed POPC(d31)/POPS(d31) LUV at pH 7.4. Actually, peptide has no effect or even slight ordering effect on POPC lipids. The result indicates that LAH4-L1 interacts preferably with POPS lipid molecules, presumably causing the lipid domain separation. Such mode of interaction was suggested previously for LAH4 peptide, when the similar order perturbation profiles were obtained upon LAH4 interaction with POPC(d31)/POPS(d31)/cholesterol=70:15:15 membranes at pH 7.5 (Mason et al., 2006a). LAH4 exhibits some order perturbation effect on POPS-d31, but no effect or even some ordering on POPC-d31 acyl chain.

At pH 5 LAH4 had a disordering effect on both POPS and on POPC lipid acyl chains, however the distortion of POPS lipid was of much greater amplitude (Mason et al., 2006a). Therefore, lipids order perturbation by LAH4 peptide is stronger at pH 5, which suggests that peptide alignment in membrane is a key in determination of the lipid order. Another elegant experiment was performed with LAH4-L1 peptide reconstituted at the concentration of 1.5*mole*% into POPC/POPS/cholesterol = 85:15:30 vesicles at varied pH conditions (pH = 4, 5, 6, 7, 8) with POPC-d31 or POPS-d31 label used in separate experiments (Iacobucci et al., 2012). The authors suggest that the change in POPC-d31 as well as POPS-31 order parameters was due to peptide rearrangement from in-planar to transmembrane alignments, rather than due to the change in peptide – membrane affinity.

In the present work we confirmed the previous finding that the membrane disordering by LAH4-L1 is determined by its alignment in lipid bilayer. We were able to compare directly the effect of peptide on ^{2}H NMR spectra of large unilamelar vesicles suspension with its membrane alignment assessed by ^{15}N NMR spectroscopy. The effect of peptide re-orientation is readily seen in ^{2}H NMR experiment on zwitterionic POPC vesicles. At 0.5*mole*% peptide concentration the perturbation of POPC vesicles by LAH4-L1 is distinctly bigger at pH 5, when at 2.5*mole*% peptide concentration the order profiles at pH 5 and pH 7.4 are rather similar (***Figure IV-8***). ^{15}N NMR spectra reveal that at low peptide concentration (1*mole*%) LAH4-L1 adopts preferably in-planar alignments at pH 5 and transmembrane – at pH 7.4. But in the condition of higher peptide surface concentration (3*mole*%) LAH4-L1 adopts both in-planar and transmembrane orientations at pH 5 as well as at pH 7.4 (***Figures III-5, III-6***). On the contrary, the increase of peptide concentration embedded into mixed POPC/POPS-d31 membranes promotes even bigger discrimination between the order profiles at pH 7.4 and pH 5 (***Figure IV-12***). And those results are consistent with peptide's orientation stabilization effect of negatively charged lipids (***Figures III-3, III-4***).

Those observations taken together reveal that in zwitterionic POPC lipid bilayer LAH4-L1 interaction with membrane can be explained by a simple partitioning mechanism whereas in mixed POPC/POPS membranes peptide selective interaction with POPS might cause the lipid reorganization. Such lipid

domains separation by antimicrobial and cell-penetrating peptides was demonstrated in various lipid mixtures and is believed to play an important role in non-endocytic CPP internalization (Epand et al., 2010; Wadhwani et al., 2012).

CONCLUSIONS.

The most important conclusions that can be made when discussing the results of ^{2}H static solid state NMR experiment on LAH4-L1 interaction with deuterated lipid vesicles (LUVs), as well as the results of ^{15}N static solid state NMR experiment on the peptide helix orientation in mechanically oriented lipid bilayers are summarized below.

- LAH4-L1 peptide interacts preferably with POPS lipids in POPC/POPS mixed vesicles at pH 7.4, which was shown by comparison of the POPS-d31 and POPC-d31 order parameter profiles. POPC-d31 order parameters were not measured for POPC/POPS vesicles at pH 5 in the current work, but it as shown previously that LAH4 peptide interacts with POPS lipids in mixed membranes at pH 5 as well (Mason et al., 2006a). The electrostatic attraction plays a great role in LAH4-L1 interaction with POPC/POPS membranes.
- LAH4-L1 perturbs the lipid order more significant at pH 5 than at pH 7.4. This conclusion is valid for POPS order perturbation in POPC/POPS mixed membranes, as well as for POPC lipid order in the membranes, which consist of zwitterionic POPC lipid only. This effect can be pretty well explained in the scope of ^{15}N NMR experimental results. At pH 7.4 and the small peptide concentrations (1-2% molar) LAH4-L1 helix adopts preferably *transmembrane* alignment when embedded into POPC/POPS and POPC oriented lipid bilayers, and at pH 5 it aligns predominantly parallel to lipid bilayer. When the peptide aligns parallel to the membranes it creates more freedom of movements for the middle and terminal segments of lipid palmitoyl chain. The model was proposed earlier for LAH4-L1 interaction with mixed POPE/POPG membranes (Mason et al., 2007c) and for LAH4 peptide interaction with mixed anionic model membranes (Georgescu et al., 2010; Mason et al., 2006a). It is schematically illustrated in a ***Figure IV-14***.

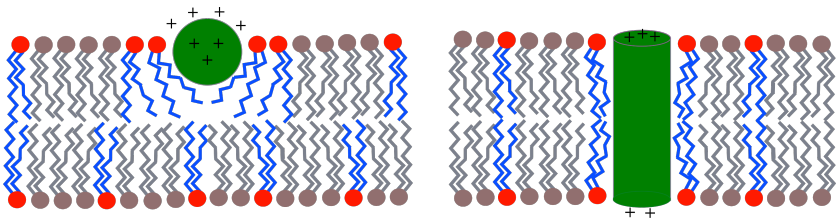

Figure IV-14. Illustration of POPC/POPS membrane perturbation by LAH4-L1 at pH 5 (left) and pH 7.4 (right). POPS lipid depicted with red ball and blue chains, POPC – brown ball, grey chain, LAH4-L1 – green cylinder.

- The peptide high surface concentration effect on the peptide alignment into membranes was tested by ^{15}N solid state NMR on mixed POPC/POPS-25% membranes, as well as on zwitterionic POPC membranes at pH 5 and at pH 7.4. The augmentation of peptide molar concentration from 2% to 4% in POPC/POPS-25% lipid bilayers encourage the peptide to adopt even more defined transmembrane alignment at pH 7.4 and more defined in-planar alignment at pH 5. In POPC oriented membranes LAH4-L1 peptide is forced to adopt both transmembrane and in-planar orientation simultaneously under the crowding conditions (3% molar peptide) at pH 7.4 and pH 5. Taking into account the quality of 15N spectra, especially one recorded with the sample at pH 5, we could exclude the presence of disordered fraction. However, in order to confirm that the peptide indeed switches its

orientation under the conditions of high peptide surface concentration, we would need to record two-dimensional ^{15}N-^{1}H heteronuclear coupling correlation spectra (broadband PISEMA) on the sample of question.

V. LAH4-L1 SECONDARY STRUCTURES STUDIED BY CIRCULAR DICHROISM

Circular dichroism spectroscopy allows assessment the peptide secondary structure when inserted into the model membranes. When large unilamellar vesicles are titrated into peptide solution in the stepwise manner, the binding isotherms can be constructed on the basis of the secondary structure changes.

A series of circular dichroism (CD) measurements was therefore performed to assess peptide association with charged and neutral *large unilamellar vesicles (LUV)*.

MATERIALS AND METHODS

Sample preparation for circular dichroism measurements.

For the circular dichroism measurement the liposomes were prepared accordingly to well established procedures (Hope et al., 1993). For the preparation of large unilamellar vesicles the lipids were mixed in the ratio POPC/POPS=3:1 (25mole% of POPS), POPC/POPS=6:1 (14mole% of POPS), POPC/ POPS=9:1 (10mole% of POPS) and POPC only (0mole% of POPS). The total of 10mg of lipid was solubilised in chloroform-methanol=4:1, vortexed and the solutions were dried under a stream of nitrogen. The samples were exposed to the high vacuum overnight in order to remove all traces of the solvents. The lipid films were rehydrated in 1mL of 10mM acetate buffer at pH≅5.0, and were subjected to five freeze-thaw cycles. The lipid solutions containing ≅13mM total lipids were passed 13 times though the syringe extruder (Avanti Polar Lipids Inc., Alabaster, AL) equipped with 100nm (pore diameter) polycarbonate membrane to obtain POPC/POPS large unilamellar vesicles of approximately 100nm diameter. The phospholipid content of vesicle preparations was determined as inorganic phosphate according to Rouser (Rouser et al., 1970).

The LAH4-L1 (KKALL AHALH LLALL ALHLA HALKKA) peptide stock solution was prepared in the same buffer at pH=5.0 and the concentration of solutions was estimated using the BCA assay (Pierce™, Thermo Scientific, https://www.piercenet.com/instructions/2161296.pdf).

The samples containing 10 (or 4.8), 10, 10 and 11μM LAH4-L1 were titrated with the corresponding amount of POPC/POPS-25%, POPC/POPS-14%, POPC/POPS-10% and POPC vesicles stock solution, respectively. 300μL of each sample was prepared with the following lipid-to-peptide molar ratios:

POPC/POPS-25%. Lipid-to-peptide molar ratios were 0:1, 2:1, 5:1, 10:1, 24:1, 48:1, 100:1, 240:1.

POPC/POPS-14%. Lipid-to-peptide molar ratios were 0:1, 2:1, 5:1, 10:1, 20:1, 50:1, 100:1.

POPC/POPS-10%. Lipid-to-peptide molar ratios were 0:1, 2:1, 5:1, 10:1, 20:1, 50:1, 100:1.

POPC. Lipid-to-peptide molar ratios were 0:1, 3.5:1, 8.6:1, 17:1, 34:1, 86:1, 170:1.

CD measurements and spectra processing.

Circular dichroism measurements were performed on the Chirascan spectrometer (Applied Photophysics Ltd, UK). CD spectra were recorded at 25°C using a 1 mm quartz cell (SUPRASIL, Hellma Analytics) at 260–195nm measurement range, with the data pitch of 1nm, 1nm bandwidth, and the response time of 12-14s/scan.

100nm vesicles without peptide produce unwanted scattering at the low wavelength. Therefore, the CD spectra of the peptides were baseline corrected by subtracting a spectrum of the corresponding LUVs in suspension of similar lipid concentration.

The data were converted to mole residue ellipticity [θ] = deg*cm2/dmol, by using the equation:

$[\theta]=0.1*\theta/(c*n*l)$,

where θ – ellipticity in mdeg, c – concentration in M, n – number amino acid residues in the sequence, l – optical path in cm.

The peptide secondary structure content was estimated using CD program kindly provided by Xiaochun Li Blatter, University of Basel. The program is essentially an MS Excel macro, performing the CD spectral deconvolution based on the least-squares method.

The calculation of percentage of the secondary structures is done using following equations.

$Y_{calc} = f_aY_a+f_bY_b+f_cY_c+f_tY_t$,

f_a - %*mole* of alpha helix, f_b - %*mole* of beta sheet, f_c - %*mole* of random coil, f_t - %*mole* of beta turn.

$f_a + f_b + f_c + f_t = 1$

$\delta^2 = (Y_{calc} - Y_{meas})^2$ least square error;

$\Sigma\delta^2 = \Sigma(Y_{calc} - Y_{meas})^2$ the sum of the least squares.

The reference database set was taken from the publication (Reed and Reed, 1997). The reference spectra are shown in a ***Figure V-1***.

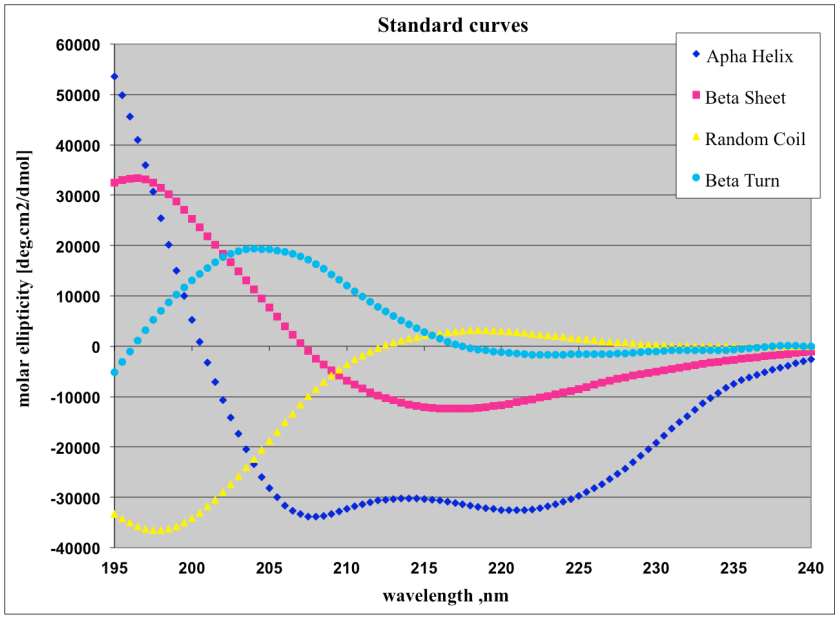

Figure V-1. A set of constructed type spectra for the estimate of peptide secondary structure from the circular dichroism data.

The ellipticity minima at 208nm and 222nm are characteristic for the α-helical structures. Further I compared secondary structures content estimate by spectra deconvolution with estimate based on absorption at 222nm. The helicity of the peptide, f_α, was determined from the mole residue ellipticity [θ] at 222nm as described by Scholtz and co-workers (Myers et al., 1997):

$$f_\alpha = \frac{[\theta]_{222} - [\theta]_{coil}}{[\theta]_{helix} - [\theta]_{coil}}$$

where $[\theta]_{helix}$ and $[\theta]_{coil}$ represent the mole residue ellipticity of a complete helix and coil, respectively.

$[\theta]_{helix} = (-42\,500*(1-3/n) + 100t) = -35096$, where n is the number of amino acid residues, and t is the temperature in °C.

$[\theta]_{coil} = 640 - 45t = -485$,

From these relationships the final formula for alpha-helix content estimate is obtained:

$f_\alpha = ([\theta]_{222} + 485)/-34611$.

RESULTS AND DISCUSSION.

The raw circular dichroism curves of LAH4-L1 titrated with POPC/POPS-10% vesicles are shown in a ***Figure V-2*** (*left*) as well as the corresponding LUV baselines (***Figure V-2***, *right*). After the CD data were corrected on the LUV absorption, the spectra shown in a ***Figure V-3*** are obtained.

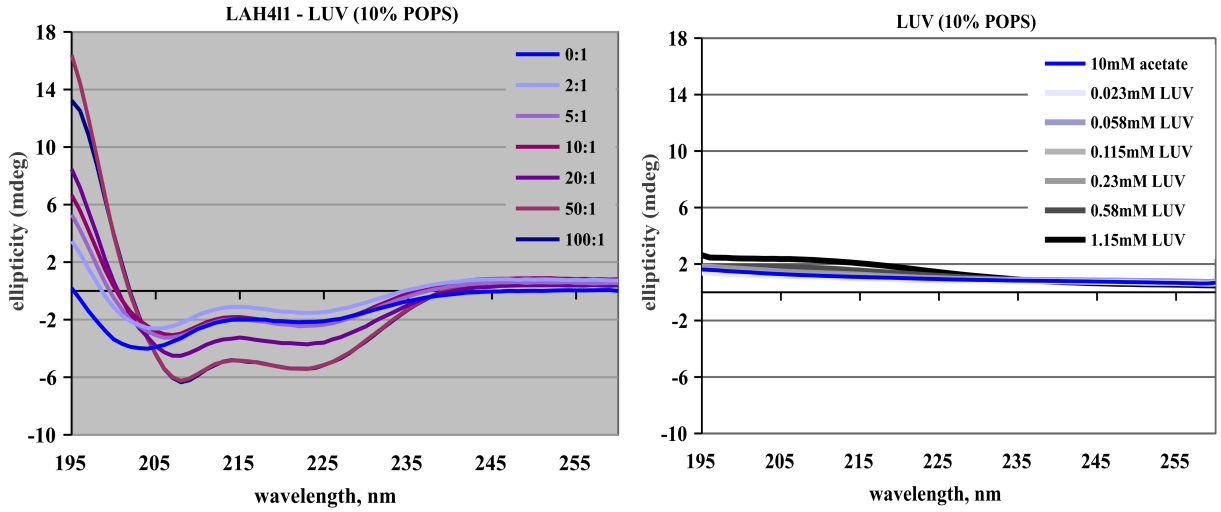

Figure V-2. Circular dichroism curves of *left*) 10µM LAH4-L1 peptide solution in 10mM acetate buffer, titrated with POPC/POPS-10% LUV. Each curve corresponds to particular lipid-to-peptide molar ratio; right) LUV absorption spectra in the range of 260nm – 195nm.

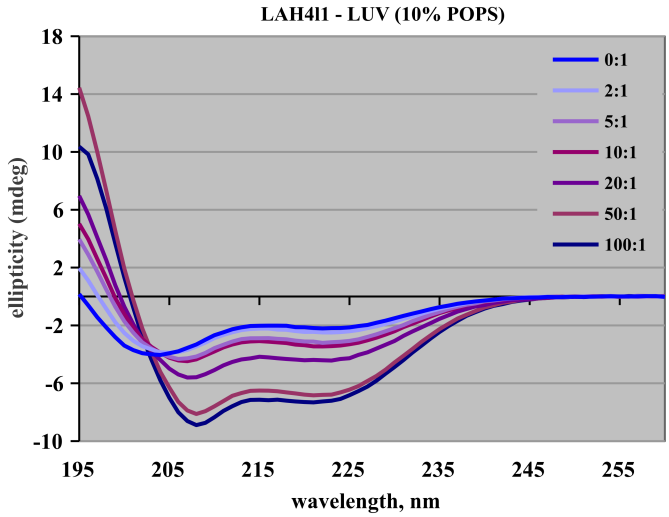

Figure V-3. Circular dichroism curves of 10µM LAH4-L1 peptide solution in 10mM acetate buffer, titrated with POPC/POPS-14% LUV and corrected for LUV absorption. Each curve corresponds to particular lipid-to-peptide molar ratio, indicated in the legend.

If the spectra are not corrected for vesicles scattering, the error in the secondary structures estimate may arise. But the scattering of 100nm lipid vesicles alone not always corresponds to the scattering of lipid vesicles in the presence of peptide. In a ***Figure V-4*** there are CD curves of LAH4-L1 titrated with POPS/POPS-25% and POPC/POPS-14%. The absorption of some curves is higher than expected. For instance the absorption of LAH4-L1 titrated with POPC/POPS-14% LUV at the ratio 1/50 (***Figure V-4***, left, pink curve) is elevated. An even more drastic shift at short wavelength is observed for LAH4-L1 absorption when titrated with POPC/POPS-25% LUV at the ratio 1/20 (***Figure V-4***, right, brown curve). At this particular lipid-to-peptide ratios vesicle aggregation may occur. In these cases the vesicle

background subtraction does not provide a sufficient correction of scattering artefacts and the curves have to be excluded from analysis.

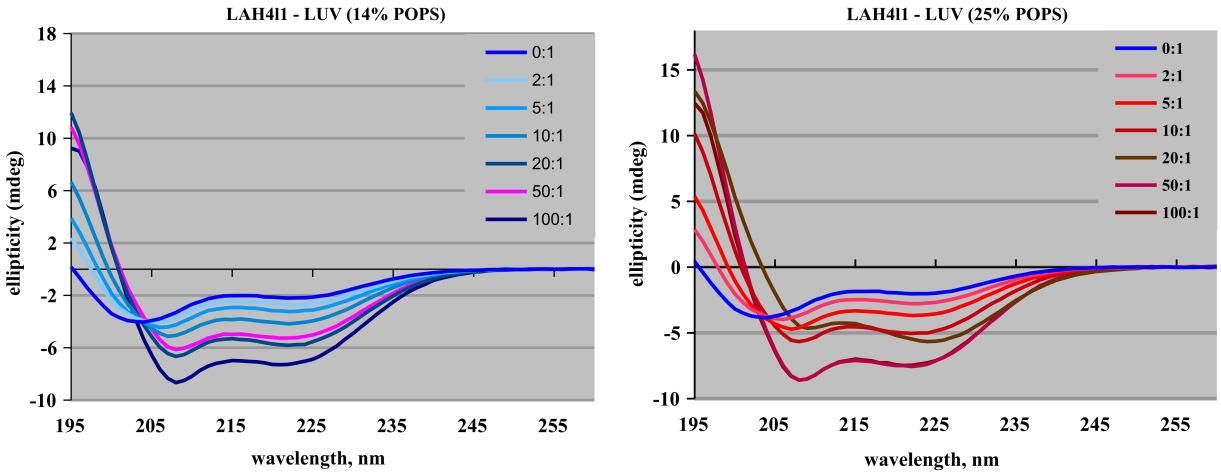

Figure V-4. Circular dichroism curves of 10μM LAH4-L1 peptide solution in 10mM acetate buffer titrated with POPC/POPS-14% LUV and POPC/POPS-25% LUV. The spectra are corrected for LUV absorption.

The vesicle aggregation is not necessarily reproducible at same lipid-to-peptide ratio. The titration of peptide with POPC/POPS-25% vesicles was repeated with 4.8μM LAH4-L1 solution. The aggregation of vesicles did not occur, or at least it didn't disturb the CD measurements (***Figure V-5***, right). It is possible that the vesicle aggregation depends on the peptide (LUV) concentration.

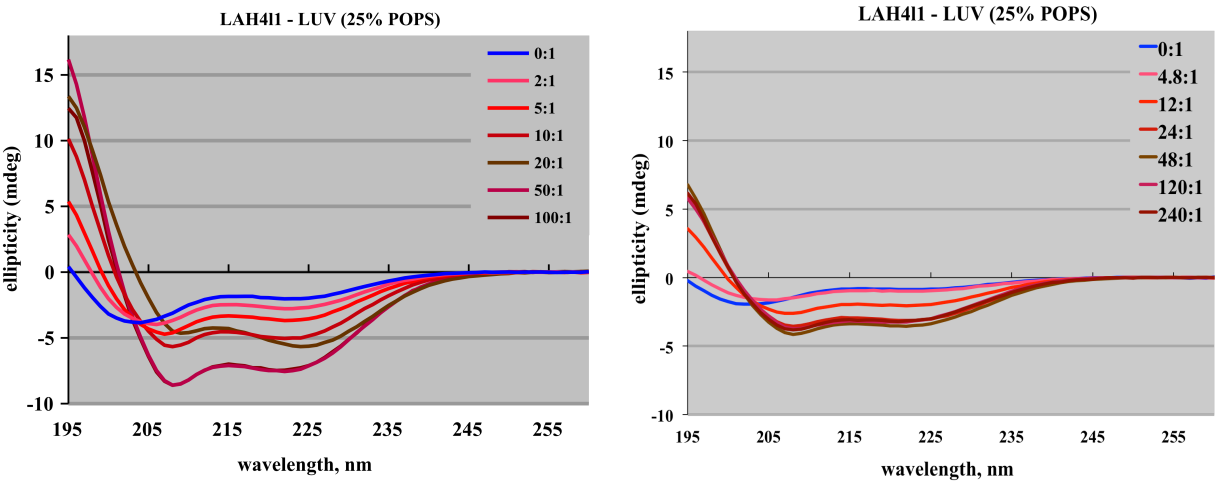

Figure V-5. Circular dichroism curves of 10μM (left) and 4.8μM (right) LAH4-L1 peptide solution in 10mM acetate buffer titrated with POPC/POPS-25% LUV. The spectra are corrected for LUV absorption.

The appearance of isosbestic point near 204nm occurs for the CD series of POPC/POPS-25% LUVs that are well corrected for the scattering effect. This isosbestic point suggests the occurrence of two peptide conformations, namely α-helix and random coil. In contrast, for the circular dichroism measurement on LAH4-L1 – POPC a well-defined isosbestic point is absent (***Figure V-6***). This could indicate two things. The vesicles were aggregating at low lipid-to-peptide ratio, such that the baseline of POPC LUV scattering didn't correspond to the actual scattering of the vesicles with bound peptide. Alternatively, LAH4-L1 could adopt another conformation, for example a β-sheet conformation.

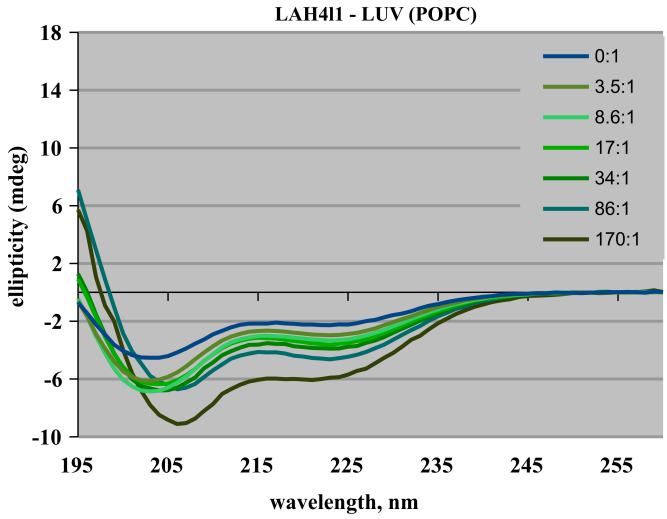

Figure V-6. Circular dichroism curves of 11μM LAH4-L1 peptide solution in 10mM acetate buffer titrated with POPC LUV. Each curve corresponds to particular lipid-to-peptide molar ratio, indicated in the legend.

The data were converted to the conventional unit *mole residue ellipticity* [deg*cm^2/dmol] and the secondary structures content was analysed. The data displayed in a ***Figure V-7*** are the combination of two POPC/POPS-25% - LAH4-L1 measurement series. The result of secondary structures content estimate is given in a ***Table V-1***, and its visual representation in a ***Figure V-8***.

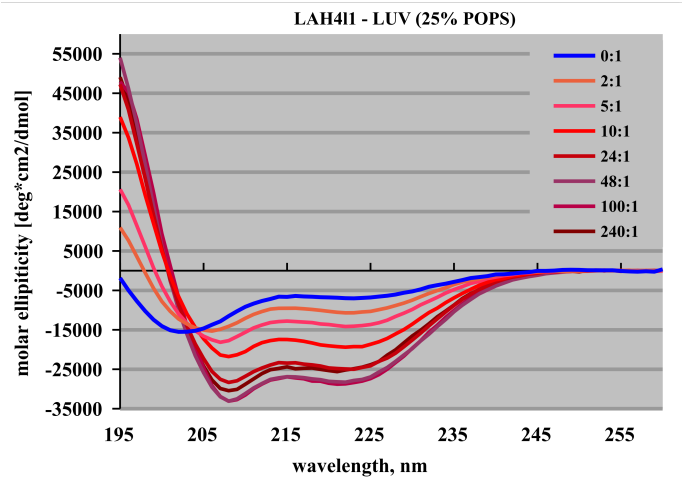

Figure V-7. Circular dichroism curves of LAH4-L1 peptide solution in 10mM acetate buffer titrated with POPC/POPS-25% LUV. Each curve corresponds to particular lipid-to-peptide molar ratio, indicated in the legend.

Table V-1. The secondary structures of LAH4-L1 peptide embedded into POPC/POPS-25% LUV as estimated from circular dichroism titration series.

Lipid-to-peptide, mole/mole	α-helix	α-helix (222nm)	random coil	β structures	sum β + α	R2
0	23,67%	21,17%	56,70%	19,63%	43,30%	99,72%
2	31,71%	29,49%	8,47%	21,76%	53,47%	99,11%
5	44,21%	39,50%	10,74%	16,29%	60,50%	99,89%
10	57,11%	54,66%	0,00%	19,31%	76,42%	99,09%
24	79,16%	70,57%	17,87%	2,97%	82,13%	99,72%
48	88,57%	80,29%	11,43%	0,00%	88,57%	99,24%
100	90,54%	81,50%	0,00%	0,00%	90,54%	99,78%
240	82,67%	71,34%	17,33%	0,00%	82,67%	99,54%

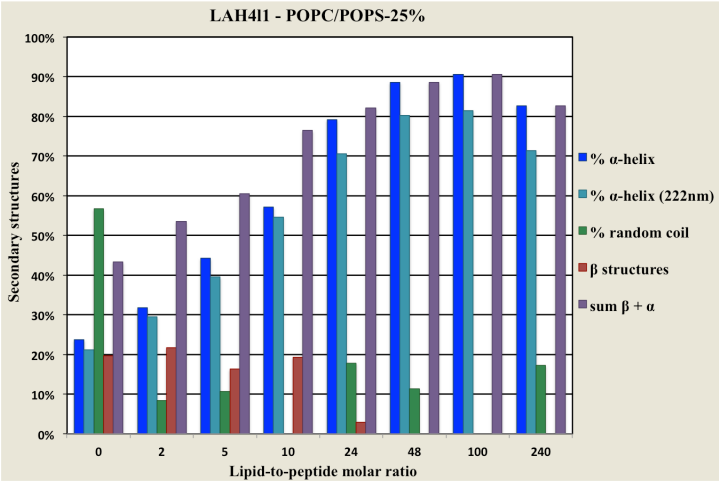

Figure V-8. The secondary structures of LAH4-L1 peptide embedded into POPC/POPS-25% LUV as estimated from circular dichroism titration series. Secondary structure content is plotted against lipid-to peptide molar ratio.

The same procedure was applied to three another data series.

Table V-2. The secondary structures of LAH4-L1 peptide embedded into POPC/POPS-14% LUV as estimated from circular dichroism titration series.

Lipid-to-peptide, mole/mole	α-helix	α-helix (222nm)	random coil	β structures	sum β + α	R2
0	28,05%	23,14%	53,90%	18,05%	46,10%	99,68%
2	31,72%	28,65%	48,42%	19,86%	51,58%	99,35%
5	37,71%	34,57%	44,53%	17,76%	55,47%	99,41%
10	47,05%	44,98%	36,24%	16,71%	63,76%	99,51%
20	69,03%	63,19%	18,74%	12,23%	81,26%	99,21%
100	84,87%	79,44%	15,13%	0,00%	84,87%	99,02%

Table V-3. The secondary structures of LAH4-L1 peptide embedded into POPC/POPS-10% LUV as estimated from circular dichroism titration series.

Lipid-to-peptide, mole/mole	α-helix	α-helix (222nm)	random coil	β structures	sum β + α	R2
0	28,05%	23,14%	53,90%	18,05%	46,10%	99,68%
2	29,08%	26,23%	49,62%	21,30%	50,38%	99,21%
5	36,68%	34,25%	44,11%	19,22%	55,89%	99,31%
10	39,14%	36,96%	41,09%	19,78%	58,91%	98,96%
20	52,22%	47,61%	36,41%	11,38%	63,59%	99,71%
50	86,19%	74,20%	13,13%	0,68%	86,87%	99,31%
100	85,24%	79,28%	14,76%	0,00%	85,24%	98,58%

Table V-4. The secondary structures of LAH4-L1 peptide embedded into POPC LUV as estimated from circular dichroism titration series.

Lipid-to-peptide, mole/mole	α-helix	α-helix (222nm)	random coil	β structures	sum β + α	R2
0	25,22%	21,22%	56,11%	18,67%	43,89%	99,75%
3,5	35,05%	28,00%	61,15%	3,80%	38,85%	99,54%
8,6	37,59%	31,41%	62,41%	0,00%	37,59%	98,27%
17	41,49%	34,25%	57,30%	1,20%	42,70%	99,03%
34	44,31%	37,19%	55,69%	0,00%	44,31%	98,36%
86	53,84%	44,30%	38,01%	8,15%	61,99%	97,33%
170	64,09%	58,48%	35,91%	0,00%	64,09%	90,42%

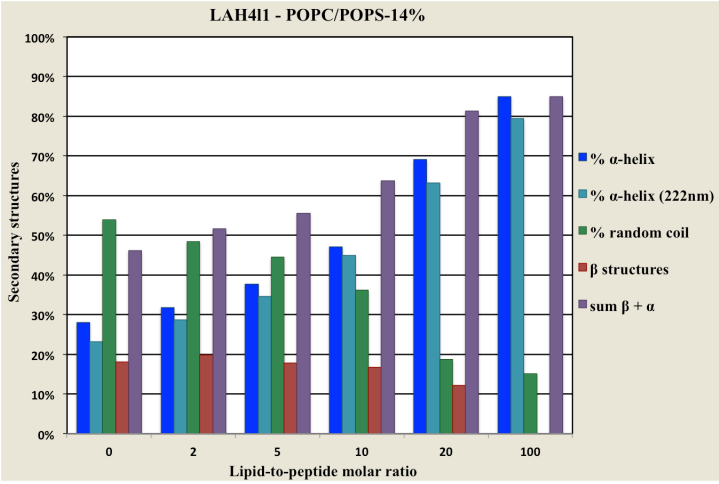

Figure V-9. The secondary structures of LAH4-L1 peptide embedded into POPC/POPS-14% LUV as estimated from circular dichroism titration series. Secondary structure content is plotted against lipid-to peptide molar ratio.

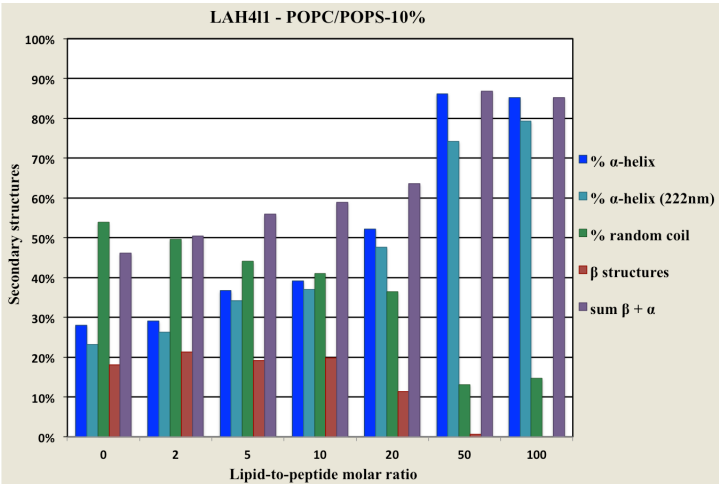

Figure V-10. The secondary structures of LAH4-L1 peptide embedded into POPC/POPS-10% LUV as estimated from circular dichroism titration series. Secondary structure content is plotted against lipid-to peptide molar ratio.

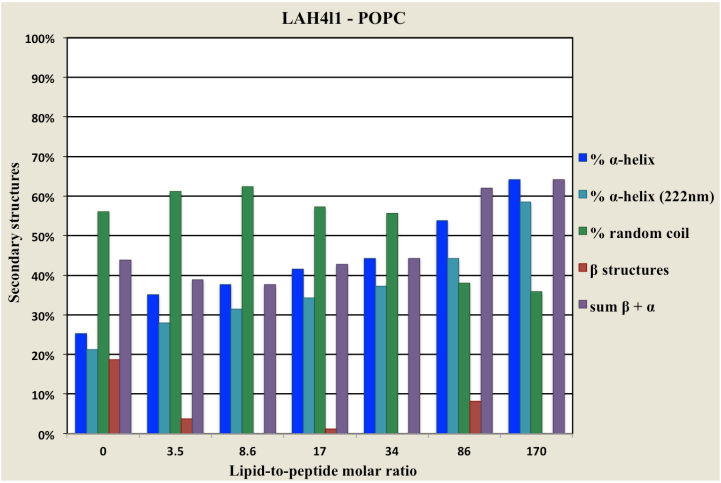

Figure V-11. The secondary structures of LAH4-L1 peptide embedded into POPC LUV as estimated from circular dichroism titration series. Secondary structure content is plotted against lipid-to-peptide molar ratio.

The spectral deconvolution of LAH4-L1 spectra in the absence of lipids (in 10mM acetate buffer) indicates the presence of a significant amount of β-sheet and β-turn. The fraction of LAH4-L1 beta-structures in POPC/POPS membranes decreases to zero when the lipid-to-peptide ratio reaches 50 (***Figures V-8, 9, 10***). The spectral deconvolution method for peptide secondary structure is more sensitive to the spectral shape and to the absorption at low wavelengths, accordingly the estimate is more affected by the LUV scattering effects, which may distort the results of simulations. But there should be no scattering artefacts that affect the LAH4-L1 spectra in 10mM acetate buffer, yet the spectral shape indicates the presence of around 18% β -sheet. It is therefore noteworthy that our analysis of the CD data covers a spectral range down to 195nm only. A detailed analysis of CD deconvolution protocols by Wallace and co-workers concludes that "the data that only extends to 200 nm contains at most two eigenvectors, and hence the results should only be interpreted in terms of two components (i.e., how much is helix and how much is not helix). Any interpretation of such data that attempts to deconvolute into more components than these will be an over-interpretation of the data" (Whitmore and Wallace, 2008).

It was shown by other biophysical methods that a peptide related to LAH4-L1 namely LAH4 does not adopt β-sheet structure. A helix-loop-helix LAH4 conformation was determined by solution NMR in DPC micelles (Georgescu et al., 2010). However β-sheet-like CD spectra shape could probably appear because the peptide forms small aggregates in hydrophilic buffer environment (Vogt and Bechinger, 1999). In a micellar environment LAH4 peptide most probably does not form any oligomeric structures, and it is mostly in α-helical form.

If we assume that the estimate of secondary structures by the deconvolution method is correct, really interesting correlations are observed. Upon peptide binding to mixed POPC/POPS vesicles at low lipid-to-peptide ratio, the fraction of β-structures increases slightly to about 21-22%. The CD spectral features indicative of β-structures disappear only at L/P >20 (***Figures V-8, 9, 10***). When LAH4-L1 interacts with zwitterionic POPC vesicles, the fraction of β-structures decreases already at low L/P. The presence of 8% of β-conformation at L/P=86 could be considered as error rather than regularity (***Figures V-11***). Taking into account that LAH4-L1 is attracted electrostatically to POPC/POPS membranes, β-structure is perhaps induced by the peptide aggregation on the lipid bilayer.

Construction of binding isotherms.

The two methods of α-helix content estimate used here, namely spectral deconvolution and following the mole residue ellipticity [θ] at 222nm, provide coherent results although the maximal helical content assessed by deconvolution method is slightly higher (***Figures V-12***, *left*). It is important to emphasize that the values of α-helix content obtained by those methods are not indicating the precise secondary structure of peptide, but rather a rough estimate of its conformational properties. However, it allows us to follow the changes in spectral properties and thereby to calculate the fraction of peptide bound to the membrane at a given lipid-to-peptide ratio (***Figures V-12***).

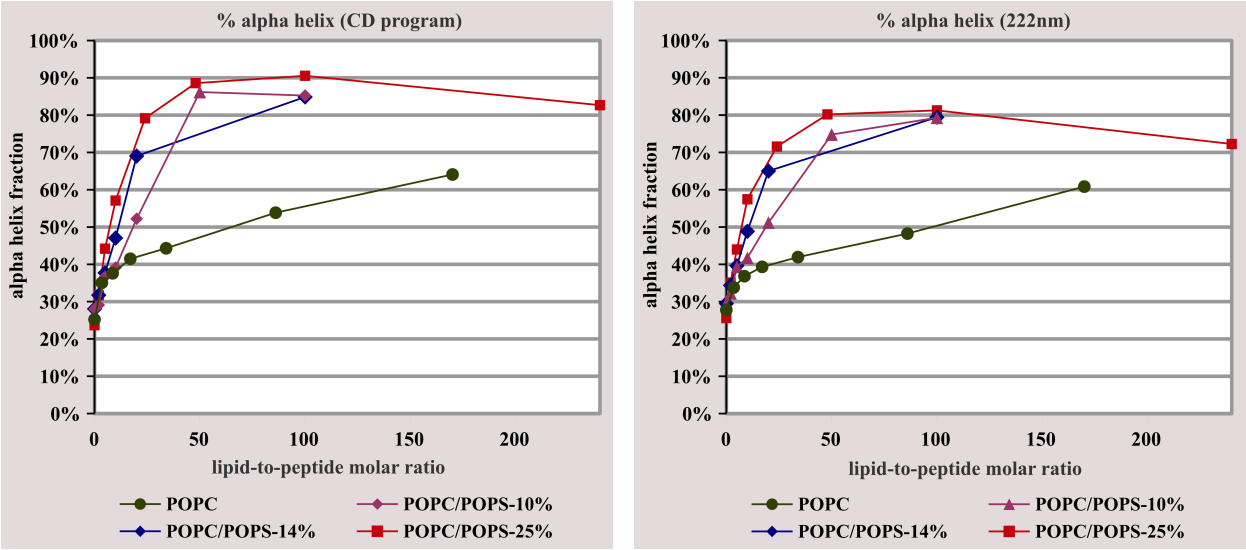

Figure V-12. LAH4-L1 α-helix content estimate by spectra deconvolution Excel program and by method based on the absorption at 222nm.

LAH4-L1 α-helix content increase quite rapidly when titrating with mixed POPC/POPS-25% LUV and reaches its maximum value at lipid-to-peptide ratio ≈50 (2mole%). Three last points form so-called plateau region, and are indicative for complete binding of peptide. For POPC/POPS-14% and POPC/POPS-10% membranes complete LAH4-L1 binding is reached at lipid-to-peptide ratio around 100. For the zwitterionic POPC membranes LAH4-L1 does not reach maximum α-helical content even at lipid-to-peptide ratio 170 (≈0.6mole% peptide).

The binding isotherms indicate that LAH4-L1 interaction with mixed vesicles at pH 5 is electrostatically driven. The peptide is attracted electrostatically to the surface of charged POPC/POPS membranes, and α-helix formation is then promoted by the peptide penetration into lipid bilayers. As it was shown previously by ^{15}N NMR spectroscopy, at pH 5 LAH4-L1 peptide adopts preferably an in-planar alignment parallel to the lipid bilayer surface. When the peptide associates with zwitterionic POPC membranes the penetration of its hydrophobic amino acids side chains into lipid bilayer stimulates the increase of the α-helical content. LAH4-L1 insertion into zwitterionic membranes is best described by a partitioning equilibrium (Wieprecht et al., 1999a).

As it was shown in the CD experiment on melittin titrated to the mixed charged POPC/POPG membranes (Fernández-Vidal et al., 2011), normalized binding isotherm can be fitted with membrane partitioning equation and the mole fraction *partition coefficient* K_X could be expressed:

$K_X = [P]_{bil} / [P]_{water}$, where $[P]_{bil}$ and $[P]_{water}$ are the bulk molar concentrations of peptide attributable to peptide in the bilayer and water.

The total peptide concentration can be expressed as $[P]_{total} = [P]_{bil} + [P]_{water}$, then:

$$f_p = \frac{K_X[L]}{[W] + K_X[L]}$$

where f_p is the fraction of peptide bound, [L] and [W] are the molar concentrations of lipid and water (55.56 M), respectively. This fraction correlates with changes in total peptide α-helical content and was determined from CD titration curves. Mole fraction partitioning coefficient K_X was then assessed by least-squares simulation of equation to plots of f_p against [L]/[P] molar ratio using the Origin 7.0 software package (OriginLab, Northampton, MA), as follows:

$$f_p = c\frac{K_X x[P]_{total}}{55.56\text{M} + K_X x[P]_{total}}$$

where K_x , c – is variable fitting parameter, $[P]_{total}$ – peptide concentration, which is constant in each separate series; x – independent variable of the function, *i.e.* lipid-to-peptide molar ratio.

In order to determine the fraction of bound peptide, the α-helical content was normalized taking that the fraction of bound peptide was zero in the absence of lipid, and the maximum fraction of α-helix observed for POPC/POPS-25% - LAH4-L1 titration was taken for 100% bound peptide. The rest of curves were normalized accordingly to POPC/POPS-25% - LAH4-L1 binding isotherm (***Figures V-13***). The variable parameter *c* was introduced in order to fit better CD-derived isotherms. By introducing this variable we assume that the max of alpha-helical content of peptide may very accordingly to lipid composition. Therefore *c* parameter was set to 1 for the simulation of LAH-L1 – LUV (PS-25%, 14%, 10%) binding isotherms, and to 0.7 for the simulation of LAH-L1 – LUV (POPC) binding isotherms, assuming that the complete bound peptide will adopt the same secondary structure when bound to PS-25%, 14%, 10% vesicles, but the fraction of α-helix of the peptide completely bound to POPC vesicles will be smaller by 0.7. The binding constants obtained by simulations are given in a ***Table V-5***.

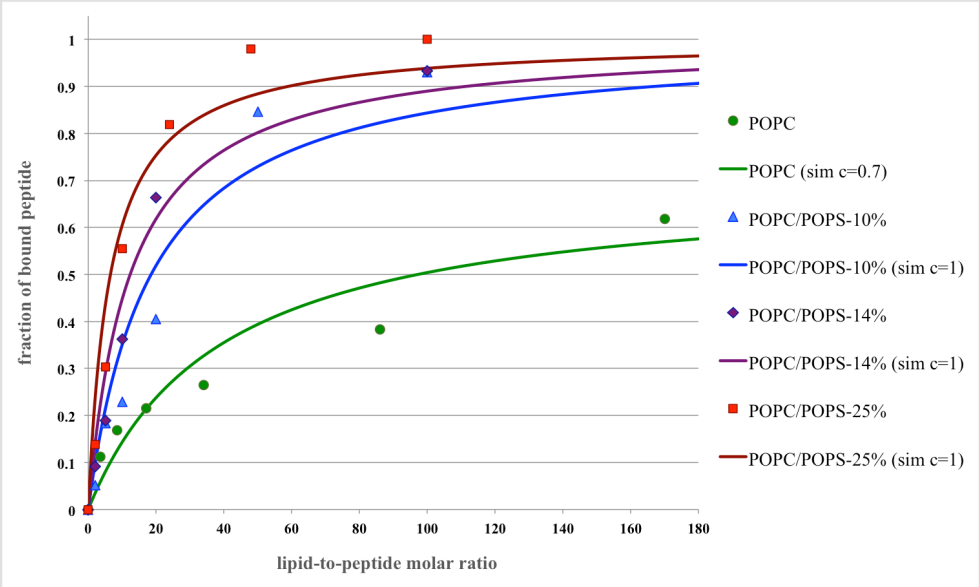

Figure V-13. LAH4-L1 - LUV binding isotherms derived from CD measurements and the corresponding membrane partitioning simulation curves.

The partitioning equilibrium was applied to simulate the CD isotherms by assuming that the fraction of peptide which is bound to membranes at a certain L/P ratio, changes its secondary structure from 18% α-helix (free peptide) to the maximum value 80% α-helix (peptide completely bound to POPC/ POPS-25% vesicles), while the fraction of LAH4-L1 which remains in solution, conserves its 18% of α-helical structure. However, this assumption can be valid only for partitioning into zwitterionic POPC

membranes. The negatively charged POPC/POPS membrane surface attracts more peptide molecules than POPC LUV at the corresponding L/P ratio (peptide concentration). First of all the electrostatic attraction effect explains much bigger apparent binding constants to PS containing membranes comparing to POPC.

Table V-5. Apparent binding constants obtained by the membrane partitioning equilibrium simulations.

Membrane composition	POPC/POPS-25%	POPC/POPS-14%	POPC/POPS-10%	POPC
K_X	850 000	450 000	300 000	13 000

The fitting using membrane partitioning equilibrium provides rather poor results. There may be several reasons for that. Fist of all the insertion of LAH4-L1 into lipid bilayer probably should be described by function more complex than membrane partitioning. For example, one can envision a situation when from this fraction of 'bound' peptide only the small part of LAH4-L1 molecules is actually immersed into hydrophobic core of lipid bilayer and adopts its maximum α-helical structure. Another part of peptides that were attracted to lipid bilayer surface forms small oligomeric structures. Therefore, not only peptide penetration into lipid core, but also peptide aggregation and oligomerization can give rise to α-helical content augmentation. If such a situation takes place, we are not able to describe CD-derived binding isotherms by simple partitioning.

Secondly, at high lipid concentrations the scattering from the vesicles may distort CD curve, then significant error may be introduced to the α-helix estimate. Notably, fitting works better at low L/P ratios.

For POPC – LAH4-L1 CD isotherm the simulation also provide poor result even though the electrostatic interactions play much smaller role in peptide binding to POPC. It confirms that there are some other contributuions to the bad fitting of CD data to partitioning model, except electrostatic effects. The most probable contributions is vesicles scattering distort the spectrum.

If our simulation approach is correct, the variable parameter *c* allows to compare the α-helical content of LAH4-L1 inserted into POPC and PC/PS membranes. The ratio of f_α between POPC and POPC/POPS-25% is 0.7. If α-helix content reaches 80% when LAH4-L1 is inserted in the POPC/POPS-25% membrane, then in POPC membranes maximum LAH4-L1 helical content will be around 56%. The random coil – to – α-helix transition of LAH4-L1 is then largely stimulated by interaction with charged POPS lipids.

The results were obtained with LAH4 (KKALLALALHHLAHLALHLALALKKA) interacting with zwitterionic and charged membranes. The helix content of LAH4 at pH 5.5 increases from 26% in the absence of membranes to 55% and 70% in the presence of POPC or POPC/POPG liposomes, respectively (Vogt and Bechinger, 1999).

VI. THERMODYNAMICS OF LAH4-L1 INTERACTION WITH MODEL MEMBRANES BY ISOTHERMAL TITRATION CALORIMETRY.

In order to assess the thermodynamic parameters of LAH4-L1 interaction with negatively charged mixed POPC/POPS and zwitterionic POPC membranes, a series of isothermal titration calorimetry (ITC) experiments was conducted. Previously ITC was used to resolve the energetics of the individual steps of membrane association with negatively charged POPC/POPG lipid vesicles of the cationic peptides melittin (Klocek et al., 2009) and antimicrobial peptide mastoparan-X (Henriksen and Andresen, 2011). The electrostatic interaction of cationic peptides to negatively charged membrane surface is not accompanied by significant enthalpy change (Klocek et al., 2009), therefore the ITC signal should arise from peptide insertion into membrane, helix formation and peptide aggregation in the membrane including pore formation (Henriksen and Andresen, 2011).

MATERIALS AND METHODS

Sample preparation for isothermal titration calorimetry.

The stock solutions of 100nm large unilamellar POPC vesicles with varied POPS content (0%, 10%, 14% and 25%) were prepared as described in Chapter III. Three type of buffers were used for sample preparation:

- 10mM acetate buffer / 0.5mM EDTA, pH≈5,
- 20mM HEPES buffer / 1mM EDTA, pH≈7.4,
- 50mM Tris buffer, pH≈7.4

The stock solutions of LAH4-L1 were prepared in the corresponding buffers and dialyzed against the same buffer. It is especially important that all the peptide samples were subjected to dialysis prior to ITC measurement in order to equilibrate pH and buffer composition between peptide stock solution and buffer itself. Otherwise the dilution enthalpy could become bigger that the enthalpy of peptide – LUV interaction. The concentrations of peptide and vesicles working solutions were adapted for each experimental condition. All working solutions were degased under low vacuum (140 mbar) prior to measurements.

Isothermal Titration Calorimetry measurements.

All measurements were taken with a MicroCal VP-ITC calorimeter (MicroCal, Northampton, MA) at the various temperature conditions (for the temperature condition for each experiment see the Tables IV.1 and IV.2). Lipid-into-peptide titrations were performed by injecting 3 to 10µL aliquots of lipid suspension into the calorimeter cell (V_{cell} = 1.4037mL) containing the peptide at a concentration between 15 and 150µM, at time intervals of 3 to 5min. Peptide-into-lipid titrations were performed by injecting 3 to 10 µL aliquots of the peptide solution (200 – 500µM) into the calorimeter cell containing the lipid suspension at a concentration of 0.3 – 1mM. The concentrations of the injectant (*or* titrant, the binding partner in the syringe $V_{syringe}$ = 300µL) as well as the concentration of titrate were optimized for each experiment in order to avoid that we run out of titrant before the binding reaction is completed. The heats of dilution were determined in the control titrations by injecting the lipid solution or the peptide solution into pure buffer and were subtracted from the calorimetric signal during the final analysis. Calorimetric response is recorded as the function of heating (*h*) received by instrument versus measurement time. This signal is then processed automatically by *Origin® ITC software*, and the result is represented as an enthalpy per mole of *injectant* (ΔH/mole, *kcal/mole*) against the *titrate-to-titrant* molar ratio.

Table VI-1 and ***Table VI-2*** summarize the conditions of all experiments, including various pH, temperature and concentration conditions.

Table VI-1. The ITC experimental conditions of LAH4-L1 interaction with LUV at **pH 5** (10mM acetate, 0.5mM EDTA).

Direction of titration	T°C	POPC / POPS-25%		POPC / POPS-14%		POPC / POPS-10%		POPC	
		V	concentration	V	concentration	V	concentration	V	concentration
L ↓ P	14	3	L: 13mM P: 15µM	3	L: 13mM P: 15µM	3	L: 13mM P: 15µM		
	25	3		10		3			
	45	3		3		3			
P ↓ L	25	5	P: 250µM L: 0.325mM	5	P: 250µM L: 0.325mM	3	P: 250µM L: 0.620mM	10	P: 250µM L: 0.670mM

Table VI-2. The ITC experimental conditions of LAH4-L1 interaction with LUV at **pH 7.4** (20mM HEPES, 1mM EDTA / 50mM Tris).

Direction of titration	T°C	POPC / POPS-25%		POPC / POPS-14%		POPC / POPS-10%		POPC	
		V	concentration	V	concentration	V	concentration	V	concentration
L ↓ P	25	10	L: 13mM P: 150µM	10	L: 13mM P: 150µM	10	L: 13mM P: 150µM		
	37	8	L: 13mM P: 150µM	8	L: 13mM P: 100µM	10	L: 13mM P: 100µM		
P ↓ L	25	5	P: 500µM L: 0.650mM	8	P: 500µM L: 1.18mM	5	P: 500µM L: 1mM	10	P: 500µM L: 0.640mM

RESULTS AND DISCUSSION.

POPC/POPS LUV titration into LAH4-L1 solution at pH 5.

ITC measurement series were started from POPC/POPS 100nm LUV titrations into 15µM LAH4-L1 solution at pH 5. As the enthalpy of LAH4-L1 association with membranes was unknown, the conditions were chosen based on the ITC titration of POPC/POPG-25% large unilamellar vesicles with another cationic amphipathic peptide *melittin* (Klocek et al., 2009).

Isothermal titration calorimetry signal is a heat flow, which corresponds to the enthalpy change per the unit of time (second). The results of the POPC/POPS-25%, POPC/POPS-14% and POPC/POPS-10% LUV titrations into 15µM LAH4-L1 solution are shown in the ***Figures VI-1, 2, 3*** correspondingly. Each set of measurements was performed at three temperature conditions (14°C, 25°C and 45°C). By performing the experiments at various temperatures we expected to discern various processes that are taking place upon LUV-peptide interaction.

A general characteristic of all LUV-to-LAH4-L1 calorimetric titration isotherms is the presence of an enthalpy minimum. An endothermic process contributes to the enthalpy at low lipid-to-peptide ratio, but the magnitude of this contribution decrease rapidly with the increase of the L/P total ratio, and contributions from exothermic process become more important. After reaching a minimum the enthalpy

comes back to 0, indicating the decay of an exothermic process (***Figures VI-1***). At the end of each ITC measurement we have some residual signal with constant intensity, corresponding to the dilution of titrant into solution in the calorimetric cell. The peptide –lipid association reaction is considered to be complete when the enthalpy is zero. The shape of calorimetric traces obtained from titration of POPC/POPS LUV vesicles into LAH4-L1 solution suggests that at least two processes that happen when the peptide binds to charged vesicles. Having a closer look on the ITC curves, one could notice that at certain titration steps the energy contributions from different processes are even time-resolved (***Figures VI-1***, A, *titration steps 11 and 12*).

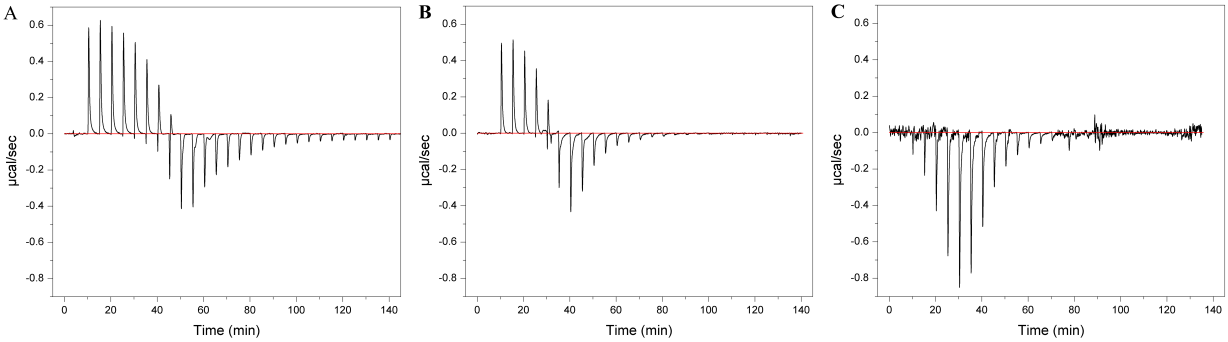

Figure VI-1. Isothermal calorimetry titration of 13mM POPC/POPS-25% LUV into 15µM LAH4-L1 solution into 10mM acetate buffer (pH 5) at 14°C (A), 25°C (B) and 45°C (C) with 3µL injections. The ITC signal is the heat change, measured in µcal/sec and plotted against measurement time.

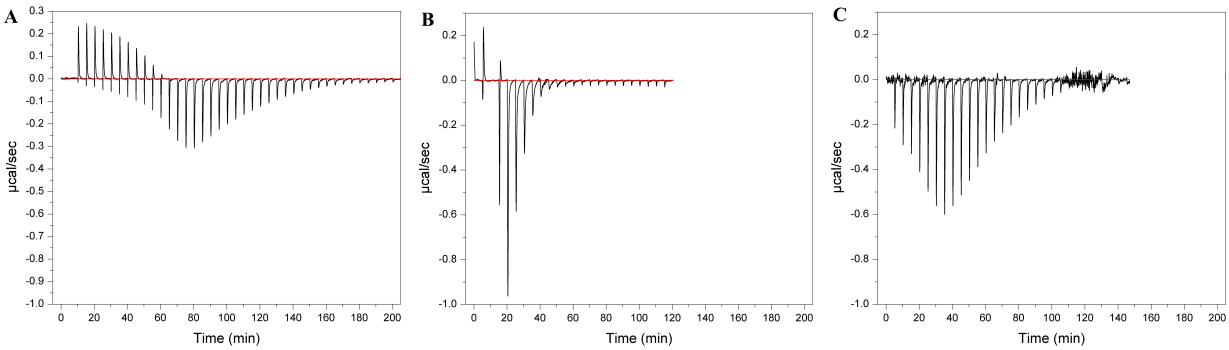

Figure VI-2. Isothermal calorimetry titration of 13mM POPC/POPS-14% LUV into 15µM LAH4-L1 solution into 10mM acetate (pH 5) at 14°C (A), 25°C (B), 45°C (C) with 3µL (A,C),10µL (B) injections. The ITC signal is the heat change, measured in µcal/sec and plotted against measurement time.

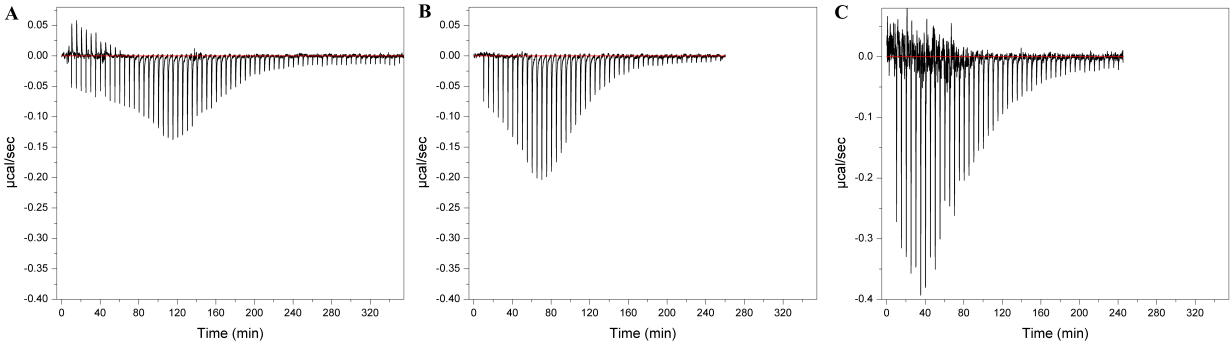

Figure VI-3. Isothermal calorimetry titration of 13mM POPC/POPS-10% LUV into 15µM LAH4-L1 solution into 10mM acetate buffer (pH 5) at 14°C (A), 25°C (B) and 45°C (C) with 3µL injections. The ITC signal is the heat change, measured in µcal/sec and plotted against measurement time.

In each of the titration experiments the intensity of the endothermic component is decreasing with temperature, so the total titration enthalpy is shifted to negative values.

The calorimetric signal is processed automatically by build-in ITC Origin® software. The initial concentrations of vesicles and the peptide and the injection volume are taken in account at the signal integration and the result of ITC measurement is expressed in kcal/mole of injectant (lipid) and plotted against the lipid-to-peptide molar ratio. A number of titration experiments were performed to assess the effect on peptide binding of temperature and of POPS content of the POPC/POPS vesicles (***Figures VI-4, 5, 6***).

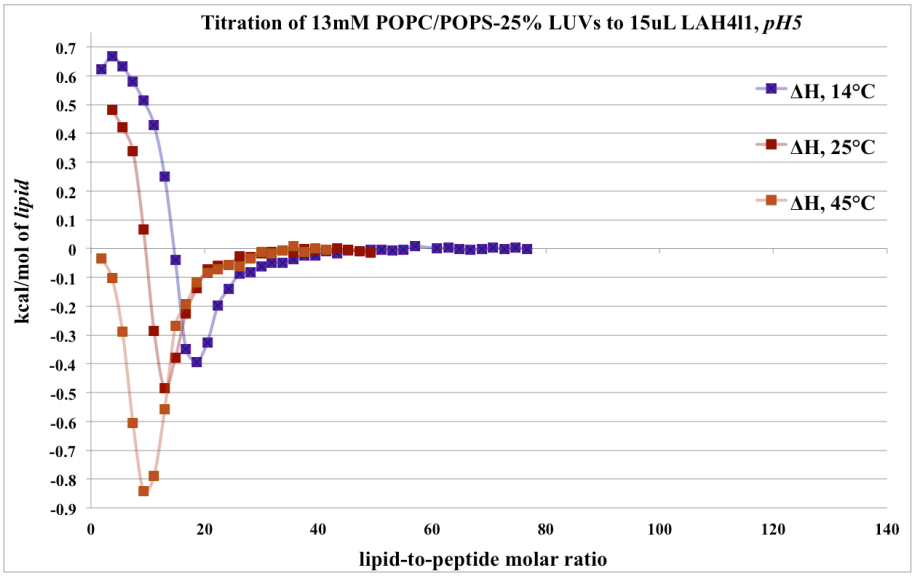

Figure VI-4. Integrated calorimetric heat (δh) of 13mM POPC/POPS-25% LUV titrated into 15μM LAH4-L1 solution into 10mM acetate buffer (pH 5) at 14°C, 25°C and 45°C. The enthalpy is expressed in kcal/mole and plotted against the lipid-to-peptide molar ratio.

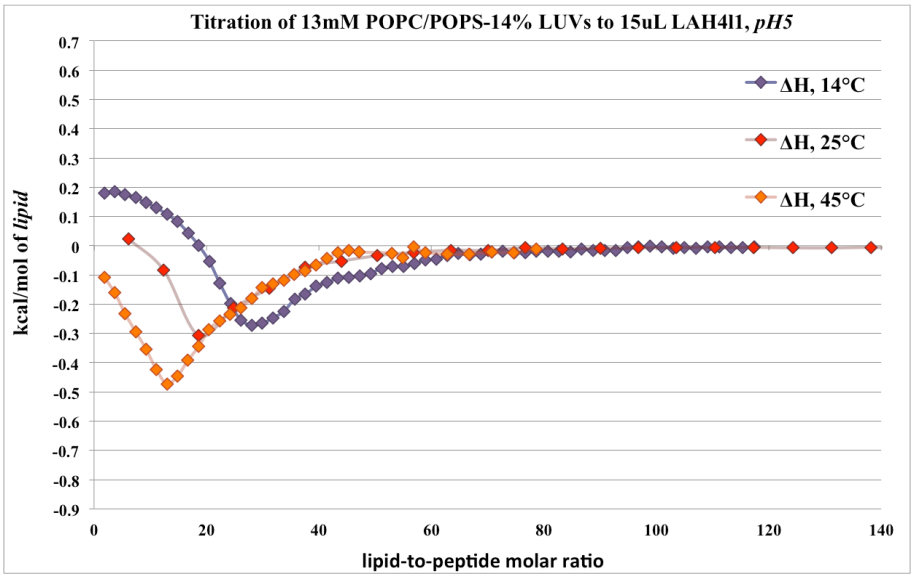

Figure VI-5. Integrated calorimetric heat (δh) of 13mM POPC/POPS-14% LUV titrated into 15μM LAH4-L1 solution into 10mM acetate buffer (pH 5) at 14°C, 25°C and 45°C.

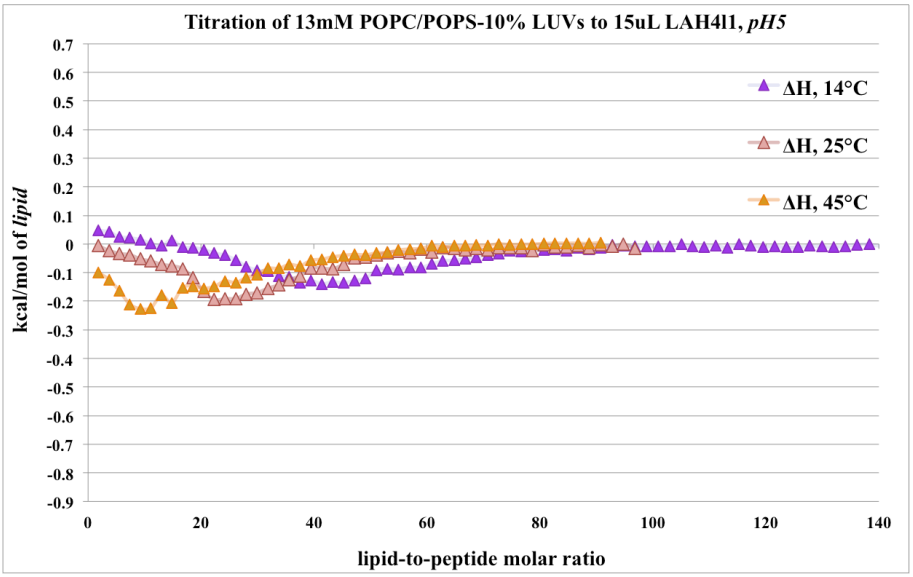

Figure VI-6. Integrated calorimetric heat (δh) of 13mM POPC/POPS-10% LUV titrated into 15μM LAH4-L1 solution into 10mM acetate buffer (pH 5) at 14°C, 25°C and 45°C. The enthalpy is expressed in kcal/mole and plotted against the lipid-to-peptide molar ratio.

All of the POPC/POPS LUV – LAH4-L1 titration isotherms have a common feature, which is the presence of at least two enthalpy components. The endothermic component is more important at low lipid-to-peptide ratio. This component possibly refers to the peptide absorption onto the membrane surface. The exact processes that may take place upon the peptide absorption to the lipid bilayer will be reviewed in General Discussion section. Briefly, the steepness of the ITC isotherm in the beginning of the titration could be explained as follows. The first injection of POPC/POPS negatively charged vesicles attracts electrostatically a large fraction of the positively charged peptide molecules. A certain fraction of peptide would be absorbed to membrane surface due to this electrostatic attraction (Wenk and Seelig, 1998) and some of the absorbed peptides will undergo the conformational changes due to membrane partitioning. Thus overall heat would be absorbed by the system. When more vesicles are injected there will be less peptide available and so on. Finally, all the peptide becomes absorbed by vesicles. Next, the addition of more vesicles would induce the peptide molecules to migrate to these 'free' vesicles, because the peptide accumulation on the surface does not allow an efficient insertion into the lipid bilayer. Thus the second, exothermic process may represent insertion of peptide and helix formation in the lipid bilayer. Considering the shape of the calorimetric isotherm, the endothermic process ends at rather low L/P ratio, whereas the exothermic process possibly takes place during the whole titration.

The quantitative description of the graphs is given in a ***Table VI-3***.

Table VI-3. The quantitative description of ITC titration curves of POPC/POPS vesicles interaction with LAH4-L1 peptide at pH 5. The lipid-to-peptide ratios at the end of reaction and at the enthalpy minimum, as well as enthalpy change are provided for each titration curve.

POPS-25%			
T°C	14°C	25°C	45°C
δh, kcal/mol	max: 0.67 min: -0.40 *diff*=1.07	max: 0.48 min: -0.49 *diff*=0.97	max: -0.03 min: -0.84 *diff*=0.81
end, l-to-p	55	40	40
min, l-to-p	18	13	10
Σ*δh, kcal/mol*	1.78	-0.54	-4.15

POPS-14%			
T°C	14°C	25°C	45°C
δh, kcal/mol	max: 0.18 min: -0.27 *diff*=0.45	max: 0.03 min: -0.3 *diff*=0.33	max: -0.08 min: -0.45 *diff*=0.37
end, l-to-p	97	85	55
min, l-to-p	28	20	13
Σ*δh, kcal/mol*	1.9	-2.9	-4.52

POPS-10%			
T°C	14°C	25°C	45°C
δh, kcal/mol	max: 0.05 min: -0.14 *diff*=0.19	max: 0 min: -0.185 *diff*=0.185	max: -0.11 min: -0.24 *diff*=0.13
end, l-to-p	105	100	85
min, l-to-p	42	23	9
Σ*δh, kcal/mol*	1.94	-2.65	-3.36

The minimum of the enthalpy is decreasing when the temperature increases. It seems that with the temperature rise it is mainly the enthalpy of the endothermic process that decreases. The latter assumption is confirmed by the fact that the enthalpy minimum is also shifted to lower lipid-to-peptide ratios. The sum of the enthalpies of all titration steps will represent the global energy taken or released by system. This total energy correlates with the temperature (***Figure VI-7***).

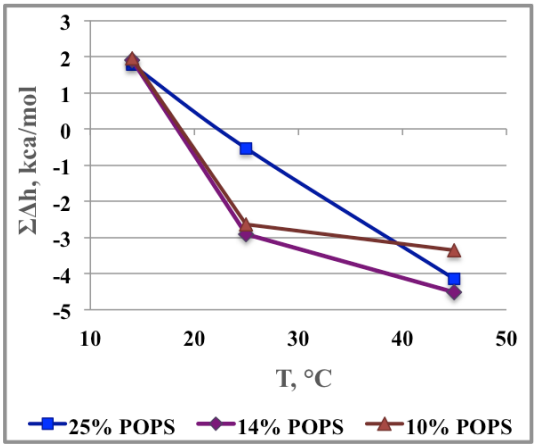

Figure VI-7. The correlation of the total enthalpy (Σδh) of POPC/POPS LUV titration to LAH4-L1 peptide solution at pH 5 with the temperature of the system. The total enthalpy of POPC/POPS-14% titrations into LAH4-L1 at 25°C was normalized by factor 10/3, because 10µL injection steps were applied in contrast to the rest of experiments, where injection volume was 3µL.

Several observations should be noticed when comparing the ITC curves of POPC/POPS vesicles with varied POPS content titration into LAH4-L1 peptide solution. The peptide – vesicles association process is finished at lower lipid-to-peptide ratios when the POPS content is higher. Secondly, the molar enthalpies of injections are smaller for peptide – LUV interaction for vesicles with smaller POPS content. This correlation is valid for endothermic and also for exothermic process. The difference between *maximum* and *minimum* value of enthalpy was measured for each titration experiment, and it correlates with POPS content too (***Figure VI-8***).

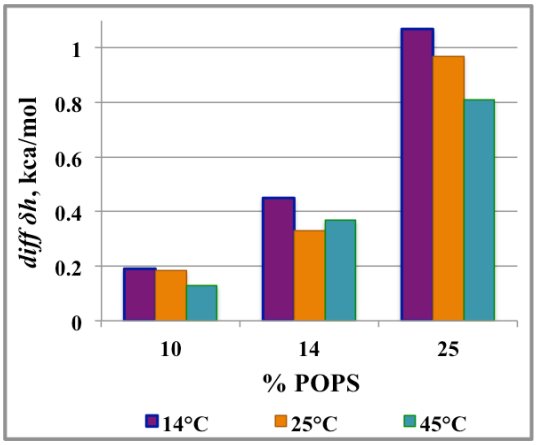

Figure VI-8. The correlation of the difference between maximum and minimum of enthalpy (diff δh) with the POPS lipid content of vesicles at three temperature conditions (14°C, 25°C and 45°C).

As the energetics of peptide association with POPC/POPS vesicles depends strongly on POPS lipid content, I compared titration curves for various ITC series by plotting them against the POPS-to-peptide molar ratio. The isotherms for various temperature conditions are given in the ***Figure VI-9, 10, 11***.

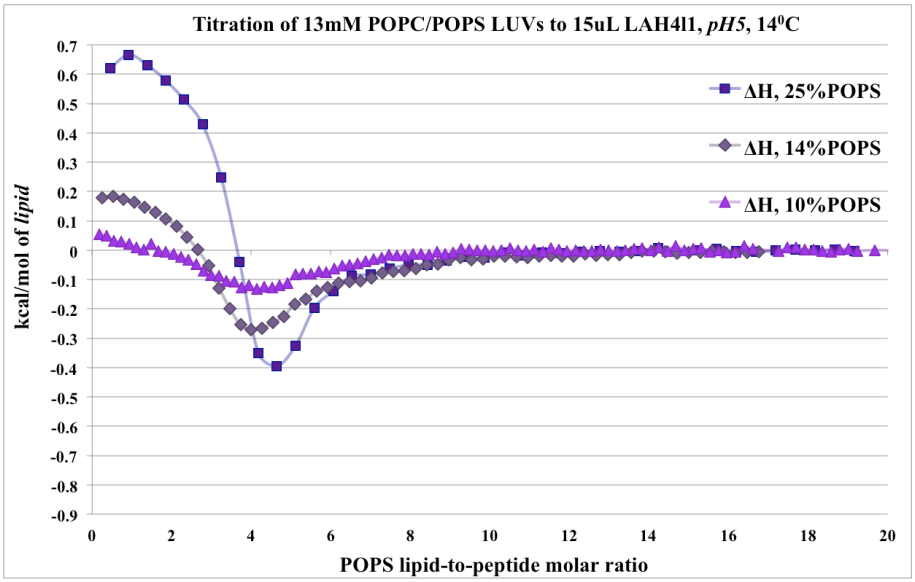

Figure VI-9. Integrated calorimetric heat (δh) of 13mM POPC/POPS LUV titrated into 15μM LAH4-L1 solution into 10mM acetate buffer (pH 5) at 14°C. The enthalpy is expressed in kcal/mole and plotted against the POPS/peptide molar ratio.

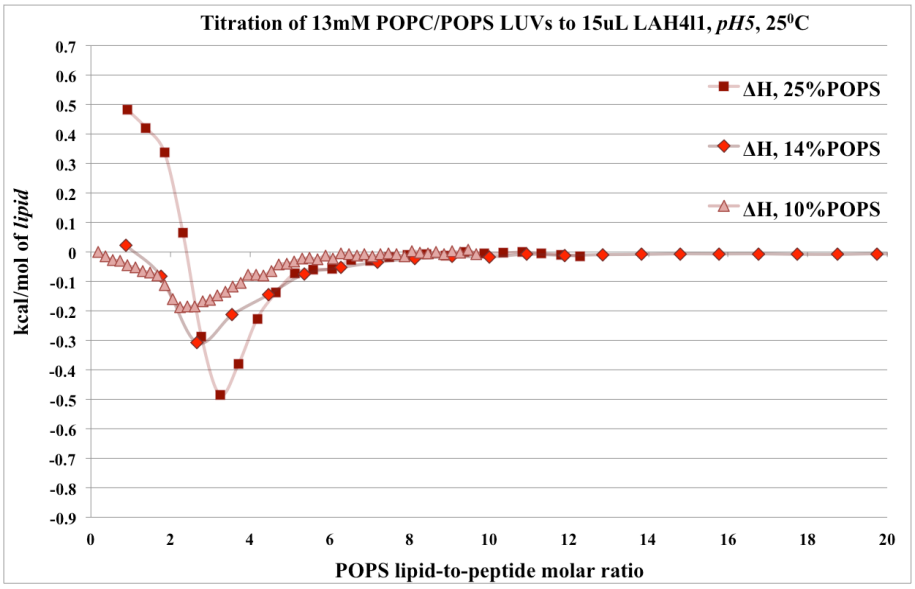

Figure VI-10. Integrated calorimetric heat (δh) of 13mM POPC/POPS LUV titrated into 15µM LAH4-L1 solution into10mM acetate buffer (pH 5) at 25°C. The enthalpy is expressed in kcal/mole and plotted against the POPS/peptide molar ratio.

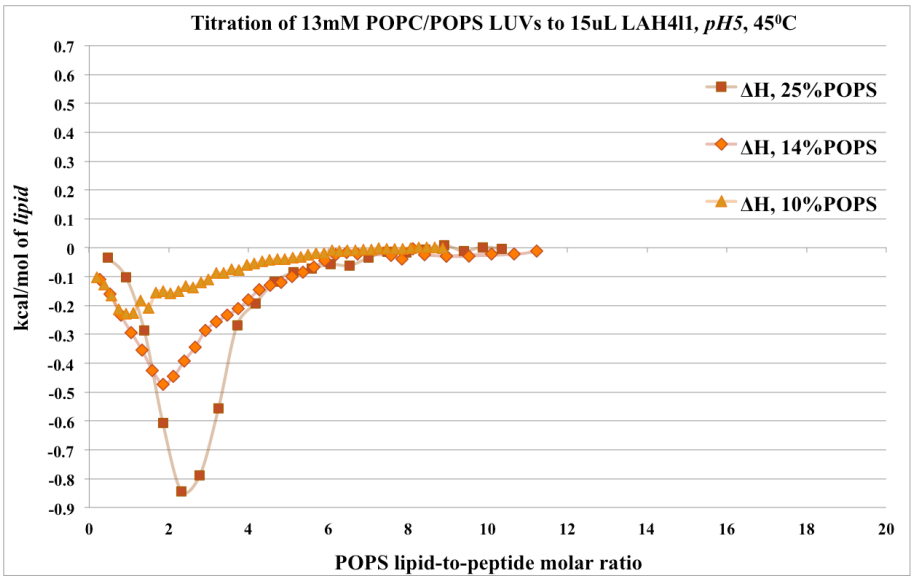

Figure VI-11. Integrated calorimetric heat (δh) of 13mM POPC/POPS LUV titrated into 15µM LAH4-L1 solution into 10mM acetate buffer (pH 5) at 45°C. The enthalpy is expressed in kcal/mole and plotted against the POPS/peptide molar ratio.

The most important conclusion that follows, is that the titration reactions are finished at the same lipid-to-peptide molar ratio when normalized on the POPS content. It takes about 11 POPS lipid molecules per LAH4-L1 peptide at 14°C, 9 POPS/LAH4-L1 at 25°C, and around 8 POPS/LAH4-L1 at 45°C. Such the heat released or absorbed upon the vesicles titration into LAH4-L1 peptide seems to be associated with peptide binding to POPS lipid molecules. It was shown also by ^{2}H NMR experiment that LAH4-L1 peptide has higher affinity to POPS than to POPC lipids when inserted into POPC/POPS membranes (*cf.* Chapter IV).

POPC/POPS LUV titration into LAH4-L1 solution at pH 7.4

A similar series of ITC measurements at pH 7.4 at two different temperature condition (25˚C and 37˚C) was conducted. Acetate buffer was no longer suitable for pH 7.4, therefore the experiment were performed in 50mM Tris buffer at 25°C. At first I tried to conduct the titration of POPC/POPS-25% LUV into peptide solution at pH 7.4 using the same concentration range as for the experiment at pH 5, *i.e.* 13mM vesicle suspension in syringe and 15µM LAH4-L1 solution in the calorimetic cell. However, the heat response was rather small, and only for the first injection sufficient signal was observed, with only the enthalpy for vesicles dilution left for most of the remainder of the titration experiment (***Figure VI-12***).

The entalpy of injections was -0.02…-0.03 µcal/mol, which is in the same range as the vesicle dilution enthalpy in ITC titrations at pH 5 (Figures IV.1-3). This observation allows us to refer all the heat changes, starting from 3rd titration step, to the vesicles dilution enthalpy. This mean that the total amount of peptide (21nmol, as concentration of LAH4-L1 was 15µM and the volume of the cell – 1.404mL) become membrane-associated during first two (maybe three) injections of vesicles, equal to 92.6 nmol of lipids. Alternatively, the binding process was still ongoing, but the calorimetric response from the peptide binding to vesicles was so small, that it was hidden under the LUV dilution enthalpy. As the heat response was very small compared to the analogous experiments at pH 5, the concentration of peptide in the calorimetric cell was increased 10 fold, and the series of titration was performed at pH 7.4 and at a temperature of 25°C (***Figure VI-13***).

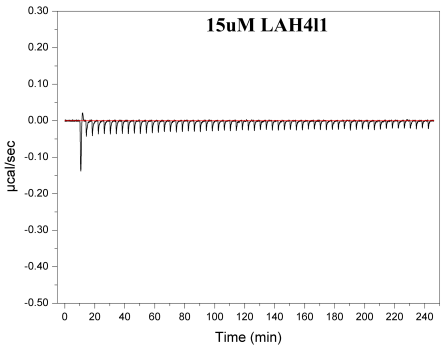

Figure VI-12. Isothermal calorimetry titration of 13mM POPC/POPS-25% LUV into 15µM LAH4-L1 solution at pH 7.4 at 25°C with 5µL injections. The ITC signal is the heat change, measured in µcal/sec and plotted against measurement time.

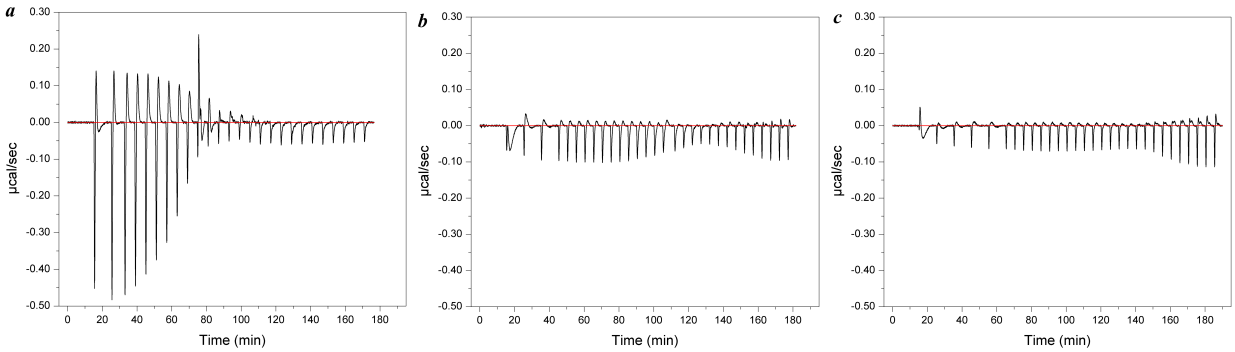

Figure VI-13. Isothermal calorimetry titration of 13mM POPC/POPS LUV into 150µM LAH4-L1 solution at pH 7.4 and 25°C. Injection volume was 10µL. a) POPC/POPS-25%, b) POPC/POPS-14%, c) POPC/POPS-10%. The ITC signal is the heat change, measured in µcal/sec and plotted agaist measurement time.

The increase of the peptide concentration in the calorimentric cell allowed us to obtain the heat response with increased intensity for POPC/POPS-25% LUV titration into LAH4-L1. For the titration of POPC/POPS-14% and POPC/POPS-10% LUV into LAH4-L1 the heat of reaction was rather small even at increased peptide concentration. The enthalpies of the last titrations were equal, however the amount of the heat observed towards the end of titration is bigger than LUV dilution enthalpy (-0.02…-0.03µcal/sec, ***Figure VI-13***). It is quite probable that there are some reaction still ongoing (***Figure VI-13*** *b,c*), but we run out of the titrant (LUV suspension in the calorimetric syringe). The shape of the signal at the last titrations steps (***Figure VI-13*** *b,c*) and the presence of endothermic and exothermic components of the signal prompts the assumption that there are still some binding events.

The experimental set up is subject to few limitations. First of all, we cannot decrease the concentration of peptide in the cell, because the signal is very small. Another way of reaching bigger lipid-to-peptide ratio at the end of titration would be vesicles concentration increase. However, after 30 injections the concentration of lipid in the calorimetric cell is 3mM. Increasing the concentration of vesicles would lead to overcrowding in the ITC solution, which might introduce the additional noise. The shape and the intensity of the POPC/POPS-25% - LAH4-L1 last titration signals are close to the calorimetric response of vesicle dilution into corresponding buffer, but for two other experiments from this series the calorimetric signals most probably is not a vesicles dilution process.

The shape of the calorimetric response at the first few injection is unusual (***Figure VI-13*** *a,b,c*). A slow process takes place at low lipid-to-peptide molar ratios, and longer time between the injections required until the calometric response reaches a stable baseline. Each individual signal is the heat coming from multiple processes that are taking place upon peptide interaction with POPC/POPS vesicles. As they are resolved in time, we could recognise those enthalpy components. Namely, a fast exothermic process is followed by fast endothermic process, and the association reaction is finished with slow exothermic process during the first titration steps (***Figure VI-13***). The last peaks of ITC isotherm represent only a slow exothermic reaction. As the signal shape changes in the course of titration it indicates that some of the processes are terminated at lower lipid-to-peptide molar ratio than others.

We attempt to better resolve the various reaction steps the similar measurements at 37°C (***Figure VI-14***).

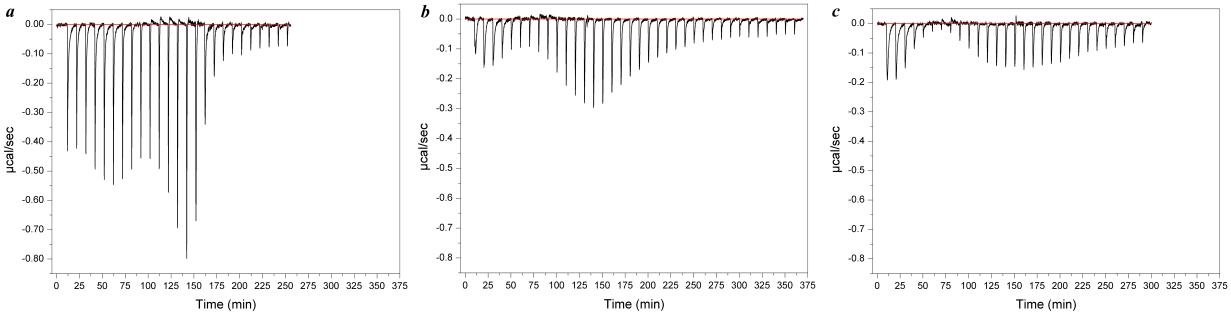

Figure VI-14. Isothermal calorimetry titration of 13mM POPC/POPS LUV into 150µM (a) and 100µM (b, c) LAH4-L1 solution at pH 7.4 and 37°C. Injection volume was 8µL (a, b) and 10µL (c). a) POPC/POPS-25%, b) POPC/POPS-14%, c) POPC/POPS-10%. The ITC signal is the heat change, measured in µcal/sec and plotted agaist measurement time.

The increase of temperature indeed helped to improve the heat response and shift the calorimetric response to the negative enthaply region. These ITC isotherms were represented as the enthalpy in kcal/mol of injectant (total lipids) plotted against lipid-to-peptide molar ratio (***Figure VI-15***) and compared with the enthalpy of POPC/POPS vesicles titration into LAH4-L1 at pH 7.4 and 25°C (***Figure VI-16***).

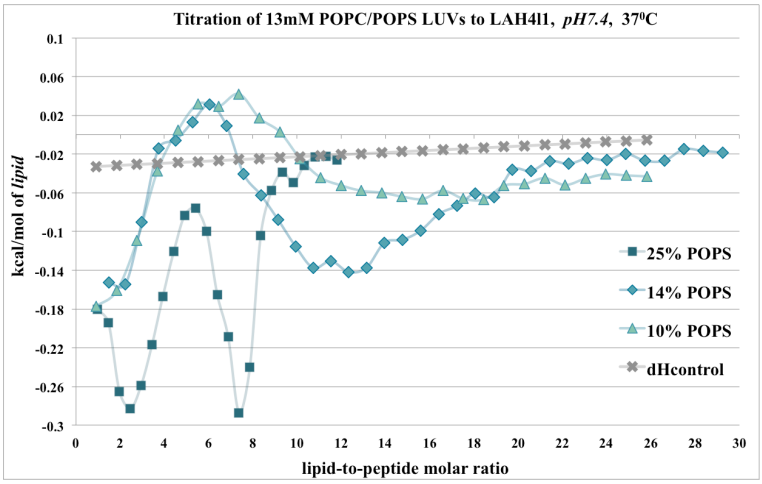

Figure VI-15. Integrated calorimetric response (δh) of 13mM POPC/POPS LUV titrated into 150μM (25% POPS) and 100μM (14% and 10% POPS) LAH4-L1 solution into 20mM HEPES buffer (pH 7.4) at 37°C. The enthalpy is expressed in kcal/mol and plotted agaist the lipid-to-peptide molar ratio.

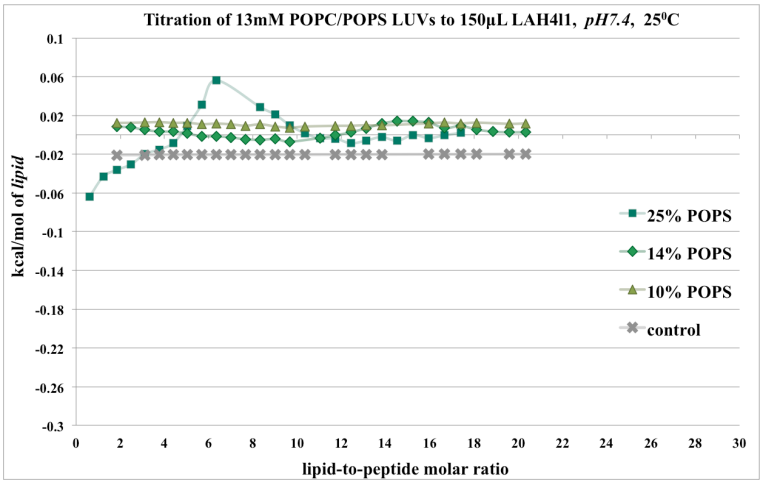

Figure VI-16. Integrated calorimetric response (δh) of 13mM POPC/POPS LUV titrated into 150μM LAH4-L1 solution into 50mM Tris buffer (pH 7.4) at 25°C. The enthalpy is expressed in kcal/mol and plotted agaist the lipid-to-peptide molar ratio.

The calorimetric signal of POPC/POPS LUV titrations into LAH4-L1 solution at pH 7.4 and 25°C is very small (***Figure VI-16***). Those calorimetric traces are already corrected for the vesicles dilution. The control experiment curve was plotted in the same graphs to give a comparable view of the heat change. The *δh* ranges of 14% and 10%-POPS LUV titration into peptide solution are comparable with that of control titrations of vesicles to buffer. Therefore, these titration isotherms could not be analysed. Based on ***Figure VI-13*** *a,b* it can be concluded that several processes occur simultaneously, which unfortunately can not be separated and quantified. Some energy contributions seem to cancel each other, thereby resulting in a weak signals. This is quite different from the ITC experiments at pH 5 (***Figure VI-11, 12, 13***, **B**). The calorimetric curves of titrations performed at pH 5 also reveal at least two processes – endothermic and exothermic, however the endothermic process dominates at low lipid-to-peptide ratios (at pH 5). Therefore the processes that could not be resolved in time, become partially resolved by changind the L/P ratio.

The ITC traces of experiments performed at 37°C are more suitable for analysis than those obtained at 25°C. However, the analysis is complicated because of irregularity of the calorimetric isotherm. The

shape of the curve confirms our previous observation that there are several processes at low L/P ratios occuring upon POPC/POPS vesicles titration into LAH4-L1 solution. This may be peptide aggregation and disaggregation on the membrane surface. It was shown previously that LAH4 peptide forms small aggregates in aqueous solutions at pH 7.4 (Marquette et al., 2008), and it will be shown by dynamic light scattering (Chapter VII) that LAH4-L1 also has this property. If the peptide forms small aggregates in the solution, these could disaggregate when exposed to a lipid bilayer.

^{15}N solid state NMR measurement on LAH4-L1 peptide reconstituted into mechanically oriented POPC/POPS membranes (Chapter I) confirmed a peptide orientation parallel to lipid bilayer surface at pH 5, and transmembrane at pH 7.4. It is therefore evident that peptide insertion into negatively charged POPC/POPS bilayers at pH 7.4 is accompagnied by the processes that have different calorimentric signature than those at pH 5.

The intensity of processes at pH 7.4 in low L/P region correlates also with the POPS content of membranes. We provide therefore the correlation of the enthalpy change on the POPS-to-peptide ratio (***Figure VI-17***) and compare it with the experiment at pH 5 (***Figure VI-18***).

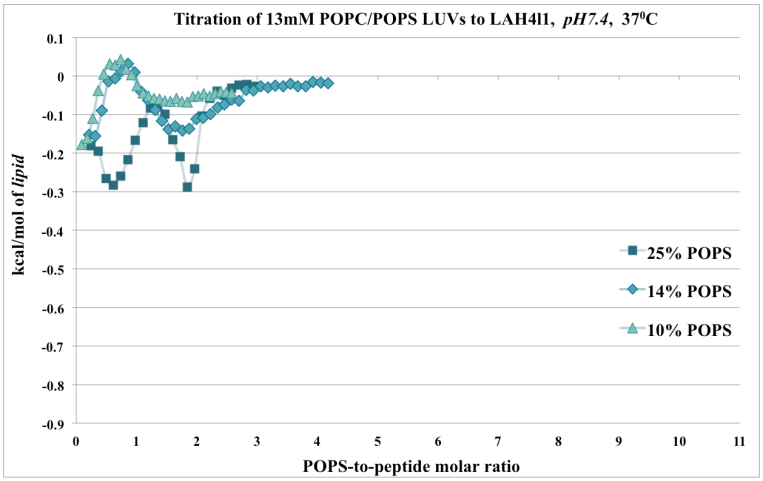

Figure VI-17. Integrated calorimetric heat of 13mM POPC/POPS LUV titrated into 150µM (25% POPS) and 100µM (14% and 10% POPS) LAH4-L1 solution into 20mM HEPES buffer (pH 7.4) at 37°C. The enthalpy is expressed in kcal/mol and plotted agaist the POPS/peptide molar ratio.

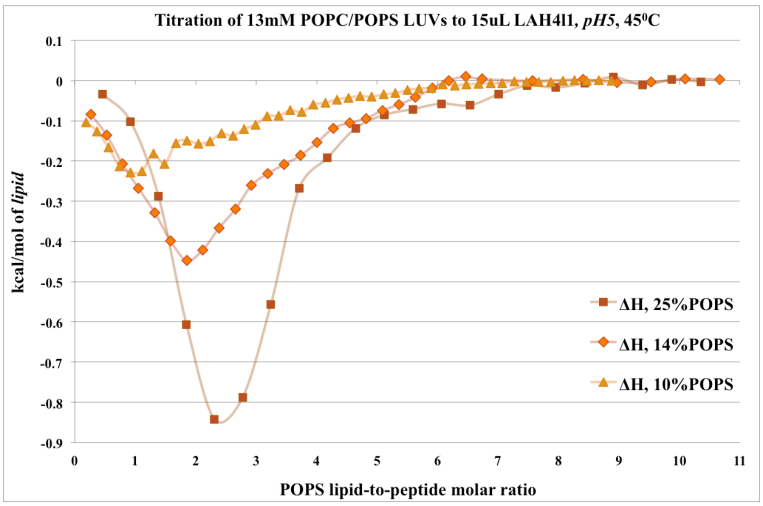

Figure VI-18. Integrated calorimetric heat of 13mM POPC/POPS LUV titrated into 15µM LAH4-L1 solution into 10mM acetate buffer (pH 5) at 45°C. The enthalpy is expressed in kcal/mol and plotted against the POPS/peptide molar ratio.

Displaying the calorimetric isotherms in this way helps us to reveal some common feature. The binding enthalpy approaches zero at the same POPS-to-peptide ratio for all three membrane compositions. This ratio is about 8 – 8.5 for the experiment at pH 5 (***Figure VI-18***). For the ITC measurement performed at pH 7.4 with POPS-10% membrane we did not reach the end of the binding processes, but with POPS-14% and POPS-25% the ratio at which the binding processes are terminated is around 3.5 POPS lipids per LAH4-L1 (***Figure VI-17***). This ratio is smaller by a factor of 2 than for experiment at pH 5. It probably means that at pH 7.4 POPC/POPS membranes are able to absorb 2x more peptides than at pH 5.

In other words, at pH 7.4 POPC/POPS-25% LUVs are capable of binding 5*mole%* of LAH4-L1, and each following portion of vesicles does not promote the peptides to leave their 'location' and to bind to this newly introduced and free of peptides vesicles. For POPC/POPS-14% membrane this value come to 2.9-3*mole%* peptide, and for POPC/POPS-10% membrane to 2mole% LAH4-L1. At pH 5 peptide binds to additional portions of POPC/POPS-25% vesicles until the concentration of embedded LAH4-L1 decreases to 2.5*mol*e%.

The magnitudes of the endothermic and the exothermic processes depend strongly on the POPS content of the membrane. *Note* that only X axes was normalized with respect to the POPS content (L/P ratio was represented as POPS/LAH4-L1), but not the enthalpy (Y axes, kcal/mol of total lipid). It is important to emphasize also that at pH 7.4 the peptide has around five positive charges (four terminal lysines and NH_3^+). At pH 5, in addition, four histidines in the central region of the peptide sequence become protonated. It was already mentioned in the introduction to this chapter that electrostatic attraction itself does not produce noticeable enthalpy change. But the formation of ion pairs between positively charged amino acids and phosphate residues of lipids head groups could produce the enthalpy change. It is difficult to decide on the basis of only ITC study if the histidines demonstrate greater affinity to POPS lipid molecules than the lysine residues, but it is clear that the presence of four additional positive charges promotes bigger enthalpy changes under peptide association with lipid bilayers.

LAH4-L1 titrations into POPC and POPC/POPS LUV at pH 5 and pH 7.4.

The addition of vesicles in small portions to LAH4-L1 solution promotes the several processes that contribute to the total enthalpy. This could be peptide aggregation on the membrane surface. Alternatively, the peptide could act as lysis agent favoring micellization of the lipid bilayer.

By reversing the titrant and titrate in calorimetric cell and syringe we start the measurement at the conditions of *high lipid-to-peptide molar ratio*. In this way we expect to obtain the calorimetric isotherm that would provide the information on peptide partitioning into the lipid bilayer rather than on some other processes. LAH4-L1 titrations into POPC/POPS vesicles were performed at pH 5 and pH 7.4, at 25°C. Futhermore, the similar titration experiments at pH 5 and pH 7.4 on LAH4-L1 interaction were made with zwitterionic POPC model membranes.

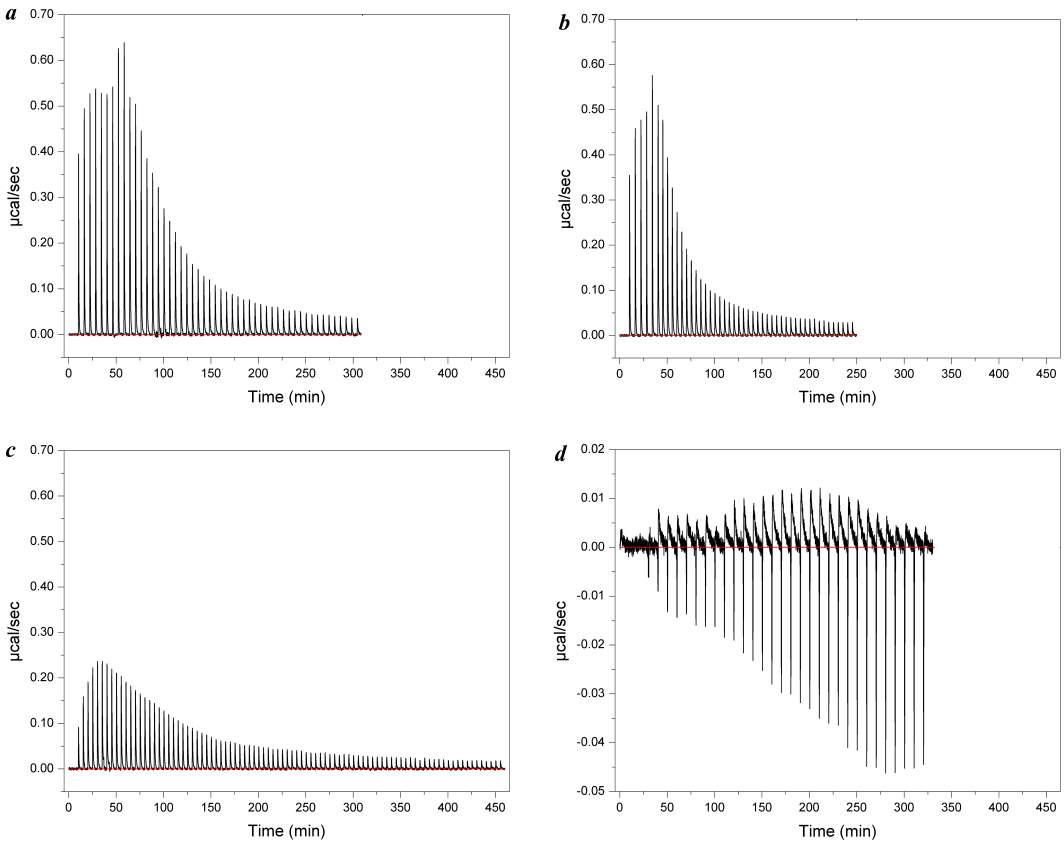

Figure VI-19. Isothermal calorimetry titration of 250µM LAH4-L1 into 325µM (a, b), 620µM (c) and 670µM (d) LUV solutions at pH 5 and 25°C. Injection volumes were 5µL (a, b) and 3µL (c) and 10µL (d). a) POPC/POPS-25%, b) POPC/POPS-14%, c) POPC/POPS-10%, d) POPC LUV. The ITC signal is the heat change, measured in µcal/sec and plotted agaist measurement time.

The calorimetric traces of the LAH4-L1 titration into POPC/POPS vesicles at pH 5 (***Figure VI-19*** *a-c*) shows narrow signals typical for fast processes. The calorimetric response is primarily endothermic. The signal does not descend to zero, but the last injections have equal intensity and are probably due to the peptide dilution enthalpy, or a small mismatch in buffer composition between peptide and the vesicles solutions. The stepwise insertion of LAH4-L1 into zwitterionic POPC lipid bilayer happens to exhibit a more complex calorimetric signature, however the intensity of the signal is much smaller and is in the range of the peptide dilution enthalpy (***Figure VI-19***, *d*). The peptide dilution control experiment was performed and the enthalpy of dilution was subtracted from the calorimetric traces. The calorimetric traces were processed and represented as heat change in kcal/mol of *peptide* plotted against the peptide-to-lipid molar ratio (***Figure VI-20***).

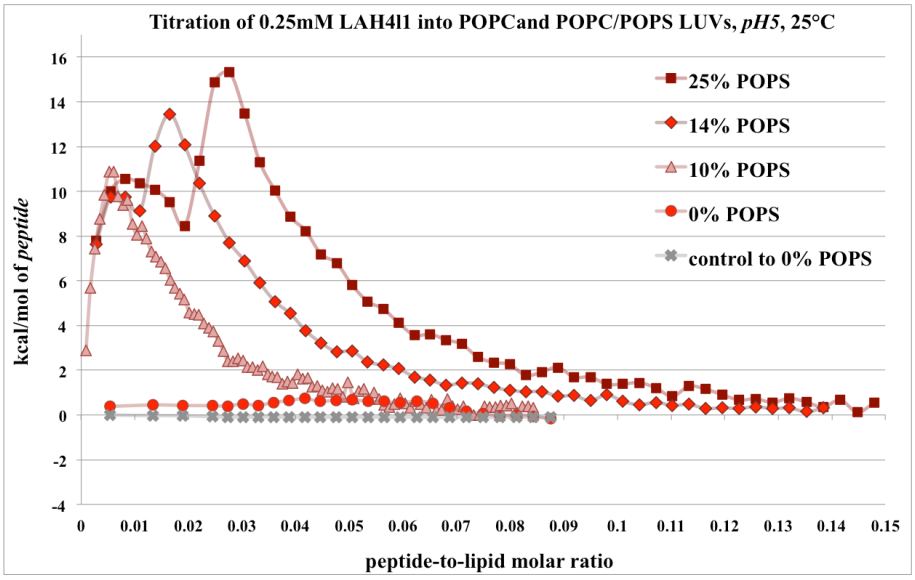

Figure VI-20. Integrated calorimetric heat of 250µM LAH4-L1 titrated into 325µM (25% and 14% POPS), 620µM (10% POPS) and 670µM (0% POPS) LUV solutions at pH 5 and 25°C. The enthalpy is expressed in kcal/mol and plotted agaist the peptide-to-lipid molar ratio.

The noticeable characteristics of the *peptide-into-vesicles* titration isotherm is that the enthalpies of peptide-vesicles interaction increase almost 20-fold (*cf.* ***Figure VI-14, 15, 16***). But it is not so striking when taking into consideration that the enthalpy is expressed now in kcal per mole of *peptide*. In other words, the energy changes in the system is monitored from the peptide 'point of view'.

In the beginning of calorimetric titration the peptide-to-lipid ratios are quite small 0.1-0.3*mole%* of LAH4-L1. At this step, all of the injected peptide is expected to bind completely to the vesicles, and each following titrant injection should give a same calorimetric response. However, we obtain a steep enthalpy increase at the P/L ratios 0…0.6*mole%*. This suggest again two simultaneous processes, (i) the peptide accumulation on the membrane leading to an endothermic signal of constant or slightly decreasing amplitude in the region of low P/L ratios, and (ii) an exothermic process of decreasing magnitude. The ITC curves (***Figure VI-19*** *a-c*) do not time-resolve the two-component calorimetric response, as we observed in the lipid-to-peptide titrations (***Figure VI-2***).

We have shown by ^{2}H NMR solid state spectroscopy that at pH 5 and a peptide concentration 1*mole%* LAH4-L1 that peptide perturbes the POPC lipids order in zwitterionic POPC membranes with the same efficiency that it affects the order of POPS lipids when inserted into POPC/POPS-10% membranes (***Figure VI-12***, C and D). It becomes obvious that huge heat release is connected to the peptide interaction with POPS lipid molecules, and most probably with the lipid headgroup phosphates. We assume that first peptide injections promote a lipid rearrangement and formation of lipid domains, as each peptide molecule prefers to interact with POPS rather than with POPC lipids (shown by ^{2}H NMR). Following portions of peptide interact with lipid bilayer releasing more heat than the previous ones. The observation concerns the region with small peptide concentration up to 1*mole%*. It is really difficult to explain the stepwise shape of POPC/POPS-25% and -14% LUV titration isotherms. The enthalpy shows a local minimum at 1.9*mole%* peptide for POPC/POPS-25% vesicles - LAH4-L1 interaction, and at 1.1*mole%* peptide for POPC/POPS-14% LUV. However those peptide-to-lipid ratios correspond to the same positive-to-negative charge ratios of 0.7 for both POPC/POPS-25% and POPC/POPS-14% membranes.

The membrane capacity to bind the peptide correlates with the POPS content. Accordingly to ITC isotherms (***Figure VI-20***), the peptide associates with POPC/POPS-10% vesicles until the total peptide

over lipid ratio in calorimetric cell reaches P/L=0.07. For POPC/POPS-14% membarnes this value makes about 0.12-0.13, and for POPC/POPS-25% membarnes ≥0.15. Those values do not mean that the total of 7*mole*%, 12*mole*% or 15*mole*% of peptide is bound to the POPC/POPS-10%, -14% or -25% vesicles, as the equilibrium between the bound and solution peptide is established. However these ratios are too high to assume only partitioning mechanism of binding. Most probably at high peptide concentrations LAH4-L1 is absorbed on the membrane surface by electrostatic interactions by not necessarily penetrate deeper in the bilayer.

It is difficult to draw unambiguous conclusions about the mechanism of LAH4-L1 interaction with **POPC** (***Figure VI-19****, d*) lipid vesicles based on the ITC curves, as the analysis is hampered by the low data quality. One reason is the small signal intensity. In addition several processes are still going on at the end of titrations, even if the peptide-to-lipid ratio reaches high value as 9*mole%*. Also, the necessary delays between the injections were a bit too short. Nevertheless some observations can be made. The individual calorimetric signal consist of two conponents (***Figure VI-19***, *d*), first fast exothermic process takes place followed by slower endothermic process. This fact exothermic signal consists mostly of the heat of peptide dilution into the buffer, which was shown in corresponding control experiment. There is also the maximum of enthalpy, but it is shifted to peptide-to-lipid ratio around 0.05.

The total enthalpy was calculated for each ITC titration of LAH4-L1 peptide into LUV suspension at pH 5 by adding the heats released in each tittration step. This total enthalpy was then normalized relative to the concentration of vesicles that were placed into calorimetric cell, given that the whole amount of vesicles participated into peptide binding.

LUV composition	c (LUV)	Σδh, kcal/mol	Σδh $_{normalized}$
POPC/POPS-25%	325	239	73,5
POPC/POPS-14%	325	162	49,8
POPC/POPS-10%	620	321	51,8
POPC	670	10,1	1,5

The analogous titrations of four types of the vesicles with LAH4-L1 solution was done at pH 7.4 as well. The calorimetric traces were processed and represented as heat change in kcal/mol of *peptide* plotted against the peptide-to-lipid molar ratio (***Figure VI-20, 21***).

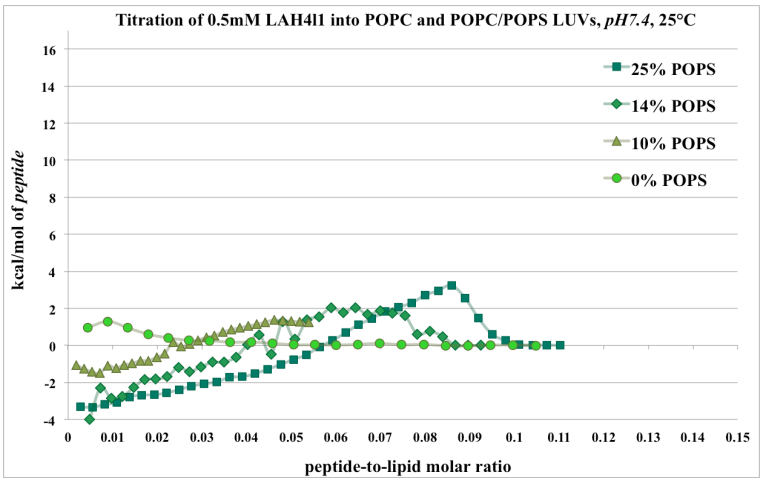

Figure VI-21. Integrated heat of 500μM LAH4-L1 into 0.65mM (25%POPS), 1.18mM (14%POPS), 1mM(10%POPS) and 400μM LAH4-L1 into 0.64mM (0%POPS) LUV solutions at pH 7.4, 25°C.

For displaying ITC isotherms of the experiment performed at pH 7.4 the same XY scale was use in order to facilitate the comparison with the isotherm at pH 5 (***Figure VI-21***). The remarkable difference is that on the initial titration steps an exothermic signal prevails. As soon as at pH 7.4 the LAH4-L1 peptide preferably adopts transmembrane alignments when inserted into POPC and POPC/POPS lipid bilayers, one could speculate that this exothermic process is connected to the on surface – to – transmembrane arrangement of peptide. Yet the penetration of the peptide into zwitterionic POPC membranes is not accompanied by that big heat absorption. At the same time it was shown by other methods that LAH4-L1 peptide penetrates POPC lipid bilayers and prefeably adopts transmembrane orientation (at peptide concentrations up to 1 – 2*mole%*), similarly as it does when interacting with mixed POPC/POPS membranes. Such it was confirmed once more time that calorimetric signal is induced primarily by LAH4-L1 interaction with POPS lipid molecules.

There is another part of calorimetric isotherm which is commom for the titrations at pH 7.4 and pH 5. This exothermic process is taking place under the titration of LAH4-L1 into zwitterionic as well as into mixed membranes. This positive enthalpy could be referred with a sustantial degree of certainty to the peptide absorption on the membrane surface. It was shown previously on the example of melittin and magainin-2 peptides that the random coil-to-α-helix conformation change is an exothermic process at the ambient temperatures (Klocek et al., 2009; Wieprecht et al., 2002). I suppose that the secondary structure change enthalpy is the major component of LAH4-L1 – POPC calorimetric signal. But for mixed POPC/POPS membranes there is obviously other exothermic component of ITC isotherm which could be referred to the interaction of peptide's positively charged amino acid sidechains with POPS lipid molecules.

Furthermore, I complete the investigation of LAH4-L1 – model membranes interaction with dynamic light scattering (DLS) and calcein release experiments.

VII. CONTROL OF VESICLES AGGREGATION UPON PEPTIDE ASSOCIATION.

The series of dynamic light scattering experiments was performed in order to assess the peptide – LUV system macroscopic behaviour such as vesicles aggregation upon the association with peptide. The experiment is used primarily as a control experiment to isothermal titration calorimetry and circular dichroism investigation. As vesicle aggregation may perturb those experiment, it is interesting to know under what conditions this aggregation takes place.

A single series of ζ-potential measurements was performed in order to determine the L/P ratio at which the vesicles surface charge is neutralized by peptides positive charge, and this ratio was correlated to the vesicles aggregation event. The ζ-potential is the surface potential measured at a distance of about 0.2 nm away from the membrane surface plane (or in general near the surface of charged particle), is such dependent on the concentration of ions that were attracted by the charged membrane surface.

MATERIALS AND METHODS

Sample preparation.

13mM stock solutions of 100nm large unilamelar POPC vesicles with varied POPS content (0%, 10%, 14% and 25%) were prepared as described in Chapter III. Two type of buffers were used for the sample preparation:

- 10mM acetate buffer / 0.5mM EDTA, pH≈5,
- 20mM HEPES buffer / 1mM EDTA, pH≈7.4,

0.5-1mM stock solutions of LAH4-L1 were prepared in corresponding buffers.

Dynamic light scattering spectroscopy.

Measurements were performed on a Zetasizer Nano ZS system (Malvern Instruments, Malvern, UK) equipped with a 4 mW He-Ne laser (λ_0=633 nm). 200µL to 500µL of the peptide/LUV solution was placed in quartz cell and the back-scattered light was collected at an angle of θ=173°.

In typical dynamic light scattering experiment the intensity of light is measured over time and represented as the time autocorrelation function of the scattered light (Frisken, 2001). The intensity autocorrelation functions were evaluated using a second-order cumulant analysis yielding the translational diffusion coefficient D. The mean hydrodynamic diameter (Z-average) was calculated from D by using the Stokes-Einstein equation. The size distributions were calculated from the diffusion coefficient distribution using the CONTIN routine built in a Malvern DTS analysis software, and the results are displayed as a set of parameters: Z-average particles size, polydispersity index (PDI) and the hydrodynamic diameters distribution by intensity, volume and numbers. More detailed explanation of principal DLS parameters can be found here:

http://www.malvern.com/en/support/resource-center/Whitepapers/WP111214DLSTermsDefined.aspx

DLS measurements are highly sensitive to particle aggregation, because larger particles produce more scattered light. Z-average particle size is the mean value of size distribution by intensity. It is standard DLS measurement parameter, but in polydispersed solutions Z-average shows rather the average size of big particles. The mathematical background of Z-average value calculation is briefly highlighted in *Appendix* part. The fundamental size distribution generated by DLS is an *intensity distribution*, which is converted, using Mie theory and taking into account sample refractive index, to a *volume distribution* (*Zetasizer Nano manual* 2004). The meaning of the principal DLS parameters will be discussed in more detail in the Results section.

Such several titration measurement series were performed in which either vesicles, or the peptide solution was placed into the measurement cuvette and the binding partner was titrated with small steps.

The samples were equilibrated at 25°C or 37°C for at least 30sec before each measurement. Each individual measurement was the result of 15 to 20 runs with ten seconds duration. The medium refractive index and the viscosity parameters were set to 1.33 and 0.8872cP (latex), respectively. The results are then presented as the set of parameters – derived count rate, Z-average size, and polydispersity index – and as a graphical distribution of hydrodynamic diameters (volume-weighted).

ζ-potential measurements were done on the same instrument using "Size & Zeta potential" folded capillary cell (DTS1060) (Malvern, UK) with at least 1mL of LAH4-L1 – LUV suspension. For each sample the instrument performed 20 scans with an initial equilibration time of 5 min at 25°C and a constant voltage of 40 mV. Values of the viscosity and refractive index were set at 0.8872 cP and 1.330, respectively. The zeta potential is calculated from the electrophoretic mobility, μ_E, by means of the Henry correction of the Smoluchowski equation (Dukhin and Semenikhin, 1970):

$$\zeta = \frac{3\mu_E\eta}{2\varepsilon_0\varepsilon_r}\frac{1}{f(\kappa a)}$$

where ε_0 is the permittivity of the vacuum, ε_r is the relative permittivity, a is the particle radius, κ is the Debye length, and η is the viscosity of water. The function $f(\kappa a)$ depends on the particle shape, which assumed to be spherical.

RESULTS AND DISCUSSION.

First of the test was done to setup the concentration range and other experimental parameters. Such DLS measurements were performed on 150μM LAH4-L1 solution in 20mM HEPES buffer, 2.5mM POPC/POPS-25% LUV in the same buffer, and on the 2.4mM LUV (25% POPS) with 138μM LAH4-L1 added. The result summary is presented in a ***Table VII-1*** and the size distribution by volume is displayed in a ***Figure VII-1***.

Table VII-1. The results of DLS measurements on LAH4-L1 peptide solution in 20mM HEPES buffer at 25°C, the POPC/POPS-25% LUV solution and 5.8mole% LAH4-L1 titrated into LUV solution.

Sample	Derived Count Rate (kcps)	Z-Average (d, nm)	PDI
150 μM LAH4-L1	459	310	0,369
2.5mM LUV (25% POPS)	155354	99	0,047
2.4mM LUV (25% POPS) + 138μM LAH4-L1 (5.8*mol* %)	167159	916	0,789

The principal DLS size measurement characteristics are provided in the ***Table VII-1*** and their description is given below.

As I mentioned in Materials and Methods section, DLS experiments generates time autocorrelation function. Cumulants method is applied to analyse this function, thus a number fitting parameters are produced. Only the first two terms derived by cumulants analysis are used in practice, a mean value for the size (so called Z-Average), and a width parameter, called polydispersity index (PdI). The Z-Average is an intensity-based calculated size value. Along with this value there is also volume-weighted size distribution displayed for comparison in a ***Figure VII-1***. The volume-weighted sizes are also calculated from autocorrelation function by taking into account the sample viscosity and refractive index, and assuming spherical shape of the particles. It is equivalent to the mass or weight distribution. In the highly monodispersed solutions mainly Z-average parameter is used to characterise the particles size. But in the

polydispersed solutions Z-average would indicate the average size of aggregates, while the distribution by volume reveals the presence of smaller particles. That is why we need to compare both parameters, intensity-weighted and volume-weighted hydrodynamic diameters. The former is presented in this work as its mean value, Z-average, and the latter – as the size distribution by mass (on the graphs). Please note, that Y-axis of the size distribution graph is relative and only informative within the single measurement. The percentage of scattered light in two different measurements cannot be compared using this value. One has to analyse the changes of *derived count rate* value instead. The X-axis, which shows the actual hydrodynamic diameters distribution, has logarithmic scale.

The polydispersity index higher than 0.3 indicates that the sample is polydispersed, if it equals to 0.05 or less – the sample is highly monodispersed.

Derived Count Rate is basically the number of photons detected per second. This parameter increases when the particles size or/and concentration increase.

The small value of derived count rate for the LAH4-L1 solution means that there is small quantity of large particles (measuring more than 100nm), despite Z-average value that says the particles diameter is 310nm. As I have already mentioned, Z-average value as well as whole DLS method is sensitive to scattering intensity produced for the most part by large particles. Basically, the result means that there are rather large oligomers presented in peptide solution, but the fraction of those particles is quite small.

For the LUV solution derived count rate is rather high, Z-average shows exactly the expected value of 100nm. The homogeneity of the sample is confirmed by the PDI value of 0.05. Adding 5.8*mole%* peptide does not cause the count rate to much increase. But Z-average rises 10-fold, as does the polydispersity index. Supposedly the vesicles undergo spontaneous aggregation when the peptide is added. The aggregates size distribution is represented in a ***Figure VII-1***.

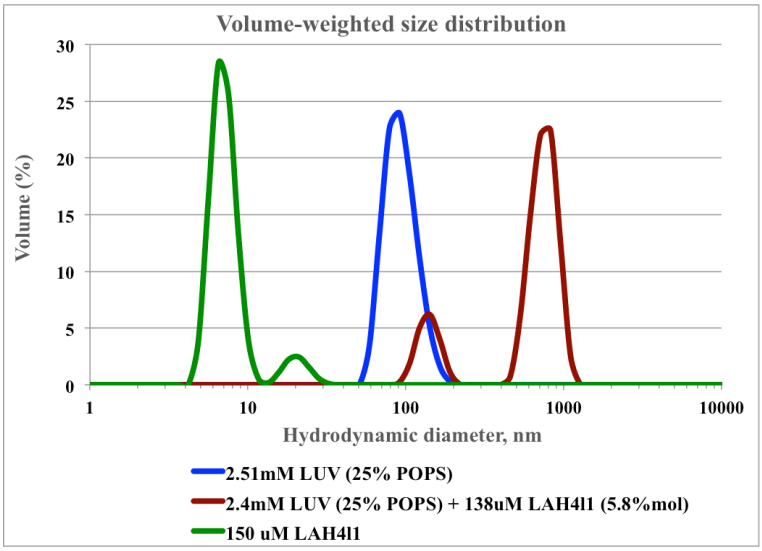

Figure VII-1. Volume-weighted particle size distribution assessed by DLS. The samples are LAH4-L1, POPC/POPS-25% LUV and 5.8% LAH4-L1 into LUV suspension.

DLS titrations of peptide with LUV and peptide into LUV suspension at pH 7.4

Furthermore the series of LAH4-L1 titrations into POPC/POPS-25% LUV was performed at 37°C in order to assess the optical properties of peptide-associated vesicles at various L/P ratios. ***Table VII-2*** provides the summary of titration conditions, as lipid-to-peptide ratio, and results summary, shown as the set of principal DLS size measurement parameters.

The lipid-to-peptide ratio decreases gradually from 216.7 to 6.2, and the positive-to-negative total charge ratio increases from 0.09 to 3.23 (***Figure VII-2***).

Table VII-2. The results of DLS measurements on POPC/POPS-25% LUV suspension in 20mM HEPES buffer at 37°C titrated with LAH4-L1 peptide. The series, which are shown in a Figure VII-2, are highlighted in gray.

Sample	L/P ratio	mole% peptide	+/- total ratio	Derived Count Rate (kcps)	Z-Average (d, nm)	PDI
1.18mM LUV (25% POPS)				80739	103	0,058
1.17mM LUV + 5.4μM LAH4-L1	216,7	0,52	0,09	79462	108	0,114
1.16mM LUV + 10.7μM LAH4-L1	108,4	0,92	0,18	80407	115	0,137
1.15mM LUV + 15.9μM LAH4-L1	72,2	1,4	0,28	80955	121	0,173
1.13mM LUV + 26μM LAH4-L1	43,3	2,3	0,46	80965	139	0,183
1.11mM LUV + 36μM LAH4-L1	31,0	3,2	0,65	80387	157	0,188
1.09mM LUV + 45μM LAH4-L1	24,1	4,2	0,83	116882	175	0,231
1.07mM LUV + 55μM LAH4-L1	19,7	5,3	1,02	148021	245	0,389
1.04mM LUV + 72μM LAH4-L1	14,4	7,1	1,38	151724	370	0,573
0.96mM LUV + 111μM LAH4-L1	8,7	11,5	2,31	93774	250	0,359
0.90mM LUV + 145μM LAH4-L1	6,2	16,7	3,23	81764	260	0,381

As soon as the vesicles suspension is highly monodispersed when there is no peptide in the solution, it is rather convenient then to use derived count rate as indicator of aggregation processes. The derived count rate displays quite stable value at around 80 000 – 80 500 kcps for non-aggregated vesicles at the concentration of 1.15mM. When total peptide concentration in the solution increases and the lipid-to-peptide ratio decreases to 24, the aggregation processes intensify, reaching the maximum at L/P=14.4. Under introduction of additional portions of peptide all three parameters (*derived count rate*, Z-average, PDI) decrease, it means that the vesicles undergo dissociation, yet not complete (***Figure VII-2***, 16.7% peptide). Derived count rate is sensitive not only to appearance of larger particles, but also to the concentration changes. Therefore, *dcr* decreases when we introduce additional sample volume under the titration with peptide. So, the approximation to initial concentration of *dcr* value has to be made. For instance, for the last titration step corrected value would be around 105384. However, the dependence is not necessarily linear, because the intensity is coming also from the aggregated particles, so I leave the value without recalculation (***Table VII-2***).

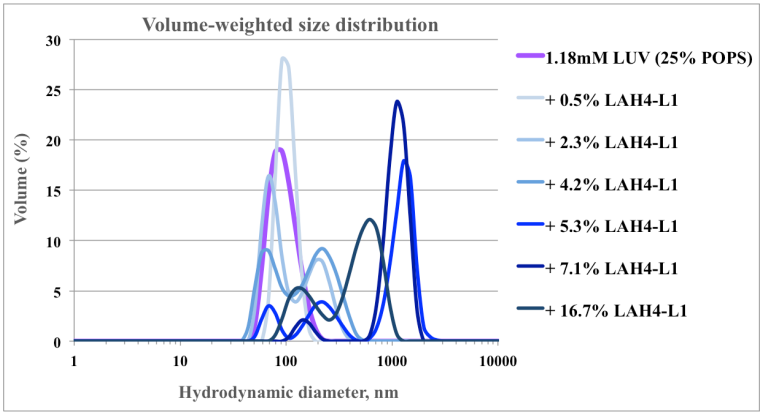

Figure VII-2. Volume-weighted particle size distribution assessed by DLS. POPC/POPS-25% LUV suspension in 20mM HEPES buffer at 37°C was titrated with LAH4-L1 peptide.

The series of reverse titration was performed with the same material, at the same temperature and pH conditions. 150µM LAH4-L1 solution was placed into the measurement cell maintained at 37°C, and titrated with POPC/POPS-25% vesicles. The same set of parameters was taken for analysis (***Table VII-3***). However, in this case derived count rate is not the most convenient parameter to follow the aggregation processes, because it increases with adding more vesicles into peptide solution.

Table VII-3. The results of DLS measurements on LAH4-L1 peptide solution in 20mM HEPES buffer at 37°C titrated with POPC/POPS-25% LUVs. The series, which are shown in a Figure VII-3, are highlighted in gray.

Sample	L/P ratio	+/- total ratio	Derived Count Rate (kcps)	Z-Average (d, nm)	PDI
150 µM LAH4-L1			578	177	0,243
149uM LAH4-L1 + 78uM LUV	0,52	38,5	4726	346	0,888
148uM LAH4-L1 + 154uM LUV	1,04	19,2	4860	425	0,414
146.5uM LAH4-L1 + 305uM LUV	2,1	9,6	13874	468	0,427
144uM LAH4-L1 + 548uM LUV	3,8	5,2	31508	393	0,371
141uM LAH4-L1 + 782uM LUV	5,6	3,6	71146	839	0,609
136uM LAH4-L1 + 1225uM LUV	9,0	2,2	68499	372	0,52
131uM LAH4-L1 + 1636uM LUV	12,5	1,6	100931	420	0,525
122uM LAH4-L1 + 2380uM LUV	19,4	1,0	229603	1795	0,999

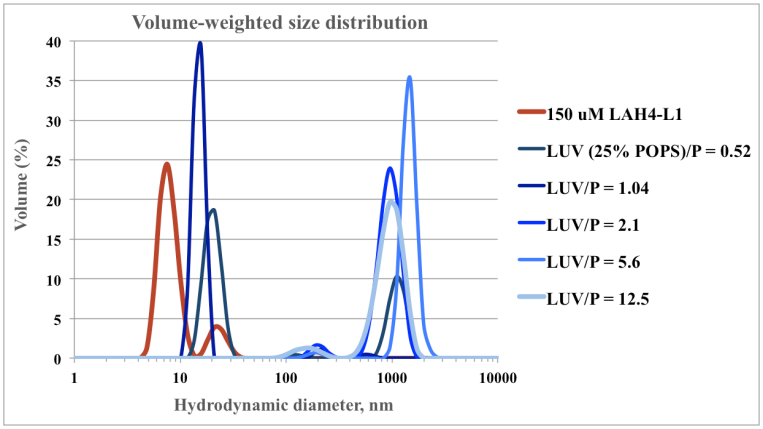

Figure VII-3. Volume-weighted particle size distribution assessed by DLS. Peptide solution in 20mM HEPES buffer at 37°C was titrated with POPC/POPS-25% LUVs.

In the case of LUV titration into peptide solution it is easier to make the conclusions about vesicles aggregation on the basis of the hydrodynamic diameter distribution by volume. Derived count rate is related to vesicles concentration, and does not provide the quantitative description of aggregation in this case.

Surprisingly, the vesicles aggregates start to form already when the first portion of vesicles was added. At the first titration step we have an important excess of peptide molecules in the solution when compare to number of LUVs. Supposedly, peptide molecules start to saturate the vesicles surface and neutralize the negative membrane surface charge, or even invert the surface charge to positive if there is a hydrophobic partitioning contribution to binding. When new portions of vesicles arrive, peptide is trying to distribute between LUVs, and to neutralize at maximum the surface negative charge. That could explain the increase of LUV aggregation at each following titration step. There is considerable fraction of peptide viewed by DLS during first titration steps when L/P ratio is still rather small (0.52 and 1.04). These particles with the size around 15-20nm are supposedly the peptide molecules, which accumulate around negatively charged lipids.

The effect of LAH4-L1 association with POPC/POPS-14% and POPC/POPS-10% LUV on vesicles aggregation was tested as well at pH 7.4 and 37°C. The results are presented in the ***Table VII-3,4*** and ***Figures VII-3,4***. Titration of LAH4-L1 peptide solution into POPC/POPS-14% and POPC/POPS-10% LUV at pH 7.4 and 37°C practically does not cause the vesicles aggregation. Principal DLS parameters, derived count rate, Z-average and PDI, stay close to the values characteristic for the vesicles suspension free of peptide. There are some aggregates observed at POPC/POPS-14% LUV-to-peptide ratio of 27.

Therefore the peptide-induced reversible vesicle aggregation depends strongly on the lipid bilayer surface charge density.

Table VII-4. The results of DLS measurements on POPC/POPS-14% LUV suspension in 20mM HEPES buffer at 37°C titrated with LAH4-L1 peptide. The series, which are shown in a Figure VII-4, are highlighted in gray.

Sample	L/P ratio	mole% peptide	+/- total ratio	Derived Count Rate (kcps)	Z-Average (d, nm)	PDI
1.18mM LUV (14% POPS)				79955	101	0,088
1.18mM LUV + 11μM LAH4-L1	108,4	0,92	0,3	85891	106	0,079
1.17mM LUV + 27μM LAH4-L1	43,3	2,3	0,8	93470	118	0,098
1.17mM LUV + 43μM LAH4-L1	27,1	3,7	1,3	99298	154	0,395
1.16mM LUV + 69μM LAH4-L1	16,7	5,9	2,1	98655	126	0,146
1.15mM LUV + 95μM LAH4-L1	12,0	8,3	2,9	102447	127	0,142
1.13mM LUV + 103μM LAH4-L1	8,7	11,5	4,0	103405	131	0,119
1.11mM LUV + 180μM LAH4-L1	6,2	16	5,7	102780	133	0,136

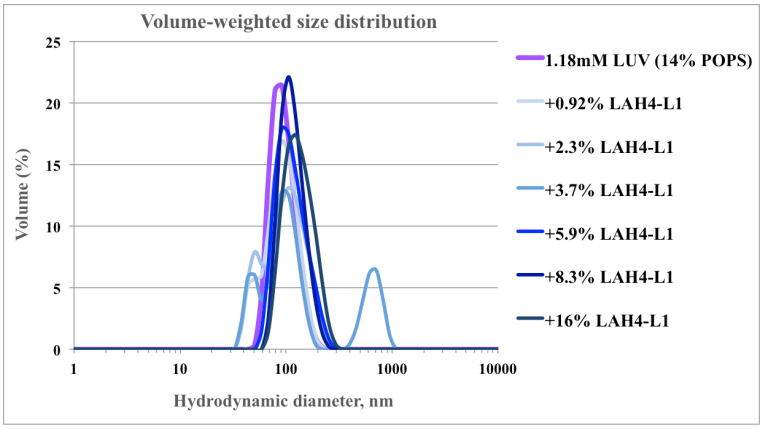

Figure VII-4. Volume-weighted particle size distribution assessed by DLS. Peptide solution in 20mM HEPES buffer at 25°C was titrated with POPC/POPS-14% LUV.

Table VII-5. The results of DLS measurements on POPC/POPS-10% LUV suspension in 20mM HEPES buffer at 37°C titrated with LAH4-L1 peptide. The series, which are shown in a Figure VII-5, are highlighted in gray.

Sample	L/P ratio	mole% peptide	+/- total ratio	Derived Count Rate (kcps)	Z-Average (d,nm)	PDI
1.2mM LUV (10% POPS)				26974	101	0,078
2.5mM LUV + 24μM LAH4-L1	104,0	0,96	0,5	182708	104	0,104
2.48mM LUV + 48μM LAH4-L1	52,0	1,9	1,0	184044	115	0,235
2.44mM LUV + 94μM LAH4-L1	26,0	3,8	1,9	172393	113	0,122
2.4mM LUV + 138.5μM LAH4-L1	17,3	5,8	2,9	175888	115	0,085
2.36mM LUV + 182μM LAH4-L1	13,0	7,7	3,8	180371	117	0,096
2.33mM LUV + 224μM LAH4-L1	10,4	9,6	4,8	183688	119	0,084
2.26mM LUV + 304μM LAH4-L1	7,4	13,5	6,7	174788	127	0,100
2.2mM LUV + 380μM LAH4-L1	5,8	17,2	8,7	144247	146	0,091

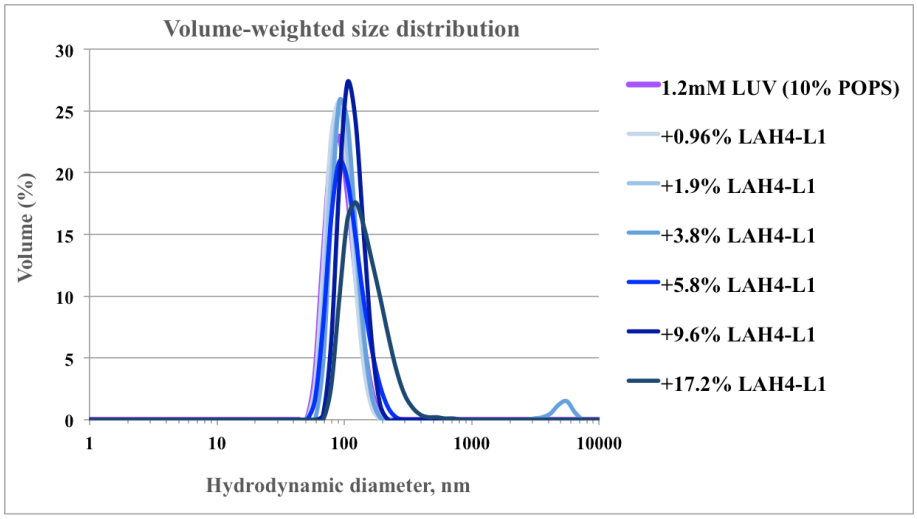

Figure VII-5. Volume-weighted particle size distribution assessed by DLS. Peptide solution in 20mM HEPES buffer at 25°C was titrated with POPC/POPS-10% LUV.

ζ-potential measurements on LAH4-L1 peptide bound to mixed POPC/POPS vesicles.

A single series of ζ-potential measurement was performed on POPC/POPS-14% LUV by titration with LAH4-L1 solution in 20mM HEPES buffer (pH 7.4) at 37°C. The average of three measurements is displayed (***Figure VII-6***).

The zeta potential is a measure of the difference in potential between the bulk fluid in which a particle is dispersed and the layer of fluid containing the oppositely charged ions that is associated with the nanoparticle surface. ζ potential of vesicles with increased fraction of bound peptide was found in the range of -44mV (in absence of peptide) to 24mV (corresponding to P/L molar ratio of 0.154). The curve crosses 0-value at *positive-to-negative total ratio* (+/-) equal to *2*, which corresponds to *L/P molar ratio = 17.5 and P/L = 5.7mole%*. For POPC/POPS-14% LUV the vesicles aggregation, observed by DLS, starts happening at total L/P ratio around 27, which corresponds to +/− = 1.3 (***Figure VII-4***). For POPC/POPS-10% only small fraction of vesicles aggregates under LAH4-L1 association at a +/− total ratio = 1.9 (***Figure VII-5***), whereas for POPC/POPS-25% vesicles aggregation takes place in a broad range of positive-to-negative total charge ratios from 0.18 to 3.2 (***Figure VII-2***). As one could observe by ζ-potential measurements, the +/− total charge ratio does not represent the charge equality on the membrane surface, as it takes into account all of membrane-associated and free peptides. Obviously at ζ=0mV the +/− ratio near membrane surface would be close to 1. On the other hand we could not state with certainty that 50% of peptide is bound to vesicles at this point. The peptide net charge is around 5 at the bulk pH 7.4, but this value can be lower when the peptide is not in solution, but is on the crowded membrane surface Thereby we are talking here about efficient +/- ratio on the membrane surface. The origin of this efficient peptide and membrane surface net charges is explained by Gouy-Chapman theory and discussed in more details on the example of melittin binding to mixed POPC/POPG vesicles (Klocek et al., 2009).

Nevertheless, zeta-potential data could be efficiently used to correlate the vesicles aggregation events with membrane surface charge. The correlation between surface charge neutralization by peptide and vesicles aggregation events was shown previously on the example of LAH4 peptide interaction with mixed POPC/POPS and zwitterionic POPC vesicles (Marquette et al., 2008, 2010).

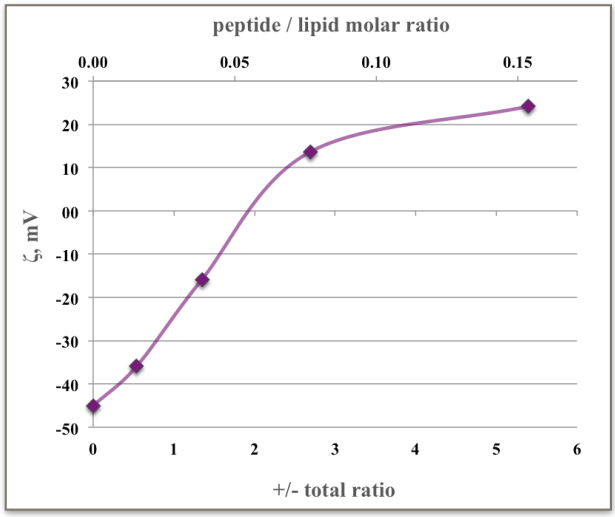

Figure VII-6. ζ-potential of 100nm POPC/POPS-14% vesicles titrated with LAH4-L1 solution in 20mM HEPES buffer (pH 7.4) at 37°C. The correlations of zeta-potential with peptide molar concentration (P/L) and positive/negative total charges ratio (+/−) are displayed.

DLS titrations of peptide with LUV and peptide into LUV suspension at pH 5

Similar investigations of lipid aggregation upon the peptide association were made at pH 5. The conditions were chosen to be close to ITC and CD titration measurements. So, in an individual experiment 15μM LAH4-L1 solution in 10mM acetate buffer was titrated with POPC/POPS large unilamelar vesicles with varied POPS content (10, 14, 25%). The principal DLS characteristics are presented in the ***Figure VII-7*** and ***Table VII-6***. PDI, Z-average and hydrodynamic diameter distribution indicate that in contrast to the vesicles behaviour at pH 7.4, at pH 5 LUVs nearly don't aggregate upon the titration into peptide solution. The only aggregation event was observed for POPC/POPS-14% at lipid-to-peptide ratio equal 20, but the aggregated disassociate at the next titration step. Unfortunately, the reproducibility of this DLS result was not checked, but there were the problems with increased scattering during POPC/POPS-14% CD titration into LAH4-L1 at L/P=50. Probably, at pH 5 there are some spontaneous aggregation events taking place when positive-to-negative total ratio is around 1-2, but those evens are may be not necessarily reproducible at the same lipid-to-peptide ratio. DLS data on 15μM LAH4-L1 indicates exclusively the presence of rather big aggregates of about 200-1000nm (***Figure VII-7***, green line). The reason for that is low concentration of peptide. At this condition the technique is not able to detect the monomers or small peptide oligomers, only big aggregates.

Table VII-6. The results of DLS measurements on POPC/POPS LUV suspension titrated into 15μM LAH4-L1 in 10mM acetate buffer (pH 5) at 25°C. The conditions where aggregation occurs are highlighted in colour.

Sample	L/P ratio	+/- total ratio	Derived Count Rate (kcps)	Z-Average (d,nm)	PDI
POPC/POPS-25%					
1.3mM LUV			47638	105,9	0,024
15μM LAH4-L1			50	1668	1
15μM LAH4-L1 + 30μM LUV	2,0	18	2129	115,8	0,042
14.9μM LAH4-L1 + 75μM LUV	5,0	7,2	5284	108,9	0,089
14.8μM LAH4-L1 + 149μM LUV	10,1	3,6	10011	109,1	0,047
14.7μM LAH4-L1 + 295μM LUV	20,1	1,8	24301	128,7	0,134
14.2μM LAH4-L1 + 713μM LUV	50,3	0,72	51623	116,9	0,057
13.4μM LAH4-L1 + 1350μM LUV	100,5	0,36	95698	109,1	0,07
POPC/POPS-14%					
1.3mM LUV			76755	111,3	0,044
15μM LAH4-L1 + 30μM LUV	2,0	31,6	2072	106,5	0,063
14.9μM LAH4-L1 + 75μM LUV	5,0	12,5	4878	108,2	0,077
14.8μM LAH4-L1 + 149μM LUV	10,1	6,3	10131	108,3	0,064
14.7μM LAH4-L1 + 295μM LUV	20,1	3,1	9264	767,8	1
14.2μM LAH4-L1 + 713μM LUV	50,3	1,25	55926	111,2	0,052
13.4μM LAH4-L1 + 1350μM LUV	100,5	0,63	63553	111,1	0,031
POPC/POPS-10%					
1.3mM LUV			48374	108,9	0,033

15µM LAH4-L1 + 30µM LUV	2,0	45	1385	107,9	0,069
14.9µM LAH4-L1 + 75µM LUV	5,0	18	2875	107,2	0,064
14.8µM LAH4-L1 + 149µM LUV	10,1	9	6887	107,7	0,067
14.7µM LAH4-L1 + 295µM LUV	20,1	4,5	14102	106,9	0,046
14.2µM LAH4-L1 + 713µM LUV	50,3	1,8	36919	114,9	0,077
13.4µM LAH4-L1 + 1350µM LUV	100,5	0,9	71405	111,4	0,024

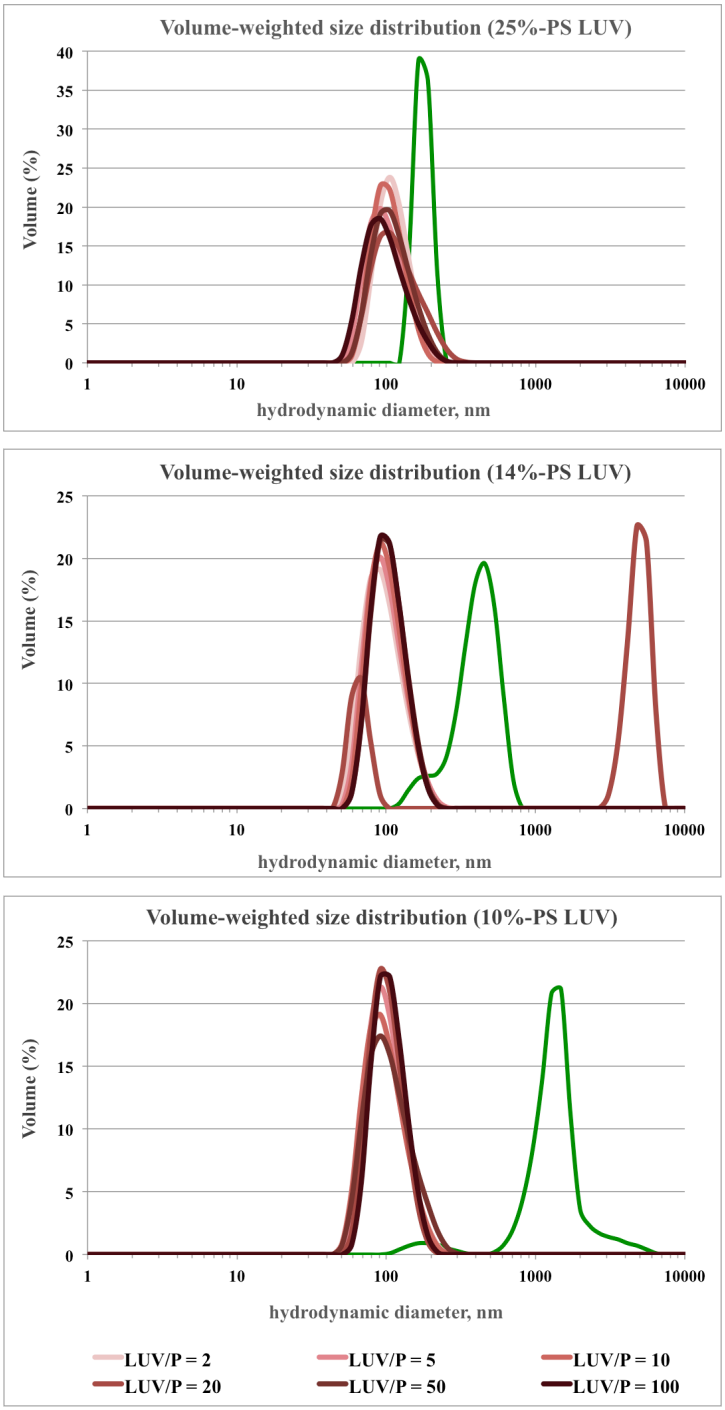

Figure VII-7. Volume-weighted particles size distribution assessed by DLS. POPC/POPS LUV suspension titrated into 15µM LAH4-L1 in 10mM acetate buffer (pH 5) at 25°C. Green line represents LAH4-L1 aggregates size distribution.

Finally, the series of DLS measurement were performed on LUV suspensions titrated with LAH4-L1 peptide solution (***Figure VII-8*** and ***Table VII-7***). The behaviour of vesicles is similar to what we observed at pH 7.4 under peptide titration to LUV, yet the aggregation rate is smaller at pH 5 in the case of POPC/POPS-25% vesicles. POPC/POPS-25% LUV start to form larger particles from lipid-to-peptide ratio of 28 to 11, which corresponds to positive/negative charge ratio range of 1.3…3.4. POPC/POPS-14% and POPC/POPS-10% aggregate only at certain L/P ratios of 50 and 83, respectively, at which +/- ratios make 1.25 and 1.09.

Table VII-7. The results of DLS measurements on POPC/POPS LUV suspension titrated with LAH4-L1 solution in 10mM acetate buffer (pH 5) at 25°C. The conditions where aggregation occurs are highlighted in colour.

Sample	L/P ratio	mole% peptide	+/- total ratio	Derived Count Rate (kcps)	Z-Average (d,nm)	PDI
POPC/POPS-25%						
6.3mM LUV				258228	120	0,083
627μM LUV + 1μM LAH4-L1	630	0,16	0,06	48678	125	0,064
621μM LUV + 3.5μM LAH4-L1	180	0,56	0,20	48820	124,6	0,086
612μM LUV + 7.3μM LAH4-L1	84	1,2	0,43	49374	126,7	0,067
600μM LUV + 11.9μM LAH4-L1	50	2	0,71	49586	125,7	0,088
578μM LUV + 20.6μM LAH4-L1	28	3,6	1,29	49843	139,7	0,161
553μM LUV + 30.7μM LAH4-L1	18	5,56	2,00	48789	146,6	0,163
508μM LUV + 48.4μM LAH4-L1	11	9,1	3,43	51444	146,8	0,224
POPC/POPS-14%						
6.3mM LUV				260788	107	0,07
627μM LUV + 1μM LAH4-L1	630	0,16	0,10	57338	104	0,067
621μM LUV + 3.5μM LAH4-L1	180	0,56	0,35	57617	104	0,082
612μM LUV + 7.3μM LAH4-L1	84	1,2	0,75	58838	105	0,065
600μM LUV + 11.9μM LAH4-L1	50	2	1,25	61100	115	0,236
578μM LUV + 20.6μM LAH4-L1	28	3,6	2,25	55619	104	0,052
553μM LUV + 30.7μM LAH4-L1	18	5,56	3,50	54529	105	0,071
508μM LUV + 48.4μM LAH4-L1	11	9,1	6,00	51230	105	0,071
POPC/POPS-10%						
6.3mM LUV				321191	107	0,08
611μM LUV + 3.5μM LAH4-L1	177	0,56	0,51	45867	104	0,054
602μM LUV + 7.3μM LAH4-L1	83	1,2	1,09	16633	206	0,439
590μM LUV + 11.9μM LAH4-L1	50	2	1,81	45115	100	0,056
569μM LUV + 20.6μM LAH4-L1	28	3,6	3,27	38755	99	0,092
544μM LUV + 30.7μM LAH4-L1	18	5,56	5,08	38846	100	0,056
500μM LUV + 48.4μM LAH4-L1	10	9,1	8,71	33582	102	0,057

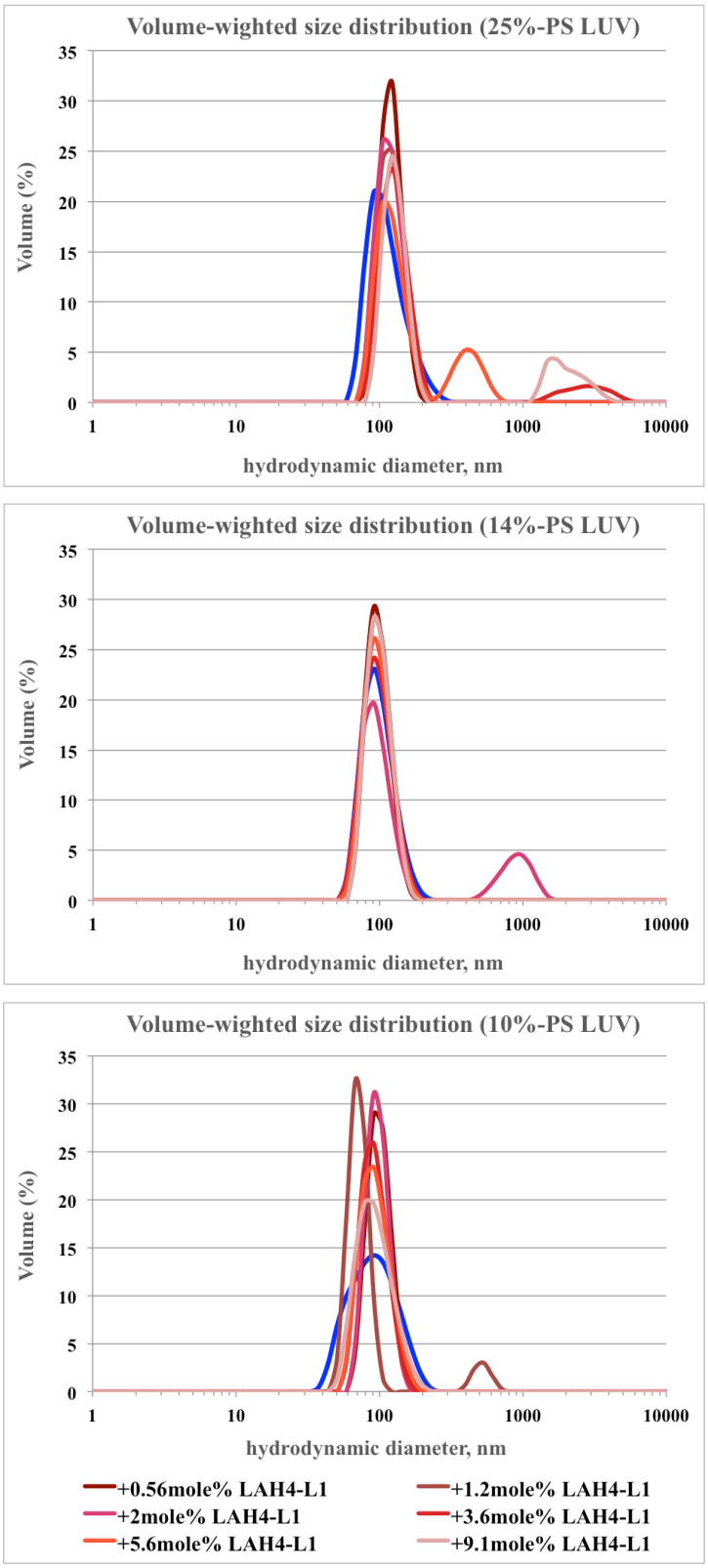

Figure VII-8. Volume-weighted particle size distribution assessed by DLS. POPC/POPS LUV suspension titrated with LAH4-L1 in 10mM acetate buffer at 25°C. Size distribution for 6.3mM LUV suspension is marked in blue.

Summary and conclusions.

Therefore it was confirmed by DLS measurements that peptide-induced vesicles aggregation is related to the membrane surface charge neutralization. POPC/POPS-25% vesicles that possess initially the highest negative surface potential are the most susceptible to the aggregation upon peptide association. Interestingly, at pH 5 we observe less aggregation of 25%-POPS LUV. At the acidic pH peptide adopts primarily parallel to membrane surface orientation, when at neutral pH – transmembrane. It means that the vesicle aggregation is also related to the peptide mode of interaction with lipid bilayer.

Vesicles aggregation does perturb strongly the circular dichroism measurements. That is why the CD experiment was conducted at pH 5 only. It remains not clear if the complex calorimetric response from LUV (25% POPS) titration into peptide solution is due to the vesicles aggregation (***Figure VII-5***), but apparently the vesicles aggregation does not affect the ITC response during the peptide titration into vesicles suspension at pH 7.4 (***Figure VI-21***), neither at pH 5 (***Figure VI-20***). Those characteristic enthalpy spikes in the ITC curve that belongs to LAH4-L1 titration into LUV (25% PS) suspension, appear at lower peptide molar concentrations (up to 3mole%) than those that induce vesicles aggregation (3,6 – 9mole%, ***Table VII-1***). Moreover, the vesicles aggregation, which leads to the particles precipitation, would augment significantly the noise level in calorimetric trace, which was not observed in out ITC experiments. The increase of the noise level was rather related to the temperature rise (45°C, ***Figure VI-1, 2, 3***).

VIII. LAH4-L1 MEMBRANE ACTIVITY ASSESSED BY THE CALCEIN EFFLUX ASSAY.

Calcein release assay is the method commonly used for assessment of pore formation and/or membrane disruption by antimicrobial and other membrane-active peptides. In typical procedure dye-loaded vesicles are titrated with the peptide solution, thus minimum concentration of the peptide required to cause the membrane disruption can be determined by measuring the fluorescence signal from released calcein. Knowing the dependence of fraction of the disrupted vesicles on the peptide concentration is helpful in revealing of the mode of peptide – membrane interaction.

MATERIALS AND METHODS

Vesicles preparation for calcein efflux assay.

For the preparation of large unilamelar vesicles the lipids were mixed in the ratio POPC/POPS=3:1w/w (25% molar of POPS), POPC/POPS=6:1w/w (14% molar of POPS), POPC/POPS=9:1w/w (10% molar of POPS). The total of 10mg of lipid was solubilised in chlorophorm-methanol=4:1, vortex and the solutions were dried under the nitrogen stream. The samples were exposed to the vacuum overnight in order to evacuate the traces of the solvents. The lipid films were rehydrated with 1ml buffer calcein containing buffer (20mM HEPES, 0.5mM EDTE, 50mM calcein disodium salt (Fluka, Switzerland), pH 7.4), and subjected to five freeze-thaw cycles. Then lipid solutions containing ≅13mM total lipids were passed 13 times though the syringe extruder (Avanti Polar Lipids Inc., Alabaster, AL, USA) equipped with 100nm (pore diameter) polycarbonate membrane (Avestin, Canada). The dye outside the calcein-loaded vesicles was removed by gel filtration through SephadexG-50 column(2.5×3.5 mm) (Sigma, USA). Eluting buffer was supplemented with 75 mM NaCl in order to compensate for the change in osmolarity induced by the presence of calcein and sodium counter ions. After the gel filtration the membranes were diluted by around 2.5-fold. The relative concentrations of the LUV suspensions was compared by measuring the dye release using fluorescence spectroscopy.

LAH4-L1 125μM stock solution was prepared in same buffer (20mM HEPES, 0.5mM EDTE, 75mM NaCl).

Calcein release measurements.

The measurements were performed on a Fluorolog 3–22 spectrometer (HORIBA Jobin-Yvon, Longjumeau, France). An aliquot of the LUV solution was added to 1mL of buffer in a quartz cuvette and equilibrated at 25°C inside the spectrometer. The vesicle suspension was kept at a constant stirring. The sample was excited at λ_{ex}=480nm and the intensity of fluorescence I_0 was recorded at λ_{em}=515 nm for about 10 min. A bandwidth of 0.5nm was set for both excitation and emission. In the following step the portion of peptide solution was added to the cuvette. The fluorescense signal was measured for 5-7min (I). Then the complete dye leakage from vesicles was caused by adding 10μL of 10%*w* Triton-100 detergent, and the fluorescence intensity was measured again (I_{max}).

The percentage of calcein released from the vesicles was calculated according to the formula :

$I\% = 100 \cdot (I - I_0)/(I_{Max} - I_0)$.

The series of measurement was recorded for all three vesicle types at various peptide concentrations. The correlation between the relative calcein fluorescence intensity (I%) and peptide-to-lipid ratio was derived (Figure IV.1).

Calcein is a small (about 1nm) fluorescent organic molecule. At high concentration calcein fluoresces very weakly because of fluorescence self-quenching. Thus, the calcein entrapped inside liposomes at high

concentrations is weakly fluorescent, while the calcein that has leaked out of the liposomes is highly fluorescent.

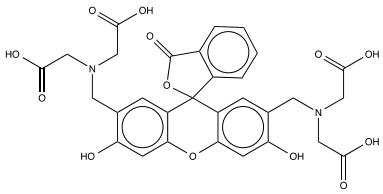

Because of this property, calcein has been widely used to probe membrane permeability (Katsu, 1999; New, 1990; Shimanouchi et al., 2009).

RESULTS.

Calcein release from POPC/POPS large unilamellar vesicles with varied POPS lipid fraction was used to characterize the pore forming or/and lytic activity of LAH4-L1 at pH 7.4. At peptide-to-lipid ratios up to 2*mole%* LAH4-L1 peptide binds to vesicles without causing significant calcein eflux. But between 2*mole%* and 4*mole%* its membrane rupture capability increases. Intrestingly the peptide's membrane rupture ability does not correlate with the POPS fraction inside the membrane in a direct manner. The hole-forming processes induced by peptide are most active for POPC/POPS-14% membranes. Therefore the efficiency of membrane rupture by peptide might be connected to lipid bilayer properties such as fluidity, not only to peptide properties.

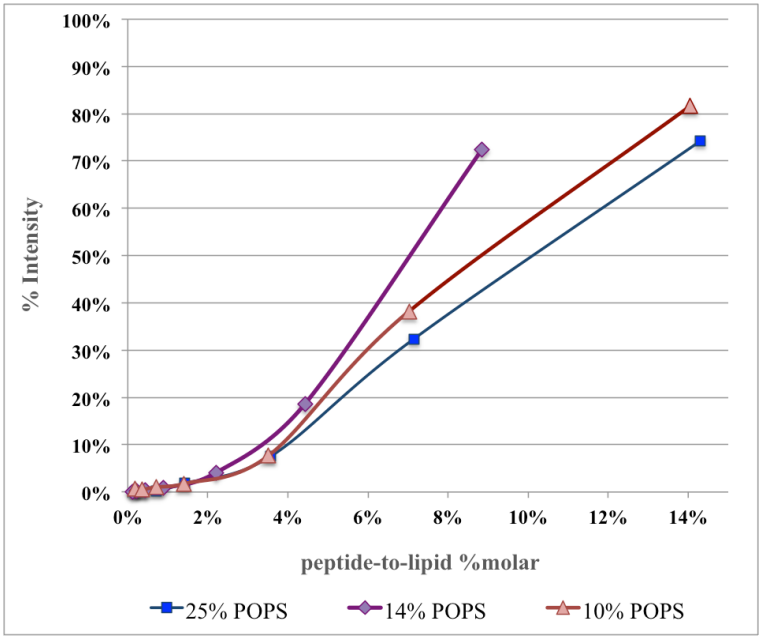

Figure VIII-1. Calcein release from POPC/POPS large unilamelar vesicles induced by LAH4-L1 peptide. The correlation between the relative calcein fluorescence intensity (I%) and peptide-to-lipid ratio is displayed.

GENERAL DISCUSSION ON THE MEMBRANE ACTIVITIES OF LAH4-L1.

As it is shown in previous chapter, LAH4-L1 cause the significant calcein efflux from mixed POPC/POPS vesicles at peptide molar concentations more than 2.5*mole%* (at neutral pH). The calcein release intensifies largely when the peptide-to-lipid total ratio rises to about 8-12*mole%* and reaches 70% (100% is complete calcein release, when the vesicles are destroyed by detergent). On the other hand there is no evidence of vesicle destruction or micellation viewed by *dynamic light scattering* in the analogous peptide-to-LUV titrational experiments (***Figure VII-2, 4, 5***), which probably means that this 70% calcein release is achieved via pore formation. Remarkably, some decrease (by 10-20nm) of the vesicle hydrodynamic diameter is observed for POPC/POPS-14% LUV when the peptide was added (0.93, 2.3 and 3.7mole% of peptide, ***Figure VII-4***), but a rather stable vesicle size (100nm) is observed at higher peptide concentrations. Interestingly, the peptide binding nearly does not change the hydrodynamic properties of POPC/POPS-10% vesicles, but as we observed in calcein release experiment, it disrupts the integrity of POPC/POPS-10% membranes as efficiently, as it does with PS-14% and PS-25% membranes (***Figure VIII-1***).

Knowledge of the membrane morphological changes during the peptide association is important as it can help considerably to understand the processes that are observed by ITC. To some extent we can claim that peptide does not cause the vesicle destruction even when the peptide is added at the concentrations as high as 15mole% in peptide-to-LUV titration experiment. Besides, in the reverse peptide-*into*-LUV ITC experiment we did not observe any processes occuring after peptide molar concentration reached 11mole % (at pH 7.4, ***Figure VI-21***). Membrane micellisation would supposedly contribute to ITC signal, as it was shown in the experiment on vescles solubilization by surfactants (Keller et al., 2006). And this process would intensify with the increase of peptide/lipid ratio, which was not observed. However, on the basis of the DLS reverse LUV-*into*-peptide titration experiment we cannot be sure whether peptide causes the LUV micellation or not. During the first two (DLS) titration steps we observed indeed the appearance of some particles of about 25nm, which may belong either to oligomeric form of peptide, or to the micellar structures (***Figure VII-3***). If those were peptide oligomers, it means that their formation was promoted by the presence of lipids. Of course, DLS is not the most suitable method to investigate the vesicles morphological changes, such as micellisation. Cryo-TEM should alternatively be used for this purpose, as it was done in similar investigation with mastoparan X peptide (Henriksen and Andresen, 2011).

When the titrations of POPC/POPS vesicles into LAH4-L1 solution were performed at pH 5, no remarkable decrease of the vesicles' hydrodynamic diameter was detected. Some minor LUV aggregation occurs at certain P/L ratios, but only an increase of the averaged hydrodymamic diameter is observed in such cases. Notably, the initial peptide concentration in solution, in addition to the lipid-to-peptide ratio, can modulate the vesicles aggregation or/and disruption processes. An LAH4-L1 concentration of 15μM was used in the experiment at pH 5, but 150μM at pH 7.4. The concentrations were chosen in a way that DLS experiment could serve as the control experiment to ITC and CD measurements.

The approach of using *direct* (LUV into peptide) and *reverse* (peptide into LUV) titrations was applied to conduct ITC and DLS experiments. The two approaches provide a different view of processes that are happening upon the peptide association with lipid vesicles. When LAH4-L1 is titrated *into* the LUV suspension, the membrane surface is gradually saturated with peptide molecules. On the initial titration steps, when the lipid-to-peptide ratio is high, all peptide molecules would supposedly adopt the most energetically favorable conformation inside the lipid bilayer. On the later titration stages, the membrane surface continues to accumulate the peptide until it is saturated, but the peptide does not necessarily penetrate *into* lipid bilayer when its surface concentration is elevated. In the case of LUV-*into*-peptide

titration, during the first titration steps there will be rather big excess of peptide molecules that are attracted electrostatically to small portiona of vesicles, which supposedly creates a high surface concentration of peptides. Such accumulation on the membrane surface may prevent the peptide to adopt the most energetically favourable conformation, and promote the peptide's dislocation to the vesicles that arrive in the next titration steps. At certain L/P ratio the reaction will stop and the additional portion of vesicles won't associate with the peptide molecules.

It is possible that at elevated concentrations LAH4-L1 peptide forms some oligomeric structures not only in the buffer solution, but also on the membrane surface or inside the lipid bilayer. Unfortunatelly, there is no direct confirmation of such peptide aggregation on the membrane surface in the experiments provided in this work. Only the increase of ζ-potential to high positive value (+24mV, ***Figure VII-6***) indicates the peptide accumulation into lipid bilayer occurs even after membrane surface charge neutralization (ζ=0).

The above-mentionned processes could be reviewed again in the scope of the ITC results. As it was already described in the Chapter VI, the ITC isotherms obtained from the LUV-into-peptide titration isotherms at pH 5 have a particular shape with an enthalpy minimum. The isotherms indicate that some endothermic process prevails at low L/P ratio, but the enthalpy descends rapidly to 0, then to negative values, and the second part of the titration curve is governed by exothermic processes. Such a shape of the calorimetric isotherm was found to be characteristic for the association of other membrane-active peptides (mastoparan X, melittin and magainin-2) with mixed negatively charged vesicles, as reported in the corresponding publications (Henriksen and Andresen, 2011; Klocek et al., 2009; Wenk and Seelig, 1998). The autors referred observed enthalpy changes to the process called *aggregation – pore formation.* According to this hypothesis the calorimetric heat trace is governed by the formation and subsequent disappearance of peptide pores, or peptide aggregates. The formation of lipid domains is also possible.

The concept was first introduced by Seelig and co-workers (Wenk and Seelig, 1998) to describe ITC isotherms from the association of magainin-2-amide with negatively charged POPC/POPG vesicles. Magainin-2- amide solutions of varied concentration were placed in the calorimeter cell and titrated with POPC/POPG small unilamelar vesicles. The binding enthalpy was purely exothermic when the concentration of peptide was low (≈ 6 μM), but a second endothermic process interfered with the calorimetric isotherm at increased peptide concentrations (≈ 20-30 μM). The endothermic process takes place mainly at the initial titration steps, when L/P ratio is small. The heat that was absorbed during this initial part of the titration is then returned as an enlarged exothermic component in the second part of titration isotherm (Figure 3 in the reference *Wenk and Seelig, 1998*). All the measurements were taken at 30°C in 10 mM Tris (pH 7.4), 100 mM NaCl buffer. At this temperature the exothermic process was prevailing at each titration step.

In two another studies ITC measurements recorded as a function of the temperature. In such a manner changes the magnitude of the enthalpy of exothermic or/and endothermic process were achieved. In order to facilitate the discussion I provide here the original calorimetric traces of the corresponding publications, adapted with permission from the authors.

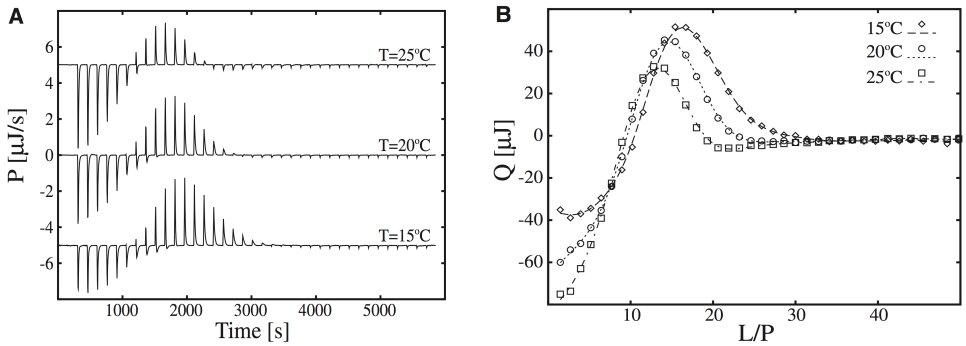

Figure Ad1. (A) Calorimetric heat traces of lipid-into-peptide titrations conducted at 15°C, 20°C, and 25°C (38×1µL 18.9 mM POPC/POPG (1:3) injected into 204µL of 100µM MPX). (B) Integrated heat trace Q of (A).
Adapted from (Henriksen and Andresen, 2011).

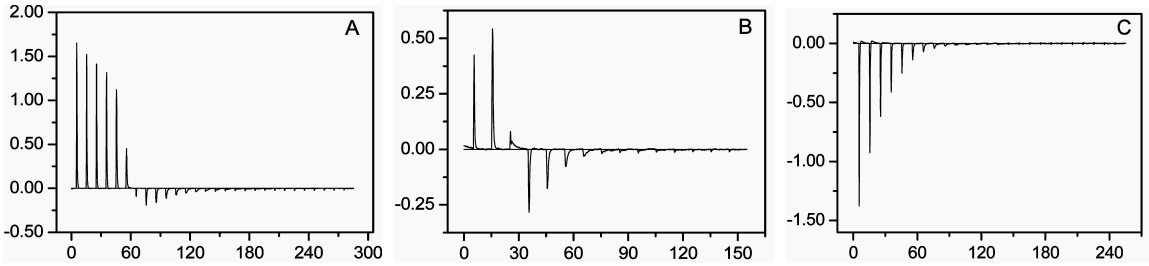

Figure Ad2. Isothermal titration calorimetry with synthetic melittin and LUVs. Melittin in buffer is titrated with 100 nm unilamellar POPC/POPG (3:1) vesicles in the same buffer. The experiment was performed at (A) 10, (B) 28, and (C) 50°C. The experimental binding enthalpy (ΔH°exp) at 28°C is zero, and the endothermic peaks of the first phase are exactly compensated by the exothermic peaks of the second phase of the titration [25 mM Tris and 50 mM NaCl (pH 7.4)]. Heat flow is measured in µcal/sec and plotted against the measurement time (min).
Adapted from (Klocek et al., 2009).

In the first study the binding of membrane-active peptide Mastoparan X (INWKG IAAMA KKLL-NH2) to mixed POPC/POPG vesicles was investigated by ITC (***Figure Ad1***), DLS and cryo-TEM.

In the second study under the similar conditions (pH, lipid composition) the binding of melittin (GIGAV LKVLT TGLPA LISWI KRKRQQ-NH2) to the mixed negatively charged vesicles was studied by ITC (***Figure Ad2***) and other biophysical methods under similar conditions (pH, lipid composition).

The common feature of this two calorimetric studies, as well as the ITC on LAH4-L1 – mixed LUV interaction at *pH 5*, is the presence of two enthalpy component with the opposite sign at the ambient temperature.

In the beginning of the vesicles-to-melittin titaration the endothermic component is dominant (Figure Ad2. A, B), then the enthalpy decreases to negative values reaching a minimum, similarly as it was observed in POPC/POPS binding with LAH4-L1. At high temperatures the endothermic component does not appear any more (Figure Ad2. C). On the contrary, the titration curve of MPX with POPC/POPG vesicles starts with exothermic process, then the enthalpy increases reaching a maximum (Figure Ad1). The authors (*Henriksen and Andresen*) refer to the first part of the titration isotherm as ‘pore formation’, and second as ‘pore desintegration’. The change of the sign of pore-forming energy comparing to mellitin the authors explain, with the reference to the work of team from Basel (Klocek et al., 2009), by a difference in length between melittin (26 residues) and MPX (14 residues) and thus in their ability to span the lipid bilayer. This assumption is consistent with behavior of LAH4-L1 under similar ITC experiment conditions if consider only the length of peptide – 26 amino acids (KKALLAHALHLLALLALHLAHALKKA-NH2) – which is close the length of melittin molecule, as

far as the hypotetic 'pore formation/peptide aggregation' enthalpy is also endothermic for LAH4-L1 at pH 5.

On the other hand, the calorimetry data have to be analysed by taking into account the mechanism of membrane penetration, which is closely related to the peptide alignment inside the lipid bilayer. In was suggested initially (for review please see *Raghuraman and Chattopadhyay, 2007*) that *melittin* induces pore formation when it adopts transmembrane alignments at high peptide-to-lipid ratios, whereas the orientation parallel to lipid bilayer, which prevails at low peptide concentrations, was generally considered as inactive. The toroidal model of pore formation by mellitin embedded into zwitterionic POPC membranes was proposed by Huang and co-workers (Yang et al., 2001). They have shown by oriented circular dichroism and neutron difraction that 85% of peptide is oriented parallel to the POPC bilayers at P/L=1/40, but 68% of peptides were transmembrane at P/L=1/15.

This finding of pore forming peptide concentration threshold was confirmed independently by Ladokhin and White by employing the membrane leakage assay. The release of entrapped fluorescent dextran markers of two different molecular masses (4 and 50 kDa) showed that mellitin-induced pores with determined diameter were formed in POPC membranes. However, melittin induced leakage from mixed POPC/POPG vesicles was not size-selective, thus a 'detergent-like' mechanism was proposed for destabilization of POPC/POPG membranes by melittin (Ladokhin and White, 2001). This mechanism of melittin interaction with mixed anionic membranes, found by Ladokhin and White, was confirmed in a more recent study (Svensson et al., 2011). The autors have shown by tryptophane fluorescence and linear dichroism (LD) methods that melittin peptide exercises its lytic activity on mixed DOPC/DOPG membranes via a carpet-like mechanism. However, their LD and fluorescence spectroscopy data on zwitterionic DOPC membrane – melittin interactions at L/P=15 were inconcistent with the pore-forming mechanism suggested earlier (Ladokhin and White, 2001; Yang et al., 2001), because they could not detect a sufficient fraction of transmembranely aligned peptides (Svensson et al., 2011). The ITC study referred above (Klocek et al., 2009) concerns the melittin interaction with charged POPC/POPG vesicles.

The *mastoparan X* peptide is adopting an α-helical conformation encompassing residues 3-14 when interacting with mixed model membranes (DPPC/DPPG=80:20, Todokoro et al., 2006), with the charged lysine sidechains forming an angle of about 100°. The orientaton of MPX into mixed anionic DMPC/DMPG 7:3 membranes was determined by NMR and is preferably in-planar with small fraction of peptide oriented perpendicular to lipid bilayer plane. The distribution of alignment was calculated from ^{15}N solid-state NMR spectra (Hori et al., 2001). At the peptide-to-lipid ratio of 10*mole%*, the two populations of 90% in-plane and 10% trans-membrane helices are characterized by a mosaic spread of ±30° and ±10°, respectively. However, binding of MPX to POPC/POPG vesicles was studied by ITC, which does not allow a direct comparison with structural data, performed in DMPC/DMPG. One should remember that DMPC/DMPG and POPC/POPG lipid bilayers possess different acyl chains, therefore have different hydrophobic thickness and area per lipid characteristics; and considerable differences in membrane alignment was observed for related peptides including LAH4 when these membranes are compared to each other (Salnikov and Bechinger. 2011, Strandberg 2013, Perrone, 2011 PhD). The hydrophobic thicknesses for the single component DMPC and POPC membranes were determined by neutron scattering and related methods, and equal to ~26.2Å (Mecke et al., 2005; Nagle and Tristram-Nagle, 2000) and ~27.7Å (Leidy et al., 2006) in their liquid crystalline phase, respectively.

The *LAH4-L1 peptide* was found to adopt preferably in-plane alignments in oriented POPC/POPS membranes as shown by ^{15}N solid state NMR spectroscopy. Peptide orientation was tested for peptide-to-lipid ratios as high as 4*mole%*, and the LAH4-L1 in-plane orientation at high peptide concentration was stabilized by the presence of 25% POPS (for details please see Chapter III). Of course, solid state NMR

experimental conditions are quite different from ITC conditions. There is practically no bulk solution in the sample that consist of stacked oriented bilayers and glass plates. Still it is a well validated method for determination of peptides alignment into lipid bilayers (Salnikov et al., 2010).

When returning to *magainin-2-amide* association with mixed POPC/POPG membranes (Wenk and Seelig, 1998), the pore formation enthalpy was reported to be positive. The structural studies show that magainin adopts essentially parallel to lipid bilayer orientation when emebedded into lipid bilayers of various compositions (Bechinger et al., 1993; Salnikov and Bechinger, 2011). Therefore, it cannot be the formation of 'classical toroidal pores' , which would require a transmembrane alignments of the peptide.

Thus the structural and calorimetric data could be shortly summarized:

- Mastoparan X: INWKGIAAMAKKLL-NH2, 14aa,
  orientation is mostly in-planar in DMPC/DMPG mixed membranes,
  supposed 'pore formation/peptide aggregation' is an exothermic process in POPC/POPG membranes;
- Melittin: GIGAVLKVLTTGLPALISWIKRKRQQ-NH2, 26aa,
  orientation is mostly in-planar in DOPC/DOPG mixed membranes even at high P/L ratio,
  supposed 'pore formation/peptide aggregation' is an endothermic process in POPC/POPG membranes;
- Magainin-2: GIGKFLHSAKKFGKAFVGEIMNS-NH2, 23aa,
  orientation – parallel to lipid bilayer in membranes of various compositions,
  supposed 'pore formation/peptide aggregation' is endothermic process in POPC/POPG membranes;
- LAH4-L1: KKALLAHALHLLALLALHLAHALKKA-NH2, 26aa,
  orientation at pH 5 – parallel to lipid bilayer in POPC/POPS 3/1, 6/1, 9/1 membranes,
  the process that dominates at high P/L ratio is an endothermic process in POPC/POPS membranes;
  orientation at pH 7.4 – mostly transmembrane in POPC/POPS 3/1, 6/1, 9/1 membranes.

It is difficult to determine the sign of supposed peptide aggregation enthalpy because of the complex calorimetric response during lipid-to-peptide titrations (***Figure VI-15***), but peptide-to-lipid ITC curve shape (***Figure VI-21***) make us believe that peptide accumulation on the membrane surface at pH 7.4 is an endothermic process too, as soon as the calorimetric signal changes the sign from – to + at high peptide-to-lipid ratio.

In ITC studies on MPX and melittin (Henriksen and Andresen, 2011; Klocek et al., 2009) the temperature was determined, at which the endothermic component of titration enthalpy compensates exothermic component resulting in total binding enthalpy equal zero ($\Sigma\delta h_i=0$). This temperature was determined by direct LUV-to-peptide titrations, as well as by the peptide into lipid reverse calorimetric titrations, at the temperature ranging from 10°C to 60°C, it makes T_{zero}=28°C for melittin and 19°C for MPX. As the enthalpy associated with the membrane partitioning reaction equals 0 at the corresponding temperature, exclusively the processes of pore formation – desintegration are observed. T_{zero} value depends on the system under investigation, *i.e.*, the peptide, lipid membrane composition and buffer system. Also, it is impotant to emphasize that all the ITC experiments disscussed here were performed with 100nm large unilamelar vesicles.

Below the recapitulation of the ITC results will be made completed by the structural details.

POPC/POPS LUV calorimetric titrations into LAH4-L1. The results of calorimetric titrations of large unilamelar vesicles into an LAH4 –L1 solution were presented and discussed in the Chapter VI. For the LAH4-L1 – vesicles interaction at pH 5, the correlation of total enthalpy with temperature was detected (***Figure VI-7b***). The total enthalpy presented here is a sum of the integrated heat released or absorbed in each titration step, normalized per mole of injected lipids. This total enthalpy correlates linearly with temperature for POPC/POPS-25% membranes, yielding zero at around 22-23°C, similarly as for the

melittin peptide (T_{zero}=28°C). However the correlation is not linear for POPC/POPS-10% and POPC/POPS-14% LUV interaction with LAH4-L1. In each of the cases the *total enthalpy* of association reaction decreases with the temperature, and is negative at 25°C and 45°C. Remarcably, at 14°C the total enthalpy observed upon vesicles association with LAH4-L1 (***Figure VI-7b***) has an identical value for each membrane composition, but the same correlation was not observed at other temperature conditions.

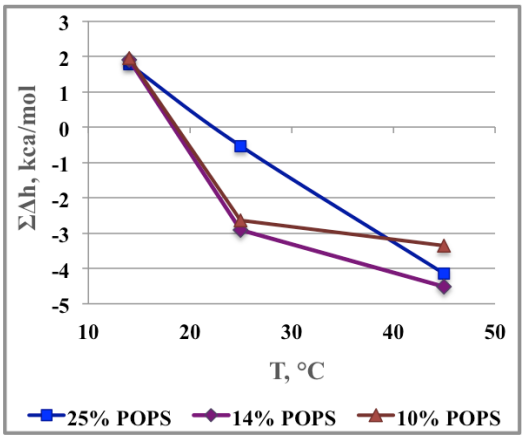

Figure VI-7b

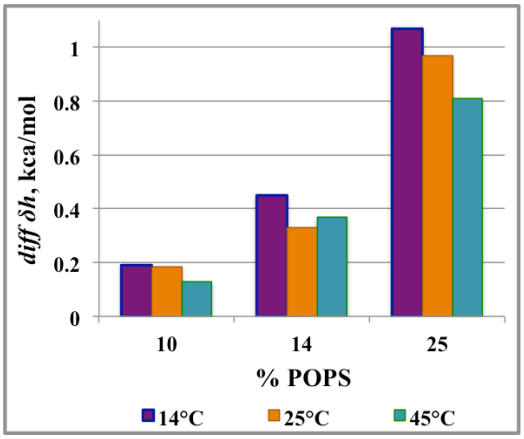

Figure VI-8b

The calorimetric profile of LUV titration into LAH4-L1 solution at pH 5 (***Figure VI-4, 5, 6***) supposedly results from the peptide accumulation (or even aggregation) on the bilayer at high P/L ratios, and subsequent desintegration of the peptide – lipid structures at lower P/L when the energy that has been absorbed in the first steps is returned (exothermic process). The magnitude of those processes depend strongly on the POPS content of membranes, which means that the peptide interacts preferably with POPS molecules. This correlation is displayed in a ***Figure VI-8b***. The enthalpy which we read on the Y axis is simply the difference between the minimum and maximum enthalpy values on the corresponding titration curves (***Figures VI-4, VI-5, VI-6***). This enthalpy difference does not bear a particular physical meaning, but helps to visualize the correlation of the enthalpy with POPS content and temperature.

Our ^{2}H NMR data also suggest the LAH4-L1 preferred association with POPS lipids (Chapter IV).

Similarly LAH4 peptide was found to be more efficient in reducing the order parameters for the acyl chain of anionic POPS, reconstituted at 15% of the total lipid, than in PC reconstituted at 70% of total lipid in PC/PS/cholesterol mixed membranes at pH 5 and at pH 7.5 (Mason et al., 2006a), which is indicative for the formation of domains enriched in POPS.

Negatively charged lipid domains separation by antimicrobial peptides was known previously and investigated by molecular dynamics simulations (Polyansky et al., 2010), ^{2}H solid state NMR (Kwon et al., 2013), differential scanning calorimetry (Wadhwani et al., 2012) and other methods (Epand et al., 2010). The lipid domains separation was even suggested as novel mechanism of action of the arginine-rich antimicrobial peptides (Arouri et al., 2009; Epand and Epand, 2009; Jean-François et al., 2008).

Interestingly, the *polylysines* induce the domain separation in mixed POPC/POPS membranes when their length exceeds n=30 (Franzin and Macdonald, 2001). Moreover it was shown by ^{2}H and ^{31}P NMR spectroscopy that *pentalysine* binds to POPC/POPS membranes only superficially, and does not disturbes the order of the lipid acyl chains (Roux et al., 1988). Therefore, it becomes evident that the mechanism of action of antimicrobial peptides that carry high positive charge (including LAH4-L1 at pH5) differs from purely electrostatic association.

If peptide accumulates around the POPS-enriched lipid domains, then this process will be obviously more intense when the POPS content is bigger. It is not necessarily that peptide forms classical toroidal

pores, the aggregates could be formed from LAH4-L1 peptide aligned parallel to lipid bilayer as well. The overview of pore-formation by antimicrobial peptides could be found in numerous publications (Aram J. Krauson, 2011; Bechinger and Lohner, 2006; Brogden, 2005; Melo et al., 2009; Yang et al., 2001). But unfortunately we don't have enough structural data to claim that LAH4-L1 peptide indeed aggregates on the membrane surface, so we use it here as an assumption.

It is possible thereafter to estimate the fraction of bound peptide at the enthalpy mimimum from the CD titration isotherms (Chapter V), on the basis of changes in peptide α-helix content. For POPC/POPS-25%−*into*−LAH4-L1 titrations at pH 5, the enthalpy minimum is observed at the lipid-to-peptide ratio equal 13 (***Figure VI-10b***). As the estimated fraction of bound peptide is 66±1%, then actual lipid-to-peptide ratio in the membranes is around 20. For POPC/POPS-14% enthalpy minimum the corresponding total lipid-to-peptide ratio makes 20, and the actual L/P = 32 (62±2% bound peptide). For POPC/POPS-10% membrane these numbers are 23 and 42 respectively (55±4% bound peptide). If we convert the L/P ratio into positive-to-negative charge ratio, the following numbers are obtained: 25% POPS LUV +/− ratio = 1.8, 14% POPS LUV – 2, 10% POPS – 2.1 . Actually the real +/− ratio on the membrane surface might be even twice bigger in the case when only the outer monolayer is accessible for peptide association. But the accessibility of the inner monolayer to peptide binding at pH 5 remains the topic for additional discussions.

For comparison, similar estimate is done for the end of calorimetric titration curve. For LAH4-L1 titration with POPC/POPS-25% LUV calorimetric isotherm indicates the termination of all processes at L/P=40 with corresponds to 85±2% of bound peptide accordingly to the CD simulation curve (***Figure V-13***, Chapter V). For POPC/POPS-14% LUV it takes place at L/P=85 which corresponds to 87±4% of bound peptide, and for POPC/POPS-10% membranes the numbers are 100 and 84±8% respectively. But the error bars between the simulation and experimental points are much bigger at the small L/P ratio, and the simulations were done so that region, where L/P is lower, was simulated with bigger accuracy (***Figure V-13***). Thereby the fraction of bound peptide can be more precisely estimated at smaller L/P ratio.

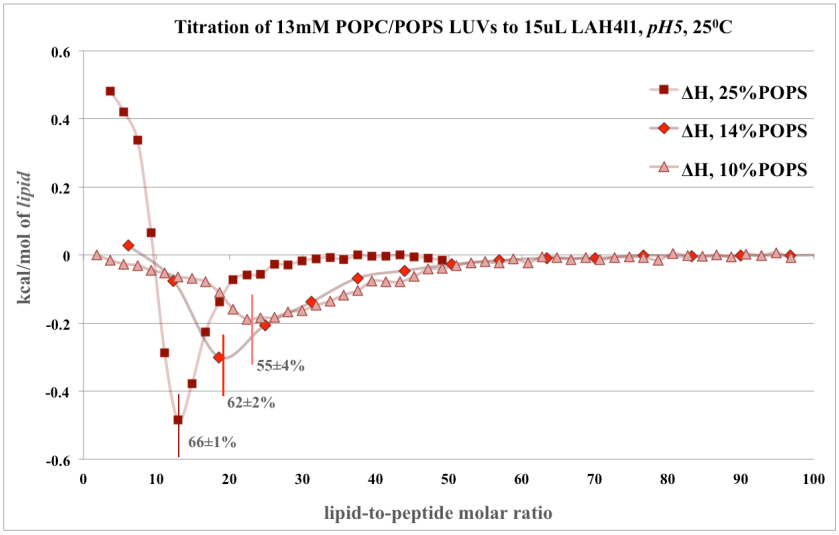

Figure VI-10b. Integrated molar heat of each titrational step is plotted against corresponding L/P ratio.

Interestingly, at *pH 7.4* when the histidines are deprotonated (pK≈6.1-6.2) and the LAH4-L1 peptide tends to adopt transmembrane configurations, we don't observe the same calorimetric profile as at pH 5, at which a preferred in-plane alignment of the peptide was detected (*cf. pH 7.4* ***Figure VI-4*** and *pH 5* ***Figure VI-15***). The titration profile is much more complex at pH 7.4 including several processes that take

place at different L/P ratio. Therefore it was rather difficult to dissect partitioning enthalpy from all the other processes.

POPC/POPS LUV calorimetric titrations with LAH4-L1 peptide.

The reverse peptide-into-LUV calorimetric titrations give better insight into peptide partitioning, because lipids are in the large excess in the beginning of the titration. The noticeable difference between ITC isotherm obtained from titrations at pH 5 and pH 7.4 is that at neutral pH the partitioning enthalpy is negative, but at pH 5 it is positive (*cf.* ***Figure VI-21*** and ***Figure VI-20***). Also the magnitude of partitioning enthalpy is bigger at pH 5. Moreover at pH 7.4 the partitioning enthalpy is nearly constant in the L/P range from 0 to 0.01. This observation concerns POPC/POPS-25% and -10% membranes, and might be the same for POPC/POPS-14% LUV – LAH4-L1 interaction, but unfortunately its titration curve is more noisy. At pH 5 the partitioning enthalpy increses quite steeply, and shows an irregular dependence with regard to the L/P ratio.

Remarkably, POPC – LAH4-L1 titration curves are pretty much different from those observed with mixed membranes. For instance LAH4-L1 partitioning enthalpy into POPC membranes is positive at pH 7.4, in contrast to POPC/POPS – LAH4-L1 partitioning. The results of ^{15}N solid state NMR spectroscopy (Chapter III) show that LAH4-L1 adopts preferably transmembrane alignments in POPC lipid bilayers at pH 7.4 and small peptide concentrations (0…2*mole%*), as it does into mixed POPC/POPS lipid bilayers. However, it shows in-planar orientations at pH 5. But somehow the peptide orientation does not correlate with partitioning enthalpy when comparing zwitterionic and charged membranes.

The magnitude of partitioning enthalpy at pH 5 is much smaller for POPC than for mixed membranes. It could be the case that T_0(partitioning) is close to 25°C for POPC membranes, but not for mixed membranes, that's why the enthalpy is close to zero.

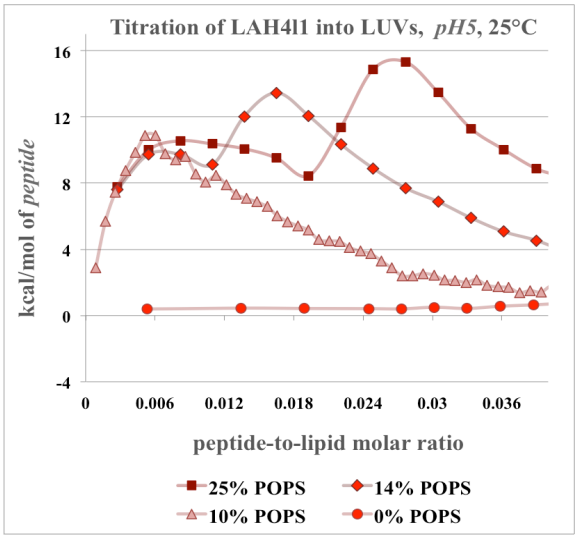

Figure IV.20b

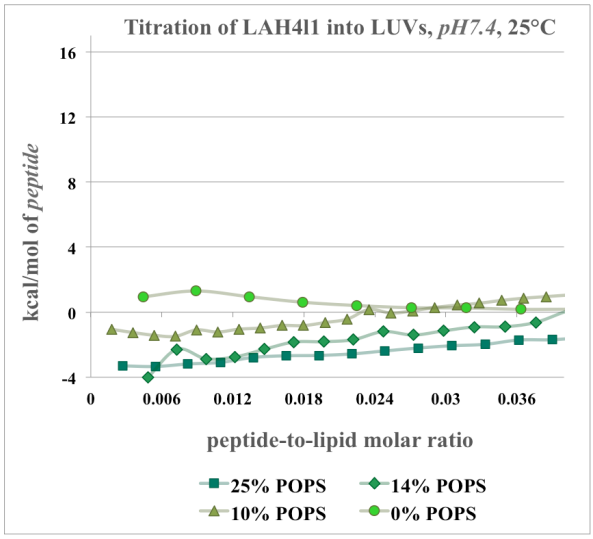

Figure IV.21b

It was already shown in the study with Mastoparan X, that peptide partitioning enthalpy into mixed POPC/POPG vesicles depends on the L/P total ratio in the P/L ratio range from 0 to 0.01 (Figure Ad3). The enthalpy of LAH4-L1 association within mixed POPC/POPS LUV at pH 5 increases drastically in the P/L range from 0 to 0.006. The peptide association with charged LUV could be characterized as cooperative at lipid-to-peptide ratios 0…0.02 at pH 5 (***Figure IV.20b***). At pH 7.4 no cooperativity was observed (***Figure IV.21b***), so we can conclude that it is not electrostatic attraction that is responsible for such a shape of ITC isotherms. Besides, similar cooperative behavior was discerned in MPX ITC

experiment (Figure Ad3). An alternative assumption can be made that at pH 5 there is no cooperativity in peptide binding neither. Just another process, which has negative enthalpy, is taking place in the same time as peptide partitioning. This process might represent the lipids rearrangements due to peptide penetration into mixed POPC/POPS vesicles.

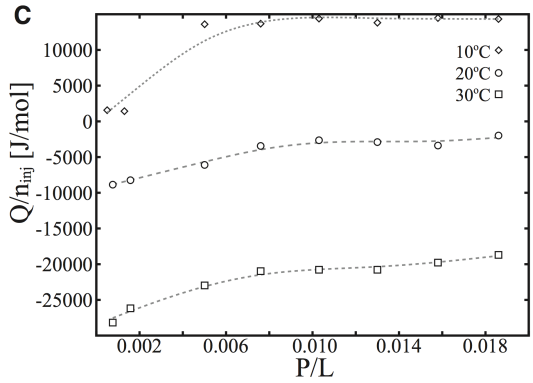

Figure Ad3. Heat of partitioning of MPX onto POPC/POPG (3:1) LUVs resolved by ITC. (C) The molar heat of partitioning is shown as a function of the peptide/lipid ratio (P/L) (n_{inj} is the amount of peptide injected). Adapted from (Henriksen and Andresen, 2011).

Supposedly the key element of understanding of processes that are observed by ITC upon LAH4-L1 peptide binding to POPC/POPS membranes is the superposition of solid-state NMR and the calorimetry results at two conditions – pH 5 and pH 7.4.

At pH 5, all the histidines of LAH4-L1 peptide are protonated, subsequently in-planar insertion into charged POPC/POPS as well as zwitterionic POPC membranes is preferable, as protonated histidines are exposed to the hydrophilic phase. An increase of the peptide/lipid ratio to 3*mole%* promotes LAH4-L1 peptide to adopt transmembrane alignment along with in-planar orientaion when embedded into POPC lipid bilayer (***Figure III.6***), while the presence of 25% POPS lipids stabilises the in-planar orientation of LAH4-L1 even at increased peptide concentration (4*mole%*, Figure I.4). The additional interaction between histidines and POPS head groups could be responsible for such stabilization.

One of the common characteristics of LAH4-L1 peptide penetration into charged and zwitterionic lipid bilayers at pH 5 and pH 7.4 is the coil-to-α-helix transition. There is no CD data on LAH4-L1 – POPC(/POPS) interaction at pH 7.4 submited in this thesis. However, oriented synchrotron radiation circular dichroism data on LAH4 (KKALLALALHHLAHLALHLALALKKA) embedded into POPC membrane shows that peptide adopts secondary structure with similar α-helix content at pH 5 and pH 7, but the precise values of helical content was not calculated (*Perrone, 2011, PhD thesis*). The α-helix content of LAH4 peptide was estimated to be 39% at neutral pH in the absence of lipids (50mM Tris/ 154mM NaCl), but only 26% in 50mM acetate buffer (pH 5) (Vogt and Bechinger, 1999). Therefore upon the binding to vesicles (zwitterionic and anionic) LAH4 increases its helicity at pH 5 and pH 7.4, however initial α-helix content is higher at pH 7.4. By extrapolating these data to LAH4-L1 we could assume that the enthalpy of random coil-to-helix transition might be smaller at pH 7.4, yet it seems unlikely that the enthalpy of coil-to-helix transition would change sign. The enthalpy of random coil – helix transition was determined to be negative for magainin peptides family which were associated with POPC/POPG membrane at 30°C (Wieprecht et al., 1999b, 2002).

Another enthalpy conponent may rise from the lipid order rearrangement upon the peptide insertion into the bilayers. As soon as insertion of peptide into mixed POPC/POPS LUV affects POPS lipids order in different manner (please see Chapter IV for more details), the calorimentric response may indeed be different. This diffrence in lipid order perturbation arises from peptide net charge and its preferable

orientation in lipid bilayer. At pH 5 peptide aligns parallel to lipid bilayer, the order perturbation by peptide is bigger for middle and terminal region of POPS palmytoil chain. While at pH 7.4, when the peptide adopts preferably a transmembrane orientation, especially at low P/L ratio, the POPS palmitoyl order is perturbed more evenly in head group region and in the middle-chain region. Interestingly, when peptide was embedded into zwitterionic POPC membranes, the perturbation of the POPC palmitoyl chain order by LAH4-L1 was also bigger at pH 5, but the order profiles look quite similar at pH 5 and pH 7.4, which clearly indicates the preferable LAH4-L1 association with charged POPS lipids. Particularly remarkable is the fact that LAH4-L1 partitioning enthalpy at pH 7.4 is positive when peptide inserts neutral POPC bilayer, and negative when some fraction of POPS lipids present, even though at low P/L ratio (up to 1*mole%*) LAH4-L1 inserts transmembrane in both types of lipid bilayer.

The transition of helical peptide from in-planar to transmembrane alignment is itself coupled with free energy change. The relative transition energies of amino acids within extended α-helical peptides when transferred from the membrane interface into the interior of phospholipid bilayers was investigated by ATR-FTIR spectroscopy on the family of designed LAH4X4 peptides (KKALL AXALH HLAXL AHXLA XHLKKA-NH2, where X_4 = L_4, T_4, V_4, W_4, A_3L, C_3L, S_3L, T_3L, Y_2L_2) embedded into POPC membranes (Aisenbrey et al., 2006). However, the free energy of transition depends strongly on the aminoacid composition of the peptide, therefore the data cannot be compared directly with ITC data on LAH4-L1 (KKALL AHALH LLALL ALHLA HALKKA-NH2). Furthermore, the presence of charged lipids is suspected to modulate the free energy of the transition of the helix alignments.

Another aspect that to my knowledge was not discussed previously in literature is the calorimetric response of positively charged amino acid side chains interaction with negatively charged lipid headgroups. A calorimetric response could rise from the non-specific interactions of functional groups, when oppositely charged moeities form ionic pairs and hydrogen bonds. However, we don't have any evidence of such specific interactions, which could be derived from the present biophysical investigations. Also, it is not clear if such interaction would produce a calorimetric response of comparable with other processes magnitude. Hence more systematic investigation should be done in order to show the possibility of some specific interaction between LAH4-L1 peptide and POPS lipids.

CONCLUSIONS AND PERSPECTIVES.

The interaction of amphiphilic cationic peptide LAH4-L1 with zwitterionic POPC and mixed POPC/POPS was investigated by various biophysical methods.

^{15}N solid-state NMR on peptide embedded into mechanically oriented lipid bilayer was employed in order to determine the LAH4-L1 pH-dependent orientation, similarly as it was determined for LAH4 peptide (Bechinger, 1996; Vogt and Bechinger, 1999). This pH-dependent membrane interaction was consolidated by wide-line ^{2}H solid-state NMR investigation on deuterated lipid vesicles.

Circular dichroism spectroscopy was applied to monitor the peptide α-helical content upon its association with POPC and POPC/POPS lipid vesicles. The preliminary values of LAH4-L1 – LUV apparent binding constants (mole fraction partitioning constants) were derived from CD binding isotherms, however with a rather small accuracy, equal 850 000, 450 000, 300 000 and 13 000 for POPC/POPS-25%, POPC/POPS-14%, POPC/POPS-10% and POPC vesicles, respectively. In order to increase the accuracy of the binding constants determination, some additional CD curves have to be recorded at larger L/P ratios (100-300) in order to estimate more precisely the α-helix content of LAH4-L1 peptide when completely bound to vesicles.

A single set of ζ-potential measurements were performed at pH 7.4 by titrating LAH4-L1 peptide into POPC/POPS-14% LUV, in order to connect the vesicles aggregation event to membrane surface neutralization, as it was done previously (Marquette et al., 2010). In perspective, LAH4-L1 absorption on lipid vesicles could be investigated using this method by titrating vesicles into peptide solution. The binding/absorption isotherms could be constructed from ζ-potential measurements, as it was done elsewhere (Freire et al., 2011). Those binding isotherms can be subsequently compared with CD –derived isotherms. However, the limited set of ζ-potential measurements, which were performed at pH 7.4, does not allow the comparison to CD data, that were taken at pH 5. Thus a more comprehensive binding analysis using this method is possible and could be done in perspective.

Isothermal titration calorimetry measurements were performed by titrating large unilamelar vesicles, consisting of POPC with varied POPS lipid content, into LAH4-L1 solution at pH 5 and pH 7.4. A set of reversed titration experiments were performed as well. The calorimetric traces give a really good insight into the energetic profiles of peptide – LUV interactions. When the vesicles are introduced into peptide solution, we detect a heat supposedly resulting from the peptide accumulation on the membrane surface and peptide penetration into hydrophobic core of lipid bilayer at high P/L ratio, but at lower P/L ratio peptide aggreagates desintegrate and penetration into the bilayer occurs. In reverse ITC experiment when the peptide was titrated into the vesicles suspension, primarily peptide penetration into lipid bilayer was observed at low P/L ratio, the enthalpy of which appeared to be pH-dependent. Even more surprisingly that at pH 5 the observed enthalpy of peptide partitioning was strongly dependent on the P/L ratio.

The experiments were performed in order to calculate the termodynamic parameters of LAH4-L1 – vesicles interaction, such as association constant K_A, free energy ΔG, enthalpy ΔH and enthropy ΔS of binding. However, the calorimetric profile was too complex to fit it with previously proposed binding models (Fernández-Vidal et al., 2011; Klocek et al., 2009; Wenk and Seelig, 1998). Thus more systematic calorimetric studies have to be performed on LAH4-L1 – membrane interaction at pH 5 and at pH 7.4. The application of simpler model compounds with a goal to discern various processes occuring in the membrane, is also possible. For example, LAH4-L1-derived peptides, with histidines in the hydrophobic core replaced by more hydrophobic (isoleucine, valine) or more hydrophilic (lysine) amino acids, can be used to study the pH-independent binding.

And finally, in order to achieve a better understanding of the processes that occur at high peptide concentration in the lipid bilayers, the knowledge of membrane morphological changes upon the peptide association is indispensable. The membrane structural investigations by NMR need to be expanded towards higher peptide-over-lipid ratios. Static non-oriented ^{31}P NMR can be used to study the morphological changes of lipid vesicles in the presence of high peptide concentration. Previously, the detergent-like properties of magainin (Bechinger, 2005) and melittin (Dufourc et al., 1986; Pott and Dufourc, 1995) were investigated by this method.

CONCLUSIONS ET PERSPECTIVES.

L'interaction du peptide cationique amphiphilique LAH4-L1 avec des membranes POPC zwitterionique et POPC/POPS mixtes a été étudiée par les méthodes biophysiques variés.

On a utilisé une RMN solide à noyau ^{15}N sur un peptide incorporé dans une bicouche lipidique orientée mécaniquement afin de déterminer l'orientation dépendante du pH de LAH4-L1, de la même manière que celle déterminée pour le peptide LAH4 (Bechinger, 1996; Vogt et Bechinger, 1999). Cette interaction membranaire dépendante du pH a été consolidée par une étude RMN de ^{2}H à large spectre sur les vésicules de lipides deutériés.

La spectroscopie de dichroïsme circulaire a été appliquée pour surveiller le contenu α-hélicoïdal du peptide lors de son association avec les vésicules lipidiques POPC et POPC / POPS. Les valeurs préliminaires des constantes de liaison apparentes LAH4-L1-LUV (constantes de partition de la fraction molaire) ont été dérivées des isothermes de liaison CD, mais avec une précision assez faible, soit 850 000, 450 000, 300 000 et 13 000 pour POPC/POPS-25 %, POPC/POPS-14%, POPC/POPS-10% et les vésicules de POPC seul, respectivement. Afin d'augmenter la précision de la détermination des constantes de liaison, certaines courbes DC supplémentaires doivent être enregistrées à des rapports L / P plus grands (100-300) afin d'estimer plus précisément la teneur en α-hélice du peptide LAH4-L1 lorsqu'il est complètement lié aux vésicules.

Un seul ensemble de mesures de potentiel ζ a été effectué à pH 7,4 en titrant le peptide LAH4-L1 dans POPV / POPS-14% LUV, afin de relier l'événement d'agrégation des vésicules à la neutralisation de la surface de la membrane, comme cela a été fait précédemment (Marquette et al., 2010). En perspective, l'absorption de LAH4-L1 sur les vésicules lipidiques pourrait être étudiée en utilisant cette méthode en titrant des vésicules dans une solution peptidique. Les isothermes de liaison / absorption pourraient être construites à partir de mesures de potentiel ζ, comme cela a été fait ailleurs (Freire et al., 2011). Ces isothermes contraignantes peuvent ensuite être comparées aux isothermes dérivées de CD. Cependant, l'ensemble limité de mesures du potentiel ζ, qui ont été effectuées à pH 7,4, ne permet pas de comparer les données CD, qui ont été prises à pH 5. Ainsi, une analyse de liaison plus complète utilisant cette méthode est possible et pourrait être effectuée respectivement.

Les mesures calorimétriques de titrage isothermes ont été effectuées en titrant de grandes vésicules unilamellaires (GVU), constituées de POPC avec une teneur lipidique POPS variée, dans une solution LAH4-L1 à pH 5 et pH 7,4. Un ensemble d'expériences de titrage inversé a également été réalisé. Les traces calorimétriques donnent un très bon aperçu des profils énergétiques des interactions peptide-GVU. Lorsque les vésicules sont introduites dans la solution peptidique, on détecte une chaleur supposée résultant de l'accumulation de peptide sur la surface de la membrane et la pénétration du peptide dans le noyau hydrophobe de la bicouche lipidique à un rapport P/L élevé, mais à un rapport P/L inférieur des agrégats peptidiques se désintègrent Et la pénétration dans la bicouche se produit. Dans l'expérience ITC inverse lorsque le peptide a été titré dans la suspension des vésicules, principalement la pénétration des peptides dans la bicouche lipidique a été observée à faible rapport P/L, dont l'enthalpie semble être dépendante du pH. Encore plus surprenant, c'est qu'à pH 5, l'enthalpie observée du partitionnement des peptides dépendait fortement du rapport P/L.

Les expériences ont été effectuées afin de calculer les paramètres thermodynamiques de l'interaction entre la LAH4-L1 et les vésicules, telles que la constante d'association KA, l'énergie libre ΔG, l'enthalpie ΔH et l'entropie ΔS de la liaison. Cependant, le profil calorimétrique était trop complexe pour l'adapter aux modèles de liaison proposés précédemment (Fernández-Vidal et al., 2011; Klocek et al., 2009; Wenk et Seelig, 1998). Ainsi, des études calorimétriques plus systématiques doivent être effectuées sur LAH4-L1 - interaction membranaire à pH 5 et à pH 7,4. L'application de composés modèles plus simples dans le but de discerner divers procédés se produisant dans la membrane est également possible. Par exemple, les

peptides dérivés de LAH4-L1, avec des histidines dans le noyau hydrophobe remplacé par des acides aminés plus hydrophobes (isoleucine, valine) ou plus hydrophiles (lysine), peuvent être utilisés pour étudier la liaison indépendante du pH.

Afin de mieux comprendre les processus qui se produisent à haute concentration de peptide dans les bicouches lipidiques, la connaissance des changements morphologiques de la membrane sur l'association peptidique est indispensable. Les études de structure membranaire par RMN doivent être étendues vers des rapports peptidiques et lipidiques supérieurs. La RMN ^{31}P non-orientée statique peut être utilisée pour étudier les changements morphologiques des vésicules lipidiques en présence d'une forte concentration de peptide. Auparavant, les propriétés détergentes de magainin (Bechinger, 2005) et de la mélitine (Dufourc et al., 1986, Pott et Dufourc, 1995) ont été étudiées par cette méthode.

BIOPHYSICAL CHARACTERISATION OF LAH4-L1 AND LAH4 INTERACTION WITH NUCLEIC ACIDS.

As it was already discussed in the previous chapters, LAH4 and LAH4-L1 peptides bear considerable promise as transfection agents. The efficiency of peptides to deliver nucleic acids into the cells relies on the peptide's membrane pH-dependent activity, but also on the strength of peptide – nucleic acids interactions. On one hand those interactions should be strong enough to assure the complex stability in the serum media, but on the other hand the nucleic acids have to be released into cytoplasm in order they exercise their function. The release of nucleic acid by LAH4 peptides is provided by the changes of peptide's net charge and subsequently its hydrophobicity upon the changes of pH conditions. It was shown previously that at pH 7.5 DNA and siRNA bind twice as much peptide as at pH 5 (Lan et al., 2010; Prongidi-Fix et al., 2007; Vidovic, 2011).

Except protection function, an efficient delivery agent has ability to condense DNA and to form particles that are readily taken up by the cell. In the living cell it is proteins that assure DNA condensation and protection. Proteins bind nucleic acids in highly specific manner. Usually the proteins that possess particular structural motifs are prone to DNA binding, which have high content of cationic amino acids (Arg, Lys). Complex stability is assured by the network of hydrogen bonds, ionic and van der Waals interactions. Transfection peptides are typically cationic peptides that don't have any specificity towards nucleic acids, but the association supposedly occurs via the same basic mechanisms – electrostatic attraction, hydrogen bond formation and changes of conformation and hydration state.

In the following chapters we will try to elucidate the mechanism of LAH4 and LAH4-L1 association with DNA by mean of biophysical techniques. Isothermal titration calorimetry reveals us the thermodynamic characteristics of peptide – nucleic acids interactions, such as enthalpy and stoichiometry of the association. Also LAH4-L1 association with model electrolyte was investigated by ITC, which allows comparing the mode of peptide interaction with model compound and with nucleic acids. Dynamic light scattering technique was employed to assess the size of DNA/siRNA-LAH4-L1 particles at different peptide-over-nucleic acid ratio, which also serves as the control of the condensation (aggregation) processes occurring in solution. And NMR was used to inspect the complex formation on the microscopic level. REDOR techniques allows measure of the interatomic distances between ^{31}P nuclei of the DNA backbone and $^{15}N(^{13}C)$ nuclei of the uniformly labeled peptide side chains, revealing the spatial proximity of those functional groups.

IX. LAH4-L1 – NUCLEIC ACID PARTICLES SIZE CONTROL BY DLS.

The series of dynamic light scattering experiments was performed in order to assess the correlation of LAH4-L1 – siRNA and LAH4-L1 – DNA complex size with peptide/nucleic acid molar ratio, pH and ionic strength of the solution. Also DLS measurements were performed as the control test of aggregation events that may occur during ITC titrations (Chapter X).

MATERIALS AND METHODS

Sample preparation for dynamic light scattering.

LAH4-L1 peptide (KKALLAHALHLLALLALHLAHALKKA-CONH2) was prepared by automated solid-phase synthesis.

siRNA was custom synthesized with the sequence (5'-gcugcaccugacgcccuuctt-3' 3'-ttcgacguggacugcgggaag-5') and purchased in its desalted form from Sigma-Aldrich Co. LLC.

Salmon testes sodium salt DNAs (≈2000bp) were purchased from Sigma-Aldrich Co. LLC.

Four type of buffers were used for the sample preparation:

- 50mM acetate buffer / 0.5mM EDTA, pH≈5,
- 20mM HEPES buffer / 1mM EDTA, pH≈7.4,
- 50mM acetate buffer / 0.5mM EDTA, pH≈5, 120mM NaCl,
- 20mM HEPES buffer / 1mM EDTA, pH≈7.4, 146mM NaCl.

Dynamic light scattering spectroscopy.

Measurements were performed on a Zetasizer Nano ZS system (Malvern Instruments, Malvern, UK) equipped with a 4 mW He-Ne laser (λ_0=633 nm). 50-70μL of the peptide solution was placed in a low-volume quartz cuvette (ZEN2112, Malvern, UK) and the back-scattered light was collected at an angle of θ=173°. In typical dynamic light scattering experiment the intensity of light is measured over the time and represented as the time autocorrelation function of the scattered light (*Frisken, 2001*). The time autocorrelation function is then processed using Malvern DTS build-in algorithms and the results are displayed as the set of parameters including Z-average size, polydispersity index and the hydrodynamic diameter distribution by intensity, volume and numbers. DLS measurements are highly sensitive to the particle aggregation. Basically, the time autocorrelation function reflects the intensity of backscattered light, which is bigger for larger particles. The Z-average particle size is the mean value calculated from the intensity-weighted distribution. The fundamental size distribution generated by DLS is an intensity distribution, which can be converted, using Mie theory and taking into account sample refractive index, to a volume distribution. This volume distribution can also be further converted to a number distribution. However, number distributions are of limited use as the small errors in gathering data for the correlation function will lead to huge errors in distribution by number (*Zetasizer Nano manual* 2004).

Four sets of titration measurements were performed in which a siRNA solution was placed into the measurement cuvette, into which the peptide solution was titrated in small steps. The samples were equilibrated at 25°C for at least 30sec before each measurement. The medium refractive index and the viscosity parameters were set to 1.33 and 0.8872cP (latex), respectively. The individual measurement is the result of 15 to 20 runs of ten seconds duration.

RESULTS AND DISCUSSION.

Figures IX.1-6 in the text and the Tables IX.2-5, which could be found in Appendix, describe the results of DLS experiments in which siRNA solution was titrated with LAH4-L1 peptide in four buffers

of different pH or salt concentration. The principal parameters of DLS size measurements, such as derived count rate, Z-average size and polydispersity index, are given in the Tables and the hydrodynamic diameter distribution by volume, as well as PDI and Z-average, volume-average size and derived count rate are displayed in the Figures. The meanings of these parameters were explained in more detail in Chapter VII.

The titration of LAH4-L1 into siRNA in 50mM acetate (pH 5) or 15mM HEPES (pH 7.4) buffer promotes the formation of suspensions, which are characterized by a large distribution of the hydrodynamic diameter of the resulting particles (***Figure IX-5***). Upon the titration of the first LAH4-L1 portions the distribution of particles hydrodynamic diameter is quite large, forming two populations with the particle sizes of about 200nm and 2000nm with, as indicated by the volume-weighted distribution profile (***Figure IX-1*** and ***Figure IX-2***). The particles size is rather big (min 200nm) already at the first titration steps, which indicates the participation of numerous siRNA and the peptides molecules in the complex formation. At higher peptide/siRNA ratio, when the siRNA negative charge is partially compensated by peptides, the particles size distribution was in a range of 800-1100nm forming only one population. That narrowing of the particles size distribution is more pronounced at pH 7.4, which is reflected by the decrease of polydispersity index to 0.25 when LAH4-L1/siRNA ratio reaches 5 (PDI, Table X-2 Appendix, ***Figure IX-6***). The final sizes of LAH4-L1 – siRNA particles formed at both pH conditions were in the same range of about 800-1100nm (pH 5) and 900-1000nm (pH 7.4) at the total +/− total ratio about 1 (***Table IX-1, Figure IX-1*** and ***Figure IX-2***).

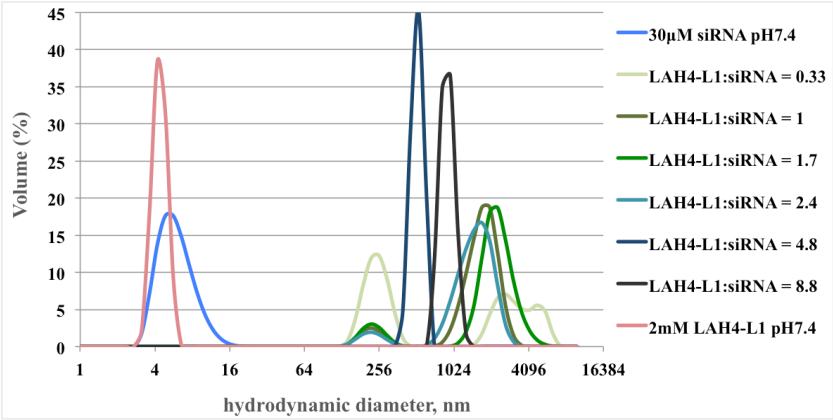

Figure IX-1. Volume-weighted particle size distribution assessed by DLS. The 30µM siRNA solution in 15mM HEPES buffer (pH 7.4) was titrated with LAH4-L1 peptide at 25°C.

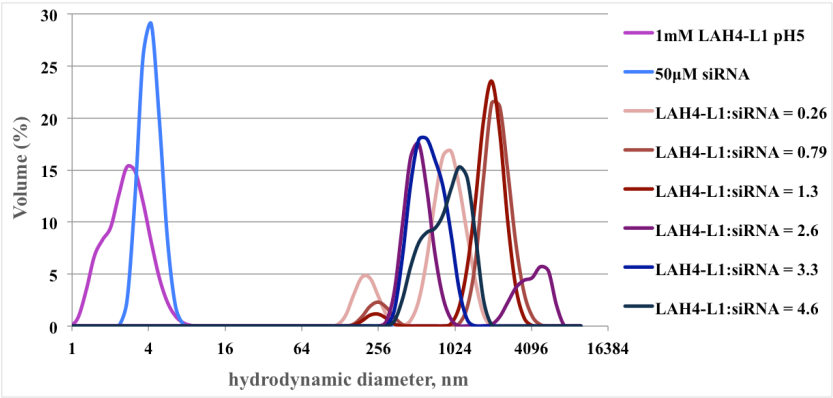

Figure IX-2. Volume-weighted particle size distribution assessed by DLS. The 50µM siRNA solution in 50mM acetate buffer (pH 5) titrated with LAH4-L1 peptide at 25°C.

When the ionic strength of solution is increased to 154mM by adding sodium chloride, the particles are formed with a quite narrow size distribution range (***Figure IX-3*** and ***Figure IX-4***). The average size (3000nm) of particles formed in the presence of salt are about three times bigger than those formed in low ionic strength buffers. The polydispersity index drops to 0.3 when the +/− ratio is about one (***Figure IX-6, Table IX-1***). Thus the particles with a more restricted polydispersity index are formed when the positive charge of peptide compensates the negative charge of nucleic acid phosphates. The hydrodynamic diameter of the particles is modulated by the ionic strength of solutions. However, the size of particles is quite large even in salt-free solutions (800-1100nm), in particular when transfection applications are considered.

It was shown in the study with the latex beads that the particles sized less than 200nm are readily uptake by the cells via endocytosis, but the particles with the sizes >1 micron generally could not be taken by the non-phagocytic cells (Rejman et al., 2004). By merely changing the peptide/siRNA ratio and/or pH it seems impossible to obtain a particles size smaller than 1 micron, however those particles show quite pronounced transfection activity (Langlet-Bertin et al., 2010). In fact, there are number of factors that influence the transfection activity of complex, and the size of particles may play a role, but it is not only factor for successful uptake. First of all the surface of peptide-siRNA particle is not inert as the latex bead. The peptide is supposedly playing an active role in cell membrane fusion. On the other hand it was shown that the activity of the complex is highest when it is prepared in the pure water rather than in the NaCl-supplied solution at the peptide-over-siRNA weight ratio of 10/1 (Langlet-Bertin et al., 2010). And this observation may be directly related to the smaller average particle size formed in the solutions with low ionic strength.

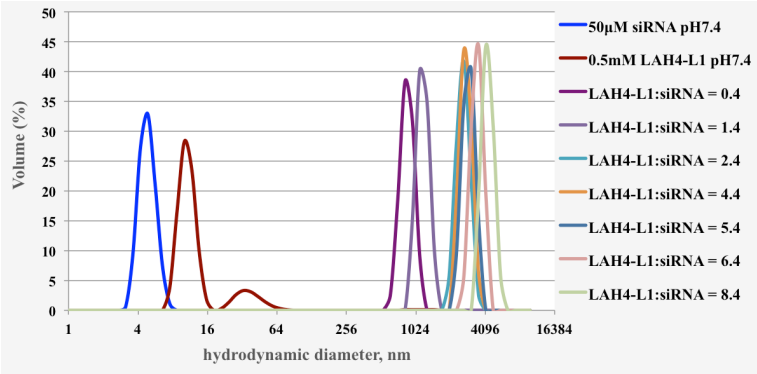

Figure IX-3. Volume-weighted particle size distribution assessed by DLS. The 50µM siRNA solution in 15mM HEPES buffer (pH 7.4), 146mM NaCl titrated with LAH4-L1 peptide, 25°C.

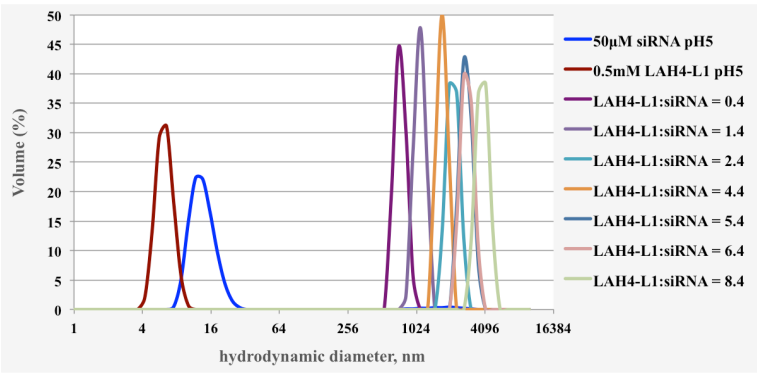

Figure IX-4. Volume-weighted particle size distribution assessed by DLS. The 50µM siRNA solution in 50mM acetate buffer (pH 5), 120mM NaCl titrated with LAH4-L1 peptide, 25°C.

The results of all DLS titration could thus be summarized (Table X-1, ***Figure X-5***). The average size of siRNA – LAH4-L1 complexes is 5-7 times bigger in saline buffers at same peptide/siRNA ratio as indicated by intensity-weighted (Z-average) and the volume-weighted mean values. Several more interesting observations can be made when analysis the summary graphs. The average size value for the volume-weighted hydrodynamic diameters distribution is about 2000nm at low peptide/siRNA ratio, but it drops to about 800nm when peptide/siRNA ratio reaches 3.3 at pH 5 and 4.8 at pH 7.4 in salt-free solutions. But accordingly to the mean value of the size distribution by intensity (Z-average) the average particles size is conserved or even increases slightly over the course of titration. Such a difference could be explained by the divergence in particle size distribution. Z-average is the value calculated directly from the scattering by the fitting of the autocorrelation function. While for calculation of the size distribution by volume the spherical shape and homogeneity of the particles are assumed. At low peptide-over-siRNA ratio, the formed complexes may be non-homogeneous and non-spherical. Moreover, at low peptide/siRNA ratio two population of particles are formed with quite differently sized particles, ~200nm and ~2000nm. As soon as scattering properties of material depend on the particles relative to light source wavelength (λ=633), it means that the particles of 200nm and 2000nm may have quite different scattering properties. This may create the divergence when the volume-weighted distribution is calculated. For instance, there is the material that has narrow particles size distribution, Z-average size of x and volume-average size of y. Then the material with wide size distribution (high PDI) and same Z-average size x, won't have the same volume-weighted average. It is the situation that we observe with siRNA – LAH4-L1 complexes. At pH 7.4 volume-weighted average size decreases when the narrower distribution observed (***Figure IX-1***, peptide/siRNA=4.8).

In saline solutions such deviations were not observed due to the narrower size distribution.

Table IX-1. The results of DLS measurements on siRNA solution titrated with LAH4-L1 peptide at 25°C in various buffers. The results are displayed for condition of +/− ratio is close to 1.

Sample	condition	peptide / siRNA molar ratio	+/− total ratio	Z-Average (d, nm)	Volume averaged size (d, nm)	PDI
19.7μM siRNA/173μM peptide	pH 7.4	8,80	1,05	844	910	0,206
29.4μM siRNA/136μM peptide	pH 5	4,62	0,99	1310	943	0,614
27.2μM siRNA/228μM peptide	pH 7.4, NaCl	8,40	1,00	7092	4318	0,315
34.7μM siRNA/153μM peptide	pH 5, NaCl	4,40	0,94	4646	1728	0,557

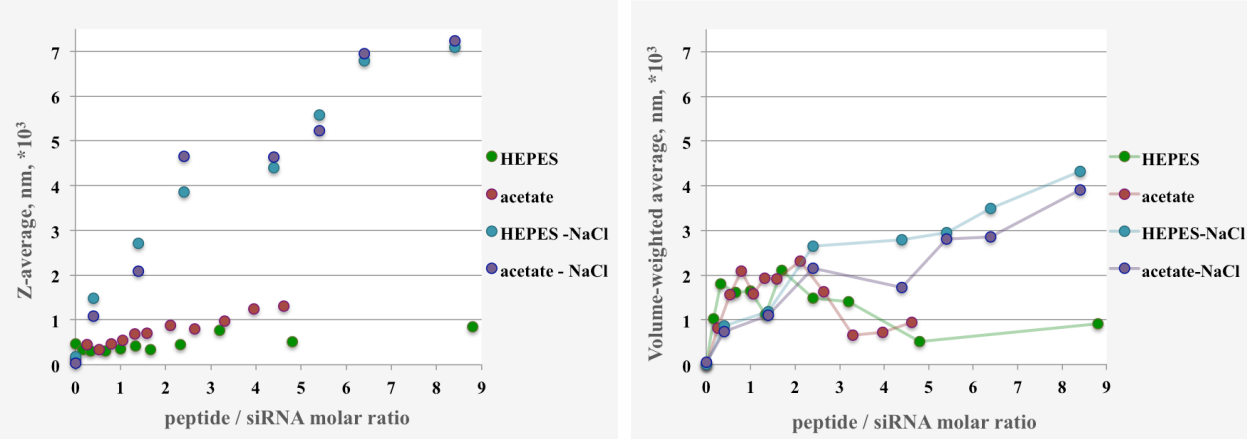

Figure IX-5. The results of DLS measurements of siRNA solution in various buffers titrated with LAH4-L1. DLS parameters are plotted against peptide-over-siRNA molar ratio *left*) Z-average size; *right*) volume-weighted average size.

The polydispersity index is quite high over the first part of titration range. Only at the peptide/siRNA ratio over 5 the PDI value drops to about 0.3, which means that the particles with narrower size distribution are formed at the higher peptide concentration.

Derived count rate is also quite sensitive indicator to track the aggregation, which reflect directly the number of photons registered from the scattered light. This value increases when the particles size or concentration increase. Derived count rate profile is characterized by the steep increase at the beginning of titrations, which indicates the phase of the active formation of new particles, and the plateau region when the aggregates are formed and subsequent addition of the peptide does not induce the increase of the scattering rate. However at Z-average graph, the increase of the particles size is observed. It means that the formation of bigger aggregated does not induce the increase of scattered light.

This examples show that the DLS results have to be analysed in complex manner by taking into accounts all the parameters.

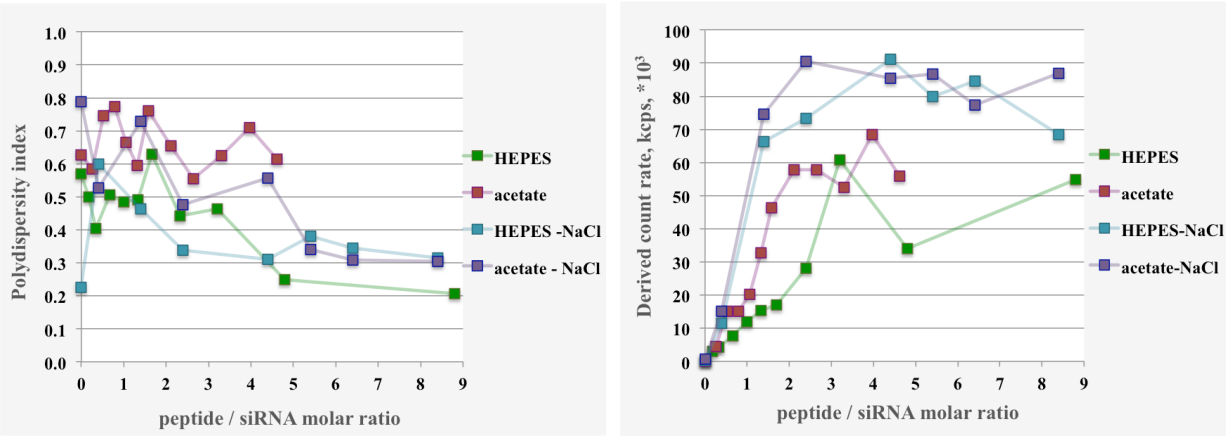

Figure IX-6. The results of DLS measurements of siRNA solution in various buffers titrated with LAH4-L1. DLS parameters are plotted against peptide-over-siRNA molar ratio *left*) polydispersity index; *right*) derived count rate.

The single series of DLS titration was performed when LAH4-L1 solution was titrated with salmon testes DNA (2000bp). The DNA solution alone is characterized by the average particles size of about 180 nm and high polydispersity index (0.7) (***Figure X-7***). When DNA is added in a stepwise manner to LAH4-L1 solution, the particles are formed with the sizes between 300nm and 1300nm. The particles sizes are approximately the same that obtained with siRNA, however the width of distribution seems to be bigger. Such broad distribution could signify that the particles formed of one DNA molecule and LAH4-L1 peptides coexist with the aggregates of such complexes.

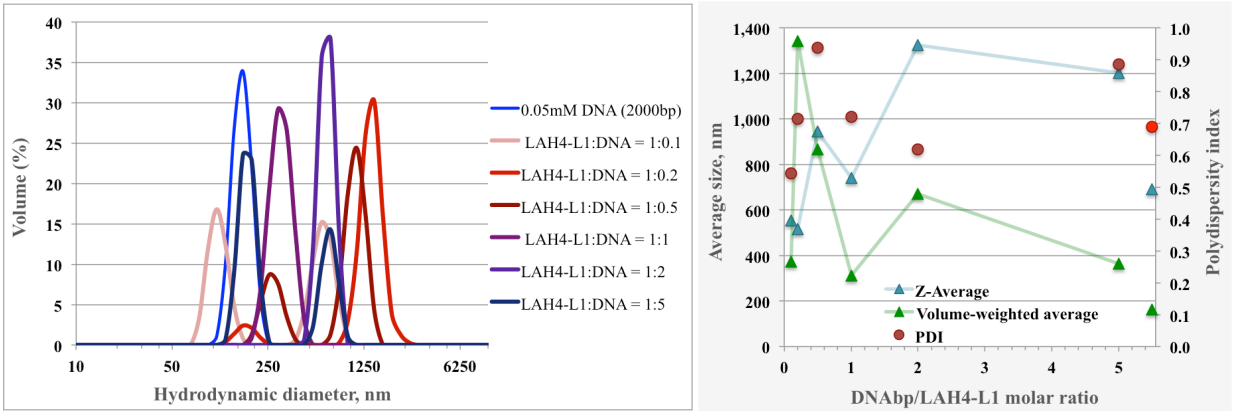

Figure IX7. The results of DLS measurements of LAH4-L1 solution in 20mM HEPES buffer (pH=7.4) titrated with DNA. DLS parameters are plotted against DNA base pairs – over – LAH4-L1 molar ratio: *left*) volume-weighted hydrodynamic diameter distribution; *right*) Z-average, volume-average size and polydispersity index. The corresponding values for DNA solution are shown on the right side of the graph.

X. THERMODYNAMICS OF LAH4-L1 INTERACTION WITH NUCLEIC ACIDS AND OTHER ELECTROLYTES BY ITC

Isothermal titration calorimetry was applied to obtain the thermodynamic profile of the interaction of LAH4-L1 with nucleic acid and a polyanionic model compound.

The method was applied previously for the investigation of the association of cell-penetrating peptides with DNA (Ziegler and Seelig, 2007), of polypeptides made of lysines and histidines or of amidoamine polymers with siRNA (Chou et al., 2014; Jensen et al., 2010), as well as various cationic polymers with DNA (Braun et al., 2005; Kim et al., 2010; Prevette et al., 2007; Samsonova et al., 2013). In some cases the whole set of thermodynamic parameters was obtained when a specific binding model was applied (Kim et al., 2010; Matulis et al., 2000; Ziegler and Seelig, 2007), however rather different approaches were employed to obtain those binding models. Very often a qualitative analysis of the isotherm along with other biophysical methods was used to elucidate the binding mechanism. In the present work the calorimetric isotherms will be analysed without applying a specific model of association.

MATERIALS AND METHODS

Sample preparation for isothermal titration calorimetry.

LAH4-L1 peptide (KKALLAHALHLLALLALHLAHALKKA-CONH2) was prepared by automated solid-phase synthesis.

siRNA was custom synthesized with the sequence (5'-gcugcaccugacgcccuuctt-3' 3'-ttcgacguggacugcgggaag-5') and purchased in its desalted form from Sigma-Aldrich Co. LLC.

Salmon testes sodium salt DNAs (≈2000bp) were purchased from Sigma-Aldrich Co. LLC.

For buffer preparation DEPC-treated water was used. In a standard procedure micro filtered water is treated with 0.1% v/v diethylpyrocarbonate for at least 2 hours at 37 °C and then autoclaved (at least 15 min) to eliminate the traces of DEPC. This procedure is necessary to inactivate RNase and DNAse, which could perturb the experiments with siRNA and DNA. This procedure could be applied to the buffers directly, except ones that contain amino groups. siRNA, DNA and LAH4-L1 stock solutions were then prepared in DEPC-treated buffers.

Poly(sodium 4-styrenesulfonate) (MW ~70,000, n=240, powder) was purchased from Sigma Aldrich and used in this experiment as a model polyelectrolyte:

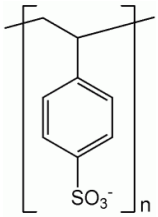

Three type of buffers were used for sample preparation:

- 60 mM acetate buffer / 0.5mM EDTA, pH≈5,
- 20mM HEPES buffer / 1mM EDTA, pH≈7.4,
- 60 mM acetate buffer / 0.5mM EDTA, pH≈5, 154mM NaCl

The stock solutions were prepared in the corresponding buffers and dialyzed against the buffer. It is especially important that all the peptide samples were subjected to dialysis prior to ITC measurement in order to equilibrate pH and buffer composition between peptide stock solution and buffer itself. Otherwise the dilution enthalpy could rise bigger that the enthalpy from reagents interaction. The concentrations of peptide and vesicles working solutions were adapted for each experimental condition. All working solutions were degased prior to measurements.

Isothermal Titration Calorimetry measurements.

All measurements were taken with a MicroCal ITC200 calorimeter (MicroCal, Northampton, MA) at the appropriate temperature conditions (25°C). ITC titrations were performed by injecting 0.5 to 2μL aliquots of peptide solution into the calorimeter cell (V_{cell} = 0.203mL) containing siRNA at time intervals of 60 to 240sec, in adequation with the kinetics of processes. The concentrations of the injectant (*or* titrant, the binding partner in the syringe, $V_{syringe}$ = 60μL) as well as the concentration of titrate were optimized for each experiment in order to ensure that enough titrant is available before the reaction is finished (δh=0). Typically 0.25 – 2mM peptide solution was in the syringe, and 30-50μM siRNA solution was placed in the calorimetric cell. About 1mM of DNA base pair was placed in the cell in analogous experiment with DNA. The heats of dilution were determined in the control titrations by injecting the lipid solution or the peptide solution into pure buffer and were subtracted from the calorimetric signal during the final analysis. Calorimetric response is recorded as a function of heating (δh) received by the instrument over measurement time. This signal is then processed automatically by the *Origin® ITC* software, and the result is represented as an enthalpy per mole of *injectant* (ΔH/mole, *kcal/mole*) against the *titrate-to-titrant* molar ratio.

RESULTS.

Calorimetric titration of LAH4-L1 into siRNA and PSS solution.

ITC experiments were performed with siRNA solutions either in 60mM acetate or in 20mM HEPES buffer placed into the calorimetric cell and titrated with LAH4-L1 in the same buffer. The calorimetric isotherms are displayed in a ***Figure X-1***. The control experiment, where the peptide solution is injected into buffer, is already subtracted from calorimetric curve. The signal from diluting the peptide solution in the buffer was quite considerable, therefore, it is displayed on the graph along with the experiment. Notably, the heat response from diluting the peptide stock solution changes with the concentration of titrant inside the calorimetric cell. Therefore this control experiment can be deconvoluted into two components. One component has a constant enthalpy for each titration step (negative for the experiment in 60mM acetate buffer, and positive in 20mM HEPES buffer), that could be due to a pH mismatch between the peptide stock solution and the buffer itself. This constant value was subtracted from the peptide-to-siRNA calorimetric isotherm as a control measurement. The second component has the opposite sign and was assigned to the peptide dilution. As shown by DLS, the peptide in solution co-exists in the monomeric and aggregated form. Therefore the desintegration of aggregates might be seen by ITC. Alternatively the signal may result from peptide protonation/deprotonation processes, which in turn may be related to the peptide disaggregation. Titration of a concentrated LAH4-L1 solution into buffer produces more monomeric peptide. This may cause a protonation or deprotonation depending on the buffer and pH. The enthalpy of peptide dilution may be different when the peptide is injected into siRNA solution. Thus only the enthalpy of the constant calorimetric signals from the control experiment was subtracted.

The calorimetric traces obtained by the titration of LAH4-L1 peptide to siRNA have complex character. At the first titration steps when the peptide-to-siRNA ratio is small, an increase of the enthalpy is observed, which is particularly steep at pH 5 (***Figure X-1***). At higher peptide/siRNA ratio the enthalpy decreases and reaches zero, indicating the termination of the binding processes. Such complex calorimetric response could result from the sum of processes accompanying the peptide association with siRNA. As soon as ITC isotherm has ascending and descending components, the attempt was made to fit this curve with mathematical model called ‘Two sets of binding sites’, which is integrated into ITC Origin® software. However, the fitting did not provide satisfactory results. The biding enthalpies had an

error up to 50%. Hence this model is not applicable to peptide – siRNA association, as there are no two different "classical" binding sites on siRNA molecule. LAH4-L1 – siRNA complex formation takes place between the oppositely charged polyelectrolytes, rather than between ligand and macromolecule.

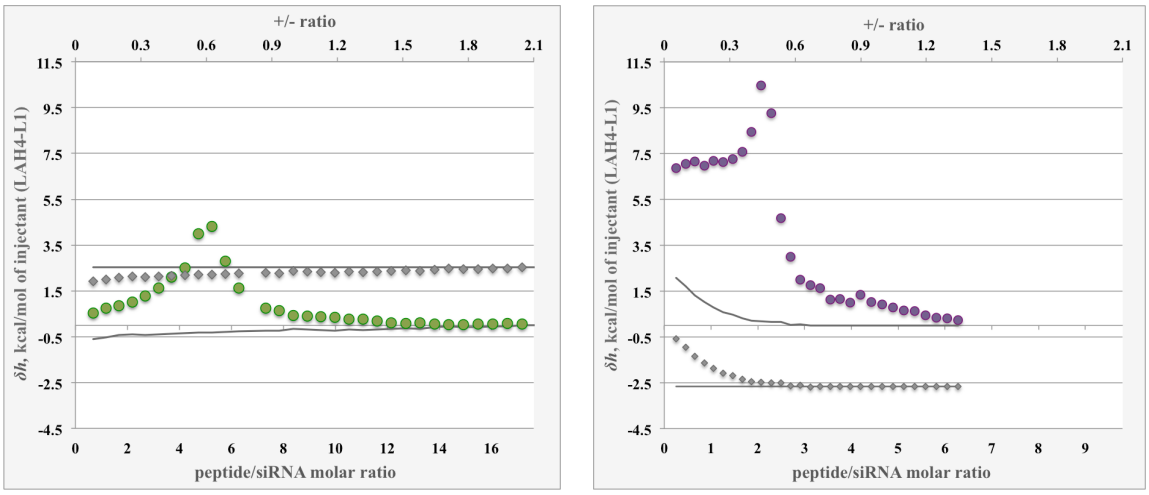

Figure X-1. Integrated calorimetric traces (Δh_i) of 30μM of siRNA titrated with 3mM LAH4-L1 in 20mM HEPES buffer (pH=**7.4**), 1μL injections, 25°C (on the *left*); and 50μM of siRNA titrated with 2mM LAH4-L1 in 60mM acetate buffer (pH=**5**), 1μL injections, 25°C (on the *right*). Corresponding control experiments are shown in grey, where the diamond symbols represent the control experiment curve, and solid lines are the estimations of two-component dilution process. The X axes scales were chosen to display the same +/− ratio values.

Alternatively, the titration isotherms can be dissected in two individual sigmoidal components. If assume that one process is described by a 'one set of identical binding site' model, then the appropriate simulation procedure yields thermodynamic parameters that describe the endothermic component of binding (***Figure X-2***). Subtracting the simulated curve from the experimental ITC data leads to the exothermic component. The exothermic process prevails at low peptide/siRNA ratio and is finished at the peptide/siRNA ratio of the enthalpy maximum. This maximum is at the same positive-to-negative total charge ratio of around 0.5 at both pH conditions. The second (endothermic) process is then terminated at total positive-to-negative ratio of 1.5, with corresponds to a peptide/siRNA ratio of 12.5 at pH 7.4, and 7 at pH 5. It is not clear however which thermodynamic processes are responsible for the appearance of such a biphasic titration isotherm. At low peptide/siRNA ratio the siRNA functional groups are easier to access. Each peptide could form close contacts with siRNA molecules, but this possibility is reduced at higher peptide/siRNA ratio. According to this interpretation (***Figure X-2***), the exothermic and endothermic processes rely on the formation of close contacts with siRNA strands. The stoichiometry of the LAH4-L1 association strongly depends on the pH, and, in turn, on the peptide net charge, which is almost twice bigger at pH 5 as at pH 7.4. In the Appendix one can find the sketch, which illustrate the siRNA molecule can associate with LAH4-L1. From the figure it becomes obvious that 8 peptides / siRNA requires a tight packing.

At pH 5 the observed enthalpies are larger than at pH 7.4. At pH 5 siRNA accommodates less peptide, but its association is accompanied by higher enthalpy. This is only possible when more bonds are created with siRNA functional groups. Alternatively, conformational changes of the peptide, such as α-helix formation, can be more pronounced at pH 5.

The parameters (stoichiometry n, binding constant K and the enthalpy H) obtained from simulation of the red curves are provided to give a preliminary idea about the strength of the interactions at various pH conditions. Thus the magnitude of both exothermic and endothermic processes becomes smaller when the

peptide net charge decreases at pH 7. However, the enthalpy of endothermic process seems to be more affected by the peptide protonation rate (***Figure X-2***).

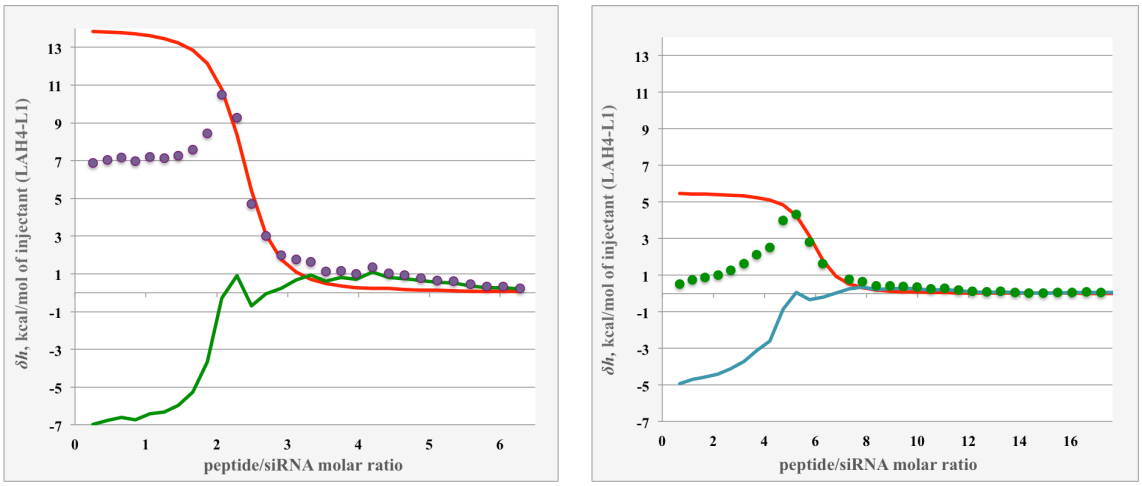

Figure X-2. Model 1. Discerning of different processes contributing to the observed enthalpy for the LAH4-L1 association with siRNA at **pH 5** (*left*) and **pH 7.4** (*right*). The simulation (red curve) was done with a single set of identical binding sites (SSIS), provided by ITC instrument manufacturer (*MicroCal Origin*®). The simulation parameters were: *left*) stoichiometry n=2.3, binding constant $K=9\times10^5$ M^{-1} and enthalpy $\Delta H=14$ kcal/mol; *right*) n=5.8, $K=3.6\times10^5$ M^{-1} and $\Delta H=5.5$ kcal/mol. The turquoise (green) line represents the difference between the observed and simulated ITC curve.

In a different interpretation, the ITC traces can be regarded as the sum of two endothermic processes (***Figure X-3***), one of which represents the binding process and can be described again by single set of identical binding sites model. The second component, obtained by subtraction of simulated curve from the ITC isotherm, has an unusual shape. The latter curve represents a process, when the enthalpy increases with the peptide/siRNA ratio, reaches a maximum, and then decreases. Such calorimetric trace could be explained by the superposition of regular association of LAH4-L1 molecules with RNA binding sites (red curve) and the aggregation of peptide-siRNA complex. To initiate the aggregation a minimum concentration of LAH4-L1 is required, and the enthalpy of process is small in the beginning of the titration. At high peptide/siRNA ratio the contribution of the aggregation processes diminishes.

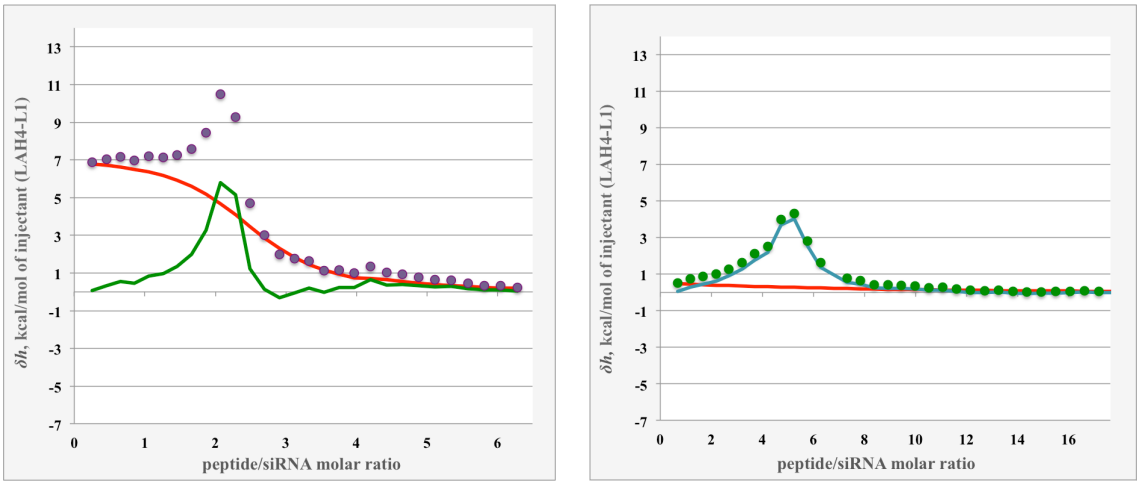

Figure X-3. Model 2. Discerning of different processes contributing to the observed enthalpy for the LAH4-L1 association with siRNA **pH 5** (*left*) and **pH 7.4** (*right*). The simulation (red curve) was done with a single set of identical binding sites (SSIS), provided by ITC instrument manufacturer (*MicroCal Origin*®). The simulation parameters were: *left*) stoichiometry n=2.5, binding constant $K=1.5\times10^5$ M^{-1} and enthalpy $\Delta H=7.2$ kcal/mol; *right*) n=5.8, $K=7\times10^3$ M^{-1}, $\Delta H=0.9$ kcal/mol. The green line represents the difference between the observed and simulated ITC curve.

The effect of the increased ionic strength on the LAH4-L1 – siRNA interaction was tested by performing the titrations in 60mM acetate buffer in the presence of 112mM sodium chloride. Integrated calorimetric traces of peptide interaction with siRNA in salt-free and saline buffer at pH 5 are displayed in a ***Figure X-4***. The control experiments are provided as well. Elevated ionic strength suppresses the electrostatic interactions, and, in turn, certain processes accompanying the LAH4-L1 – siRNA interaction.

The ITC isotherm can be decomposed in two components by simulation of one of the hypothetical contributions to the isotherm (***Figure X-5****, left*), or by fitting of the isotherm with single set of identical sites model (***Figure X-5****, right*).

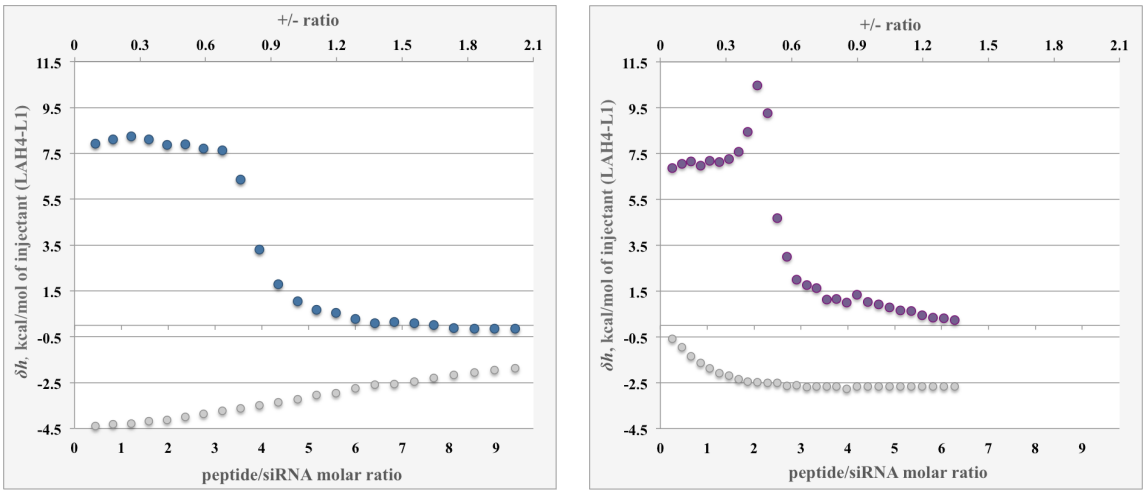

Figure X-4. Integrated calorimetric traces (Δh_i) of 30μM of siRNA titrated with 1.5mM LAH4-L1 in 60mM acetate buffer (pH=5), 112mM NaCl, 1.5μL injections, 25°C (on the ***left***); and 50μM of siRNA titrated with 2mM LAH4-L1 in 60mM acetate buffer (pH=5), 1μL injections, 25°C (on the ***right***). Corresponding control experiments are shown in grey. The x axes scales were chosen to display the same +/− ratio values.

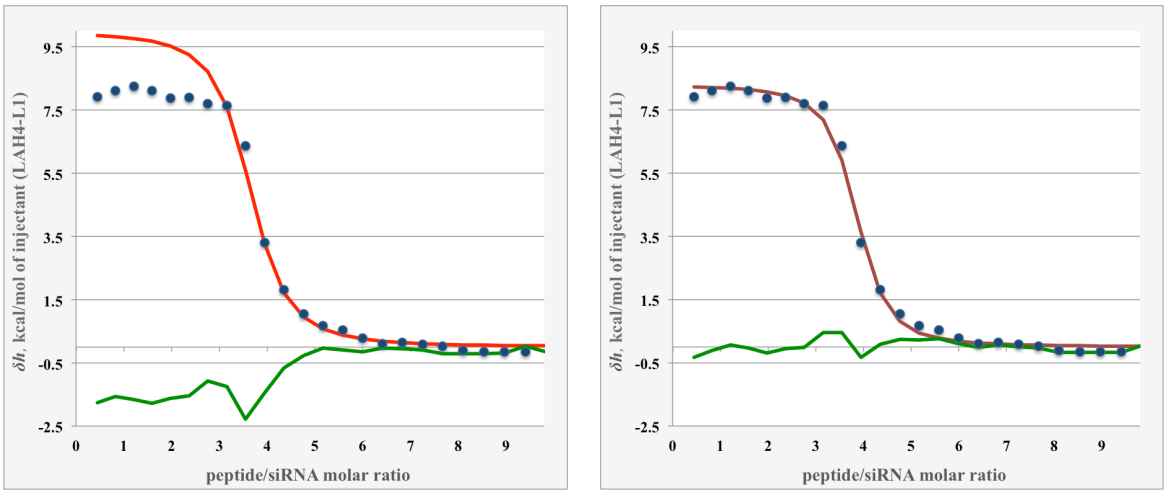

Figure X-5. Discerning of different processes contributing to the observed enthalpy for the LAH4-L1 association with siRNA at pH 5 and the increased ionic strength (154mM). The red curve on the ***left*** figure represents the result of simulation done with a single set of identical binding sites (SSIS). The simulation parameters were set as follows: stoichiometry n=3.5, binding constant $K=8\times10^5$ M^{-1} and enthalpy $\Delta H=10$ kcal/mol. The dark red curve on the ***right*** figure represents the result of fitting of experimental data with a SSIS model. The obtained thermodynamic parameters were n=3.73±0.02, $K=(15 \pm 2.4)\times10^5$ M^{-1}, $\Delta H=8.2 \pm 0.09$ kcal/mol, $T\Delta S=16.6$ kcal/mol. The green line represents the difference between the observed and simulated ITC curve.

High ionic strength is known to suppress electrostatic interaction between charged moieties. Therefore the endothermic component of the titration isotherm seems to be more affected by charge suppression (simulation type I, ***Figure X-5****, left*). If one assumes that the LAH4-L1 – siRNA titration isotherm consists of two endothermic components, one of which related to the aggregation or condensation of the complex, it follows that the enthalpy of such an aggregation process is equal to zero in the solutions of high ionic strength. The LAH4-L1 association with siRNA can thus be fitted with SSIS model (***Figure X-4****, right*).

Similar experiments were performed previously with low molecular weight salmon sperm DNA and LAH4 peptide (Prongidi-Fix et al., 2007). The thermodynamic parameters of the peptide – DNA association were determined by fitting the titration curves with the single set of identical sites model. The reported values were $\Delta H=12 \pm 2$ kcal/mol, $T\Delta S = 19.6 \pm 2$ kcal/mol, $K=(28 \pm 10)\times10^6$ M^{-1}, $n = 98 \pm 10$ peptides per DNA molecule (~300bp). With siRNA and LAH4-L1 peptide the fitting parameters are $\Delta H=8.2 \pm 0.09$ kcal/mol, $T\Delta S=16.6$ kcal/mol, $K = (1.5 \pm 0.24)\times10^6$ M^{-1} and $n=3.73\pm0.02$ LAH4-L1 per siRNA (21bp). The stoichiometry of complex formation can be expressed in peptide per nucleic base pair ratio, which is equal to 0.33 for the LAH4 – DNA and 0.18 for the LAH4-L1 – siRNA interaction.

In order to assess whether the LAH4-L1 interaction with siRNA is governed mainly by the non-specific attractions, LAH4-L1 was titrated into poly-sodium 4-styrenesulfonate (PSS, MW ~70,000) solution. This polymeric molecule is simpler than siRNA, as it contains only one type of functional group, the sulfonate moiety. The siRNA molecule possesses multiple sites for hydrogen bonding (phosphate group, -OH of sugars, tertiary nitrogen).

The calorimetric traces of LAH4-L1 interaction with PSS are also biphasic curves (***Figure X-6***), and the sum of exothermic and endothermic processes. The exothermic process dominates at low peptide/PSS molar ratio, similar to siRNA titrations. Remarkably, the dependence on pH, or more precisely on the peptide net charge, is exactly the same as for the peptide – siRNA interaction. Even the magnitude of the endothermic component is very close to the values obtained with siRNA (***Figure X-1***). One can conclude that the enthalpy of the association process depends on the peptide properties rather than on the nature of the negatively charged counterpart. In other words, the peptide 'feels' both siRNA and PSS as a network of negative charges.

The LAH4-L1 – PSS association reaction is terminated when the positive-to-negative charge ratio reaches 1.4, which is very close to the value obtained for siRNA.

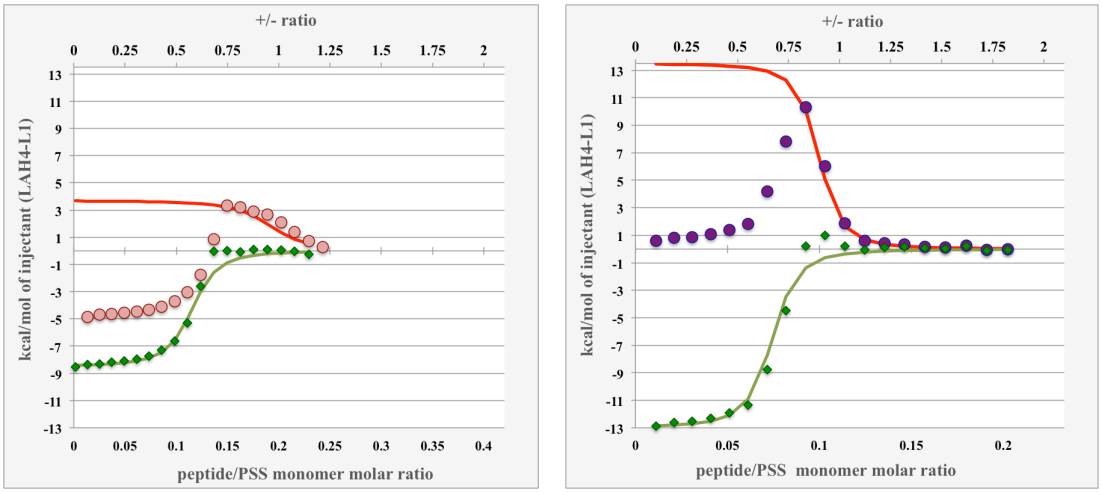

Figure X-6. Integrated calorimetric traces (Δh_i, round symbols) of ***left***) 1.7mM of PSS (the concentration is presented as per monomer) titrated with 2mM LAH4-L1 in 20mM HEPES buffer (pH=**7.4**), 2µL injections, 25°C; ***right***) 2mM of PSS (monomers) titrated with 2mM LAH4-L1 in 60mM acetate buffer (pH=**5**), 2µL injections, 25°C. The X axes scale was chosen to display the same +/− ratio values.
The red curve represents the result of the simulation with single set of identical sites model of the second part of titration isotherm with the following parameters: ***pH7.4***) n=0.2, K=4×10^5 M^{-1}, H=3.7 kcal/mol; ***pH5***) n=0.095, K=15×10^5 M^{-1}, H=13.5 kcal/mol.
The green diamond symbols represent the difference between the experimental titration isotherm and the simulated red curve. The light green curve represents the simulation of this differential curve with SSIS model. The parameters for simulation were following: ***pH7.4***) n=0.12, K=5×10^5 M^{-1}, H=−8.5 kcal/mol; ***pH5***) n=0.07, K=8×10^5 M^{-1}, H=−13 kcal/mol.

The LAH4-L1 – siRNA and LAH4-L1 – PSS interaction differs in the exothermic process, which is larger for PSS than for siRNA (***Figure X-6*** *vs.* ***Figure X-1***). Considering only the electrostatic interactions, the differences between PSS and siRNA are their size and conformation. The PSS molecule consists of about 240 monomers and is flexible, while siRNA has 21 base pairs and is rather rigid. The physical character of PSS and siRNA condensation is presumably quite different, as the siRNA molecule is not able to bend. The condensation reaction could also be an aggregation of the siRNA – peptide particles (Jensen et al., 2010). The formation of large particles, sized at least 200nm, in the peptide - siRNA solution indicates that many siRNA and peptide molecules participate in the complex. Therefore peptide condenses siRNA by interconnecting the neighbouring strands, while with flexible PSS peptide can interact by compacting the same polymer molecule.

Calorimetric titration of PSS and DNA into LAH4-L1 solution.

The interaction of DNA with LAH4-L1 peptide was tested at pH 7.4 and its thermodynamic profile was compared with the analogous isotherm of the PSS – LAH4-L1 interaction. In this study the DNA and PSS macromolecules were titrated *into* the LAH4-L1 solution (***Figure IX-7***). The observed calorimetric isotherms have a biphasic character. In the following the heat response is represented as a function of DNA (PSS) monomer / peptide ratio.

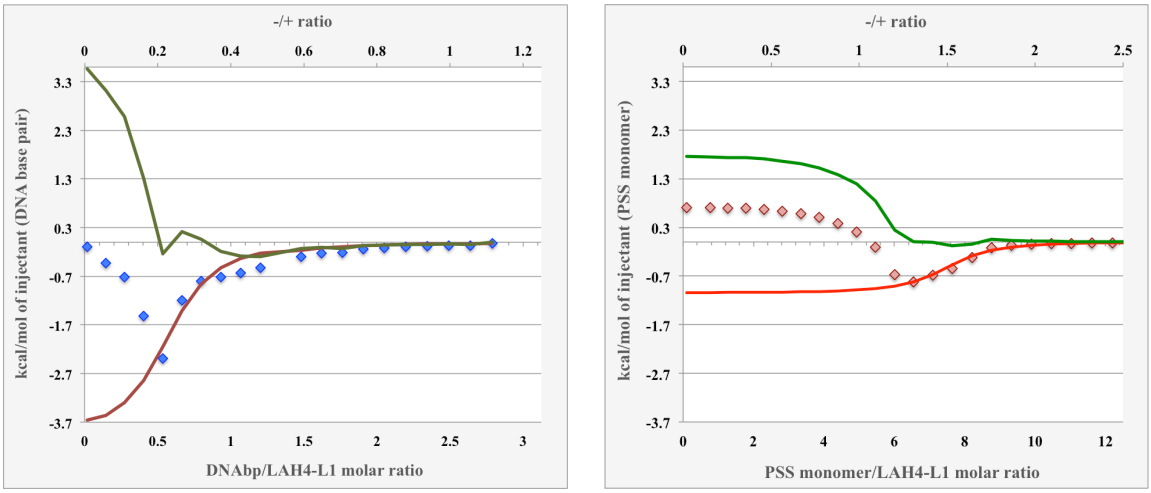

Figure X-7. Integrated calorimetric traces (Δh_i, diamond symbols) of ***left***) 5.13mM of salmon testes **DNA** (as per base pair) titrated *into* 2mM LAH4-L1 in 20mM HEPES buffer (pH=**7.4**), 1.5µL injections, 25°C; ***right***) 60µM of **PSS** (the concentration as per monomer is 20.3mM) titrated *into* 0.3mM LAH4-L1 in 20mM HEPES buffer (pH=**7.4**), 2µL injections, 25°C.
The red curves represent the simulation curves (single set of identical sites) with the following parameters: ***DNA***) $\Delta H = -4$ kcal/mol, $K = 5\times10^4$ M^{-1}, n = 0.55 DNA base pairs per LAH4-L1; ***PSS***) $\Delta H = -1.05$ kcal/mol, $K = 6\times10^4$ M^{-1}, n = 7.3 PSS monomers per LAH4-L1. The green curves represent the difference between the experimental isotherm and the simulated curve.

Interestingly, the enthalpy changes in an opposite way compared to the peptide-to-siRNA (PSS) titration. The enthalpy decreases to some minimum negative value, and then increases reaching zero (***Figure IX-7***). The calorimetric curve can be decomposed into two components of the opposite sign. An endothermic process prevails at low DNA (PSS) / peptide ratio, followed by an exothermic process. Both endothermic and exothermic curves are steeper for DNA – LAH4-L1 interaction than for PSS – peptide interaction. Therefore DNA – LAH4-L1 interaction is characterized by a rather strong association.

About 2.5 DNA base pairs are needed to completely bind the LAH4-L1 peptide. This corresponds to the −/+ ratio of about 1, whereas about 10 PSS building blocks are required to associate with the peptide (−/+ = 2). These values indicate the total DNA(PSS)-to-peptide ratio required to terminate the binding processes, but they do not necessarily represent the stoichiometry of the DNA(PSS) – peptide association.

The enthalpy minimum for DNA - peptide interaction is observed at the negative/positive charge ratio of 0.2, while for PSS – LAH4-L1 interaction the enthalpy minimum is at −/+ ratio of about 1.3. About 6.5 PSS monomers are needed to terminate the binding process, while only 0.5 DNA base pairs are required. Therefore, the DNA binding capacity is much larger than that of the PSS polymer.

The PSS-*into*-peptide titration isotherm has a common feature with peptide-*into*-PSS titration curve, that is an endothermic signal which is observed at low PSS/peptide ratio, and an exothermic process at high PSS/peptide ratio. However, when PSS is titrated into the LAH4-L1 solution the endothermic process seems to dominate over the exothermic (***Figure X-7****, right*). When LAH4-L1 is titrated into PSS the exothermic process has the larger enthalpy (***Figure X-6****, left*).

The LAH4-L1 – PSS titration isotherms can also be decomposed with model 2 (see ***Figure X-3*** for simulation of LAH4-L1 – siRNA association), *i.e.* a sigmoidal binding isotherm and strong endothermic peak-like signal from an assumed condensation processes (***Figure X-8,*** *left*). When LAH-L1 is titrated into a PSS solution, the endothermic condensation process requires a minimum concentration of the peptide to begin (*cf.* Kim et al., 2006). But upon the reverse concentration, the peptide is in excess. Therefore the condensation takes place at each titration step (green curve on the right figure) until certain PSS/LAH4-L1 ratio is reached.

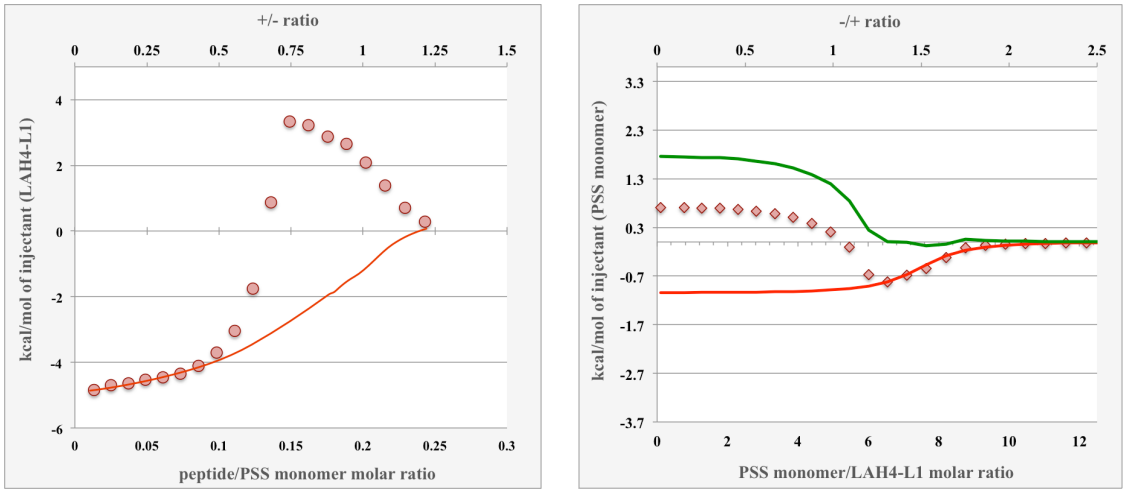

Figure X-8. left) Integrated calorimetric traces (Δh_i, round symbols) 1.7mM of PSS (monomer concentration) titrated *with* 2mM LAH4-L1 in 20mM HEPES buffer (pH=**7.4**), 2μL injections, 25°C. The red line illustrates the exothermic binding process (in contrast to previous figures, red line here is just drawing, not simulation curve). ***right***) 60μM of **PSS** (the concentration as per monomer is 20.3mM) titrated *into* 0.3mM LAH4-L1 in 20mM HEPES buffer (pH=**7.4**), 2μL injections, 25°C. The red curves represent the simulation curves (single set of identical sites) with the following parameters: ΔH = −1.05 kcal/mol, K = 6×104 M-1, n = 7.3 PSS monomers per LAH4-L1. The green curves represent the difference between the experimental isotherm and the simulated curve.

For the PSS – LAH4-L1 system the condensation process involves a bending of the PSS polymer leading to a compact complex. The term 'condensation' was proposed to describe the DNA compaction by various cations and cationic polymers (Matulis et al., 2000). However when translating the same principle to the siRNA – peptide complex, the 'condensation' of siRNA occurs without bending . The individual siRNA molecules with attached peptides undergo aggregation processes. The formation of big particles of at least 200 nm diameter is observed, when the sizes of siRNA and peptide alone are about 5-6 and 3-4 nm (***Figures IX-1*** and ***IX-2***). The aggregation is usually accompanied with water and counter-ions depletion from the aggregating surfaces. These processes are entropy-driven and could tolerate the endothermic heat changes.

SUMMARY AND DISCUSSION.

ITC experiments were performed in which LAH4-L1 peptide was titrated into siRNA solution or into the solution of the anionic polymer polystyrenesulfonate (PSS) at pH 5 and pH 7.4. *Reverse* calorimetric titrations were also performed, where PSS or salmon testes DNA (2000bp) were titrated into LAH4-L1 solution at pH 7.4. The aggregation rate of siRNA – LAH4-L1 and DNA – LAH4-L1 particles upon titration was monitored by the dynamic light scattering. The complexes formation results in highly polydisperse suspension. However, at the sufficiently high peptide/siRNA ratio (about 5-6) it was possible to obtain particles with a lower polydispersity index (0.3), suggesting a rather homogenous suspension.

The calorimetric traces were rather similar for LAH4-L1 – siRNA and LAH4-L1 – PSS systems. In the course of the titration the enthalpy increases, reaching a positive maximum value, and then decreases to zero. By applying the Origin® 'one set of sites' binding model (SSIS), it was possible to discern two components of the binding enthalpy. According to this simulation, the endothermic component represents the regular sigmoidal binding curve. The exothermic process (difference between observed enthalpy and simulated with SSIS model) occurs at low peptide/siRNA (PSS) ratios and is largely suppressed by increasing the ionic strength of the buffer (to 154mM) (***Figure X-4***). Electrostatic processes are supressed

by high salt concentrations. The enthalpy of the endothermic process seems to be more dependent on the peptide charge than the enthalpy of the exothermic process.

A second interpretation of LAH4-L1 titration into siRNA solution was shown in a ***Figure X-3***, *i.e.* the ITC curve is composed of the sigmoidal binding isotherm and a peak-like isotherm that results from the particles aggregation process. As it was shown by DLS technique the aggregation of the particles accompany the LAH4-L1 binding to siRNA at each titration step. However, on molecular level it is possible that the extent of the aggregation increases upon the peptide binding, reaching some maximum value, and then decreases at high peptide/siRNA ratios. Indeed, the maximum of the enthalpy peak at the peptide/siRNA ratio of 2 at pH 5 correlates with the stabilisation of derived count rate parameter, provided by the DLS. The stabilization of derived count rate at the constant value signifies that the formation of the peptide-siRNA particles is finished, or retarded. The aggregation/condensation processes with respect to the PSS – LAH4-L1 direct and reverse calorimetric titrations were discussed already in the RESULTS section.

The molecular interpretation of exothermic and endothermic components of the LAH4-L1 association with nucleic acids and anionic polymer is difficult. Similar ITC titration profiles were obtained for other compounds, such as cationic polymers and peptides interacting with nucleic acids. At same time quite divergent hypotheses are found in literature to explain the shape of such isotherms (see the discussion in the Introduction part, p.43).

The most common assumption is that the association process with nucleic acids consist of complexation of ligand with the nucleic acid and the condensation of nucleic acid strands (Kim et al., 2010; Matulis et al., 2000). These two processes are not necessarily occurring simultaneously. For instance, when small polyvalent cations are interacting with a long DNA strand (as plasmid DNA), complexation occurs first. When all binding sites on DNA molecule are saturated, the condensation process begins. Both processes are endothermic in this case. Kim and co-workers showed that the two processes are well-resolved in the ITC isotherm (Kim et al., 2006). However, when long polymers such as polylysines interact with DNA, complexation and condensation processes occur simultaneously (Kim et al., 2010). In other publications, where a biphasic calorimetric isotherm was observed upon titration of DNA with cationic polymers or peptides, the *exothermic* component of the observed enthalpy was assigned to the condensation process (Matulis et al., 2000; Québatte et al., 2013).

As multiple factors contribute to the thermodynamics of the interaction of macromolecules, the analysis is complicated for the following reasons. 1) The condensation mechanism and energetics would vary from DNA to siRNA considerably if the conformation change is a major contributor to the enthalpy; 2) the change of ligand conformation should be taken into account, as the peptides, depending on the external conditions, change the conformation from random coil to α-helix upon association. This process results in an exothermic enthalpy, as new hydrogen bonds are formed; 3) the type of bond formed during association influences the sign and the magnitude of observed enthalpy (e.g. hydrogen bonding vs. hydrophobic interactions); 4) depletion of hydration water and counter-ions makes a considerable contribution to the entropy, and should be taken into account; 5) and most important, the proton transfer also contributes to the enthalpy (Ghai et al., 2012). The observed enthalpy depends on number of the proton donors and acceptors of the macromolecule and of the ligand. These protonation – deprotonation processes depend, in turn, on the buffer ionization properties. Therefore performing the titration in several buffers should allow to calculate the intrinsic enthalpy of binding (as described in the Chapter II).

Chou and co-workers (Chou et al., 2014) have suggested that the exothermic signal, which appears upon siRNA titration with lysine-histidine polypeptides, results from hydrogen bond formation.

Moreover, the authors have concluded that *only* histidines form the hydrogen bonds, and that protonation of histidines at *pH 5* enhances the histidine hydrogen bonding capacity as the exothermic enthalpy increased at pH 5. When siRNA was titrated with polylysine (17 residues) only the endothermic ITC signal was obtained (Chou et al., 2014), which the authors explained by incapability of lysine for hydrogen bonding. Therefore, the formation of ion pairs was accompanied by an endothermic signal.

However, statistical analysis of the DNA−protein complexes structural database shows that arginines and lysines form much more contacts with nucleic acids via hydrogen bond formation than histidines (Luscombe et al., 2001). Moreover, as it is discussed elsewhere in the literature (Anderson et al., 2013) the salt bridge between lysine residues and DNA phosphates combines short range electrostatic interaction is combined with hydrogen bond formation. Under these conditions, the amine functional groups of the lysine residue remain 'mobile', which is entropically favorable. Privalov and co-workers also showed that the protein-DNA interaction in the non-sequence-specific complexes is accompanied by positive enthalpic and entropic terms (Privalov et al., 2011). Non-specific binding in DNA – protein complexes relies mostly on the interaction of the backbone phosphates with the positively charged amino-acids. In contrast, non-electrostatic hydrogen bonding is often accompanied by the negative enthalpy (major groove binders, ***Figure X-9***).

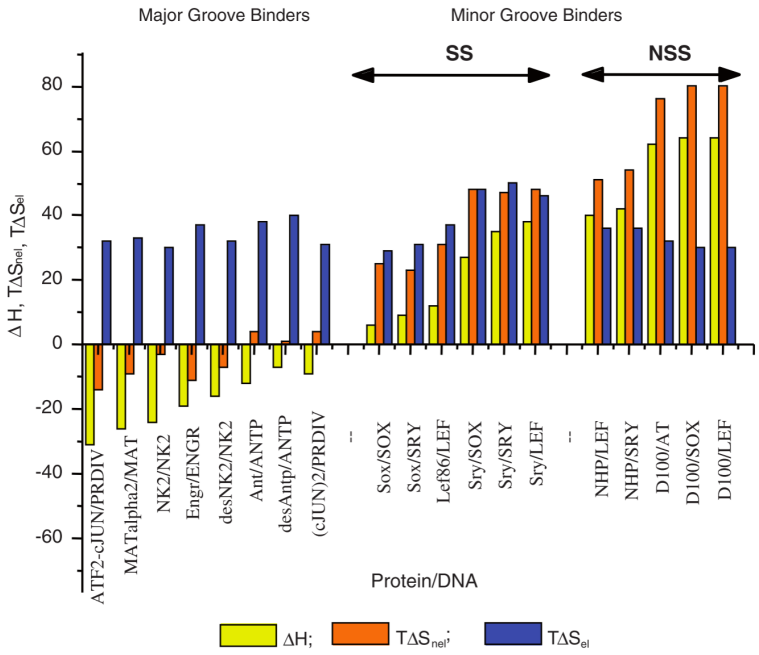

Figure X-9. Enthalpies (ΔH) and entropy factors (TΔS: nel, non-electrostatic; el, electrostatic) of binding proteins to the minor and major groove of their optimal and sub-optimal DNAs. SS=sequence-specific, NSS=non-sequence-specific DNA binding domains. Each data set is labeled with the name of the protein DBD followed by the DNA designation. Adapted from (Privalov et al., 2011).

Schaefer and co-workers have shown by REDOR NMR distance measurements that in bacteriophage T4 it is the lysine, not the arginine or histidine residue that forms the hydrogen bonds with the DNA phosphate groups (Yu and Schaefer, 2008). It was shown also by REDOR NMR for the complex of DNA with $^{15}N/^{13}C$ uniformly labeled pLAH4 peptide, prepared at pH 5, that the lysine residues are in a close contact with the phosphate groups of DNA, but not the histidines, which are positively charged at pH 5 (Vidovic, 2011). In view of these results, it is no longer obvious that only histidines are responsible for hydrogen bonding and the corresponding exothermic signal, as suggested by Chou and co-workers.

In our work we deal with histidine and lysine−containing polypeptide, and we observe the biphasic exothermic−endothermic ITC signal as well. However, our investigation is extended by measurements of peptide – anionic polymer interactions. One could imagine that for the flexible PSS polymer it is energetically advantageous if positively charged histidines (at pH 5) also participate in the interaction. Therefore it remains an *open question* whether binding $–SO_2$ groups to histidines would result in an endothermic or exothermic signal at ambient temperature.

The exothermic process of LAH4-L1 – siRNA association depends on the ionic strength of the solution (***Figure X-5***), the endothermic process to lesser extent. However, the thermodynamic analysis of the DNA−protein association shows that the enthalpy of hydrogen bond formation is independent from the NaCl concentration (Privalov et al., 2011). The electrostatic interactions are usually suppressed by the salt presence.

Exactly the same dependence on the ionic strength was observed by Kim and co-workers for binding of PEG-PLL polymer to plasmid DNA (Kim et al., 2010). A complex endothermic ITC curve was obtained, where the enthalpy increased to a maximum and then decreased to zero (***Figure II-20***). The enthalpy of binding was affected by salt presence, similarly as in siRNA – LAH4-L1 system. Different from our work, Kim *et al.* assigned the beginning of the calorimetric isotherm to complexation, and the second part to condensation process. The binding model proposed by Kim and co-workers is based on the combination of the SSIS models. The authors showed that both complexation and condensation were affected by the presence of salt, but none of the reaction was completely suppressed.

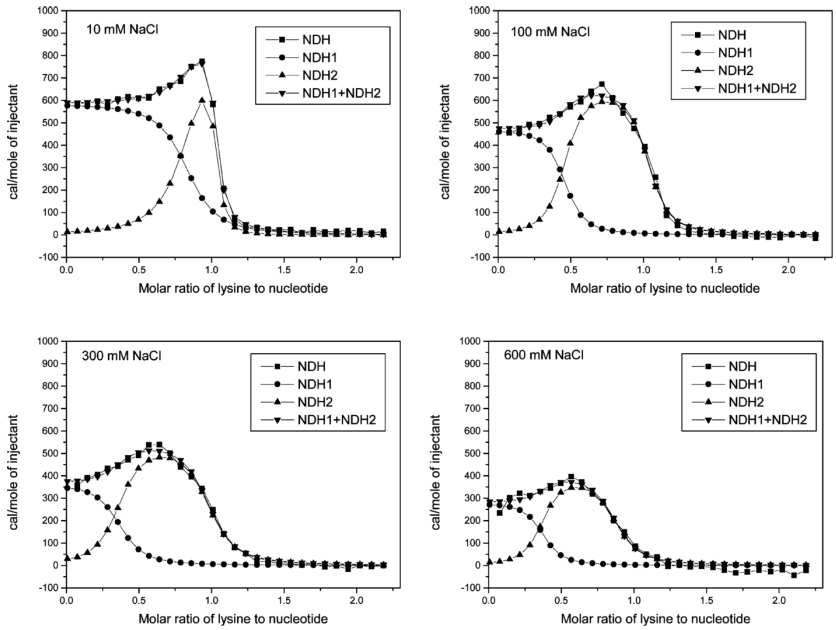

Figure X-10. Representative resolution of ITC curves of PEG-PLL (*12-109*) binding into two parts using the fitting method proposed by Kim et al.: (a) 10 mM, (b) 100 mM, (c) 300 mM, and (d) 600 mM NaCl. NDH: experimental ITC curves; NDH1: curves corresponding to the binding of PEG-PLL to pDNA without DNA condensation (first binding stage); NDH2: curves corresponding to the binding of PEG-PLL during DNA condensation (second binding stage); NDH1 + NDH2 – resulting fitting curve. Adapted from (Kim et al., 2010).

Another source for an exothermic signal are conformational changes of the peptide. It was shown by ITC investigation of the peptide – membrane interactions that α-helix formation is essentially exothermic process due to the hydrogen bond formation (Seelig, 2004). It is possible that the random coil-to-α-helix transition is enhanced when the peptide is tightly interacting with siRNA, i.e. at low peptide/siRNA ratio.

On the other hand it was shown by circular dichroism spectroscopy (Prongidi-Fix et al., 2007) that LAH4 peptide at the concentration of 18μM adopts the secondary structure with only 5% of α-helical conformation at pH 5.5, but 41% α-helical at pH 7.5 (10mM phosphate buffer was used to maintain both pH conditions). When DNA was added at a concentration equivalent of 10 DNA base pairs per LAH4 peptide, the helical content of the peptide increased to 35% at pH 5.5, but didn't change at pH 7.5 (Prongidi-Fix et al., 2007). If we assume that LAH4-L1 behaves the same upon association with siRNA, we must expect to obtain a larger exothermic component at pH 5 than at pH 7.4.

The exothermic process is strongly affected by the increased ionic strength. It was shown that presence of the salt promotes the increase of the LAH4 α-helix formation (Prongidi-Fix et al., 2007). Therefore it is possible that the peptide secondary structure is not altered upon the siRNA association in *saline* buffer.

Endothermic enthalpies may result from the entropically favorable processes. This could be water and the counter-ions depletion, which accompany the interaction of the positively charged lysines with the phosphate groups of siRNA and DNA, or the sulfonate groups of PSS.

The accurate calculation of the thermodynamic parameters of LAH4-L1 association with the nucleic acids and polystyrene sulfonate (ΔH, ΔS, K_D, n) was not possible with the binding models provided by the instrument manufacturer. The model proposed by Kim and co-workers (Kim et al., 2006, 2010) is based on the combination of 'single set of identical sites' simulations for several parallel processes. The principle is similar to the 'two sets of binding sites (TSS)' model, but the former is free of the limitations, imposed by TSS algorithm. For instance, Kim's model allows ligand (cationic polymer or monomer) to participate in several binding processes, in particular, the ligand bound on the first step (complexation), could also participate in the second binding step (condensation).

In this work the binding parameters were estimated by simulating certain region of calorimetric isotherm with SSIS model. This approach was used previously by Quebatte and co-workers for the analysis of ITC isotherm of melittin-lipid nanoparticles binding to DNA (Québatte et al., 2013). This method allows us to visualize 'quantitatively' the hypothesis that the binding isotherms consist of the endothermic and exothermic components. We obtain approximate thermodynamic parameters. The enthalpy and the association constant of the endothermic process, accompanying LAH4-L1 binding to siRNA, are about 2.5 larger at pH 5 than at pH 7.4, but the stoichiometry is 2.5 times smaller (5.8 peptides per siRNA at pH 7.4 against 2.3 peptides/siRNA at pH 5, ***Figure X-2***). The enthalpy of exothermic process decreases 1.4 times when the pH changes from 5 to 7.4.

Table X-1. The estimated thermodynamic parameters of LAH-L1 association with siRNA, DNA and the anionic polymer PSS.

System / method	Component 1	Component 2
LAH4-L1 – siRNA pH = 5 method 1	n = 2.3 peptide/siRNA K = 9×10 ΔH = 14 kcal/mol of peptide	no simulation ΔH = −7 kcal/mol of peptide
LAH4-L1 – siRNA pH = 7.4 method 1	n = 5.8 peptide/siRNA K = 3.6×10 ΔH = 5.5 kcal/mol of peptide	no simulation ΔH = approx. −4.5 kcal/mol of peptide
LAH4-L1 – siRNA pH = 5 method 2	n = 2.5 peptide/siRNA K = 1.5×10 ΔH = 7.2 kcal/mol of peptide	no simulation peak-like signal

LAH4-L1 – siRNA pH = 7.4 method 2	n = 5.8 peptide/siRNA K = 7×10 ΔH = 0.9 kcal/mol of peptide	no simulation peak-like signal
LAH4-L1 – siRNA pH = 5 − NaCl method 1	n = 3.5 peptide/siRNA K = 8×10 ΔH = 10 kcal/mol of peptide	no simulation ΔH = approx. −1.5 kcal/mol of peptide
LAH4-L1 – siRNA pH = 5 − NaCl method 2	Fitting: n = 3.73 ± 0.02 peptide/siRNA K = (15 ± 2.4)×10 ΔH = 8.2 ± 0.09 kcal/mol of peptide TΔS = 16.6 kcal/mol of peptide ΔG = - 8.4 kcal/mol of peptide	second component is close to zero
LAH4-L1 – PSS pH = 5 method 1	n = 0.095 peptide/PSS monomer K = 15×10 ΔH = 13.5 kcal/mol of peptide	n = 0.07 peptide/PSS monomer K = 8×10 ΔH = −13 kcal/mol of peptide
LAH4-L1 – PSS pH = 7.4 method 1	n = 0.2 peptide/PSS monomer K = 4×10 ΔH = 3.7 kcal/mol of peptide	n = 0.12 peptide/PSS monomer K = 5×10 ΔH = 8.5 kcal/mol of peptide
PSS − LAH4-L1 reverse titration pH = 7.4 method 1	n = 7.3 PSS monomer/peptide K = 6×10 ΔH = −1.05 kcal/mol of PSS monomer	no simulation ΔH = approx. 1.7 kcal/mol of PSS monomer
DNA − LAH4-L1 reverse titration pH = 7.4 method 1	n = 0.55 DNA base pair/peptide K = 5×10 ΔH = −4 kcal/mol of DNA base pairs	no simulation ΔH = approx. 3 kcal/mol of DNA base pairs

LAH4-L1 titration into PSS solution results in a larger exothermic component compared to analogous ITC experiment with LAH4-L1 and siRNA (***Figure X-6***). At pH 7.4 the exothermic component is twice larger for LAH4-L1 - PSS interaction (***Figure X-6****, left*), but in the reverse titration experiment the endothermic process was larger. In the course of the direct titration the PSS charged groups become gradually saturated with bound peptide, but in the reverse titration the new portions of PSS groups are available for binding during the whole titration experiment.

Thereafter we can compare the ITC results with other experiments on transfection complexes *in vitro* and *in vivo*. Accordingly to calorimetric trace (pH 7.4, ***Figure X-1***) at most 12 peptide equivalents are required to be introduce into siRNA solution to completely bind the nucleic acids. The following peptide addition does not lead to a heat response. However, in the gel electrophoresis experiment 8.5 *weight* equivalents of the LAH4-L1 peptide were required to retard the migration of siRNA (Langlet-Bertin et al., 2010), which corresponds to about 20 peptides per siRNA molecule. Interestingly that about the same amount of peptide (8.5μM/1μM siRNA) is required for the efficient transfection (Langlet-Bertin et al., 2010), which may signify that the additional peptides are needed to interact with the cell membranes and enhance the complex uptake. Therefore ITC can be used for the design of transfection experiments, along with other biophysical methods.

In summary, further ITC experiments should be performed for a better understanding of the LAH4-L1 association with nucleic acids and polyelectrolytes, namely:

(i) conducting the measurements at various salt concentration may allow discrimination between electrostatic and non-electrostatic components of binding;

(ii) the role of protonation, and the protonation enthalpy can be estimated by conducting measurement using the buffers with varied ionization enthalpy.

(iii) the temperature dependence of the binding enthalpy, called heat capacity change of binding (ΔC_p), can be measured as well. The magnitude of ΔC_p is related to the solvent accessible surface area (ASA) of the macromolecule and is widely to distinguish the mechanisms of protein – ligand or DNA – ligand binding (Gallagher and Sharp, 1998; Sharp et al., 1991).

XI. STRUCTURAL INVESTIGATION OF DNA – LAH4 COMPLEXES BY ssNMR.

As it was discussed in the introductory part of the manuscript, REDOR (Rotational Echo Double Resonance) is a versatile method for the distance and orientation determination in biological solids. Phosphorus of the nucleic acids phosphate residue is a suitable nucleus for use in REDOR experiments, as it is 100% abundant and has rather high sensitivity. $^{19}F–^{31}P$ is a widely used spin pair for REDOR application, for instance for measurements of DNA-drug (Olsen, 2003) and peptide-membrane interactions (Grage et al., 2004; Webb et al., 2006). The method requires more elaborated synthesis schemes for the peptide or the drug, however, as a result it is possible to deal essentially with an isolated pair of interacting spins, which makes analysis of the results more straightforward.

Very often the labeling with ^{19}F is not possible or not practical as in the case of proteins. Schaefer and co-workers studied the DNA packaging in bacteriophage T4 by measuring the distances between lysine residues of the protein and the DNA phosphate groups (Yu and Schaefer, 2008). The protein in the complex was obtained by recombinant expression and therefore uniformly labeled with ^{15}N. Thus the distances were evaluated by REDOR NMR experiment on multispin systems.

Cationic transfection peptides, such as LAH4 and LAH4-L1, are also capable of DNA packaging. The condensation of DNA strands most probably occurs via the same mechanism as in bacteriophages, *i.e.* unspecific interactions between positively charged cationic amino acids and phosphate residues of DNA. In order to test this hypothesis a series of REDOR experiments were performed by Vidovic and co-workers (Vidovic, 2011). At first LAH4 peptide was labeled with ^{13}C within the hydrophobic core, namely at the β-position of 6^{th} and 13^{th} alanines, respectively (*i.e.* two peptides with one label at a time were prepared). The complexes with salmon sperm DNA were prepared at pH 5, where the molar ratio between peptide and DNA base pairs was 2/13. However, no REDOR effect, i.e. no changes in signal intensity which would indicate a close proximity between the labeled sites and the DNA phosphates was detected. Therefore, $^{13}C/^{15}N$ uniformly labeled peptide was prepared by recombinant bacterial expression. The peptide contained one extra proline at N-terminus due to the cleavage procedure from the fusion protein which was produced during over-expression (PKKALLALALHHLAHLALHLALALKKA). Three nitrogen peaks were resolved in the ^{15}N solid-state NMR MAS experiment: about 35 ppm, 180 ppm and 120 ppm corresponding to lysine, histidine side chains and all the backbone nitrogens (Vidovic, 2011). Among those signal only one at 35 ppm (lysine side chains) showed detectable dephasing by interactions with the phosphorus atoms. In contrast, the imidazole moieties of histidines are not affected by the DNA phosphates, even though they are protonated at pH 5. When ^{31}P-{^{15}N} REDOR curves were measured and simulated with a model encompassing one pair of isolated spins, the average distance to the nearest nitrogens was found to be 4Å. However when ^{15}N-{^{31}P} REDOR was performed, the average distance was detected equal 5.5Å. It was concluded that all of the phosphate groups have the lysine residues in close proximity, whereas not all of the lysines are in direct contact with the DNA. In order to investigate further the structure of LAH4-DNA complex, the series of peptides was prepared, where one lysine residue at the time was uniformly labeled with $^{13}C/^{15}N$ (***Figure XI-1***):

LAH4k1: KKALLALALHHLAHLALHLALALKKA-NH2
LAH4k2: KKALLALALHHLAHLALHLALALKKA-NH2
LAH4k24: KKALLALALHHLAHLALHLALALKKA-NH2
LAH4k25: KKALLALALHHLAHLALHLALALKKA-NH2

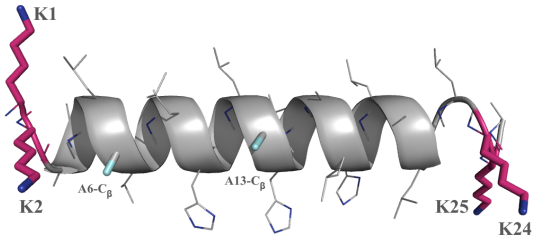

Figure XI-1. The LAH4 peptide is shown in an alpha-helical conformation with the labeled residues highlighted in color (lysines in magenta, β-carbons of alanines in light turquoise).

In the case of uniformly labeled peptide, all NMR-active nuclei interact with each other with different strength. The dipolar interaction depends on the internal properties of nuclei (gyromagnetic ratio) and the distance between the interacting species, and is described by the dipolar coupling constant (Hz):

$$d_{IS} = \frac{\mu_0 \gamma_I \gamma_S \hbar}{8\pi^2 r_{IS}^3}$$

where $\mu_0 = 4\pi \times 10{-}7$ H·m^{-1} is the permeability of free space, γ – gyromagnetic ratio (rad s^{-1}·T^{-1}), ħ – reduced Plank constant (1.0546×10^{-34} J·s), r_{IS} – distance between nuclei.

Given that $\mu_0 \cdot \hbar/2 = 66.178 \times 10^{-12}$ (T^2·Å^3/Hz) the dipolar couplings (Hz) at 1Å distance can be estimated for various spin pairs.

Nucleus	γ/2π (	^{1}H	^{13}	^{15}	^{19}	^{31}
^{1}H	42.576	119 962	30 162	-12 161	112 853	48 561
^{13}	10.705	30 162	7 584	-3 058	28 375	12 210
^{15}	−4.316	-12 161	-3 058	1 233	-11 440	-4 923
^{19}	40.053	112 853	28 375	-11 440	106 166	45 684
^{31}	17.235	48 561	12 210	-4 923	45 684	19 658

The strongest interactions with the most abundant proton nuclei are removed by the ^{1}H decoupling procedure during the REDOR pulses and acquisition. The homonuclear interactions between the carbon spins (around 7500 Hz) are normally averaged by magic angle spinning at the angular speed that exceeds the dipolar coupling (typically between 15 and 22 kHz).

The REDOR curves were similarly constructed for the DNA-LAH4(k1/k2/k24/k25) complexes (Vidovic, 2011), and the distances were estimated using simulations based on isolated spin pairs method. The results are summarized in a Table XI-1 (the percentage between the brackets indicates the amount of peptide for which such distance was detected; * – ^{15}N signals were not resolved):

Table XI-1. The results of distance measurement in transfection complexes prepared at pH 5.5, using REDOR NMR and isolated spin pair analysis method.

Observed nucleus	P-LAH4, Å	LAH4k1, Å	LAH4k2, Å	LAH4k24, Å	LAH4k25, Å
^{15}N	5.5	>10	4 (100%)	4 (90%)	5 (40%)
^{15}N (120 ppm)			5	7	7
^{31}	4	4.6	5.5	6	7

The numbers indicated in Table represent the REDOR distances (in Å) averaged over the molecular assembly. Surprisingly enough, the shortest distances were measured with 2nd and 24th lysines, and not

with terminal ones. Furthermore, ^{13}C-^{31}P REDOR measurements were performed with the same material, *i.e.* on the complexes prepared at pH 5.

In the present work the pH of LAH4-Kx – DNA complexes was changed to pH 7.4 and the series of ^{13}C-^{31}P and ^{15}N-^{31}P REDOR experiments was performed. The distances obtained previously and in the current experiments were reviewed with multispin system model using custom –build software (not published, author Dr. Philippe Bertani).

Please note that LAH4 peptide was used in the series of REDOR experiments, but LAH4-L1 peptide was the main subject for the investigation in the rest work. Those two homologues peptides have similar amino acid sequence and properties (*cf.* Chapter I). They only differ in the position of histidines, which determines the angle subtended by the histidines in peptide's α-helical form, and which consequently defines more pronounced transfection activity of LAH4-L1 peptide. Therefore, the difference in the primary structure of these two peptides is more crucial in the context of the membrane interaction, and supposedly less important for peptide - nucleic acids interactions.

The primary reason of using LAH4 in REDOR experiment was the availability of the labelled peptide, prepared previously by Dr. Verica Vidovic and Dr. Philippe Bertani, who initiated those studies.

MATERIALS AND METHODS.

Preparation of Tranfection complexes for REDOR solid-state NMR spectroscopy

The LAH4 peptide series with one $^{13}C/^{15}N$ labeled lysine at time were prepared by solid-phase synthesis using standard Fmoc chemistry on a Millipore 9050 automated peptide synthesizer. Labeled lysines were from EURISO-TOP (Saint Aubin, France). The purity and identity of the products was controlled by MALDI-TOF mass spectrometry (MW=2787,5) and HPLC. After the purification by reverse phase liquid chromatography (Gilson inc., Middleton, UK) with ProntoSIL 60-3-C18 H column (BISCHOFF Chromatography, Leonberg, Germany), the trifluoroacetate counterions were exchanged with acetate counterions as follows. The peptide powders were placed into 4% acetic acid, the solutions were frozen with liquid nitrogen and subjected to lyophilization at high vacuum overnight.

The low molecular weight salmon sperm DNA (200-1000bp) were purchased from Fluka (Buchs, Switzerland).

The complexes of LAH4-Kx and salmon sperm DNA was prepared by Dr. Vidovic (Vidovic, 2011) at pH 5.5. In a typical procedure, 14mg of each peptide was dissolved in 7mL of 10mM acetate buffer, and 20mg of DNA in 2mL of acetate buffer. The solutions were combined and vigorously mixed, the samples were left overnight at the ambient temperature. Thereafter, the complexes were precipitated by centrifugation at 10 000 g and 20°C for 20min (Eppendorf 5804R, Eppendorf). The pellets were lyophilized at high vacuum overnight. The pellets were placed in 3.2mm MAS zirconia rotors (Bruker, Karlsruhe, Germany). The supernatants were tested for the presence of peptide and DNA. The liquid chromatography test have shown no peptide presence in supernatants, also no DNA was detected by the absorption at 260nm. Therefore the ratio between LAH4 and DNA in complex was 2 peptides per 13 base pairs, or 6.5 DNAbp/LAH4-Kx.

In order to change the pH of complexes, about 17mg of DNA – LAH4-K1, -K24 and –K25 samples were recovered from the MAS rotor, placed in 20mL of DNAse-free Milli-Q water, mixed and sonicated for 30min in a water bath sonicator (Bandelin Sonorex, Berlin, Germany). Then the pH value was measured (pH=4.9) and changed to pH 7.4 by adding 0.1M NaOH. No additional buffer was used for the complex preparation at pH 7.4. Afterwards the suspension of the complexes was left for about 4-5h under constant agitation at 25°C. When complexes were formed, the suspension was centrifuged (Eppendorf

5804R) for 20 min at 20 °C and 13 000 g. The supernatant was stored at 4°C The pellet was lyophilized overnight and placed back in 3.2mm MAS rotor.

The complexes of DNA with LAH4-K2 peptide were prepared anew. Thus 19.6 mg DNA salmon testes (Na^+, 2000 bp, Sigma) were diluted in 22mL of DNAse-free Milli-Q water. Then the sample was placed in the ice bath and sonicated 5 times for 15sec (with a break of 15-20sec each time) with a tip sonicator (Bandelin Sonopuls HD200, Bandelin, Berlin) in order to obtain smaller fragments of 200 – 1000 base pairs. 14.6mg of peptide was added to sonicated DNA solution, diluted previously in 2mL of Milli-Q water. The suspension was vigorously mixed and the pH was adjusted to 7.4 with 0.1M NaOH. Afterwards the sample was left for agitation at 25 °C, 200 rpm for 4h; centrifuged at 20 °C, 13 000 g for 20 min. The pellet was lyophilized and placed in a rotor, and the supernatant was stored. The supernatant was subsequently analyzed for the presence of DNA and peptide. The careful DNA concentration determination by absorption at 260nm (MultiScan Go, ThermoScientific) showed that 10.1 mg of DNA was left in the supernatant. And the peptide quantification performed with CBQCA Protein quantitation kit (Life technologies) revealed that about 1.8 mg of LAH4-K2 was present in supernatant. The recalculation of the DNA and peptide quantities in the pellet provide us with DNA base pairs – over – LAH4-K2 ratio of **3.6**, which is almost twice smaller than obtained previously at pH5 (6.5).

Similar quantification tests were performed with supernatants from the DNA – LAH4-K1, -K24, -K25 preparations at pH 7.4. It was found that about 35-40% of DNA (3.5-4mg) was released from the complexes, but only about 6-8% of the peptide, which leads us to the estimated DNA basepairs / peptide ratio of **4**.

Solid-state NMR experiments

All the NMR experiments were performed on a Bruker Avance DSX500 spectrometer equipped with a BL3.2 X/Y/H DVT probe, and operating at frequencies of 50.67, 202.42 and 500.03 MHz for ^{15}N, ^{31}P and ^{1}H resonance respectively. The same probe was used for performing the ^{13}C-^{31}P REDOR and CP MAS experiments by changing the stop circuit coil (^{13}C resonance at 125.75 MHz). All measurements were made at the magic angle spinning conditions at 22000 Hz or 17000 Hz. Spinning speeds were regulated to ±5 Hz using a pneumatic control unit. To suppress DNA and the peptide motions, which reduce dipolar couplings, all REDOR experiments were performed at 245 to 255 K. The temperature of the sample was maintained with cooled air obtained with Bruker BCU Extrem unit (the final temperature depends on the performance of the unit).

Cross-polarization magic-angle spinning (CPMAS) and ^{15}N-^{31}P REDOR NMR experiments of LAH4-Kx/DNA complexes.

Before starting the REDOR measurements 1D ^{15}N and ^{31}P MAS spectra were recorded. ^{31}P and ^{15}N chemical shifts were referenced externally to the ^{31}P signal of 85% phosphoric acid at 0 ppm and the ^{15}N signal of $^{15}NH4Cl$ at 41.5 ppm, respectively. Proton-decoupled ^{15}N CP MAS NMR spectra were performed using a cross-polarization (CP) pulse sequence with a spectral width, acquisition time, contact time, and recycle delay of 17 kHz, 30 ms, 1500 µs and 1.5 s, respectively. Proton-decoupled ^{31}P CP MAS NMR spectra were performed using a cross-polarization (CP) pulse sequence with a spectral width, acquisition time, contact time, and recycle delay of 17 kHz, 30 ms, 1500 µs and 2.5 s, respectively. For all the CP MAS experiments, the ^{1}H $\pi/2$ pulse and SPINAL64 heteronuclear decoupling field strengths B_1 corresponded to a nutation frequency of 125 kHz. The CP conditions were optimized directly on the LAH4-Kx/DNA sample.

Furthermore the accurate values for ^{31}P and ^{15}N π-pulses were determined by performing 2D NMR nutation experiments (Samoson and Lippmaa, 1988).

$^{15}N\{^{31}P\}$ REDOR experiments were accomplished for each 10-30-60 rotor cycles of dipolar evolution with an increasing number of scan from 1k to 48k. $^{31}P\{^{15}N\}$ REDOR experiments were performed for each 10 rotor cycles of dipolar evolution (τ) until τ = 15 msec with 64 scans, then each 100 rotor cycles with increasing number of scans. Typically, the acquisition of a REDOR curve takes 8-24 hours and up to 2 hours for the $^{15}N\{^{31}P\}$ and $^{31}P\{^{15}N\}$ experiment, respectively. Other parameters included 6.17 μs 31P π-pulses (81 kHz), 10.4 μs ^{15}N π-pulses (48 kHz), and proton decoupling of 125 kHz. Standard REDOR scheme, used in the experiment, include repeated π-pulses on the dephasing nucleus and one central π-pulse on the observed nucleus. Pulse sequence scheme and pulse program can be found in the Appendix. Standard xy8 phase cycling was used for 31P and 15N channels. An exponential apodization function corresponding to a line broadening of 150 Hz and 50 Hz was applied to transform ^{15}N and ^{31}P spectra, respectively.

Cross-polarization magic-angle spinning (CP MAS) and ^{13}C-^{31}P REDOR NMR experiments of LAH4/ DNA complexes.

Proton-decoupled ^{13}C CP MAS NMR spectra were recorded using a cross-polarization (CP) pulse sequence with a spectral width, acquisition time, contact time, and recycle delay of 25 kHz, 10 ms, 3000 μs and 3 s respectively and 1024 scans. For all the CPMAS experiments, the 1H π/2 pulse and spinal64 heteronuclear decoupling field strengths B1 corresponded to a nutation frequency of 77 kHz. The ^{13}C NMR spectra were referenced relative to adamantine, which has two peaks at 38.2 and 29 ppm.

The accurate values for ^{31}P and ^{13}CE π-pulses were determined by performing 2D NMR nutation experiment, therefore REDOR experiment was 'tuned' for ^{13}CE resonance frequency.

$^{13}C-\{^{31}P\}$ REDOR experiments were performed for each 10 rotor cycles of dipolar evolution with 1024 scans till evolution time = 12 msec and each 20 - 40 rotor cycles scans after this time with increasing number of scans. $^{31}P-\{^{13}C\}$ REDOR experiments were performed for each 10 rotor cycles of dipolar evolution with 128 scans till evolution time = 35 msec, then at 600, 650, 700, 750 and 800 rotor cycles (rotor period T = 0.059msec) with increasing number of scans. Other parameters included 4.63 μs 31P π-pulses (108 kHz), 3.8 μs ^{13}C π-pulses (132 kHz), and proton decoupling of 77 kHz. Standard REDOR scheme, used in the experiment, include repeated π-pulses on the dephasing nucleus and one central π-pulse on the observed nucleus. Pulse sequence scheme and pulse program can be found in the Appendix. Standard xy8 phase cycling was used for 31P and 13C channels. An exponential apodization function corresponding to a line broadening of 50 Hz was applied before Fourier transformation to both ^{31}P and ^{13}C spectra .

REDOR simulations of multispin system.

For the analysis of the REDOR experimental results which are recorded on the system of multiple interacting nuclei, such as DNA - LAH4 transfection complex, more elaborated approach is required than for the analysis of the REDOR data on the isolated pair of the interacting nuclei. For this purpose the simulation program was written by Dr. Philippe Bertani. The program uses analytical solution of the Hamiltonian for multiple interacting spin system in the conditions of heteronuclear decoupling of the dipolar interactions (REDOR conditions). The program is working with the spin system file, which has to be preliminary created. The spin system file is made using SIMMOL program http://nmr.au.dk/software/simpson/ (Bak et al., 2000), which in turn uses the pdb coordinates (text file). Unfortunately, SIMMOL program does not recognises the phosphorus atoms. In order to create the multiple spin system,

containing the interactions between the phosphorus nuclei and carbon or nitrogen nuclei, all the phosphorus in the pdb file were substituted with protons, and all other protons were deleted. Once the final spin system file is created using SIMMOL (text file, usually .spinsys), the ^{1}H - ^{13}C (^{15}N) dipolar constants are substituted with ^{31}P - ^{13}C (^{15}N) dipolar constants, and resulting file is used by the simulation program to produce the REDOR curve.

RESULTS AND DISCUSSION

First of all the performance of ^{15}N-^{31}P REDOR experiment was tested on the *model compound*. O,O-diethyl-N-phenylphosphoramidate was kindly provided by Dr Hologne (UMR 5180 Sciences Analytiques, Villeurbanne, France). The compound is ^{15}N labeled and the length of single N−P bond is 1.702Å.

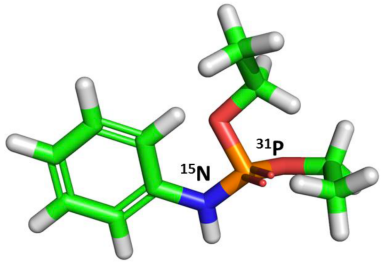

Figure XI-2. The structure of O,O-diethyl-N-phenylphosphoramidate. The picture is adapted from the reference (Vidovic, 2011).

^{15}N and ^{31}P CP MAS measurements result both in narrow nitrogen and phosphorus signals for diethyl-N-phenylphosphoramidate. The chemical shifts and the peak width at the half-height were 24.8 ppm and 110 Hz for the ^{31}P signal and 89 ppm and 133Hz for ^{15}N respectively (spectra not shown).

The REDOR curves were constructed by integrating the corresponding signals, and plotting the ratio Int (S)/Int(S_0) against the evolution time (= the number of rotor cycles × T – rotor period). The signal-over-noise ratios and the calculated error bars (ε (S/S_0)) for the first and the last point of corresponding dephasing curve (S/S_0) are shown in a Table. The error bars were estimated using a formula:

$\varepsilon (S/S_0) = S/S_0 \times \mathrm{sqrt}(\varepsilon_S^2 + \varepsilon_{S_0}^2)$, where $\varepsilon_{S\,(S_0)} = 1/\,\mathrm{sino}$ (S or S_0); sino – signal-over-noise ratio.

Table XI-2. The calculation of the error bars of REDOR dephasing curves. The parameters as signal-over-noise ratio (s/n) for each of the series (S and S_0), as well as S/S_0 ratio and the error bar values are presented for the chosen evolution times.

nucleus / rotor cycle	s/n (S	s/n (S)	S/S	ε (
15N				
2 (0.12msec)	59	68.1	0,969	0.022
80 (4.7msec)	14	2.56	0,108	0.043
31P				
2 (0.12msec)	422	238	0,973	0.005
110 (6.47msec)	344	28.1	0,053	0.002

The corresponding REDOR curves are shown in a ***Figure XI-3***.

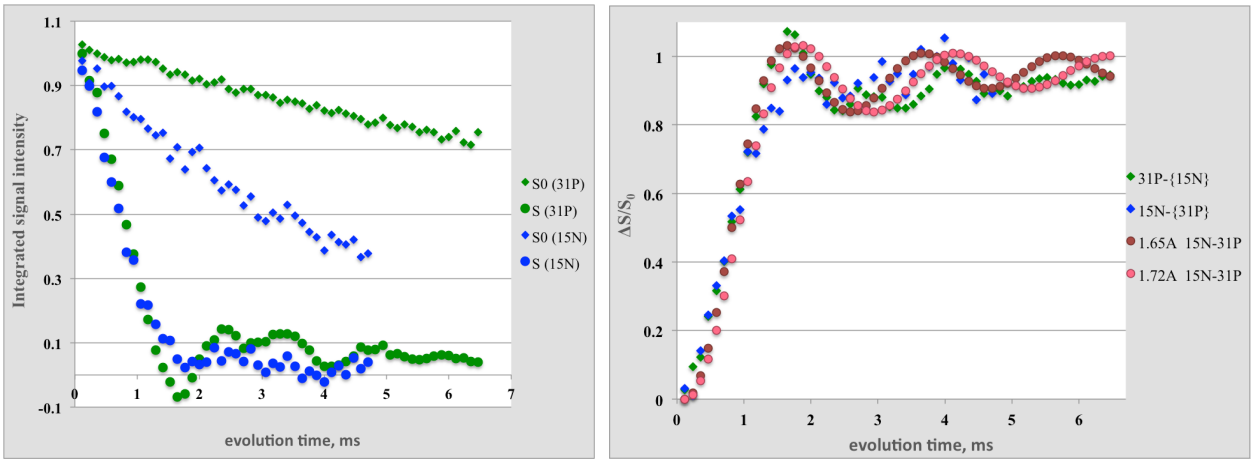

Figure XI-3. The results of REDOR measurements on O,O-diethyl-N-phenylphosphoramidate. *left*) The dephasing curve (S) and control curve (S_0) were measured for each of the observed nuclei (indicated in the brackets). The signal intensity in control experiment decreases due to transversal relaxation (T_2). The intensity of the dephasing curve decreases due to relaxation and the effect of π-pulse on the non-observed interacting nuclei. *right*) ^{31}P-{^{15}N} and ^{15}N-{^{31}P} REDOR curves (1−S/S_0). The non-observed nucleus is indicated in the curved brackets. The simulations for ^{15}N-^{31}P isolated spin pair were performed for the distances 1.65 and 1.72Å using a SIMPSON/SIMMOL software (Bak et al., 2000).

Despite the excellent signal-to-noise ratio for ^{15}N and ^{31}P spectra, the integrated curves S and S_0 (for ^{15}N only) are a bit noisy, which results in the small uncertainty of the distance determination. Thus the REDOR curves can be simulated with the REDOR spectra corresponding to the distances in a range of 1.65 - 1.72Å. However, the error of ±0.04Å is not crucial for the distance measurement in LAH4-DNA complexes, provided that the spectral signal-to-noise ratio is the same.

^{15}N–^{31}P REDOR on the LAH4-Kx−DNA complex prepared at pH 7.4.

First of all ^{15}N and ^{31}P cross polarization magic angle spinning spectra were recorded on each of the DNA−LAH4-Kx complex. ^{31}P CP MAS spectra result in a single peak at about 20 ppm and the width at half-height of 1300Hz for each of the complexes (spectra not shown). ^{15}N CP MAS spectra are shown in a ***Figure XI-4***. Two peaks are obtained for each of DNA−LAH4-K2, 24, 25 complexes at pH 7.4 (green) as well as at pH 5 (violet), and a single ^{15}N signal for DNA−LAH4-K1, where the lysine is placed at the N-terminus and the protonation states of ε-NH_3^+ and terminal NH_3^+ group are in the equilibrium. The peak at about 50 ppm corresponds to the ε-NH_3^+ side chain group and the peak at about 135 – 140 ppm is backbone nitrogen. The peaks half-widths are indicated in a Figure (K1 and K24). The ^{15}N chemical shifts of lysine backbone –NH− and ε-NH_3^+ do not change upon the pH increase, only the signal of ε-NH_3^+ group of the 25th lysine is shifted slightly downfield.

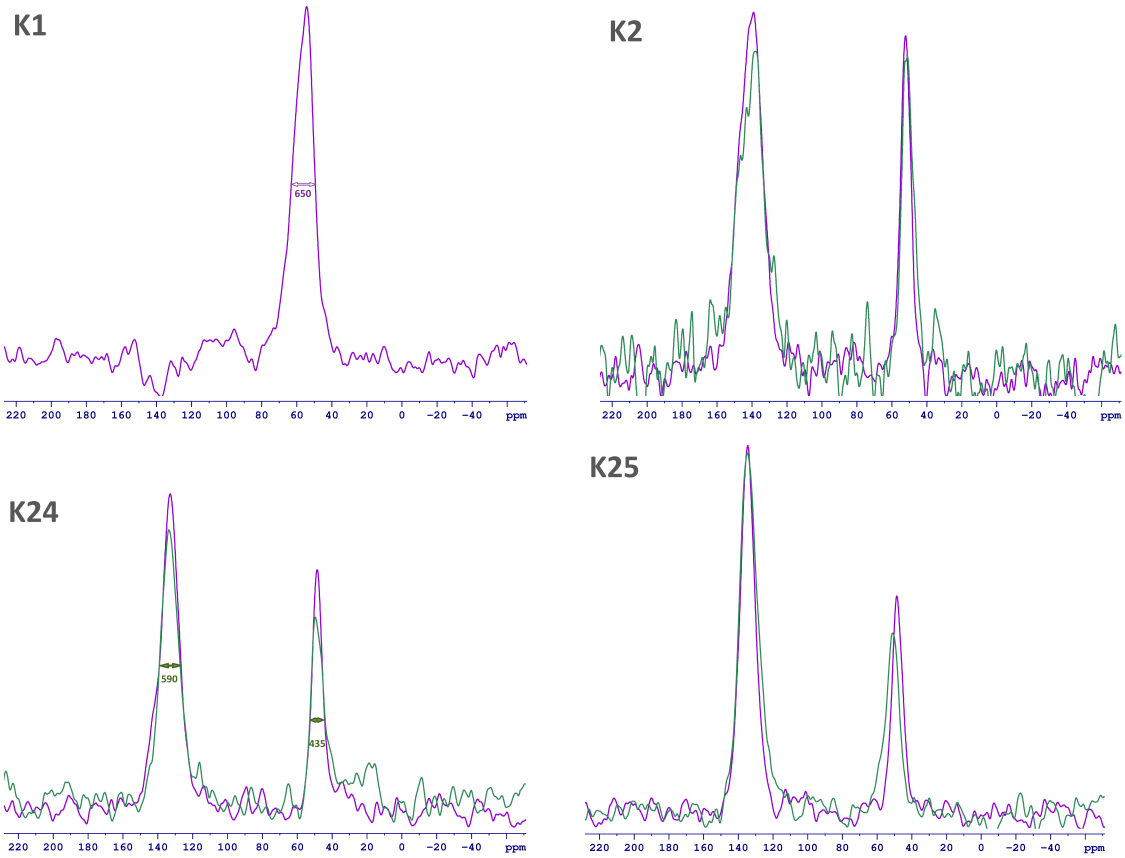

Figure XI-4. ^{15}N CP MAS spectra of DNA−LAH4-Kx complexes. In a single experiment the nitrogen signal from corresponding uniformly labeled lysine is observed. The peak at about 50 ppm corresponds to the ε-$NH3^+$ side chain group and the peak at about 135 – 140 ppm is backbone nitrogen (K2, K24, K25). The peak at 55 ppm for DNA−LAH4-K1 complex is a signal from both ε-$NH3^+$ side chain and N-terminal $NH3^+$ group. Green spectra were recorded for complexes at pH 7.4, and the violet spectra at pH 5 (by Verica Vidovic and Philippe Bertani). Numbers indicate the peak width at half-height.

The series of one-dimentional ^{15}N and ^{31}P CP MAS spectra without (S_0) and with (S) the dephasing on the non-observed nucleus (^{31}P and ^{15}N respectively) were recorded after a given number of rotor cycles. The REDOR curves were constructed by integrating the corresponding signals, and plotting the ratio Int (S)/Int (S_0) against the evolution time. The REDOR spectra were not recorded for DNA−LAH4-K1 complex at pH 7.4 as two ^{15}N can not be resolved and the analysis is complicated, as it was shown previously for the data obtained at pH 5 (Vidovic, 2011). The representative ^{31}P−{^{15}N} and ^{15}N−{^{31}P} REDOR curves for DNA−LAH4-K24 complex are shown in a ***Figure XI-5***. The error bars were estimated for each spectral set and are plotted along. The error bars are much bigger for ^{15}N−{^{31}P} REDOR curves, because the ^{15}N nuclei are less sensitive and less abundant in the sample. It takes much more time to record a ^{15}N−{^{31}P} REDOR series than to acquire a ^{31}P−{^{15}N} REDOR set, that is why conditions were chosen to optimize the 'signal/noise – over – time cost'.

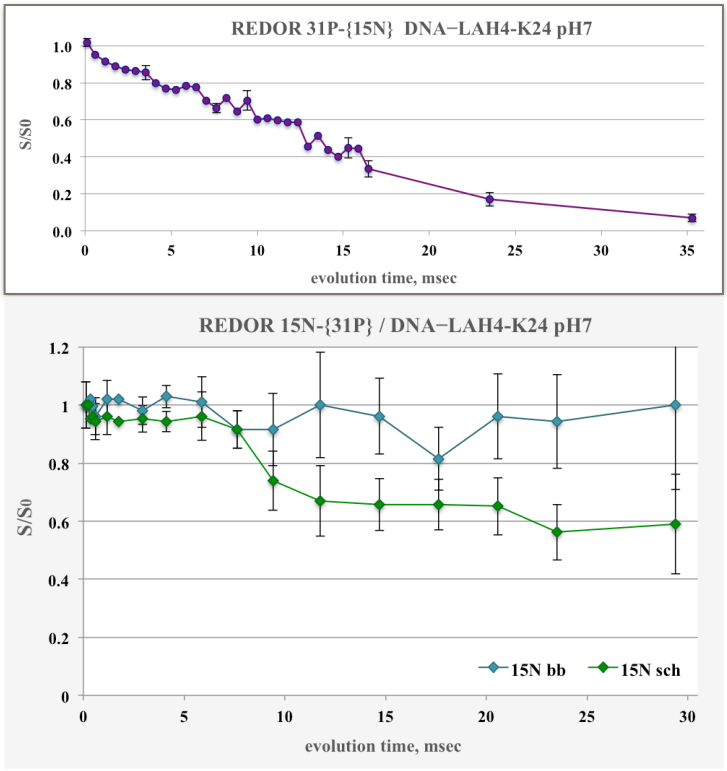

Figure XI-5. $^{31}P-\{^{15}N\}$ (top) and $^{15}N-\{^{31}P\}$ (bottom) REDOR curves for DNA−LAH4-K24 complex, prepared at pH 7.4. The error bar were calculated for each point as : ε (S/S0) = $S/S_0 \times \mathrm{sqrt}(\varepsilon_S^2 + \varepsilon_{So}^2)$, where $\varepsilon_{S\,(So)} = 1/$ sino (S or S_0); sino – signal-over-noise ratio. Evolution time is number of rotor cycles multiplied by rotor period (rotor period T = 1/ 17000 Hz). bb refers to backbone NH group, sch to side chain NH_3^+ group.

The REDOR curves were constructed for each of the DNA−LAH4-Kx complexes at pH 7.4 and pH 5.5 (***Figure XI-6***). The spectra for complexes prepared at pH 5.5 were recorded by Dr. Verica Vidovic and Dr. Philippe Bertani. The K1 graph in a left figure represents the signal from from the added intensities of the side chain and the N-terminal NH_3^+ as the signals are not resolved. $^{15}N-\{^{31}P\}$ REDOR data for DNA −LAH4-K1 are not taken into account as soon as it represents the signal from two types interacting with phosphorus nuclei, which could have however different relaxation properties. This results in such irregular curve. Otherwise we observe following correlation for the lysine side chains proximities to phosphates K2 > K24 > K25 at pH 5.5, and K2 = K24 > K25.

When comparing the REDOR curves at pH 5.5 and pH 7.4, the dephasing is more efficient at pH 5.5. In fact, there are two factors that influence the observed dephasing rate, namely the promixity of the observed nuclei to the dephasing nuclei, and the fraction of the nuclei that participate in the interactions. In the REDOR experiment we measure the intensity of ^{15}N signal from the whole population of the ^{15}N spins, even those that are not interacting directly with phosphates. As soon as ^{15}N signals from interacting and not interacting lysine NH_3^+ group are not resolved in solid-state NMR spectrum (data not shown), it was not possible to exclude non-interacting spins from the analysis. As far as about 40% of DNA are released from the complex during the sample pH change from 5.5 to 7.4 (Meterials and Methods), it seems quite rational that there will be almost twice less peptides that are interacting directly with phosphate groups. For $^{31}P-\{^{15}N\}$ REDOR the correlation is K1 > K2 > K24 at pH 5.5, but K2 < K24! Unfortunately not whole data set was recorded to present for the comparison, but it is obvious that the $^{31}P-\{^{15}N\}$ REDOR data for K2 at pH 7.4 do not correlate with the rest of the curve. When the portion of DNA is released from complex, then there will be more phosphate groups remaining in the complex,

which are in the close contact with peptides (1 LAH4 per 3.5 DNA bp at pH 7.4, and 1 LAH4 per 6.5 DNA bp at pH 5.5). It is difficult to determine then the reasoning for such dephasing behaviour for K2 complex. The reason may be purely technical as well, *i.e.* the probe condition may change in the course of the experiment. For information, the time required to record the $^{15}N-\{^{31}P\}$ and $^{31}P-\{^{15}N\}$ REDOR dataset is about two weeks.

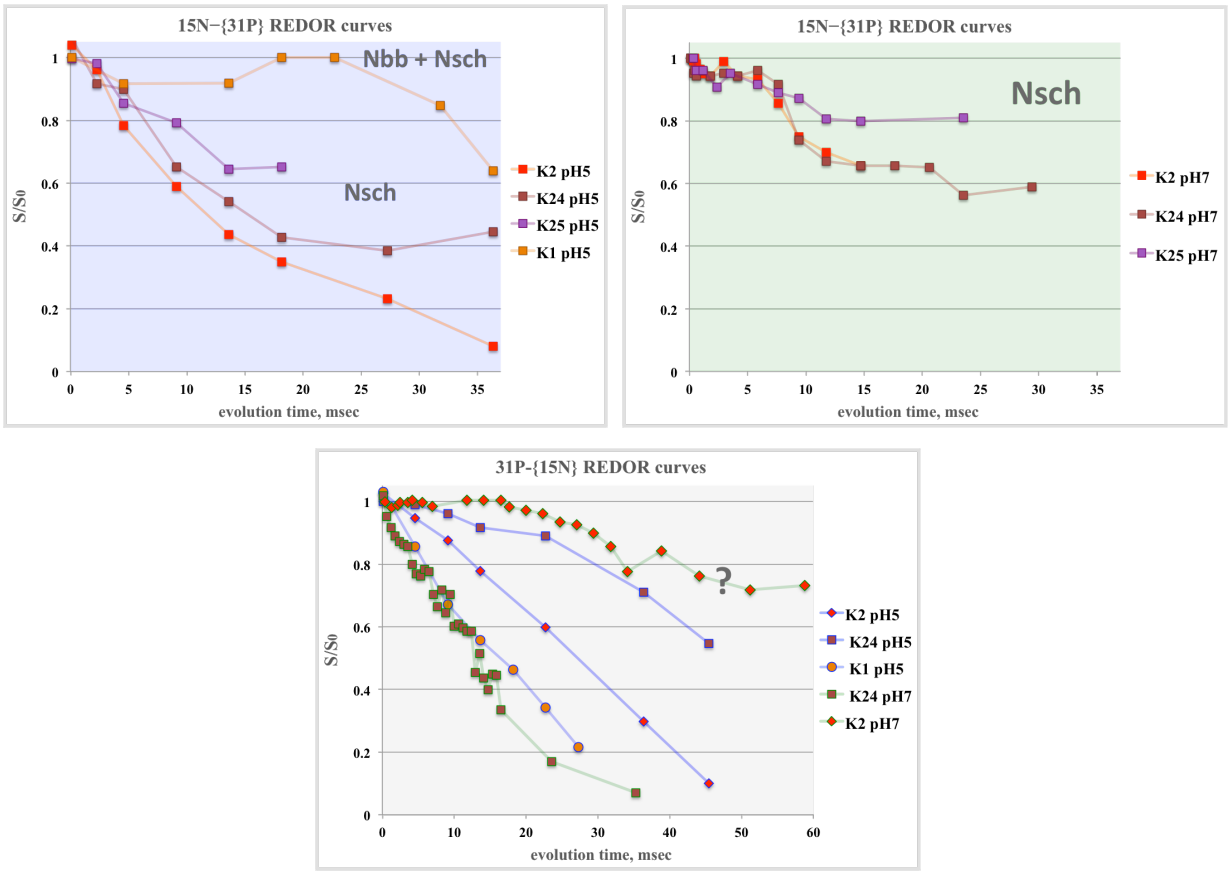

Figure XI-6. $^{15}N-\{^{31}P\}$ (top) and $^{31}P-\{^{15}N\}$ (bottom) REDOR curves for DNA−LAH4-Kx complexes, prepared at pH 7.4 and pH 5.5. REDOR data at pH 5.5 were recorded by Dr. Vidovic and Dr. Bertani, as reported earlier (Bechinger et al., 2011; Vidovic, 2011).

$^{13}C-^{31}P$ REDOR on the LAH4-Kx−DNA complex prepared at pH 7.4

Similarly the series of one-dimensional ^{31}P and ^{13}C CP MAS spectra were recorded, then $^{31}P-\{^{13}C\}$ and $^{13}C-\{^{31}P\}$ REDOR curves were constructed for all four DNA−LAH4-Kx complexes. As it was indicated in the previous paragraph ^{31}P CP spectra of the DNA−peptide complex represents a single peak at about 20 ppm. In contrast, the ^{13}C CP spectra contain multiple peaks from the uniformly labelled lysine, but also the natural abundance background from the DNA and peptide molecules, which is 1.1% for the ^{13}C isotope. The MAS spectra of free peptides in powder were recorded and the ^{13}C signals were assigned.

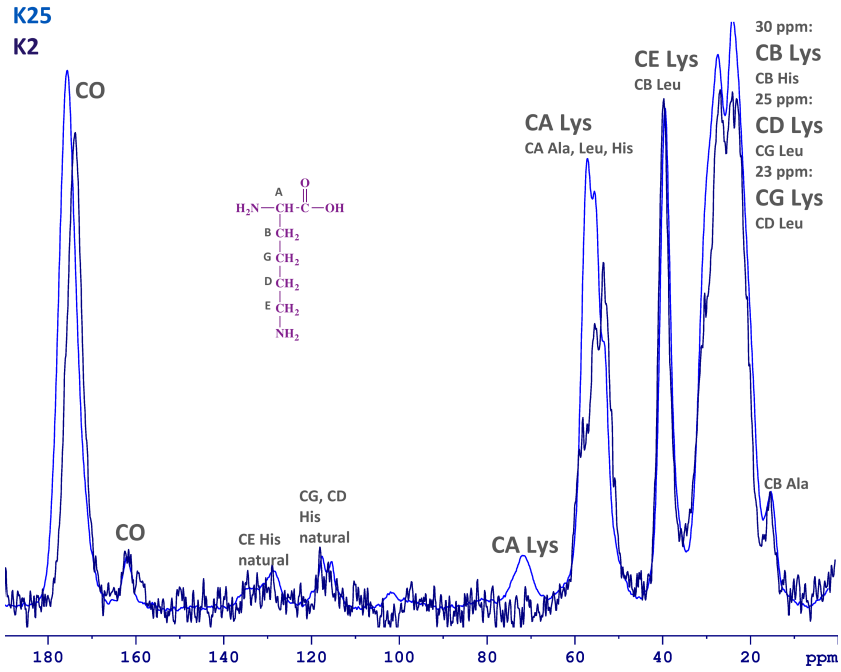

Figure XI-7. ^{13}C CP MAS spectra of dry powders of LAH4-K2 and LAH4-K25 peptides. The peaks were assigned by simulating of the spectra for LAH4 peptide with MNova NMR software (http://mestrelab.com/). The simulations are based on the averaged ^{13}C chemical shifts of amino acids, available in the corresponding databases. The extra signal at 72 ppm was observed for LAH4-K25 (powder) exclusively and was tentatively assigned to the carbon in α-position of isomeric form of peptide.

The ^{13}C NMR spectra were recorded for the complexes at pH 7.4 and pH 5 and compared with the spectrum of free peptide (***Figure XI-8***). Neither the signal line width, nor the chemical shifts change significantly upon the peptide association with DNA at pH 7.4 and pH 5, as revealed by ^{13}C MAS spectra.

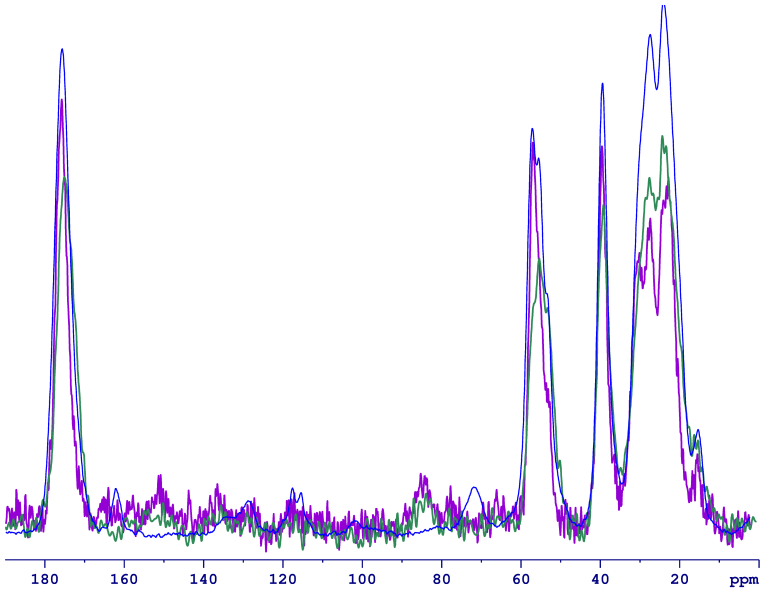

Figure XI-8. ^{13}C CP MAS spectra of LAH4-K25 peptide in powder (blue) and DNA−LAH4-K25 complex at pH 7.4 (green) and pH 5 (violet, recorded by Dr. Philippe Bertani).

For constructing the REDOR curves the series of ^{13}C and ^{31}P CP spectra were recorded as described previously with and without applying the 180° dephasing pulse on the non-observed nucleus. ^{13}C nuclei of lysine residue have different relaxation rates as shown in a ***Figure XI-9***, and therefore different limits

for the REDOR curve construction and the distance determination. We can see already by comparing S_0 and S MAS spectra that the carbon nuclei which is directly bound to ε-NH_3^+ group (CE) undergo the fastest dephasing, thereby showing the closest proximity to the DNA phosphates. After 328 rotor cycles (τ = 19.3 msec) only a residual signal intensity is observed at 38 ppm, corresponding to the natural abundance signal of ^{13}C-β nuclei of leucine residues and some contribution from DNA (the DNA background at 38 ppm is about three times smaller than the DNA ^{13}C signal at 85 ppm, data not shown). The ^{13}CE signal is the most reliable indicator of the phosphate group proximity, because it is bound directly to the interacting group (ε-NH_3^+), but also because it contains the smallest background from naturally abundant ^{13}C nuclei.

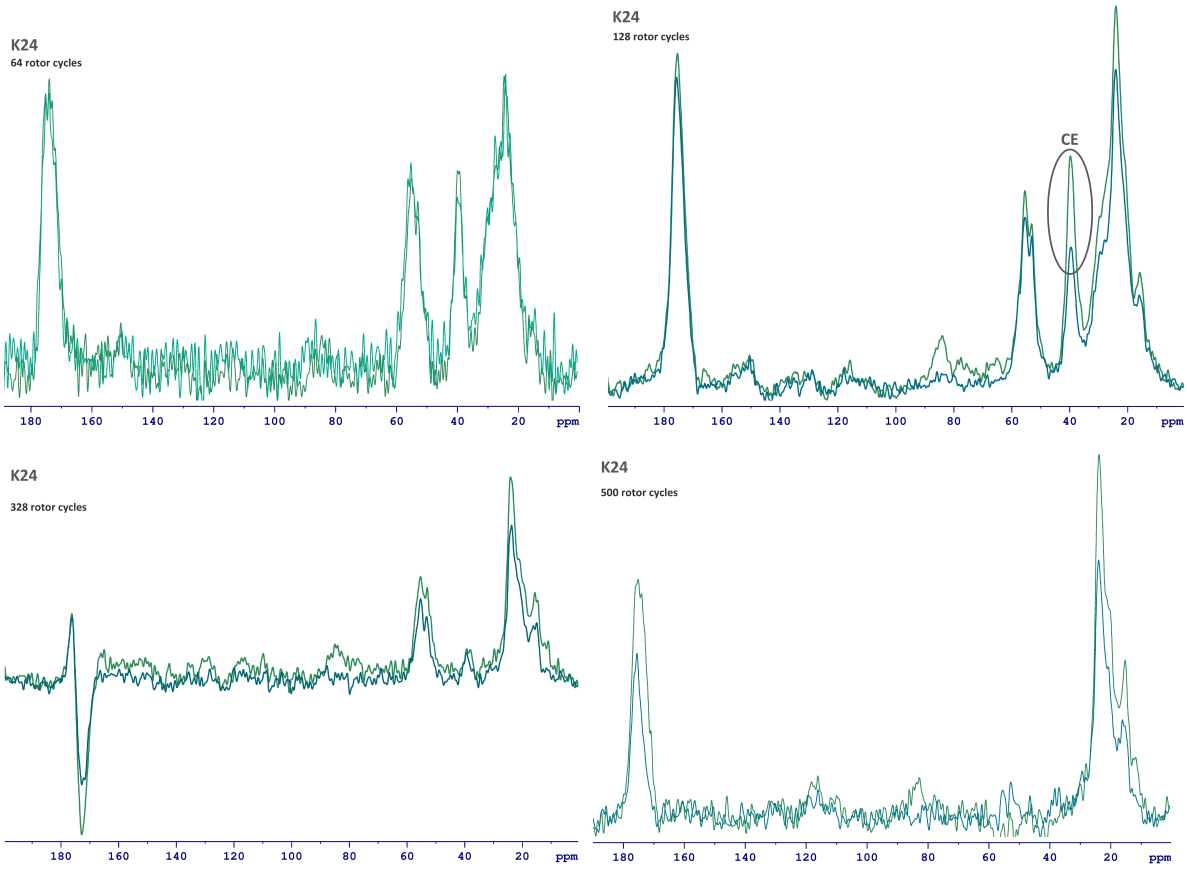

Figure XI-9. ^{13}C CP spectra of the DNA−LAH4-K24 complex recorded at various evolution times. Green curves correspond to the MAS spectra without dephasing (S_0), and the green-blue curves represent the ^{13}C spectra with ^{31}P dephasing.

The REDOR curves were obtained by integrating of the corresponding ^{13}C signals (CA, CE and CB – CD regions) and plotting S/S_0 against evolution time and shown in a ***Figure XI-10***. The error bars were calculated as described previously. The ^{13}C – ^{31}P REDOR curves were recorded for each of the DNA −LAH4-Kx complexes at pH 7.4. The lower S/S_0 values are indicative of the the closest proximity of the observed nucleus (^{13}C) to the dephasing nucleus (^{31}P) in this case (*i.e.* CE nuclei are closer to phosphates than CD, CG, CB, CA nuclei). The relation between the shape of dephasing curve and the distance between the nuclei will be discussed later in more detail. The REDOR curve for CE nuclei is going up at the long evolution times, which indicates that the nuclei contributing to the residual signal at 38 ppm have long relaxation times, and that they do not interact with phosphorus (thereby S/S_0 approaches 1). The same shape of S/S_0 (CE) dephasing curve was obtained with other DNA−LAH4-Kx complexes at both

pH. This point where the REDOR curve has its minimum was defined as a limit of $^{13}C-\{^{31}P\}$ detection, and the extra points were excluded from the analysis.

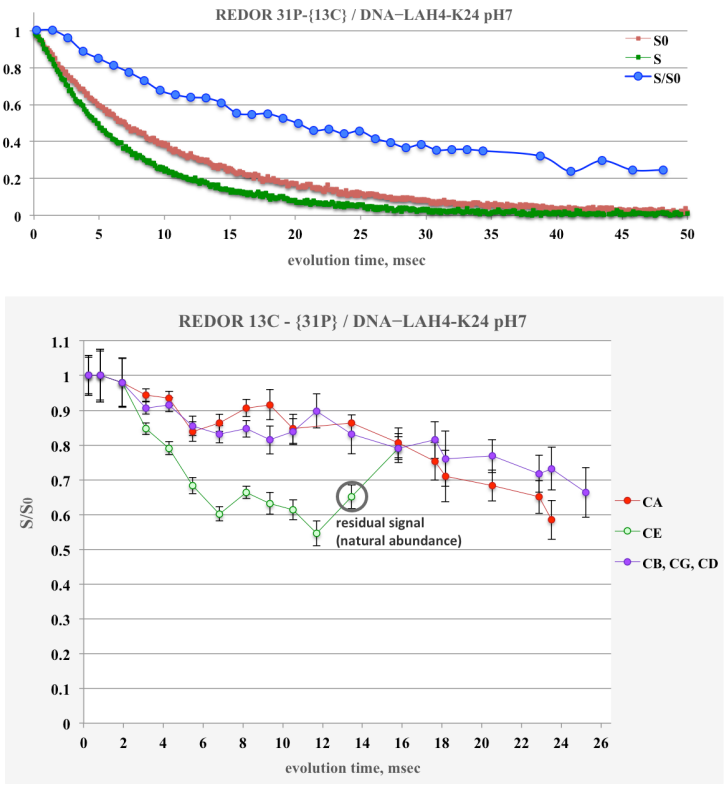

Figure XI-10. $^{31}P-\{^{13}C\}$ (top) and $^{13}C-\{^{31}P\}$ (bottom) REDOR curves for DNA−LAH4-K24 complex, prepared at pH 7.4. The error bar were calculated for each point as following: ε (S/S0) = $S/S_0 \times \mathrm{sqrt}(\varepsilon_S^2 + \varepsilon_{S_0}^2)$, where $\varepsilon_{S\,(S_0)} = 1/\,\mathrm{sino}$ (S or S_0); sino – signal-over-noise ratio. The error bars for $^{31}P-\{^{13}C\}$ curve were the same as in $^{15}N - ^{31}P$ experiment, and not shown in a figure. Evolution time is number of rotor cycles multiplied by rotor period (rotor period T = 1/ 17000 Hz). The figure on the top shows also the integrated intensities of the series of ^{31}P CP MAS spectra without (S_0) and with (S) dephasing on the ^{13}C nuclei, recorded after each two rotor cycles.

The REDOR curves were constructed for each of the DNA−LAH4-Kx complexes at pH 7.4 and pH 5.5 (***Figure XI-11*** and ***Figure XI-12***). In contrast to the REDOR data obtained with $^{15}N - ^{31}P$ interacting spin pair, the $^{13}C-\{^{31}P\}$ REDOR curves are rather similar for each of the lysines (K1, K2, K24, K25), especially with respect to ^{13}CE dephasing curve, which has the best confidence interval (see ***Figure XI-10***) and is the most reliable measure, as discussed above. Moreover, there is no substantial difference between two pH conditions. However when analysing the $^{31}P-\{^{13}C\}$ REDOR curves (***Figure XI-12***) we could assume that there are slightly more phosphate groups in direct contact with 25th lysines (K25) at pH 7.4 than at pH 5.5, or they make tighter contact. The same is probably valid for K24, but the noisy curve doesn't allow making the unambiguous conclusion. The phosphorus nuclei dephase more efficiently on K2 lysines at pH 5, but is the same as K24 and K25 at pH7.4 (***Figure XI-12****, right*). Moreover, the phosphorus nuclei dephase slightly better in the presence of uniformly labelled N-terminal lysine (K1) at pH 7.4 (***Figure XI-12****, left*). In fact, lysine 1 contains two positively charged groups, namely ε-NH_3^+ and the terminal NH_3^+. It is possible therefore that this residue is interacting more efficiently with the DNA phosphates and the N-terminal NH_3^+ is spatially closer to phosphates than any of the backbone -NH- groups of the other lysine residues.

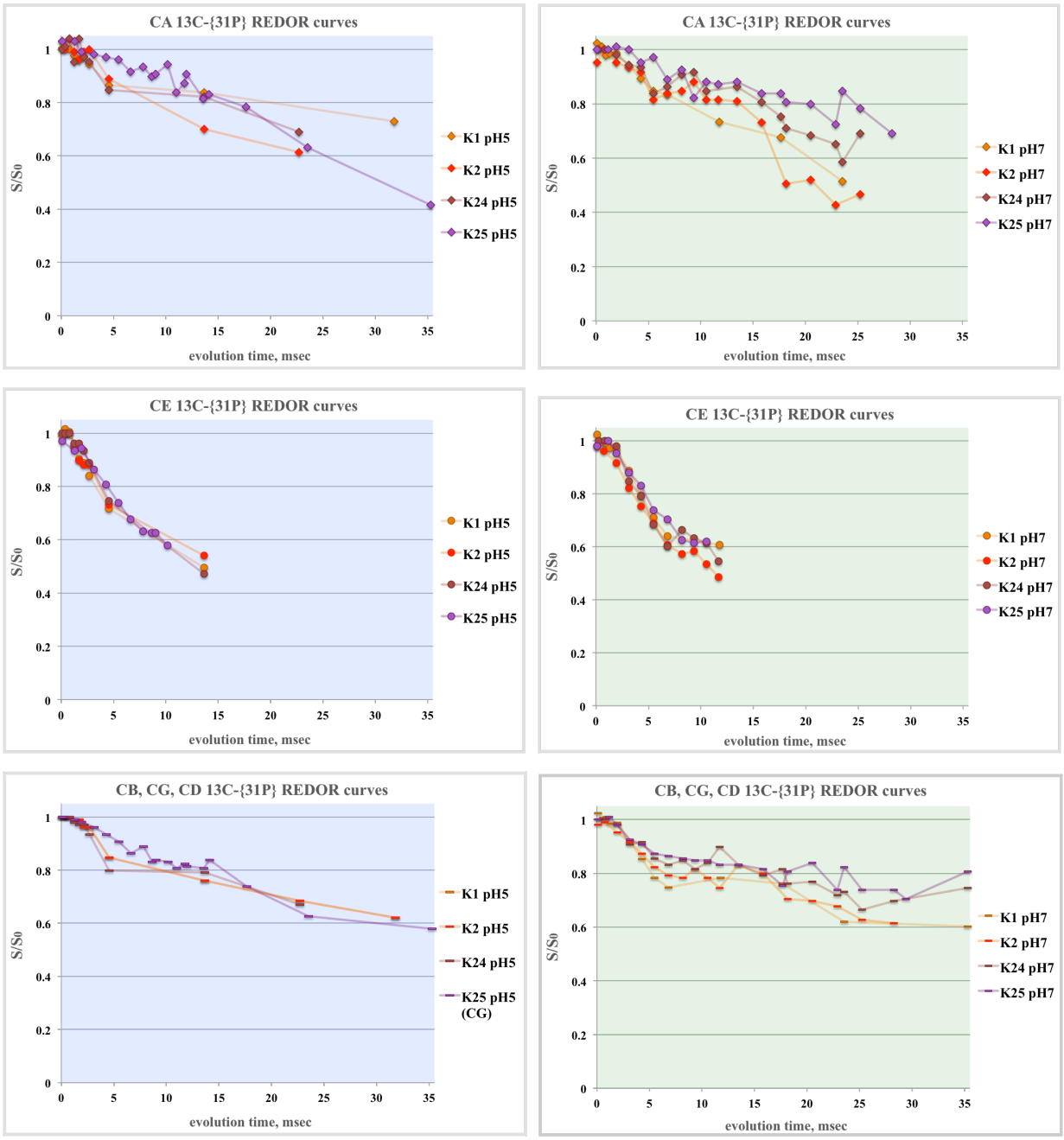

Figure XI-11. $^{13}C-\{^{31}P\}$ REDOR on DNA−LAH4-Kx complexes at pH 7.4 and pH 5.5. S/S_0 curves were obtained by integrating corresponding regions on ^{13}C dephased and non-dephased CP MAS spectra and by plotting the quotient against the evolution time. The REDOR spectra at pH 5.5 were recorded by Dr. Philippe Bertani.

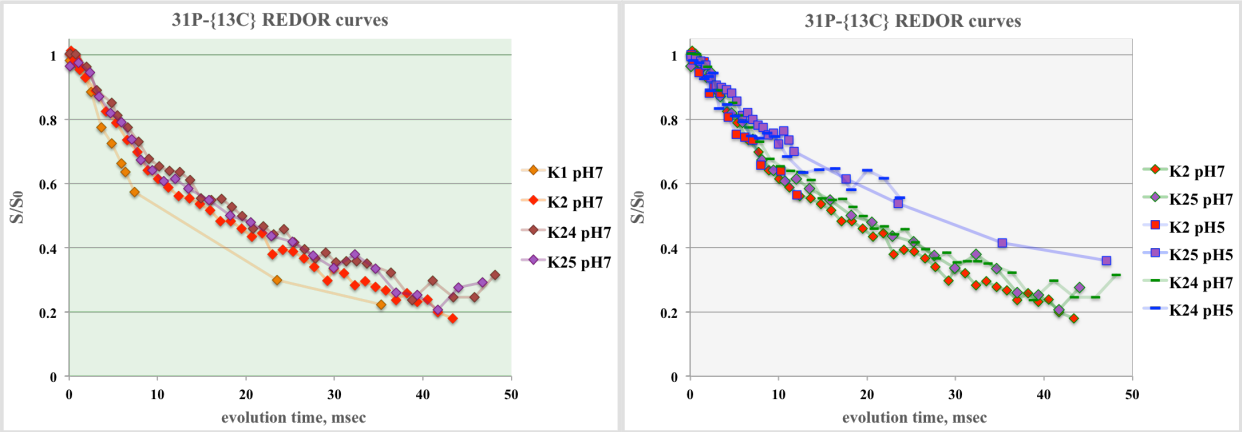

Figure XI-12. $^{31}P-\{^{13}C\}$ REDOR on DNA−LAH4-Kx complexes at pH 7.4 (*left*) and comparison of the phosphorus REDOR curves at pH 7.4 and pH 5.5 (*right*). S/S_0 curves were obtained by integrating ^{31}P dephased and non-dephased CP MAS spectra and by plotting the quotient against the evolution time. The REDOR spectra at pH 5.5 were recorded by Dr. Philippe Bertani.

In order to clarify the correlation (or the absence of the correlations) of the dephasing curves obtained in REDOR experiment with pH and lysine position, the distance simulation were performed using the appropriate multispin systhems.

Distance determination from the REDOR curves using multispin simulation approach.

When $^{13}C/^{15}N$ uniformly labelled lysine residue interacts with the phosphate group of DNA, then in the sphere of 15Å we can find at least 3 phosphorus nuclei that reside in closest proximity to this lysine residue. Each of the phosphorus nuclei interacts with six carbon nuclei or two nitrogen nuclei. As the distances from the phosphorus nucleus to each of the carbons are in the close range, then probably all six carbons will participate in the dephasing, not equally, but depending on the distance. In the current approach we exclude the participation of CO group. The reason is following. In order to perform an efficient REDOR experiment, the precise value of dephasing 180º pulse was determined. This value was slightly different for ^{13}C nuclei of CO group, that is why the efficiency of the interaction of ^{31}P with this nuclei will be less pronounced.

Let us imagine the (realistic) spin system, where the lysine residue is placed in close proximity to the DNA strand. There will be several phosphorus nuclei (shown as white stars) near ^{13}CE nucleus. The shortest distances are between ^{13}CE and ^{31}P are 3.7, 4.9 and 9.0 Å. There were up to 18 P nuclei used in the simulations. The further phosphorus nuclei were 11 Å and more away. The simulations were performed in order to show how REDOR curve shape is determined by number of the dephasing spins used in simulations (4, 6 or 18).

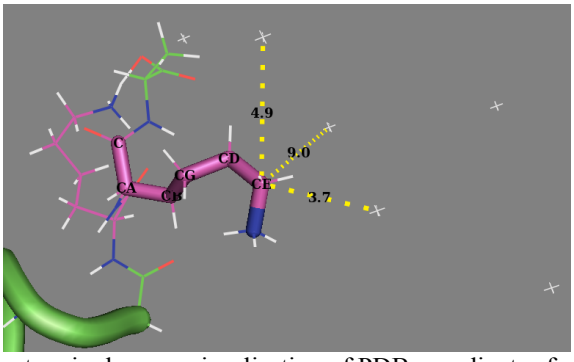

Figure XI-13. ^{13}C - ^{31}P spin system is show as visualisation of PDB coordinates for DNA and LAH4.

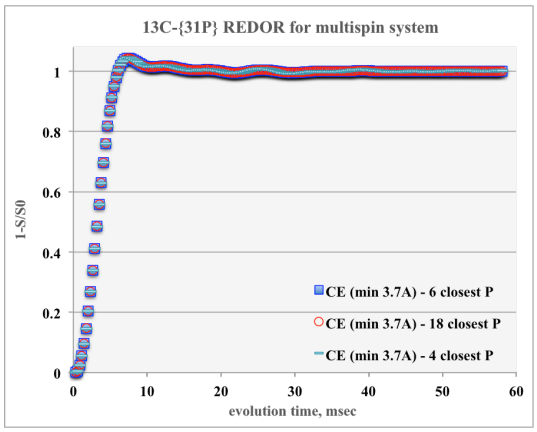

Figure XI-14. Results of ^{13}C - $\{^{31}P\}$ REDOR simulations using multispin approach. The simulations result in the same REDOR curve when 4, 6 or 18 dephasing nuclei were used.

The results show that the ^{13}C - $\{^{31}P\}$ REDOR curve is governed by the interactions with the closest neighbours, so that simulations can be performed with limited number of the closely interacting nuclei. But do we need to perform the multispin simulations, which are more time consuming, or we could use simpler one spin pair model and simulate the REDOR curve only for the interaction with closest neighbour? The test was performed in order to answer this question and the results are shown in a ***Figure XI-15***. Thus, the steepness of the dephasing curve is indeed determined by the strongest interaction, but the oscillations disappear because the interaction with each separate nucleus will result in different phases of REDOR curve oscillation, and they cancel each other. Therefore, multispin interactions result in the REDOR curve with different shape, and multispin simulations are providing us the model, which describes more realistically the experimental data.

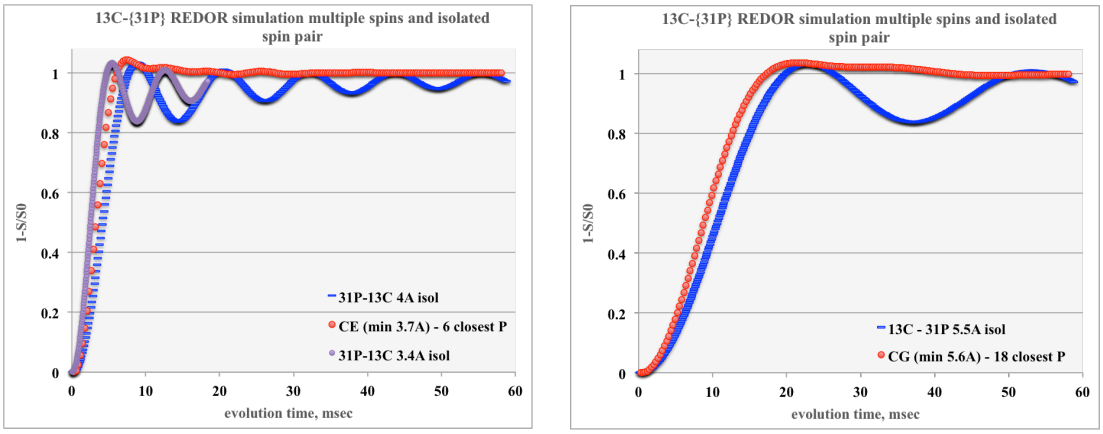

Figure XI-15. Comparison of the REDOR curves, obtained by the isolated spin pair and the multiple spins simulation methods.

In order to begin the simulation on such a complex spins system as DNA and uniformly labelled peptide, some starting point should be determined. As it is was shown already by analyzing the ^{15}N - ^{31}P REDOR data on the transfection complexes with isolated spin pair simulation method, performed previously by Dr. Vidovic and Dr. Bertani, the lysine residues indeed interact closely with phosphate groups of DNA.

The formation of the direct contact hydrogen bonds or ion pair implies that the nitrogen atom of lysine ε-NH_3 group will be found at the distance of at least 3.7 Å (Yu and Schaefer, 2008). If solvent separated bonds are formed, the this distance will be bigger. There is about 18% of the solvent separated hydrogen bonds and ion pairs found in the natural DNA - protein complexes (Luscombe et al., 2001).

In the case of direct contact of the functional groups the distance between CE atom of lysine and phosphorus atom would be approx. 4.5 - 4.7 Å, but of course it depends on the geometry of hydrogen bond and on the lysine residue conformation.

It is possible to see how the close interactions between lysine residues and the phosphate backbone of DNA are realised in the natural DNA - protein complexes by analysing the corresponding PDB entries. One should remember however that the resolution of the crystal structures of such big complexes is about 2 Å in average, so the residue conformations and the distances provided in the pdb file may deviate. Another reason for uncertainty is that hydrogen bonding does not imply rigidly determined geometry, a donor−hydrogen−acceptor angle is between 90° and 180° (Hubbard and Haider, 2010).

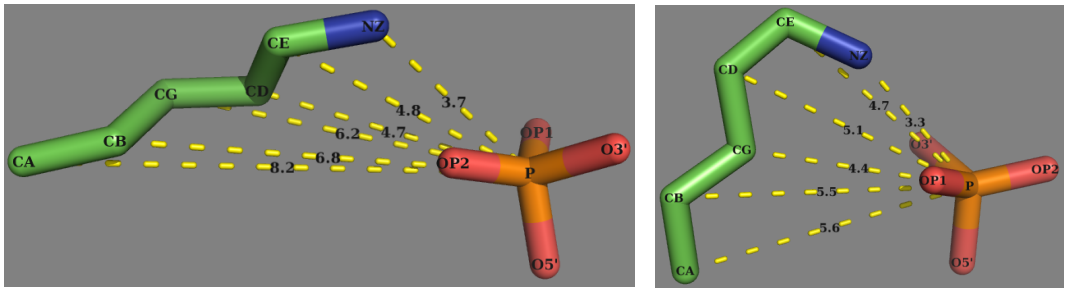

Figure XI-16. The illustration of the lysine residue (green) interacting with the phosphate group of DNA (yellow). The selection is taken from the pdb coordinates of the following DNA - protein complexes: **1PUF** (K42, ***left***) and **1CKT** (K292, ***right***).

Two possible conformations of lysine - phosphate interaction are shown in a ***Figure XI-16***. The other distances between NZ of lysine (ε-NH_3) and P of DNA / CE and P, found in pdb structures, were 3.7 Å / 4.8 Å, 3.8 Å / 4.1 Å, 3.6 Å / 4.6 Å, 3.3 Å / 4.7 Å, 4.0 Å / 4.5 Å.

Therefore, for the simulation of ^{13}C - {^{31}P} and ^{31}P - {^{13}C} experimental REDOR curve, the system was chosen, where the closest to lysine residue P atom is 4.9 Å away from the CE. The two more distant phosphates are at the of 7.9 and 9.8 Å from CE, and the others are further away. CG and CA atoms of the lysine residue were 5.6 and 8.4 Å away from the nearest phosphate.

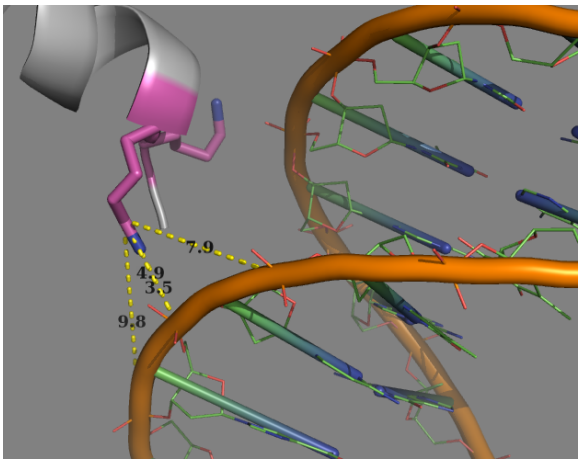

System A
One central 31P and 5*13C
Dipole P-CE (1): 4.9 A
Dipole P-CD (2): 5.9 A
Dipole P-CG (3): 6.5 A
Dipole P-CB (4): 7.8 A
Dipole P-CA (5): 8.2 A

System B
Dipole P-CE (1): 7.9 A
Dipole P-CD (2): 7.8 A
Dipole P-CG (3): 7.4 A
Dipole P-CB (4): 8.7 A
Dipole P-CA (5): 8.7 A

System C
Dipole P-CE (1): 9.8 A
Dipole P-CD (2):11.1 A
Dipole P-CG (3): 12.2 A
Dipole P-CB (4): 13 A
Dipole P-CA (5): 13.3 A

Figure XI-17. *left*) The model used for the multispin simulation of the experimental ^{13}C - ^{31}P REDOR data. The closest to the lysine residue phosphorus atom is 4.9 Å away from the CE atom. *right*) description of the multispin system, used in the P-nC multispin simulation.

Thus the ^{31}P - {^{13}C} REDOR simulations were performed on the three multispin systems, which contains one central phosphorus atom and five carbons, as described in a ***Figure XI-17.*** According to this model all phosphate groups of DNA molecule can be divided into three groups. One groups has the lysine residue in close proximity by making a direct contact (for instance, hydrogen bonding), and the distance

between CE and P atoms are 4.9 Å. Two other groups of phosphate residues don't make direct contacts with lysine residue and the P atoms are 7.9 and 9.8 Å away from CE. The fourth group represents the phosphates that don't have the lysine residue in close proximity (no lys in the sphere of 15 Å with the P atom in the center). The experimental ^{31}P - {^{13}C} curve can be theoretically decomposed onto several dephasing curves : ^{31}P (group one) - {^{13}C}, ^{31}P (group two) - {^{13}C}, and so on. What interactions govern the shape of the observed REDOR curve is not clear, but can be verified by looking for the best fit of the simulated curve to the experimental one. The results of ^{31}P - {^{13}C} REDOR experiment on the DNA - LAH4-K25 complexes prepared at pH 7.4 and pH 5.5 are shown in a ***Figure XI-18.***

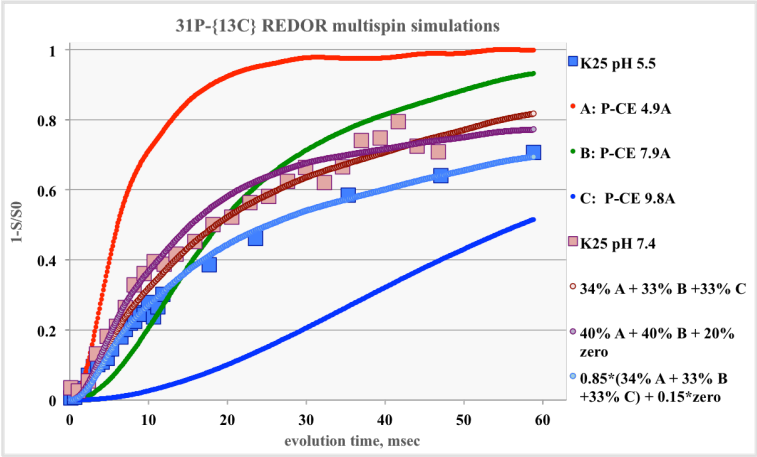

Figure XI-18. The experimental ^{31}P - {^{13}C} REDOR data an the curves simulated with P-nC multispin method, where the central nuclei (P) interacts with all five carbon nuclei of the lysine residue (CE, CD, CG, CB and CA). The distance between CE atom of lysine residue and phosphorus atom is indicated in the legend, and the complete description of the simulation system can be found in a Figure XI-17.

As we can see from the simulation results, any of the models which comprise one central atom and several carbons, does not give satisfactory results alone. But the linear combination of the dephasing curves, provided by each of the simulation system, does. Simulation system B gives the results, which in fact are the closest to the experimental curve, but the shape of this curve is quite different from one obtained experimentally. The steepness of the REDOR curve in the beginning implies that there is C - P distances smaller than 7.9 Å. Therefore, the sum of the contribution from the different phosphorus populations provides more realistic picture of the interactions in the sample. The experimental REDOR curve for DNA - LAH4-K25 complex prepared at pH 7.4 can be equally well fitted with two simulation approaches. One comprises the equal contribution from each of the systems A, B, C, *i.e.* in the DNA - peptide complex the will be the phosphate groups that have lysine residue at the distance of at least 9.8 Å. Another way of simulation comprises two populations of phosphates, one interacting directly with the lysine moiety (4.9 Å), and other which is neighbouring (7.9 Å), plus 20% contributions from the phosphates that don't have labelled lysine residue at the distance closer than 15 Å. Such situation is envisagable, provided that only one lysine is labelled at time.

The REDOR curve for DNA - LAH4-K25 complex prepared at pH 5.5 shows that the participation from the phosphate groups, which have the labelled lysine residue at longer distances, is slightly bigger. Thus the experimental curve was simulated with the model where the participation from three closest phosphates was equal 28%, and the participation from the phosphate groups that don't have any labelled lysine in the proximity was fixed to 15%.

The result of simulations is consistent with the information about the peptide - DNA stoichiometry, which is obtained by other methods (ITC, gel electrophoresis, photometric quantification), *i. e.* that DNA binds twice more LAH4-L1 (LAH4) peptides at pH 7 than it does at pH 5.

Of course, the described approach is still quite simplistic. The multispin interactions in the DNA - peptide sample that have no specific interactions, neither defined three-dimensional structure, could be way more complex. But it allows us to have a first look on how these interactions could be seen experimentally using REDOR NMR technique.

Furthermore, those results were compared with the simulations performed on the ^{13}C - $\{^{31}P\}$ experimental REDOR curve on DNA - LAH4-K25 complex prepared at pH 7.4. In order to keep it simple, the simulations were done on exactly the same model system, but it this case the model implies the interaction of one carbon nucleus with 18 phosphorus nuclei. According to this system, the closest phosphate atom is 4.9 Å from CE, 5.6 Å from CG and 8.4 Å from CA. The results of C - 18P simulations are presented in a ***Figure XI-17*** (right). The experimental curves are depicted as the circles, and the results themselves were explained in more details in the previous section. Multispin simulations with one central carbon atom (CE, CG, or CA) and 18 phosphorus are shown as the diamonds. As we can see once more, only ^{13}CE - $\{^{31}P\}$ experimental curve can be simulated with the satisfactory results. However, the REDOR curve for CE nuclei could be recorded only to rather short evolution time, about 8 msec. Also, we don't know whether all labelled lysines make direct contacts with the phosphate groups. CE experimental curve can be equally well fitted with 5.6 Å (minimum) multispin simulation system, and with 4.9 Å (minimum) system, if only 60% of the labelled lysines participate in the bond formation with the phosphates. The latter assumption is more consistent with the results of the simulation performed with ^{31}P - $\{^{13}C\}$ REDOR results, which show that there is indeed the close contact of the phosphate groups with lysine residue, and this contact corresponds to the hydrogen bond or/and ionic pairs formation.

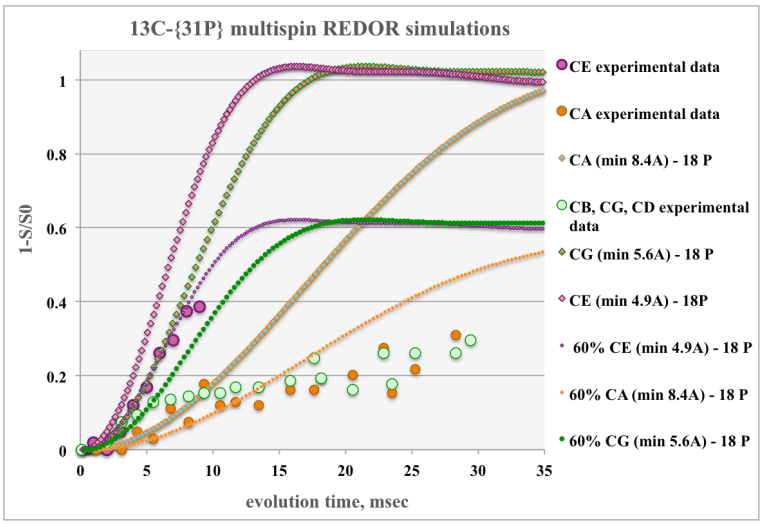

Figure XI-19. The results of the REDOR experiment on DNA - LAH4-K25 complex (pH 7.4) simulated using the multispin model system with one central carbon atom and several phosphates. The central atoms in current system were CE, CG and CA carbons of the lysine residue. The experimental ^{13}C - $\{^{31}P\}$ REDOR results are presented as the circles, and the simulations - as the diamonds and the small circles. More detailed explanation of the graph can be found in the text.

The REDOR curves obtained for the other two groups of carbon nuclei, namely CE and CB-CG-CD, which could be similarly analysed only till really short evolution times (only about 5 msec). At the longer evolution times, the background from the naturally abundant ^{13}C nuclei become more important and interfere more with the REDOR results. The steepness of ^{13}C (B, G, D) - $\{^{31}P\}$ REDOR curve at the short

evolution times (up to 5 msec) tells us that these nuclei have the phosphate group in close proximity, and the REDOR curve can be fitted with model, which has 60% of CG nuclei at 5.6 Å from the phosphorus atom of the phosphate group.

On the other hand, when having a closer look on the ^{13}C (E) - $\{^{31}P\}$ REDOR curves for each of the complex prepared at pH 7.4, it become evident that determined in previous experiments distance between ^{13}C (E) and the closest ^{31}P nuclei in the complex is not a single solution. The REDOR data for DNA - LAH4-K25 complex can be fitted with the simulation curve corresponding to 60% of the lysine residues for which the distance between CE and P is 4.9 Å, but also it can be simulated with the curve corresponding to 40% of the lysine residues for which the distance between CE and P is 4 Å. It does not mean however that the results of simulations of ^{13}C - $\{^{31}P\}$ and ^{31}P - $\{^{13}C\}$ REDOR curves are inconsistent. There are simply much many solutions to perform the fitting of the experimental curves than ones that were proposed. The results are less unambiguous for the CE carbon nuclei of the lysine residues. There is one population of those ^{13}CE carbon atoms that belong to the lysine residues, which are in a direct contact with the phosphate groups, and the interaction of ^{13}CE nuclei with the spatially closest phosphorus nuclei determines the shape of the experimental REDOR curve. Another population of the ^{13}CE nuclei belong to the lysine residues that do not interact with the phosphate groups and are spatially remote form the phosphate groups. The contribution of those lysines are observed as the lowering of REDOR curve by xx% (***Figure XI-20***). ^{31}P - $\{^{13}C\}$ REDOR curve simulation has more solutions because there exist several populations of the phosphate groups. One population does not have labelled lysines in close proximity (<15Å). Other three populations of ^{31}P correspond to the phosphate groups that (i) bind directly the lysine residues, (ii, iii) adjacent phosphate groups. The distances between CE and P atoms could vary depending on the conformation of the hydrogen bond and the lysine residue itself. However, the shortest distance determines the steepness of REDOR curve. ^{13}C - $\{^{31}P\}$ and ^{31}P - $\{^{13}C\}$ REDOR simulations show that the shortest distances between CE and P atoms are in a range of 4 - 4.9 Å, thus confirming the bond formation between the functional groups.

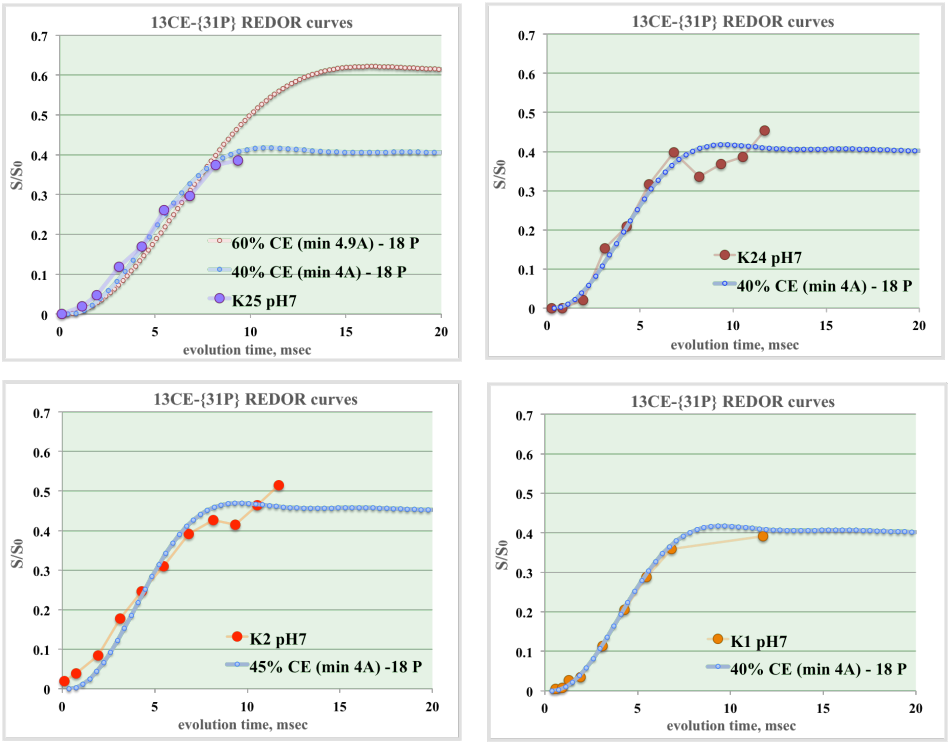

Figure XI-20. The results of the REDOR experiment on DNA - LAH4-Kx complexes (pH 7.4) simulated using the multispin model system with one central carbon atom (CE) and several phosphates.

Similarly, the simulations can be performed for ^{15}N - $\{^{31}P\}$ REDOR experiment. As it is shown in a ***Figure XI-21***, the shape of REDOR curves are very similar whether it is simulated with isolated spin pairs method, or with multispin system with one central NZ atom and three closest neighbouring phosphorus (violet and green curves respectively, ***Figure XI-21***, top).

The large error bars (***Figure XI-5***) do not allow such precise fitting of the experimental REDOR data to simulated curves, as it was done for ^{13}CE - $\{^{31}P\}$ REDOR data. Nevertheless, the steepness of the curves at the small evolution times indicates that the the distances between NZ atoms of the lysine residues and P atoms of phosphate residues are in the range of 3.4 - 3.8 Å, which underlines the close contact between this functional groups. ^{15}NZ - $\{^{31}P\}$ REDOR curve reaches the plateau at 1 - S/S_0 value of about 0.6 at pH 5 and 0.4 at pH 7.4 for DNA - LAH4-K2 and -K24 complexes. Those values for DNA - LAH4-K25 complex are lower at pH 5 (0.35), as well as at pH 7.4 (0.25). It means that there is only 35% (or 25% respectively) of the labelled lysine groups (K25) that are in a close contact with DNA strands. These values are different from that obtained in the ^{13}CE - $\{^{31}P\}$ REDOR simulation experiment. According to carbon - phosphorus REDOR data there is no substantial difference between the DNA association by 25th lysine and other lysine residues (***Figure XI-21***). This difference may be related to the experimental setup or the NMR probe condition, and should be further investigated.

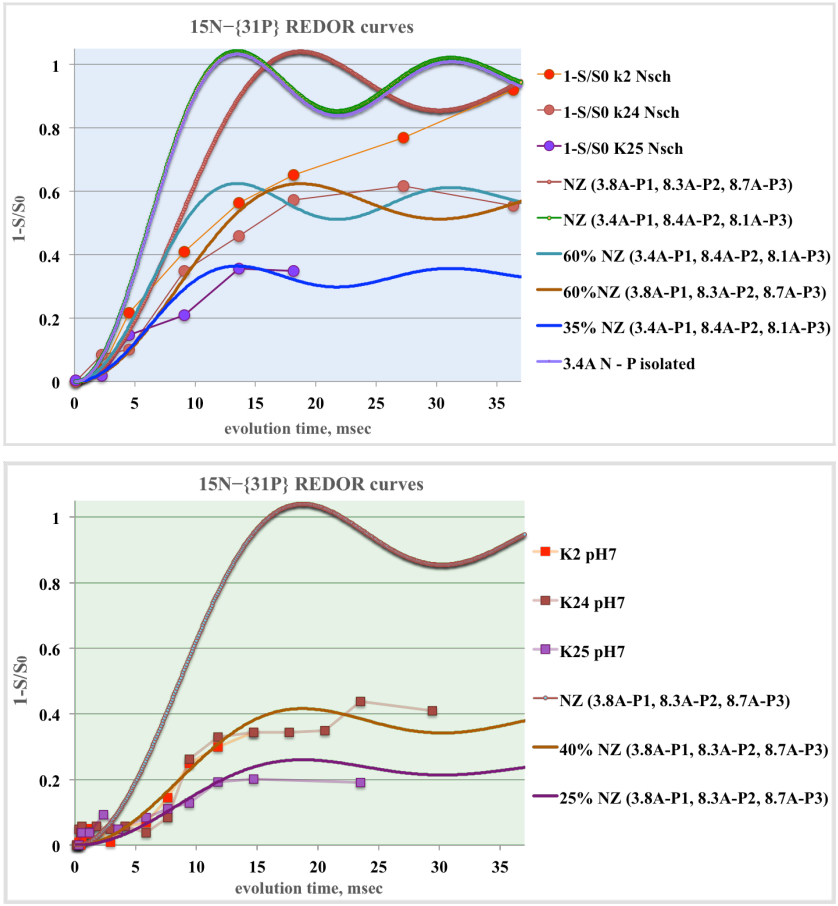

Figure XI-21. ^{15}NZ - $\{^{31}P\}$ experimental and simulated REDOR curves for DNA - LAH4-K2, 24, and 25 complexes at pH 5.5 (top) and pH 7.4 (bottom).

CONCLUSIONS

The series of ^{15}N - ^{31}P and ^{13}C - ^{31}P REDOR NMR experiment were performed on the DNA - LAH4 complexes, where the whole peptide was uniformly $^{13}C/^{15}N$ labelled, or contained the uniformly labelled lysine residue.

The results of the measurements, performed previously, indicate that in the DNA - pLAH4 ($^{13}C/^{15}N$ UL) complex, prepared at pH 5.5, only lysine residues are in the close contact with the DNA phosphates, but not histidines (Vidovic, 2011, PhD thesis). Furthermore, the REDOR experiments were performed on the DNA - peptide complex, in which one of four lysines is $^{13}C/^{15}N$ uniformly labelled. By conducting these experiments we intended to gain more insight into the structure of the transfection complex, and to determine the preferred binding sites.

The distance simulations of ^{13}C - ^{31}P REDOR dephasing curves shows that the terminal carbon atom (CE) of the lysine is found at the distances as close as 4.9 Å, which implies the formation of the direct contact hydrogen bonds / ionic pairs. However, only certain fraction (40-60%) of the labelled lysine residues was found to be in the direct contact with the phosphate groups of DNA. Multispin simulations can not provide us the accurate measure of distances between the lysine and phosphate residues and of the fraction of labelled lysine residues that participate in the bond formation with the phosphate groups. Thus the closest distance between phosphorus (P) and carbon (CE) can be in the range of 4 - 4.9 Å, and the fraction of bound lysine residues varies between 40 and 60%, as determined by simulation of the ^{13}C - ^{31}P REDOR curves.

There are few sources of the ambiguity. First of all there exist multiple conformations of the hydrogen bonding, and multiple conformations of lysine residue itself. Secondly, in the multiple spin system multiple solutions can be found to fit the experimental REDOR curve. Both these factors make the interpretation of the phosphorus REDOR curves especially difficult, as there exist several fractions of the phosphorus nuclei that interact with the ^{13}C and ^{15}N nuclei of labelled lysine residues. One fraction belongs to phosphates that interact directly with the lysine, hence the distance between P and CE atom should be in the range of 4 to 5 Å, depending on the configuration of the hydrogen bonds (ionic pairs). The other fractions belong to neighbouring phosphate groups, for which the distances between P and C (E, D, G, B, A) depend on the configuration of the lysine moiety. Also, there may be a fraction of the phosphates that do not have labelled lysines in the close proximity, as in the peptide sample there is only one lysine residue of four is labelled at time.

On the carbon nuclei side, there will be only one fraction of the lysine residues that determine the shape of ^{13}C - $\{^{31}P\}$ REDOR, those fraction consists of the labelled lysines that interact directly with the phosphate groups. However, the accurate $1 - S/S_0$ values determination is obscured by the presence of rather high content of naturally abundant ^{13}C nuclei from other amino acids and the DNA.

^{15}N nuclei natural content is much smaller, thus ^{15}N-$\{^{31}P\}$ REDOR data should provide more accurate measure of the phosphate and lysine residues proximity. However, ^{15}N nucleus has rather low sensitivity, and the $1 - S/S_0$ were obtained with substantial error bars (up to ÷10%). Also, some divergence was found between the fraction of bound lysine residues in DNA - LAH4-K25 complex, obtained by the simulating of the ^{15}N - $\{^{31}P\}$ and ^{13}C - $\{^{31}P\}$ REDOR curves, which should be further investigated. The distances between NZ and P atoms were in a range of 3.4 - 3.9 Å, as determined by the multispin simulation method.

Despite all this ambiguities, REDOR curve shape is mostly determined by the closely interacting spins, and the steepness of the curve at short evolution times is a good indicator of the close distances.

Therefore, it was possible to show that LAH4 peptide interacts with DNA by forming the direct contacts (hydrogen bonds / ion pairs) with the DNA phosphates.

Also, the multiple spin simulations approach is interesting itself, as it provide us much better insight of what the REDOR data look like when recorded in the system of multiple interacting nuclei. It allows to obtain more accurate shapes of the dephasing curves and also provide us a mean to relate the REDOR curve shape to the geometry of the spin system.

DNA - LAH4-Kx transfection complexes could be further investigated by REDOR NMR technique. In order to avoid the ambiguities in the calculation of 1 - S/S_0 values due to the low sensitivity (^{15}N) or rather high natural abundance (^{13}C), the labelling of the peptide with fluorine-19 may be considered. For example when the C-terminus of the LAH peptide is associated with DNA strand, it is supposedly bound to the minor groove of the DNA, as bigger negative electric potential is accumulated in the minor groove of the regular B-form of DNA. It is possible therefore to incorporate a fluorinated alanine residue in the α- or β-position of the 26th alanine residue (***Figure XI-22***). The 24th and 25th lysine residue will supposedly be associated with the phosphate groups of the DNA, thus C-terminal alanine residue appears to be in a close proximity to the DNA backbone functional groups as well. Therefore, by performing ^{19}F - $\{^{31}P\}$ REDOR experiment, we could learn more about the peptide - DNA binding mode. At the same time more accurate fitting to the multispin model system might be possible, and in this way we can better translate the results of the multispin system REDOR simulations to the experimental data.

Mono- or trifluorinated Fmoc-protected alanine building blocs could be obtained from Sigma Aldrich (http://www.sigmaaldrich.com/catalog/product/aldrich/615927?lang=fr&region=FR), or PolyPeptide (Strasbourg, France, http://www.polypeptide.com/assets/002/5204.pdf).

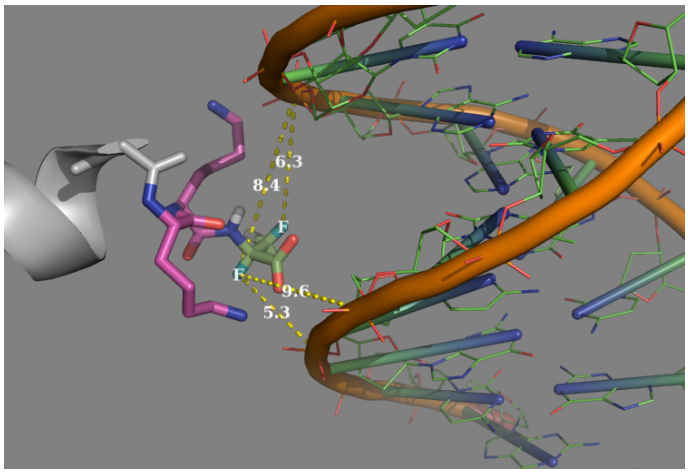

Figure XI-22. ^{19}F - ^{31}P REDOR experiment can be performed with the LAH4 peptide, which possesses mono-, di-, or trifluorinated C-terminal alanine. In case if LAH4 binds to minor groove of the DNA, the fluorine atoms will appear in the close proximity to the phosphorus atoms of DNA backbone.

XII. PRINCIPAL FINDINGS AND PERSPECTIVES

In the present work we have investigated the membrane and nucleic acids associations of the designed transfection peptide LAH4-L1. First of all it was determined using ^{15}N static solid-state NMR spectroscopy that LAH4-L1, similarly to LAH4 peptide, associates with model membranes in pH-dependent manner. In particular, it adopts predominantly transmembrane alignments in mixed POPC/POPS and zwitterionic POPC lipid bilayers at pH 7.4, but mostly in-planar orientation at acidic pH (around 5). Moreover, using various peptide concentrations we were able to show that the presence of negatively charged lipids stabilises a given orientation: transmembrane at pH 7 and in-planar pH 5.

It was shown by ^{2}H static ssNMR technique that LAH4-L1 peptide perturbes lipid acyl chains order more efficiently at pH 5 than at pH 7.4, which is related to the orientation of the peptide permeation into the bilayer. Enchanced membrane order destabilisation is also related to the increased lytic activity at pH 5.

LAH4-L1 peptide promotes a lipid domains separation in the mixed membranes by associating preferably with negatively charged species. LAH4-L1 perturbs the order of POPC lipids in zwitterionic membranes as efficiently as it disturbs POPS lipids order in mixed membranes. It means that even if peptide associates almost exclusively with negatively charged lipids in mixed bilayers, it still penetrates the zwitterionic membranes because of its extended hydrophobic surface, and is embedded there in pH-depended manner.

Secondary structure of LAH4-L1 was determined using circular dichroism spectroscopy. Thus in mixed negatively charged membranes at pH 5 peptide adopts about 80% α-helical structure, while in zwitterionic membranes it is only about 55% α-helical. The binding isotherms were constructed by plotting changes in the helical content against the total lipid-to-peptide ratio. Fitting the binding isotherms with partitioning model allowed determining the apparent peptide - membrane association constants. For POPC membrane this constant was about 20, 35 and 65 times smaller than corresponding binding constants for POPC/POPS-10%, POPC/POPS-14% and POPC/POPS-25%. The binding isotherms should be furthermore analysed with the binding model that accounts for the electrostatic attraction to the membrane surface. This approach will allow calculation of the intrinsic association constants.

In order to investigate the thermodynamics of the LAH4-L1 association with model membranes and nucleic acids we have employed isothermal titration calorimetry. Calorimetric signature of the peptide association with negatively charged membranes has quite complex character. Based on the investigation of the similar systems, available in the literature, the ITC traces at pH 5 were tentatively assigned to the sequence of process occurring upon LUV titration into the LAH4-L1 solution, namely peptide accumulation on the membrane surface and peptide partial partitioning at low lipid-to-peptide ratios, then disassociation of peptide aggregates and complete penetration into membrane at higher lipid-to-peptide ratios. It was shown also that partitioning enthalpy sign depends on the pH, which indicates that there exists a relation between the peptide - membrane binding energy and peptide alignments into lipid bilayers. Notably, none of the above-listed relations was valid for LAH-L1 association with zwitterionic POPC membranes. First of all, the calorimetric signal was rather feeble, and secondly the enthalpy sign did not show the expected correlation with pH. Therefore, the magnitude of the observed enthalpy depends on the peptide association with negatively charged lipids.

In order to obtain the complete set of the thermodynamic parameters, as ΔG, ΔH, ΔS, K and n, the appropriate binding model should be applied. Due to the complexity of the calorimetric data, it was not possible at the present step to elaborate the mathematical model of LAH4-L1 association with the

membrane. Subsequent ITC experiments may be suggested hence, such as using simpler peptide model or the series of peptides with the sequential mutations.

LAH4-L1 association with nucleic acids results also in the complex biphasic calorimetric isotherm. By applying simple model, which implies that the exothermic and endothermic processes occurs simultaneously upon peptide titration into nucleic acids and that nucleic acid double strand possesses *n* independent equivalent binding sites, it was possible to obtain the preliminary thermodynamic parameters. Interestingly, the thermodynamic characteristics of peptide - siRNA association were rather similar to those obtained with LAH4-L1 and styrenesulfonate polymer, which suggests that the same types of the interactions are involved. Those interactions supposedly involve the hydrogen bonds / ionic pairs formation, as well as the conformational changes of peptide, anionic polymer / nucleic acid, or the conformational changes of the complex as a whole.

In order to estimate the strength of LAH4-L1 association with nucleic acids (DNA and siRNA) and compare with thermodynamic characteristics of peptide - membrane interaction, it is essential to understand which molecular processes contribute to the observed enthalpy. This, in turn, will allow the development of the appropriate mathematical description of the association processes.

Knowing the binding parameters will help to obtain clearer picture of how the peptidic vector distribute between the transfection complex and the outer plasma membrane during cellular uptake, also how the redistribution between the complex and endosomal membrane occurs at the endosome maturation step, leading to the nucleic acid release. It will allow also to design more efficient peptidic vectors.

It was shown previously and in the present work by various biophysical techniques, including ITC, that about half of peptides are released from the transfection complex when pH of the solution is changed from about 7.5 to pH 5. Those peptide become therefore available for the binding with endosomal membrane. The increased lytic activity of the peptide at pH 5 assures more efficient endosome destabilisation.

LAH4-L1 - DNA and LAH4-L1 - siRNA complexes are rather big structures, with the sizes ranging from 200 nm to 1 micron. The particles are readily taken by the cells via endocytosis if their size does not exceeds 500nm, ideally it should be around 100 nm. Possessing the particles of the right size would supposedly help us to increase significantly the uptake of the genetic material. It is not possible to reduce the complexes size by merely changing the media (buffer/ionic strength). Therefore, it can be reached by the modification of one of the peptide termini, for instance by incorporating the residues that would prevent the aggregation of the transfection complexes. At the same time, the structural features responsible for the pH-dependent mode of the peptide interaction with membranes should be preserved, as soon as this mechanism assures peptide's low toxicity towards cell together with enhanced endosome disruption activity.

Finally, we have accomplished the series of the REDOR NMR experiments in order to access the distances between the lysine residues and phosphate moiety in the LAH4 - DNA complex. We have determined on the basis of previous and present studies that the peptide associates with nucleic acids by forming hydrogen bonds (ionic pairs) between lysine residues and phosphate moiety at pH 5.5 and at pH 7.4. The simulations of REDOR curves with multispin model system shows that about 40 - 60% of labelled lysine residues (K1, K2, K24 or K25) are directly bound to the phosphate group. Also the simulations show that the complex is more densely packed at pH 7.4 than at pH 5.5, which confirms the previous findings that the fraction of peptide is getting released from the complex when the pH of the media changes from neutral to acidic.

CONCLUSIONS

La série des expériences 15N - 31P et 13C - 31P REDOR RMN a été réalisée sur les complexes ADN - LAH4, où le peptide entier était uniformément marqué au 13C / 15N ou contenait le résidu de lysine uniformément marqué.

Les résultats des mesures effectuées précédemment indiquent que, dans le complexe DNA-pLAH4 ($^{13}C/^{15}N$ UM), préparé à pH 5,5, seuls les résidus de lysine sont en contact étroit avec les phosphates d'ADN, mais pas les histidines (Vidovic, 2011, Thèse de doctorat). En outre, les expériences REDOR ont été effectuées sur le complexe ADN-peptide, dans lequel l'une des quatre lysines est $^{13}C/^{15}N$ uniformément marquée. En menant ces expériences, nous avons l'intention de mieux comprendre la structure du complexe de transfection et de déterminer les sites de liaison préférés.

Les simulations à distance des courbes de déphasage ^{13}C - ^{31}P REDOR montrent que l'atome de carbone terminal (CE) de la lysine se trouve à des distances aussi proches que 4,9 Å, ce qui implique la formation des liaisons hydrogène à contact direct / paires ioniques. Cependant, seule une certaine fraction (40-60%) des résidus de lysine marqués était au contact direct avec les groupes phosphate de l'ADN. Les simulations multispines ne peuvent pas nous fournir une mesure précise des distances entre les résidus de lysine et de phosphate et de la fraction de résidus de lysine marqués qui participent à la formation de liaison avec les groupes phosphate. Ainsi, la distance la plus proche entre le phosphore (P) et le carbone (CE) peut se situer entre 4 et 4,9 Å, et la fraction des résidus de lysine liés varie entre 40 et 60%, déterminée par la simulation des courbes REDOR ^{13}C - ^{31}P.

Néanmoins, il existe quelques sources d'ambiguïté. Tout d'abord, il existe des conformations multiples de la liaison hydrogène et des conformations multiples du résidu de lysine lui-même. Deuxièmement, dans le système de spin multiple, des solutions multiples peuvent être trouvées pour s'adapter à la courbe REDOR expérimentale. Ces deux facteurs rendent particulièrement difficile l'interprétation des courbes REDOR de phosphore, car il existe plusieurs fractions de noyaux de phosphore qui interagissent avec les noyaux ^{13}C et ^{15}N des résidus de lysine marqués. Une fraction appartient à des phosphates qui interagissent directement avec la lysine, d'où la distance entre l'atome de P et CE doit être comprise entre 4 et 5 Å selon la configuration des liaisons hydrogène (paires ioniques). Les autres fractions appartiennent à des groupes phosphate voisins, pour lesquels les distances entre P et C (E, D, G, B, A) dépendent de la configuration de la fraction lysine. En outre, il peut y avoir une fraction des phosphates qui n'ont pas de lysines marquées à proximité, comme dans l'échantillon peptidique il n'y a qu'un seul résidu de lysine de quatre est étiqueté au moment.

Sur le côté des noyaux de carbone, il n'y aura qu'une seule fraction des résidus de lysine qui déterminent la forme de 13C - {31P} REDOR, cette fraction consiste en les lysines marquées qui interagissent directement avec les groupes phosphate. Cependant, la détermination précise des valeurs 1 - S / S0 est obscurcie par la présence d'un contenu assez élevé de noyaux 13C naturellement abondants provenant d'autres acides aminés et de l'ADN.

Le contenu naturel des noyaux 15N est beaucoup plus petit, donc 15N- {31P} Les données REDOR devraient fournir une mesure plus précise de la proximité des résidus de phosphate et de lysine. Cependant, le noyau 15N a une sensibilité assez faible, et le 1 - S / S0 a été obtenu avec des barres d'erreur substantielles (jusqu'à ÷ 10%). En outre, une certaine divergence a été trouvée entre la fraction de résidus de lysine liée dans le complexe ADN - LAH4-K25, obtenue en simulant les courbes REDOR 15N - {31P} et 13C - {31P}, qui devraient être étudiées plus avant. Les distances entre les atomes NZ et P se situaient dans une gamme de 3,4 à 3,9 Å, déterminée par la méthode de simulation multispine.

Malgré toutes ces ambiguïtés, la forme de la courbe REDOR est principalement déterminée par les spins étroitement interactifs, et la pente de la courbe à des temps d'évolution courts est un bon indicateur des distances proches.

Par conséquent, il a été possible de montrer que le peptide LAH4 interagit avec l'ADN en formant les contacts directs (liaisons hydrogène / paires d'ions) avec les phosphates d'ADN.

De plus, l'approche des simulations de spin multiple est intéressante elle-même, car elle nous permet de mieux comprendre ce que ressemblent les données REDOR lorsqu'elles sont enregistrées dans le système de noyaux interactifs multiples. Il permet d'obtenir des formes plus précises des courbes de déphasage et nous fournit également un moyen de relier la forme de la courbe REDOR à la géométrie du système de spins.

Les complexes de transfection ADN-LAH4-Kx pourraient être étudiés plus avant par la technique REDOR de RMN. Afin d'éviter les ambiguïtés dans le calcul des valeurs 1 - S / S0 en raison de la faible sensibilité (15N) ou de l'abondance naturelle assez élevée (13C), l'étiquetage du peptide avec le fluor-19 peut être considéré. Par exemple, lorsque l'extrémité C-terminale du peptide LAH est associée à un brin d'ADN, elle est supposée liée à la rainure mineure de l'ADN, car un potentiel électrique négatif plus important s'accumule dans la rainure mineure de la forme B normale de l'ADN. Il est donc possible d'incorporer un résidu d'alanine fluoré dans la position α ou β du 26ème résidu d'alanine (Figure XI-22). Le résidu de lysine 24e et 25e sera supposé être associé aux groupes phosphate de l'ADN, de sorte que le résidu d'alanine C-terminal semble être également proche des groupes fonctionnels du squelette ADN. Par conséquent, en effectuant une expérience REDOR de 19F - {31P}, nous pourrions en apprendre davantage sur le mode de liaison peptide - ADN. En même temps, un ajustement plus précis au système modèle multispin pourrait être possible, et de cette façon, nous pouvons mieux traduire les résultats des simulations REDOR du système multispin aux données expérimentales.

Des blocs de construction d'alanine protégés par Fmoc mono- ou trifluorés pourraient être obtenus auprès de Sigma Aldrich (http://www.sigmaaldrich.com/catalog/product/aldrich/615927?lang=fr&region=FR), soit PolyPeptide (Strasbourg, France, http://www.polypeptide.com/assets/002/5204.pdf).

XII. CONSTATATIONS PRINCIPALES ET PERSPECTIVES

Dans le présent travail, nous avons étudié les associations d'acides nucléiques et nucléiques du peptide de transfection conçu LAH4-L1. Tout d'abord, il a été déterminé en utilisant une spectroscopie RMN statique 15N à l'état solide, que LAH4-L1, de manière similaire au peptide LAH4, s'associe aux membranes modèles de manière dépendante du pH. En particulier, il adopte principalement des alignements transmembranaires dans des POPB / POPS mixtes et des bicouches lipidiques POPC zwitterioniques à pH 7,4, mais principalement à l'orientation plane au pH acide (environ 5). En outre, en utilisant diverses concentrations de peptides, nous avons pu montrer que la présence de lipides chargés négativement stabilise une orientation donnée, transmembranaire à pH 7 et planaire à pH 5.

Il a été démontré par la technique ssNMR statique 2H que le peptide LAH4-L1 perturbe les chaînes acyles lipidiques de manière plus efficace à pH 5 qu'à pH 7.4, ce qui est lié à l'orientation de la perméation peptidique dans la bicouche. La déstabilisation de l'ordre des membranes enchaîné est également liée à l'activité lytique accrue au pH 5.

Le peptide LAH4-L1 favorise une séparation des domaines lipidiques dans les membranes mixtes en associant de préférence à des espèces chargées négativement. LAH4-L1 perturbe l'ordre des lipides POPC dans les membranes zwittérioniques aussi efficacement qu'il perturbe l'ordre des lipides POPS dans les membranes mixtes. Cela signifie que même si le peptide associe presque exclusivement à des lipides chargés négativement dans des bicouches mixtes, il pénètre encore dans les membranes zwitterioniques en raison de sa surface hydrophobe étendue et est intégré dans la manière dépendante du pH.

La structure secondaire de LAH4-L1 a été déterminée en utilisant une spectroscopie de dichroïsme circulaire. Ainsi, dans des membranes mixtes chargées négativement à un peptide de pH 5 adopte environ 80% de structure hélicoïdale α, alors que dans les membranes zwittérioniques, elle est seulement d'environ 55% α-hélicoïdale. Les isothermes de liaison ont été construites en traçant des changements dans le contenu hélicoïdal par rapport au rapport lipide-peptide total. Le montage des isothermes de liaison avec un modèle de partitionnement a permis de déterminer les constantes apparentes de l'association peptide-membrane. Pour la membrane POPC, cette constante était d'environ 20, 35 et 65 fois inférieure aux constantes de liaison correspondantes pour POPC / POPS-10%, POPC / POPS-14% et POPC / POPS-25%. Les isothermes de liaison devraient en outre être analysées avec le modèle de liaison qui explique l'attraction électrostatique de la surface de la membrane. Cette approche permettra le calcul des constantes d'association intrinsèque.

Afin d'étudier la thermodynamique de l'association LAH4-L1 avec des membranes modèles et des acides nucléiques, nous avons utilisé une calorimétrie de titrage isotherme. La signature calorimétrique de l'association peptidique avec des membranes chargées négativement a un caractère assez complexe. Sur la base de l'étude des systèmes similaires, disponibles dans la littérature, les traces de l'ITC au pH 5 ont été provisoirement assignées à la séquence de processus se produisant lors du titrage LUV dans la solution LAH4-L1, à savoir l'accumulation de peptide sur la surface de la membrane et la partition partielle peptidiques à faible rapport lipide-peptide, puis dissociation des agrégats peptidiques et pénétration complète dans la membrane à des rapports lipides-peptides plus élevés. Il a également été démontré que le signe d'enthalpie de partition dépend du pH, ce qui indique qu'il existe une relation entre l'énergie de liaison peptidique-membranaire et les alliages de peptides en bicouches lipidiques. Notamment, aucune des relations énumérées ci-dessus était valable pour l'association LAH-L1 avec les membranes POPC zwitterioniques. Tout d'abord, le signal calorimétrique était plutôt faible et, d'autre part, le signe d'enthalpie n'a pas montré la corrélation attendue avec le pH. Par conséquent, la magnitude de l'enthalpie observée dépend de l'association peptidique avec des lipides chargés négativement.

Afin d'obtenir l'ensemble complet des paramètres thermodynamiques, comme ΔG, ΔH, ΔS, K et n, le modèle de liaison approprié doit être appliqué. En raison de la complexité des données calorimétriques, il

n'était pas possible à l'étape actuelle d'élaborer le modèle mathématique de l'association LAH4-L1 avec la membrane. Des expériences d'ITC subséquentes peuvent être suggérées, par exemple, en utilisant un modèle peptidique plus simple ou la série de peptides avec les mutations séquentielles.

L'association LAH4-L1 avec des acides nucléiques résulte également de l'isotherme calorimétrique biphasique complexe. En appliquant un modèle simple, ce qui implique que les processus exothermiques et endothermiques se produisent simultanément lors du titrage des peptides en acides nucléiques et que le double brin d'acide nucléique possède n sites de liaison équivalents indépendants, il était possible d'obtenir les paramètres thermodynamiques préliminaires. Fait intéressant, les caractéristiques thermodynamiques de l'association peptide-siRNA étaient plutôt similaires à celles obtenues avec le polymère LAH4-L1 et styrènesulfonate, ce qui suggère que les mêmes types d'interactions sont impliqués. Ces interactions impliquent supposément la formation de paires d'hydrogène / couples ioniques, ainsi que les changements conformationnels du peptide, du polymère anionique / acide nucléique ou des changements conformationnels du complexe dans son ensemble.

Afin d'estimer la force de l'association LAH4-L1 avec les acides nucléiques (ADN et siARN) et de comparer avec les caractéristiques thermodynamiques de l'interaction peptide-membrane, il est essentiel de comprendre les processus moléculaires qui contribuent à l'enthalpie observée. Ceci, à son tour, permettra le développement de la description mathématique appropriée des processus d'association.

La connaissance des paramètres de liaison aidera à obtenir une image plus claire de la répartition du vecteur peptidique entre le complexe de transfection et la membrane plasmatique externe lors de l'absorption cellulaire, ainsi que la redistribution entre le complexe et la membrane endosomale à l'étape de maturation de l'endosome, conduisant au nucléique Sortie acide. Il permettra également de concevoir des vecteurs peptidiques plus efficaces.

Il a été montré précédemment et dans le présent travail par diverses techniques biophysiques, y compris l'ITC, qu'environ la moitié des peptides sont libérés du complexe de transfection lorsque le pH de la solution est changé d'environ 7,5 à pH 5. Ces peptides deviennent donc disponibles pour la liaison Avec une membrane endosomale. L'activité lytique accrue du peptide au pH 5 assure une déstabilisation des endosomes plus efficace.

LAH4-L1 - DNA et LAH4-L1 - Les complexes d'siARN sont des structures assez grandes, avec des tailles allant de 200 nm à 1 micron. Les particules sont facilement prises par les cellules par endocytose si leur taille n'excède pas 500 nm, idéalement, elle devrait être d'environ 100 nm. Posséder les particules de la bonne taille nous aiderait à augmenter considérablement l'utilisation du matériel génétique. Il n'est pas possible de réduire la taille des complexes en changeant simplement le support (amortissement / force ionique). Par conséquent, il peut être atteint par la modification de l'une des extrémités peptidiques, par exemple en incorporant les résidus qui empêcheraient l'agrégation des complexes de transfection. Dans le même temps, les caractéristiques structurelles responsables du mode dépendant du pH de l'interaction peptidique avec les membranes devraient être préservées, dès que ce mécanisme garantit la faible toxicité du peptide vis-à-vis de la cellule avec une activité améliorée d'interruption des endosomes.

Enfin, nous avons accompli la série des expériences REDOR RMN afin d'accéder aux distances entre les résidus de lysine et la fraction de phosphate dans le complexe LAH4 - ADN. Nous avons déterminé sur la base d'études antérieures et présentes que le peptide associe avec des acides nucléiques en formant des liaisons hydrogène (paires ioniques) entre les résidus de lysine et la fraction phosphate à pH 5,5 et à pH 7,4. Les simulations des courbes REDOR avec système modèle multispin montrent qu'environ 40 à 60% des résidus de lysine marqués (K1, K2, K24 ou K25) sont directement liés au groupe phosphate. De plus, les simulations montrent que le complexe est plus densément emballé à pH 7,4 qu'à pH 5,5, ce qui confirme les résultats précédents que la fraction de peptide est libérée du complexe lorsque le pH du milieu passe de neutre à acide.

Bibliography

A

Abbate, V., Liang, W., Patel, J., Lan, Y., Capriotti, L., Iacobucci, V., Bui, T.T., Chaudhuri, P., Kudsiova, L., Vermeer, L.S., et al. (2013). Manipulating the pH response of 2,3-diaminopropionic acid rich peptides to mediate highly effective gene silencing with low-toxicity. J. Control. Release 1–11. 10.1016/j.jconrel.2013.09.033

Aisenbrey, C., and Bechinger, B. (2004). Tilt and rotational pitch angle of membrane-inserted polypeptides from combined 15N and 2H solid-state NMR spectroscopy. Biochemistry *43*, 10502–10512. 10.1021/bi049409h

Aisenbrey, C., Goormaghtigh, E., Ruysschaert, J.-M., and Bechinger, B. (2006). Translocation of amino acyl residues from the membrane interface to the hydrophobic core: thermodynamic model and experimental analysis using ATR-FTIR spectroscopy. Mol. Membr. Biol. *23*, 363–374. 10.1080/09687860600738742

Aisenbrey, C., Bertani, P., and Bechinger, B. (2010). Solid-state NMR investigations of membrane-associated antimicrobial peptides. Methods Mol. Biol. *618*, 209–233. 10.1007/978-1-60761-594-1_14

Alatorre-Meda, M., Taboada, P., Krajewska, B., Willemeit, M., Deml, A., Klösel, R., and Rodríguez, J.R. (2010). DNA-poly(diallyldimethylammonium chloride) complexation and transfection efficiency. J. Phys. Chem. B *114*, 9356–9366. 10.1021/jp1016856

De Almeida, R.F.M., Fedorov, A., and Prieto, M. (2003). Sphingomyelin/phosphatidylcholine/cholesterol phase diagram: boundaries and composition of lipid rafts. Biophys. J. *85*, 2406–2416. 10.1016/S0006-3495(03)74664-5

Anderson, K.M., Esadze, A., Manoharan, M., Brüschweiler, R., Gorenstein, D.G., and Iwahara, J. (2013). Direct observation of the ion-pair dynamics at a protein-DNA interface by NMR spectroscopy. J. Am. Chem. Soc. *135*, 3613–3619. 10.1021/ja312314b

Aoki, Y., Hosaka, S., Kawa, S., and Kiyosawa, K. (2001). Potential tumor-targeting peptide vector of histidylated oligolysine conjugated to a tumor-homing RGD motif. Cancer Gene Ther. *8*, 783–787. http://www.nature.com/cgt/journal/v8/n10/abs/7700362a.html

Aram J. Krauson (2011). Mechanisms of Pore Formation in Membranes. PhD dissertation. TULANE UNIVERSITY

Aravind, L. (1998). AT-hook motifs identified in a wide variety of DNA-binding proteins. Nucleic Acids Res. *26*, 4413–4421. 10.1093/nar/26.19.4413

Arouri, A., Dathe, M., and Blume, A. (2009). Peptide induced demixing in PG/PE lipid mixtures: a mechanism for the specificity of antimicrobial peptides towards bacterial membranes? Biochim. Biophys. Acta *1788*, 650–659. 10.1016/j.bbamem.2008.11.022

Van Asbeck, A.H., Beyerle, A., McNeill, H., Bovee-Geurts, P.H.M., Lindberg, S., Verdurmen, W.P.R., Hällbrink, M., Langel, U., Heidenreich, O., and Brock, R. (2013). Molecular parameters of siRNA--cell penetrating peptide nanocomplexes for efficient cellular delivery. ACS Nano *7*, 3797–3807. 10.1021/nn305754c

B

Bak, M., Rasmussen, J.T., and Nielsen, N.C. (2000). SIMPSON: a general simulation program for solid-state NMR spectroscopy. J. Magn. Reson. *147*, 296–330. 10.1006/jmre.2000.2179

Baker, B.M., and Murphy, K.P. (1996). Evaluation of linked protonation effects in protein binding reactions using isothermal titration calorimetry. Biophys. J. *71*, 2049–2055. 10.1016/S0006-3495(96)79403-1

Ball, V., and Maechling, C. (2009). Isothermal microcalorimetry to investigate non specific interactions in biophysical chemistry. Int. J. Mol. Sci. *10*, 3283–3315. 10.3390/ijms10083283

Bechinger, B. (1996). Towards membrane protein design: pH-sensitive topology of histidine-containing polypeptides. J. Mol. Biol. *263*, 768–775. 10.1006/jmbi.1996.0614

Bechinger, B. (2005). Detergent-like properties of magainin antibiotic peptides: a 31P solid-state NMR spectroscopy study. Biochim. Biophys. Acta *1712*, 101–108. 10.1016/j.bbamem.2005.03.003

Bechinger, B., and Lohner, K. (2006). Detergent-like actions of linear amphipathic cationic antimicrobial peptides. Biochim. Biophys. Acta *1758*, 1529–1539. 10.1016/j.bbamem.2006.07.001

Bechinger, B., and Salnikov, E.S. (2012). The membrane interactions of antimicrobial peptides revealed by solid-state NMR spectroscopy. Chem. Phys. Lipids *165*, 282–301. 10.1016/j.chemphyslip.2012.01.009

Bechinger, B., and Sizun, C. (2003). Alignment and structural analysis of membrane polypeptides by15N and31P solid-state NMR spectroscopy. Concepts Magn. Reson. *18A*, 130–145. 10.1002/cmr.a.10070

Bechinger, B., Zasloff, M., and Opella, S.J. (1993). Structure and orientation of the antibiotic peptide magainin in membranes by solid-state nuclear magnetic resonance spectroscopy. Protein Sci. *2*, 2077–2084. 10.1002/pro.5560021208

Bechinger, B., Ruysschaert, J.M., and Goormaghtigh, E. (1999). Membrane helix orientation from linear dichroism of infrared attenuated total reflection spectra. Biophys. J. *76*, 552–563. http://dx.doi.org/10.1016/S0006-3495(99)77223-1

Bechinger, B., Aisenbrey, C., and Bertani, P. (2004). The alignment, structure and dynamics of membrane-associated polypeptides by solid-state NMR spectroscopy. Biochim. Biophys. Acta *1666*, 190–204. 10.1016/j.bbamem.2004.08.008

Bechinger, B., Bertani, P., Werten, S., De, C.M., Mason, A.J.J., Aisenbrey, C., Perrone, B., Prudhon, M., Vidovic, V., De, I., et al. (2008). The structural and topological analysis of membrane polypeptides by oriented solid-state NMR spectroscopy : Sample preparation and theory. In Structure and Function of Membrane-Active Peptides" (Ed. M. Castanho), (Internat'l University Line), pp. 193–216.

Bechinger, B., Vidovic, V., Bertani, P., and Kichler, A. (2011). A new family of peptide-nucleic acid nanostructures with potent transfection activities. J. Pept. Sci. *17*, 88–93. 10.1002/psc.1318

Beck, A.W., Luster, T. a, Miller, A.F., Holloway, S.E., Conner, C.R., Barnett, C.C., Thorpe, P.E., Fleming, J.B., and Brekken, R. a (2006). Combination of a monoclonal anti-phosphatidylserine antibody with gemcitabine strongly inhibits the growth and metastasis of orthotopic pancreatic tumors in mice. Int. J. Cancer *118*, 2639–2643. 10.1002/ijc.21684

Bello Roufaï, M., and Midoux, P. (2001). Histidylated polylysine as DNA vector: elevation of the imidazole protonation and reduced cellular uptake without change in the polyfection efficiency of serum stabilized negative polyplexes. Bioconjug. Chem. *12*, 92–99. 10.1021/bc0000738

Bergqvist, S., Williams, M.A., O'Brien, R., and Ladbury, J.E. (2004). Heat capacity effects of water molecules and ions at a protein-DNA interface. J. Mol. Biol. *336*, 829–842. 10.1016/j.jmb.2003.12.061

Beschiaschvili, G., and Seelig, J. (1992). Peptide binding to lipid bilayers. Nonclassical hydrophobic effect and membrane-induced pK shifts. Biochemistry *31*, 10044–10053.

Beusen, D.D., McDowell, L.M., Slomczynska, U., and Schaefer, J. (1995). Solid-State Nuclear Magnetic Resonance Analysis of the Conformation of an Inhibitor Bound to Thermolysin. J. Med. Chem. *38*, 2742–2747. http://pubs.acs.org/doi/pdf/10.1021/jm00014a025

Binder, H., and Lindblom, G. (2003). Charge-dependent translocation of the Trojan peptide penetratin across lipid membranes. Biophys. J. *85*, 982–995. 10.1016/S0006-3495(03)74537-8

Bobone, S., Gerelli, Y., De Zotti, M., Bocchinfuso, G., Farrotti, A., Orioni, B., Sebastiani, F., Latter, E., Penfold, J., Senesi, R., et al. (2013). Membrane thickness and the mechanism of action of the short peptaibol trichogin GA IV. Biochim. Biophys. Acta *1828*, 1013–1024. 10.1016/j.bbamem.2012.11.033

Braun, C.S., Vetro, J.A., Tomalia, D.A., Koe, G.S., Koe, J.G., and Middaugh, C.R. (2005). Structure/function relationships of polyamidoamine/DNA dendrimers as gene delivery vehicles. J. Pharm. Sci. *94*, 423–436. 10.1002/jps.20251

Breukink, E., Ganz, P., de Kruijff, B., and Seelig, J. (2000). Binding of Nisin Z to Bilayer Vesicles As Determined with Isothermal Titration Calorimetry. Biochemistry *39*, 10247–10254. 10.1021/bi000915q

Brogden, K. a (2005). Antimicrobial peptides: pore formers or metabolic inhibitors in bacteria? Nat. Rev. Microbiol. *3*, 238–250. 10.1038/nrmicro1098

Brooks, H., Lebleu, B., and Vivès, E. (2005). Tat peptide-mediated cellular delivery: back to basics. Adv. Drug Deliv. Rev. *57*, 559–577. 10.1016/j.addr.2004.12.001

Brown, A. (2009). Analysis of cooperativity by isothermal titration calorimetry. Int. J. Mol. Sci. *10*, 3457–3477. 10.3390/ijms10083457

Burnett, L.J. (1971). Deuteron Quadrupole Coupling Constants in Three Solid Deuterated Paraffin Hydrocarbons: C2D6, C4D10, C6D14. J. Chem. Phys. *55*, 5829. http://dx.doi.org/10.1063/1.1675758

C

Cai, S., Zhu, L., Zhang, Z., and Chen, Y. (2007). Determination of the three-dimensional structure of the Mrf2-DNA complex using paramagnetic spin labeling. Biochemistry *46*, 4943–4950. 10.1021/bi061738h

Campagne, S., Saurel, O., Gervais, V., and Milon, A. (2010). Structural determinants of specific DNA-recognition by the THAP zinc finger. Nucleic Acids Res. *38*, 3466–3476. 10.1093/nar/gkq053

Campagne, S., Gervais, V., and Milon, A. (2011). Nuclear magnetic resonance analysis of protein-DNA interactions. J. R. Soc. Interface *8*, 1065–1078. 10.1098/rsif.2010.0543

Chan, J.C.C., Oyler, N.A., Yau, W.-M., and Tycko, R. (2005). Parallel beta-sheets and polar zippers in amyloid fibrils formed by residues 10-39 of the yeast prion protein Ure2p. Biochemistry *44*, 10669–10680. 10.1021/bi050724t

Chen, Q.-R. (2002). Optimal transfection with the HK polymer depends on its degree of branching and the pH of endocytic vesicles. Nucleic Acids Res. *30*, 1338–1345. http://www.ncbi.nlm.nih.gov/pmc/articles/PMC101355/

Chen, B., Jiang, Y., Zeng, S., Yan, J., Li, X., Zhang, Y., Zou, W., and Wang, X. (2010). Endocytic sorting and recycling require membrane phosphatidylserine asymmetry maintained by TAT-1/CHAT-1. PLoS Genet. *6*, e1001235. 10.1371/journal.pgen.1001235

Chen, L., Glover, J.N., Hogan, P.G., Rao, A., and Harrison, S.C. (1998). Structure of the DNA-binding domains from NFAT, Fos and Jun bound specifically to DNA. Nature *392*, 42–48. doi:10.1038/32100

Cheng, J.T.J., Hale, J.D., Elliot, M., Hancock, R.E.W., and Straus, S.K. (2009). Effect of membrane composition on antimicrobial peptides aurein 2.2 and 2.3 from Australian southern bell frogs. Biophys. J. *96*, 552–565. 10.1016/j.bpj.2008.10.012

Chou, S.-T., Hom, K., Zhang, D., Leng, Q., Tricoli, L.J., Hustedt, J.M., Lee, A., Shapiro, M.J., Seog, J., Kahn, J.D., et al. (2014). Enhanced silencing and stabilization of siRNA polyplexes by histidine-mediated hydrogen bonds. Biomaterials *35*, 846–855. 10.1016/j.biomaterials.2013.10.019

Clifton, L.A., Skoda, M.W.A., Daulton, E.L., Hughes, A. V, Le Brun, A.P., Lakey, J.H., and Holt, S.A. (2013). Asymmetric phospholipid: lipopolysaccharide bilayers; a Gram-negative bacterial outer membrane mimic. J. R. Soc. Interface *10*, 20130810. 10.1098/rsif.2013.0810

Cokol, M., Nair, R., and Rost, B. (2000). Finding nuclear localization signals. EMBO Rep. *1*, 411–415. 10.1093/embo-reports/kvd092

Copolovici, D.M., Langel, K., Eriste, E., and Langel, U. (2014). Cell-penetrating peptides: design, synthesis, and applications. ACS Nano *8*, 1972–1994. 10.1021/nn4057269

D

Dathe, M., Meyer, J., Beyermann, M., Maul, B., Hoischen, C., and Bienert, M. (2002). General aspects of peptide selectivity towards lipid bilayers and cell membranes studied by variation of the structural parameters of amphipathic helical model peptides. Biochim. Biophys. Acta *1558*, 171–186. 10.1016/S0005-2736(01)00429-1

Davis, J.H., Jeffrey, K.R., Bloom, M., Valic, M.I., and Higgs, T.P. (1976). Quadrupolar echo deuteron magnetic resonance spectroscopy in ordered hydrocarbon chains. Chem. Phys. Lett. *42*, 390–394.

Drechsler, A., and Separovic, F. (2003). Solid-state NMR structure determination. IUBMB Life *55*, 515–523. 10.1080/15216540310001622740

Drin, G., Déméné, H., Temsamani, J., and Brasseur, R. (2001). Translocation of the pAntp Peptide and Its Amphipathic Analogue AP-2AL. Biochemistry *40*, 1824–1834. 10.1021/bi002019k

Dufourc, E.J., Smith, I.C., and Dufourcq, J. (1986). Molecular details of melittin-induced lysis of phospholipid membranes as revealed by deuterium and phosphorus NMR. Biochemistry *25*, 6448–6455. 10.1021/bi00369a016

E

Eeman, M., and Deleu, M. (2010). From biological membranes to biomimetic model membranes. *14*, 719–736. http://popups.ulg.ac.be/1780-4507/index.php?id=6568

Ehtezazi, T., Rungsardthong, U., and Stolnik, S. (2003). Thermodynamic Analysis of Polycation−DNA Interaction Applying Titration Microcalorimetry. Langmuir *19*, 9387–9394. 10.1021/la0268799

Epand, R.M., and Epand, R.F. (2009). Lipid domains in bacterial membranes and the action of antimicrobial agents. Biochim. Biophys. Acta *1788*, 289–294. 10.1016/j.bbamem.2008.08.023

Epand, R.F., Maloy, W.L., Ramamoorthy, A., and Epand, R.M. (2010). Probing the "charge cluster mechanism" in amphipathic helical cationic antimicrobial peptides. Biochemistry *49*, 4076–4084. 10.1021/bi100378m

F

Falconer, R.J., and Collins, B.M. (2010). Survey of the year 2009: applications of isothermal titration calorimetry. J. Mol. Recognit. *24*, 1–16. 10.1002/jmr.1073

Fernández-Vidal, M., White, S.H., and Ladokhin, A.S. (2011). Membrane partitioning: "classical" and "nonclassical" hydrophobic effects. J. Membr. Biol. *239*, 5–14. 10.1007/s00232-010-9321-y

Fojan, P., Kr, J., and Gurevich, L. (2011). Label-free detection of Biomolecular Interaction – DNA - Antimicrobial peptide binding. 0–4, In Wireless Communication, Vehicular Technology, Information Theory and Aerospace & Electronic Systems Technology (Wireless VITAE), 2011 2nd International Conference. http://ieeexplore.ieee.org/xpl/articleDetails.jsp?arnumber=5940906

Frantz J.-F., Castano, S., Desbat, B., Odaert, B., Roux, M., Metz-Boutigue, M.-H., and Dufourc, E.J. (2008). Aggregation of cateslytin beta-sheets on negatively charged lipids promotes rigid membrane domains. A new mode of action for antimicrobial peptides? Biochemistry *47*, 6394–6402. 10.1021/bi800448h

Franzin, C.M., and Macdonald, P.M. (2001). Polylysine-induced 2H NMR-observable domains in phosphatidylserine/phosphatidylcholine lipid bilayers. Biophys. J. *81*, 3346–3362. 10.1016/S0006-3495(01)75968-1

Freire, E., Mayorga, O.L., and Straume, M. (1990). Isothermal titration calorimetry. Anal. Chem. *62*, 950A–959A. 10.1021/ac00217a002

Freire, J.M., Domingues, M.M., Matos, J., Melo, M.N., Veiga, A.S., Santos, N.C., and Castanho, M.A.R.B. (2011). Using zeta-potential measurements to quantify peptide partition to lipid membranes. Eur. Biophys. J. *40*, 481–487. 10.1007/s00249-010-0661-4

Freyer, M.W., and Lewis, E.A. (2008). Isothermal titration calorimetry: experimental design, data analysis, and probing macromolecule/ligand binding and kinetic interactions. Methods Cell Biol. *84*, 79–113. 10.1016/S0091-679X(07)84004-0

Frisken, B.J. (2001). Revisiting the Method of Cumulants for the Analysis of Dynamic Light-Scattering Data. Appl. Opt. *40*, 4087. http://dx.doi.org/10.1364/AO.40.004087

Fu, R., and Cross, T. a (1999). Solid-state nuclear magnetic resonance investigation of protein and polypeptide structure. Annu. Rev. Biophys. Biomol. Struct. *28*, 235–268. 10.1146/annurev.biophys.28.1.235

G

Galdiero, S., Falanga, A., Cantisani, M., Vitiello, M., Morelli, G., and Galdiero, M. (2013). Peptide-lipid interactions: experiments and applications. Int. J. Mol. Sci. *14*, 18758–18789. 10.3390/ijms140918758

Gallagher, K., and Sharp, K. (1998). Electrostatic contributions to heat capacity changes of DNA-Ligand Binding. *75*, 769–776. 10.1016/S0006-3495(98)77566-6

Garvie, C.W., and Wolberger, C. (2001). Recognition of Specific DNA Sequences. Mol. Cell *8*, 937–946. 10.1016/S1097-2765(01)00392-6

Gawrisch, K., Gaede, H.C., Mihailescu, M., and White, S.H. (2007). Hydration of POPC bilayers studied by 1H-PFG-MAS-NOESY and neutron diffraction. Eur. Biophys. J. *36*, 281–291. 10.1007/s00249-007-0142-6

Gehman, J.D., and Separovic, F. (2008). Solid-State NMR of Membrane-Active Proteins and Peptides. 305–311. In Advances in Biological Solid-State NMR: Proteins and Membrane-Active Peptides (Frances Separovic, Akira Naito). http://www.rsc.org/shop/books/2014/9781849739108.asp

Georgescu, J., Munhoz, V.H.O., and Bechinger, B. (2010). NMR structures of the histidine-rich peptide LAH4 in micellar environments: membrane insertion, pH-dependent mode of antimicrobial action, and DNA transfection. Biophys. J. *99*, 2507–2515. 10.1016/j.bpj.2010.05.038

Georgi Beschiaschvili, J.S. (1990). Melittin Binding to Mixed Phosphatidylglycerol/Phosphatidylcholine Membranes. Biochemistry *29*, 52–58. 10.1021/bi00453a007

Ghai, R., Falconer, R.J., and Collins, B.M. (2012). Applications of isothermal titration calorimetry in pure and applied research--survey of the literature from 2010. J. Mol. Recognit. *25*, 32–52. 10.1002/jmr.1167

Goparaju, G.N., Satishchandran, C., and Gupta, P.K. (2009). The effect of the structure of small cationic peptides on the characteristics of peptide-DNA complexes. Int. J. Pharm. *369*, 162–169. 10.1016/j.ijpharm.2008.10.028

Grage, S.L., Watts, J. a., and Watts, A. (2004). 2H-{19F} REDOR for distance measurements in biological solids using a double resonance spectrometer. J. Magn. Reson. *166*, 1–10. 10.1016/j.jmr.2003.10.005

Gruschus, J.M., Tsao, D.H., Wang, L.H., Nirenberg, M., and Ferretti, J.A. (1997). Interactions of the vnd/NK-2 homeodomain with DNA by nuclear magnetic resonance spectroscopy: basis of binding specificity. Biochemistry *36*, 5372–5380. 10.1021/bi9620060

Gullion, T., and Schaefer, J. (1989). Rotational-echo double-resonance NMR. J. Magn. Reson. *81*, 196–200. 10.1016/0022-2364(89)90280-1

Guo, X., and Huang, L. (2012). Recent advances in nonviral vectors for gene delivery. Acc. Chem. Res. *45*, 971–979. 10.1021/ar200151m.

Gupta, K., Jang, H., Harlen, K., Puri, A., Nussinov, R., Schneider, J.P., and Blumenthal, R. (2013). Mechanism of membrane permeation induced by synthetic β-hairpin peptides. Biophys. J. *105*, 2093–2103. 10.1016/j.bpj.2013.09.040

H

Hall, K., Lee, T.-H., and Aguilar, M.-I. (2011). The role of electrostatic interactions in the membrane binding of melittin. J. Mol. Recognit. *24*, 108–118. 10.1002/jmr.1032

Hatefi, a, Megeed, Z., and Ghandehari, H. (2006). Recombinant polymer-protein fusion: a promising approach towards efficient and targeted gene delivery. J. Gene Med. *8*, 468–476. 10.1002/jgm.872

Heerklotz, H. (2004). The microcalorimetry of lipid membranes. J. Phys. Condens. Matter *16*, R441–R467. 10.1088/0953-8984/16/15/R01

Henriksen, J.R., and Andresen, T.L. (2011). Thermodynamic profiling of peptide membrane interactions by isothermal titration calorimetry: a search for pores and micelles. Biophys. J. *101*, 100–109. 10.1016/j.bpj.2011.05.047

Hong, M., and Su, Y. (2011). Structure and dynamics of cationic membrane peptides and proteins: insights from solid-state NMR. Protein Sci. *20*, 641–655. 10.1002/pro.600

Hong, M., Zhang, Y., and Hu, F. (2012). Membrane protein structure and dynamics from NMR spectroscopy. Annu. Rev. Phys. Chem. *63*, 1–24. 10.1146/annurev-physchem-032511-143731

Honig, B., and Nicholls, A (1995). Classical electrostatics in biology and chemistry. Science *268*, 1144–1149. http://www.sciencemag.org/content/268/5214/1144.long

Hope, M.J., Nayar, R., Mayer, L.D., and Cullis, P.R. (1993). Reduction of liposome size and preparation of unilamellar vesicles by extrusion techniques. In Liposome Technology, G. Gregoriadis, ed. (Boca Raton, FL: CRC Press), pp. 124–139. http://www.liposomes.ca/publications/167%20Hope%20et%20al%201993.pdf

Hori, Y., Demura, M., Iwadate, M., Ulrich, A.S., Niidome, T., Aoyagi, H., and Asakura, T. (2001). Interaction of mastoparan with membranes studied by 1H-NMR spectroscopy in detergent micelles and by solid-state 2H-NMR and 15N-NMR spectroscopy in oriented lipid bilayers. Eur. J. Biochem. *268*, 302–309. 10.1046/j.1432-1033.2001.01880.x

Hoyer, J., and Neundorf, I. (2012). Peptide vectors for the nonviral delivery of nucleic acids. Acc. Chem. Res. *45*, 1048–1056. 10.1021/ar2002304

Hsu, C.-H., Chen, C., Jou, M.-L., Lee, A.Y.-L., Lin, Y.-C., Yu, Y.-P., Huang, W.-T., and Wu, S.-H. (2005). Structural and DNA-binding studies on the bovine antimicrobial peptide, indolicidin: evidence for multiple conformations involved in binding to membranes and DNA. Nucleic Acids Res. *33*, 4053–4064. 10.1093/nar/gki725

Huang, W., Seo, J., Willingham, S.B., Czyzewski, A.M., Gonzalgo, M.L., Weissman, I.L., and Barron, A.E. (2014). Learning from host-defense peptides: cationic, amphipathic peptoids with potent anticancer activity. PLoS One *9*, e90397. 10.1371/journal.pone.0090397

Huang, X., Yin, Y., Ye, D., Brekken, R., and Thorpe, P. (2013). Phosphatidylserine-targeting antibody induces M1 macrophage polarization, promotes myeloid derived suppressor cell differentiation and boosts tumor-specific immunity. J. Immunother. Cancer *1*, P154. 10.1186/2051-1426-1-S1-P154

Hubbard, Roderick E; and Kamran Haider, Muhammad (February 2010) Hydrogen Bonds in Proteins: Role and Strength. In: Encyclopedia of Life Sciences (ELS). John Wiley & Sons, Ltd: Chichester. 10.1002/9780470015902.a0003011.pub2

Huotari, J., and Helenius, A. (2011). Endosome maturation. EMBO J. *30*, 3481–3500. 10.1038/emboj.2011.286

I

Iacobucci, V., Di Giuseppe, F., Bui, T.T., Vermeer, L.S., Patel, J., Scherman, D., Kichler, A., Drake, A.F., Mason, A.J., and Giuseppe, F. Di (2012). Control of pH responsive peptide self-association during endocytosis is required for effective gene transfer. Biochim. Biophys. Acta *1818*, 1–33. 10.1016/j.bbamem.2011.12.018

J

Jamin, N., and Toma, F. (2001). NMR studies of protein–DNA interactions. Prog. Nucl. Magn. Reson. Spectrosc. *38*, 83–114. 10.1016/S0079-6565(00)00024-8

Jaroniec, C.P. (2009). Dipolar Recoupling: Heteronuclear. In eMagRes, R.K. Harris, and R.L. Wasylishen, eds. (Chichester, UK: John Wiley & Sons, Ltd). 10.1002/9780470034590

Jensen, L.B., Mortensen, K., Pavan, G.M., Kasimova, M.R., Jensen, D.K., Gadzhyeva, V., Nielsen, H.M., Foged, C., and Pamam, G. (2010). Molecular characterization of the interaction between siRNA and PAMAM G7 dendrimers by SAXS, ITC, and molecular dynamics simulations. Biomacromolecules *11*, 3571–3577. 10.1021/bm101033g

Jin, E., Zhang, B., Sun, X., Zhou, Z., Ma, X., Sun, Q., Tang, J., Shen, Y., Van Kirk, E., Murdoch, W.J., et al. (2013). Acid-active cell-penetrating peptides for in vivo tumor-targeted drug delivery. J. Am. Chem. Soc. *135*, 933–940. 10.1021/ja311180x

Judge, P.J., and Watts, A. (2011). Recent contributions from solid-state NMR to the understanding of membrane protein structure and function. Curr. Opin. Chem. Biol. *15*, 690–695. 10.1016/j.cbpa.2011.07.021

K

Kaptein, R. (2013). NMR studies on protein-nucleic acid interaction. J. Biomol. NMR *56*, 1–2. 10.1007/s10858-013-9736-8

Katsu, T. (1999). Application of calcein-loaded liposomes for the determination of membrane channel size. Biol. Pharm. Bull. *22*, 978–980. http://www.ncbi.nlm.nih.gov/pubmed/10513625

Kaur, T., Tavakoli, N., Slavcev, R., and Wettig, S. (2011). Calorimetric Investigations of Non-Viral DNA Transfection Systems. In Thermodynamics - Kinetics of Dynamic Systems, D.J.C. Moreno, ed. (InTech),. http://www.intechopen.com/books/thermodynamics-kinetics-of-dynamic-systems/

Keller, M., Tagawa, T., Preuss, M., and Miller, A.D. (2002). Biophysical characterization of the DNA binding and condensing properties of adenoviral core peptide mu. Biochemistry *41*, 652–659. 10.1021/bi0156299

Keller, S., Heerklotz, H., Jahnke, N., and Blume, A. (2006). Thermodynamics of lipid membrane solubilization by sodium dodecyl sulfate. Biophys. J. *90*, 4509–4521. 10.1529/biophysj.105.077867

Kichler, A., Pages, J.C., Leborgne, C., Druillennec, S., Lenoir, C., Coulaud, D., Delain, E., Le Cam, E., Roques, B.P., and Danos, O. (2000). Efficient DNA transfection mediated by the C-terminal domain of human immunodeficiency virus type 1 viral protein R. J. Virol. *74*, 5424–5431. http://www.pubmedcentral.nih.gov/articlerender.fcgi?artid=112026&tool=pmcentrez&rendertype=abstract

Kichler, A., Leborgne, C., März, J., Danos, O., Bechinger, B., and Ma, J. (2003a). Histidine-rich amphipathic peptide antibiotics promote efficient delivery of DNA into mammalian cells. Proc. Natl. Acad. Sci. U. S. A. *100*, 1564–1568. 10.1073/pnas.0337677100

Kichler, A., Bechinger, B., and Danos, O. (2003b). Des peptides cationiques antibactériens comme vecteurs de transfert de gènes. 1046–1047. http://dx.doi.org/10.1051/medsci/200319111046

Kichler, A., Leborgne, C., Danos, O., and Bechinger, B. (2007). Characterization of the gene transfer process mediated by histidine-rich peptides. J. Mol. Med. (Berl). *85*, 191–201. 10.1007/s00109-006-0119-4

Kim, W., Yamasaki, Y., and Kataoka, K. (2006). Development of a fitting model suitable for the isothermal titration calorimetric curve of DNA with cationic ligands. J. Phys. Chem. B *110*, 10919–10925. 10.1021/jp057554e

Kim, W., Yamasaki, Y., Jang, W.-D., and Kataoka, K. (2010). Thermodynamics of DNA condensation induced by poly(ethylene glycol)-block-polylysine through polyion complex micelle formation. Biomacromolecules *11*, 1180–1186. 10.1021/bm901305p

Kim, Y., Geiger, J.H., Hahn, S., and Sigler, P.B. (1993). Crystal structure of a yeast TBP/TATA-box complex. Nature *365*, 512–520. 10.1038/365512a0

Klocek, G., Schulthess, T., Shai, Y., and Seelig, J. (2009). Thermodynamics of melittin binding to lipid bilayers. Aggregation and pore formation. Biochemistry *48*, 2586–2596. 10.1021/bi802127h

Koppel, D.E. (1972). Analysis of Macromolecular Polydispersity in Intensity Correlation Spectroscopy: The Method of Cumulants. J. Chem. Phys. *57*, 4814. 10.1063/1.1678153

Korolev, N., Berezhnoy, N. V, Eom, K.D., Tam, J.P., and Nordenskiöld, L. (2009). A universal description for the experimental behavior of salt-(in)dependent oligocation-induced DNA condensation. Nucleic Acids Res. *37*, 7137–7150. 10.1093/nar/gkp683

Kovacs, F.A., Fowler, D.J., Gallagher, G.J., and Thompson, L.K. (2007). A practical guide for solid-state NMR distance measurements in proteins. Concepts Magn. Reson. Part A *30A*, 21–39. 10.1002/cmr.a.20071

Kucerka, N., Kiselev, M. a, and Balgavý, P. (2004). Determination of bilayer thickness and lipid surface area in unilamellar dimyristoylphosphatidylcholine vesicles from small-angle neutron scattering curves: a comparison of evaluation methods. Eur. Biophys. J. *33*, 328–334. 10.1007/s00249-003-0349-0

Kwon, B., Waring, A.J., and Hong, M. (2013). A 2H solid-state NMR study of lipid clustering by cationic antimicrobial and cell-penetrating peptides in model bacterial membranes. Biophys. J. *105*, 2333–2342. 10.1016/j.bpj.2013.08.020

L

Ladbury, J.E. (2004). Application of isothermal titration calorimetry in the biological sciences: things are heating up! Biotechniques *37*, 885–887. http://www.biotechniques.com/BiotechniquesJournal/2004/December/Application-of-Isothermal-Titration-Calorimetry-in-the-Biological-Sciences-Things-Are-Heating-Up/biotechniques-117556.html?pageNum=3

Ladokhin, a S., and White, S.H. (2001). “Detergent-like” permeabilization of anionic lipid vesicles by melittin. Biochim. Biophys. Acta *1514*, 253–260. 10.1016/S0005-2736(01)00382-0

Lam, J.K.W., Liang, W., Lan, Y., Chaudhuri, P., Chow, M.Y.T., Witt, K., Kudsiova, L., and Mason, A.J. (2012). Effective endogenous gene silencing mediated by pH responsive peptides proceeds via multiple pathways. J. Control. Release *158*, 293–303. 10.1016/j.jconrel.2011.11.024024

Lan, Y., Langlet-Bertin, B., Abbate, V., Vermeer, L.S., Kong, X., Sullivan, K.E., Leborgne, C., Scherman, D., Hider, R.C., Drake, A.F., et al. (2010). Incorporation of 2,3-diaminopropionic acid into linear cationic amphipathic peptides produces pH-sensitive vectors. Chembiochem *11*, 1266–1272. 10.1002/cbic.201000073

Langlet-Bertin, B., Leborgne, C., Scherman, D., Bechinger, B., Mason, A.J., and Kichler, A. (2010). Design and Evaluation of Histidine-Rich Amphipathic Peptides for siRNA Delivery. Pharm. Res. 1426–1436. 10.1007/s11095-010-0138-2

Leavitt, S., and Freire, E. (2001). Direct measurement of protein binding energetics by isothermal titration calorimetry. Curr. Opin. Struct. Biol. *11*, 560–566. 10.1016/S0959-440X(00)00248-7

Leidy, C., Linderoth, L., Andresen, T.L., Mouritsen, O.G., Jørgensen, K., and Peters, G.H. (2006). Domain-induced activation of human phospholipase A2 type IIA: local versus global lipid composition. Biophys. J. *90*, 3165–3175. 10.1529/biophysj.105.070987

Lejeune, D., Delsaux, N., Thomas, A., and Brasseur, R. (2005). Protein – Nucleic Acid Recognition : Statistical Analysis of Atomic Interactions and Influence of DNA Structure. Proteins: Structure, Function, and Bioinformatics, *271*, 258–271. 10.1002/prot.20607

Leventis, P.A., and Grinstein, S. (2010). The distribution and function of phosphatidylserine in cellular membranes. Annu. Rev. Biophys. *39*, 407–427. 10.1146/annurev.biophys.093008.131234

Liang, W., Mason, A.J., and Lam, J.K.W. (2013). Western Blot Evaluation of siRNA Delivery by pH Responsive Peptides. Methods Mol Biol. *986*, 73–87. 10.1007/978-1-62703-311-4_5

Lin, Q., and London, E. (2014). Preparation of artificial plasma membrane mimicking vesicles with lipid asymmetry. PLoS One *9*, e87903. 10.1371/journal.pone.0087903

Lo, S.L., and Wang, S. (2008). An endosomolytic Tat peptide produced by incorporation of histidine and cysteine residues as a nonviral vector for DNA transfection. Biomaterials *29*, 2408–2414. 10.1016/j.biomaterials.2008.01.031

Loth, K., Pelupessy, P., and Bodenhausen, G. (2005). Chemical shift anisotropy tensors of carbonyl, nitrogen, and amide proton nuclei in proteins through cross-correlated relaxation in NMR spectroscopy. J. Am. Chem. Soc. *127*, 6062–6068. 10.1021/ja042863o

Luo, P., and Baldwin, R.L. (1997). Mechanism of helix induction by trifluoroethanol: a framework for extrapolating the helix-forming properties of peptides from trifluoroethanol/water mixtures back to water. Biochemistry *36*, 8413–8421. 10.1021/bi9707133

Luscombe, N.M., Austin, S.E., Berman, H.M., and Thornton, J.M. (2000). An overview of the structures of protein-DNA complexes. Genome Biol. *1*, REVIEWS001. 10.1186/gb-2000-1-1-reviews001

Luscombe, N.M., Laskowski, R.A., and Thornton, J.M. (2001). Amino acid-base interactions: a three-dimensional analysis of protein-DNA interactions at an atomic level. Nucleic Acids Res. *29*, 2860–2874. 10.1093/nar/29.13.2860

M

Ma, P.L., Lavertu, M., Winnik, F.M., and Buschmann, M.D. (2009). New insights into chitosan-DNA interactions using isothermal titration microcalorimetry. Biomacromolecules *10*, 1490–1499. 10.1021/bm900097s

Madani, F., Lindberg, S., Langel, U., Futaki, S., and Gräslund, A. (2011). Mechanisms of cellular uptake of cell-penetrating peptides. J. Biophys. *2011*, 414729. http://dx.doi.org/10.1155/2011/414729

Mann, A., Thakur, G., Shukla, V., and Ganguli, M. (2008). Peptides in DNA delivery: current insights and future directions. Drug Discov. Today *13*, 152–160. 10.1016/j.drudis.2007.11.008

Marquette, A., Mason, A.J.J., and Bechinger, B. (2008). Aggregation and membrane permeabilizing properties of designed histidine-containing cationic linear peptide antibiotics. Journal of peptide science : an official publication of the European Peptide Society, *14*, 488–495. 10.1002/psc.966

Marquette, A., Lorber, B., and Bechinger, B. (2010). Reversible liposome association induced by LAH4: a peptide with potent antimicrobial and nucleic acid transfection activities. Biophys. J. *98*, 2544–2553. 10.1016/j.bpj.2010.02.042

Mason, a J., Leborgne, C., Moulay, G., Martinez, A., Danos, O., Bechinger, B., and Kichler, A. (2007a). Optimising histidine rich peptides for efficient DNA delivery in the presence of serum. J. Control. Release *118*, 95–104. 10.1016/j.jconrel.2006.12.004

Mason, A.J., Glaubitz, C., Danos, O., Kichler, A., Bechinger, B., and Martinez, A. (2006a). The antibiotic and DNA-transfecting peptide LAH4 selectively associates with, and disorders, anionic lipids in mixed membranes. FASEB J. *20*, 320–322. 10.1096/fj.05-4293fje

Mason, A.J., Gasnier, C., Kichler, A., Prévost, G., Aunis, D., Metz-Boutigue, M.-H., Bechinger, B., and Pre, G. (2006b). Enhanced membrane disruption and antibiotic action against pathogenic bacteria by designed histidine-rich peptides at acidic pH. Antimicrob. Agents Chemother. *50*, 3305–3311. 10.1128/AAC.00490-06

Mason, A.J., Marquette, A., and Bechinger, B. (2007b). Zwitterionic phospholipids and sterols modulate antimicrobial peptide-induced membrane destabilization. Biophys. J. *93*, 4289–4299. 10.1529/biophysj.107.116681

Mason, J., Bechinger, B., and Kichler, A. (2007c). Rational design of vector and antibiotic peptides using solid-state NMR. Mini Rev. Med. Chem. *7*, 491–497. 10.2174/138955707780619563

Matulis, D., Rouzina, I., and Bloomfield, V. a (2000). Thermodynamics of DNA binding and condensation: isothermal titration calorimetry and electrostatic mechanism. J. Mol. Biol. *296*, 1053–1063. 10.1006/jmbi.1999.3470

McDermott, A. (2009). Structure and dynamics of membrane proteins by magic angle spinning solid-state NMR. Annu. Rev. Biophys. *38*, 385–403. 10.1146/annurev.biophys.050708.133719

McGhee, J.D., and von Hippel, P.H. (1974). Theoretical aspects of DNA-protein interactions: Co-operative and non-co-operative binding of large ligands to a one-dimensional homogeneous lattice. J. Mol. Biol. *86*, 469–489. 10.1016/0022-2836(74)90031-X

Mecke, A., Lee, D.-K., Ramamoorthy, A., Orr, B.G., and Banaszak Holl, M.M. (2005). Membrane thinning due to antimicrobial peptide binding: an atomic force microscopy study of MSI-78 in lipid bilayers. Biophys. J. *89*, 4043–4050. 10.1529/biophysj.105.062596

van Meer, G., Voelker, D.R., and Feigenson, G.W. (2008). Membrane lipids: where they are and how they behave. Nat. Rev. Mol. Cell Biol. *9*, 112–124. 10.1038/nrm2330

Melinda J. Duer (2002). Solid-state NMR spectroscopy. Principles and Applications. http://eu.wiley.com/WileyCDA/WileyTitle/productCd-0632053518.html

Melo, M.N., Ferre, R., and Castanho, M. (2009). Antimicrobial peptides: linking partition, activity and high membrane-bound concentrations. Nat. Rev. Microbiol. *7*, 245–250. 10.1038/nrmicro2095

Midoux, P., and Monsigny, M. (1999). Efficient gene transfer by histidylated polylysine/pDNA complexes. Bioconjug. Chem. *10*, 406–411. 10.1021/bc9801070

Midoux, P., Pichon, C., Yaouanc, J.-J., and Jaffrès, P.-A. (2009). Chemical vectors for gene delivery: a current review on polymers, peptides and lipids containing histidine or imidazole as nucleic acids carriers. Br. J. Pharmacol. *157*, 166–178. 10.1111/j.1476-5381.2009.00288.x

Mitchell, D.J., Steinman, L., Kim, D.T., Fathman, C.G., and Rothbard, J.B. (2000). Polyarginine enters cells more efficiently than other polycationic homopolymers. J. Pept. Res. *56*, 318–325. 10.1034/j.1399-3011.2000.00723.x

Murphy, E.C., Zhurkin, V.B., Louis, J.M., Cornilescu, G., and Clore, G.M. (2001). Structural basis for SRY-dependent 46-X,Y sex reversal: modulation of DNA bending by a naturally occurring point mutation. J. Mol. Biol. *312*, 481–499. 10.1006/jmbi.2001.4977

Murray, D.T., Das, N., and Cross, T.A. (2013). Solid state NMR strategy for characterizing native membrane protein structures. Acc. Chem. Res. *46*, 2172–2181. 10.1021/ar3003442

Myers, J.K., Pace, C.N., and Scholtz, J.M. (1997). A direct comparison of helix propensity in proteins and peptides. Proc. Natl. Acad. Sci. *94*, 2833–2837. 10.1073/pnas.94.7.2833

N

Nagle, J.F., and Tristram-Nagle, S. (2000). Structure of lipid bilayers. Biochim. Biophys. Acta - Rev. Biomembr. *1469*, 159–195. http://www.ncbi.nlm.nih.gov/pmc/articles/PMC2747654/

Neeraj Sinha, M.H. (2003). X–1H rotational-echo double-resonance NMR for torsion angle determination of peptides. Chem. Phys. Lett. *380*, 742–748. 10.1016/j.cplett.2003.09.088

New, R.R.C. (1990). Liposomes : A Practical Approach (Oxford: IRL Press (Oxford University Press)).

O

Ogris, M., Steinlein, P., Carotta, S., Brunner, S., and Wagner, E. (2001). DNA/polyethylenimine transfection particles: influence of ligands, polymer size, and PEGylation on internalization and gene expression. AAPS PharmSci *3*, E21. 10.1208/ps030321

Okhrimenko, O., and Jelesarov, I. (2008). A survey of the year 2006 literature on applications of isothermal titration calorimetry. J. Mol. Recognit. *21*, 1–19. 10.1002/jmr.859

Olsen, G.L. (2003). Determination of DNA minor groove width in distamycin-DNA complexes by solid-state NMR. Nucleic Acids Res. *31*, 5084–5089. 10.1093/nar/gkg720

Olsen, G.L., Edwards, T.E., Deka, P., Varani, G., Sigurdsson, S.T., and Drobny, G.P. (2005). Monitoring tat peptide binding to TAR RNA by solid-state 31P-19F REDOR NMR. Nucleic Acids Res. *33*, 3447–3454. 10.1093/nar/gki626

Op den Kamp, J.A. (1979). Lipid asymmetry in membranes. Annu. Rev. Biochem. *48*, 47–71. 10.1146/annurev.bi.48.070179.000403

Opella, S.J. (1994). SOLIID-STATE NMR STRUCTURAL STUDIIES OF PROTEINS. Annu. Rev. Phys. Chem. *45*, 659–683. 10.1146/annurev.pc.45.100194.003303

P

Perrone, B. (2011). NEW METHODOLOGIES OF SOLID STATE NMR AND BIOPHYSICAL STUDIES OF ANTIMICROBIAL AND DESIGNED PEPTIDES IN MODEL AND NATURAL MEMBRANES. PhD dissertation (University of Strasbourg).

Persson, D., Thorén, P.E.., and Nordén, B. (2001). Penetratin-induced aggregation and subsequent dissociation of negatively charged phospholipid vesicles. FEBS Lett. *505*, 307–312. 10.1016/S0014-5793(01)02843-5

Pervushin, K., Riek, R., Wider, G., and Wüthrich, K. (1997). Attenuated T2 relaxation by mutual cancellation of dipole-dipole coupling and chemical shift anisotropy indicates an avenue to NMR structures of very large biological macromolecules in solution. Proc. Natl. Acad. Sci. U. S. A. *94*, 12366–12371. http://www.ncbi.nlm.nih.gov/pmc/articles/PMC24947/

Peters, W.B., Frasca, V., and Brown, R.K. (2009). Recent developments in isothermal titration calorimetry label free screening. Comb. Chem. High Throughput Screen. *12*, 772–790. 10.2174/138620709789104889

Polyansky, A. A., Volynsky, P. E., Arseniev, A. S., Efremov R. G. (2006). Computer Simulations of Anionic Unsaturated Lipid Bilayer—A Suitable Model to Study Membrane Interactions with A Cell-Penetrating Peptide, In Bioinformatics of Genome Regulation and Structure II. 235-246. 10.1007/0-387-29455-4_24

Polyansky, A.A., Ramaswamy, R., Volynsky, P.E., Sbalzarini, I.F., Marrink, S.J., and Efremov, R.G. (2010). Antimicrobial Peptides Induce Growth of Phosphatidylglycerol Domains in a Model Bacterial Membrane. J. Phys. Chem. Lett. *1*, 3108–3111. 10.1021/jz101163e

Poschner, B.C., Reed, J., Langosch, D., and Hofmann, M.W. (2007). An automated application for deconvolution of circular dichroism spectra of small peptides. Anal. Biochem. *363*, 306–308. 10.1016/j.ab.2007.01.021

Pott, T., and Dufourc, E.J. (1995). Action of melittin on the DPPC-cholesterol liquid-ordered phase: a solid state 2H- and 31P-NMR study. Biophys. J. *68*, 965–977. 10.1016/j.ab.2007.01.021

van Pouderoyen, G., Ketting, R.F., Perrakis, A., Plasterk, R.H., and Sixma, T.K. (1997). Crystal structure of the specific DNA-binding domain of Tc3 transposase of C.elegans in complex with transposon DNA. EMBO J. *16*, 6044–6054. 10.1093/emboj/16.19.6044

Prevette, L.E., Kodger, T.E., Reineke, T.M., and Lynch, M.L. (2007). Deciphering the role of hydrogen bonding in enhancing pDNA-polycation interactions. Langmuir *23*, 9773–9784. 10.1021/la7009995

Privalov, P.L., Dragan, A.I., and Crane-Robinson, C. (2011). Interpreting protein/DNA interactions: distinguishing specific from non-specific and electrostatic from non-electrostatic components. Nucleic Acids Res. *39*, 2483–2491. 10.1093/nar/gkq984

Prongidi-Fix, L., Sugawara, M., Bertani, P., Raya, J., Leborgne, C., Kichler, A., and Bechinger, B. (2007). Self-promoted cellular uptake of peptide/DNA transfection complexes. Biochemistry *46*, 11253–11262. 10.1021/bi700766j

Q

Québatte, G., Kitas, E., and Seelig, J. (2013). riDOM, a Cell-Penetrating Peptide. Interaction with DNA and Heparan Sulfate. J. Phys. Chem. B *117*, 10807–10817. 10.1021/jp404979y

R

Raghuraman, H., and Chattopadhyay, A. (2007). Melittin: a membrane-active peptide with diverse functions. Biosci. Rep. *27*, 189–223. 10.1007/s10540-006-9030-z

Rance, M., and Byrd, R.A. (1983). Obtaining high-fidelity powder spectra in anisotropic media: Phase-cycled Hahn echo spectroscopy. J. Magn. Reson. *52*, 221–240. 10.1016/0022-2364(83)90190-7

Recktenwald, D.J., and McConnell, H.M. (1981). Phase equilibria in binary mixtures of phosphatidylcholine and cholesterol. Biochemistry *20*, 4505–4510. http://www.ncbi.nlm.nih.gov/pubmed/6269591

Reddy, C.K., Das, a, and Jayaram, B. (2001). Do water molecules mediate protein-DNA recognition? J. Mol. Biol. *314*, 619–632. 10.1006/jmbi.2001.5154

Reed, J., and Reed, T. a (1997). A set of constructed type spectra for the practical estimation of peptide secondary structure from circular dichroism. Anal. Biochem. *254*, 36–40. 10.1006/abio.1997.2355

Rejman, J., Oberle, V., Zuhorn, I.S., and Hoekstra, D. (2004). Size-dependent internalization of particles via the pathways of clathrin- and caveolae-mediated endocytosis. Biochem. J. *377*, 159–169. 10.1042/BJ20031253

Ren, J., Jenkins, T.C., and Chaires, J.B. (2000). Energetics of DNA Intercalation Reactions. Biochemistry *39*, 8439–8447. 10.1021/bi000474a

Reshetnyak, Y.K., Andreev, O.A., Segala, M., Markin, V.S., and Engelman, D.M. (2008). Energetics of peptide (pHLIP) binding to and folding across a lipid bilayer membrane. Proc. Natl. Acad. Sci. U. S. A. *105*, 15340–15345. 10.1073/pnas.0804746105

Reuter, M., Schwieger, C., Meister, A., Karlsson, G., and Blume, A. (2009). Poly-l-lysines and poly-l-arginines induce leakage of negatively charged phospholipid vesicles and translocate through the lipid bilayer upon electrostatic binding to the membrane. Biophys. Chem. *144*, 27–37. 10.1016/j.bpc.2009.06.002

Rice Phoebe (1996). Crystal Structure of an IHF-DNA Complex: A Protein-Induced DNA U-Turn. Cell *87*, 1295–1306. 10.1016/S0092-8674(00)81824-3

Rittner, K., Benavente, A., Bompard-Sorlet, A., Heitz, F., Divita, G., Brasseur, R., and Jacobs, E. (2002). New basic membrane-destabilizing peptides for plasmid-based gene delivery in vitro and in vivo. Mol. Ther. *5*, 104–114. 10.1006/mthe.2002.0523

Rohs, R., West, S.M., Sosinsky, A., Liu, P., Mann, R.S., and Honig, B. (2009). The role of DNA shape in protein-DNA recognition. Nature *461*, 1248–1253. 10.1038/nature08473

Rouser, G., Fleischer, S., and Yamamoto, A. (1970). Two dimensional thin layer chromatographic separation of polar lipids and determination of phospholipids by phosphorus analysis of spots. Lipids *5*, 494–496. 10.1007/BF02531316

Roux, M., Neumann, J.-M., Bloom, M., and Devaux, P.F. (1988). 2H and 31P NMR study of pentalysine interaction with headgroup deuterated phosphatidylcholine and phosphatidylserine. Eur. Biophys. J. *16*. 10.1007/BF00254062

S

Saitô, H., Ando, I., and Ramamoorthy, A. (2010). Chemical shift tensor - the heart of NMR: Insights into biological aspects of proteins. Prog. Nucl. Magn. Reson. Spectrosc. *57*, 181–228. 10.1016/j.pnmrs.2010.04.005

Salnikov, E.S., and Bechinger, B. (2011). Lipid-Controlled Peptide Topology and Interactions in Bilayers: Structural Insights into the Synergistic Enhancement of the Antimicrobial Activities of PGLa and Magainin 2. Biophys. J. *100*, 1473–1480. 10.1016/j.bpj.2011.01.070

Salnikov, E., Aisenbrey, C., Vidovic, V., and Bechinger, B. (2010). Solid-state NMR approaches to measure topological equilibria and dynamics of membrane polypeptides. Biochim. Biophys. Acta *1798*, 258–265. 10.1016/j.bbamem.2009.06.021

Salnikov, E.S., Mason, a J., and Bechinger, B. (2009). Membrane order perturbation in the presence of antimicrobial peptides by (2)H solid-state NMR spectroscopy. Biochimie *91*, 734–743. 10.1016/j.biochi.2009.01.002

Samoson, a, and Lippmaa, E. (1988). 2D NMR nutation spectroscopy in solids. J. Magn. Reson. *79*, 255–268. 10.1016/0022-2364(88)90218-1

Samsonova, O., Glinca, S., Biela, A., Pfeiffer, C., Dayyoub, E., Sahin, D., Klebe, G., and Kissel, T. (2013). The use of isothermal titration calorimetry and molecular dynamics to show variability in DNA transfection performance. Acta Biomater. *9*, 4994–5002. 10.1016/j.actbio.2012.10.006

Schaefer, J. (1999). REDOR-determined distances from heterospins to clusters of 13C labels. J. Magn. Reson. *137*, 272–275. 10.1006/jmre.1998.1643

Schiffer, M., and Edmundson, B. (1967). Use of helical wheels to represent the structures of proteins and to identify segments with helical potential. Biophys. J. *7*, 121–135. 10.1016/S0006-3495(67)86579-2

Schutters, K., and Reutelingsperger, C. (2010). Phosphatidylserine targeting for diagnosis and treatment of human diseases. Apoptosis *15*, 1072–1082. 10.1007/s10495-010-0503-y

Seelig, J. (1977). Deuterium magnetic resonance: theory and application to lipid membranes. Q. Rev. Biophys. *10*, 353–418. http://dx.doi.org/10.1017/S0033583500002948

Seelig, J. (1997). Titration calorimetry of lipid-peptide interactions. Biochim. Biophys. Acta *1331*, 103–116. 10.1016/S0304-4157(97)00002-6

Seelig, J. (2004). Thermodynamics of lipid-peptide interactions. Biochim. Biophys. Acta *1666*, 40–50. 10.1016/j.bbamem.2004.08.004

Seelig, A, and Seelig, J. (1974). The dynamic structure of fatty acyl chains in a phospholipid bilayer measured by deuterium magnetic resonance. Biochemistry *13*, 4839–4845. 10.1021/bi00720a024

Seelig, J., and Seelig, A. (1980). Lipid conformation in model membranes and biological membranes. Q. Rev. Biophys. *13*, 19–61. http://dx.doi.org/10.1017/S0033583500000305

Seelig, J., Nebel, S., Ganz, P., and Bruns, C. (1993). Electrostatic and nonpolar peptide-membrane interactions. Lipid binding and functional properties of somatostatin analogues of charge z = +1 to z = +3. Biochemistry *32*, 9714–9721. 10.1021/bi00088a025

Seeman, N.C., Rosenberg, J.M., and Rich, A. (1976). Sequence-specific recognition of double helical nucleic acids by proteins. Proc. Natl. Acad. Sci. *73*, 804–808. 10.1073/pnas.73.3.804

Shao, C., Novakovic, V.A., Head, J.F., Seaton, B.A., and Gilbert, G.E. (2008). Crystal structure of lactadherin C2 domain at 1.7A resolution with mutational and computational analyses of its membrane-binding motif. J. Biol. Chem. *283*, 7230–7241. 10.1074/jbc.M705195200

Sharp, K. a, Nicholls, a, Friedman, R., and Honig, B. (1991). Extracting hydrophobic free energies from experimental data: relationship to protein folding and theoretical models. Biochemistry *30*, 9686–9697. 10.1021/bi00104a017

Shimanouchi, T., Ishii, H., Yoshimoto, N., Umakoshi, H., and Kuboi, R. (2009). Calcein permeation across phosphatidylcholine bilayer membrane: effects of membrane fluidity, liposome size, and immobilization. Colloids Surf. B. Biointerfaces *73*, 156–160. 10.1016/j.colsurfb.2009.05.014

Soubias, O., and Gawrisch, K. (2007). Nuclear magnetic resonance investigation of oriented lipid membranes. Methods Mol. Biol. *400*, 77–88. 10.1007/978-1-59745-519-0_6

Sreerama, N., and Woody, R.W. (2000). Estimation of protein secondary structure from circular dichroism spectra: comparison of CONTIN, SELCON, and CDSSTR methods with an expanded reference set. Anal. Biochem. *287*, 252–260. 10.1006/abio.2000.4880

Stefl, R., Wu, H., Ravindranathan, S., Sklenár, V., and Feigon, J. (2004). DNA A-tract bending in three dimensions: solving the dA4T4 vs. dT4A4 conundrum. Proc. Natl. Acad. Sci. U. S. A. *101*, 1177–1182. 10.1073/pnas.0308143100

Su, Y., Li, S., and Hong, M. (2013). Cationic membrane peptides: atomic-level insight of structure-activity relationships from solid-state NMR. Amino Acids *44*, 821–833. 10.1007/s00726-012-1421-9

Svensson, F.R., Lincoln, P., Nordén, B., and Esbjörner, E.K. (2011). Tryptophan orientations in membrane-bound gramicidin and melittin-a comparative linear dichroism study on transmembrane and surface-bound peptides. Biochim. Biophys. Acta *1808*, 219–228. 10.1016/j.bbamem.2010.10.004

T

Terzi, E., Hölzemann, G., and Seelig, J. (1995). Self-association of beta-amyloid peptide (1-40) in solution and binding to lipid membranes. J. Mol. Biol. *252*, 633–642. 10.1006/jmbi.1995.0525

Thapa, N., Kim, S., So, I.-S., Lee, B.-H., Kwon, I.-C., Choi, K., and Kim, I.-S. Discovery of a phosphatidylserine-recognizing peptide and its utility in molecular imaging of tumour apoptosis. J. Cell. Mol. Med. *12*, 1649–1660. 10.1111/j.1582-4934.2008.00305.x

Thomas, J.C. (1987). The determination of log normal particle size distributions by dynamic light scattering. J. Colloid Interface Sci. *117*, 187–192. 10.1016/0021-9797(87)90182-2

Todokoro, Y., Yumen, I., Fukushima, K., Kang, S.-W., Park, J.-S., Kohno, T., Wakamatsu, K., Akutsu, H., and Fujiwara, T. (2006). Structure of tightly membrane-bound mastoparan-X, a G-protein-activating peptide, determined by solid-state NMR. Biophys. J. *91*, 1368–1379. 10.1529/biophysj.106.082735

Toke, O., and Cegelski, L. (2010) REDOR Applications in Biology : An Overview. Chapter 28, in eMagRes. 59–67. 10.1002/9780470034590.emrstm1152

U

Utsugi, T., Schroit, A.J., Connor, J., Bucana, C.D., and Fidler, I.J. (1991). Elevated Expression of Phosphatidylserine in the Outer Membrane Leaflet of Human Tumor Cells and Recognition by Activated Human Blood Monocytes. Cancer Res. *51*, 3062–3066. http://cancerres.aacrjournals.org/content/51/11/3062

Utsuno, K., and Uludağ, H. (2010). Thermodynamics of polyethylenimine-DNA binding and DNA condensation. Biophys. J. *99*, 201–207. 10.1016/j.bpj.2010.04.016

V

Vance, J.E. (2008). Phosphatidylserine and phosphatidylethanolamine in mammalian cells: two metabolically related aminophospholipids. J. Lipid Res. *49*, 1377–1387. 10.1194/jlr.R700020-JLR200

Vega, S. (2005). Nuclear Distance Measurements in Solid State NMR Spectroscopy. ChemInform *36*, 3–11. 10.1002/chin.200511300

Velázquez-Campoy, A. (2006). Ligand binding to one-dimensional lattice-like macromolecules: analysis of the McGhee-von Hippel theory implemented in isothermal titration calorimetry. Anal. Biochem. *348*, 94–104. 10.1016/j.ab.2005.10.013

Vermeer, L.S., de Groot, B.L., Réat, V., Milon, A., and Czaplicki, J. (2007). Acyl chain order parameter profiles in phospholipid bilayers: computation from molecular dynamics simulations and comparison with 2H NMR experiments. Eur. Biophys. J. *36*, 919–931. 10.1007/s00249-007-0192-9

Vidovic, V. (2011). Thèse Production du peptide P-LAH 4 chez E . coli et études par RMN de ses propriétés antibactérienne et de transfection d ' ADN.

Vogt, T.C.B., and Bechinger, B. (1999). The interactions of histidine-containing amphipathic helical peptide antibiotics with lipid bilayers. The effects of charges and pH. J. Biol. Chem. *274*, 29115–29121. 10.1074/jbc.274.41.29115

W

Wadhwani, P., Epand, R.M.F., Heidenreich, N., Bürck, J., and Ulrich, A.S. (2012). Membrane-active peptides and the clustering of anionic lipids. Biophys. J. *103*, 265–274. 10.1016/j.bpj.2012.06.004

Wann, M.-H., and Harbison, G.S. (1994). Axial asymmetry in the nuclear magnetic resonance spectra of deuterated methyl groups: An alternative explanation. J. Chem. Phys. *101*, 231. 10.1063/1.468174

Watkins, S., van Pouderoyen, G., and Sixma, T.K. (2004). Structural analysis of the bipartite DNA-binding domain of Tc3 transposase bound to transposon DNA. Nucleic Acids Res. *32*, 4306–4312. 10.1093/nar/gkh770

Waugh, J.S. (1976). Uncoupling of local field spectra in nuclear magnetic resonance: determination of atomic positions in solids. Proc. Natl. Acad. Sci. *73*, 1394–1397. http://www.ncbi.nlm.nih.gov/pmc/articles/PMC430300/

Webb, G.A., Grage, S.L., and Watts, A. (2006). Applications of REDOR for Distance Measurements in Biological Solids. Annu. Reports NMR Spectrosc. *60*, 191–228. 10.1016/S0066-4103(06)60005-7

Weingarth, M., and Baldus, M. (2013). Solid-state NMR-based approaches for supramolecular structure elucidation. Acc. Chem. Res. *46*, 2037–2046. 10.1021/ar300316e

Wenk, M.R., and Seelig, J. (1998). Magainin 2 amide interaction with lipid membranes: calorimetric detection of peptide binding and pore formation. Biochemistry *37*, 3909–3916. 10.1021/bi972615n

Wettig, S. (2012). Thermodynamic Studies of DNA-Cationic Components Interactions Using Titration Calorimetry. J. Thermodyn. Catal. *04*, 1–6. 10.4172/2157-7544.1000121

White, S.H. (1998). Protein Folding in Membranes : Determining Energetics of Peptide – Bilayer Interactions. In Biochemistry, Chapter 4, pp. 62–87. http://www.tulane.edu/~biochem/faculty/facfigs/M_Enzym_PepBiEnerg.pdf

Wieprecht, T., Beyermann, M., and Seelig, J. (1999a). Binding of antibacterial magainin peptides to electrically neutral membranes: thermodynamics and structure. Biochemistry *38*, 10377–10387. 10.1021/bi990913+

Wieprecht, T., Apostolov, O., Beyermann, M., and Seelig, J. (1999b). Thermodynamics of the alpha-helix-coil transition of amphipathic peptides in a membrane environment: implications for the peptide-membrane binding equilibrium. J. Mol. Biol. *294*, 785–794. 10.1006/jmbi.1999.3268

Wieprecht, T., Apostolov, O., Beyermann, M., and Seelig, J. (2000a). Membrane binding and pore formation of the antibacterial peptide PGLa: thermodynamic and mechanistic aspects. Biochemistry *39*, 442–452. 10.1021/bi992146k

Wieprecht, T., Apostolov, O., and Seelig, J. (2000b). Binding of the antibacterial peptide magainin 2 amide to small and large unilamellar vesicles. Biophys. Chem. *85*, 187–198. 10.1016/S0301-4622(00)00120-4

Wieprecht, T., Beyermann, M., and Seelig, J. (2002). Thermodynamics of the coil-alpha-helix transition of amphipathic peptides in a membrane environment: the role of vesicle curvature. Biophys. Chem. *96*, 191–201. 10.1016/S0301-4622(02)00025-X

Williamson, P., and Schlegel, R.A. (2002). Transbilayer phospholipid movement and the clearance of apoptotic cells. Biochim. Biophys. Acta *1585*, 53–63. 10.1016/S1388-1981(02)00324-4

Wiseman, T., Williston, S., Brandts, J.F., and Lin, L.-N. (1989). Rapid measurement of binding constants and heats of binding using a new titration calorimeter. Anal. Biochem. *179*, 131–137. 10.1016/0003-2697(89)90213-3

Wu, G.Y., and Wu, C.H. (1987). Receptor-mediated in vitro gene transformation by a soluble DNA carrier system. J. Biol. Chem. *262*, 4429–4432. http://www.jbc.org/content/262/10/4429.full.pdf+html

Wu, Y., Tibrewal, N., and Birge, R.B. (2006). Phosphatidylserine recognition by phagocytes: a view to a kill. Trends Cell Biol. *16*, 189–197. 10.1016/j.tcb.2006.02.003

Wyman, T.B., Nicol, F., Zelphati, O., Scaria, P. V, Plank, C., and Szoka, F.C. (1997). Design, synthesis, and characterization of a cationic peptide that binds to nucleic acids and permeabilizes bilayers. Biochemistry *36*, 3008–3017. 10.1021/bi9618474

Y

Yamasaki, K., Kigawa, T., Inoue, M., Tateno, M., Yamasaki, T., Yabuki, T., Aoki, M., Seki, E., Matsuda, T., Tomo, Y., et al. (2004). Solution structure of the B3 DNA binding domain of the Arabidopsis cold-responsive transcription factor RAV1. Plant Cell *16*, 3448–3459. 10.1105/tpc.104.026112

Yan, J., Wang, K., Dang, W., Chen, R., Xie, J., Zhang, B., Song, J., and Wang, R. (2013). Two hits are better than one: membrane-active and DNA binding-related double-action mechanism of NK-18, a novel antimicrobial peptide derived from mammalian NK-lysin. Antimicrob. Agents Chemother. *57*, 220–228. 10.1128/AAC.01619-12

Yandek, L.E., Pokorny, A., Florén, A., Knoelke, K., Langel, U., and Almeida, P.F.F. (2007). Mechanism of the cell-penetrating peptide transportan 10 permeation of lipid bilayers. Biophys. J. *92*, 2434–2444. 10.1529/biophysj.106.100198

Yandek, L.E., Pokorny, A., and Almeida, P.F.F. (2009). Wasp mastoparans follow the same mechanism as the cell-penetrating peptide transportan 10. Biochemistry *48*, 7342–7351. 10.1021/bi9008243

Yang, L., Harroun, T.A., Weiss, T.M., Ding, L., and Huang, H.W. (2001). Barrel-stave model or toroidal model? A case study on melittin pores. Biophys. J. *81*, 1475–1485. 10.1016/S0006-3495(01)75802-X

Yeung, T., Heit, B., Dubuisson, J.-F., Fairn, G.D., Chiu, B., Inman, R., Kapus, A., Swanson, M., and Grinstein, S. (2009). Contribution of phosphatidylserine to membrane surface charge and protein targeting during phagosome maturation. J. Cell Biol. *185*, 917–928. 10.1083/jcb.200903020

Yu, T.-Y., and Schaefer, J. (2008). REDOR NMR characterization of DNA packaging in bacteriophage T4. J. Mol. Biol. *382*, 1031–1042. 10.1016/j.jmb.2008.07.077

Z

Zauner, W., Ogris, M., and Wagner, E. (1998). Polylysine-based transfection systems utilizing receptor-mediated delivery. Adv. Drug Deliv. Rev. *30*, 97–113. 10.1016/S0169-409X(97)00110-5

Zhao, X. (2012). Protein structure determination by solid-state NMR. Top. Curr. Chem. *326*, 187–213. 10.1007/128_2011_287

Ziegler, A., and Seelig, J. (2007). High affinity of the cell-penetrating peptide HIV-1 Tat-PTD for DNA. Biochemistry *46*, 8138–8145. 10.1021/bi700416h

Ziegler, A., Blatter, X.L., Seelig, A., and Seelig, J. (2003). Protein transduction domains of HIV-1 and SIV TAT interact with charged lipid vesicles. Binding mechanism and thermodynamic analysis. Biochemistry *42*, 9185–9194. 10.1021/bi0346805

Zwaal, R.F. a, Comfurius, P., and Bevers, E.M. (2005). Surface exposure of phosphatidylserine in pathological cells. Cell. Mol. Life Sci. *62*, 971–988. 10.1007/s00018-005-4527-3

(2000). Structure of the Plasma Membrane. http://www.ncbi.nlm.nih.gov/books/NBK9898/

(2004). Zetasizer Nano Series User Manual.

Appendix.

Appendix 1.

Dynamic light scattering.

The introduction to the DLS method is adapted from 'A Basic Guide to Particle Characterization', Malvern Instruments http://golik.co.il/Data/ABasicGuidtoParticleCharacterization(2)_1962085150.pdf.

Dynamic light scattering (DLS), sometimes referred to as Photon Correlation Spectroscopy (PCS) or Quasi-Elastic Light Scattering (QELS), is a non-invasive, well-established technique for measuring the size of particles and macromolecules typically in the submicron region down to below 1 nanometre. It can be used to measure samples which consist of particles suspended in a liquid e.g. proteins, polymers, micelles, carbohydrates, nanoparticles, colloidal dispersions, and emulsions

Key advantages include:

• particle size range ideal for nano and biomaterials

• small quantity of sample required

• fast analysis and high throughput

• non-invasive allowing complete sample recovery.

Principles. Particles in suspension undergo Brownian motion caused by thermally induced collisions between the suspended particles and solvent molecules. If the particles are illuminated with a laser, the intensity of the scattered light fluctuates over very short timescales at a rate that is dependent upon the size of the particles; smaller particles are displaced further by the solvent molecules and move more rapidly. Analysis of these intensity fluctuations yields the velocity of the Brownian motion and hence the particle size using the Stokes-Einstein relationship.

The diameter measured in Dynamic Light Scattering is called the hydrodynamic diameter and refers to the way a particle diffuses within a fluid. The diameter obtained by this technique is that of a sphere that has the same translational diffusion coefficient as the particle being measured. The translational diffusion coefficient will depend not only on the size of the particle 'core', but also on any surface structure, as well as the concentration and type of ions in the medium. This means that the size will be larger than measured by electron microscopy, for example, where the particle is removed from its native environment. It is important to note that dynamic light scattering produces an intensity weighted particle size distribution, which means that the presence of oversized particles can dominate the particle size result.

What is Z-average and how it is calculated.

The following information is adapted from the Horiba Scientific educational resource (http://www.horiba.com/fr/scientific/products/particle-characterization/education/sz-100/particle-size-by-dynamic-light-scattering-resources/what-is-z-average/).

Dynamic light scattering (DLS) results are often expressed in terms of the Z-average. The Z-average arises when DLS data is analyzed by the use of the technique of cumulants (Koppel, 1972). Since the calculation of the Z-average is mathematically stable, the Z-average result is insensitive to noise, and that makes it a preferred DLS size parameter. The Z-average can be expressed as the intensity based harmonic mean (Thomas, 1987):

$$D_z = \frac{\sum S_i}{\sum {S_i}/{D_i}}$$

Here, S_i is the scattered intensity from particle *i* and D_i is the diameter of particle *i*. Note that the result is in the form of a harmonic mean. Since this mean is calculated from the intensity weighted distribution, leading to the statement that the Z-average size is the intensity weighted harmonic mean size. In the case of sufficiently small particles known as Rayleigh scatterers, $S_i \sim D_i^6$. Therefore, the Z-average can be approximated as:

$$D_z \approx \frac{\sum D_i^6}{\sum D_i^5}$$

How is the Z-average calculated from raw DLS data?

The Z-average size value is calculated by the methods of cumulants. Since this technique relies on numerically stable least squares fitting, it is relatively insensitive to experimental noise. In cumulants analysis the baseline subtracted autocorrelation function, C, is treated as an exponential decay of the following form:

$$C(\tau) = A\exp(-2\bar{\Gamma}\tau + \mu_2\tau^2 - \cdots)$$

Here, C is the baseline subtracted autocorrelation function and τ is delay time. Values for A, Γ, and μ_2 can be readily obtained by a least squares fit. One then finds the intensity weighted average diffusion coefficient $D_{t,avg.}$ with the relation $\Gamma = D_{t,avg.} * q^2$. Here q is the scattering vector given by $q = (4\pi n/\lambda)\sin(\theta/2)$. The refractive index of the liquid is n. The wavelength of the laser light is λ, and scattering angle, θ. Finally, one uses the Stokes-Einstein relation to go from Dτ to Z-average particle size, D_z:

$$D_z = \frac{k_B T}{3\pi\eta D_{t,avg}}$$

where D_z is the hydrodynamic diameter (particle size)

$D_{t,avg}$ is the translational diffusion coefficient (measured by DLS)

k_B is Boltzmann's constant (known)

T is thermodynamic temperature (known)

η is dynamic viscosity (known).

The weighting of the average is somewhat convoluted. The decay constant is proportional to the diffusion coefficient. So, by DLS one has determined the intensity weighted diffusion coefficient. The diffusion coefficient is inversely proportional to size. Therefore, the "Z-average size" is the intensity weighted harmonic mean size.

Size distribution. (From 'A Basic Guide to Particle Characterization', Malvern Instruments).

Intensity weighted distributions. Dynamic light scattering techniques will give an intensity weighted distribution, where the contribution of each particle in the distribution relates to the intensity of light scattered by the particle. For example, using the Rayleigh approximation, the relative contribution for very small particles will be proportional to $(\text{size})^6$.

When comparing particle size data for the same sample measured by different techniques, it is important to realize that the types of distribution being measured and reported can produce very different

particle size results. This is clearly illustrated in the example below, for a sample consisting of equal numbers of particles with diameters of 5nm and 50nm. The number weighted distribution gives equal weighting to both types of particles, emphasising the presence of the finer 5 nm particles, whereas the intensity weighted distribution has a signal one million times higher for the coarser 50nm particles. The volume weighted distribution is intermediate between the two.

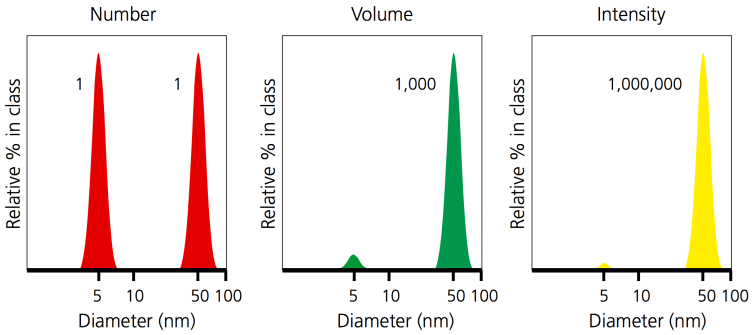

It is possible to convert particle size data from one type of distribution to another, however this requires certain assumptions about the form of the particle and its physical properties.

Dynamic light scattering measurements on LAH4-L1 – siRNA complexes.

Table X-2. The results of DLS measurements on siRNA solution in 15mM HEPES buffer (pH 7.4) titrated with LAH4-L1 peptide at 25°C.

Sample	peptide / siRNA molar ratio	+/– total ratio	Derived Count Rate (kcps)	Z-Average (d, nm)	Volume-averaged size (d, nm)	PDI
30μM siRNA in 15mM HEPES			190	462	16	0,569
2mM LAH4-L1			745	258	4	0,346
29μM siRNA + 4.9μM LAH4-L1	0,17	0,02	2988	342	1019	0,499
29μM siRNA + 9.6μM LAH4-L1	0,33	0,04	4203	299	1803	0,405
28μM siRNA + 18.5μM LAH4-L1	0,67	0,08	7765	311	1605	0,507
27μM siRNA + 26.8μM LAH4-L1	1,00	0,12	11927	360	1637	0,486
26μM siRNA + 34.5μM LAH4-L1	1,33	0,16	15346	426	1112	0,492
25μM siRNA + 42μM LAH4-L1	1,67	0,20	16959	343	2114	0,629
23μM siRNA + 55μM LAH4-L1	2,43	0,28	28185	448	1481	0,442
22μM siRNA + 71μM LAH4-L1	3,20	0,38	60742	771	1411	0,464
21.6μM siRNA + 103μM LAH4-L1	4,80	0,57	34023	516	521	0,249
19.7μM siRNA + 173μM LAH4-L1	8,80	1,05	54868	844	910	0,206

Table X-3. The results of DLS measurements on siRNA solution in 50mM acetate buffer (pH 5) titrated with LAH4-L1 peptide at 25°C.

Sample	peptide / siRNA molar ratio	+/– total ratio	Derived Count Rate (kcps)	Z-Average (d, nm)	Volume-averaged size (d, nm)	PDI
50μM siRNA in 50mM acetate			179	318	4	0,500
1mM LAH4-L1			68	124	3	0,628
48μM siRNA + 12.7μM LAH4-L1	0,26	0,06	4435	456	817	0,584
46.3μM siRNA + 24.4μM LAH4-L1	0,53	0,11	15153	344	1571	0,745
44.6μM siRNA + 35.4μM LAH4-L1	0,79	0,17	15038	462	2095	0,774
43μM siRNA + 46μM LAH4-L1	1,06	0,23	20211	550	1578	0,666
42μM siRNA + 55μM LAH4-L1	1,32	0,28	32742	690	1930	0,595
40μM siRNA + 64μM LAH4-L1	1,58	0,34	46278	706	1915	0,762
38μM siRNA + 80μM LAH4-L1	2,11	0,45	57835	877	2315	0,655
35.7μM siRNA + 94μM LAH4-L1	2,64	0,57	57907	804	1626	0,555
33.3μM siRNA + 110μM LAH4-L1	3,30	0,71	52477	981	655	0,626
31.3μM siRNA + 124μM LAH4-L1	3,96	0,85	68396	1240	716	0,709
29.4μM siRNA + 136μM LAH4-L1	4,62	0,99	55867	1310	943	0,614

Dynamic light scattering measurements on LAH4-L1 – siRNA complexes in saline buffers.

Table X-4. The results of DLS measurements on siRNA solution in 15mM HEPES buffer (pH 7.4), 146mM NaCl titrated with LAH4-L1 peptide at 25°C.

Sample	peptide / siRNA molar ratio	+/– total ratio	Derived Count Rate (kcps)	Z-Average (d, nm)	Volume-averaged size (d, nm)	PDI
50μM siRNA			185	180	5	0,226
0.5mM LAH4-L1			1219	38	20	0,310
48μM siRNA + 19.2μM LAH4-L1	0,40	0,05	11565	1478	866	0,600
44μM siRNA + 61.4μM LAH4-L1	1,40	0,17	66403	2706	1182	0,464
40μM siRNA + 97μM LAH4-L1	2,40	0,29	73324	3866	2644	0,338
34.7μM siRNA + 153μM LAH4-L1	4,40	0,52	91118	4396	2792	0,310
32.5μM siRNA + 175μM LAH4-L1	5,40	0,64	79948	5571	2945	0,380
30.5μM siRNA + 195μM LAH4-L1	6,40	0,76	84632	6794	3489	0,344
27.2μM siRNA + 228μM LAH4-L1	8,40	1,00	68479	7092	4318	0,315

Table X-5. The results of DLS measurements on siRNA solution in 50mM acetate buffer (pH 5), 120mM NaCl titrated with LAH4-L1 peptide at 25°C.

Sample	peptide / siRNA molar ratio	+/– total ratio	Derived Count Rate (kcps)	Z-Average (d, nm)	Volume-averaged size (d, nm)	PDI
50μM siRNA			629	35	53	0,789
0.5mM LAH4-L1			1462	577	6	0,544
48μM siRNA + 19.2μM LAH4-L1	0,40	0,09	15105	1080	741	0,528
44μM siRNA + 61.4μM LAH4-L1	1,40	0,30	74492	2091	1099	0,729
40μM siRNA + 97μM LAH4-L1	2,40	0,51	90508	4656	2150	0,476
34.7μM siRNA + 153μM LAH4-L1	4,40	0,94	85388	4646	1728	0,557
32.5μM siRNA + 175μM LAH4-L1	5,40	1,16	86629	5227	2811	0,341
30.5μM siRNA + 195μM LAH4-L1	6,40	1,37	77372	6956	2858	0,309
27.2μM siRNA + 228μM LAH4-L1	8,40	1,80	87000	7229	3902	0,304

Appendix 2.

A spatial view of siRNA – LAH4-L1 interactions. The lysines are shown in magenta, charged histidines in violet, and deprotonated histidines in grey.

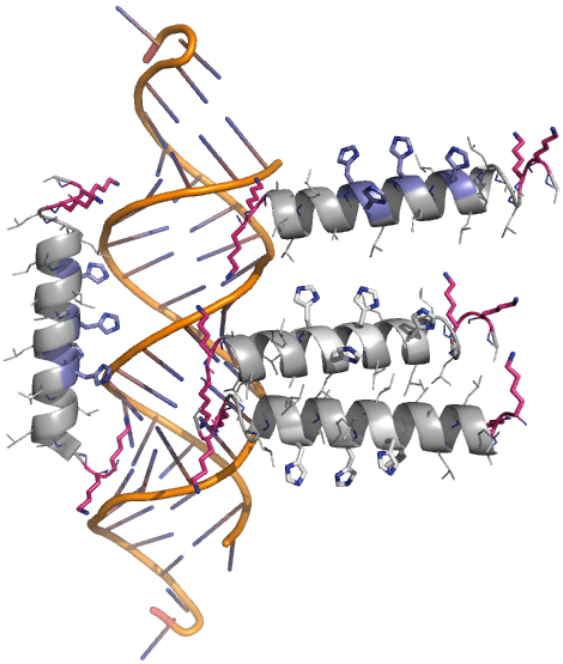

Appendix 3.

REDOR pulse program and its schematic representation.

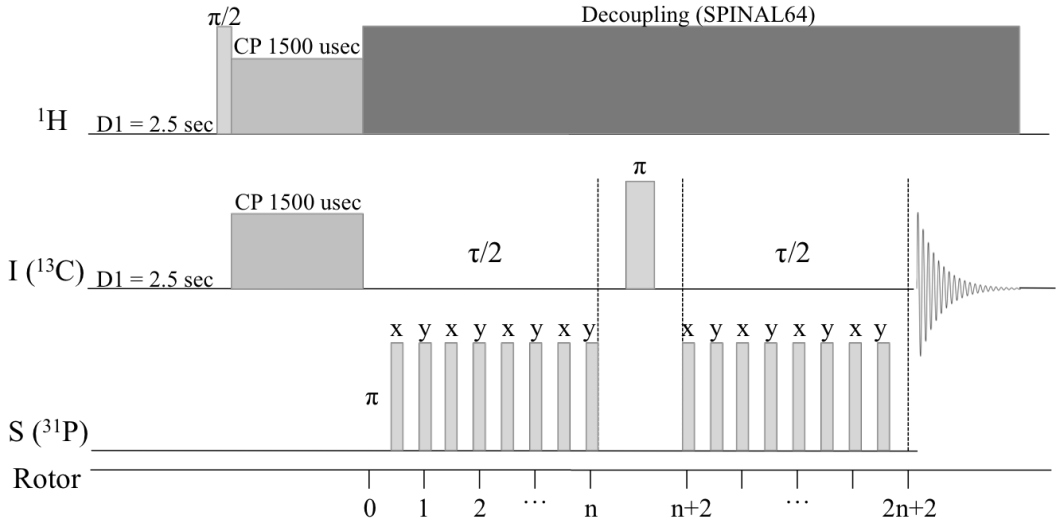

Pulse program.

```
;2D REDOR  experiment

;parameters:
;d1 : recycle delay
;d31 : =1s/cnst31, 1 rotor period
;p2 : X 180 degree pulse
;p3 : H 90 degree pulse
;p12 : Y 180 degree pulse
;p15 : contact time
;d20 : delay in saturation pulse train
;p30 : =p31-0.4u -> calculated pulse for cpd
;p31 : pulse length in decoupling sequence
;pl1 : X power level for CP
;pl2 : proton contact power level
;pl3 : Y power level (for H to Y CP)
;pl5 : Y power level for Y to X CP
;pl11 : power level for X pulses
;pl12 : power level for H 90 and standard proton decoupling
;pl13 : e.g. used in tppm13
;spnam0 : file name for variable amplitude CP
;l0 : =1, must be odd
;l20 : number of pulses in saturation pulse train, 0 if undesired
;cnst31 : spinning frequency
;cpdprg2 : sequence used for decoupling (tppm15, cw, etc.)
;FnMode : QF

;$COMMENT=REDOR  experiment, cp for excitation
;$CLASS=Solids
;$DIM=pseudo 2D
;$TYPE=cross polarisation
;$SUBTYPE=REDOR
;$OWNER=Bruker
define delay del25 ;calculate sync. delays
"del25=(0.25s/cnst31)"
define delay del26
"del26=(0.25s/cnst31)-(p12/2)"
define delay del27
"del27=(0.25s/cnst31)-(p2)"
```

```
"p1=p2/2"
"d31=1s/cnst31"                         ;allow protection for misset cnst31

#include <tppm.incl>
#include <trigg.incl>
;10 usec trigger pulse at TCU connector I cable 6


1 ze

2 10m do:f2
saturate, d20
  (p3 ph1):f2
  lo to saturate times l20
  d1
  d31

  10u pl2:f2 pl1:f1 pl3:f3
  2u rpp9
  2u rpp8
  p3:f2 ph1 ;proton 90 pulse
  0.3u pl22:f2
  (p15:spf1 ph2):f1 (p15:spf2 pl22 ph10):f2
  del25  cpds2:f2
3 del26 pl12:f2
  (p12 ph8^):f3
  del26
  lo to 3 times l0
  del27
  (p1 pl11 ph4):f1
  (p2  ph5):f1
  (p1 ph4):f1
  del27
4 del26
  (p12 ph9^):f3
  del26
  lo to 4 times l0
  del25
  go=2 ph31
  1m do:f2
  10m mc #0 to 2 F1QF(1m iu0 & 1m iu0)
HaltAcqu, 1m
exit

ph1= 1 3
ph2= 0 0 1 1 2 2 3 3
ph4= 0 0 1 1 0 0 1 1
ph5= 1 1 2 2 1 1 2 2
ph8= 0 1 0 1 1 0 1 0
ph9= 0 1 0 1 1 0 1 0
ph10= 0
ph31= 0 2 1 3 2 0 3 1
```

Nataliia VOIEVODA

Etudes des Interactions entre la Membrane et les Acides Nucléiques aves le Peptide de Transfection LAH4-L1

Résumé

La thérapie génique et l'interférence par l'ARN sont des méthodes pleines de promesses pour le traitement de nombreux troubles génétiques et infections virales, mais ce sont aussi des outils polyvalents pour l'étude des mécanismes génétiques et épigénétiques à la base du bon fonctionnement ou dysfonctionnement des cellules et des organismes complexes. Toutefois, la délivrance intracellulaire d'acides nucléiques reste un obstacle majeur pour la mise en œuvre de ces thérapies. En dépit des progrès récents dans le domaine, il existe un nombre limité d'agents de transfection non viraux qui ont passé à la phase clinique de la mise au point de médicaments.

Un agent de transfection efficace forme un complexe (généralement non-covalent) avec des acides nucléiques, qui est stable dans l'environnement extracellulaire, en particulier dans le plasma sanguin. En outre, il doit favoriser la délivrance cellulaire en interagissant avec la membrane plasmique ou avec des glycosaminoglycanes chargés négativement et induire l'absorption par endocytosedu complexe de transfection. Enfin, l'agent de transfection devrait améliorer l'échappement de l'endosome et le dépaquetage des acides nucléiques à partir du complexe.

Les peptides amphiphiles et cationiques, qui ont la capacité de pénétrer dans les cellules, possèdent toutes les caractéristiques ci-dessus nommées. En effet, ils s'associent aux acides nucléiques via des liaisons électrostatiques, ils se lient de manière efficace et traversent la membrane plasmique en favorisant l'absorption de la cargaison. LAH4-L1 est le peptide de la famille LAH4 riche en lysines et histidines , possédant une activité de transfection d'ADN et de pARNi prometteuse. ce qui a été montré dans des expériences biologiques sur des cellules en culture. Le peptide LAH4-L1 présente des modes d'interaction différents avec les membranes à pH neutre et acide, ce qui est l'une des caractéristiques les plus importantes puisqu'elle assuret une libération efficace des acides nucléiques dans le cytoplasme.

Ce travail est dédié à l'étude des caractéristiques structurales et thermodynamiques de l'association LAH4-L1 avec des membranes modèles et des acides nucléiques, comme l'ADN générique et de pARNi. Une grande variété de techniques biophysiques, telles que la résonance magnétique nucléaire, le dichroïsme circulaire, la calorimétrie de titration isotherme, la diffusion dynamique de la lumière et le dosage d'efflux de la calcéine, a été utilisée pour élucider le mécanisme de la transfection cellulaire efficace par le peptide LAH4-L1.

Mots clés : peptide de transfection LAH4-L1, ADN, pARNi, membranes, méthodes biophysiques, RMN, TCI, DC.

Résumé en anglais

Gene and RNA-based therapies have a great promise as the methods for the treatment of variety of the genetic disorders and viral infections, but also it is a versatile tool for the investigation of the genetic and epigenetic mechanisms underlying the proper functioning or dysfunctioning of the cells and complex organisms. However, intracellular delivery of nucleic acids remains a major hurdle for the implementation of these therapies. In spite of the recent progress in the field, there is limited number of the non-viral transfection agents that passed to the clinical phase of the drug development.

An efficient transfection agent forms a complex (usually non-covalent) with nucleic acids, which is stable in the extracellular environment, in particular in the blood plasma. Furthermore, it should promote the cellular delivery by interacting with the plasma membrane or negatively charged glycosaminoglycans and inducing the endocytic uptake of the transfection complex. Finally transfection agent should enhance the endosomal escape and unpacking of the nucleic acids from the complex.

Cationic amphipathic cell-penetrating peptide comprise all above-named features as they associate electrostatically with the nucleic acids, they bind efficiently and translocate plasma membrane promoting the cargo uptake. LAH4-L1 is the lysine and histidine-rich designed peptide from LAH4 family, possessing a promising DNA and siRNA transfection activity, which was shown in biological experiments on the cell culture. LAH4-L1 peptide displays different modes of interaction with the membranes at neutral and acidic pH, which is one of the most important features that assure an efficient nucleic acid release to the cytoplasm.

This works is dedicated to the investigation of structural and thermodynamic characteristics of the LAH4-L1 association with model membranes and nucleic acids, such as generic DNA and siRNA. The variety of the biophysical techniques, as nuclear magnetic resonance, circular dichroism, isothermal titration calorimetry, dynamic light scattering and calcein efflux assay, were used to unravel the mechanism of efficient cellular transfection by LAH4-L1 peptide.

Key words : transfection peptide LAH4-L1, DNA, siRNA, membranes, biophysical methods, NMR, ITC, CD.